CALIFORNIA POLYTECHNIC STATE UNIVERSITY (CALPOLY)

Technical Turbine Design Report

2021 DOE Collegiate Wind Competition

May 23, 2021

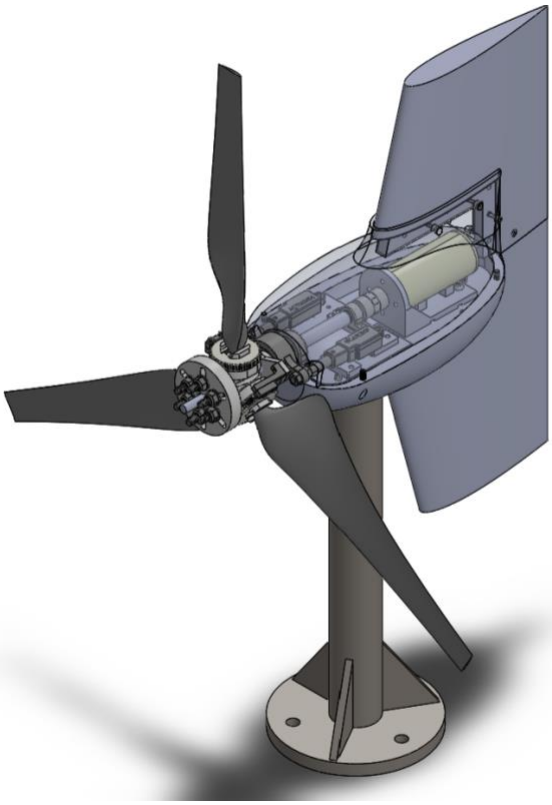
Aero Team
Jessica Dent (Lead)
Josephine Maiorano

Electrical Team
Grayson Capers (Lead)
Shane Alayvilla
Jonathan Yu
Matthew Renati

Sophie Spencer – **Team Lead**

Mechanical Team
Zachary Dunkleberger (Lead)
Elizabeth Costley
Jeff Larson
Kinsale Sproule
Milo Klein
Nora Riedinger

Advisors
Dr. Andrew Kean – Principal Investigator
Prof. Ali Dehghan Banadaki – Faculty Advisor
Dr. Patrick Lemieux – Faculty Advisor
Paulo Iscold & Nandeesh Hiremath – Wind Tunnel Managers



WIND POWER
CAL POLY, SAN LUIS OBISPO, CA

TABLE OF CONTENTS

1.0 Executive Summary 3

2.0 Technical Design 4

2.1 Overall Design Objective 4

2.2 Blade Design Objective 4
2.2.1 Blade Design 4
2.2.2 Blade Structural Analysis 6
2.2.3 Aerodynamic Analysis 7

2.3 Pitching Mechanism 8
2.3.1 Pitching Mechanism Design 8
2.3.2 Pitching Mechanism Analysis 9

2.4 Drive Train Components 9
2.4.1 Shaft Design 9
2.4.2 Shaft Analysis 10
2.4.3 Bearings 10
2.4.4 Rotor Balancing Mechanism 10

2.5 Support Structures and Yaw 11
2.5.1 Tower Design and Analysis 11
2.5.2 Yawing Mechanism and Vane Design 12

2.6 Electrical Systems Objectives 12
2.6.1 Electrical Systems Overview 12
2.6.2 Generator Design and Testing 13
2.6.3 Hall Effect and Current Sensors 15
2.6.4 Load Design and Analysis 16
2.6.5 Buck Boost and Voltage Regulation 17
2.6.6 Controls Analysis and Software Documentation 17

3.0 Testing 18

3.1 Field Testing 19

3.2 Wind Tunnel Testing 19

4.0 Conclusion 21

5.0 References 22

1.0 EXECUTIVE SUMMARY

In this report, the California Polytechnic State University, San Luis Obispo Wind Power team (CPWP) outlines the technical design decisions, analysis, and testing results of the turbine development component of the Department of Energy's 2021 Collegiate Wind Competition (CWC). The CWC has tasked CPWP with designing, manufacturing, and testing a small-scale wind turbine to meet the dimensional and loading engineering specifications outlined in the CWC Rules and Requirements [1]. The turbine should ideally meet a set of performance tasks: cut-in wind speed, power curve performance, control of rated power, safety, and durability tasks. Given the disruptions from 2020-2021 public health restrictions, the turbine should also be designed for distributed manufacturability.

Section *2.0 Technical Design* presents detailed information on the aerodynamic, mechanical, and electrical design decisions and analyses made by CPWP. This section outlines the overall design objectives as well as those specific to each subsection. First, the rotor aerodynamics design process is outlined presenting the methods used to achieve the final airfoil, chord, and twist distribution. Additionally, both the structural and aerodynamic analysis is provided to ensure the turbine meets the CWC safety requirements and optimizes rotor performance. Subsequently, the design of the mechanical systems including, the pitching system, drivetrain, support structures, and yawing system, is showcased with both structural and functional analysis. Next, the electrical system section documents the design, build, and test of each of the components that make up the electrical subsystem. In addition, the controls analysis and software documentation are outlined including how each subsystem will satisfy each of the turbine testing tasks.

Section *3.0 Testing* outlines the field and wind tunnel testing CPWP has been able to accomplish and their respective results. With limited lab and wind tunnel accessibility this year, field testing has been largely utilized to ensure the functional and structural performance of the turbine as well as for design iteration for optimizing aerodynamic performance. Wind tunnel testing results are outlined as well as how the results influenced the team's next steps in improving performance.

Section *4.0 Conclusion* summarizes CPWP's accomplishments and turbine performance results. Additionally, this section illustrates what the team learned from their first year competing in the CWC and outlines future steps that will be taken to optimize turbine performance.

2.0 TECHNICAL DESIGN

The Cal Poly Wind Power (CPWP) team was challenged by the CWC to design, build, and test a wind turbine that could produce power under the various testing conditions outlined in the CWC Rules and Requirements [1]. A wind turbine is designed to extract as much energy out of the wind as possible by utilizing blade aerodynamics to rotate a shaft, which in turn drives a generator to produce electricity. The technical design of the turbine outlined in the following sections are broken down by the main components of the turbine: the blades, pitching mechanism, drivetrain, support structures and yaw mechanism, and finally the electrical and controls systems.

2.1 Overall Design Objective

Like most teams, the CPWP team needed to overcome unique limitations due to limited access to the campus machine shops and testing facilities as well as limited ability to meet up in person to work on the design. Being a brand-new team to the competition, the Cal Poly team also needed to complete all design work from scratch. A majority of this competition year was dedicated to the technical design of the turbine. The team did extensive research through the turbine design reports of previous competition teams. Common challenges previous teams experienced were noted when determining the design objectives for the CPWP 2021 turbine. Challenges identified include difficulty achieving low cut-in wind speeds and stalling in high wind speeds.

The winning report from the 2020 competition influenced the team's design decisions by encouraging the ambitious design of a variable pitch turbine to optimize the power output of the turbine, especially at low speeds. The pitching mechanism would also allow the turbine to increase the angle of attack at lower wind speeds and aid in reducing the cut in wind speed. Additionally, it could be used to pitch the blades to limit the rotor speed in the control of rated rotor speed task and "park" the turbine in extreme wind conditions. The team emphasized selecting a generator which exhibited low startup torque and thus provided a low cut in wind speed. The 2021 Cal Poly turbine was designed to be a 40-Watt variable-pitch horizonal axis wind turbine. The theoretical maximum power available in the wind is higher than this, however the team assumed that this first turbine attempt would have significant losses on top of the Betz limit due to lack of experience, so the goal power production was set at 40W.

2.2 Blade Design Objective

The blade design is integral to producing the desired turbine performance, so the team placed emphasis on iteration of this aspect of the turbine to optimize the aerodynamic performance of the blades. Throughout the blade design process, the team emphasized repeated testing to produce blades with a low cut-in wind speed and reliable performance in variable wind conditions. The team chose 11 m/s as the rated wind speed for the turbine, which affected the chosen tip speed ratio (TSR) and blade geometry.

The team originally chose a TSR of 5 since the generator was not yet fully specified, however later learned through experimentation that lower tip speed ratios perform better with real-world conditions for turbines this small and fast moving. The final TSR selected was 3.75, to align the peak power producing performance of the blades with the design generator speed of about 2100 rpm.

2.2.1 Blade Design

The first consideration was which airfoil to use. After extensive research through research papers and available small wind turbine data, the team used the software Q-Blade to compare the lift, drag, lift over drag coefficients (C_L/C_D) versus alpha, and power coefficients of each airfoil. The airfoil which exhibited the highest C_L/C_D versus alpha at low angles of attack was selected. The blades were designed using blade element momentum theory [2, 3]. This method was built into a MATLAB script which was developed entirely by the student team. The MATLAB code uses a numerical method [3] to iterate the angle of attack

for each blade element by solving for the intersection of that individual element's lift coefficient (black) with the empirically derived C_L versus alpha curve for that airfoil (blue), as shown in Figure 1.

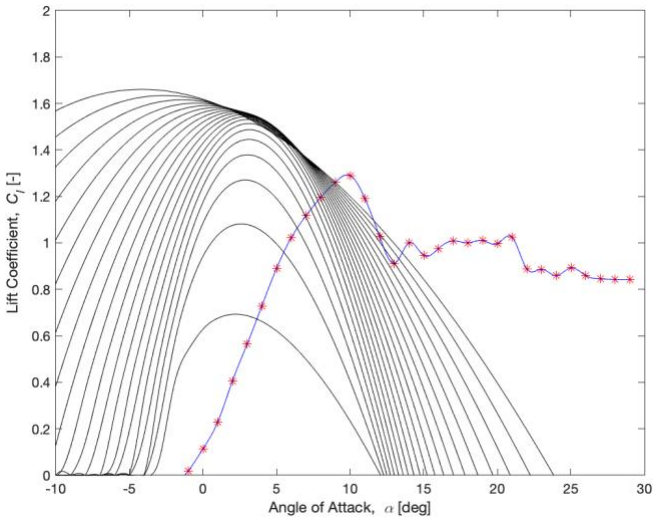


Figure 1. C_L and Angle of Attack Iteration at Each Blade Element to Solve for Blade Twist Distribution.

Additionally, the code outputs the necessary chord lengths and twist angles for the inputs of the desired tip speed ratio (TSR), and the predicted lift, drag, and moment coefficients produced via QBlade for the specified airfoil. The code was designed to analyze the blade with 2 or more different airfoils, such as a thicker root airfoil for greater structural integrity. The Reynolds number that the team used was about 50,000, which was determined using an average chord length which could be reasonably manufactured and withstand the loads induced at 22 m/s wind speeds.

The Cp-Lambda plot using the chosen airfoil for blade design, SD7043, defines the performance of the turbine's theoretical performance over a range of tip speed ratios. The Cp-Lambda plot of the final rotor design is shown in Figure 2. For most blade designs, the power coefficient peaked at a TSR of about 7, however with the incredibly small rotor diameter restrictions, the team determined that a lower rpm was necessary for both safety and practicality. The team chose a design TSR of 3.75 instead.

The blade manufacturing process was considered by a senior project team, and it was concluded that due to the limited machine shop access, experience with composites, and CNC milling, the most reliable route for blade manufacture would be to 3D print them. The team determined that the best materials for 3D printing were ABS or an SLA resin. The ABS was determined to be more lightweight and less brittle, however less structurally sound, and with significantly rougher surface finish. The application of a coating to smooth the surface finish was considered, however, the risk of significant mass imbalance was of concern. The team decided to use the SLA resin printed blades for final prototypes.

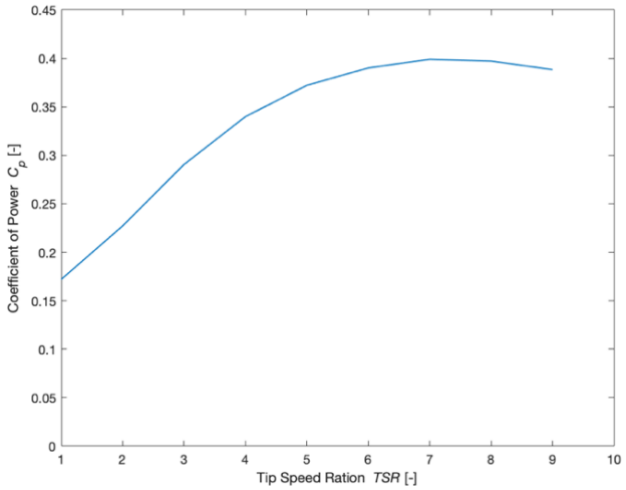


Figure 2. Power Coefficient versus Tip Speed Ratio of Turbine Using SD7043 Airfoils.

2.2.2 Blade Structural Analysis

The team assessed that the most critical loading would be at the cut-out wind speed during the safety test, at 22 m/s. Since this is the team's first time competing in the Collegiate Wind Competition, conservative values were used and a broad safety factor of 2.0 was applied to estimated maximum loads. This made the safety factor even higher on the turbine when in a static conditions, such as parked in high winds, and during conditions at or below the rated speed. The loads were calculated using the thrust, torque, drag, and lift coefficients from the BEM analysis at 22 m/s and are listed in Table 1.

Table 1. Loading on Blades Operating at Maximum Wind Speed.

Load	Magnitude	Units
F_A – Axial Force	33.5	N
F_N – Flapwise (Lift) Force	16.0	N
F_T - Edgewise (Drag) Force	3.1	N
M_P - Pitching Moment	-0.8	N-m
M_X - Edgewise Moment	0.4	N-m
M_Y - Flapwise Moment	0.2	N-m

The combined loading on each blade while operating can be broken down into three forces and three moments, characterized by being axial, flapwise, or edgewise. The diagram in Figure 3 shows the direction of these loads with reference to the naming convention in Table 1.

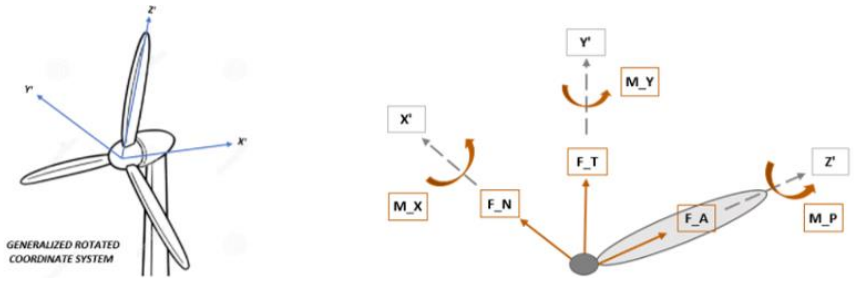
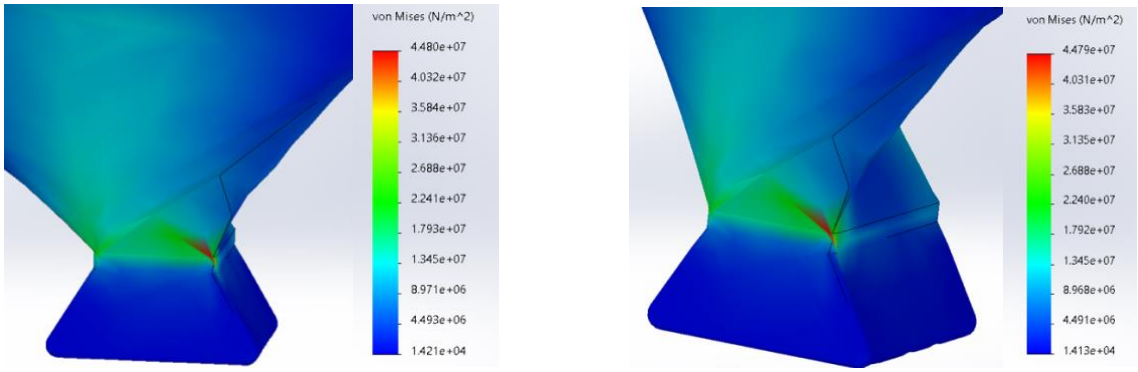


Figure 3. Diagram of External Forces and Moments Applied to Each Blade.

To analyze the effects of this loading, the team conducted finite element analysis (FEA) on the blade geometries, with both operational and parked loading conditions, to ensure that they would not experience stresses greater than the yield strength of the material. The loads used in FEA also utilize the same safety factors as previously mentioned. Torsion induced in the shaft from the blades being parked was taken under consideration in the shaft design, see 2.4.1 Shaft Design for more details. During the stationary analysis, the drag force on the blades in the edgewise direction from rotational motion were negligible.



(a) Operational Loading (b) Stationary Loading

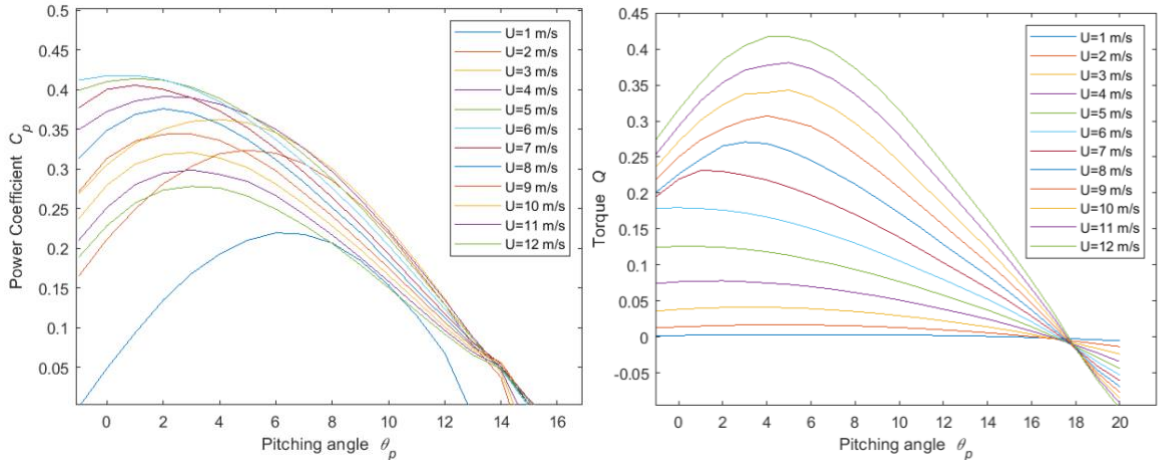
Figure 4. Results of the Operational and Parked Loading FEA Studies at 22 m/s Wind Speed.

The blades were assessed using a 60% reduced material strength for the ABS resin, the material properties for which were estimated from the manufacturer's datasheets. The reduction in strength is to account for the loss of strength due to the material being 3D printed. The highest stress concentrations were around the root as expected, as seen in Figure 4. The highest expected stresses were well below the yield strength of the material. The blades passed both simulations and real-world testing, leading the team to confirm that the rotor design was structurally sound.

2.2.3 Aerodynamic Analysis

Most of the aerodynamic analysis was done first by simulation and then validated in real-world testing. The majority of the real testing was done on a fixed-pitch turbine, leading to insights about the aerodynamic behavior of the turbine. With the focus on reducing the cut-in speed, the team found that increasing the angle of attack for low wind speeds would increase the torque produced by the rotor and thus lead to a lower cut-in wind speed with slightly higher power. This was validated during simple comparative testing of a set of blades early in the design process, using static hubs with either 0 or 15 degrees angle of attacks.

Since the turbine was designed as a variable pitch, further aerodynamic analysis of the blade performance at a range of pitch angles was necessary. This was again performed using the team's custom MATLAB script. To evaluate the best pitching angle for each wind speed, plots of the torque and power coefficient versus a range of pitch angles was used and are shown in Figure 5. The team found that the effects of the pitch angle on torque becomes more pronounced as the wind speeds increase, while the optimum pitch angle for a high power coefficient decreases with increased wind speeds. This led the team to determine that the turbine should start at higher pitch angles at low wind speeds, and then decrease the pitch to zero degrees when the turbine hits the rated wind speed of 11 m/s.



(a) Power Coefficient vs. Pitch Angle (b) Torque vs. Pitch Angle

Figure 5. Plots of Cp vs. Pitch Angle and Torque vs. Pitch Angle.

Various blade geometries were compared by 3D-printing a fixed-pitch rotor set and documenting the performance at low and high wind speeds. Comparative tests were completed with a high-powered fan. The team printed six different rotor sets to test, including ones with a factor applied to uniformly increase the blade's chord length. The team had noticed in prior testing that blades with larger chords operated at higher rpms. The results of the testing showed that blades with a large chord factor produced the most power.

As a result of final testing, the blades chosen for the team's final turbine used blades with only SD7043 airfoils and a chord factor of 4.25 applied to uniformly increase the length of the chords. With more time available, the team would have liked to further iterate root airfoils within the same family to further improve performance by generating more lift at the root of the blade.

2.3 Pitching Mechanism

A blade pitching system on a turbine can improve its efficiency and reduce the likelihood of failure when operating in extreme wind speeds. Primarily, the pitching system helps maintain a constant mechanical power from the rotor to maximize the power generation of the turbine's generator. The designed pitching mechanism achieves this by adjusting each blade's angle of attack with respect to the wind simultaneously. The angle of attack directs the lift and drag forces induced by the wind, which then controls the rotor speed. This enables the generator to produce consistent electrical power at or above its rated rotational speed.

2.3.1 Pitching Mechanism Design

To maintain reliable power, the pitching mechanism must pitch accurately and rapidly and maintain a low power draw to improve the efficiency of the turbine. Key structural considerations include reducing inertia about the rotational axis as well as reducing the moment on the cantilevered end of the turbine shaft. The final pitching system subassembly is shown in Figure 6.

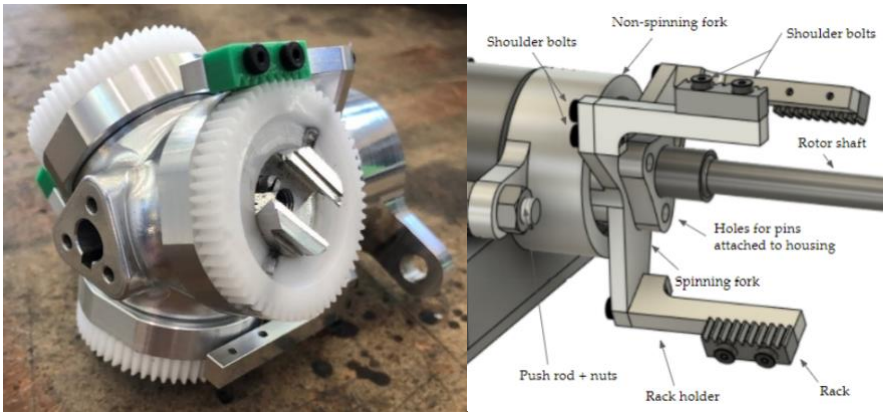


Figure 6. Assembled Pitching Mechanism Subassembly

The pitching mechanism design was evaluated using the technical specifications given in Table 2. Ultimately, the rack-and-pinion design was chosen to focus on mechanical simplicity and reliability, rather than making the assembly more compact. The final design of the pitching mechanism is a system that is actuated by two linear actuators mounted inside the nacelle, which are connected by pushrods to the relative motion subassembly outside the nacelle.

Table 2. Pitching Mechanism Technical Requirements.

Requirement	Value	Unit
Pitch Rate	2	deg/s
Pitch Torque	0.8	N-m
Pitch Range	20	deg
Active Power Draw	5	W
Standby Power Draw	1	W
Subsystem Mechanical Efficiency	90	%
Pitch Resolution	0.5	deg

The relative motion subassembly allows the collars connected to the actuators to slide along the rotor shaft axis. While the rack and pinions spin, the relative motion sub assembly allows for linear movement of the racks and causes pitching of the blades. The blade mounting subassembly then constrains the blades in all degrees of freedom, except for rotation about the pitch axis, and establishes the primary load path from the blades to the rotor shaft.

While the team focused on mechanical reliability, CPWP also worked to limit the hub's diameter to achieve better aerodynamic performance by decreasing the radial distance from the axis of the rotor shaft to the start of the blade. This also lowers the rotational inertia of the outboard turbine system. The relative motion subassembly rack mounting was designed for easy manufacturability and emphasized using stock material that is low cost. In addition, three pins were used in the hub housing to constrain rotational degrees of freedom of the spinning fork. Using pins helped shorten the tolerance stack for the assembly so that the angular position of the racks relative to the pinions could be better controlled.

To select the linear actuators, calculations were performed for the linear travel, linear velocity, and tangential force required from the actuator for various pinion radii. Ultimately, the 6 V DC Actuonix L12-R Micro Linear Servos for RC and Arduino with 210:1 gear reduction were chosen as the actuators for the final design. The L12-R also features closed-loop position feedback that easily interfaces with an Arduino control system.

2.3.2 Pitching Mechanism Analysis

The pitching mechanism underwent static testing to ensure the blade connection subassembly and entire rotating subassembly would withstand the loads they would experience during operation. This was done by applying loads using fish scales in the directions of the anticipated maximum loads. The static testing setup can be seen in Figure 7. The static testing resulted in the failure of the 3D printed dovetail base, used to attach the blades to the hub. The team addressed this issue by machining the final dovetail bases out of aluminum.



Figure 7. Pitching Mechanism Static Loading Apparatus

2.4 Drive Train Components

The drive train consists of the shaft, bearings, rotor balancing mechanism, couplings, and appropriate mounting and housing hardware for the listed components. The drive train needs to efficiently transmit power from the hub to the generator while withstanding the cyclic loads created during operation, avoiding vibration, and providing sufficient alignment so as not to impart undue stresses or wear on the components.

2.4.1 Shaft Design

When designing the shaft, the team began by analyzing the expected loads the shaft would be subjected to. These can be separated into parked loads which are always present, and operational loads. The torque from the wind, T_w, the gyroscopic moment caused by the interaction between the rotation of the shaft and the rotation of the yaw and the reactionary torque, T_r, are the only additional operational loads. The loading diagram can be seen in Figure 8.

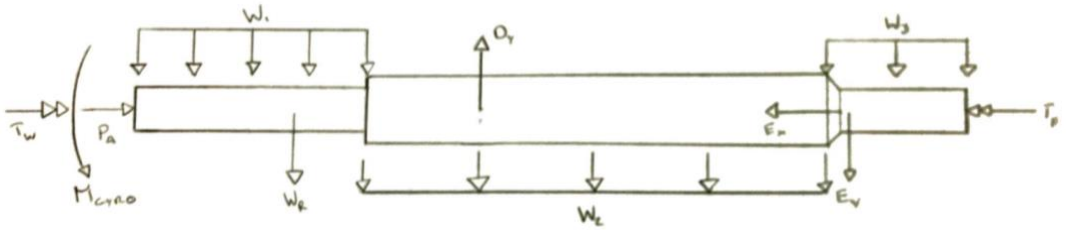


Figure 8. The Loads Used in the Shaft Design.

The values for all these loads are listed in Table 3. The stresses induced by the combined loading of the shaft were used to determine the necessary diameter. The highest stress concentrations of concern were found at the steps in the shaft. The steps were necessary to locate the hub and to take the axial load on the

shaft. The turbine experiences relatively small loading, so a minimum shaft diameter of 8mm was chosen for the purposes of machinability. The shaft design provides a safety factor of 24.8 for the determined loads. The thicker shaft means deflections will be minimized, which also reduces the vibrations in the turbine. The distance between the bearings is maximized to decrease the loads on the bearings. The material chosen for the shaft was 1566 Carbon steel for its strong material properties, cost, machinability, and relatively high endurance limit. For ease of assembly, a wrench flat was included on the shaft.

Table 3. Applied and Reactionary Forces on the Shaft.

Load	Value	Units
Weight force of the front portion of the shaft until the first step	0.012	N
Weight force of the shaft from the first step to the first bearing	0.036	N
Weight force of the shaft between the two bearings	0.063	N
Weight force of the shaft after the second bearing	0.0080	N
Weight of the rotor components	5.56	N
Axial force from the wind	29.80	N
Gyroscopic moment	0.17	N*m
Torque due to the wind	0.40	N*m
Vertical reaction at the first bearing	12.10	N
Vertical reaction at the second bearing	6.37	N
Axial reaction at the second bearing	29.80	N
Torque applied by the generator	0.40	N*m

2.4.2 Shaft Analysis

The critical operational limits on the shaft are the allowable deflections at the bearings, rotor, and coupling. Based on the loading conditions described in Table 3 above, the deflections, stresses, and fatigue on the shaft were found iteratively using an Excel code. The calculated deflections were less than 0.001 degrees for both bearing locations, which are well within the limits specified by the bearing manufacturers. Additionally, the team aimed to minimize deflection of the shaft at the tip as this will lead to whirl. The deflection at the tip of the shaft was also determined to be less than 0.001 degrees, which is sufficiently low to be considered negligible. Lastly, the deflection at the coupling to the generator shaft was also found to be less than 0.001 degrees, well within the tolerance of the coupling. The deflection and yield strength were tested using static load testing, where no deflections or yielding were observed.

2.4.3 Bearings

The shaft required two bearings to accommodate both the axial and radial loading on the shaft. The front bearing needed to hold a 12-millimeter shaft and take a radial load of 15.3 Newtons, while the rear bearing had to hold an 8-millimeter shaft, take an axial load of 29.8 Newtons and a radial load of 9.6 Newtons. Because the loading on the turbine is small, acceptable bearing types narrowed to high-speed ball bearings. This can be an issue at higher loads but is negligible for this design. After selecting NTN radial deep groove ball bearings that fulfilled the loading and sizing requirements, CPWP analyzed the fatigue life. The team found the loading would provide a life far larger than the required design life.

2.4.4 Rotor Balancing Mechanism

The objective of the rotor balancing system is to minimize mass imbalance in the wind turbine's rotor assembly and optimize power collection while meeting safety requirements. The team assumed the sliding

masses were in the plane of the rotor to significantly simplify the analysis. This was accomplished using a grooved plate mounted on the main shaft of the turbine and secured to the hub, which is shown in Figure 9.

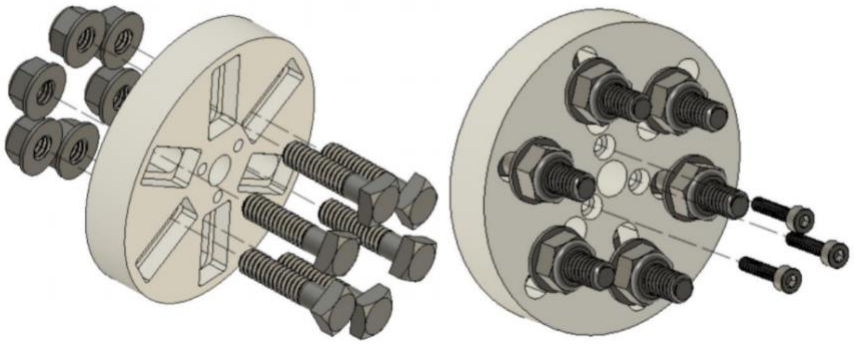


Figure 9. Grooved Plate Rotor Balancing Mechanism Exploded View.

The grooves in the plate allow CPWP to adjust sliding masses in a controlled way, using increments as small as can be measured and accurately maneuvered. The imbalance is measured using an accelerometer mounted to the bearing block, and that information is then fed into a MATLAB program to determine which masses to move and where to move them.

2.5 Support Structures and Yaw

The support structures on the turbine include the tower, base connection to the wind tunnel, nacelle baseplate, and nacelle covers. The yaw mechanism was integrated with the support structure and nacelle.

2.5.1 Tower Design and Analysis

The tower of the turbine consists of a tower column, a tower base dimensioned to the competition requirements, and three ribs to connect the column to the base. The ribs are thin sheet metal cut into triangles, welded to the base and tower to support the tower column. The tower column consists of a steel circular tube to house wires and connect to the yawing mechanism. The tower system was principally concerned with deflection, vibrations, and buckling; finite element analysis was performed, as seen in Figure 10, and it was verified that the system would be functional and meet required deflection limits.

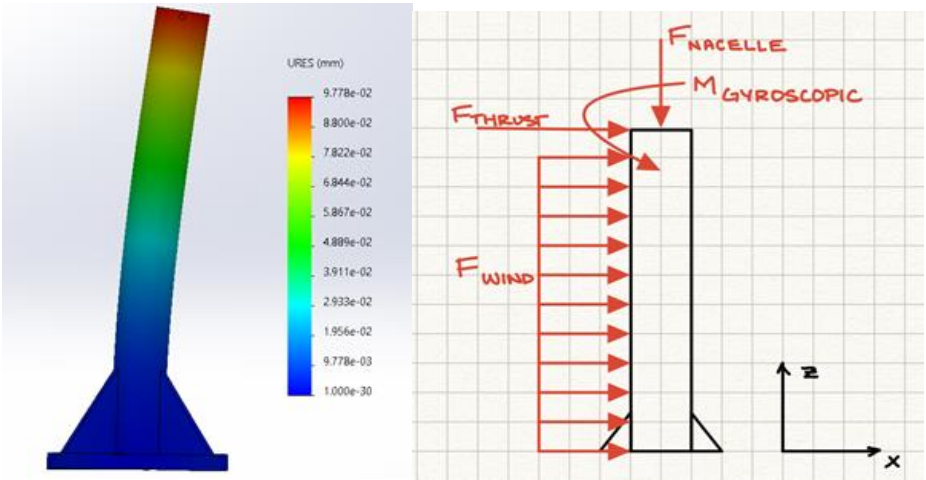
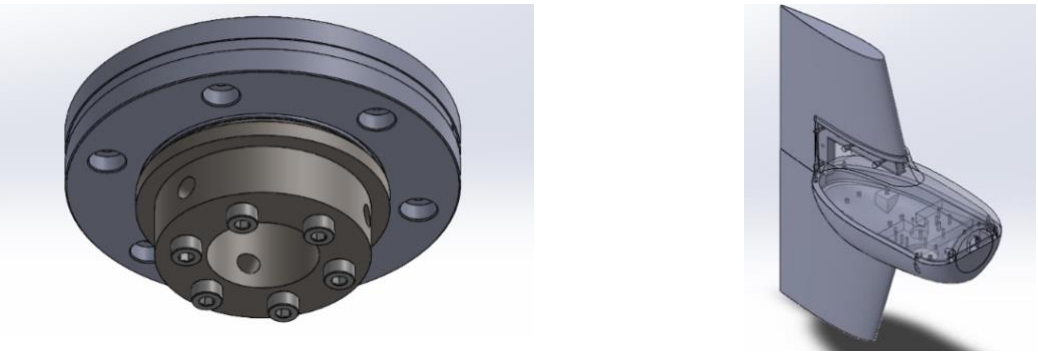


Figure 10. FEA for the Tower, Ribs, and Baseplate. Includes a Radial Thrust Force, Axial Force from the Nacelle, and Pressure Force from the Wind.

2.5.2 Yawing Mechanism and Vane Design

A passive yawing mechanism, which included a rotational mechanism and yaw vane, was utilized to ensure the turbine is oriented into the wind, minimizing yaw error and maximizing power production. For the rotational mechanism shown in Figure 11a, a slew bearing was chosen because it could handle radial, axial, and moment loads with a high factor of safety and minimal friction while also minimizing the number of custom parts needed to be manufactured. The slew bearing connected directly to the nacelle's baseplate, using washers as spacers to eliminate component rubbing, and an internal flange was designed to interface between the slew bearing and tower. The slew bearing was sized based on the static and dynamic loads calculated as well as the tower diameter and wire clearances.



(a) Slew Bearing and Flange Subassembly (b) Yaw Vane and Nacelle Integration

Figure 11. Yaw Mechanism System Components.

Moreover, forces on a yaw vane create a restoring moment that is critical for orienting the turbine. The yaw vane, shown in Figure 11b, was designed to achieve a high drag force when experiencing yaw error by maximizing the surface area with an integrated attachment into the nacelle. Additionally, the yaw vane utilizes a symmetric airfoil cross section, NACA 0015, rather than a flat plate to provide an additional lift force in order to reorient the turbine. The nacelle covers and vanes were produced via a 3D printer and are made of polylactic acid (PLA).

2.6 Electrical Systems Objectives

The turbine's electrical system allows the mechanical rotational power harnessed by the blades to be converted into electrical power. This electrical power is then dissipated across an electrical load. In addition, the electrical system needs to be able to control the speed of the turbine rotor to ensure the system does not exceed its rated rotor speed during high wind speeds. It also must also be able to stop the blades from moving in the event of an emergency. This requires the turbine to continuously sense the power output and rotor speeds to detect if the wind exceeds 11 m/s or a load disconnection has occurred.

2.6.1 Electrical Systems Overview

The electrical system converts rotational mechanical power to electrical power in a controlled and safe manner that completes the turbine testing tasks. On the turbine side of the electrical system, there is a three phase Permanent Magnet Synchronous Generator (PMSG), a rectifier, and an output capacitor. These components will produce a DC voltage with minimal voltage ripple. To best complete the competition tasks, the turbine side of the electrical system is equipped with an Arduino Uno microcontroller. This microcontroller is powered by a buck boost converter that draws from the output of the rectifier. There is a DC voltage, DC current, and a hall effect rotor speed sensor, allowing the microcontroller to monitor these values. The microcontroller can actuate the pitching motors to set the blades to the desired angle.

The load side of the generator contains a dynamic load. The dynamic load is a resistive load whose resistance can be varied by changing the duty cycle of a pulse width modulation signal input. The load side

of the system has an Arduino Uno microcontroller with its own set of DC current and DC voltage sensors. It is powered by a standard 9V cell battery. This microcontroller can change the resistance of the dynamic load by varying the duty cycle of the input.

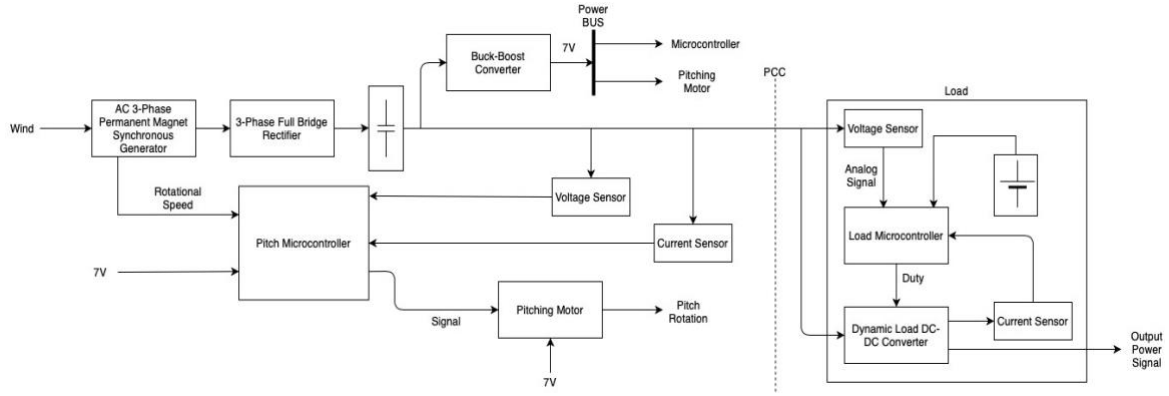


Figure 12. Turbine Electrical System Canonical Model

The electrical system canonical model is shown in Figure 12 and the one-line diagram of the electrical system is shown in Figure 13. The diagram includes the open circuit voltage of the generator (E_G), and the winding resistance. The two diodes represent the pair of diodes that are on at any given point to rectify the three-phase output. The capacitor is used to smooth the voltage ripple. On the load side, a simple potentiometer is used to represent the dynamic load. Both the turbine side and load side of the PCC have a shunt resistor used to sense current.

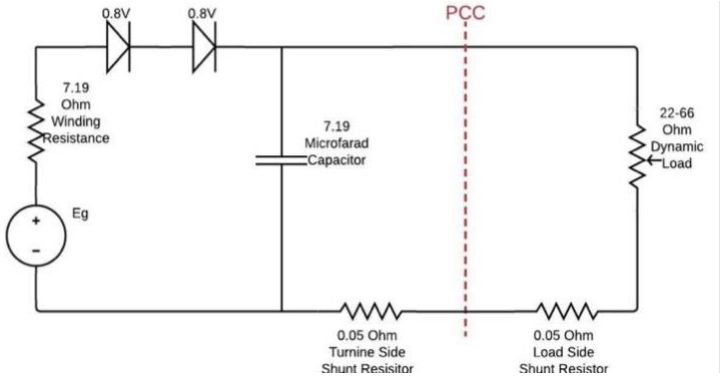


Figure 13. Turbine Electrical System One Line Diagram.

2.6.2 Generator Design and Testing

The generator is the system which converts mechanical rotational power into electrical three-phase AC power. Ideally, the team would have designed and manufactured a generator in house to meet the desired specifications, however, it was decided to purchase this component off the shelf due to uncertainty in the team's ability to secure the lab space needed to manufacture a generator, and as a freshman team in the competition, CPWP wanted to spend more time on other parts of the turbine design. Learning from all-team calls and past competition reports, the team was able to assemble a set of criteria that the generator should meet. The primary concerns noted at the all-team call for off-the-shelf generators were the inability for some generators to produce enough voltage and generators with high cut-in wind speeds. To make sure the generator is producing enough voltage to power a microcontroller, the team wanted to choose one with a low K_V rating. To ensure that the generator could cut in at a low wind speed, a generator with a slotless stator was needed. A slotless stator eliminates the iron teeth that coils are typically wound around, virtually eliminating the cogging torque that could prevent the rotor from spinning at low wind speeds.

In addition to these criteria, the team wanted the generator to have a hall effect sensor. This sensor gives the microcontroller measurements on how fast the rotor is spinning. This information is critical for the control of rated rotor speed task and determining the estimated wind speed. To regulate PCC voltage to at or below 48V, the simplest and most efficient option was to have a generator that would never produce a voltage that high. Since the design of the turbine was to pitch the blades to regulate the rotor speed at wind speeds greater than 11 m/s, the maximum rotor speed the generator should spin at is the optimal TSR rotor speed at 11 m/s. The rotor speed at optimum TSR during an 11 m/s wind speed was expected to be 2100 RPM. To add room for error, the generator should not reach 48 V until the rotor is spinning at more than 3200 RPM. If the K_V rating of the generator is $K_V > \frac{3200\,RPM}{48V}$, thus $K_V > 67\frac{RPM}{V}$, the voltage at the PCC should never reach 48V. The generator selected that met all of these criteria is manufactured by Maxon Motors. The key specifications are listed in Table 4.

Table 4. Maxon EC-Max 40 120W Generator Part# 283873

Specification	Value
K_V [rpm/V]	76.1
Terminal Resistance Phase to Phase [Ω]	7.19
Rated Power [W]	120
Rated Voltage [V]	48

The team used an at home dynamometer test setup built in house, pictured in Figure 14, to spin the shaft of the generator. Although the generator was purchased off-the-shelf, this test setup was useful to verify that the generator was operating in agreement with the specifications laid out in the data sheet. In addition, this setup enabled the team to test the hall effect sensor integrated into the generator body.

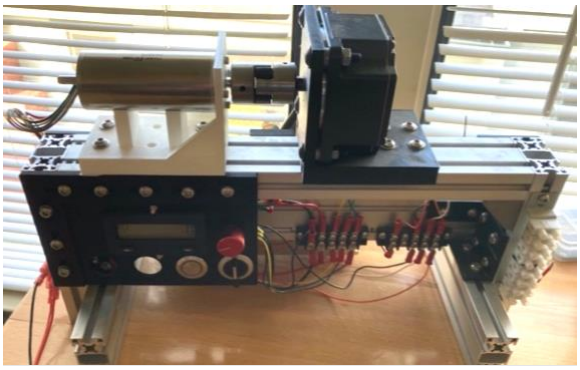
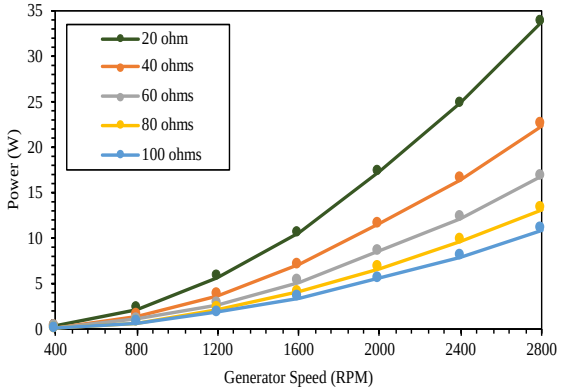
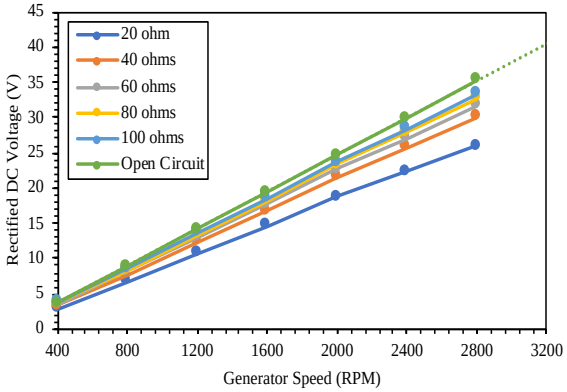


Figure 14. Cal Poly's Custom Dynamometer Test Setup. Generator (left) Coupled to Dynamometer (right).

The results of the dynamometer testing are shown in Figure 15. The generator power output and rectified DC voltage were measured at various rotor speeds and resistive loads. The dynamometer was only capable of spinning up to a speed of 2800 RPM, so to verify that the PCC voltage would never exceed 48V, a trendline was extrapolated to 3200 RPM as shown in Figure 15b.



(a) Load Power vs. Generator Speed



(b) DC Voltage vs. Generator Speed

Figure 15. Dynamometer Testing Results

2.6.3 Hall Effect and Current Sensors

A hall effect sensor provides generator rotor speed information from magnetics inputs. The team utilized the hall effect sensor that was included with the generator to acquire information about the turbine's rotor speed in RPM. These RPM measurements are essential in the control of rated rotor speed task. A basic voltage divider was built to allow the Arduino Uno microcontroller to measure the voltage at the output of the rectifier without damaging it. Additionally, a current sensor was included to measure power by multiplying the sensed voltage and current, and to sense load disconnection. If voltage is detected at the output of the rectifier, but no current is sensed, the microcontroller knows the load was disconnected and shuts down the system.

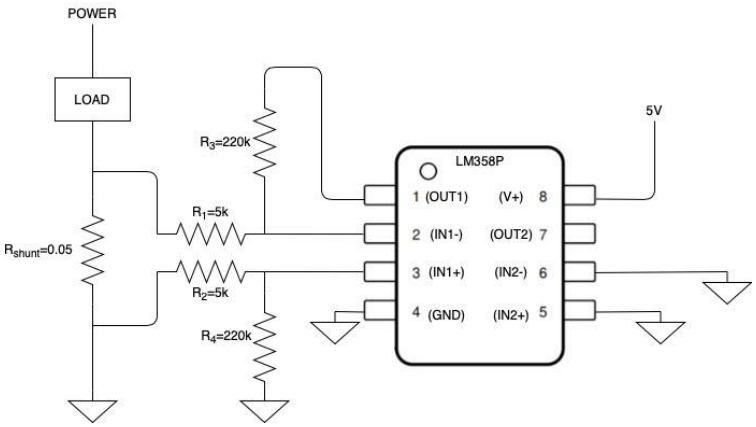


Figure 16. Circuit Schematic of Shunt Resistor Based Current Sensor.

The current sensor was designed and built-in house. The circuit schematic is shown in Figure 16. The design utilizes a low-side shunt resistor and a differential amplifier. This design allows the turbine and load side microcontrollers to sense up to 1.75 Amps of DC current flowing through the PCC.

Figure 17 shows the testing results of the shunt DC current sensor. The testing results demonstrate that the sensor saturates at a current of approximately 1.75A, which is greater than the highest expected current. Additionally, the plot shows the power loss as a function of current. It is important that the current sensor undergoes minimal losses to maximize the turbine's performance in the power performance curve task. The power loss reaches a value of about 150 mW at 1.75A.

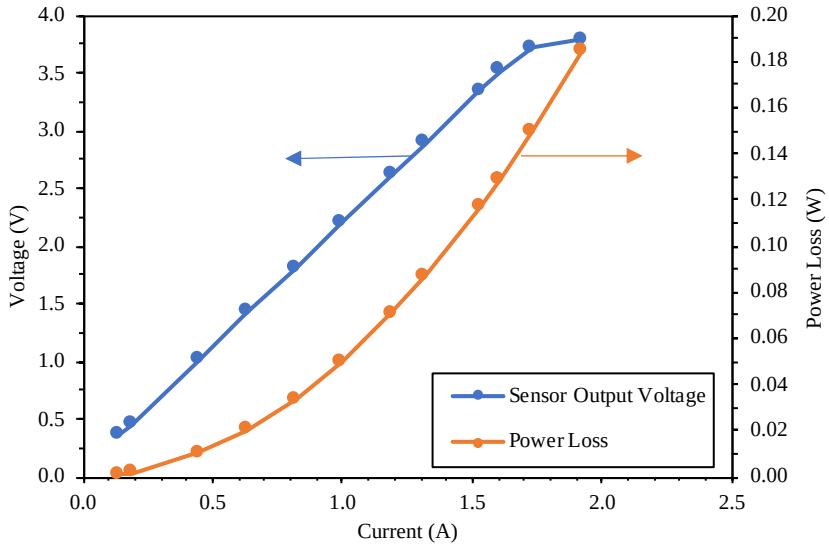
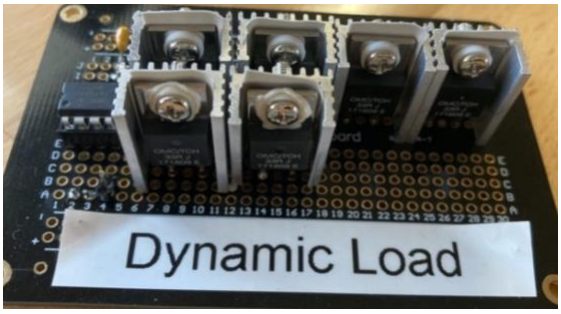
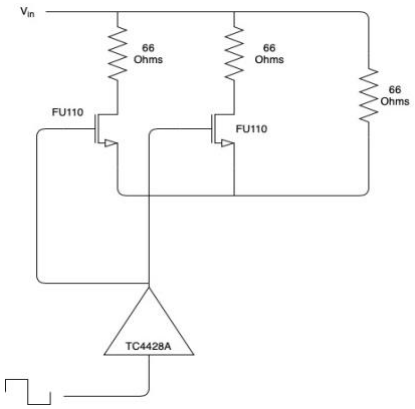


Figure 17. Power Loss and Output Voltage vs. Current Testing Results of Current Sensor

2.6.4 Load Design and Analysis

As the wind speed changes, the resistance that will produce the greatest output power changes as well. In order to maximize the output power, a dynamic load, as shown in Figure 18a, whose resistance can be varied was designed. A resistance range of $66\Omega - 22\Omega$ was chosen by reviewing loads successful teams have chosen in the past, and by analyzing the wind tunnel test data.





(a) Manufactured Component (b) Circuit Schematic

Figure 18. Dynamic Load Component and Circuit Schematic

A circuit schematic of the dynamic load can be seen in Figure 18b. The system changes the average resistance by quickly switching on and off two resistors in parallel with the third. When the NMOS devices are on, the equivalent resistance is 22Ω. When the NMOS devices are off, the equivalent resistance is 66Ω. As the duty cycle increases from 0% to 100%, the resistance drops from 66Ω to 22Ω. This relationship can be seen in the testing data plotted in Figure 19. The FU110 power NMOS was chosen because it could operate in saturation mode with a gate voltage of 5V, the output voltage of the Arduino that will be driving them. In addition, a gate driver was needed to switch the gates on and off quickly.

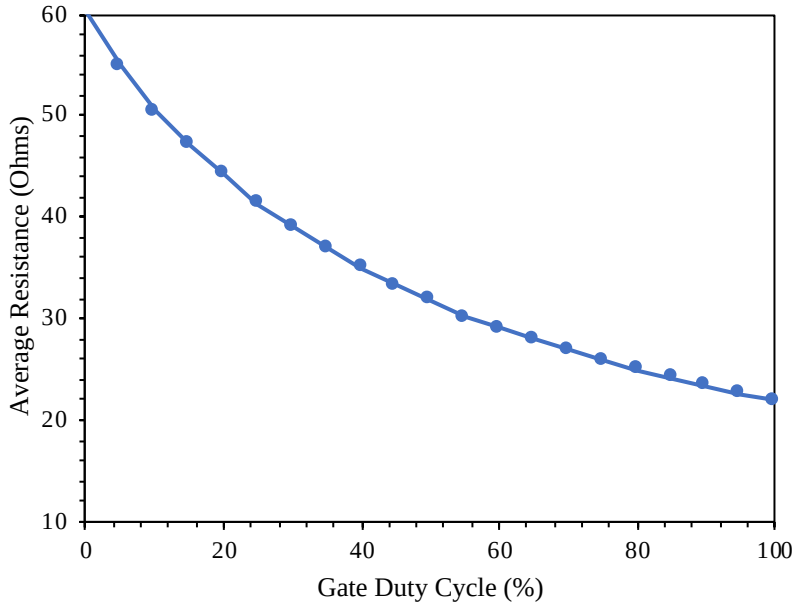


Figure 19. Dynamic Load Average Resistance vs. Gate Duty Cycle Testing Results

2.6.5 Buck Boost and Voltage Regulation

To supply sufficient power and regulate voltage to the control electronics, a buck-boost controller was selected. Specifically, the LM5145RHFEVM-HD 4-Switch Buck-Boost Controller Evaluation Module from Texas Instruments was chosen. This controller was selected for turbine-side voltage regulation because it has a wide-range input voltage range: $5.5V\ -\ 42V$. This allows for power to be drawn from the main power (generation) line post-rectification to supply voltage to the turbine side Arduino and pitching actuators. This module offers adjustable feedback control to deliver constant voltage at its output. The control system and pitching actuators require $7V$ to be delivered from the Buck-Boost controller. This output is adjusted by changing feedback resistor values. According to the user manual, the appropriate feedback resistor for the desired output voltage can be achieved using the following equation.

$$R_{FB1} = \frac{R_{FB2}V_{ref}}{V_{out} - V_{ref}} = \frac{(100{,}050\ [\Omega])(0.8\ [V])}{7\ [V]\ -\ 0.8\ [V]} = 12.910\ [k\Omega]$$

A feedback resistance of $13k\Omega$ was selected to yield an output voltage of $7V$. This resistor was soldered onto the Buck-Boost Controller Evaluation Module to tune the output voltage.

2.6.6 Controls Analysis and Software Documentation

In order to complete the turbine testing tasks to the best of the team's ability, the electrical system is equipped with a turbine and a load side microcontroller. The function of these microcontrollers is to mimic the power output vs wind speed curve shown in Figure 20 by altering blade pitch and load resistance.

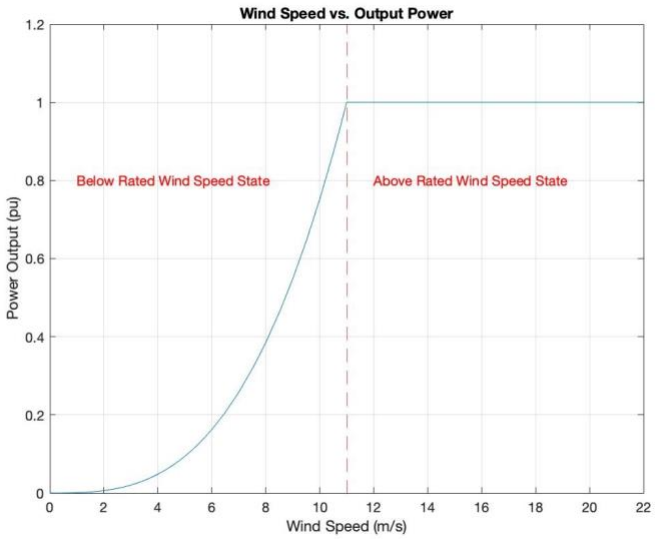


Figure 20. Plot of Ideal Wind Speed vs. Power Output

The turbine side microcontroller is programmed as a finite state machine with three states: below rated wind speed state, above rated wind speed state, and the shutdown state. A microcontroller finite state machine diagram is shown in Figure 21. The microcontroller switches between the below and above rated wind speed states when the power crosses above or below the rated power threshold. This threshold is the experimentally determined power output of the wind turbine at 11 m/s. At any time during the below or above rated wind speed states, the E-stop button may be pressed, or the load may be disconnected. If this happens, the load microcontroller transitions to the shutdown state where the blades are pitched out of the wind indefinitely, slowing the rotor to a standstill. In the below rated wind speed state, the blade pitch is held at a constant angle of attack.

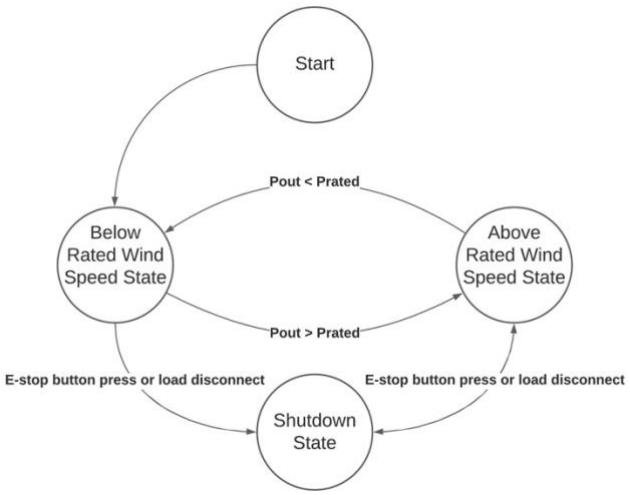


Figure 21. Load Side Microcontroller Finite State Machine Diagram

In the above rated wind speed state, a Proportional and Integrative (PI) control loop scheme, as shown in Figure 22, is used to regulate both rotor speed and output power at the same values measured during an 11 m/s wind speed. In this PI loop utilizes the blade pitch mechanism as an actuator and the hall effect rotor speed sensor as the feedback path. The PI system is able to correct disturbances, such as the wind speed increasing from 12 m/s to 13 m/s, to settle the rotor speed to the "rated" 11m/s value. By regulating the rotor speed of the generator, the voltage output will remain constant, and therefore the power due to the resistive load will also remain constant.

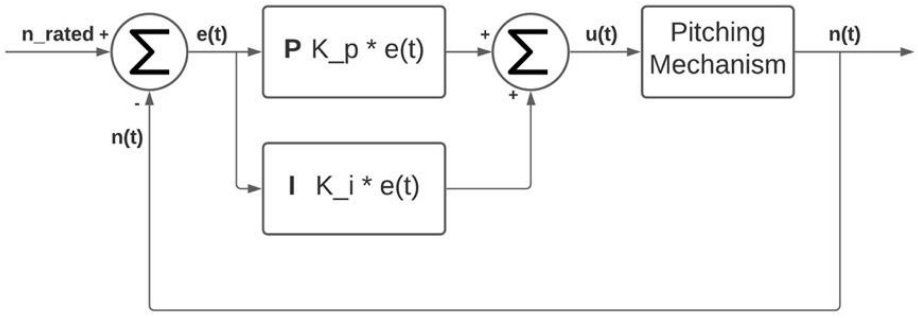


Figure 22. Turbine Side Microcontroller Above Rated Wind Speed State Control System

The load side microcontroller uses its current and voltage sensors to calculate the power being supplied to the load. The microcontroller can change the resistance of the load to increase the power output. It utilizes a lookup table that will be populated with optimum resistances at each integer wind speed. These optimum resistances are found by varying the resistance of the load at various wind speeds and pitching the value which yields the greatest power.

3.0 TESTING

Testing of the turbine and its subsystems was one of the major challenges the team faced because of the health restrictions and severely limited access to campus facilities and labs. Despite this, the team utilized some creative methods to validate the designs and assess the overall turbine performance.

3.1 Field Testing

Most of the testing performed on the turbine can be considered as field testing, since it was done in less controlled environments like students' backyards and out of car sunroofs. Subsystem and component tests are discussed in their relative report sections and in the Testing Milestone Report. At the beginning of the competition, the team did not have access to a wind tunnel, so a small setup was built in a student's garage with a large cardboard box propped in front of a fan. Using a handheld anemometer, the team was able to measure the wind speed exiting the box and placed the chosen rotor set on a basic unloaded turbine setup at varied distances from the end of the box to measure the approximate cut-in wind speed. Originally, the team was interested in maximizing the startup torque of the turbine, and as such chose to continue to refine the best performing blade since it had lower cut-in wind speed in this initial test.

The next set of testing was done with the electrical system connected to the turbine and a dynamic variable load. This test was performed by placing the turbine nacelle components out of the top of a car sunroof. The voltage and amperage produced at various resistances was measured using a multimeter, and the car was driven slowly up to about 14 m/s, verifying that the prototype was capable of withstanding the wind speeds it would later experience in the Cal Poly aerospace department's wind tunnel. This also verified that the blade and rotor design was capable of producing power properly.

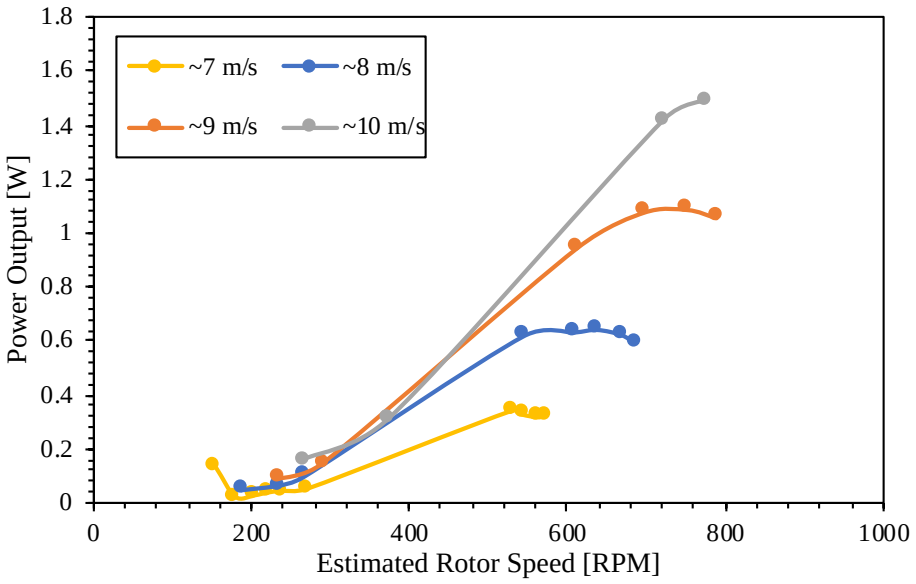
With the new capacitors in place, the team was able to test the turbine with a new more powerful fan up to about 10 m/s. This test was inherently variable since the team did not have access to the tunnel to streamline the airflow, but it was powerful enough to show that the rpm of the blades needed to nearly double to reach the power output desired for the given generator. Since the blades were 3D printed, the team decided to go back to the drawing board and re-design the blade airfoils and TSR. The team found a new set of airfoils to evaluate in QBlade. The resulting theoretical best performing airfoil was placed in the in-house blade design code and new geometries were defined. Six different blade geometry variations were printed and tested again in front of the powerful fan to determine the best rotor geometry for the turbine.

The ability of the turbine to have a stable yaw in variable wind speeds was evaluated on the Cal Poly campus during a particularly gusty day. The passive yaw system was able to realign the turbine quickly when manually rotated out of the incoming wind direction, quickly aligning itself to the incoming wind direction within the 180º per second rule requirement.

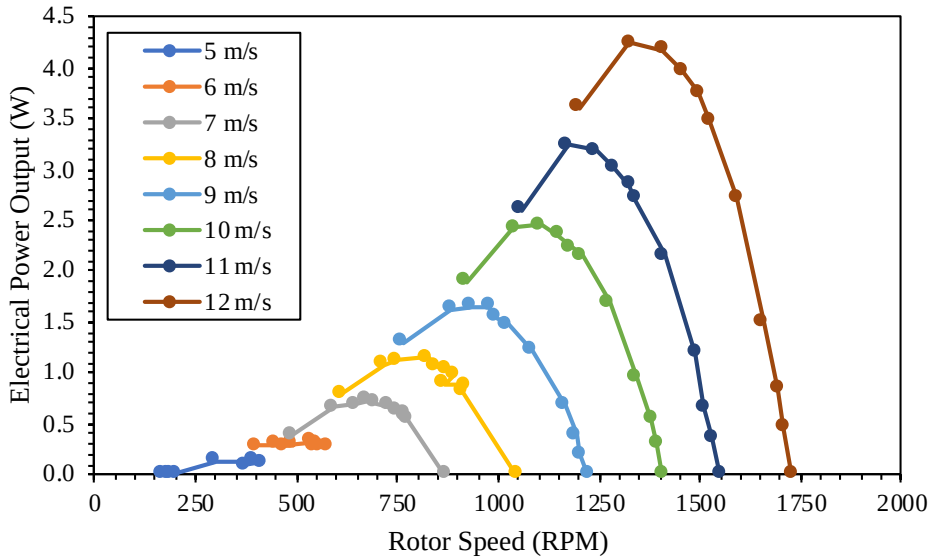
3.2 Wind Tunnel Testing

Following the car sunroof testing, the fixed-pitch prototype turbine was tested for the first time within the actual wind tunnel. This was again effective at showing that the fixed-pitch rotor could produce power, albeit lower than desired by the team. The data collected was used to optimize the resistance of the load at various wind speeds and showed a significant amount of oscillation in recorded power. This was identified as a ripple effect from the rectified three phase AC voltage and was addressed by adding the capacitors to the system (they were still being shipped at the time of first testing). The data is plotted in Figure 23a.

The final wind tunnel test at the time of this report again utilized a fixed hub turbine, but with the final blade geometry determined using the large fan testing mentioned above. A laser tachometer was also used to verify that there was no slippage between the drivetrain and the generator, and to gather data to associate the wind speed with the rotor rpm. The power curves produced are shown in Figure 23b.



(a) Wind Tunnel Test #1 with SG6043 Airfoil



(b) Wind Tunnel Test #2 with New SD7043 Airfoil

Figure 23. Wind Tunnel Testing Turbine Performance Results – Output Power vs. Rotor Speed

An important thing to note about the second wind tunnel test is that the blades were about 1.5 cm undersize in length. This was due to the accessible 3D printer beds not having a large enough build volume to print the full length blades. This also indicates that the turbine should be able to generate more lift and thus higher rotational speeds. With the full-size blades, the turbine is assumed to generate more power.

At the time of this report the team was not able to complete full wind tunnel testing with the pitching mechanism installed due to unexpected shipping issues for necessary bearings; however, the pitching mechanism and the turbine with a static hub were tested extensively and perform as anticipated.

4.0 CONCLUSION

Through testing, the team has learned what caused the turbine to produce less power than anticipated: namely the selection of a rated speed for a generator that was higher than the blades can achieve. The tradeoff of establishing a low cut-in wind speed in place of higher power at the rated was emphasized too heavily. The team now knows how to change the generator selection and blade tip speed ratio in future iteration of the design. Despite these issues, CPWP was able to make marked improvements in the performance of the turbine over the course of the current testing up to this point. The team plans to fully incorporate the pitching mechanism to improve performance even further before the end of the competition.

The wind turbine designed by Cal Poly Wind Power was successful in meeting most of the design goals outlined by the team and competition. It produced less power than desired, however, the design process undertaken by the first-year team has provided an excellent groundwork which can be taken and improved to reach the power production goals. Analytical tools such as the electrical and controls schematics, and rotor optimization MATLAB script can be modified and utilized by future Cal Poly CWC teams. The turbine paved the way for Cal Poly to use a variable-pitch system in the future which can be optimized with further testing.

5.0 REFERENCES

[1] US Department of Energy. (2020) CWC 2021 Rules and Requirements. Collegiate Wind Competition 2021

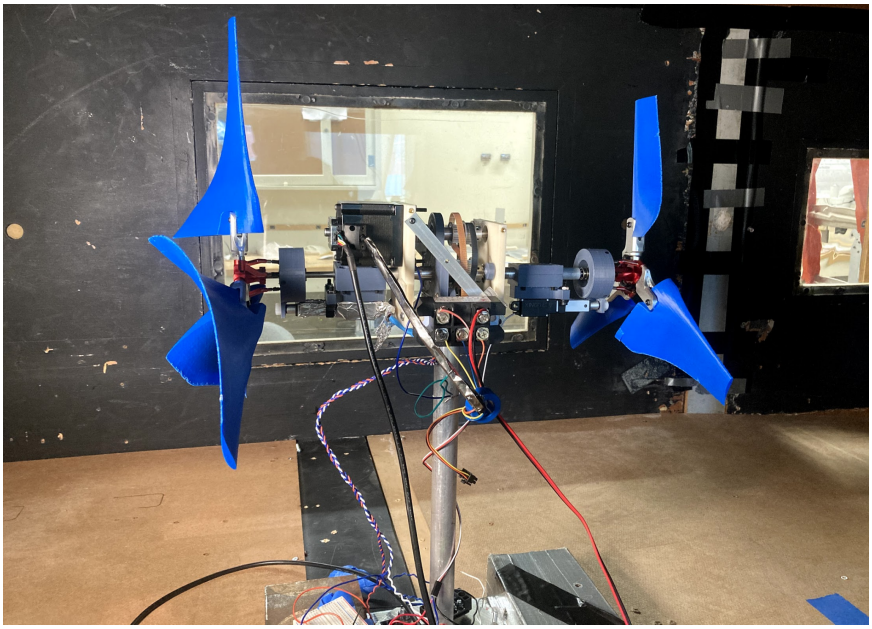
[2] Manwell, James F., et al. (2011) *Wind Energy Explained: Theory, Design and Application*. Wiley.

[3] Anderson, Collin G. (2020). *Wind Turbines: Theory and Practice*. Cambridge University Press.

HOPKINS STUDENT WIND ENERGY TEAM

Technical Design Report

Johns Hopkins University
Collegiate Wind Competition 2021



Generator Team:
Willa Grinsfelder (Generator, Structures Lead)
Zach Galvarro

Aerodynamics Team:
Owen Friesen (Aerodynamics Lead)

Structures Team:
Kathy Cao, Ebuka Ezekwesili,
Evan Latourrette-Ghez, and Isaac Lee

Electronics & Controls:
Annika Torp (Electronics & Controls Lead)
Shivanie Ally, Caitlyn Bernhard, Eleni
Daskopoulou, Yared Kokeb, and Daniel Okereke

With Assistance from Prof. Nathan Scott, PI

JOHNS HOPKINS UNIVERSITY

COLLEGIATE WIND COMPETITION
U.S. DEPARTMENT OF ENERGY

Table of Contents:

1.0 Executive Summary **2**

2.0 Technical Design **3**
- **2.1 Blade Design** **3**
  - **2.1.1 Aerodynamic Design** **3**
  - **2.1.2 Aerodynamic Analysis** **4**
  - **2.1.3 Yaw Design & Analysis** **6**
  - **2.1.4 Structural Design** **7**
- **2.2 Structure Design** **7**
  - **2.2.1 Rotor Shaft Supports** **7**
  - **2.2.2 Chassis** **8**
  - **2.2.3 Passive Yaw Bearing Assembly** **8**
  - **2.2.4 Brazed Aluminum Joint at Turbine Base** **9**
- **2.3 Generator Design** **9**
  - **2.3.1 Numerical Simulation** **9**
  - **2.3.2 Simulation Validation** **9**
  - **2.3.3 Selected Generator and Predicted Performance** **10**
- **2.4 Transmission Design** **11**
- **2.5 Electrical Design** **11**
  - **2.5.1 Variable Load** **12**
  - **2.5.2 Voltage Regulation** **13**
  - **2.5.3 Power Smoothing** **13**
  - **2.5.4 Safety System** **13**
- **2.6 Control Model** **14**

3.0 Testing **17**
- **3.1 Commissioning Checklist** **17**
- **3.2 Results** **17**

4.0 Conclusion **18**

5.0 Enumeration of Influence of Previous Design Reports **18**

6.0 Appendices **19**
- **6.1 Full Circuit Diagram** **19**
- **6.2 Table of Safety Factors** **19**

7.0 References **R1**

1.0 Executive Summary

For our inaugural entry to the Collegiate Wind Competition, the JHU team aimed to maximize the efficiency of a turbine that complies with the space requirements of the competition. To do so, we developed a novel dual-rotor counter-rotating turbine design that allows us to extract more power from a limited swept area than a comparable single-rotor design. Dual rotor turbines have a higher theoretical efficiency than single-rotor variants, with a maximum efficiency of 81.4% compared to the 59.3% Betz Limit [1].

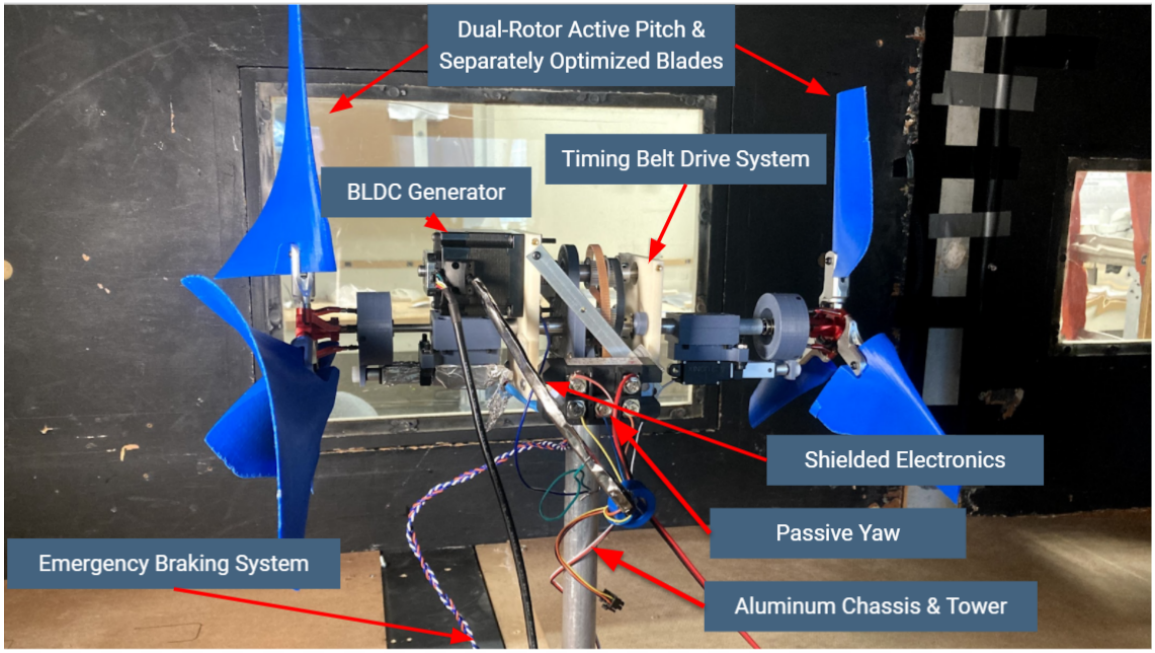


Figure 1: Overview Schematic of our Final Prototype.

Our blades are derived from the S1210 airfoil which was originally designed for RC aircraft. This airfoil is well suited to our low-Reynolds number application [2]. We separately optimized the front and rear sets of blades for the applicable flow conditions. We then 3D printed the blades from ABS and smoothed them with acetone to even out the surface finish.

Our controls employ two variable pitch mechanisms, one for each rotor, to control and brake the turbine. This system uses two linear actuators mounted to our chassis, which, with intelligent programming, minimizes power consumption while allowing us greater control over turbine performance.

We use a timing belt transmission system to combine the mechanical power from the two rotor shafts and step-up the generator shaft speed. By stepping up the shaft speed of the generator, we are able to better achieve the maximum efficiencies of both our blade design and generator. We selected a commercial brushless 3-phase motor to drive as a generator by using the weighted average of generator power production over competition wind speeds.

In an attempt to improve upon prior art, we decided to design a safety system that can brake the turbine without a functioning microcontroller by using low-level logic gates and other simplistic electrical devices, with the goal of improving robustness. This design struggled with the multiple conditions under which it had to execute different functions (which is why others in the past have preferred controlling

braking with a microcontroller); however, this system could be hugely successful with improvements in future years.

Finally, we built a tower and chassis using a combination of machined metal parts and 3D printed parts to improve the overall manufacturability of our design in highly uncertain times, when the availability of machining equipment and the consistency of our access to lab spaces were changing with the global pandemic.

The peak efficiency measured in testing our turbine was 21.8%. This efficiency was lower than the theoretical levels predicted in literature for dual-rotor counter-rotating wind turbine designs, but we were able to build a working dual-rotor design for this application. In future years we hope to continue developing our counter-rotating wind turbine design with the ultimate goal of breaking through the Betz limit.

2.0 Technical Design

For the 2021 Collegiate Wind Competition, our team was tasked with researching, designing, and building a miniature wind turbine for highly uncertain times. We specifically sought to maximize our turbine's power production between 5 and 11 m/s using novel counter-rotating wind turbine prototype. Individual team members spearheaded the development of our four key subsystems — blades, structure, generator, and electronics — while working from home during the fall semester. In the spring, our team came together to integrate our components and test them in our university's one-meter wind tunnel. The following sections detail the design, analysis, and testing of each of these key sub-components.

2.1 Blade Design

We designed and built our turbine blades to accommodate the unique opportunities and challenges of a counter-rotating wind turbine. For the competition, we developed a pair of rotors with separately optimized blade geometries to match the unique flow conditions present at the front and rear of the turbine. These rotors also work in concert to provide passive yaw control for our system, negating the need for a separate tail. With separate active pitch control systems for each rotor, we are able to tailor the turbine characteristics to produce optimal performance under a wide range of conditions.

2.1.1 Aerodynamic Design

The core of our aerodynamic system is a pair of rotors which, working together, extract mechanical energy from the wind. Both rotors are based off of the S1210 airfoil, shown in Figure 2, which we chose for its high C_L/C_D ratio at low Reynolds numbers ($Re < 100{,}000$).

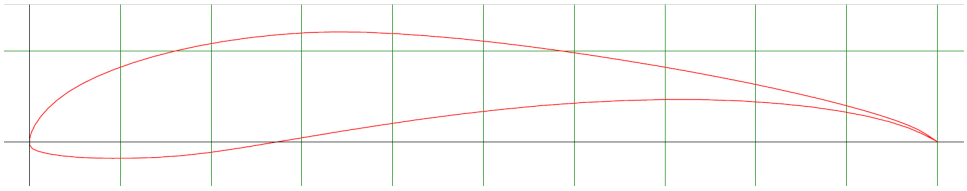


Figure 2: The S1210 airfoil [3].

The S1210 airfoil was originally designed for low-Reynolds number applications in RC aircraft, and is therefore well suited for use in small length scales [2]. Because of these favorable properties, this airfoil

has been adopted by a number of research teams for small scale wind turbines, and it was our choice for the 2021 competition [2, 4].

Once we selected our airfoil, we constructed our blade geometries in QBlade. The overall dimensions of our blades were informed by our yaw system (see below). To accommodate passive yaw, we designed our front blades with a diameter of 35 cm and our rear blades with a diameter of 45 cm. Our active pitch hub had a 3.5 cm radius, allowing an overall blade length of 14 cm for the front blades and 19 cm for the rear blades. Our blades also experienced different flow conditions because of turbulence and their different geometries. Through an iterative process based on the analysis described below, we determined that our front blades are subject to flow at Re = 90,000 and our rear blades are subject to flow at Re = 70,000.

The last key input for our QBlade optimization was the tip-speed ratio (TSR). Based on iterative testing with our generator, we chose to use a TSR of 3 for both rotors for our final set of blades. With our geometry and flow parameters established, we were able to use the Betz optimization process in QBlade to determine an ideal twist and chord length array for the two sets of blades. We could then conduct further aerodynamic analysis in QBlade and extract STL files with the blade geometry for further structural design in Solidworks.

2.1.2 Aerodynamic Analysis

To perfect this blade geometry, we conducted both computational analysis and iterative testing. This was essential to account for the unique flow conditions present in a dual-rotor system, which is not natively supported by QBlade nor well-researched. We did most of our computational analysis using QBlade's native lifting-line theory (LLT) function, shown in Figure 3, which provides more detailed flow data than blade element momentum (BEM) analysis without the computational cost of computational fluid dynamics (CFD). To model our system, we conducted two separate sets of analysis. First, we modeled our front rotor at the chosen wind speed and TSR. We then extracted the velocity field 45 cm behind that rotor to model the wake that the rear rotor experiences. In Excel, we could process this data to obtain the average flow velocity in the swept area of the rear rotor, and use that as the input for a second LLT simulation to model the rear rotor. This simulation provided useful data for design, but its accuracy was limited by the use of the single x-velocity variable to model the interaction between the two systems, as well as the fact that we could not model the counter-rotation of the rear rotor this way.

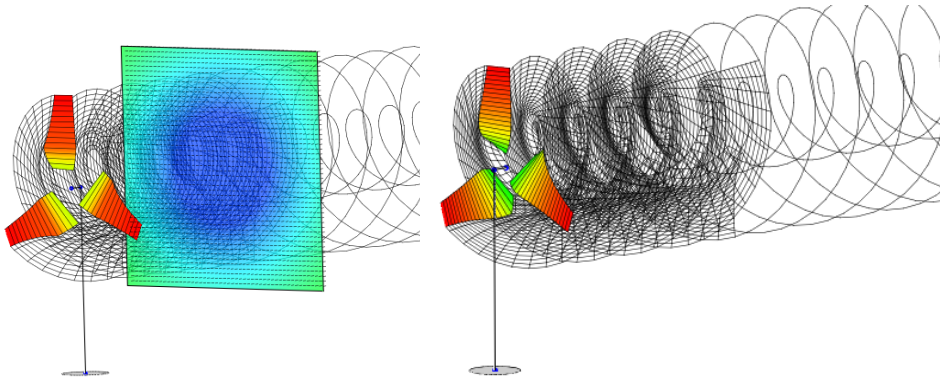


Figure 3: LLT simulation of the front (left) and rear (right) rotor with the velocity plane behind the front.

The lifting-line theory model predicted an 11% average drop in the flow velocity as a result of the front rotor. This decreases the efficiency of the rear rotor, but the additional rotor still significantly improves the overall coefficient of performance of the system. As shown in Figure 4, we predicted a total power output of up to 75 W with the dual rotor system at 11 m/s.

	Front	Rear	Combined
Inlet Velocity (m/s)	11	9.8	11
Power (W)	37	38	75
C_p	0.47	0.41	0.58

Figure 4: An example of the results of the LLT simulations, at 11 m/s.

This simulation likely has significant error, because of the aforementioned simplifications in the LLT model and the fact that the model does not incorporate feedback from the generator. As a result, we sought a lot of physical testing to validate our models and refine our optimizations.

Over the course of the year, we went through 15+ iterations of the blade design, shown in Figure 5. This allowed us to test our blades independently and in combination with various generators.



Figure 5: A series of blade prototypes produced and tested throughout the year.

During these tests, we gathered wind speed, power, and RPM data from our data acquisition system, which allowed us to finetune the flow characteristics and TSR we used for our optimization, as discussed above. Our final testing yielded a pair of power coefficient (Cp) vs. TSR curves shown in Figure 6, which illustrates that our peak performance is obtained at higher TSRs. We were able to control the TSR with our load and blade pitch. This shows that we did a good job of matching the TSRs of the two rotors, with the rear rotor operating at only slightly higher TSRs than the front one. As expected, the experimental power coefficient did not reach our ideal values from the LLT simulations but showed significant improvement as we continued to iterate, reaching an average of 21.8% under our final set of conditions.

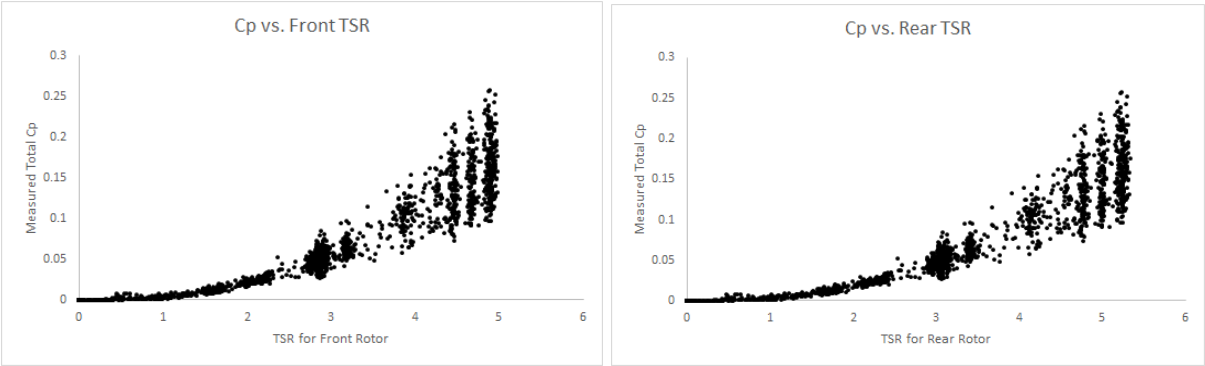


Figure 6: Cp vs. TSR plots for our front (left) and rear (right) rotors during testing at 11 m/s.

2.1.3 Yaw Design & Analysis

We achieved passive yaw through a size differential between our two rotors and a yaw bearing, which allowed our full system to self-center in the flow. The objective for the passive yaw system is to have the turbine respond to yaw rates of 180° per second at wind speeds between 6 m/s and 13 m/s. The transient response of the yawing turbine was modeled using MATLAB and a series of simplifying assumptions.

The net torque acting on the turbine over time was calculated as the sum of the torque from the drag on the front blades, the torque from the drag on the back blades, and the rolling frictional torque in the two bearings at each timestep. We used the SKF model to approximate the rolling frictional torque [5]. The net torque was used to derive the angular acceleration, angular velocity, and yaw angle over time.

Figure 7 shows the transient response of the yawing turbine for yaw angles of 1° and 179° at a wind speed of 9 m/s. The results suggest that the yaw system is able to respond to yaw rates of 180° per second at wind speeds between 6 m/s and 13 m/s. Additionally, as shown in Figure 7, a larger initial yaw angle is predicted to take the turbine longer to equilibrate at 0°. In practice, we saw the turbine equilibrate more quickly than predicted by the model, likely because of additional rolling frictional torque. Note that this model cannot accommodate initial yaw angles of 90° and 180° since the net torque would be calculated as zero for those angles.

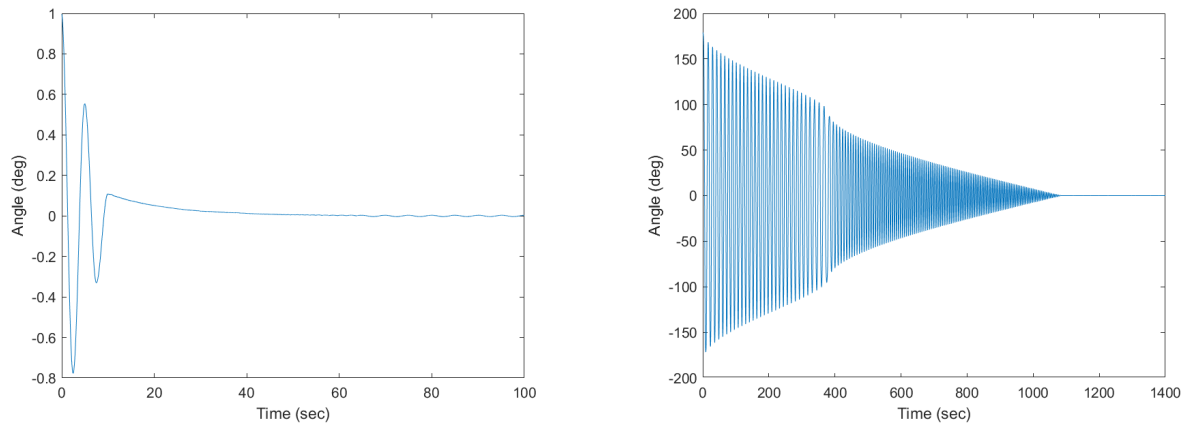


Figure 7: Transient response of yaw angle for initial yaw angle of 1° (left) and 179° (right) at 9 m/s.

2.1.4 Rotor Hub Design

For our rotor hub, we chose to use a modified hub from a JCZK 300C RC helicopter, shown in Figure 8, to achieve active pitch control. We epoxied a linear bearing in line with the shaft to limit the pitch control to one degree of freedom and ensure that the three blades on each rotor pitched together. This pitch system is attached to our Actuonix L12 linear actuator with a 3D printed coupler to obtain precise control.



Figure 8: JCZK 300c Rotor Hub [6]

In order to mount the blades to the rotor hub, we imported the blade geometry from QBlade to Solidworks. We could then add in appropriate mounting geometry that lined up with the neutral plane. Therefore, when the active pitch system is at a neutral position, the blades are pitched appropriately.

All of our blades and other 3D printed parts were 3D printed from ABS with a solid infill. We chose ABS for its ease of printability and relatively high strength and heat tolerance compared to other 3D printed materials. Parts that did not require high degrees of accuracy were printed on a Qidi X-plus home 3D printer. More accurate parts for the blades and chassis were printed on both a UPrint SE Plus and a Stratasys F370 in university-managed facilities, still from ABS. We post-processed the blades in an acetone vapor bath to ensure a smooth surface.



Figure 9: Assembly drawing of turbine structure including rotor and blade shaft and support structures (green) and major chassis and tower components (red).

2.2 Structural Design

The objective of the structural design of our wind turbine is to adequately support all wind turbine components in both parked conditions and the maximum operating conditions of wind speeds of 22 m/s. We also designed for a small frontal area of the chassis in order to minimize power losses over the chassis. Finally, we included a thrust and radial ball bearing assembly to passively yaw the turbine.

The major loading conditions on the turbine are a thrust load on both sets of blades of 5.3 lbf per rotor in wind speeds of 22 m/s, a maximum rotor rotational speed of 2500 rpm, and a bending moment of 50 N·m at the base of the turbine. In the “parked” case both the front and rear blades of the turbine are feathered. The frontal area of the feathered blades is 12% of the area of the blades during operation. This indicates that the turbine’s major mode of failure will be due to loads manifesting during operation. The minimum safety factor in the design is 12.5 in the back rotor shaft due to fatigue loading conditions. A complete table of calculated safety factors is available in Appendix A.2.

2.2.1 Rotor Shaft Supports

The rotor shaft support assembly consists of the two 6 mm 416 Stainless Steel rotor shafts supported by machined 6061-T6 aluminum support arms. This design was chosen for the smaller form

factor it allowed us with the dual-rotor design, as well as ensuring quick and easy assembly of key parts. after our team noticed significant walking in earlier bearing mount assemblies during testing. In addition, the support arm allows the rotor to be assembled to the final chassis with ease.

2.2.2 Chassis

The chassis was designed out of three 6061-T6 machined aluminum brackets and four cross braces. The objective of the design is to support the bending moment from the cantilevered rotor support arms and accurately position the transmission assembly while minimizing frontal area. The chassis brackets clamp to the passive yaw bearing housing using four M5 screws for ease of subsystem assembly and disassembly. The stresses in the chassis brackets were modeled in ANSYS. For testing, the turbine chassis was fabricated from 3D Printed ABS so that we could perform fit checks and quickly adjust our design. The final prototype of the turbine structure is designed to be professionally machined from 6061 Aluminum.

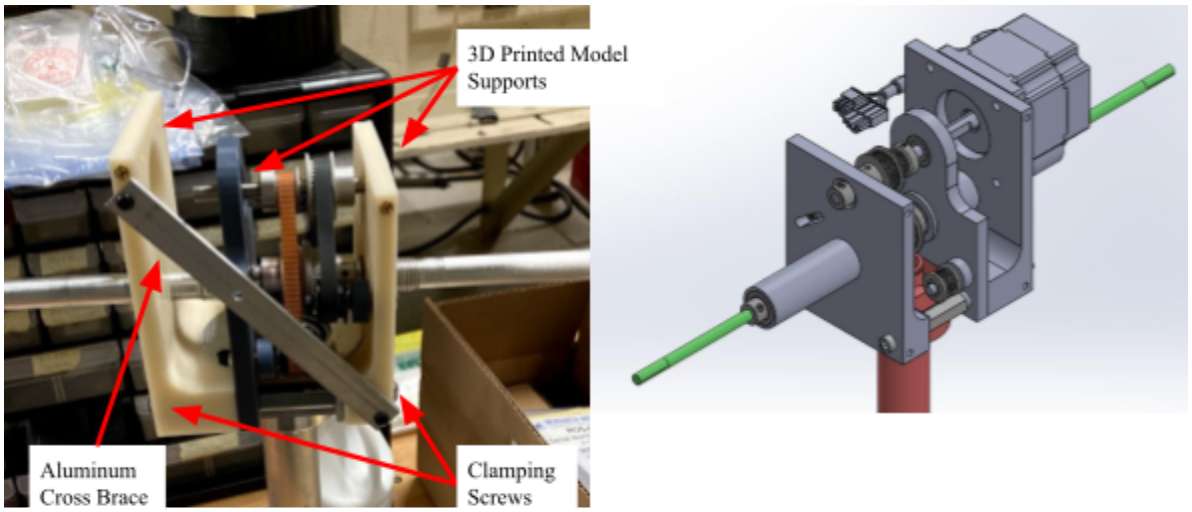


Figure 10: Annotated image of the major components of the chassis structure when test assembly produced (left) and CAD model of completed assembly sans aluminum cross bars (right) to the turbine tower.

2.2.3 Passive Yaw Bearing Assembly

The design objective for the passive yaw bearing assembly is to minimize friction in the yawing assembly while ensuring our design is robust enough to withstand unpredictable vibrational loading of the turbine blades. In addition, the design was completed such that the cross sectional area projected on the flow is minimized, which minimizes power losses due to impingement on the flow. The design uses a 3220JR Tapered Roller Bearing and a 60/22 deep groove ball bearing to allow for free rotation of the turbine in variable loading conditions. The mounting assembly is designed such that the tapered roller bearing takes the

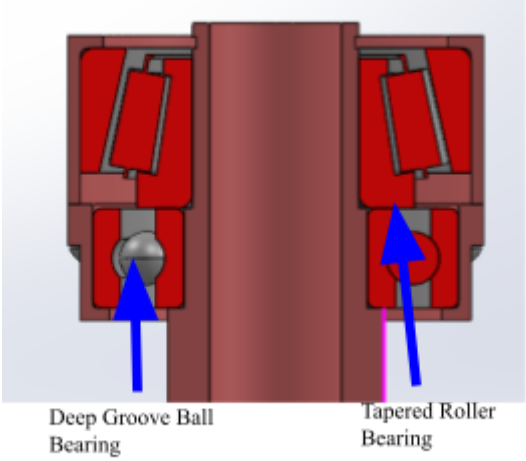


Figure 11: Cross Section of Yaw Bearing Assembly

majority of the axial load, and the roller bearing resists any bending moment caused by the thrust on the turbine blades.

2.2.4 Brazed Aluminum Joint at Turbine Base

The design objective for the tower and base plate is to create an easily replicable assembly that withstands at least 50 N·m of bending moment. Since the height of the wind tunnel on the JHU campus is significantly smaller than the height of the competition wind tunnel, we needed to design a turbine tower that could easily be swapped depending on our circumstances. To accomplish this goal our team minimized machining operations for the 6061-T6 aluminum tower and used brazing to permanently fasten the base plate to the tower. This allowed our team to avoid threading or milling bolt holes into the base plate after turning it to size and maintained the strength of our joint. We found that the brazed aluminum joint on the 1" diameter tower withstood more than 70 N·m of force in laboratory testing, indicating that the design was appropriate for the competition requirements.

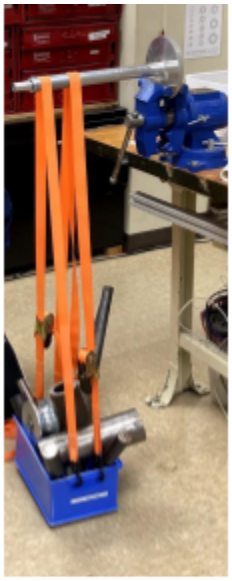


Figure 12: Brazed aluminum tower in laboratory testing.

2.3 Generator Design

The objective of our generator design is to maximize the weighted power performance of our turbine between wind speeds of 5 and 11 m/s.

2.3.1 Numerical Simulation

The operating parameters of the generator were determined using a simplified actuator disk model of a dual rotor wind turbine [1]. The optimal generator rotational speed was defined by the blade TSR and wind speed. The maximum torque on the generator was derived from the mechanical power equation for a rotating shaft and the theoretical maximum power harvestable from the wind. A transmission system was included in the generator design to step up/down the input speed and torque from the rotor blades to the generator. The main purpose of the transmission system is to combine the mechanical power from the two sets of turbine blades. To evaluate the optimal transmission ratio and generator combination, power production was estimated over the operating range of wind speeds given incremental changes in the transmission ratio. The weighted score for generator and transmission performance was calculated based on the Collegiate Wind Competition's scoring rubric [7]. The generator and transmission combination with the highest weighted score was chosen for our generator design.

2.3.2 Simulation Validation

The simulation of generator performance was verified using an in-house dynamometer and Maxon RE 50 generator, one of the first generators our team identified as a viable option. While we discovered a load mis-match between our turbine blades and generator which led us to revisit alternative generator options, the dynamometer testing allowed us to use the MATLAB generator performance simulation with confidence in our generator selection.

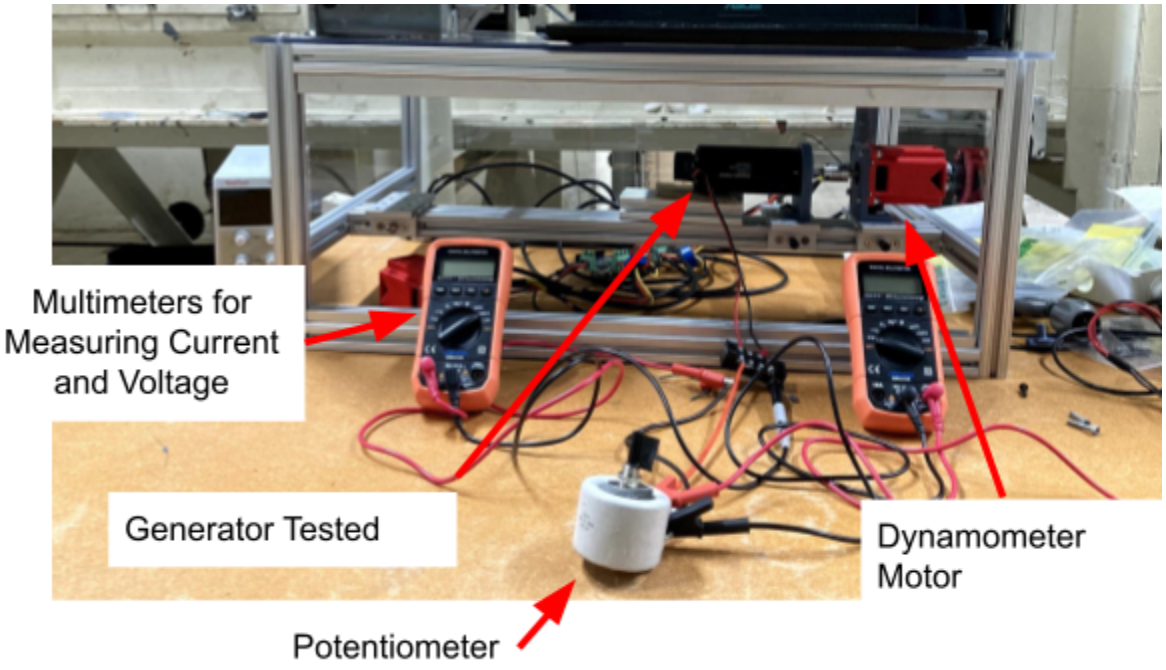


Figure 13: Dynamometer assembly used for validating generator numerical simulations.

2.3.3 Selected Generator and Predicted Performance

A range of brushless DC motors and brushed DC motors' power performance were used to identify the optimal combination of motor constants for generator selection. To achieve a maximum generator efficiency, our team aimed to select a generator that would spin quickly, demand low torque from the drive shaft, and minimize copper losses in the windings of the generator. Parameters that played a role in our final design included motor speed constant, motor speed-torque constant, terminal resistance in motor windings, and cogging torque when available from data sheets. For the competition this year our team decided to use the Lin Engineering BL23E22-02 brushless DC motor. The optimal transmission for both startup wind speed and power curve performance was a transmission ratio of 0.8 from the front blades to the generator shaft. This translated to an increase in rotational speed of 1.25, and a decrease in torque of 0.8 from the front shaft to the generator. The following table outlines the key parameters that this generator satisfies.

Table 1: Outline of generator predicted performance over range of operating wind speeds.

Condition	Lin Engineering Generator Performance
Startup Wind Speed between 2.5 and 5 m/s	Predicted to startup at 4.5 m/s and produce 3.83 W
Maximize Power Curve Performance between 5 and 11 m/s	Predicted to achieve a maximum power production of 23.3 W at 11 m/s, and total weighted performance score of 46 out of 50

2.4 Transmission Design

The objective of the transmission system in the wind turbine design is to efficiently combine the mechanical power of the two rotor blades into a single input for the generator. For the turbine this year, our team decided to use a timing belt system as our transmission system. The timing belt system was ideal for our team as we experimented with varying transmission ratios, chassis designs, and blade-generator combinations because built-in tensioning mechanisms allowed for ease of adjustment while keeping overall costs low.

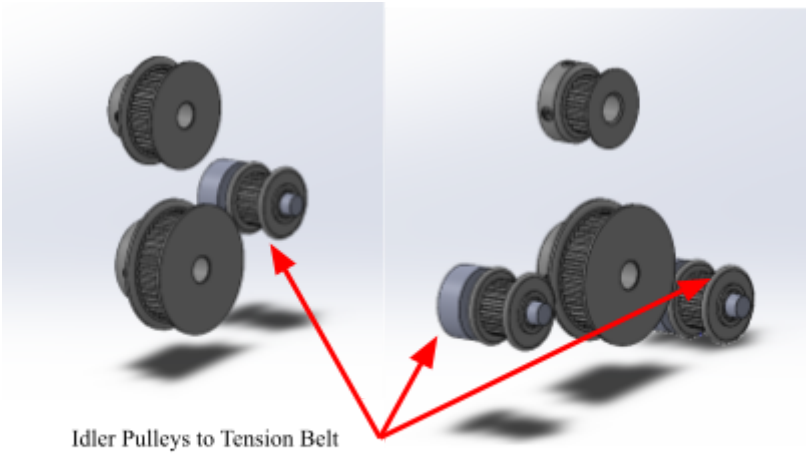


Figure 14: The front rotor pulley assembly (left) and the back rotor pulley assembly (right) including the idler pulleys with adjustable position.

The MXL series timing belt pulleys were used for their small size and weight. The gear ratios used in the final design were based on the generator modeling simulation, as well as the assumed aerodynamic relationships between the front and back rotor. The following table outlines the gear ratios:

Table 2: Tooth counts on pulleys in wind turbine transmission system.

	Tooth Count on Rotor Shaft Pulleys	Tooth Count on Generator Shaft Pulleys
Front	40	32
Back	40	20

Thus the ratio of the front rotor shaft speed to the generator shaft speed was a ratio of 1.25, and the ratio of the front rotor shaft speed to the back rotor shaft speed was 1.2. Both timing belts were manufactured with Kevlar tensioning chords, with a maximum yield strength of 1865 N, well above the calculated maximum tension of 39 N for this design [8].

2.5 Electrical Design

The purpose of the electrical system is to regulate and optimize the power produced by the generator. To accomplish this, the electrical system is controlled by a single microcontroller unit (MCU), which pitches both sets of blades, reads sensor and state data, and controls the variable load. The electronics design also features a safety system that has the intention of improving robustness by braking the turbine without the input or processing power of the MCU.

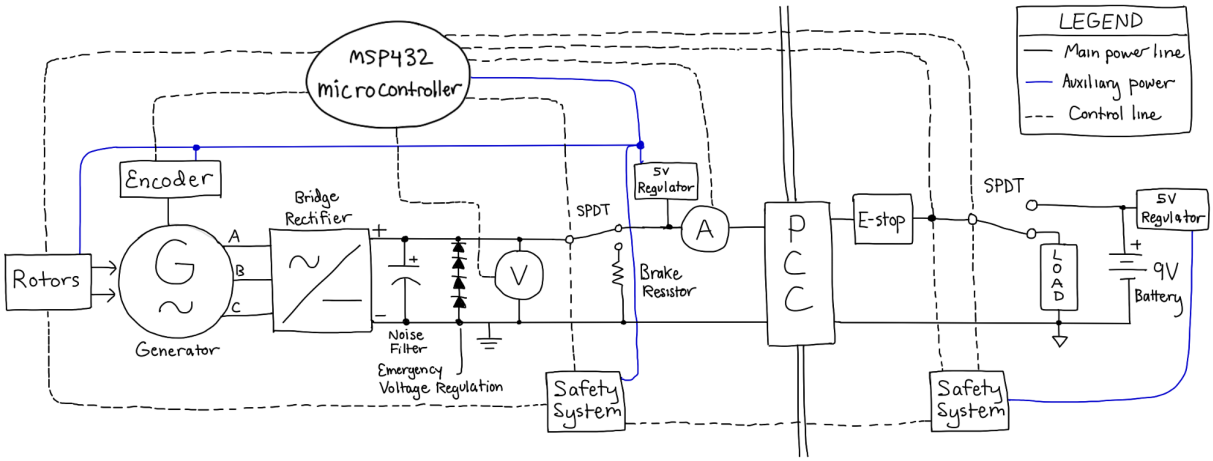


Figure 15: Overview of the electronics system. Full circuit diagram in Appendix 2.

The Texas Instruments MSP432 LaunchPad was chosen as our MCU for its low power consumption and because it is Arduino-compatible. We chose early on to only use one MCU with the goal of reducing complexity and the chance for error. The MCU measures the generated voltage through a voltage divider and the current using a current shunt monitor breakout board. Both of these measurements are read as an analog input voltage and a rolling average is taken of the last ten measurements to mitigate noise effects, then that average is used by the MCU to make decisions. Generator speed is measured by a quadrature encoder, the signal of which the MCU uses to count the number of rotations in a given time period. The MCU pitches the two sets of blades during normal operation by sending pulse-width modulation (PWM) signals to the linear actuators.

While the goal of only using one MCU to reduce complexity was a good one, this increased our power consumption on the turbine-side of the PCC due to the increased number of optically isolated signals that needed to cross the PCC, and a solution to this problem should be found in future years.

2.5.1 Variable Load

Ahead of the necessary information to choose the appropriate resistor values for a variable load system, we designed one that allowed for up to eight different resistance values, intended for seven different wind speed bins and a startup load resistance. Power resistors are added in parallel to each other with power MOSFETs controlled by the MCU. These resistances would be determined by thorough testing at various wind speeds, blade pitches, and load resistances.

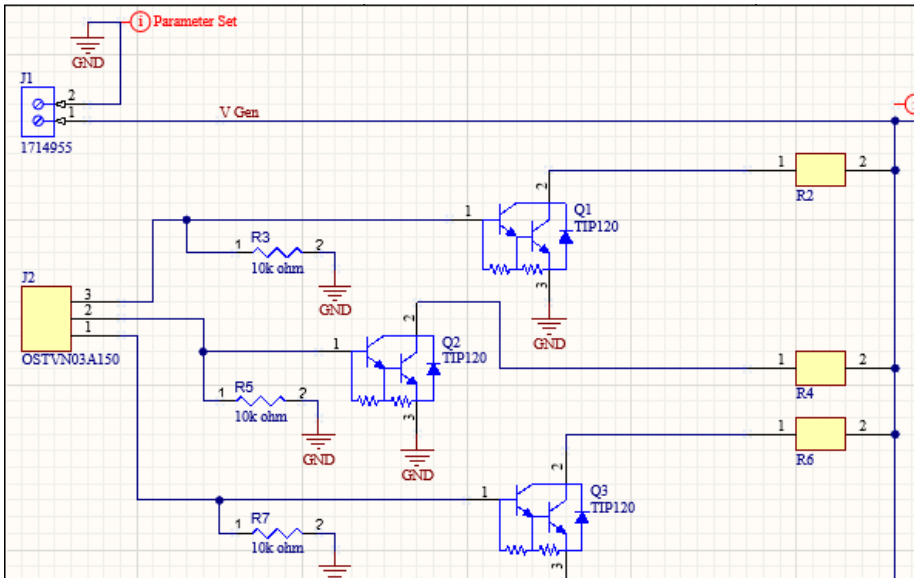


Figure 16: Part of the variable load circuit -- signals come in from the turbine side (left of the image) and control MOSFETs that add power resistors in parallel (right of the image)

2.5.2 Voltage Regulation

We only anticipate reaching ~30V in testing, however, should the generated voltage reach 45V as measured by the sensors, the control system will pitch the blades to reduce the power output of the turbine. In case of a control malfunction at high voltages, we also have four 12V diodes in series that span the output of our bridge rectifier, which would short the generator at 48V.

2.5.3 Power Smoothing

The power output of the three-phase generator was modeled using MATLAB. The necessary capacitance was selected based on the stability criteria of the competition rules and regulations. A smoothing capacitor was included in series with the full-wave bridge rectifier to ensure power stability over the full operating range of the generator. The minimum capacitance was selected based on the calculated frequency of the rectified power output to be 30 mF. To account for any unexpectedly low frequency operating points, a smoothing capacitor with a value of 50 mF was chosen for our design.

2.5.4 Safety System

The goal of our safety system design is to brake the turbine independently of whether or not the MCU is functioning for improved safety and robustness upon prior art. This is achieved by “reading” states at different points in the circuit, and using low-level logic gates to actuate the braking of the turbine. Figure 17 below shows the “safety” part of the circuit, with unnecessary information removed to better illustrate how the system functions.

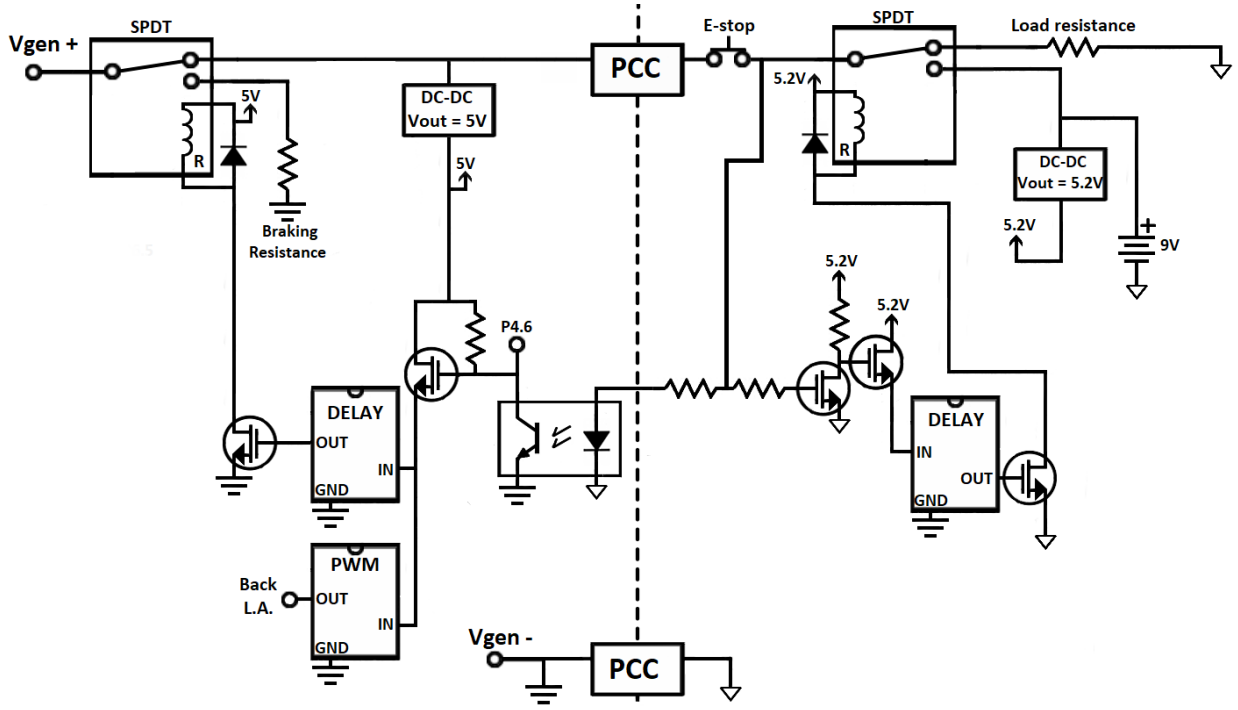


Figure 17: The safety system with no microcontroller intervention (extraneous information removed).

For our prototype and testing setup, we are able to place our emergency stop button in series with the PCC, as our button is rated to ~460V and 10A, and our generator is not rated to produce more than 1.6A.

The system works by converting the generated voltage at a node on the load side of the PCC down to a logic-level 5V, and using this "HIGH" or "LOW" condition to begin the braking process. If this node is "LOW" (load disconnect or E-stop button press), the logic gates on either side of the PCC begin the braking process -- on the turbine side, the rear rotor blades pitch to a predetermined braking angle from a PWM signal generated by a 555 timer IC. On either side of the PCC, a separate 555 timer circuit begins a delay for a latching relay. The turbine side relay resets first, and disconnects the generator from the main power line and to a braking power resistor. The load side relay resets second and disconnects the main power line from the variable load, and switches it to a backup battery pack. Meanwhile, the rear blades have been pitched and the turbine is slowing to a halt. With the selection of an appropriate battery pack (we are using 6 AA batteries in series), the system can wait indefinitely like this, until the emergency stop button is unpressed or the PCC reconnected. Once this happens, the MCU is operating off of the backup battery, and will begin a restart, which is described in the Control Model Analysis section. Importantly, there is an additional, small latching ("first run") relay on the load side that is reset before a testing session begins, which prevents the safety system from triggering upon the first startup (every other startup within a testing session is presumed to be from a purposeful brake). See Appendix 2 for the full circuit diagram.

2.6 Control Model

As mentioned previously, we chose the MSP432 LaunchPad for its low power consumption, and this board remained on the turbine-side of the PCC. The MCU has two primary decision-making loops and three operational states it must traverse. Upon powering on, it must first go through the loop within the *STARTUP* state, which it will only exit if it has enough power for the safety system to run properly

(assumed to be at or below 5 m/s). It will then enter into the *NORMAL OPERATION* state, where it optimizes or limits the power to the load. It's here that the MCU also monitors whether or not the circuit has entered into the *SAFETY* state, in which the MCU does nothing.

Figure 18 shows the finite state machine that indicates how the MCU navigates the information it reads in during *STARTUP*, and Figure 19 shows how it operates in *NORMAL OPERATION* or *SAFETY*. The specifics of the change conditions between states and the microcontroller functions of each state are in Table 4.

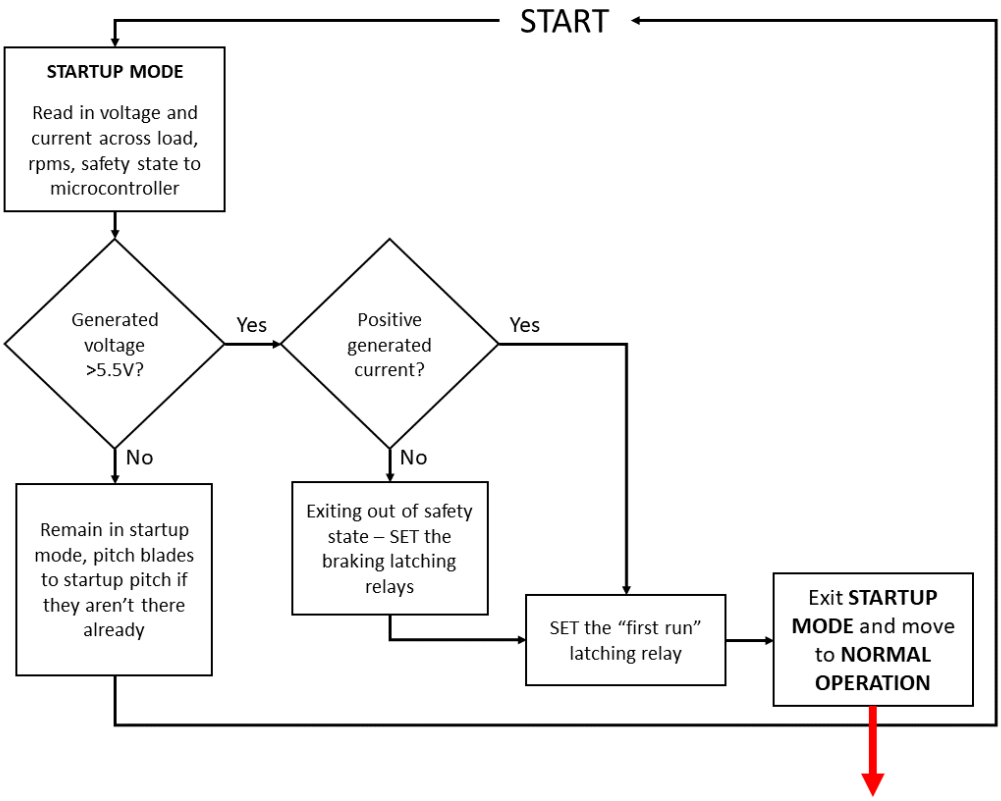


Figure 18: Finite state diagram within *STARTUP* state. The system cannot enter the safety state from startup, which complies with testing requirements assuming startup at or below 5 m/s.

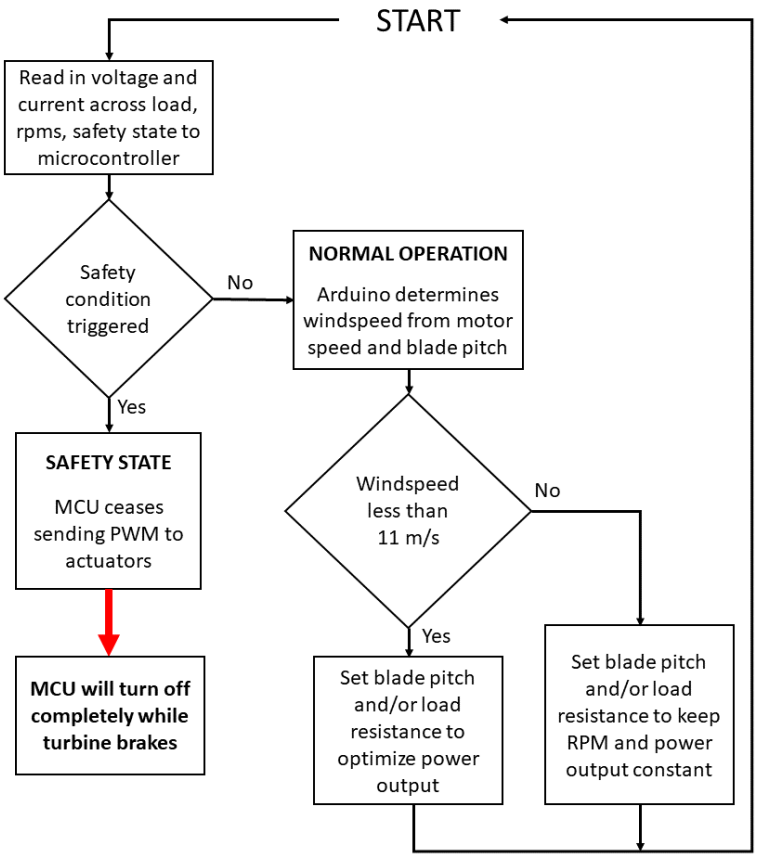


Figure 19: Finite state diagram for the *NORMAL OPERATION* and *SAFETY* states. The MCU has no function during the *SAFETY* state.

Table 3: List of states, their functions, and their change conditions.

State	Description of State Functions	Change Conditions
Startup	• Starting state when MCU powers on • Pitch blade to startup if necessary • Set all latching relays before exiting	Go to normal operation when voltage is >5.5V and there is positive current

Normal Operation	• Read in voltage, current, motor speed, and safety condition
	• "Calculate" wind speed and make decisions based upon it
	• If below 11 m/s:
	  ○ Optimize power output by pitching blades and changing variable load
	• If above 11 m/s:
	  ○ Limit power output by pitching blades
		Go to safety state when safety condition is read in as true

Safety	• Cease PWM output to linear actuators	MCU turns off completely when the turbine is braked

In order to optimize the power curve of the turbine, the MCU must estimate the wind speed by using known power curve data from testing of the final turbine. It takes the two blade pitches and encoder data and compares it to data hard-coded into the MCU program through a series of if/else statements. If the current blade pitches and load setting are not the optimal ones for the current wind speed, the MCU will change those settings.

3.0 Testing

For our final validation testing, our team used the Corrsin Wind Tunnel, a low speed wind tunnel located on the Johns Hopkins campus seen in Figure 20. We were able to characterize the flow in the tunnel to test our turbine at wind speeds of 2.5 m/s to 13 m/s. Our final prototype successfully produced positive power at a wind speed of 4.5 m/s, meeting the startup condition. The turbine was also able to yaw effectively in the flow, and continue producing positive power throughout the yawing events simulated. We collected power and encoder data at multiple speed bins, and collected the results seen in Figure 21 to characterize the system.

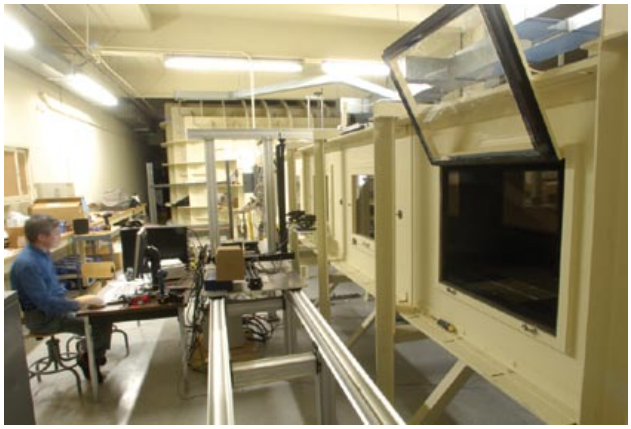


Figure 20: Corrsin Wind Tunnel

3.1 Commissioning Checklist

- ❑ Assemble all mechanical components of the wind turbine outside of the wind tunnel
- ❑ Place the turbine in the center of the wind tunnel, threading wire from the base of the turbine through appropriate channels
- ❑ Secure the turbine to the wind tunnel (using metal weights in the Corrsin wind tunnel, or fasteners provided by the Collegiate Wind Competition)
- ❑ Attach electrical leads from the positive and negative generator terminals to the turbine electronics
- ❑ Attach electrical leads for the linear actuators (5V, signal, ground) to the turbine electronics
- ❑ Attach electrical lead from the turbine electronics ground to the turbine tower
- ❑ Attach electrical lead from the turbine tower to the earth-grounded wind tunnel structure
- ❑ Confirm continuity of all electronics using digital multimeter, beginning with grounds
- ❑ Turn on the power to the wind tunnel, and switch it on to its lowest wind speed (2.5 m/s)
- ❑ Adjust wind speed as needed for operation and testing (in the JHU Corrsin wind tunnel)

3.2 Results

Our system produced positive power at a range of wind speeds above 4.5 m/s. We compared our results to those from some previous competitions, and found that our power curve was comparable to a mid-range performance, with a maximum average output of 21 W at 11 m/s. We did have some significant

problems with noise in our system, which we corrected in generator design by adding a smoothing capacitor to our system.

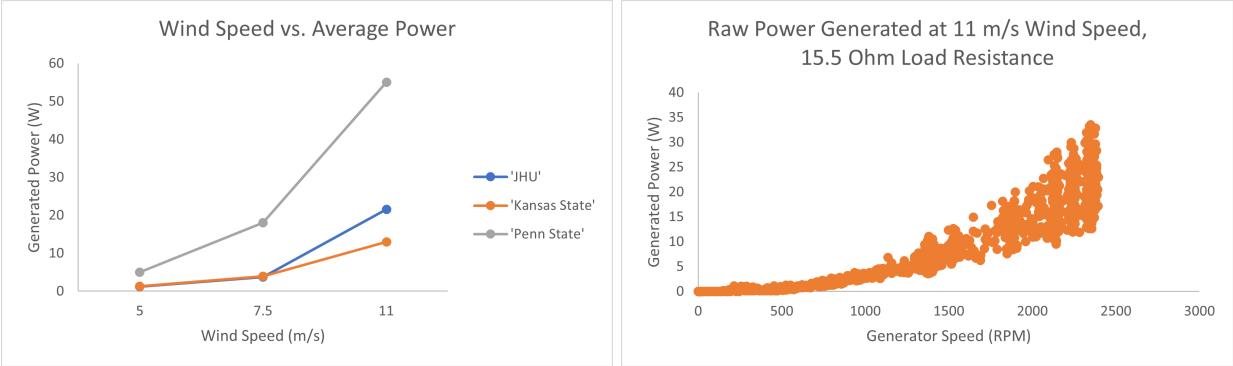


Figure 21: Our team's performance compared to other teams in 2019 (left) and our noise issue (right).

4.0 Conclusion

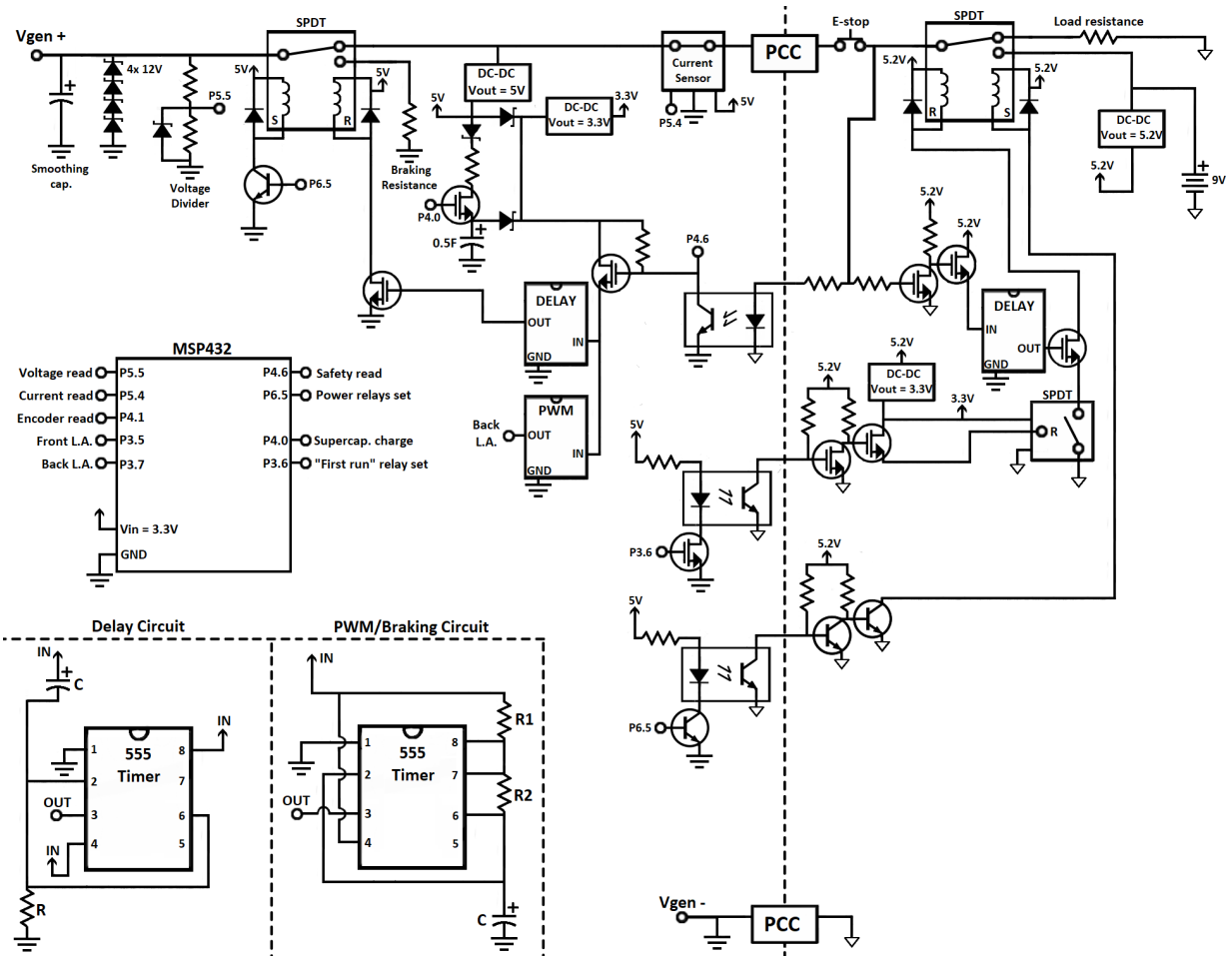
This year, our team successfully designed, built, and tested a working miniature counter-rotating wind turbine in a distributed fashion. While we did not meet all of our goals for our system's performance, we met the key competition specifications for size, safety, and design. With a cut-in wind speed below 5 m/s and a power coefficient of up to 21.8% at 11 m/s we would expect to perform well if the competition was able to include a testing component this year. As our school's first entry to the Collegiate Wind Competition, we believe we have set a solid foundation with an innovative design that future years can build on to achieve even better performance.

5.0 Enumeration of Influence of Previous Design Reports

As a first-year team, we pulled extensively from previous design reports to gain a foundational understanding of miniature wind turbine designs. From the winning teams in 2019 and 2020, Penn State University and California Maritime University, we gained an understanding of some of the key off-the-shelf components that exist and are useful in miniature turbine design, including the use of off-the-shelf pitching mechanisms, linear actuators with microcontroller libraries. We also built our dynamometer and generator testing assembly based on previous team's design reports, selected a variable load system based on Penn State's electronics diagram, and adopted the practice of monitoring wind speed and power output using rpms and voltage instead of wind speed sensors. These are a few of the many lessons that our team learned from previous team's reports, and we are grateful that these reports were provided as reference materials.

6.0 Appendices

6.1 Full Circuit Diagram



6.2 Table of Safety Factors

A complete table of calculated safety factors in tower design, based on FEA simulations and hand calculations.

Location	Maximum Stress	Calculated Safety Factor
Tower	11.16 MPa	49.4
Braze (tower-base joint)	11.16 MPa	35.84 - 85.13
Base plate	5.7317 MPa	48.52
Front Rotor Shaft	20.1 MPa	17.3575
Back Rotor Shaft	27.9 MPa	12.508
Front Rotor Support Arm	0.89044 MPa	309.72
Front Chassis	1.2284 MPa	224.51
Back Chassis	0.48528 MPa	568.31

7.0 References

[1] Sundararaju, Lo, K.H., Metcalfe, R., and Wang, S., 2017, "Aerodynamics and CFD analysis of equal size dual-rotor wind turbine," Journal of Renewable and Sustainable Energy, 9(043305), from https://aip.scitation.org/doi/pdf/10.1063/1.4999500

[2] Chen, S., 2020, "Numerical Investigation of Wind Turbine Airfoils under Clean and Dusty Air Conditions," Ph.D. thesis, Washington University in St. Louis, from https://openscholarship.wustl.edu/cgi/viewcontent.cgi?article=1577&context=eng_etds

[3] "S1210 12%", from http://airfoiltools.com/airfoil/details?airfoil=s1210-il

[4] Singh, R.K., Ahmed, M. R., Zullah, M. A., and Lee, Y. H., 2012, "Design of a low Reynolds number airfoil for small horizontal axis wind turbines," Renewable Energy, Volume 42 66-76, from https://doi.org/10.1016/j.renene.2011.09.014

[5] "The SKF model for calculating the frictional moment." SKF. From: https://www.skf.com/binaries/pub12/Images/0901d1968065e9e7-The-SKF-model-for-calculating-the-frictional-movement_tcm_12-299767.pdf

[6] "JCZK 300C RC Helicopter Parts Main Rotor Head Set" From: https://usa.banggood.com/JCZK-300C-RC-Helicopter-Parts-Main-Rotor-Head-Set-p-1653921.html?cur_warehouse=CN&ID=513344

[7] "US Department of Energy Collegiate Wind Competition 2021 Rules and Regulations" National Renewable Energy Lab, October 9th 2021. From: https://www.energy.gov/eere/collegiatewindcompetition/downloads/collegiate-wind-competition-rules-and-requirements

[8] "Belt and Chain Drives" SDP/SI Catalog. From: https://sdp-si.com/D820/PDFS/Belt-and-Chain-Drives.pdf

The Pennsylvania State University
Wind Energy Club

Technical Design Report

Submitted to
2021 Collegiate Wind Competition
NREL Competition Operations Manager Elise DeGeorge

Aerodynamics Team

Joshua Forrest	Lead
Joshua Bannon	Member
Allison Karp	Member
Akhilesh Mulgund	Member
Jeremy O'Connor	Member
Joseph Snider	Member
Colin Welch	Member

Circuits and Controls Team

Jackie Cheng	Lead
Satyam Patel	Lead
Mohammed Aal Abdulla	Member
James Leandri	Member

Generator Team

Eric Sarbacker	Lead
Eric Folmar	Member
Tara Presnall	Member
Zoe Shu	Member

Strategic Advisors

Dr. Mark Miller
Dr. Susan Stewart
Dr. Yan Li
Mr. Richard Auhl
Jason Cornelius
Costa Kandias
Sean Wang

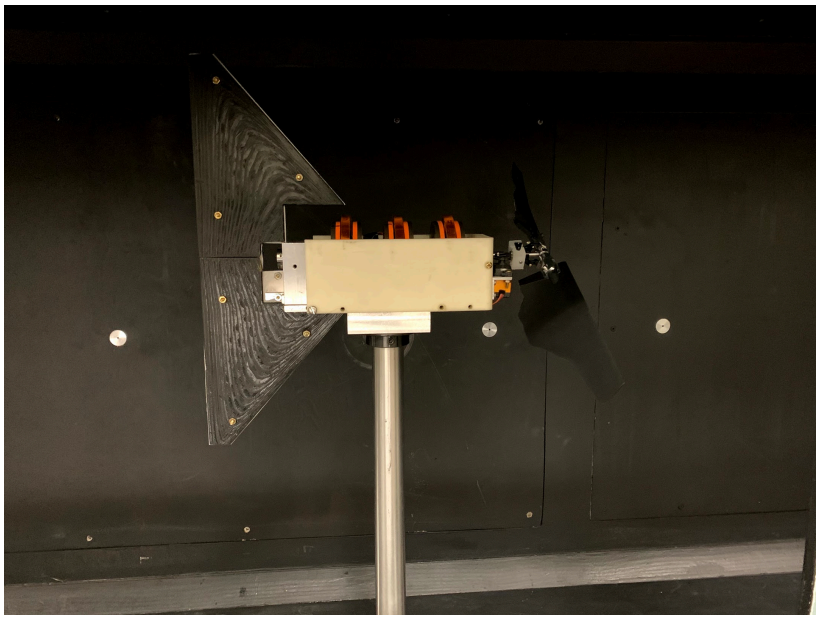


Table of Contents

1 Executive Summary **2**

2 Technical Design **2**

2.1 Rotor System Design 2

2.1.1 Rotor Design 3

2.1.2 Rotor Structural Testing 6

2.1.3 Hub Strength Testing 7

2.1.4 Blade Collective Pitch System 7

2.1.5 Yaw Control System 8

2.2 Generator Design 9

2.3 Turbine Nacelle 10

2.4 Circuits and Control Design 11

2.4.1 Voltage Rectification 11

2.4.2 Control Circuit Voltage Regulation 11

2.4.3 Control Circuit Logic 12

2.4.4 Control Model Analysis 13

2.4.5 Load Circuit 13

3 Turbine Testing **14**

3.1 Testing Objective 14

3.2 Testing Procedure 14

3.3 Testing Results 15

4 Commissioning Checklist **16**

5 Building on Previous Years' Work **16**

6 Conclusions **17**

References **i**

1 Executive Summary

In this document, the Pennsylvania State University Wind Energy Club describes the research, design, construction, and analysis of a wind turbine during the Covid-19 pandemic. The team divided the turbine system into three primary categories: aerodynamics, generator, and circuits and control. The team overcame many challenges derived from the pandemicand also had to make many compromises. In particular, the inability to access any laboratory spaces until the middle of March hindered progress in the assembly and experimentation for the turbine. However, the team made significant strides in the system's design.

The wind turbine system features a newly-designed two-bladed rotor with the potential for increased torque at startup and higher power coefficients across Region II operation. The turbine's pitching servo has transitioned from a radial to linear servo to more precisely and accurately control the pitching of the blades. The generator used is an axial-flux three-stage generator that minimizes the torque required. The control circuit for the turbine uses an arduino to control the pitching servo and also varies the circuit load to maximize and control the power produced by the turbine as well as meet the competition requirements for voltage.

Overall, the 2021 competition turbine builds upon the team's previous successes with turbine design and features an improved rotor, pitching system, and control circuit.

2 Technical Design

The Turbine was split into 3 subsystems/sub-teams: The Aerodynamics team was responsible for the design of the blades, the Circuits and Control team was responsible for controlling the pitch and electrical systems, and the Generator team was responsible for the generator's physical design and optimization. Each sub-team met on their own once per week in addition to meeting with the entire team to discuss their work and progress on their subsystem of the turbine.

2.1 Rotor System Design

This year, the Aero sub-team decided to switch to a 2-bladed rotor design. Much of the fall semester was focused on determining whether this was the right choice, and additionally was tasked with finding a suitable airfoil for the blades. This process was done first using XFOIL to determine which airfoil would have the best lift-to-drag characteristics and secondly in XTURB (a Blade Element Momentum performance code developed at Penn State) to narrow down the shape of our blades [2, 3]. Once we had the shape determined, we began to create a SolidWorks model of the blade by outlining the shape of the blade along the span, pasting the airfoil coordinates along 52 planes of the blade, and rotating each airfoil to the ideal twist according to our simulations in XTURB. Once the model was complete around the middle of the spring semester, the blades were ready to be 3D printed. The initial prints of our blades were flimsy and tessellated near the thin trailing edge, and they

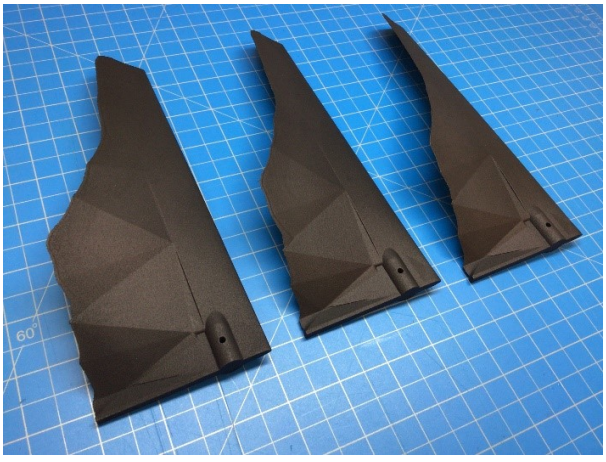


Figure 1: The Nylon 12 material blades experienced high tip deflections and were prone to flutter

tended to flutter when tested in the wind tunnel. As such, another company was chosen for printing a second batch using a different material, and these new blades were stronger and much more accurate when compared with the CAD model (Figure 2).

2.1.1 Rotor Design

Wind turbine rotor design depends heavily on the scale of the rotor which drives the limiting design factors. The scale of utility wind turbines is so large that the primary limiting design factors are the maximum allowable tip speed and blade structural design. The industry has converged primarily on 3-bladed rotors because they effectively produce power while meeting requirements for noise and relatively affordable construction. However, the CWC rotors are only 45 cm in diameter, which makes the aerodynamics of the rotor the limiting factor rather than the rotor structure or tip speeds. More specifically, a large contributor to the rotor's deviation from a rotor's optimal performance is the low blade chord Reynolds numbers. At lower Reynolds numbers, airfoils have significantly higher drag coefficients. For the MA 409 airfoil used in this turbine, the drag coefficient at the airfoil's most efficient point (or maximum glide ratio) is 0.0221 at 50,000 Reynolds number and 0.0134 at 110,000 Reynolds number, obtained from XFOIL [2]. That is a 39% decrease in relative drag due to the increase in Reynolds number. Because the drag decreases with increasing Reynolds number, the glide ratio, or the ratio of lift to drag, also increases with Reynolds number. The rotor's aerodynamic performance increases with an increase in the glide ratio, so the rotor design emphasized maximizing the glide ratio of the blades.



Figure 2: Accura60 material blades are stiffer than the Nylon 12 blades.

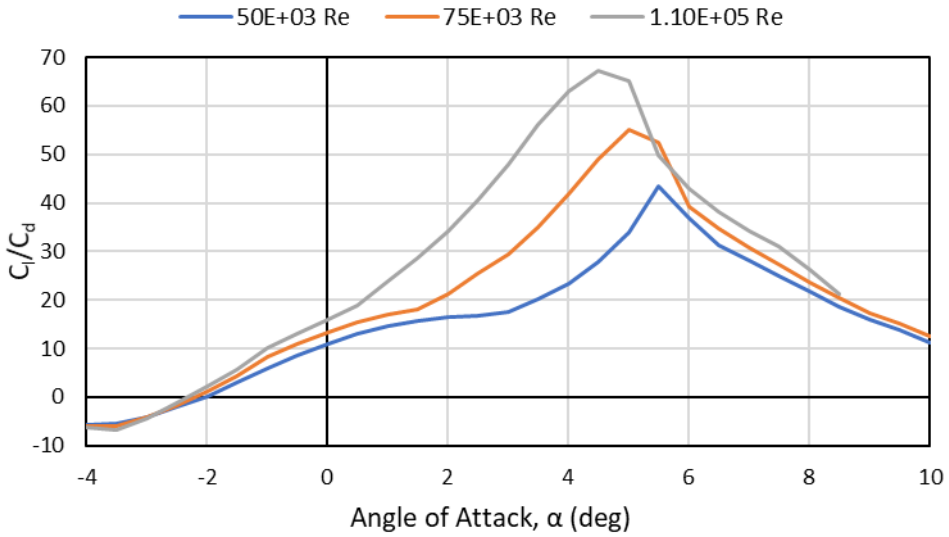


Figure 3: MA 409 airfoil "Glide Ratio" for expected Reynolds numbers

Increasing Reynolds number can be achieved in four different ways: an increase in the fluid density, a decrease in the fluid viscosity, an increase in the fluid flow speed, or an increase in the length scale of the aerodynamic body. In the competition, the only parameter that can be adjusted is the length scale of the aerodynamic body: the blade chord length. However, increasing the blade chord length changes the rotor solidity and reduces the maximum power coefficient tip speed ratio. From Aerodynamics of Wind Turbines, the best design tip speed ratio depends upon the average expected airfoil glide ratios along the blade in the design case [4]. For the competition, the highest-scoring category in the power curve task is 8 m/s, for which the rotor is expected to have chord Reynolds numbers of approximately 40,000 to 70,000 along the blade for the club's 3-bladed rotor from 2020. At these Reynolds numbers, most airfoils achieve glide ratios of 25 to 40 according to XFOIL. This corresponds to a design tip speed ratio of approximately 3.5, which is the 2020 rotor design point ([4], figure 3.14). If the average glide ratio is increased by increasing the Reynolds number, the rotor will have a higher power coefficient across all tip speed ratios. However, simply increasing the chord of the blades will increase the solidity and decrease the maximum power coefficient tip speed ratio and the rotor will under perform. Instead, reducing the number of blades to two and increasing the chord allows for the solidity to be slightly decreased while increasing Reynolds number. This allows for the tip speed ratio to be 4, which was determined to be the design case after evaluating available airfoils at the expected Reynolds numbers, discussed later on.

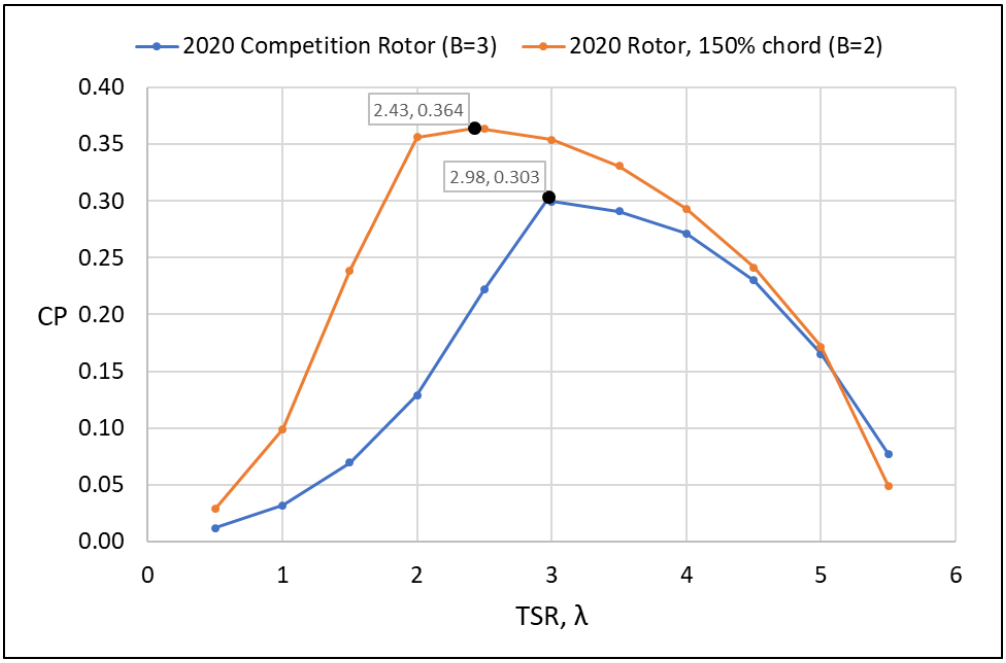


Figure 4: Power curves for the PSU 2020 3-blade competition rotor and 2-blade change

Changing to a two-bladed rotor with a longer chord length increases the Reynolds numbers to improve rotor performance but also increases the tip losses which decrease rotor performance. To investigate the tradeoffs between the two effects, the 2020 competition rotor design was analyzed in XTURB in the original 3-bladed configuration and a comparison 2-bladed case with chord of the blades increased by 50% to match the solidity. The two designs were compared at a fixed pitch which was optimized for the design tip speed ratio of the 3-bladed rotor. As shown in Figure 4, the maximum power coefficient increased by 20.1% from 0.303 to 0.364. Importantly, the power coefficient was increased across all tip speed ratios, notably at low tip speed ratios. This is due to the increased Reynolds number delaying the onset of stall, which occurs for a fixed-pitch turbine at low tip speed ratios. This indicates the potential for more torque at low wind speeds

with the two-bladed rotor compared to the three-bladed rotor.

The two-bladed rotor was designed using a procedure based on the ideal Blade number, tip speed ratio, lift coefficient, and chord relation described by in [4]. Given a defined blade number, design tip speed ratio, and design lift coefficient distribution, the chord distribution of the blades can be determined.

$$\mathrm{B}\lambda c_l * \mathrm{c}(r/R) = \left(\frac{4}{3}\right)^2 \pi \frac{1}{\lambda_r} \tag{1}$$

Once an airfoil is selected, the pitch distribution can also be obtained by determining the design angle of attack required to achieve the design lift coefficient. The design lift coefficient is determined by choosing the optimal glide ratio lift coefficient for the chosen airfoil.

To select the optimal airfoil, a number of different airfoils from the Selig Airfoil Database were analyzed using XFOIL. The glide ratios vs angles of attack were plotted for the lower Reynold's number of 50,000. It was found that the MA 409 airfoil had the highest peak glide ratio compared to other airfoils [5]. Further optimization to the design could involve searching for airfoils that have a more rounded peak at the higher glide ratios rather than the sharp peak found in the MA 409.

Once the MA409 airfoil was selected, the blade was designed using Equation 1 as a first-pass. The design was altered to reduce the chord towards the inboard sections to a more reasonable chord length and rounding the tip off to reduce tip losses. The resulting design was analyzed in XTURB to determine the expected performance (Figure 5).

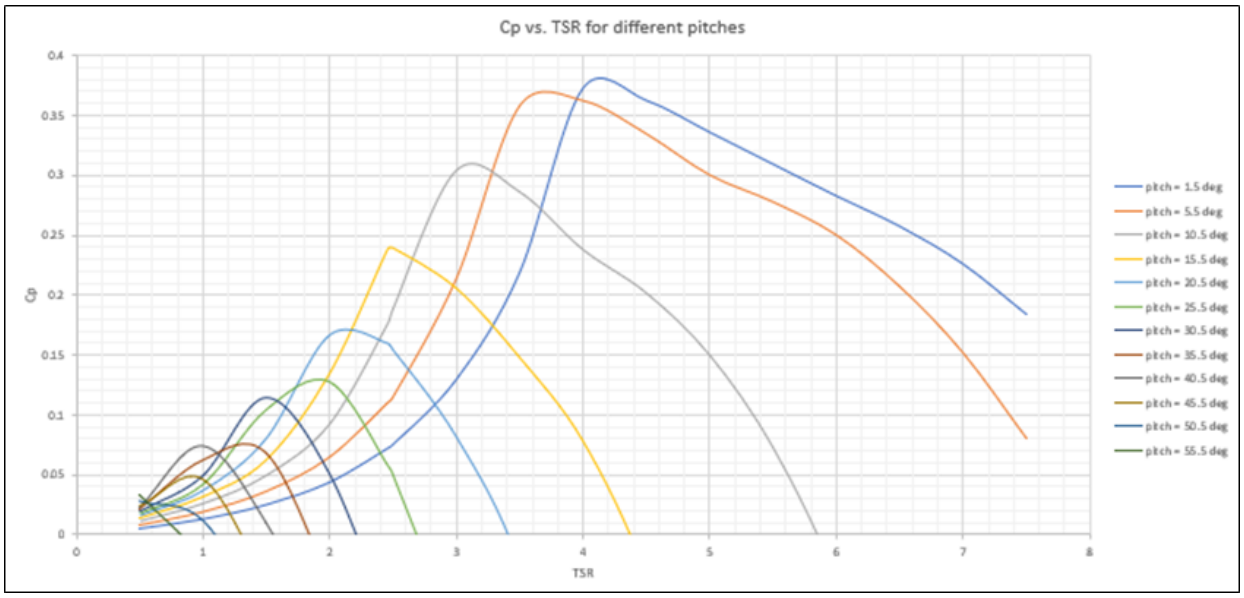


Figure 5: Power curves for the PSU 2021 two-bladed competition rotor with varying collective pitches.

The power coefficient curve was determined for a variety of collective pitches. The results show that the optimum power coefficient of 0.38 is achieved for a collective pitch of 1.5 degrees for a tip speed ratio of 4.1. This is a significant improvement of 25.4% in peak power coefficient compared to the 2020 rotor design. Increasing the collective pitch of the blades increases the rotor's power coefficient at lower tip speed ratios. This clearly indicates the control procedure for the turbine when in operation in regions 2 and 3. The startup pitch is likely to be much higher, so pitching the blades out of the wind from the startup pitch will increase the rotor speed to the optimum tip speed ratio. However, experimentation to determine the exact pitches is required to verify the results from XTURB. Performing these experiments is the goal of the club for the 2022 Competition due to limited access to on-campus activities for the 2021 Competition.

2.1.2 Rotor Structural Testing

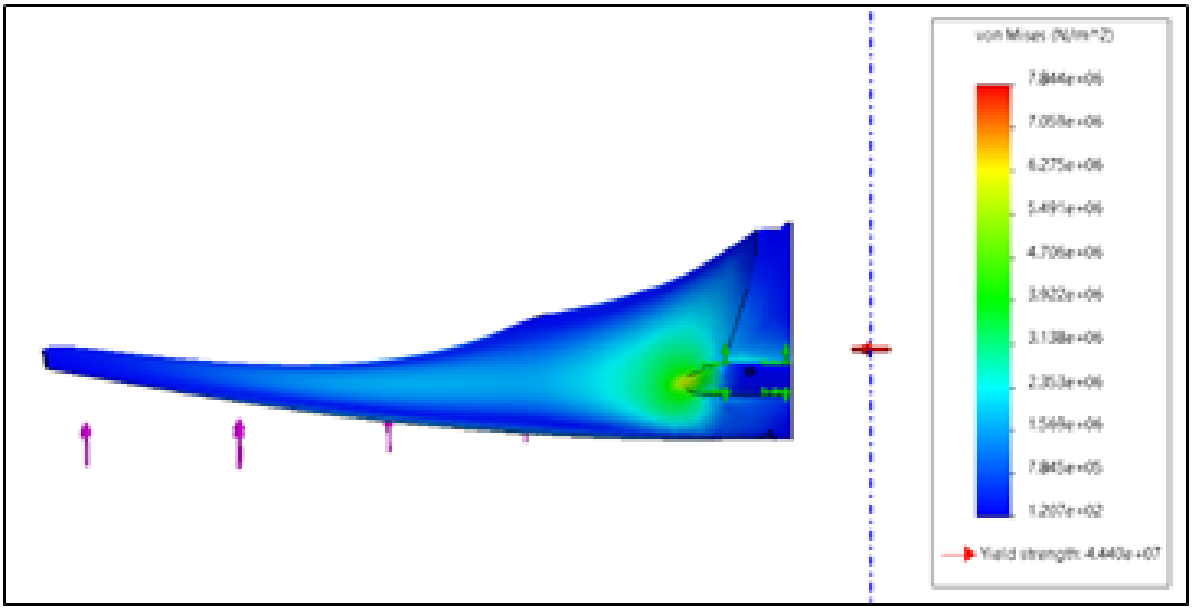


Figure 6: Visualization of blade stresses for the highest load case, 23 m/s freestream and 1867 RPM. There is a stress concentration at the gripped location but the stress is below the yield stress by a factor of 5.66.

From our SolidWorks testing of our blade design, it was clear that the most stress would be at the end of the circular piece that connects the blade to the hub. The loads applied were informed by XTURB results. XTURB gives a distribution of lift coefficient, from which the spanwise lift distribution was determined. A fifth-order polynomial was curve-fit to the spanwise distribution of lift with an R^2 value of 0.985. The loads were applied normal to a strip centered at the blade's quarter-chord, which was estimated to be the approximate aerodynamic center. The total scaling of the loads applied was changed to match the total thrust from aerodynamic forces, in this case 45 N for each blade for the 23 m/s case. Then, the centripetal load from rotating 1867 RPM was applied and the resultant stresses analyzed for stress concentrations and factors of safety. Our strength results, with a Nylon 12 material imported in, demonstrated a factor of safety of 5.66 (Figure 6) for the max load of 45 N.



Figure 7: Blade strength testing to verify the factor of safety. The load applied was resolved to the spanwise location of the resolved lift distribution at the quarter chord. The Nylon 12 blades had high strain but did not yield.

To confirm the SolidWorks simulations, the blades were tested physically in person. The blades used in this experiment contain the same airfoil used in the model and have the same shape, but they are not the final blades used for our turbine. Due to limited time and restrictions on in-person work due to the pandemic, only a single set of blades were available for testing and these had a manufacturing defect on the pressure side of the blade. However, it was expected that this discrep-

ancy would not significantly affect the performance of the test and would still produce useful validation data for our final product. The setup involved fixing the blade at the hub location with a clamp. This was done in order to straighten the other end of the blade to easily add weights at the resultant force location to accurately represent the aerodynamic blade loads. From here, weights were added one at a time until the point of failure. However, the failure occurred due to the clamping system, not by breakage of the blade. Until this point, the blade was able to withstand over 62 N which guarantees a factor of safety of at least 1.77. However, the competition rules state that the maximum testing done in competition will be 13 m/s, not 23 m/s. This means that the maximum aerodynamic loading will be 11.2 N in the actual competition testing. Compared to this loading case, the factor of safety is at least 5.53. It is noted in the image of the test that the blade was bending significantly which is undesirable for a wind turbine. Because of this we decided to reconsider our material to Accura 60, which is significantly stiffer. However, the team was unable to test the new Accura 60 blades and will look to analyze their structural factor of safety for the 2022 competition.

2.1.3 Hub Strength Testing

The hub testing was completed in a similar way to past competition rotors. A block with a rod on one end is clamped to an I-beam attached to the wall. This rod took the place of the generator driveshaft and locates the hub piece. A sacrificial bolt was used where the blade would normally be clamped in case of damage it could be easily removed. Once the bolt was in place with the hub on the rod, a chain hoist was used to apply an upward force on the hub assembly, with the resulting force being read out by a dial gauge between the hoist and hub. From the SolidWorks model, it was predicted that the hub needed to withstand approximately 110 N on each side to fully support the blades at their maximum speed. The hub was tested up to 890 N with only minor damage to the screw. This creates a factor of safety of at least 8.09 which means our strength test proved to be very successful and the blades will be held without damage.

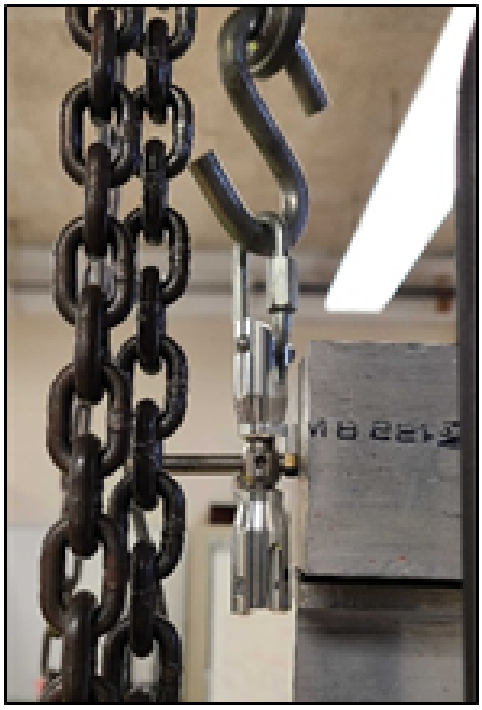


Figure 8: Testing the strength of the hub for radially applied tension force equal to the blades spinning at 1867 RPM.

2.1.4 Blade Collective Pitch System

The rotor hub was changed to support the shift to the two-bladed design. A re-purposed RC helicopter tail rotor (Align 700) was used [1]. This device, when paired with the two linear servos, will be able to pitch the blades at a variety of different angles for the cut in wind speed, power curve performance, and safety tasks. In the past, radial servos have been used, with preliminary investigations also exploring using linear servos. It was found that two linear servos in parallel would draw similar power to the single radial servo. The two linear servos will be located on either side of the nacelle. This will ensure that no bending moment is created on the shaft of the nacelle when setting the blade pitch, a problem that was faced in previous years' designs. These designs were made remotely using CAD software, with measurements of the different parts taken by team members who were in-person.

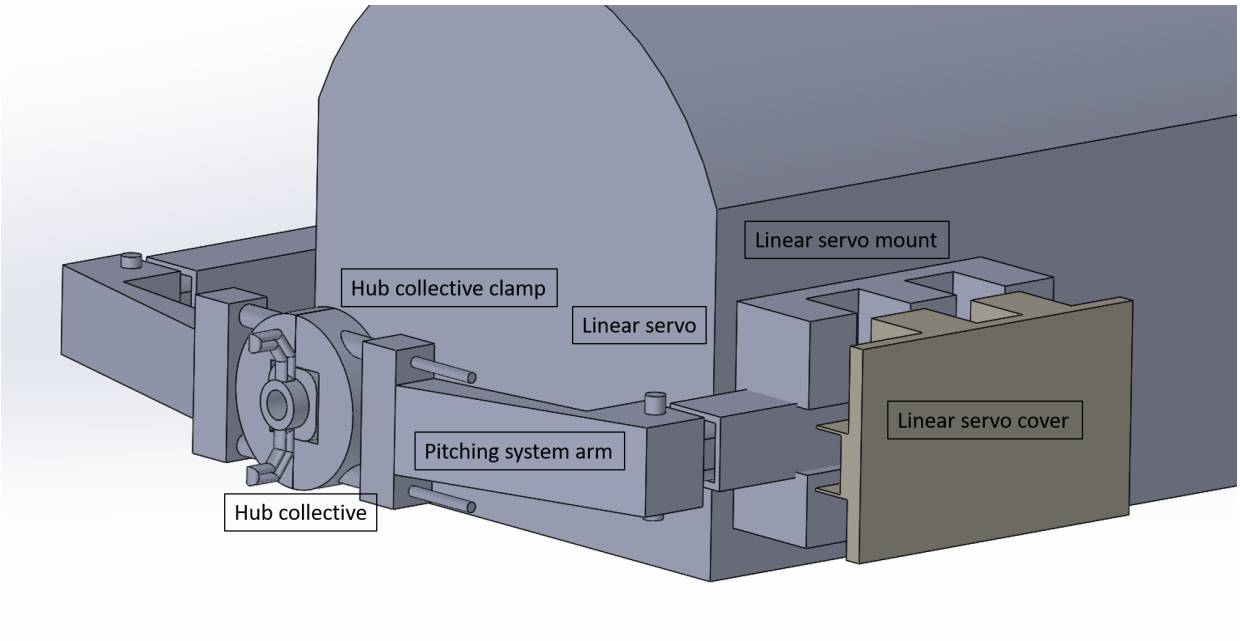


Figure 9: Linear servo pitching system with dual linear servos controlled simultaneously by the arduino.

2.1.5 Yaw Control System

Our yaw system is entirely passive and unpowered. It relies on a tailfin, composed of steel and a 3D printed NACA 009 airfoil. This design is more than capable of moving our turbine into the direction of the freestream air, and it does so without needing any active control or power. Two halves of the airfoil sandwich the metal plate, which is attached to the rear of our turbine nacelle via screws. An in-depth analysis of how quickly the tailfin can yaw the turbine depending on the velocity of the oncoming air has not been performed as of the writing of this report. However, based on how the turbine performs in the wind tunnel, it appears return the nacelle to the freestream direction within 1-2 seconds.

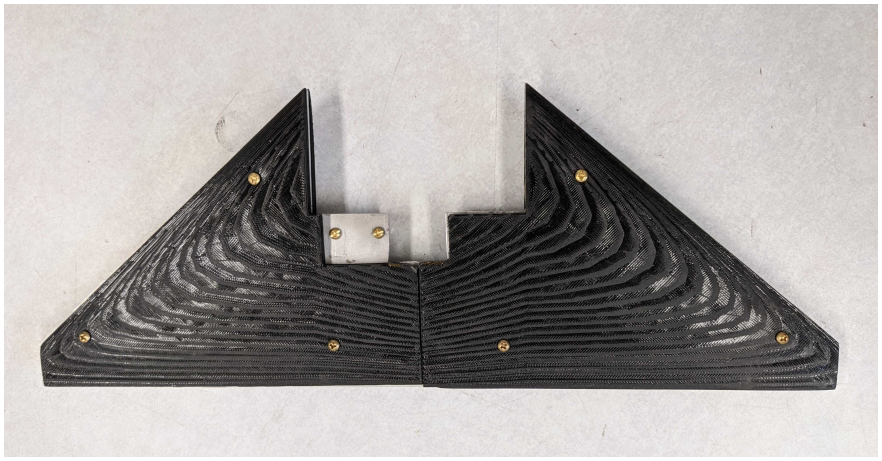


Figure 10: The turbine tailfin, which is a flat metal plate with 3D printed NACA 009 covers.

2.2 Generator Design

For the generator sub-team, much of the year was spent with the generator inaccessible, so most of the efforts were focused on improving the generator design code that is used to predict performance. The generator code was redesigned so that new members of the team would understand how to use it. This came in the form of adding additional graphs as well as explanations of what the code uses for its calculations. With all these additions to the code, we hope that new members will be able to use the code, understand what it is outputting, and be able to more systematically change the variables to see how it would affect generator performance.

Prediction of Voltage, Current, Electrical Power

	Voltage			Current			Power			
RPM	1	2	3	1	2	3	1	2	3	
200	1.05	2.09	3.14	0.180	0.180	0.180	0.19	0.38	0.57	
400	2.09	4.18	6.27	0.360	0.360	0.360	0.75	1.51	2.26	
600	3.14	6.27	9.41	0.540	0.540	0.540	1.70	3.39	5.09	
800	4.18	8.36	12.55	0.721	0.721	0.721	3.01	6.03	9.04	
1000	5.23	10.45	15.68	0.901	0.901	0.901	4.71	9.42	14.13	
1200	6.27	12.55	18.82	1.081	1.081	1.081	6.78	13.56	20.34	
1400	7.32	14.64	21.95	1.261	1.261	1.261	9.23	18.46	27.69	
1600	8.36	16.73	25.09	1.441	1.441	1.441	12.05	24.11	36.16	
1800	9.41	18.82	28.23	1.621	1.621	1.621	15.26	30.51	45.77	
1900	9.93	19.86	29.80	1.712	1.712	1.712	17.00	34.00	50.99	
2000	10.45	20.91	31.36	1.802	1.802	1.802	18.83	37.67	56.50	
2200	11.50	23.00	34.50	1.982	1.982	1.982	22.79	45.58	68.37	Target
2400	12.55	25.09	37.64	2.162	2.162	2.162	27.12	54.24	81.37	
2600	13.59	27.18	40.77	2.342	2.342	2.342	31.83	63.66	95.49	
2800	14.64	29.27	43.91	2.522	2.522	2.522	36.92	73.83	110.75	
3000	15.68	31.36	47.05	2.702	2.702	2.702	42.38	84.76	127.13	
3200	16.73	33.45	50.18	2.883	2.883	2.883	48.22	96.43	144.65	
3400	17.77	35.55	53.32	3.063	3.063	3.063	54.43	108.86	163.30	
3600	18.82	37.64	56.45	3.243	3.243	3.243	61.02	122.05	183.07	
3800	19.86	39.73	59.59	3.423	3.423	3.423	67.99	135.99	203.98	
4000	20.91	41.82	62.73	3.603	3.603	3.603	75.34	150.68	226.02	

$$V = \frac{2\,\pi\,q\,k\,\emptyset}{120} * \frac{N}{\sqrt{2}} * Stators$$

$$I = \frac{V}{2 * R} * Stators$$

$$P = I * R * Stators$$

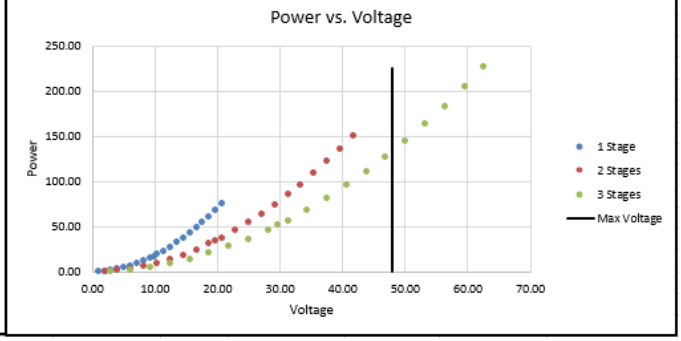


Figure 11: Updated V, I, P section of the generator code includes range of values along various RPM values, highlighting the target value for the turbine at max RPM. Now also includes how the values were calculated as well as important graphs highlighting range of power in compliance with competition safety.

The prediction of voltage, current, and electrical power is just one small portion of the generator code. The updated version gives a clearer picture of the design process and accomplished what we aimed for in making the design good looking as well as more accessible.

Although the generator code is helpful in the prediction of how the generator will perform, all calculations should be backed up by rigorous testing. Testing is not only important to validate the predictions of the generator code, but also ensure the generator can withstand the conditions it is required to undertake. If any components of the generator are not working properly, then it is much easier to fix the problem outside of the wind tunnel, for this reason we did most testing on a dynamometer test bench.

To improve on generator testing this year, upgrades were made to our dynamometer test stand to

allow for testing and changes to be made to the generator on the fly. Compared with previous years, the generator is placed upright on the test stand. Additionally, this new design is more secure than in previous years. By using bolts and machined aluminum rather than metal straps, there are less vibrations and less unwanted torques on the generator and dynamometer.

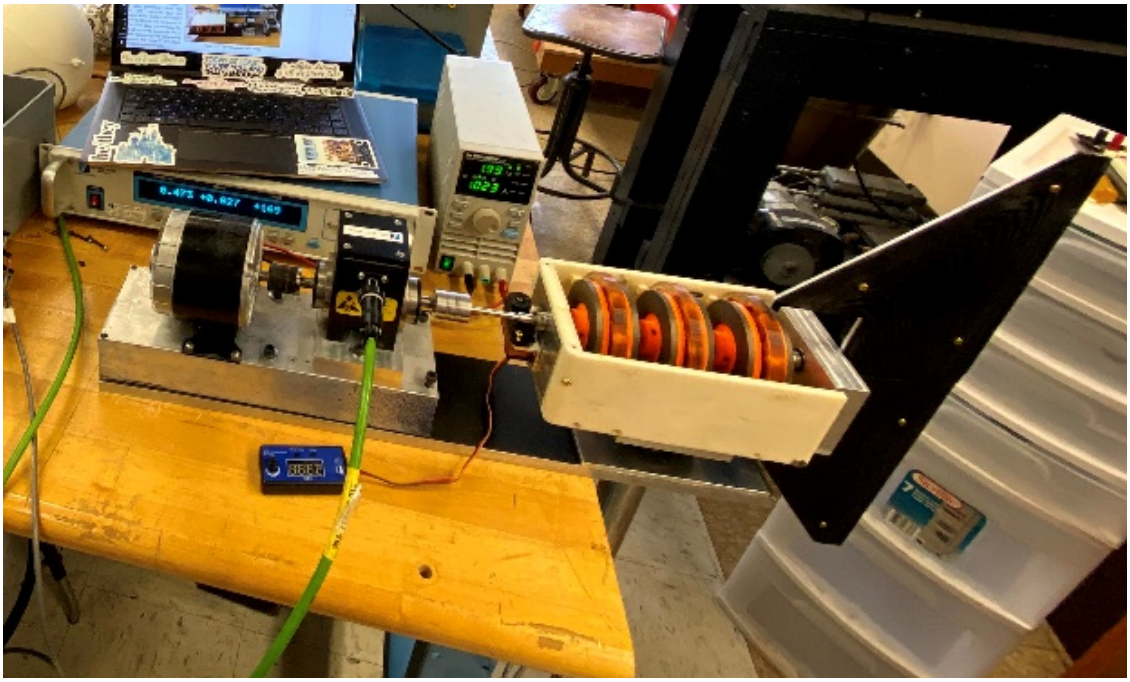


Figure 12: Generator dynamometer testing set up.

The data collected from the dynamometer testing was limited due to lab access being restricted, but the test did validate the generator code and proved that the generator performs as required, even outside the range that is necessary for competition. The data collected on variable resistance will be helpful in optimizing load resistance and power output for possible automation in the future.

Since the generator was mostly unavailable, the parts of the generator were reused from last year. The turbine structure was made from aluminum and steel parts and constructed using traditional machining techniques. This includes the tower baseplate, nacelle structure, shaft, and servo connector. The housing, and generator rotors were best constructed out of ABS plastic with fused deposition modeling 3D printing, which is very accurate but does not produce as strong a final product as traditional machining does with metals. For this reason, the plastic parts are designed not to be structural and take minimal loads. During testing, imperfections were found in the nacelle that hinder the performance and accessibility of the stators. Plans were made to improve the housing to relieve these issues, but they were never realized as getting initial testing done was deemed more important.

2.3 Turbine Nacelle

The turbine structure was constructed using traditional machining techniques, with high-strength aluminum and steel parts with relatively simple geometries. The tower baseplate, nacelle structure, shaft, and servo connector were made using this technique. The housing, and generator rotors however, have very complex geometries that are best constructed out of ABS plastic with fused deposition modeling 3D printing. This technique is very accurate but does not produce as strong a final product as traditional machining does with metals. For this reason, the plastic parts are designed not to be structural and take minimal loads.

2.4 Circuits and Control Design

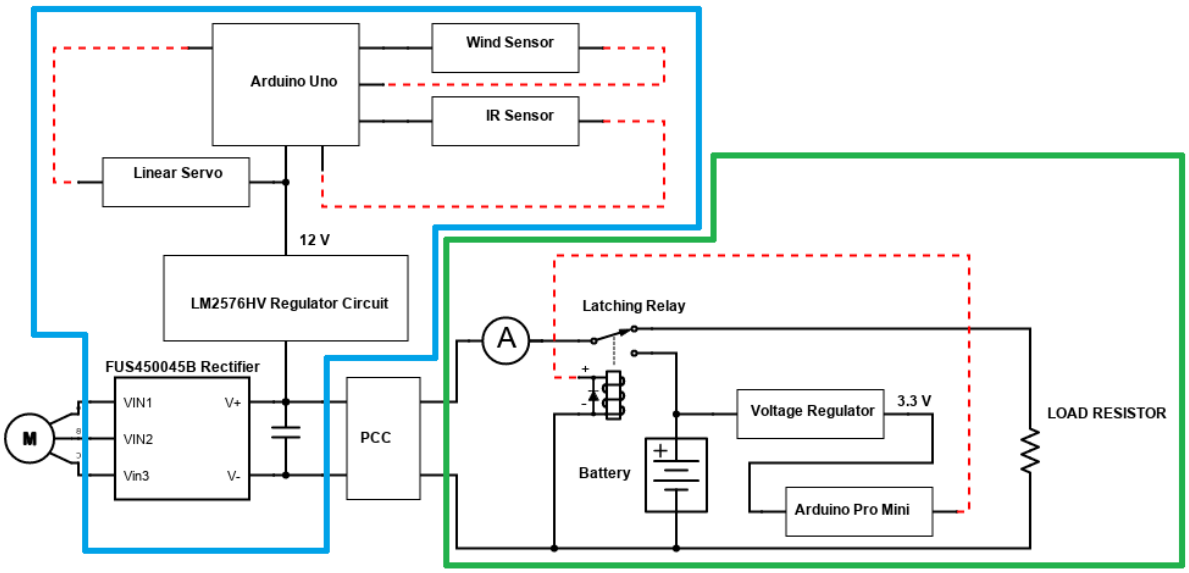


Figure 13: Complete Electrical Diagram- the blue outline encompasses the control circuit and the green outline encompasses the load circuit.

2.4.1 Voltage Rectification

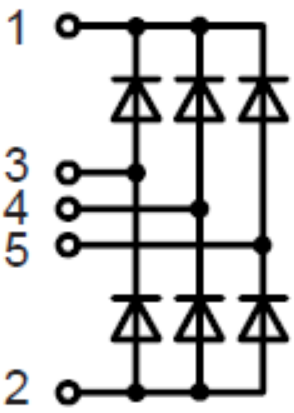


Figure 14: Diagram of FUS45-0045B

The generator produces an AC signal with nine total phases of output voltage. A total of three Schottky Three Phase Bridge Rectifiers inside a FUS45-0045B IC are used to convert the 9 phased AC signal to a single DC signal. A single 3 phase rectification circuit is shown in Figure 14. The maximum input of the rectifier is 45VRRM outputting up to 63V DC. This is well within the range of operation because the voltage across the PCC cannot exceed 48V. This DC signal can now be used to feed the computers and sensors within the turbine, and most importantly, power the turbine load. The complete electrical diagram of the turbine control and load circuit is shown in Figure 13.

2.4.2 Control Circuit Voltage Regulation

The rectifier in the control circuit can output a DC voltage which varies from 0V to 48V. This raw DC signal can easily exceed the maximum input voltage of the sensors and microcontrollers. To mitigate this, a voltage regulation circuit was used. This circuit contains the LM2576HV regulation IC configured to limit the voltage from the rectifier to 12V.

To configure the LM2576HV regulator output to a peak output voltage of 12V, the following formula from the datasheet was utilized:

$$V_{\text{out}} = 1.23\left(1 + \frac{R_2}{R_1}\right),\ R_2 = 8.7\text{k}\Omega,\ R_1 = 1\text{k}\Omega \tag{2}$$

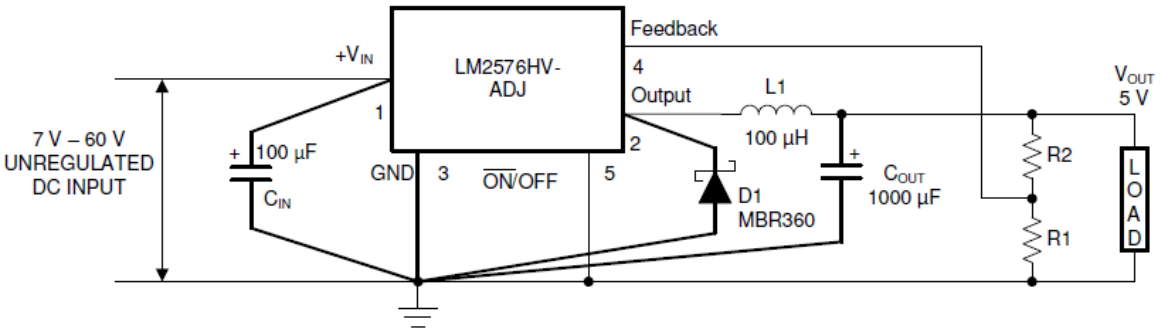


Figure 15: Diagram of General LM2576HV Regulator Circuit

This 12V signal from the regulator is then used to power the servo motor and control Arduino. The servo motor can then control the blade pitch which is crucial for controlling turbine operation and safety tasks. The control Arduino also has its own built in voltage regulators outputting 5V and 3.3V. The 5V regulated output from the Arduino Uno is used to power a wind speed sensor which uses a digital hot-wire technique as opposed to a traditional anemometer to obtain wind speed. The 3.3V regulated output from the Arduino is used to power the RPR220 IR Sensor. This IR sensor is embedded inside the generator assembly on top of one of the coil magnets. As the coil magnet rotates, a the RPR sensor will output a low value when it detects a dark surface (the magnet), and then output a high value when it detects a white dote painted on the magnet. The Arduino can then calculate the RPM of the turbine by identifying the number of high signals in a period of time.

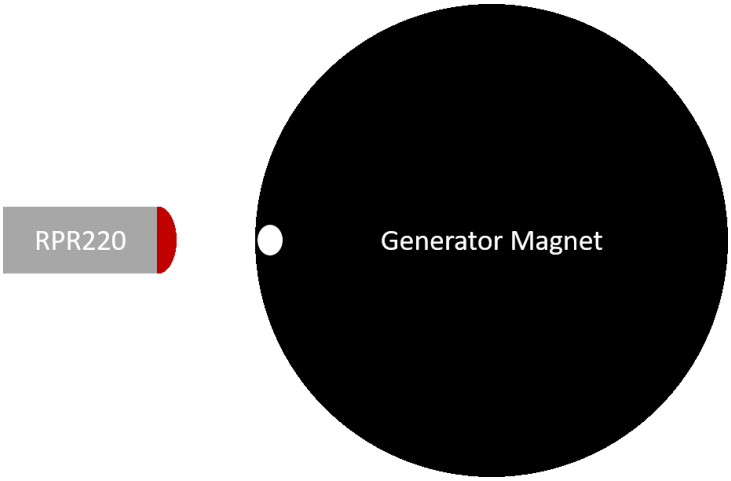


Figure 16: The RPR220 IR sensor is used to measure the generator RPM.

of the turbine by identifying the number of high signals in a period of time. The wind speed sensor works by heating up a resistor coil, and then calculates the wind speed by determining how much power is required to keep coil at a certain temperature. This process can draw a high level of current at high wind speeds. To account for this factor, the team chose to power the Arduino Uno with a 12V DC signal - which is the maximum input voltage it can handle - to make sure the Arduino has enough power to run at full capacity while also operating both the wind speed and RPM sensors.

2.4.3 Control Circuit Logic

During the turbine testing phase, a simplified version of the control circuit code was utilized. This code enabled quick changes of the blade pitch directly from the serial monitor of the control Arduino. An IR sensor was used to monitor generator RPM, and a wind speed sensor was included in the circuit design, but they both have not been fully integrated into the code of the control Arduino.

The primary control circuit code functions as the following: when the turbine is producing enough power to activate the control circuit computer, it will begin to pitch the turbine blades to the enable position.

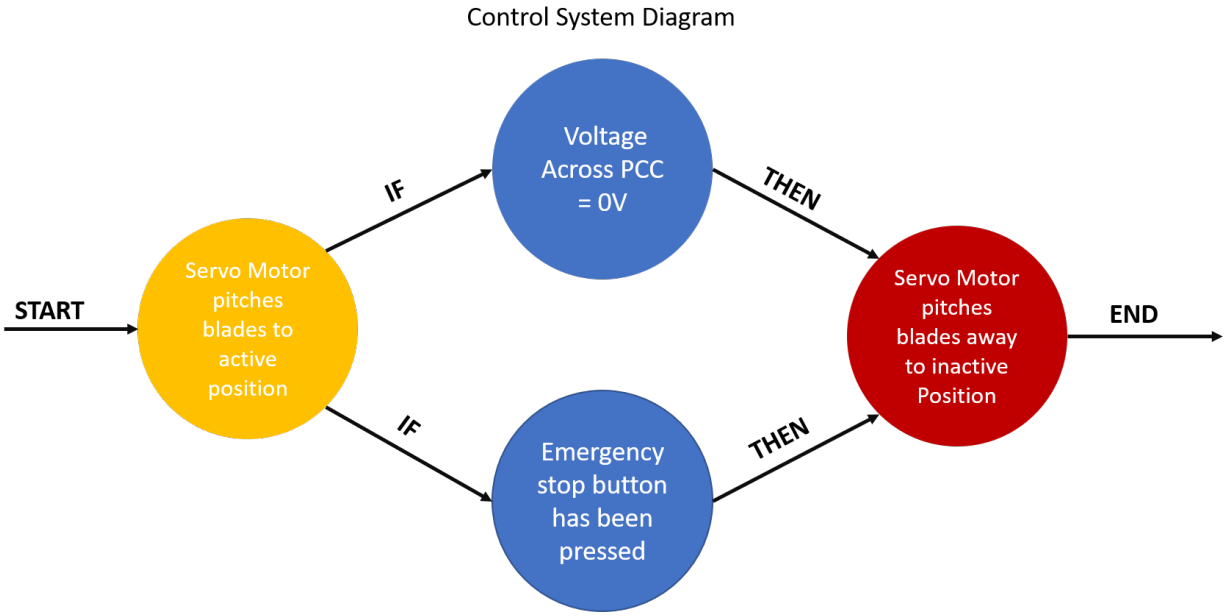


Figure 17: Visualization of the control circuit logic

This is the pitch that will produce maximum power. At this state, the computer will continuously loop to check the status of the voltage across the PCC, as well as monitor the status of the emergency stop button. If the voltage across the PCC is detected to be 0V or if the emergency stop bump switch has been activated, the servo motors will pitch the blades to the maximum forward position, so that the blades act as an air brake thus slowing the turbine to a stop.

2.4.4 Control Model Analysis

The functionality of the turbine will vary greatly depending on the environment it is placed in. There are four total functional states that are determined based on the physical wind speed of the environment. In region 1, the wind speed will be low ranging from 2.5 to 4.5 m/s. Region 2 is the “normal” operational state and it occurs when the wind speed ranges from 4.5 m/s to 11 m/s. Region 3 occurs at high wind speeds greater than 11 m/s. Finally, Region 4 is set when the turbine needs to immediately shut down.

2.4.5 Load Circuit

The load circuit consists of a current sensor, latching relay, LiPo battery, voltage buck/boost regulator, Arduino Pro Mini, and 50-ohm load resistor. The purpose of the current sensor is to detect when the load is disconnected. The latching relay is used to deliver power from the battery to the linear servos during the safety task. The LiPo battery and voltage buck/boost regulator are used together to power the load Arduino during all modes of operation and the linear servos when the load is disconnected or when the emergency stop button is depressed. The Arduino Pro Mini was chosen for its low power consumption and is used to toggle the latching relay and communicate with the current sensor. Lastly, the 50-ohm resistor is the main power dissipating element of the load. Due to limited lab access, the team was not able to determine the new optimal value for the resistor. As a result, the team elected to use the 50-ohm value, which was used in the 2019 competition.

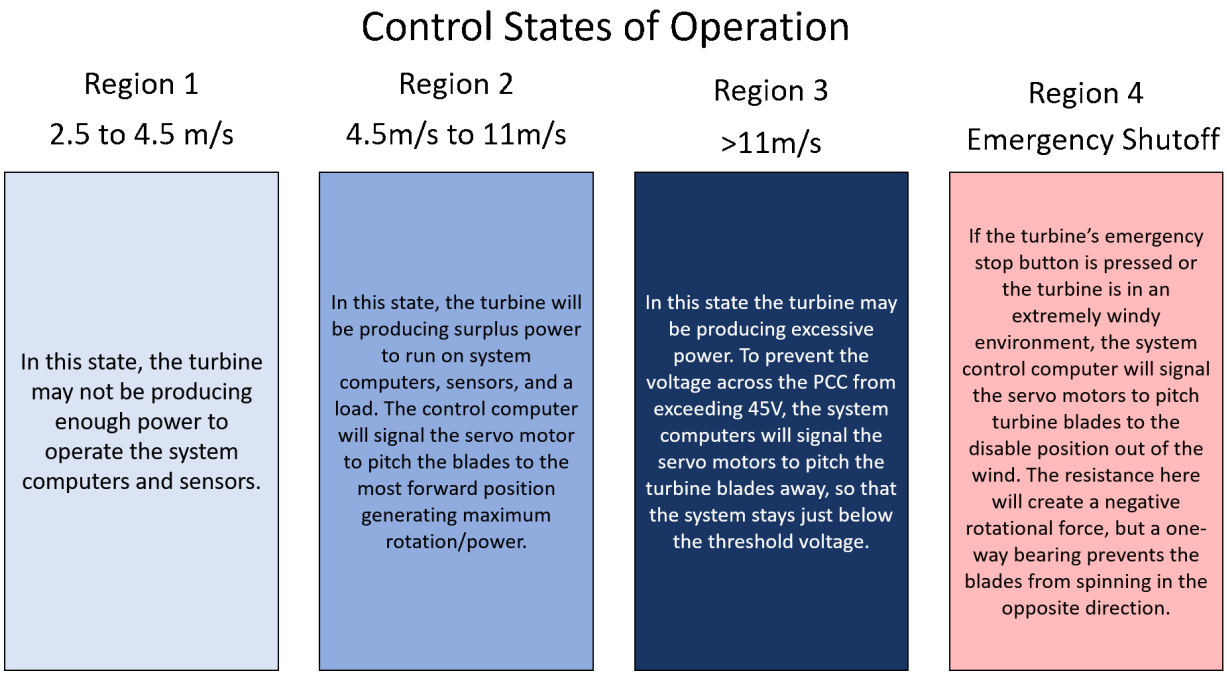


Figure 18: Description of control states for each of the turbine's three regions, plus emergency shutoff (Region 4).

3 Turbine Testing

For most of the year testing was unavailable due to the risks associated with the pandemic, fortunately, some initial testing was completed before the end of the year. The turbine underwent wind tunnel and dynamometer testing to gather data on the performance of the turbine. This data would both give insight on how the turbine as a whole can be optimized with the new two-bladed rotor, and ensure the generator is performing appropriately as compared to how it has performed in the past. The main issue faced in preparing the turbine was that one of the coil housings had a broken foot, which prevented it from sitting in the stator in a secure fashion. This issue was remedied by preparing a new housing and replacing the broken one.

3.1 Testing Objective

Since lab access was limited, the main objective for testing was to understand how the turbine performs with a two-bladed rotor and within the parameters of the competition. Wind tunnel testing was done to better understand how the new rotor performs under various conditions. Dynamometer testing was done to see how the generator performs compared to last year as well as to see how the generator performs at the extremes of the competition. One final objective it to ensure the turbine produces enough voltage at cut-in velocity to power an Arduino, which will be used to control the pitch of the blades.

3.2 Testing Procedure

Wind tunnel testing was done qualitatively, with the exception of completing the Arduino objective, so data points were not extensively collected. The two-bladed rotor was fitted with the nylon-12 blades and the output current, voltage, and power were monitored during testing on an electric load. The RPM was

kept within the predicted parameters of optimal performance and measured using a strobe light.

The cut-in velocity was determined to be 2.5 m/s, which is an improvement from the three-blade rotor design. At this velocity the turbine produced 5V, which is enough to power an Arduino. To determine how the behavior of the rotor speed, the wind velocity was increased to a maximum of 9 m/s (uncorrected) and the turbine did not exceed the predicted threshold for optimal tip speed ratio (TSR) of 1900 RPM.

Since dynamometer testing was more readily accessible, additional general and specific testing was done. General testing showed that the generator was performing comparably to previous years, therefore no immediate repairs had to be made after replacing a coil housing. The next round of testing was strength testing. In this round of testing, we tested the limits of the generator within the parameters of the competition. Our results indicated that the limits of the turbine system are mainly controlled by the maximum current allowable through the stators, which indicates that the voltage limit of the competition will be satisfied if the current is monitored.

3.3 Testing Results

Figure 19 is the culmination of the dynamometer testing. It shows the power curves produced by the dynamometer at various load resistances. The results show that the generator is still performing as well as in previous years . If more time was available for testing, wind tunnel data would be provided showing power output in comparison to the predicted power output. This data would be crucial to deter mining the turbine's operating range and finding the optimal electronic load resistance, which could be programmed into the control Arduino to optimize power production.

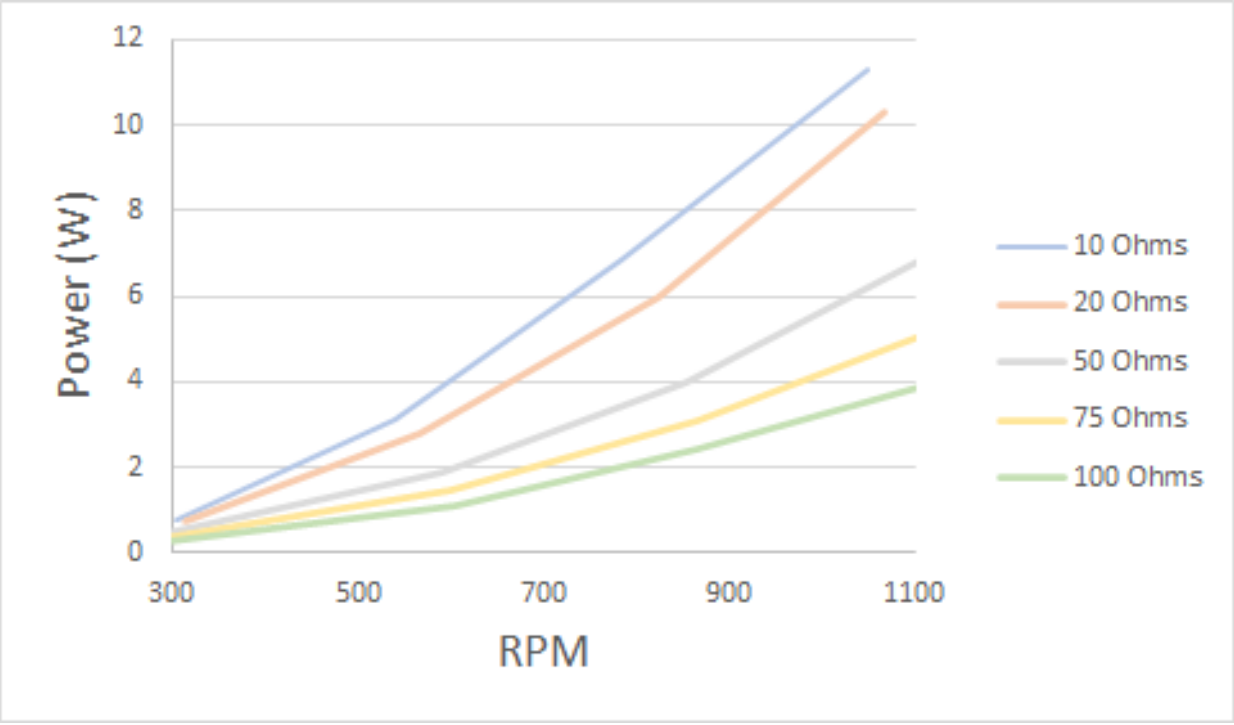


Figure 19: Generator code predicted power (red) overlaid with results from dynamometer testing.

4 Commissioning Checklist

For wind tunnel testing, the following commissioning checklist can be used to ensure that the turbine is fully operational. The critical parts to check are that the rotor is correctly secured and that the control circuit can be used to change the rotor pitch to prevent the rotor from spinning uncontrollably in the high wind speed test.

PSU Wind Energy Club
Commissioning Checklist for Wind Tunnel Testing

Activity (once the turbine is installed, double-check each of these)	Completed?	
Attach the test stand to the nacelle		
Assemble the generator in the nacelle		
Position the rotors and stators so the stators line up with the holders on the nacelle cover		
Thread the rotor shaft through the nacelle, rotors, and stators and secure with a one-way clutch bearing and two-way bearings		
Use the aluminum foil slips to space the rotors and stators appropriately before screwing in		
Attach servos to nacelle		
Connect wires to generator stages and servos and run through the test stand pipe		
Assemble the rotor, attaching the hub and pithing mechanism before the blades		
Thread the rotor onto the shaft and position the hub so that the pitching mechanism has an effective range of motion		
Assemble the servo-pitching subsystem		
Attach the collar to the pitching mechanism		
Attach the subsystem arms to the collar using the pins		
Attach the arms to each linear servo		
Attach the tailfin to the rear of the nacelle		
Secure the nacelle cover onto the top of the nacelle		
Assemble the circuits and controls box		
Put the turbine in the wind tunnel, threading the wires through the hole in the floor. Bolt the turbine down		
Connect the wires to the load and controls circuit for the generator stages and servo		
Calibrate the linear servos for control		

5 Building on Previous Years' Work

The Penn State Wind Energy Club has a strong history in the Collegiate Wind Competition, particularly with regards to the physical turbine. The team has continued to use components developed in previous years. Notably, the team's in-house generator continues to be used since it has a very low startup torque compared to off-the-shelf generators available. In the 2022 year, the team aims to reconsider the generator design and further optimize the axial flux design. Additionally, the team is using the same nacelle as in

previous years since it is already designed with the current generator in mind. The nacelle also allows for the same rotor shafts to be used as previously, which are compatible with the new hub for the two-bladed rotor. The team has also continued to use the same tailfin as in previous years since its dimensions still fit within the box, and it attaches easily to the nacelle. Within the circuits and controls subsystem, the framework of the control and load circuit is much like that of the 2019 competition year. This is because a redesign would not be feasible due to issues obtaining lab access during the pandemic. Despite this, some improvements have been made to design, specifically in the control circuit. A wind speed sensor and RPM sensor were implemented to provide data to optimize pitch angle for maximum turbine performance. In the past, optimal pitch angle values were determined through extensive experimental testing. Specifically, the turbine computers would estimate wind speed from the voltage being produced by the Turbine, but this system only works well in one specific geographic location where air density is constant. By directly obtaining the generator RPM, and wind speed, a more accurate method of optimized pitch control can be obtained. The team also modified the voltage regulation circuit within the control circuit to improve circuit stability.

6 Conclusions

The Penn State Wind Energy Club's 2021 competition turbine is an improvement upon previous years' turbine systems. Most notably, the rotor has changed from three blades to two blades, which has two primary advantages. It increases the Reynolds number experienced by the blades which results in higher airfoil glide ratios and increased power production. It also reduces the effects of stall, making the rotor more consistent in startup at low tip speed ratios where the pitch is fixed because the turbine is not producing enough power to control the Arduino. Another important design change is the replacement of the radial servo with a pair of linear servos, which allows for more precise and accurate control of the blade collective pitch for turbine control. The control circuit has also been simplified and documented for use in future years. The team has been able to improve upon the club's existing turbine despite the numerous challenges presented by the past year's remote working conditions. Testing and experimentation was extremely limited due to restrictions on lab availability, especially not gaining access to any lab space until mid March. The majority of the work was completed across video calls, slack, and shared documents.

References

[1] Align 700. http://www.align.com.tw/helicopter-en/trex700/. Accessed: 05-23-2021.

[2] Mark Drela. XFOIL: An analysis and design system for low Reynolds number airfoils. Low Reynolds number aerodynamics lecture notes, 1989.

[3] Sven Schmitz. XTURB-PSU, 2017.

[4] Sven Schmitz. *Aerodynamics of Wind Turbines: A Physical Basis for Analysis and Design*. John Wiley & Sons, 2020.

[5] Michael S Selig. *Summary of low speed airfoil data*. SOARTECH publications, 1995.

Trident Wind Collaborative
Collaborate Innovate Generate

APRIL
2022

Technical Design Report Milestone

Prepared for the 2022 Collegiate Wind Competition Organizers and the U.S. Department of Energy

COLLEGIATE
WIND COMPETITION
U.S. DEPARTMENT OF ENERGY

JAMES MADISON
UNIVERSITY

Faculty Advisors

Dr. Stephen Keith Holland
Dr. Jonathan Miles
Mr. Edwin Clamp

Joshua Bautch
Secondary Lead of Electronic Design

Alexandra Davis
Primary Lead of Controls and Electronic Design

Garrett Downs
Primary Lead of Generator and Electronic Design

Ban Mansoor
Secondary Lead of Electronic Design

Nicole Peterson
Secondary Lead of Electronic Design

Matthew Porchetta
Secondary Lead of Generator and Structure & Foundation Design

Colby Schneider
Primary Lead of Structure & Foundation Design

Brian Sweet
Primary Lead of Rotor Design

Table of Contents

Executive Summary 2

1.0 Design Objectives 3

2.0 Rotor Design 3
- **2.1 Rotor and Blade Design** 3
- **2.2 Blade Pitch** 6
- **2.3 Rotor Fabrication** 7

3.0 Generator Design 7
- **3.1 Generator and Rotor Pairing** 7
- **3.2 Generator Fabrication** 8

4.0 Structural and Foundational Design 9
- **4.1 Structural Design** 9
- **4.2 Foundation Design** 11

5.0 Electronics and Controls 13
- **5.1 Rectification** 14
- **5.2 Power Regulation and Energy Storage** 14
- **5.4 Load Configuration** 15
- **5.5 Controls** 15

6.0 New for 2022 Design 17

7.0 Full Turbine Assembly 17
- **7.1 Safety Inspection** 18
- **7.2 Cut-in Wind Speed** 18
- **7.3 Power Curve Performance** 18
- **7.4 Safety Task** 19

8.0 Prototype Testing Commissioning Checklist 19

References 21

Executive Summary

With the focus of the CWC 2022 competition being on offshore development, the Trident Wind Collaborative (TWC), from James Madison University (JMU), identified three primary objectives of enhancing prototype control using a wind speed sensing device, reducing thrust at high wind speeds through implementing a blade pitch mechanism, and designing a mounting structure to address the sand bed anchoring requirements. An existing prototype from the 2021 JMU team served as a reference design to modify for alignment with the CWC 2022 Rules and Regulations (R&R). The identified objectives served to enhance the capabilities of prior JMU prototype designs for the revised competition requirements.

The team began with the planning and information gathering phase of the design process by learning wind concepts, understanding requirements, benchmarking prior competition designs, and identifying challenges encountered by prior JMU competition teams. While several alternatives were considered, the team identified a three-blade, active pitch, horizontal axis rotor as the design most suited to meet competition objectives. The blade concept that was ultimately selected for competition was a Wortmann FX60-126 root airfoil with a SG6042 tip profile designed for a tip-speed ratio of 3.0. The blades were 3D printed with Onyx filament, a strong and flexible carbon fiber reinforced nylon material. An active pitching mechanism consisting of lever arms, ball joints, and a push plate attached to a Actuonix PQ12 linear servo, was designed to adjust the angle of attack at wind speeds greater than 11m/s to maintain constant power output and reduce rotor thrust. The pitching system will be a broad power regulator and will be fine tuned by the digitally controlled current sink.

Electrical power is produced from a team-designed direct drive, three-phase axial flux permanent magnet generator composed of two magnetic rotors, each with 12 neodymium magnets and 9-coil stator. The hand wound stator coils, each with 200 turns of 26-gage magnet wire, were designed to match required generator torque with simulated blade rotor torque and rotational speed characteristics to maximize power production. The three phase AC generated power is rectified, regulated to a constant voltage and distributed throughout the system to an actuator, sensors, microcontroller, the PCC, and load using commercially available connectors and wires. A digitally controlled current sink into a load resistor serves as the turbine system's maximum power point tracking load.

For turbine safety tasks a second Actuonix PQ12 linear servo was incorporated into the nacelle to pull a cabled disc brake. When the turbine is in a state of emergency, such as when power is lost or the emergency stop button is pressed, the brake system brings the turbine rotors to a complete stop. Similar to the 2021 JMU team, TWC has incorporated three current-voltage sensors, a wide-input 12 V output buck-boost converter, and 120 VAC - 12 VDC power supply for restart conditions. New this year is the incorporation of a Rev. C wind speed sensor to better identify state conditions and stop relying on an optical encoder and power output for state recognition.

The prototype is controlled by two Arduino Pro Minis, one in the load-side NEMA enclosure and the other in the turbine NEMA enclosure. The two microcontrollers communicate via optically isolated serial communications through HCPL 2200 ICs. The turbine controller monitors generator power, buck-boost converter power, rotor rotational speed, and emergency stop conditions. The load controller serves as the primary controller, incorporating information from the turbine to implement control algorithms that monitor the state conditions of the turbine and adjust load and pitch settings.

This report details the TWC team's design decisions, control scheme, testing results, and commissioning checklist to be implemented at the competition. Due to planning and design for manufacturing, a fully functional turbine was fabricated and demonstrated at JMU, as seen in Figure 1. Testing results indicated that the balanced design objectives were achieved.



Figure 1: Fully assembled turbine prototype.

1.0 Design Objectives

Three primary objectives for the TWC prototype were to enhance controls using wind speed measurements, to reduce thrust at high wind speeds by implementing a blade pitch actuation system, and to design a robust mounting structure to anchor the turbine in a sand bed. To address the safe operation and turbine control, the team opted to use a wind speed sensing device for better state recognition capabilities. To reduce thrust, the team decided to implement an active blade pitching system to control the turbine at high wind speeds and eliminate reliance on a disc brake, except for stopping the turbine during emergencies. With the offshore focus, the team explored and tested numerous pile configurations and sand mat designs to ensure stability during testing.

2.0 Rotor Design

The rotor blade designs were extensively modeled using QBlade and team-designed modeling tools to optimize the design for maximum power production from 5 - 11 m/s. Fabrication of all rotor components was completed in-house. Testing occurred in JMU's wind tunnel and allowed the team to calibrate power production prior to the competition.

2.1 Rotor and Blade Design

A three-bladed horizontal-axis rotor configuration was selected to maximize power production potential of the prototype, due to a high power coefficient (C_p) relative to other configurations. Three blades were chosen for stability and desired torque and rotational speed characteristics over 4 or 5 blade designs. Several candidate rotor blades were designed using QBlade [1], based on airfoils with high glide (C_l/C_d) ratios at low Reynolds number flows (approx. Re = 50,000). Candidate airfoil profiles considered included Wortmann FX60-126 and Wortmann FX63-137 root profiles, and SG6040, SG6042, SG6043, and SG6050 tip profiles. Blade twist was used to achieve the optimal angle of attack to maximize airfoil lift relative to the apparent wind vectors along the length of the blade.

To evaluate and select a rotor blade design, the team compared QBlade simulations of different blade designs and tip speed ratio (TSR) optimizations. A team generated MATLAB script was developed to predict the expected generator voltage and power outputs at different steady state rotational speeds and generator loads when driven by candidate rotor configurations. The power curve performance of each blade was calculated and compared using score weights from Table A-5 in the R&R [2], shown in Table 1. Blades with higher performance scores became the focus of selection. Rotational speeds and

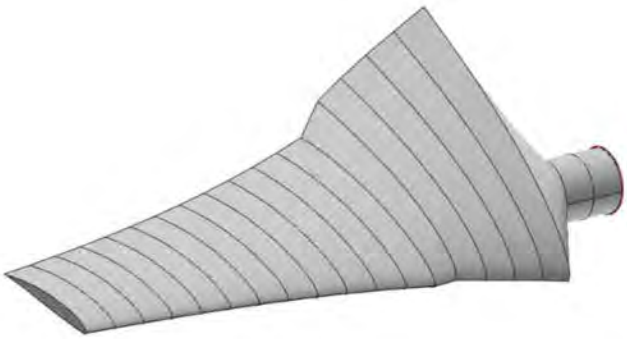
voltage outputs were also considered, to ensure safe operation of the rotor, blades, and electronics with a primary constraint of not exceeding the maximum 60 V input of the selected buck-boost converter.

The selected rotor blade design consists of a Wortmann FX60-126 root airfoil, with a 12.6% chord thickness for structural support, and a SG6042 tip profile, which provides a large lift-to-drag ratio demonstrated in Figure 2 and the associated table. The FX60-126, SG6042 design iterations had higher weighted scores than their counterparts while minimizing highlighted voltage output values. 190-turn and 180-turn generator iterations were not considered due to questionable voltage output modeling results.

Table 1: Modeling results including power output, weighted score, and voltage output predictions at wind speeds from 5 - 11 m/s.

Blade Design	Blade Parameters	Windspeed (m/s)							Total Weighted Score
200 Turn Generator		5	6	7	8	9	10	11	
FX63-137 Root, SG6042 Tip	Power Output	4.64	7.58	12.17	18.10	25.19	33.31	42.28	
	Weighted Score	3.25	6.06	9.73	12.67	10.08	9.99	4.23	56.01
	Voltage Output	49.20	53.00	53.30	55.00	55.00	55.00	55.00	
SG 6050 Root and Tip	Power Output	4.48	7.61	11.89	17.44	24.26	32.00	40.62	
	Weighted Score	3.14	6.09	9.51	12.21	9.71	9.60	4.06	54.32
	Voltage Output	33.80	41.30	50.40	54.00	55.00	55.00	55.00	
FX60-126 Root, SG6042 Tip	Power Output	4.94	8.06	12.94	17.04	23.38	31.36	41.01	
	Weighted Score	3.46	6.45	10.35	11.93	9.35	9.41	4.10	55.04
	Voltage Output	25.70	31.30	35.70	41.20	48.00	54.70	55.00	
FX60-126 Root, SG6043 Tip	Power Output	4.07	7.07	11.45	17.31	24.75	33.76	43.99	
	Weighted Score	2.85	5.65	9.16	12.11	9.90	10.13	4.40	54.20
	Voltage Output	29.20	34.30	39.60	46.90	53.30	55.00	55.00	
190 Turn Generator									
FX60-126 Root, SG6042 Tip	Power Output	4.93	8.03	12.88	18.05	24.58	31.05	40.61	
	Weighted Score	3.45	6.43	10.30	12.63	9.83	9.31	4.06	56.02
	Voltage Output	34.80	43.10	50.00	55.00	53.60	48.50	52.00	
FX60-126 Root, SG6043 Tip	Power Output	4.10	7.11	11.49	17.34	24.73	33.78	44.19	
	Weighted Score	2.87	5.69	9.19	12.14	9.89	10.13	4.42	54.33
	Voltage Output	21.70	29.80	37.50	46.10	51.30	53.20	55.00	
180 Turn Generator									
FX60-126 Root, SG6042 Tip	Power Output	4.91	8.01	12.84	19.19	25.39	31.44	40.23	
	Weighted Score	3.44	6.41	10.28	13.44	10.16	9.43	4.02	57.16
	Voltage Output	32.80	40.70	47.10	53.10	54.70	52.60	54.10	
FX60-126 Root, SG6043 Tip	Power Output	4.07	7.07	11.42	17.23	24.56	33.55	44.08	
	Weighted Score	2.85	5.65	9.13	12.06	9.82	10.07	4.41	53.99
	Voltage Output	20.40	28.10	35.30	43.40	48.20	52.70	55.00	

A similar design, using a SG6043 tip was selected by the 2021 JMU team. At high wind speeds, the observed torque and rotational speed was higher than predicted by QBlade models due to blade roughness and airflow quality. This year's design accounts for these effects to ensure that the rotor does not operate at a speed exceeding generator or power electronics design limits. The rotor was optimized for a TSR of approximately 3.0. Although a larger C_p may be achieved with a higher TSR, the 3.0 design provided the torque necessary to drive the selected loaded generator while limiting operating rotational speeds to approximately 1,750 RPM, thus reducing centripetal forces on the rotor and drive train. Figure 3 shows the simulated C_P-λ performance for the chosen blade design at 0° pitch. Figure 4 shows simulated steady state power production for the selected blade design. At 11 m/s wind speeds, this rotor design is predicted to produce approximately 51 W.



Pos (m)	Chord (m)	Twist (deg)	Foil
0	0.025	0	Circular Foil
0.01	0.025	0	Circular Foil
0.02	0.025	0	Circular Foil
0.03	0.1	36.77	Wortmann FX60-126
0.04	0.096	32.07	Wortmann FX60-126
0.05	0.092	28.19	Wortmann FX60-126
0.06	0.087	24.97	Wortmann FX60-126
0.07	0.081	22.26	Wortmann FX60-126
0.08	0.075	16.96	SG6042
0.09	0.072	15	SG6042
0.1	0.068	13.3	SG6042
0.11	0.065	11.82	SG6042
0.12	0.062	10.53	SG6042
0.13	0.059	9.38	SG6042
0.14	0.056	8.36	SG6042
0.15	0.054	7.45	SG6042
0.16	0.052	6.62	SG6042
0.17	0.049	5.88	SG6042
0.18	0.047	5.21	SG6042
0.19	0.046	4.59	SG6042
0.2	0.044	4.03	SG6042

Figure 2: CAD image of final blade design and detailed design breakdown table - Wortmann FX60-126 Root, SG6042 tip.

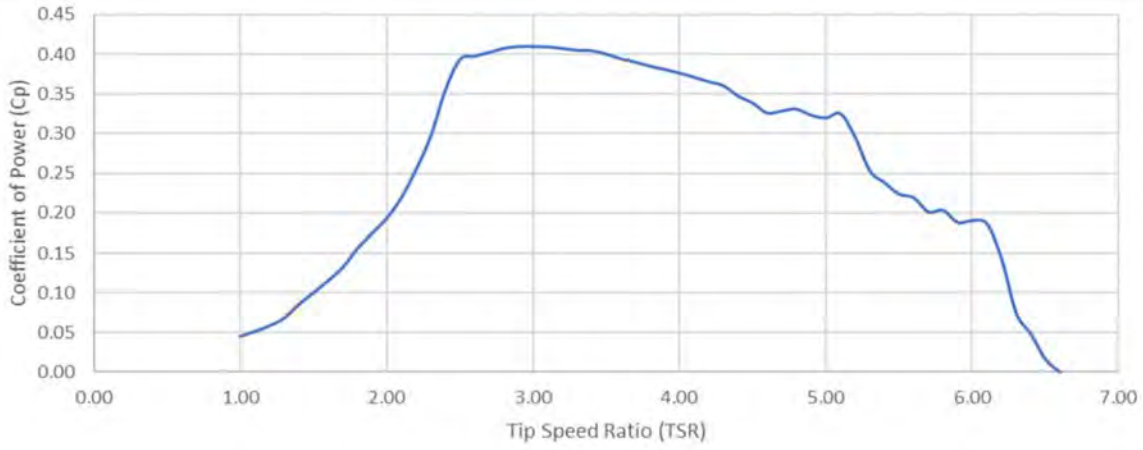


Figure 3: CP vs. TSR for chosen blades demonstrating a Cp of ~0.4 at a TSR of 3.

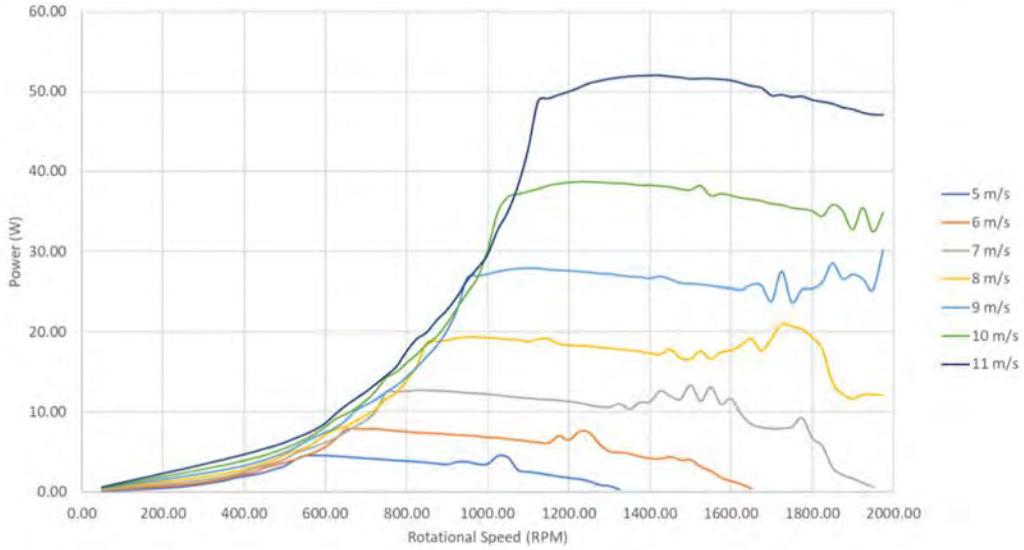


Figure 4: Steady state model of power production for selected blade design.

Blades were 3D printed from Onyx filament [3], a strong and flexible carbon fiber reinforced nylon material, which has been extensively modeled, tested, and demonstrated to withstand required loads. The maximum thrust force experienced by the turbine blades was projected by QBlade to be 10 N at 11 m/s

wind speeds. Deflection testing was performed by drilling holes in the blades, affixing them horizontally, and suspending progressively heavier weights to simulate the thrust force. The point of failure was defined as “deflection that would cause the blades to hit the nacelle” and occurred at 88 N shown in Figure 5, providing a safety factor of 8.8.



Figure 5: Point of failure at 20 lbf (88N) during blade deflection testing.

A maximum centripetal force of 162 N was estimated, assuming a maximum rotational speed of 1800 RPM and measured 28.5 g blades. The 4-40 alloy steel screws affixing the blades have a tensile strength of 170,000 psi, ensuring that the design will withstand the maximum estimated shear forces of 47 psi. To test the integrity of the shoulder bolts holding the blades in place, the rotor was spun at 2500 RPM for 5 minutes at a time. This testing and analysis confirmed that the blades and rotor can withstand the peak thrust and centripetal forces experienced during operation.

2.2 Blade Pitch

To improve turbine control, reduce thrust forces on the tower, and limit overturning forces at the mounting structure, an active pitch system was designed to regulate the rotational speed of the rotor in wind conditions above 11 m/s. A custom designed blade pitching hub, shown in Figure 6, was fabricated to induce blade pitch with a linear actuator.

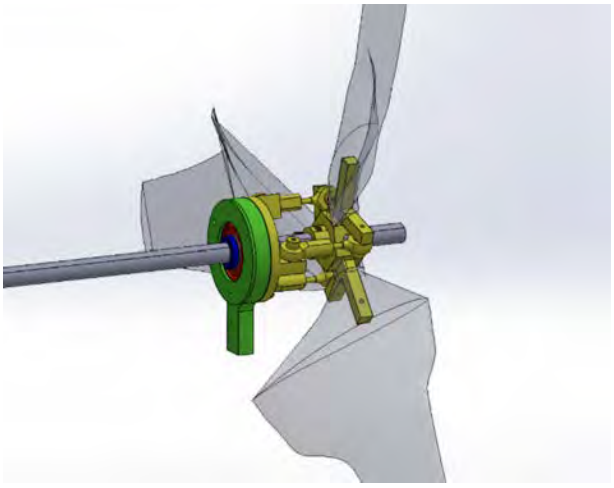


Figure 6: Color coded CAD model of the turbine pitching system. Yellow components rotate with the driveshaft; all other colored pieces do not.

Blades are mounted onto l-shaped aluminum lever arms and fixed using 4-40 thread steel screws. The lever arms are fixed to a hexagonal 6061 aluminum hub with shoulder bolts which allow the lever arms to rotate. Ball joint rods connect the lever arms to a linear-rotary ball bearing based push plate. A non-rotating push-plate is mounted around a rotary ball bearing highlighted in red in Figure 6, which in turn was press-fit onto a linear-rotary bearing colored blue. This configuration allows a non-rotating actuator to vary the blade angle of attack by changing the distance between the fixed hub and push-plate. QBlade was used to simulate the impact of blade pitching on reducing thrust forces at high wind speeds. Figure 7 shows the expected blade pitch angle required to maintain a constant power output for wind speeds greater than 11 m/s. Similarly, this figure shows the anticipated rotor thrust as a function of wind speed when the blades are pitched at these angles. Rotor thrust reaches a maximum of 10 N at 11 m/s and then continues to decrease as the blades are pitched to maintain rotational speed and power output at higher wind speeds.

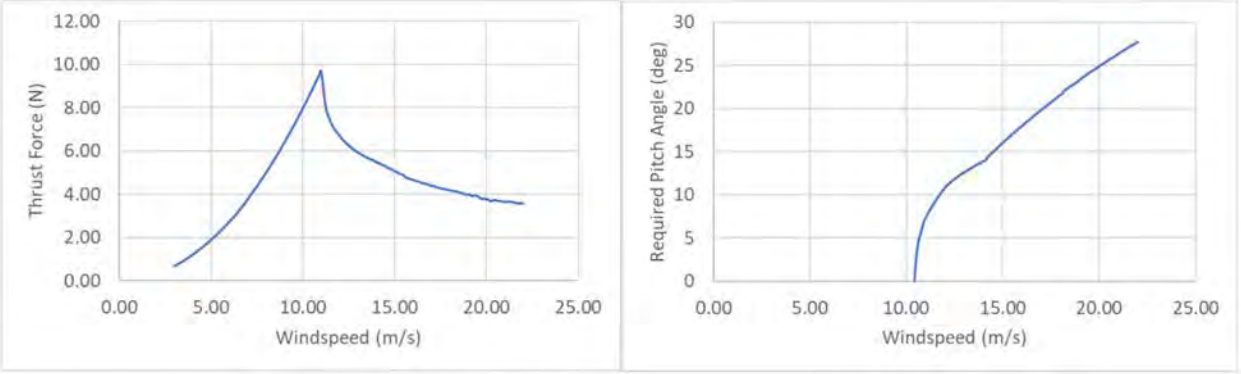


Figure 7: Estimated thrust force experienced by the turbine compared to the angle of blade pitch and pitch angle required at each wind speed

2.3 Rotor Fabrication

The pitching mechanism was fabricated in JMU's machine shop. The circular pitching components and hub were mainly constructed using a lathe and CNC machine. Holes were tapped mainly for 4-40 thread screws, with the exception of the set screw affixing the hub to the driveshaft. 6061 Aluminum was the chosen material because of its lightweight, non-magnetic, and mechanical properties.

3.0 Generator Design

During the conceptual phase of design, the team elected to design and fabricate a three-phase, axial flux permanent magnet generator (AFPMG) because it allowed for optimization of power production when matched with the selected blade design [4]. Although alternatives, including off the shelf motors were considered, an AFPM generator was chosen due to ease of fabrication and customization. The configuration allowed the team to modify the generator voltage output range and efficiency by changing the coil winding density and magnetic air gap [5]. Such flexibility in design allowed the team to match the required torque to power output characteristics of the generator to the chosen rotor blade and electronics design. The generator was the first component manufactured by the team because it represents the critical interaction point between the mechanical and electrical subsystems. All subsequent electronics tests with the system utilized this generator. The size of the generator also influenced all other component dimensions included in the nacelle.

3.1 Generator and Rotor Pairing

A mathematical model, implemented in MATLAB code, was developed to estimate the power produced by a generator and rotor blade design combination at competition wind speeds [6]. The model compared rotor torque and rotational speed characteristics at each wind speed, generated from QBlade models, to the torque required to drive a generator under different resistive loads. In this model, generator design parameters, such as coil winding density and magnetic air gap spacing, were varied to study the impact on power production. The team developed multiple potential generator designs using simulated

data from the preliminary rotor design. To identify the optimal generator configuration, an anticipated power-curve task score, computed using the scoring factors provided in the Rules and Requirements document, was estimated for each candidate generator and rotor pairing configuration. For all simulations, the rectified generator output was limited to 55 V, so as not to exceed the maximum 60 V input of the selected power conditioning electronics. Based on these simulations, the rotor design described above was best paired with a stator consisting of 9-coils, each with 200 turns of 26-gauge magnet wire, wired in a three-phase (3 coils per phase) Wye configuration. This differed from prior JMU design by reducing the number of wire turns per coil to reduce generator voltage and increasing the wire gauge to reduce resistance loss and increase generator efficiency.

3.2 Generator Fabrication

The two generator rotors consist of annular-shaped 416 stainless steel plates with twelve 1 in. x 0.25 in. x 0.25 in. N52 neodymium magnets, arranged in alternating polarities, affixed to one side. Magnetic 416 stainless steel was selected for the plate as it provides low magnetic resistance to close the magnetic circuit and strengthen the magnetic flux through the stator air gap. The team utilized JMU's Machine Shop to fabricate an aluminum hub that affixes each plate to the drive shaft with a set screw and serves as a guide for magnet positioning. The generator stator consists of nine magnetic wire coils, with three sets of three coils soldered together in series to form a phase. The phases were connected in a Wye configuration to produce three-phase alternating current. The hand-wound 26-gauge, 200 turn magnet wire coils were inserted into a laser-cut mold and filled with epoxy resin to solidify the stator's shape. The stator is positioned between the generator rotors using a 3D printed ABS plastic mount. An aluminum spacer was placed between the two magnetic rotors to obtain a fixed magnetic air gap of 1.4 cm.

A focus of this year's effort was to validate the team-designed MATLAB mathematical model by testing the generator on a testing stand that incorporates an AC motor coupled with a torque sensor, shown in Figure 8. These tests allowed the team to verify how generator design variables including magnetic air gap, coil winding density, and flux density impact the loaded generator's drive torque requirements. Figure 9 compares the MATLAB model predictions for torque as a function of rotational speed at different constant operating voltages with experimental measurements of the team fabricated generator design.

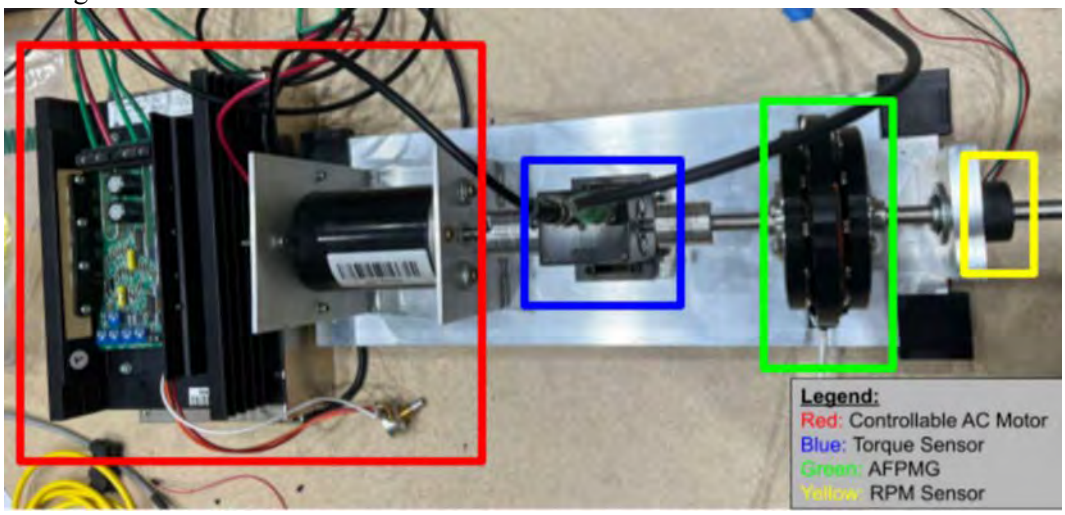


Figure 8: Controllable DC motor powered dynamometer generator test stand.

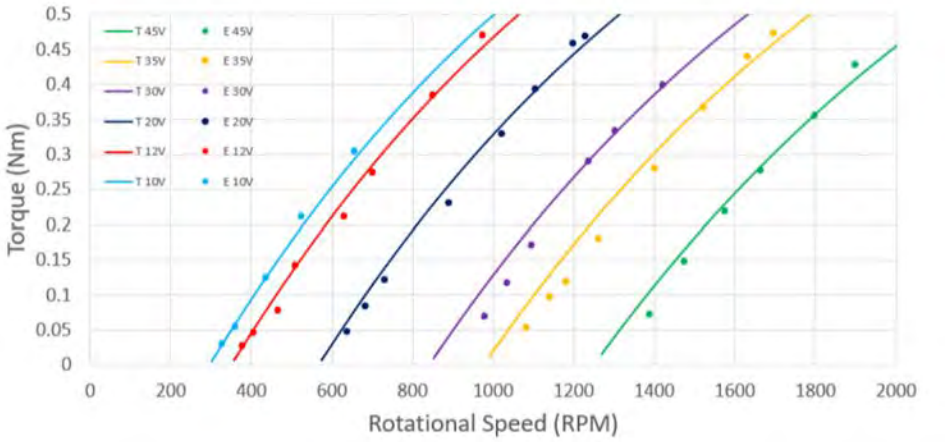


Figure 9: Theoretical (T, solid) and measured (E, points) plot of torque required to drive the AFPMG at different load resistances and voltages as a function of rotational speed.

4.0 Structural and Foundational Design

A new aspect of the competition this year is the inclusion of the fixed-bottom offshore foundation for the turbine prototype. To account for this addition, the team separated nacelle substructure design into two sections: structural design and foundational design, as illustrated in Figure 10. Structural design refers to all non-rotor and non-electronic components that are oriented in the wind tunnel. Foundational design refers to all components located outside of the wind tunnel including the competition-provided transition stub and the team designed fixed-bottom foundation.

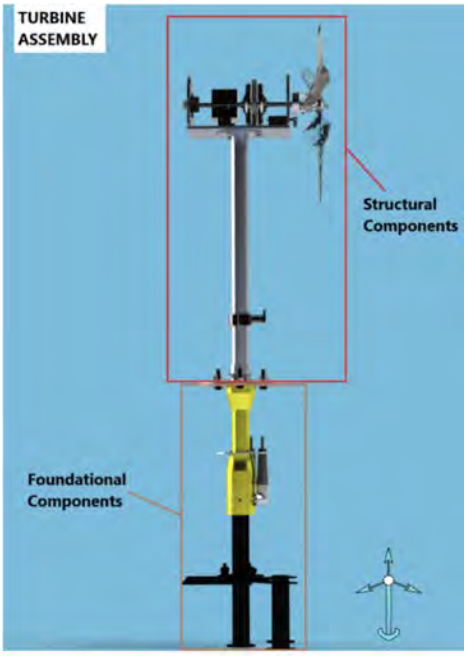


Figure 10: Structural and foundational component callouts of complete turbine assembly.

4.1 Structural Design

The structural components of the turbine include the nacelle, the manually adjustable yaw, the tower, the wind sensor mount, and the baseplate as seen in Figure 11. All structural components, excluding the wind sensor mount, were fabricated from 6061 aluminum.

The nacelle consists of a front, a rear, and a bottom plate that provides structure for mounting the driveshaft, generator, brake system, optical encoder, linear actuators, and Schottky Diode rectifier, as shown in Figure 11. Prior to fabrication and assembly, the nacelle was modeled in SolidWorks to ensure

proper spacing, wire routing, and size. Components are fastened to the nacelle plates using 4-40 thread size, 1/2 in. long button head screws. A D-profile rotary shaft was selected for the drivetrain to reduce the slipping of rotary components. Two sealed ball bearings are press-fit into the front and rear nacelle plates. The turbine's braking system is a cable driven brake caliper, actuated with an Actuonix PQ12 linear servo motor, with an aluminum brake rotor mounted to the driveshaft.

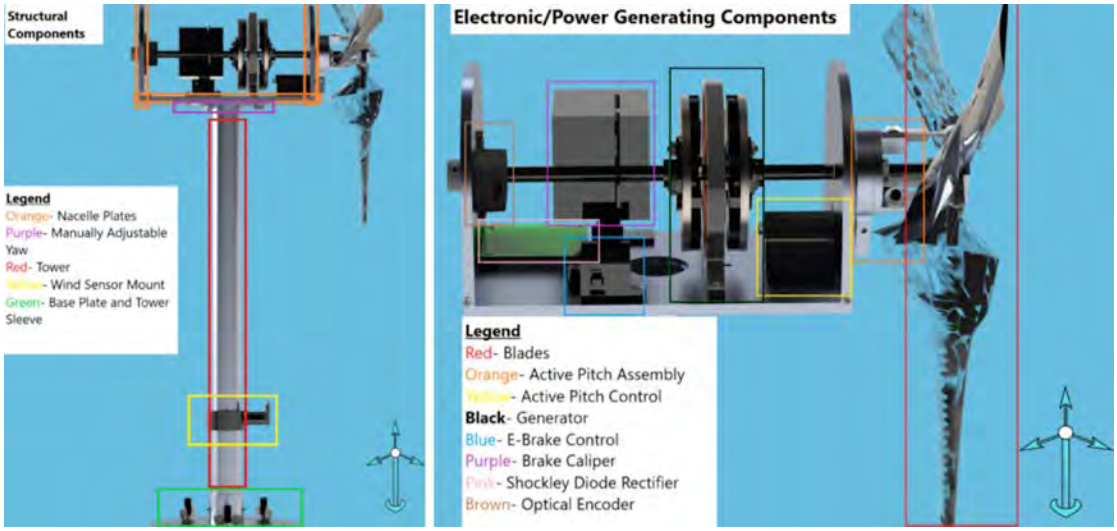


Figure 11: Structural, electronic, and power generating component diagram.

The nacelle rests and pivots upon a flange that is welded to the top of a 54 cm tall tower, which positions the rotor hub 60 cm above the bottom of the wind tunnel. Upon placement within the wind tunnel, the rotor can be oriented in the upwind direction and locked into place. A secondary plate below the flange and the bottom plate of the nacelle exert a compression force on the flange when fastened together by three screws. When the yaw locking screws were tightened to a torque of 1.1 N-m (10 in-lbf), test results, shown in Figure 12, indicated that the nacelle orientation did not change until a moment of 75 in-lbf was applied. The maximum moment expected to be applied to the nacelle is 19.5 in-lbs, yielding a safety factor above 3.5.

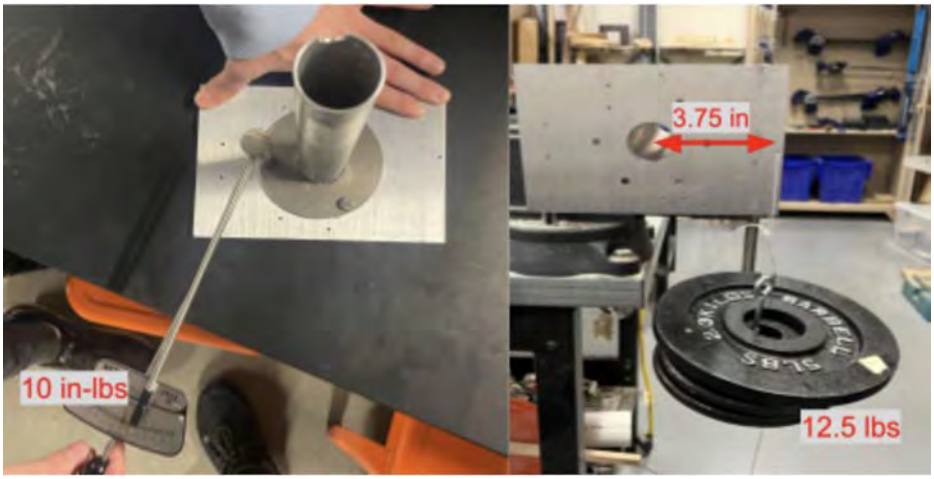


Figure 12: Nacelle lock with safety factor above 3.5.

The turbine tower slides into a metal sleeve that has been welded onto the baseplate. It is then locked into the sleeve via two set screws. There is a hole in the base of the tower and sleeve that allow for the electronic components in the nacelle to be grounded to the baseplate.

The wind sensor mount is located 9 cm from the base of the tower. QBlade wind flow simulations predicted minimal flow velocity reduction at 15 cm below the rotor blades. Similarly, the boundary layer

created from the bottom of the wind tunnel was determined to have an insignificant effect on the wind speeds above 2 cm. Thus, the wind speed sensor mounting location was selected to fall within this height range.

4.2 Foundation Design

To address the new foundation challenge for this year, the team performed a literature review to understand the types of offshore foundations, geotechnical principles, and design parameters. The team opted to focus on a pile-supported structure, eliminating suction caisson, gravity base, floating, monopile, and jacket foundation types from consideration based on competition requirements and the literary review [7]. Current data and equations used to mathematically model offshore foundation design is primarily based on empirical data gathered from tests and large-scale case studies. These modeling techniques were not applicable to a foundation of this project's scale, so the team conducted numerous tests to inform their design.

The team's fixed-bottom foundation is shown below in Figure 13. The team recognizes that on a large-scale application, offshore foundations undergo winds from multiple directions and are typically axisymmetric. However, this foundation was designed for single direction wind flow because the team can infer the wind direction prior to foundation installation, and a single flow design allows for a reduction of weight of the foundation. Based on simulations on rotor thrust, the maximum expected moment the foundation will be subjected to is approximately 10 N-m (7.14 ft-lbf). The design contains three main features: the sand mat, flanged piles, and the foundation tower. All of the main features were constructed from 4130 alloy steel because of its ferrous and machinable properties.

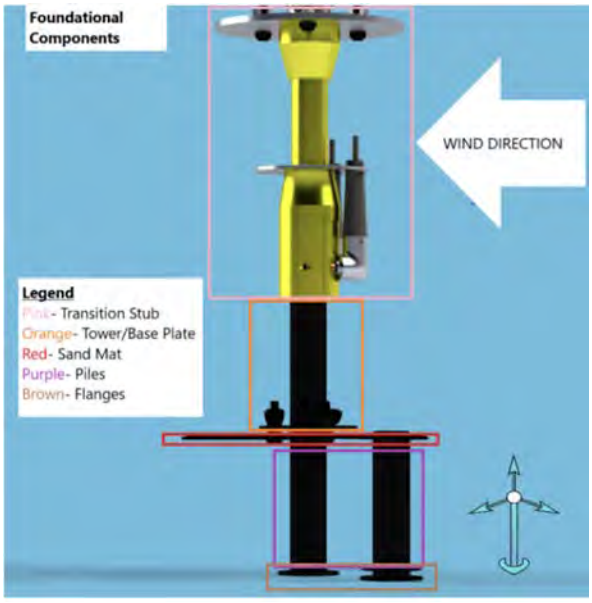


Figure 13: Foundational component diagram.

The sand mat design was fabricated from a 24 cm x 24 cm steel plate. On the upwind half of the plate, sections of plate were removed that were not needed to support the piles to reduce the weight of structure. The downwind half of the plate was left unaltered to generate a greater normal force as the plate drives into the sand.

Three piles were welded to the sand mat; one collinear with the turbine tower and two in the upwind corners of the sandmat. This configuration of piles was determined by using the pile configuration testing fixture seen in Figure 14.

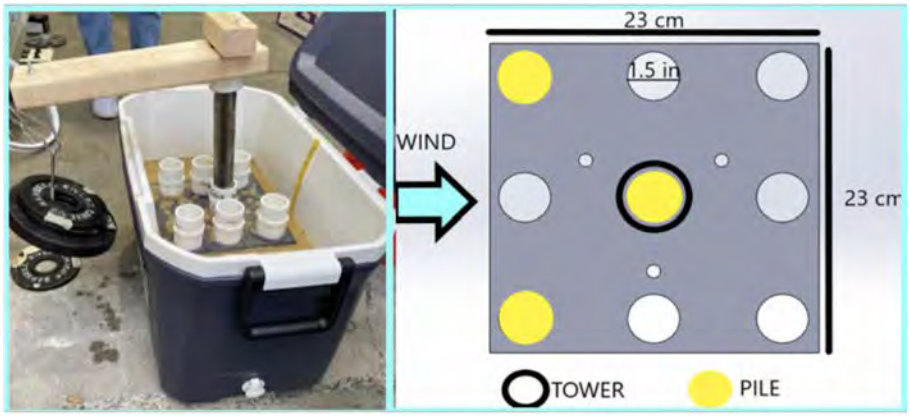


Figure 14: Pile arrangement testing fixture and chosen pile arrangement.

The piles used for testing were 5.75 in. long, 1.5 in. diameter tubing with .058 in. thick walls. The length was chosen because longer piles generate greater lateral loads and the maximum depth of insertion is 6 in. A 1.5 in. diameter pile was selected for consistency with the tower diameter. A thin wall was chosen to decrease the weight of the piles and increase the surface area for generating skin friction. A variety of pile arrangements were tested to their failure point using a torque arm. The chosen three-pile configuration contained the least number of piles that resulted in a safety factor of at least 1.5. The maximum overturning moment the foundation could withstand was 12.5 ft-lbf. Three full scale foundations were then 3D printed with this pile arrangement and tested for uplift force resistance as seen in Figure 15; one with unaltered piles, one with a meshing at the base of the piles, and one with flanges at the base of the piles.

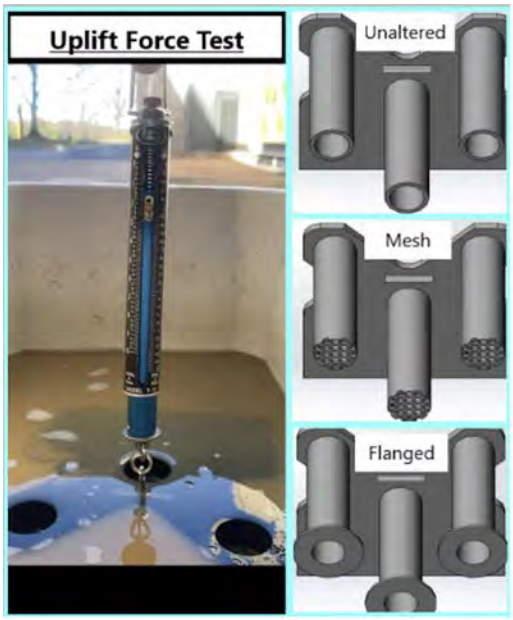


Figure 15: Uplift force test and three pile types.

The flanged pile configuration outperformed the unaltered pile configuration by a factor of 2. From the results of this test, the team decided to weld a flange to the base of each of the piles. The final foundation design was tested to withstand an overturning moment of 32.5 N-m (24 ft- lbf). The addition of the piles had a tradeoff of increasing the weight to increase the safety factor, however the piles only increased the weight of the foundation by 6.7%, but increased the safety factor by about 100%.

The pile supported sand mat is connected to the transition stub by a tower that is welded to a baseplate. The baseplate is secured to the sandmat by three nuts and bolts. There is an opening at the base of the tower so that wires can be routed from the controls to the nacelle. The entire foundation is

assembled and inserted via vibrations generated from a 20 V battery powered Dewalt sheet sander. The sander transfers the vibrations to one pile at a time via metal tubing and 3D printed connections as seen in Figure 16. This method has consistently required approximately 2 minutes for insertion and leveling. The removal of the foundation has consistently taken about thirty seconds.



Figure 16: Process for inserting foundation into sand.

Finite element analysis was conducted on the foundational components to identify weak points in the design. From the von Mises stress distribution diagram, as seen in Figure 17, the areas under the most stress include the upwind base of the foundation tower, and the three fasteners that connect the foundation base plate to the sand mat. The maximum stresses on the foundation are estimated to be 11,620,000 N/m^2. The yield strength of 4130 alloy steel is approximately 460,000,000 N/m^2 yielding a safety factor of 40.

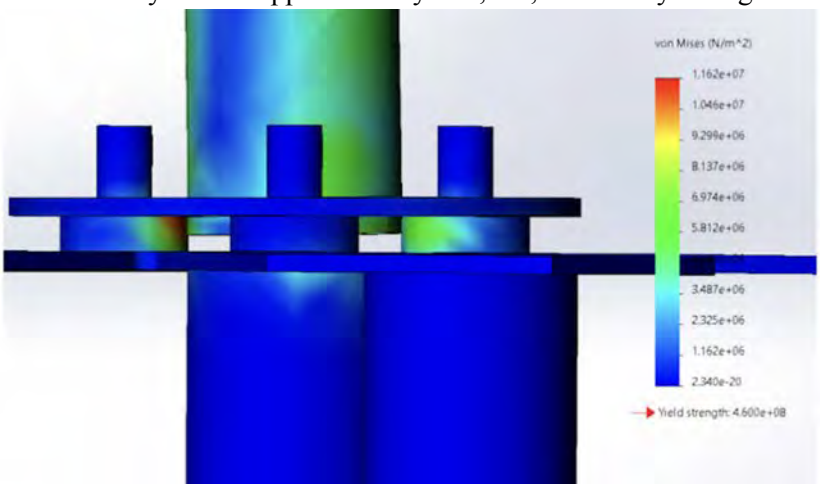


Figure 17: Finite element analysis on foundational components due to oncoming winds.

5.0 Electronics and Controls

The electrical system is designed to safely and efficiently supply maximum power produced by the turbine to the load. Figure 18 presents a simplified schematic of the electronics of the prototype turbine. Three-phase AC power is produced by the AFPMG and rectified to an unregulated DC output with a three-phase Schottky rectifier. The unregulated DC power is then measured by a current and voltage (IV) sensor before being regulated to 12 VDC by a wide range input buck-boost converter. The electronic load is a controlled current sink and power resistor. The power switch and load side motherboard are continuously powered by a 120 VAC to 12 VDC converter that is plugged into a wall outlet. The power switch allows this 12 V supply to be directed to the turbine through the PCC as required for restart control actions, such as releasing the brake, repositioning the pitch actuator after emergency stop actions, and monitoring sensor outputs when the turbine is not producing sufficient power.

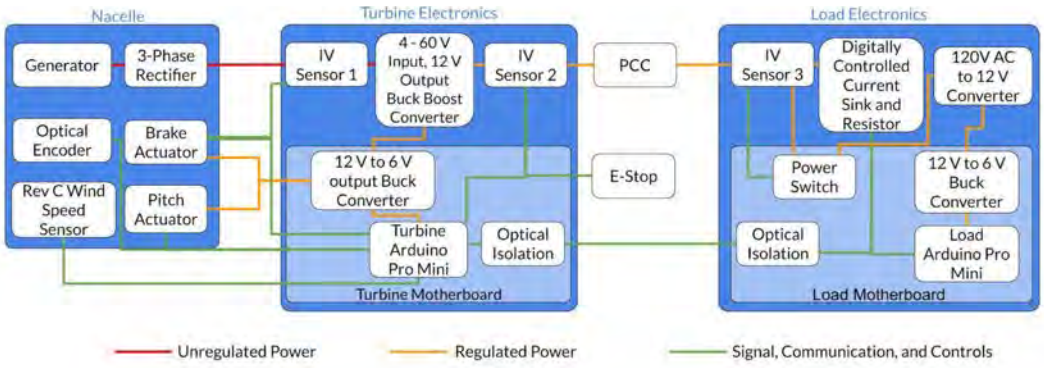


Figure 18: Single line diagram of electrical components and controls.

5.1 Rectification

The three-phase AC output of the AFPM generator required rectification to DC. A MOSFET based ideal diode rectifier specified by the 2020 team and a Schottky diode rectifier were considered for this function. Although less efficient, a Schottky diode rectifier was selected due to ease of manufacturing, reliability, and component availability. Six 60 V, 5 A Schottky diodes, having a forward voltage of 0.52 V, were arranged on a custom designed circuit board in a full wave rectification configuration. At a wind speed of 11 m/s, the generator is expected to produce a current of approximately 0.8 A, resulting in 0.83 W of dissipation by the rectifier.

5.2 Power Regulation and Energy Storage

Unregulated output from the generator is passed from the rectifier to a wide range buck boost converter and is regulated to a constant 12 V. The 12 V output is then distributed to sensors, microcontrollers, actuators, and the load. An off-the-shelf LT8390 buck converter, with an input range of 4-60 V and a constant 12 V output with 4 A output capacity, allows the system to operate over a wide range of rotational speeds without exceeding the 48 V limit at the point of common coupling (PCC). Two additional buck converters are used on each motherboard to step the 12 V input down into 6 V to power the Arduino microcontrollers and each servo motor for the braking and pitching systems. The Arduino then powers all sensors from its onboard regulator supplying 5 V to the IV, RPM, and wind speed sensors. Energy storage on the turbine side electrical system consists of 42 capacitors and 4 inductors on the buck-boost converter, generator and load IV sensors, and motherboard. The inductors range from 1.5 µH to 22 µH and capacitors range from 10 pF to 120 µF. The total energy storage capacity on the turbine side is 0.3 J, well below competition requirements of < 10 J of combined energy storage.

5.3 Sensors

Three custom current and voltage sensors, designed by the 2021 team, monitor crucial points of the system's power path. The first sensor is placed to measure current and voltage immediately after the rectifier, the next following the buck boost converter, and the third on the load side after the PCC. The boards are designed with voltage divider configurations and shunt current amplifiers to condition measurements for the Arduino's analog input.

U.S. Digital E5 optical encoder with a 100 count per revolution resolution is used to measure the rotational speed of the drive shaft. The Arduino can measure the square output waves and convert them into an estimated rotational speed. Due to the timing resolution of the Arduino Pro Mini, the team can read measurements ranging from 10 RPM to over 10,000 RPM, well over prototype operating conditions.

New for the 2022 team, a Modern Device Rev C. Wind Sensor [8] will be introduced to have a direct measurement of incoming wind speeds. The sensor operates based on a hot-wire anemometer principle, measuring the current required to maintain the temperature of a resistive element. Sensor voltage output is sent to the microcontroller, where calibration data is already in place to accurately identify the incoming

wind speed. The sensor will assist in state identification for control and positioning of the active pitching mechanism.

5.4 Load Configuration

The load system, represented schematically in Figure 19, is an analog controlled current sink with a 2.7 Ω resistor. The load system consists of an error amplifier with two inputs; a digital-to-analog signal commanded by the Arduino and the output of an instrumentation amplifier used to measure the potential difference across a 5 mΩ shunt resistor. The output of the error amplifier controls the gate voltage of an N-channel MOSFET to make the difference between the two inputs as close to zero as possible. This makes the current measured through the MOSFET and power resistor match the current command sent from the Arduino. A heat sink is used on the MOSFET to remove the increase in temperature as it is simulating a resistor. The power resistor used as the load is rated for 100 W with high current handling and no current derating. This configuration is the same as the 2021 team as it was proven to ensure power quality and stability to the load.

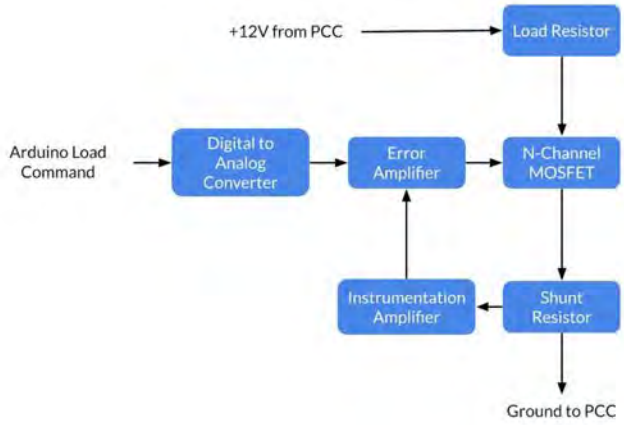


Figure 19: Load schematic for the analog controlled system.

5.5 Controls

Initially the controls subteam was planning to use Python to run calibration and control programs, but with a long history of Arduino knowledge and familiarity, the team decided to use two Arduino Pro Mini microcontrollers. The Pro Minis have 6 analog input pins that allow the team to incorporate the wind speed sensor into the design and enhance state identification capabilities. The Pro Minis are considerably smaller, consume less power, and maintain the required functionality as the previously used Pro and Uno boards in the 2021 turbine prototype. The load side controller is always powered and is the primary system controller. The turbine side controller monitors sensor outputs, sends control signals to the brake and pitch actuators, and tracks emergency conditions. The two controllers exchange information and commands via a 57,600 baud serial connection that is optically isolated with two HCPL 2200 ICs.

The main operating states are briefly described below and schematically shown in Figure 20.

- Start/Restart State (States A, B, or X): Identified by lack of power to the turbine, no communications from the turbine, or serial communications disconnected. If emergency stop conditions are not present, power is provided from load to release the brake and reposition pitch to startup state.
- Cut-in (State C): Wind speeds below 5 m/s, low rotor rotation speed. No load, power with +12 V from turbine. Slight pitch to feather to increase torque experienced at the generator.
- Power Curve (States D, E, and F): Wind speeds between 4.5 m/s - 11 m/s. Pitch to zero, control load to maximize power, and maintain rotational speed.
- Control of Rated Power (State G): Wind speeds 11-22 m/s. Adjust pitch based on measured wind speed to reduce rotational speed and rotor thrust. Adjust load to maintain rated operating speed and maximum power.

- Cut out (State H): Above 22 m/s. Pitch turbine rotor, activate parking brake.
- Emergency Stop (State K): When emergency stop button disconnect is detected, activate the disc brake. Initiate restart once the emergency stop condition is removed.
- Power Disconnect (State L): Monitor turbine output voltage and load input voltage. If there is a significant difference between the two, active brake. Initiate restart state.

For every cycle, the main controller validates if communications from the turbine have been received. If there is no communication the load understands that the turbine is either in the parked position, communications have been disconnected, or the wind speed is insufficient to power the turbine electronics. When these conditions are observed, the primary controller provides power to the turbine, commands the controller to release the brake, and return the active pitching actuator to the starting position.

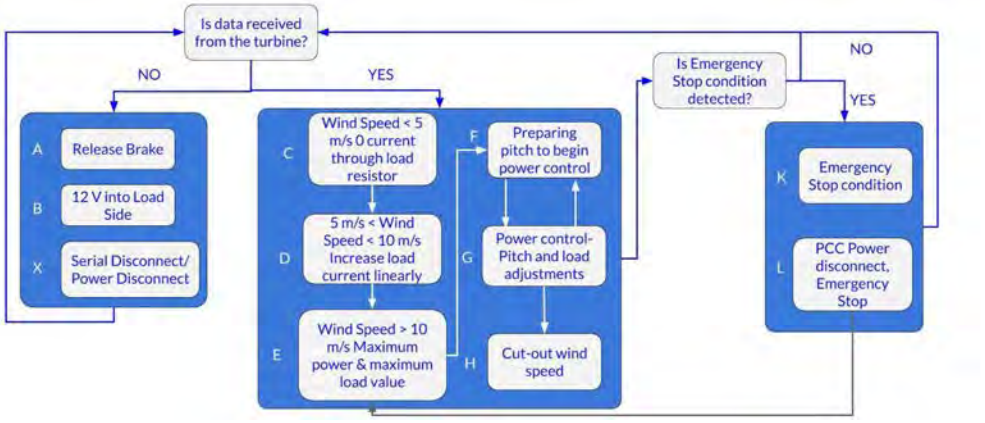


Figure 20: Turbine control states diagram.

When communication is received, the controller determines the operating state based on the wind speed and adjusts the load current, brake, and pitch settings accordingly. During pre cut-in wind speeds, the load acts as an open circuit to allow all generated power to be consumed by the turbine electronics. Once cut-in is reached, the controller gradually increases the current setting in a linear progression as wind speeds increase. Above 6 m/s, the controller enters a maximum power tracking state. Adjustment of the load is achieved by monitoring the wind speed and rotational speed measured. The load current command is adjusted proportionally to the difference between the observed and optimal rotational speed. If the measured speed is higher than anticipated, the load will allow more current to pass and slow the rotor. Similarly, with a slower expected rotational speed, the load will reduce the amount of current that is passed to the load and speed up the rotor to make up the difference.

When wind speeds above 11 m/s are measured by the wind speed sensor. The active pitching system engages and begins to pitch the rotor. The pitch position is determined based on the measured wind speed. Once the pitch is set, the load algorithm acts as a fine tuner to match the expected rotational speed at each wind speed above 11 m/s. The final state the turbine checks is the emergency stopping condition. The manual E-stop is identified by a change in the button state monitored by the primary load side controller. The PCC power disconnect is identified by the voltage difference on both sides of the PCC. If either emergency condition is observed, the brake is engaged fully to stop the rotor by a disc brake.

6.0 New for 2022 Design

JMU has been a regular participant in CWC since 2018. The TWC team's prototype is the product of each subsequent team's experiences and knowledge. As a result of this, the 2022 TWC team's design differs from the 2021 design in most aspects. The rotor is a combination of two airfoils, the Wortmann FX60-126 & SG6042, the previous team also incorporated the Wortmann FX60-126 but with a different tip profile. Never achieved by previous teams, this year's design will pitch the blades at high wind speeds with an active pitching mechanic. The AFPM generator design was opted to be used again like previous

teams but the parameters changed to 9-coil 26-gauge wire with 200 turns to optimally match our rotor selection instead of 28-gauge wire with 225 turns used by the 2021 team.

With a focus on offshore development, the team identified the critical functions and requirements for the structural and foundational components. The 2021 team incorporated a passive yaw system that was replaced by a fixed yaw with a manual locking system. The electronics incorporated in this year's design are identical with the exception of the wind speed sensor for better state identification abilities. As a result of the wind speed sensor and active pitching mechanic, the control algorithm for the prototype is vastly different from previous years. A power tracking algorithm was developed for the 2021 team that determined the state of the turbine. At high wind speeds, the brake was engaged to slow the driveshaft. The 2022 team can identify state conditions through the wind speed sensor and encoder data. At high wind speeds, the active pitch will engage to stall the rotor and control the rated power produced.

7.0 Full Turbine Assembly

Full turbine assembly was achieved by constant communication between the subteams and step wise integration techniques to consistently test the functionality of subsystems. The mechanical drawing and exploded view of each turbine component can be seen in Figure 21. The team was able to successfully complete most competition contests in the JMU home-built wind tunnel with the exception of tests requiring wind speeds above 9.5 m/s and the Control of Rated Power Task. The team documented all calibration and testing data to estimate performance and score according to the R&R scoring rubric.

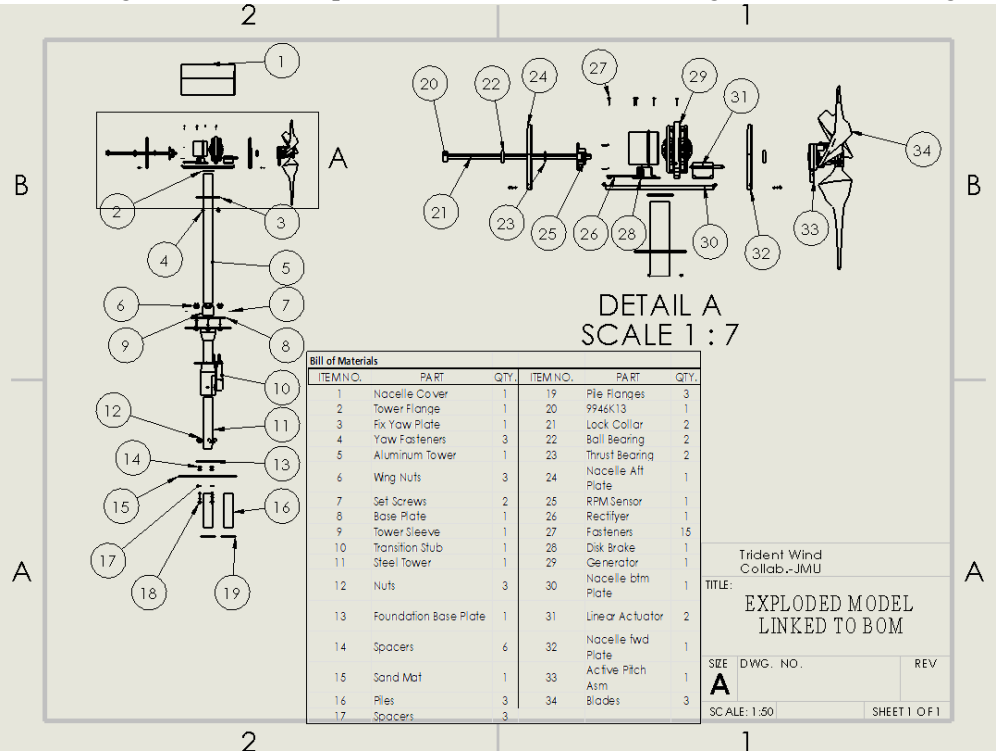


Figure 21: Full turbine exploded view.

7.1 Safety Inspection

The team initiated several safety checks at various stages of integration. Dr. Keith Holland, the team's capstone advisor, conducted initial safety inspections prior to testing in the in-house wind tunnel. The team also enlisted the help of Computer Engineer and Associate Professor Dr. Jason Forsyth and Engineering Lab manager, John Wild, to conduct the Safety and Tech Inspection Sheet provided in Appendix B of the R&R.

7.2 Cut-in Wind Speed

Sporadic power was observed at 4.5 m/s while reliable power was recorded at 4.7 m/s. Therefore, the cut-in speed of the turbine is 4.7 m/s. Considering drivetrain friction, electrical load, and a cut-in speed of 4.7 m/s, QBlade estimates that a torque of 0.08 N*m is required to begin producing power. With the active pitching system, the team can slightly feather the blades to cut-in at lower wind speeds and return to a zero pitch angle after power is observed.

7.3 Power Curve Performance

The turbine was tested in the in-house wind tunnel at a range of wind speeds up to 9 m/s to determine the maximum power curve. At each wind speed from 4.7 - 9 m/s the voltage, current, power output, wind speed, and rotational speed were recorded. Figure 22 presents the measured and projected generator power in blue and the measured and projected power delivered to the load in orange. Note that the measured generator power is similar to that anticipated through modeling while the power delivered to the load is reduced due to electrical and mechanical losses.

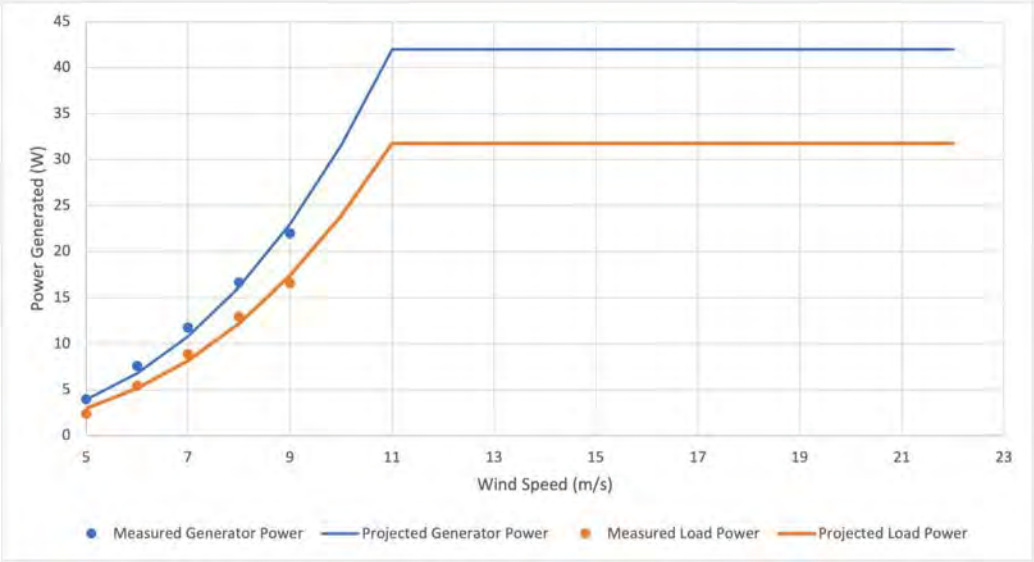


Figure 22: Measured and anticipated power production at competition wind speeds.

The measured results indicate an end-to-end wind power to load power efficiency of 24.5%. Assuming a rotor C_p of 0.38, the generator mechanical-to-electrical power conversion efficiency was estimated to be 85%, consistent with model predictions. This suggests an electrical conversion and transfer efficiency of 76%. These measurements and estimates are reasonable due to the power consumption from the turbine electronics, sensors, actuators, and the anticipated 85% buck-boost converter efficiency [9]. Through calibration testing, the team also identified that the simulated TSR values were close to the observed values, shown in Table 2.

Table 2: Comparison of expected and measured RPM and TSR.

Wind Speed	**5 m/s**	**6 m/s**	**7 m/s**	**8 m/s**	**9 m/s**
Simulated	765.80 RPM TSR = 3.0	1024.81 RPM TSR = 3.0	1199.36 RPM TSR = 3.0	1415.10 RPM TSR = 3.0	1674.38 RPM TSR = 3.0
Measured	824.21 RPM TSR = 3.22	1017.62 RPM TSR = 2.97	1188.43 RPM TSR = 2.97	1408.21 RPM TSR = 2.98	1652.32 RPM TSR = 2.96

7.4 Safety Task

The turbine was run through one of the two safety tests by demonstrating a safe stop during the E-stop shutdown. The turbine was able to successfully come to a complete stop when the E-stop switch was initiated. Following each shutdown condition, the turbine was able to successfully restart and return to a power producing state. Prior to competition, the team will test the second shutdown condition by disconnecting the load and turbine electronics.

8.0 Prototype Testing Commissioning Checklist

A checklist to verify each step of assembling the turbine during the competition is provided in Table 3. This checklist includes a team member responsible for performing each verification step and a person responsible for verifying that each step is performed correctly.

Table 3: Commissioning checklist for turbine assembly.

Verification Step	**Initiating Team Member Initials**	**Verification Team Member Initials**
Gather foundation and insertion materials: Pile-supported sand mat, tower and baseplate, spacers, sander with fully charged 20 V battery, and vibration transfer tubes	**CS**	**MP**
Place electrical cable through the foundation tunnel and base plate.	**CS**	**MP**
Fasten the base plate to the sand mat.	**CS**	**MP**
Place vibration transfer tubes onto upwind piles.	**CS**	**MP**
Place the assembled foundation into the tank with piles facing in the upwind direction.	**CS**	**MP**
Apply vibration from sander to one pile at a time until the sand mat is flush with sand bed.	**CS**	**MP**
Check the top of the tower for levelness and make adjustments with sander to make the foundation level.	**CS**	**MP**
Attach a transition stub so that one bolt of the flange assembly is pointing in the downwind direction.	**CS**	**MP**
Slide foundation tank under the center of the wind tunnel.	**CS**	**MP**
Connect wires from the nacelle to the foundation connection point	**CS**	**MP**
Fasten the turbine base plate so that the wind sensor is perpendicular to the incoming wind flow.	**CS**	**MP**
Ensure the nacelle is oriented in the upwind direction, then tighten the fasteners on the manually adjustable lock plate to 10 in-lbs	**CS**	**MP**
Connect and verify Anderson Power Pole Connection from tower to turbine electronics.	**AD**	**GD**

Connect and verify Anderson Power Pole Connection power connection to PCC from the turbine.	**AD**	**GD**
Connect and verify Anderson Power Pole Connection power from PCC to load	**AD**	**GD**
Connect and verify Serial communications cable	**AD**	**GD**
Plug load AC/DC adapter to outlet	**AD**	**GD**
Confirm receipt of Serial communications and startup state of turbine	**AD**	**NP**
Engage E-stop to verify servo operations	**AD**	**NP**
Remove E-stop	**AD**	**NP**
Verify cut-in at 4.7 m/s wind speed	**AD**	**NP**
Verify receipt of wind speed measurements.	**AD**	**NP**
Verify the voltage and current readings through all IV sensors	**AD**	**NP**
Confirm receipt of rotational velocity measurements	**AD**	**NP**
Alert judges to commence testing sequence.	**AD**	**BS**

References

[1] Hermann Föttinger Institute of TU Berlin. (2014). QBlade: an Open Source Software Version (v0.8).

[2] "Rules and Regulations." US Department of Energy. September 2021. https://www.energy.gov/eere/collegiatewindcompetition/articles/collegiate-wind-competition-rules-and-requirements

[3] "800cc Onyx Filament Spool." *Markforged*, 11 Dec. 2021, https://markforged.com/product/onyx-filament/.

[4] Price, G., Batzel, T., Comanescu, M., & Muller, B. (2014). Design and testing of a permanent magnet axial flux wind power generator (Paper 190, ENT 202). International Association of Journals & Conferences.

[5] Kao, J. –Hsiang, Lin, Y.-J., & Huang, Y.-W. (2020a). Apply blade element momentum theory in matching a wind turbine system. International Journal of Smart Grid and Clean Energy, 44–51. https://doi.org/10.12720/sgce.9.1.44-51

[6] Kao, J.-H. (2016). Developing the process in matching a wind turbine system to attain optimal performance. Advances in Mechanical Engineering, 8(11), 168781401667469. https://doi.org/10.1177/1687814016674697

[7] Lavanya, C., & Kumar, N. D. (2020, August 19). *Foundation types for land and offshore Sustainable Wind Energy Turbine Towers*. E3S Web of Conferences. Retrieved March 11, 2022, from https://www.e3s-conferences.org/articles/e3sconf/abs/2020/44/e3sconf_icmed2020_01094/e3sconf_icmed2020_01094.html

[8] "Wind Sensor Rev. C." Modern Device. April 18, 2022. https://moderndevice.com/product/wind-sensor/

[9] "Demo Manual DCA - Analog Devices." April 24, 2022, https://www.analog.com/media/en/technical-documentation/user-guides/DC2457AF.PDF

Final Turbine Design Report

Collegiate Wind Competition 2022

Wildcat Wind Power at Kansas State University

Officers

Eric Christman – President, Student Lead
Hayden Dillavou - Vice President, Student Lead
Brianna Wagoner - Secretary
Caleb Stuber -Treasurer
Jakob Long – Project Development Lead
Lane Lundeen – Connection Creation Lead
Matthew Monsion – Electrical Design Lead
Michael Brosseit – Electrical Design Lead
Kavian Kalantari – Mechanical Design Lead
Josh Meurer – Mechanical Design Lead

Advisor

Dr. Hongyu Wu, Associate Professor, Electrical and Computer Engineering

Mechanical Design Team

Kavian Kalantari
Josh Meurer
Chase Eccles
Jacob Lowe
Rafael Lopez Barraza
Stephen Kielhofner
Wesley Smith

Electrical Design Team

Matthew Monsion
Michael Brosseit
Brianna Wagoner
Andrew DuLac
Andy Freshnock
David Pierson
Kent Detarding
Macie Sexten
Patrick Flett
Tyler Schooley

Contact

echris018@ksu.edu or hongyuwu@ksu.edu

Mike Wiegers Department of Electrical and Computer Engineering
3108 Engineering Hall
1701D Platt St.
Manhattan, KS 66506
785-532-560

Wildcat Wind Power dedicates our work this year to our longtime advisor, Dr. Warren White, who passed away in May of 2021. Dr. White cared deeply about our mission, and his presence is sorely missed.

Table of Contents

Executive Summary 3
Design Objective 3
Mechanical Design 4
Blades 4
Nacelle 5
Mechanical Loading 6
Foundation System 7
Active Pitch System 8
Electrical Design 10
Generator Selection 10
Turbine Controls 10
Load Controls 11
Power Systems 12
Software 13
Assembly of Systems 15
Mechanical Assembly 15
Electrical Assembly 16
Commissioning Checklist 17
Operation 18
Operational Modes and States 18
Testing of Systems 19
Review from 2021 Competition 21
References ..... Ref. 1

Executive Summary

This report details the design, construction, and testing of a small-scale wind turbine for the 2022 Collegiate Wind Competition, by the Wildcat Wind Power team at Kansas State University. Our primary design motivation was to design a wind turbine that could withstand the more rigorous testing conditions specified in the competition this year, and we developed a variety of control features to ensure that the turbine would meet the necessary operational requirements.

We used in-house analytical tools to design blades that would maximize the turbine's performance along its power curve, and continued to utilize 3D-printing for blade and nacelle construction. One of our most critical design efforts was that of an active pitching system, which used a pair of linear actuators in the turbine nacelle to pitch each of the three blades through a bearing which encircled the driveshaft. The active pitch system, which was also constructed out of largely 3D-printed components, provides more than 100° of rotation to each blade, and is used to regulate RPM and power production at high wind speeds. The turbine foundation, a new addition to the competition this year, was designed as an open-topped box constructed out of steel sheets and a steel plate, to be filled with sand during installation before connecting the competition stub piece.

The turbine electrical systems include sensors and controls on both the turbine and load sides of the PCC, with each unit containing its own microcontroller and mounted on a PCB. The turbine-side system contains a three-phase bridge rectifier, switching converters to power the various controls and a microcontroller, and the ability to receive power from the load during braking procedures. The load-side system contains a similar arrangement of sensors, converters, and microcontroller, as well as a variable resistance load system designed around MOSFETs. The two systems communicate through isolated UART communication lines, and share data regarding the position of the active system, electrical variables like power and voltage, and control variables like the load resistance and braking conditions.

Software for the system runs on Teensy microcontrollers for both the load and turbine systems, and tracks the turbine's operation to force it to operate through its simple control scheme. The load system was designed to communicate with our wind tunnel for testing purposes, which allowed for iterative, automated testing to collect data for power curve and regulation parameters.

Design Objective

The overarching objective for this design was to create a scaled wind turbine to operate in a wind tunnel that mimics the operational parameters of fixed-bottom offshore turbines. Key design parameters include a shallow-water foundation and turbine operation at any wind speed up to 22 m/s. These parameters create new requirements for turbine durability and reliability, introduce new manufacturing techniques for the foundation, and provide for increased control flexibility as turbine power and RPM regulation is not measured outside of the safety task. We see the increased 22 m/s wind speed as the primary motivator for design decisions. In building a regulation system, we prioritized the utilization of the system to optimize the turbine's power production throughout its power curve and minimize its cut-in wind speed, while ensuring it could limit turbine rotational speeds when needed. In building a foundation, we wanted to remain cautious of the destructive ability of the wind, and set out to build a foundation that could keep the turbine stable at 22 m/s, even if it weighed

more than a leaner design. Non-operational aspects of our design objective include designing a turbine and foundation that was easy to maintain and install, designing an electrical system that could operate full-system testing through a single control interface, and building a complete system that followed all design requirements set in the competition Rules and Regulations.

Mechanical Design

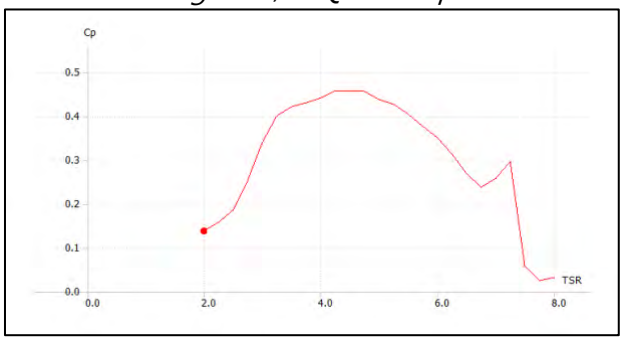
Blades

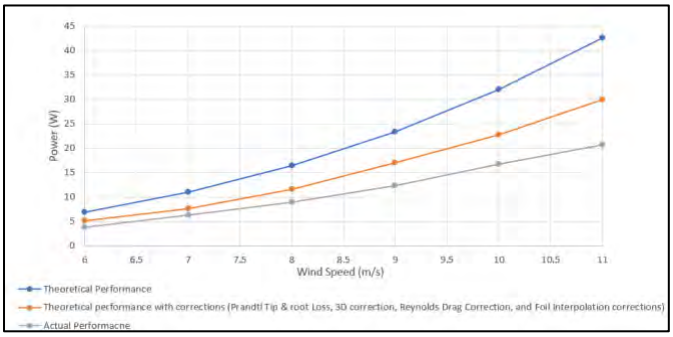
For this year's competition, we wanted to redesign our previous year's blade with more optimized airfoils and blade angles. Based on our research into blade element momentum (BEM) theory [1], we designed our new blade around a constant tip speed ratio (TSR), as the angle of airflow over a blade element at any wind speed is constant if the TSR is constant. To find the best airfoil at every blade element, we decided we would simulate every airfoil at every blade element position and write a program to select the best performing airfoil for each position.

Originally, we planned to use QBlade to run airfoil simulations, but a second piece of software was needed to calculate the Reynolds numbers and Mach airflow speeds for each simulation. MATLAB was chosen because of our familiarity with the software, and the simplicity of coding arrays in MATLAB compared to other coding languages. We designed our MATLAB program to calculate the Reynolds numbers and Mach speed for each blade element based on the number of blade elements, minimum and maximum blade radius, chord lengths, wind speed, and TSR. The program calculates data for QBlade extremely quickly, which along with QBlade's multi-threaded batch analysis, expedited the otherwise very lengthy process of running simulations for each airfoil. By exporting simulation data from QBlade as comma separated value (CSV) files, we could input the simulation data directly into MATLAB for analysis. We faced some problems with the simulation data importing correctly, but those problems were solved by writing a simple python script to edit the format of the CSV files into a format MATLAB could more easily read. Our MATLAB program compares each airfoil based on the maximum coefficient of force it produces in the direction of rotation, and outputs the best airfoil and angle for each blade element along the blade. Additionally, the program also keeps track of the optimum angle and calculates the ideal blade twist for each blade element along the blade.

Our analysis focused on NACA airfoils. These airfoils are generated from only 3 variables: the maximum camber, position of maximum chamber, and the maximum thickness ratio [2]. With only three variables, NACA airfoils allowed us to test a wide variety of different airfoils very quickly. The optimum blade according to our analysis is made of the airfoils: NACA 6809, 6806, 6206, and 6306, and has an average maximum coefficient of lift to drag ratio of 35.9. The program also calculated the optimum twist angle for each airfoil, considering the optimum angle of attack as well as relative wind angles. We chose to compare the performance of every airfoil at a wind speed of 8 m/s, as it was halfway between the maximum and minimum wind speeds used in the power curve test. Also shown is the actual power production, in comparison to the theoretical maximum production, and theoretical production when considering a number of different loss types. We recorded an increase in our power output from last year of 17.5 W to 20.5 W at a wind speed of 11m/s.

Figure 1, 2: QBlade Cp-λ Curve at 8 m/s, Theoretical vs Actual Performance





We chose to 3D-print the blades as it was the easiest and fastest way to produce the geometry accurately. Below is the 3D model in SolidWorks and the same blade 3D-printed.

Figure 3, 4: Blade SolidWorks Rendering, Photo





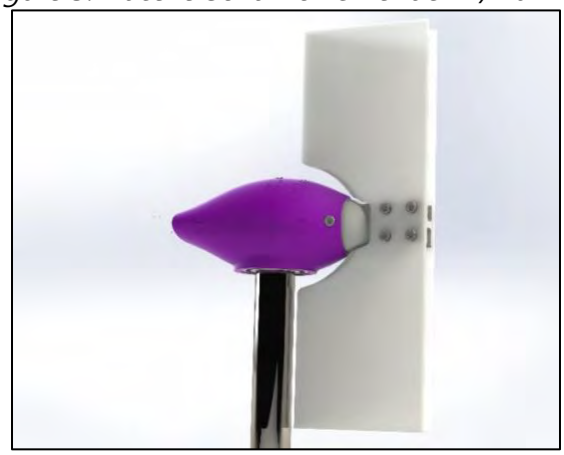
Calculation of the turbine annual power production was performed with data taken from the Galveston offshore area analyzed in the Project Development portion of the competition. The turbine power curve, from testing, was compared to a 5-minute time series of wind speeds in the location, and a final number of 91.74 kWh of yearly production was calculated. We did compare this metric to an onshore location in North Texas for the same year and hub height, for the sake of analysis, and found similar yearly production at 91.87 kWh.

Nacelle and Yaw Mechanism

The nacelle design was largely determined by the components that the nacelle must enclose or connect to, largely the active pitch hub mechanism, generator, and linear actuators. Our original nacelle design was cylindrical, with a rounded face facing the wind and a large acrylic tailfin on the opposite side. It had to be wider than we would have liked, due to the linear actuators for the active pitch system mounted on either side of the generator. The fin, coupled with a bearing between the nacelle and turbine tower, allow for simple passive yawing to ease in installation and testing. Comparison of the turbine testing results to simulated blade data showed that the turbine was not as efficient as it could be, and we believed this may have been due to large frontal area of nacelle. We attempted to reduce

the area by narrowing the top and bottom of that face, and smoothing the curve up to the top of the nacelle. This improved design, along with the acrylic tailfin and a connector piece, is shown below. The turbine tower was recycled from previous years, and is an aluminum tube welded to a flat aluminum base, with holes drilled for connection to the competition stub, and the yaw bearing set at the top.

Figure 5: Nacelle SolidWorks Render w/ Tail Fin

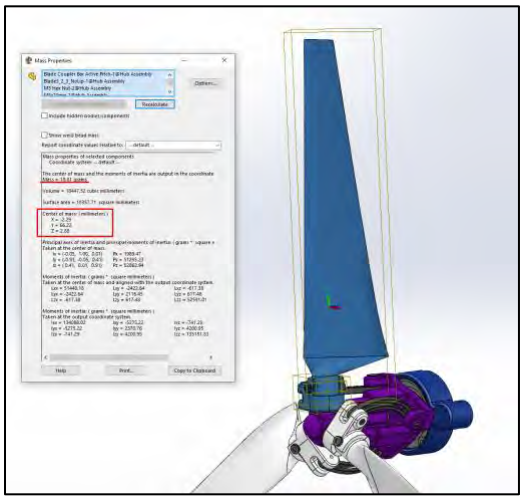


Mechanical Loading

Due to the nature of conducting stress analysis of 3D-printed parts, much of the review of our turbine relies on testing new designs in our wind tunnel, then making appropriate modifications and retesting. For example, one of the major issues with creating a finite element method (FEM) model of a 3D-printed part in SolidWorks is the way infill percentage is handled. Infill refers to the percentage of the inside of a part that has mass and is not empty space. To save time, material, and weight, parts are printed with a preset number of perimeter layers, and then the remaining cavity is filled in based on the given infill percentage (meaning that most of the interior is hollow save for some support structures). A known workaround to modeling the physical part involves creating a shell of the modeled part, making it completely hollow. This is usually the best approximation for parts created with low infill percentage, but it still doesn't consider the small, stiffening, webbed structures that make up the interior. Another issue with conducting an analysis of a 3D-printed part comes from how the layers are stacked. For traditional fused deposition modeling (FDM), the major weakness is along the layer lines. As a part is created, weaknesses are formed between layers due to the temperature differential in the cooled previous layer and the hot, viscous, current layer. This weakness makes print orientation a major factor for loading direction, as having these layer lines perpendicular to the major forces on the system make the part significantly weaker. Because of all these reasons, we mainly relied on physical testing data and component failure to be the driving factor for design considerations related to mechanical loading.

When testing different versions of our active pitch design, we noticed that one of the major points of failure involved the connection of the blades to the nosecone. With our mechanism, each blade is mounted to a bearing to allow for blade rotation, and then attached into a round peg on the nosecone. As RPM increases, the centrifugal force of the blades pulling on the nosecone was overcoming the glue we had used to keep it in place. This original design resulted in blades becoming detached from the turbine (catastrophic failure) at around 1500 RPM. Our target max RPM was 3500, so with some analysis in SolidWorks, using the center of mass of the blades relative to our axis of rotation, we translated this RPM into a max tension force that would be put onto the blades.

Figure 6: SolidWorks Mass Properties of Constructed Blade Assembly



$$T = mr_{COM}\omega^2 = \wedge.01881kg(.06626m)\left(\frac{3500\frac{rev}{min}}{60\frac{s}{min}} * 2\pi\frac{rad}{rev}\right)^2 = 170N$$

To remedy this issue and increase the maximum tension we could put on the assembly, we incorporated heat set metal inserts into the design. These inserts are heated (usually with a soldering iron) and then press fit into an undersized hole in a 3D-printed part, re-forming plastic around the grooves of the insert and solidifying it into the part.

Figure 7: Heat Set Insert Installed on Nosecone



We found through research that we could expect to resist a force of at least ~1300 N in tension on the insert [3]. The testing done doesn't incorporate the exact length, inner and outer diameter, or the surrounding geometry of our part, but we figured it to be a good enough estimate. This loading force was well over the 170 N that we expected to see at our target RPM from the simulation. This result was also backed up to an extent by the fact that we could max out our wind tunnel and run our turbine at over 4900 RPM, giving us a tension on the blade assembly of 330N.

Foundation System

The design of a fixed-bottom foundation presented a very new challenge to us this year, especially given our lack of experience in working with machined or welded components. We began the foundation design process by setting up a testing environment with sand in a plastic tub. After testing a variety of designs made from wood and other materials, we settled upon a design that resembled a box

with an open top, in which the tube that connected the foundation to the connection stub came up from the bottom of the box and out of the open top. The constructed design is shown in Figure 8. For installation, the wiring for the turbine will enter the top portion of the tube through the stub connector, and exit through a hole on the side of the steel tube 10cm from the top. This design weighs just under 8 lbs, which may be more than the weight of other team's foundations but should ensure it performs well at higher wind speeds.

Figure 8: Turbine Fixed-Bottom Foundation



The primary advantage of this design, which we first discovered by testing a flat base foundation without any sides, is that it uses the weight of the sand to anchor the turbine down, without weighing more than necessary as a standalone structure. The sides prevent the wet sand from acting like a fluid and shifting when the torque of the turbine is applied on the foundation due to the force of the wind. The sand cannot flow over the top of the anchor, and translation and rotation of the stub piece is prevented.

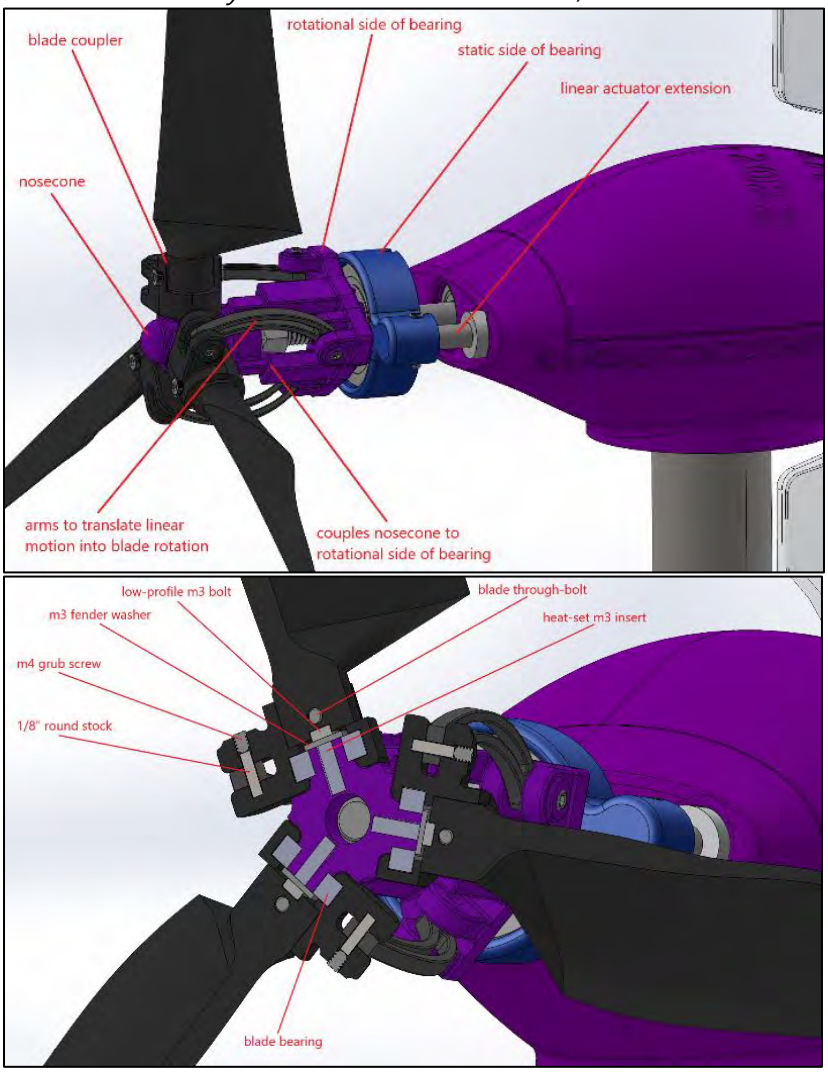
We considered many designs that included vertical plates parallel or perpendicular to the direction of wind flow and torque on the anchor, and tried to consider how the sand-water mixture would react to torque being applied on each foundation. We believe that it was imperative that the foundation contain some vertical structures perpendicular to the direction of wind flow, and the more cross-sectional area these structures have, the better resistance against torque they can provide. But, it can also be important for the foundation to have some resistance against any twisting motion, hence structures parallel to the wind flow need to be introduced as well. Even with all of these considerations, the best possible anchor would be an extremely heavy one that weighs the turbine down against any and all moment applied to the nacelle. We know, and our testing showed, that finding some way to use the weight of the sand to weight the turbine down would be critical. Our design was created to do this while minimizing the weight of the foundation itself.

Active Pitch System

The active pitch system is the turbine's primary mechanical actuator, and is the most technically significant subsystem design that we attempted this year. Originally, we wanted to implement an RC helicopter swashplate, but struggled to find one available for purchase that was rated for parameters

we expected the turbine to see, or had the same number of arms as the number of blades of our turbine. Through our research into swashplates and pitch systems, we also learned that our system did not need separate degrees of freedom for each blade, as a swashplate would, so an in-house system might require reduced complexity. We settled on a design in which two linear actuators, placed in the nacelle and aligned with the driveshaft, will push outwards on a plate that wraps around the rotating shaft. A bearing in the plate transfers this linear force to the rotating blades through curved arms connected to each blade. Each of the three blades are on their own bearing and free to rotate, and the outward or inward push of the actuators will pitch the blades over 100 degrees. Individual components of the assembly were 3D-printed, aside from the bearings and brass pin joints to attach moving components together. The linear actuators chosen were Progressive Automations PA-12 7.4V models, and while they proved difficult to program, they provide very strong precision in linear motion and perform well even under high windspeeds. A labelled SolidWorks screenshot of the full final design is shown below, along with a diagram of the blade coupling and connection.

Figure 9, 10: Active Pitch System Mounted on Nacelle, Blade Connection Diagram



Although the fundamental concepts of the design remained the same throughout the testing process, it went through many iterations before it performed as we had hoped. The first iterations of the design used print-in-place joints rather than discrete bearings and pin joints, and while they afforded a great deal of design flexibility, they produced too much friction during the pitching motion under load. Further iterations replaced the print-in-place joints with bearings and pins, which performed better under load, but oscillated during operation due to unequal loading between each blade and a high overall moment of inertia of the hub. The curved pitching arms were introduced to increase the total range of angles for the blades, and the size of the nosecone was reduced to limit oscillation. This system performed much better and operated much smoother under load. However, when wind speeds were increased, the blade bearings connections demonstrated a tendency to destructively slip out while the blades were pitching. To remedy this, additional fasteners were introduced to secure the blades to the nosecone, and the entire system held up much better at high wind speeds.

Electrical Design

Generator Selection

We selected a Nanotec DB42L01 Brushless DC Motor to act as the turbine generator, rated at 4000RPM and 75W. Brushless DC motors are widely available at the RPM and power ratings our turbine operates at, and tend to last longer than their brushed counterparts. The motor was selected after calculating the RPM and power values the turbine might see during operation at an efficient tip speed ratio and C_p. Although perfect RPM and power regulation would allow the motor to be sized to the values corresponding to 11 m/s operation, some leeway was given for imperfect regulation, and the motor was sized to values corresponding to 13.5 m/s operation. A smaller motor would be lighter and more efficient at lower RPM, which is why sizing was limited to this value. One benefit of this model is that it is equipped with a set of Hall-Effect sensors that output a signal alongside the main AC output. There are individual lines for each phase of the motor, and they produce a square wave in phase with the rotation of the motor. This signal is used for the measurement of RPM. The presence of the Hall-Effect sensors meant that we didn't have to design a standalone RPM sensor in the nacelle, as we have done in previous years.

Turbine Controls

The turbine-side control system includes a passive rectifier, power measurement sensors, communication equipment, and a microcontroller to run the controls and communicate with the turbine's other subsystems.

We originally planned to design and build a controllable (also known as PWM) rectifier for the competition turbine. We did succeed in building a working prototype that was able to efficiently rectify the three-phase AC signal from the generator into DC, and regulate its voltage by delaying the firing signals by adjusting phase. However, once we began to integrate it into the rest of the turbine-side systems, we discovered that it interacted very poorly with the control power circuitry designed to power the sensing and communications systems. The presence of a powered controllable rectifier on the system required a separate passive rectifier during start-up, and the rectifiers interfere with each other during normal operation, as well as interfering with the various buck-boost converters we used to power the rest of the controls. We were only able to make the decision to move away from the controllable rectifier after building and attempting to integrate it, hence its presence in previous design

reports. We chose to use a single monolithic diode rectifier instead, an IXYS chip mounted on the PCB that the active rectifier was designed on. The diodes conduct at 0.55V, a less-than ideal voltage but a necessary efficiency loss given that the passive bridge rectifier requires no external power source to operate. The signal produced sees minimal voltage ripple during normal operation, which ensures power ripple under 10% as required by competition specifications. We included two small LC filters, with total energy storage capacity under 2J, on the rectifier output to minimize the ripple as much as possible. A 5V buck/boost converter powers the turbine control systems from the output of the rectifier, and feeds directly in to the 7.4V boost converter used to power the linear actuators. The 5V rail has a 5V, 0.47F (5.875J) supercapacitor attached to it, which is charged during normal operation and used during the discontinuity safety task to briefly keep the controls powered while the pitch is pulled back.

The turbine-side system includes one major sensor, a power sensing INA260 IC. This IC measures current, voltage, and can calculate power. The INA260 reports this information to the turbine side system's microcontroller through the I2C protocol. Many breakout boards and libraries have been designed around the INA series ICs which made it very easy to implement a custom version right into our design. In addition to receiving signals from the hall effect sensor and I2C from the INA260, the turbine side microcontroller also has transmit and receive lines to the microcontroller on the load side system and to a TISN74 dual buffer/driver. The SN74 controls the two linear actuators which move our active pitch system. Using this IC allows us to have separate data transmit and receive lines going to the microcontroller but only one line to the linear actuators in the nacelle. On the other transmit line, information such as the RPM, voltage, current, power, and position of the linear actuators can be sent to the load side system via optically isolated UART. This information will help inform the load side system about what changes to make to either maximize power or control RPM. The load side system will then send instructions for the turbine side system on its receiving line.

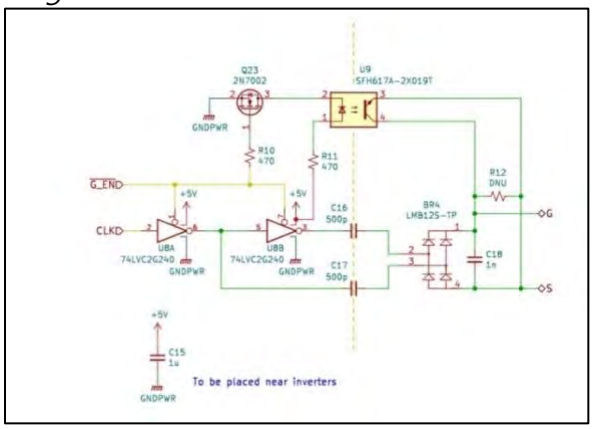
The main microcontroller chosen for the turbine was a Teensy 4.0. While the microcontroller is required to perform many tasks, the defining requirement was that it must send control signals to the linear actuators in the nacelle. The actuators were specified for their robustness and precision, not their communications compatibility, so they required a very large code library that took up a lot of space in the ATmega328P chips in the microcontrollers that we typically gravitate towards. The Teensy, with its larger memory and faster processor, can handle the actuator closed-loop controls much better, and thus was chosen for the turbine-side controls. The specific 4.0 model was chosen because of its smaller form factor and lower power consumption compared to the Teensy 4.1, which was used in the load side controls. Operating at 3.3V, both Teensys introduced a new level of complexity to the system, as we traditionally design sensors and controls at 5V, and the linear actuators require 7.4V.

Load Controls

We designed a variable resistance load for the 2020-2021 turbine, and consider it a genuine success. We wanted to build off that work, continue to innovate, and design a better variable resistance load for this turbine. It would provide the same benefits in optimization, regulation, and testing, although the overall control burden of this specific control system would be reduced with the introduction of the active pitch system alongside it. The load uses MOSFETs in combination with resistors increasing in a binary fashion, and creates different resistances by combining different combinations of resistors together. As the resistance of each set in the series doubles, a full linear range of resistances is achieved, ranging from 0.25 Ohms to 63.75 Ohms with a precision of 0.25 Ohms. Because the load must be able

to change resistance regardless of the power flowing through it, the FETs require a separate, isolated firing circuit (or gate driver circuit) to operate, which was the main challenge of implementing this system. The gate drivers accept a clock and enable signal as inputs. The clock line is common to all drivers and is switching at 200kHz by default. While the clock line could be used as a master disable to all the gate drivers, the enable pins (active low) are used to control the drivers. When the enable pins are set low, the back-to-back inverters begin switching at the clock frequency, which essentially pumps current through the 500pF coupling capacitors and bridge rectifier, which develops a DC voltage across the gate and source of the load FET. This voltage will allow the load FET to conduct through its channel, effectively shorting out the resistor associated with it. Conversely, when the enable pin is set high, the inverters cease to switch and the small-signal FET will allow current to pass through the diode of the optocoupler. The isolated NPN BJT of the optocoupler will then begin to conduct, which will tie the gate and source of the load FET together. This will cause the load FET to stop conducting through its channel and "unshort" the resistor associated with it. The gate driver was designed in this fashion (capacitively and optically isolated) so that the load and the driver circuit could use separate ground planes. Relays could have been used instead of FETs, but FETs are an overall more energy-efficient and modern component that reflects the sustainable nature of this competition. A schematic representation of the gate driver circuit is shown in Figure 11.

Figure 11: Gate Driver Circuit used in Load



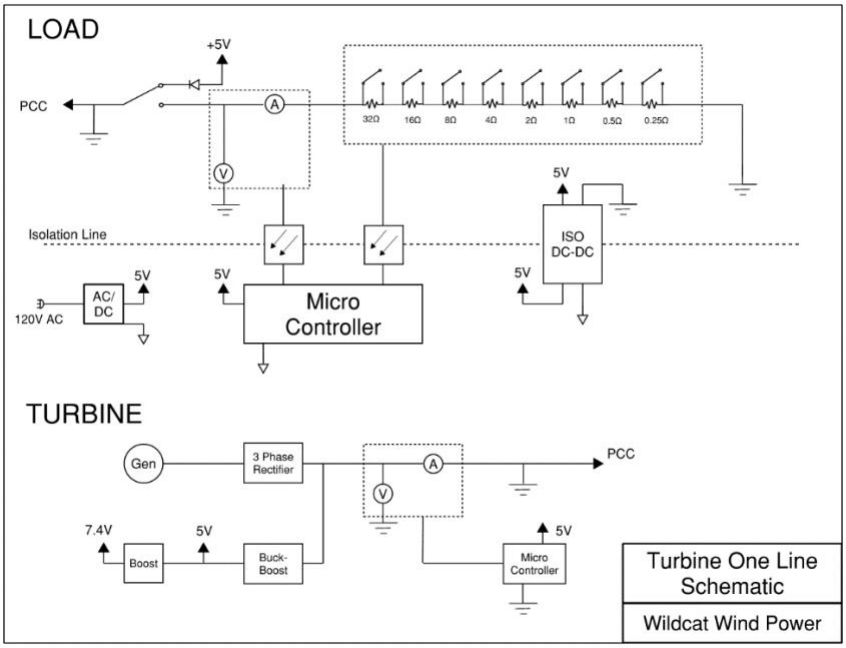
The load system includes its own set of communications circuitry and sensors. Communications between the load and turbine utilize the UART protocol. A dedicated isolating IC was used to only allow the incoming or outgoing data to pass without any power transfer. This IC is placed on the load-side system but could have been placed on the turbine-side system with the same outcome. Because the team did not opt to design or use differential line drivers, which is preferred for long board-to-board communications, the baud rate used in our system was set to a minimum to ensure no data corruption. The load system communicates with the INA260 power sensing IC via I2C protocol, rather than UART.

The load system will be controlled by a Teensy 4.1 microcontroller, which was chosen primarily to improve the team's data-logging and data-tracking capabilities during testing. The load has access to almost all of the turbine data through its communications systems, and the Teensy 4.1 is able to log testing data to a MicroSD card during testing for later analysis. The load also contains its own DC power supplies, such that it can and will be powered through a 120VAC wall outlet. The wall outlet will power the load controls and microcontroller, and supply power to the system for re-start after braking.

Power Systems

The generator, wiring, rectifier, filter, and load comprise the essential power system of the turbine during operation. The generator is rated at 24VDC for pulsed DC operation, and in use as a generator we have never seen it produce AC voltages beyond 18Vpp. At these lower voltages, the turbine should never produce above 48Vdc at the PCC. The filter is comprised of two LC (1uH, 3.3mF) filters in series on the DC side of the rectifier, to smooth the signal and limit high-frequency noise on the system. This filter combination provided the smoothest filtering and lowest losses during simulation of the rectifier system. Power wiring from the turbine nacelle to the electronics is a single 4-stranded 14 AWG cable, which should minimize wire losses even at the low voltages at which the generator operates. A simplified one-line diagram to illuminate the turbine power system is shown below.

Figure 12: Turbine One-Line Diagram



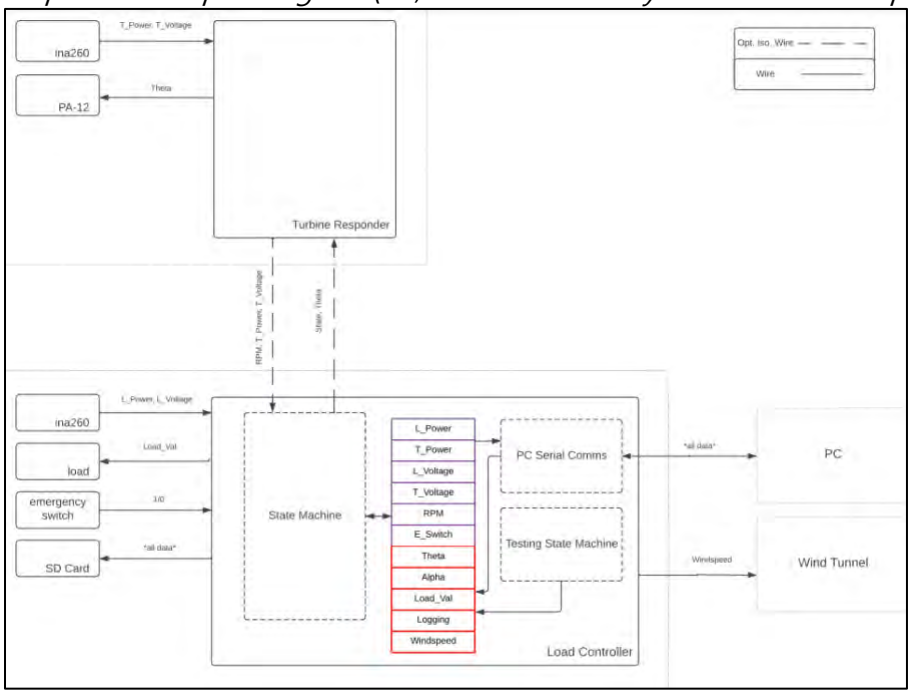
Software

The software development process is like previous years, but has been improved to simplify testing, data acquisition, and code collaboration. In the past, software would first be designed, written, and tested for individual electrical components to then be incorporated into the production code (for competition) to run on the microcontroller, and this year is similar. Turbine-load communication, variable load control, and peak tracking are all component level modules that have been adopted from last year's design. Off-the-shelf components such as the INA260 and PA12 came with libraries which made interfacing with these devices as easy as a method call. The Teensy 4.1 board has an on-board SD card interface and libraries are available for this as well. Once all component level modules and libraries were confirmed to work, a base level program was developed for the Teensy 4.1 on the load board to facilitate the development of an automated testing and data acquisition configuration, as well as the production code configuration. Alongside this, production code was developed for the Teensy 4.0 on the turbine board.

Turbine-load communication allowed a controller/responder setup where all inputs would be managed by the load controller and outputs forwarded to the turbine responder. As mentioned previously, the turbine responder's code could remain the same for both automated tests and production runs. However, on the load controller, there would be two configurations: one for automated testing and one for production code. For the sake of simplicity and clarity, these two configurations would be different codebases adapted from the same base level program.

The testing and data acquisition configuration for the load controller enables the system to interface with our wind tunnel and either automatically sweep through system parameters (pitch, resistance, wind speed) while logging data or take user input to specify system parameters. We designate theta as the pitch angle of the blades. The automatic tests are accomplished with a state machine which sweeps each parameter through a preset range. The step size, range to be swept through, and step time to account for transients can all be set prior to testing for each parameter. If the option is made to manually enter parameters, then the input is received via a serial connection to a PC. In this case, the user also has the option to log data or not. During data logging, all the system inputs and outputs are written to an SD card in .csv format for later export and analysis.

Figure 13: System Input and Output Diagram (PC, Wind Tunnel only used for Data Acquisition purposes)



When connection is made between the load controller and the turbine responder, the controller reads inputs [RPM, turbine voltage, turbine power, load voltage, load power, emergency switch] and produces outputs [state, theta, load resistance, PCC relay]. It will receive the first three inputs [RPM, turbine voltage, and turbine power] from the turbine responder via serial communication, read the remaining inputs via onboard sensors, determine the state of the system, generate outputs, then forward the first two outputs [state, theta] to the turbine responder. Similarly, the turbine responder will receive those two outputs, read the turbine voltage and power, update the pitch angle with theta, and then send its outputs back to the load.

All component level modules, libraries, configurations, and example code are stored in a GitHub repository. It is organized to have different examples for each component used, code from the previous year, all libraries used, and project folders for both the load controller and turbine responder. In each project folder, copies of the required libraries for that project are provided in the /src folder so it is easy for anyone to pull the code, open it in the Arduino IDE, and upload it without installing dependencies. Data archiving is performed by uploading test data to a shared drive for analysis and later use.

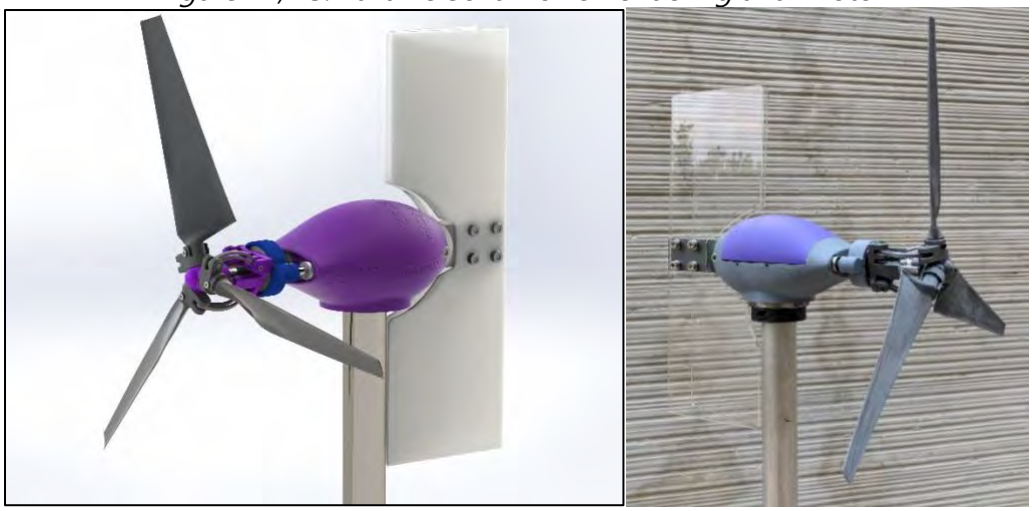
Assembly of Systems

Mechanical Assembly

The blades and nacelle were both 3D-printed, a manufacturing technique that we are comfortable using due to its ease of use in iterative design and manufacturing. Although we gained access to a Stereolithography (SLA) printer, we determined that both the blades and nacelle should be printed using our FDM printer, as it produces stronger, larger, and more reliable components. The main concern we faced with 3D-printing blades was the tendency of 3D-printed parts to fail along layer lines. To mitigate the risk of blade breakage, we printed the blades so that the layer lines were normal both to the shear force caused by the wind and the shear flow caused by the blade bending. We found it advantageous to conduct 3D design in SolidWorks through a shared file database on Microsoft Teams, so that different team members could work on separate turbine components at the same time. The nacelle yaw fin connector was 3D-printed, with the acrylic plating being laser cut. The active pitch system was constructed out of 3D-printed components and off-the-shelf bearings and fasteners.

To assemble the nacelle, hub, and blades, first each arm of the active pitch mechanism was attached to the rotating side of the bearing plate with pins and set screws, and then the other end of the arm was attached in a similar manner near the base of each blade. The blades were set in their respective rotating holders (allowed to rotate through a bearing), and the entire assembly was placed over the driveshaft and locked in rotation with it through a nut under the nosecone. The linear actuators were set on either side of the generator, and their arms attached to each arm on the nonrotating side of the main bearing plate. The cap of the nacelle, which contains printed brackets to hold each actuator in place, snugly fits on top of it after the actuators are mounted. The nacelle yaw fin is held in place behind the nacelle with a 3D-printed piece that is secured to the nacelle with fasteners. Care is taken during assembly to ensure that wiring for the actuators and generator will not be disturbed by the movement of the actuators or placement of the nacelle cap. The assembled turbine, along with its full SolidWorks model, is shown below.

Figure 14, 15: Turbine SolidWorks Rendering and Photo

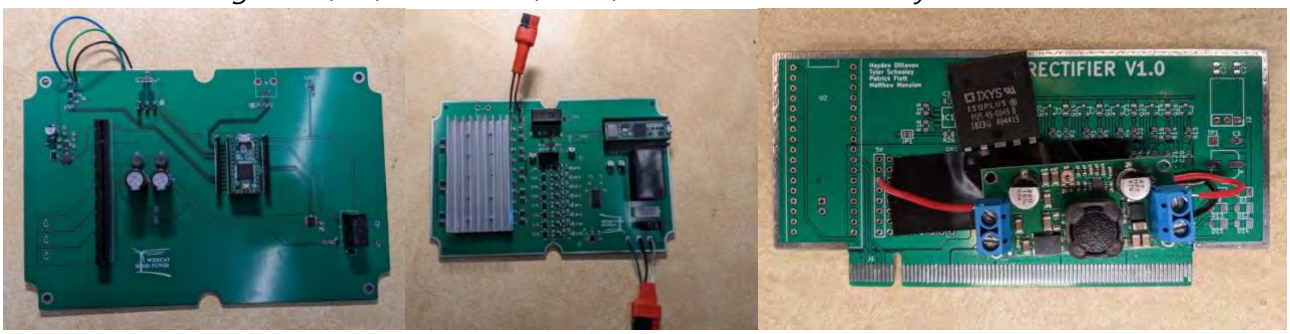


The assembly of the foundation began after testing of wooden mockups was complete. We chose to construct the design out of steel, due to it being the most easily available ferrous metal to us. For the thick metal base, we used 3/16" steel. To cut the steel, we used a plasma cutter to make a rough cut and then used an angle grinder to square out the sides. We then welded on a 1.5" outer diameter, 0.035" thick steel round tube to the center of the base. The sheet metal casing was made from 30-gauge steel. The steel that we bought was slightly too short to make it around the perimeter of the base, so we cut it into two pieces and aligned them opposite of each other around the base. This allowed for most of the perimeter to be twice as thick as the single sheet. We then drilled holes into the base and connected the casing to the base using steel rivets. We also used the same steel rivets to connect the two separate pieces of the casing on the top.

Electrical Assembly

All electrical circuits and systems outside of the turbine nacelle were designed on printed circuit boards (PCBs). We separated our systems into a load board, a turbine board, and a controllable rectifier board. All boards were ordered in early February along with their respective components and assembled mainly through a surface-mount assembly process in a PCB oven. As part of planning for the assembly process, a small test board was designed, ordered, and assembled in November using surface-mount components so that the team could learn how to assemble a surface-mount board. Surface-mount assembly presents the opportunity for the use of a wider variety of components for design, which is useful given the semiconductor shortages seen across the industry this year. The controllable rectifier system was designed to fit in a PCIExpress slot on the main turbine board, so that if the active system did not perform it could be replaced with a diode bridge rectifier. When it did not perform, it was replaced with a diode bridge rectifier soldered on to an unpopulated PCB. Images of the front sides of all three completed PCBs are shown below.

Figure 16, 17, 18: Turbine, Load, and Rectifier PCBs Fully Assembled



Wiring for the system was separated into two strands, power and communications. The turbine PCC was mounted in a NEMA-rated box contained with wire glands to connect the power strand and an inset RJ-45 connector for the communications wiring (Figure [D]). A 4-strand 14-gauge wire was used for the power transfer, and CAT5 cables were used for communications between the turbine and turbine electronics, as well as between the turbine and load. The load PCB was mounted in a similar container to the turbine-side board, and used similar connectors. The major non-SMT assembly of the board was the power resistors and necessary heat sink. The TO-247 package resistors were mounted with their thermal pads facing upwards, and an off-the-shelf aluminum heatsink was cut and then mounted over the resistors. Machine screws coming up through the bottom of the PCB secure the heatsink to the resistors through holes tapped at regular intervals in the heatsink.

Commissioning Checklist

The system was designed to be mobile with ease of commissioning in mind. While mobility is important, durability and reliability were not to be sacrificed. The integration of subsystems both electrically and mechanically was achieved with connections that are easy to install and uninstall. The commissioning checklist provides detailed instructions for the implementation of our system, and is shown below.

Step #	Process
1.	Run power and control wires through the hole in the foundation tubing, pull through to keep connectors away from water.
2.	Fill foundation with sand using shovels, move sand from center of container.
3.	Place foundation, wobble to move deeper down to competition depth, fill around foundation with sand, level the entire mechanism.
4.	Install stub and run wires upwards through it.
5.	Bolt the base plate of the tower to competition-provided stub, pulling wires up through tower.
6.	Attach three-phase power and control cables to nacelle base connectors.
7.	Attach nacelle to tower through compression fit on yaw bearing. Ensure compression fit of nacelle lid is secure. Check alignment of nacelle on tower, and use provided level to ensure tower is vertically aligned. Adjust foundation if necessary.
8.	Connect 3-phase power wires from the turbine to the APPs connected to the turbine control box labeled “3-Phase Power".
9.	Plug in the RJ-45 connector from the turbine to the female connector labeled “Turbine Controls”.

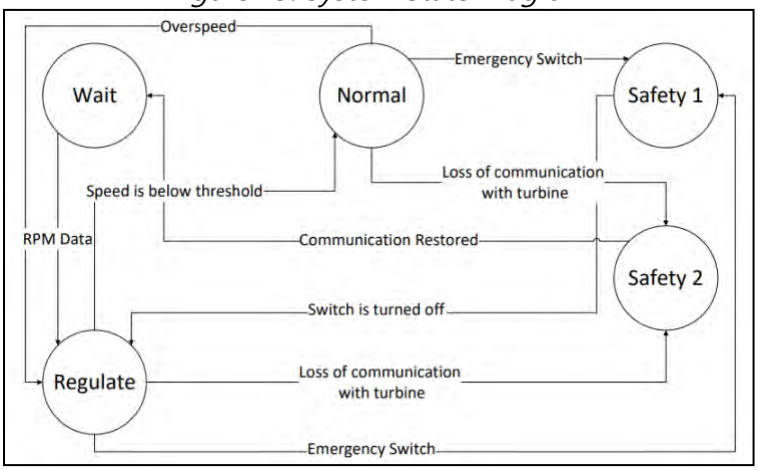
10.	Connect rectified power cord labeled "Turbine DC Power" from the turbine control box to the PCC via APPs. Connect the other side of the PCC to the load control box labeled "Turbine DC Power" using APPs as well.
11.	Using an ethernet cord, connect the load to turbine controls. The female RJ45 connectors are labeled "Load Controls" on both sides.
12.	Connect the emergency stop cable labeled "E-Stop" on the load control box to the competition provided stop button via a JST RCY connector.
13.	Plug the load control board into 120V wall power using the IEC connection cord.
14.	Ensure control box lids are secure and boards are powered.

Operation

Operational Modes and States

The turbine is set to operate between five different states, the relationship between the states is shown in the following figure. Because the competition does not require full power and RPM regulation at wind speeds above 11 m/s, the control system does not attempt to estimate the tunnel wind speed during operation, and the decision to regulate power and RPM is triggered by an RPM threshold. The speed threshold after which the turbine begins to regulate is 3500RPM, chosen because it reflects roughly a 12 m/s wind speed cutoff, ensuring regulation does not occur during the power curve task. The turbine has operated at over 4900RPM safely, so the 3500RPM cutoff is well within the margin of safe operation. Our experience working with 3D-printed blades tells us that they would fail due to internal stresses at roughly 5500RPM, so the safety margin should provide enough leeway.

Figure 19: System State Diagram



The operational functions of the turbine, and how each state is related to others, is explained in the following table. We define separate turbine states for each of the competition safety tests, as they are triggered by different system conditions. Regulation during the 'Regulate' state is achieved through a simple proportional controller that adjusts the blade pitch to keep the turbine between 2850 and 3450RPM. After the transition from the 'Wait' to 'Normal' state, the load resistance is adjusted to maintain the turbine-side voltage at 3.3V, high enough to continue to power the turbine controls and linear actuators, and this functionality is maintained until the turbine produces enough power to run the linear actuators regardless of load resistance. Only then does the load set a constant resistance at a

point to maximize power production. Discontinuity detection to enter the 'Safety 2' state is defined as the combination of nonzero RPM and a load voltage much greater than the turbine voltage.

State	Function	Enter Case	Exit Case	Operation
Wait	Wait until Cut-In	Default	Turbine-Side electronics on	Blades pitched to cut-in pitch, Load at max resistance
Normal	Power Curve	Turbine-Side electronics on OR Wind Speed < 12	Wind Speed > 12	Load Resistance Constant, Blades pitched to maximum power pitch
Safety 1	Emergency Stop	E-Stop Closed	E-Stop Open	Power turbine from load, feather blades, wait for E-Stop
Safety 2	Disconnect Brake	Discontinuity Detected	Continuity Detected	Power turbine from load, feather blades, wait for continuity
Regulate	Keep turbine at safe RPM	RPM > 3500	RPM < 2850	Regulate RPM through pitch control

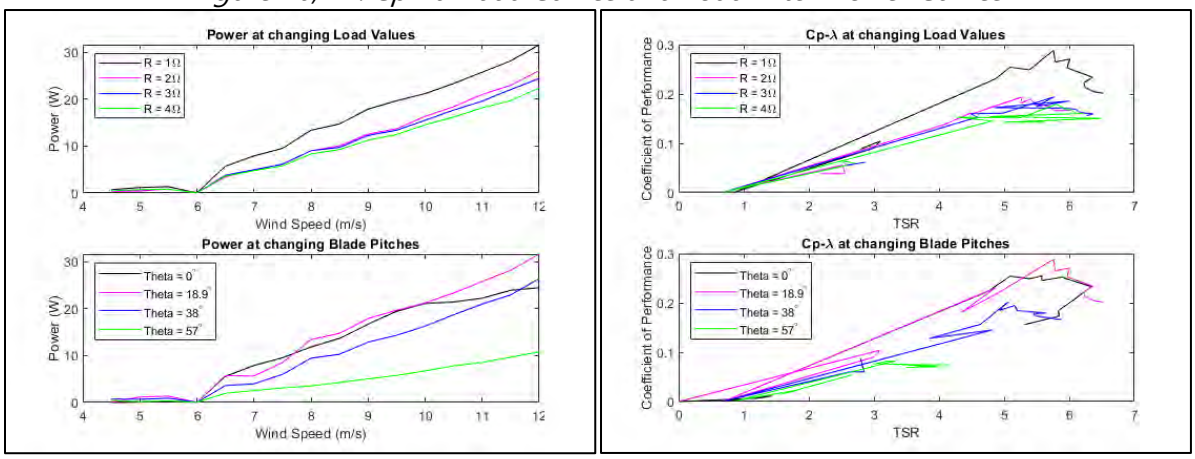
Testing of Systems

Subsystem testing was carried out throughout the design process, culminating in significant subsystem testing in February and March for the foundation system, blades, electrical systems, and active pitch mechanism. Once we began to connect subsystems and assemble the entire-turbine, we could begin full-system testing.

Preliminary full-system tests showed that the original active pitch mechanism could theoretically brake the turbine and regulate its power production and RPM, but higher-speed testing showed that the mechanism was unwieldy and oscillated heavily at higher wind speeds. The oscillations caused some joints to disconnect and the blades to shatter at one point, so we decided to go back and redesign the pitch mechanism to reduce the moment of inertia and dampen the oscillations. We also strengthened the connection between the blades and the hub, as mentioned previously. After reducing the diameter of the nosecone and the radius of the pitching arms, further testing showed reduced oscillations and operation without mechanical failure. After fixing these issues with the active pitch system, we turned our attention to our controllable rectifier design. Testing of the rectifier with the turbine and other electrical systems showed that, although it could operate cleanly if powered externally, its control power setup interfered heavily with its operation when it had to power itself. We eventually determined that fixing the control power issues would require new PCBs of the rectifier and turbine, and made to decision to switch back to a passive rectifier.

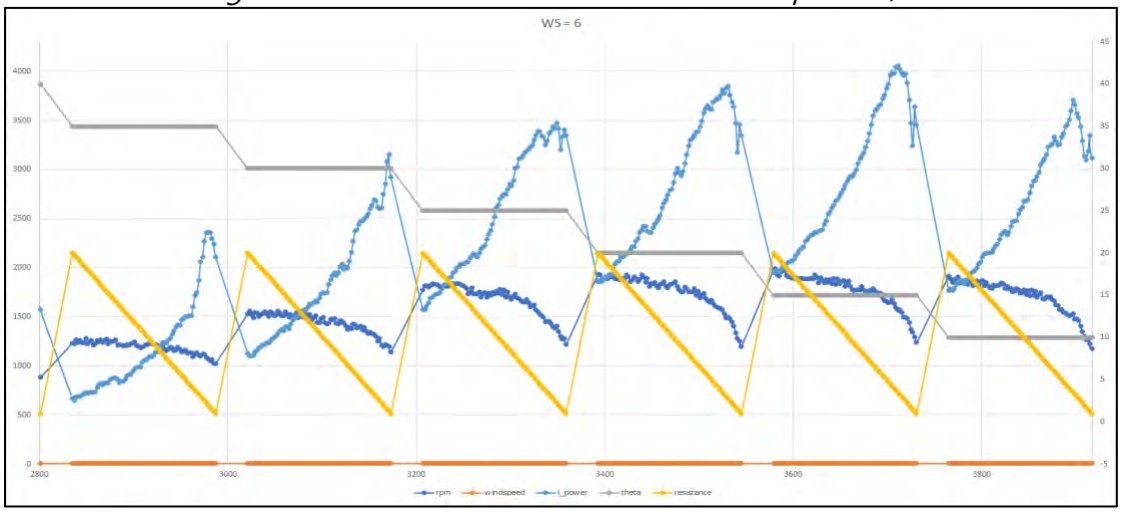
Once these decisions had been made, it was time to move into full-system testing to determine the operational parameters of the turbine control scheme. We developed a fully automated testing platform that integrated with our wind tunnel, such that we were able to automate a test that ran through multiple variables and track data, or manually change system parameters to see how the turbine reacted. We used the automated system to first determine a maximum operational RPM for the turbine, by operating it without RPM regulation to the highest wind speed our tunnel could produce. We determined it to be upwards of 4900RPM, well above our planned regulation cutoff of 3500RPM. Next, we set out to collect data on the pitch and load relationships, in order to determine the best pitch and load setpoints for the Power Curve task. The results from this round of data collection are shown as Cp-Lambda and Power Curve plots below, although they do not represent the final turbine data that we collected. This data served to validate our control scheme.

Figure 20, 21: Cp-Lambda Curves and Load-Pitch Power Curves



Next, we began to run through the competition safety tasks and develop RPM regulation for the higher wind speeds in the durability tasks. Tests of each saw strong performance in our regulation scheme, but we saw some minor issues during the safety tasks with our turbine-side microcontroller not always turning back on. We were able to fix the issue with a combination of software and hardware changes, and tested turbine braking up to 16 m/s in both the disconnect and E-stop conditions to ensure it would reliably brake. With the fundamental secure operations of the turbine (braking, regulating), we continued analyzing the relationship between load resistance, pitch, power, and RPM. Data collection showed that pitch angle and load resistance played a major role in power production, as seen in Figure 22 below, where a variety of load and pitch angles and their respective power outputs are shown at a single wind speed.

Figure 22: Load-Pitch-Power-RPM Relationship at 6m/s



Testing of the foundation system was conducted separately from turbine testing, due to the fixed floor of our wind tunnel, and focused on maximizing the torque that the anchor could withstand while set in wet sand. A model of the competition setup was created in a plastic tub filled with 200lbs of sand and filled with water, and a spring scale was attached to a wooden dowel to allow for measurement of torque. Designs, both preliminary wooden ones and the final steel mechanism, were installed in the

sand, and torque was applied to the base until it failed. Under this setup, we found our final box design could withstand 15-20 N*m before it began to shift, and more than 30 N*m before it failed. The testing setup in use is shown below. We also developed a platform in the wind tunnel to test the torque that the turbine will apply to the foundation. An arrangement of PVC pipes with a tiltable pivot point on the bottom was attached to the turbine base, and a pulley system along with spring scale was rigged in our wind tunnel to measure the tilt of the turbine against the scale under wind. The setup is also shown below, and showed loading near 1 N*m at 14 m/s, that decreased as the blades pitched out of the wind.

Figure 23, 24: Foundation System Testing





Review from 2021 Competition

Some design concepts, mainly the variable resistance load, were carried over from the turbine designed for the 2021 competition, but most of the work this year was spent on designing new turbine elements and controls. Even the variable resistance load itself was redesigned with power electronics to be more efficient and more accurate. The active pitch system was a completely new actuator that we had not formally attempted to design ever before, and the turbine blade design was fully revamped. A new style of generator was used, and obviously the foundation system involved many new lines of thinking. Although the system controls and operational states are similar to the system designed for the 2021 competition, the overall control requirements lessened, and degree of state estimation that was needed for the previous turbine was not implemented this year. One system, the turbine nacelle fin and yaw control system, was somewhat recycled from years past, but a new tailfin was still designed in the same style. The turbine tower was fully re-used from previous turbines.

References

[1] T. Burton, D. Sharpe, N. Jenkins, and E. Bossanyi, *Handbook of Wind Energy*. Chichester: John Wiley & Sons, Ltd, 2001.

[2] R. S. Shevell, *Fundamentals of Flight*. Englewood Cliffs, NJ: Prentice Hall, 1982.

[3] S. Hermann. Threaded Inserts for 3D Prints – Cheap vs Expensive. Dec. 7th, 2019. Accessed on: April 21st, 2022. [Online]. Available: https://www.cnckitchen.com/blog/threaded-inserts-for-3d-prints-cheap-vs-expensive

Northern Arizona University

2022 Collegiate Wind Competition

Turbine Team

Technical Design Report

For the United States Department of Energy

4/24/2022

Prepared by,

Owen Murphy	Mikela Petersen	Lucas Johnson	Graham Burnside	Dario DeDonato	Ben Coulter
ME Team Lead	Blades	Pitching	Foundation	Tower & Yaw	Brakes
jom28@nau.edu	mmp378@nau.edu	lbj38@nau.edu	gfb32@nau.edu	dgd53@nau.edu	bsc226@nau.edu

Samantha Nearing	Chase Hughes	Andrew Harper	Tyler Schwartz	Maxwell Fawcett
EE Team Lead	Diversion Load	DC/DC Converter	PCB Design	Arduino Control
sdn63@iris.nau.edu	cmh789@nau.edu	andrew.harper@nau.edu	tms579@nau.edu	mbf95@nau.edu

WindJa Energy Club at NAU

1 Contents

2 Executive Summary 3
3 Design Objectives 3
3.1 Turbine Objectives 3
3.2 Foundation Objectives 4
4 Blade Design 4
4.1 Geometry & Airfoil Selection 4
4.2 Aerodynamic Analysis 5
4.3 Composite Manufacturing 5
4.4 Blade and Hub Stress Analysis 6
5 Foundation Design 7
5.1 Initial Axial Thrust and Tower Drag Calculations 7
5.2 Axial Drag Reductions 8
5.3 Load Cell Testing 9
5.4 Design Iterations 9
5.5 Installation Procedure 10
5.6 Foundation Testing 11
6 Mechanical Design 12
6.1 Nacelle 12
6.2 Pitching 12
6.3 Brakes 14
6.4 Tower and Yaw 15
7 Electrical System Design & Analysis 16
7.1 Generator 16
7.2 AC/DC 16
7.3 DC/DC Boost Converter 16
7.4 Diverter Load 17
7.5 Printed Circuit Board 18
7.6 Load 18
8 Software Implementation and Testing 18
9 Field Testing 19
9.1 Procedure 19
9.2 Results 19
10 Changes from Last Year 20
11 References 21
12 Appendix/Photo Collection 22

2 Executive Summary

Northern Arizona University's WindJax team designed, analyzed, and tested a micro-wind turbine and foundation system for the 2022 Collegiate Wind Competition. This report discusses the design choices that the team made, what analysis methods were used to estimate turbine performance, and the testing procedures used to validate the design.

The turbine design consists of a three bladed horizontal axis wind turbine with composite blades, an active pitching system, and a disk brake. The airfoil selected was the GOE79, and the blades were manufactured by vacuum bagging a flax seed based composite structure called BComp around 3D printed cores.



Figure 1: Wind Turbine Full CAD Model Isometric

The variable pitch design was initially based on last year's swash plate system. However, the team made multiple design changes in order to improve performance and reliability. These changes included a hub diameter reduction, swash plate size reduction, switching from a PLA bearing to stainless steel, and directly mounting a linear actuator in place of last year's rack and pinion system.

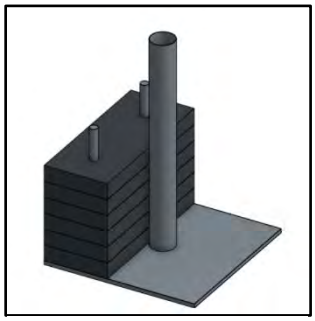


Figure 2: Foundation CAD Model

Due to the introduction of the foundation design requirements for this year's competition, the team prioritized early design prototypes and testing for this system. Additionally, significant efforts were put towards streamlining the turbine and tower to reduce drag forces. After thorough testing, the team settled on a gravity based, directional foundation design. This decision was made as none of the earlier designs tested met the expected moment produced in competition, and the team found that having a heavier foundation that is stable would provide more points than otherwise.

3 Design Objectives

3.1 Turbine Objectives

Looking at the three tasks that will be completed at competition that are specifically focused on the turbine, the team developed design specific objectives to optimize performance in each task. For the power curve performance task our turbine must produce maximum power between wind speeds of 5 m/s to 11 m/s. To accomplish this task, the team's main design objective is to maximize the turbine's coefficient of power. In order to meet this design objective, the team designed blades that maximize the lift coefficient to drag coefficient ratio at the expected Reynolds numbers based on the known wind speeds. The blade shape also maximizes the swept area, optimizing the energy captured from the wind. While the cut-in wind speed is not a measured task in the competition, the team is cognizant of our turbines cut-in wind speed and is aiming to have turbine startup in wind speeds less than 5 m/s. The turbines pitching system will reduce the cut-in wind speed, as well as improve the power output between 5 m/s to 11 m/s.

For the safety task, the wind turbine must be able to reach "shutdown" at wind speeds up to 22 m/s [1]. The design objective for the safety task is to have a braking system that can overcome the moment

created by the shaft at 22 m/s. The team accomplished this design objective by designing a disk brake system that works in conjunction with the pitching system. The pitching system in the stall position slows the rotation of the blades while the disk brake can further decelerate the turbine as necessary.

The durability task of the competition measures the change in foundation position after the completion of the previously mentioned tasks. The main design objective for this task is to minimize the drag on the nacelle and the tower. The design objective was accomplished by creating the most compact nacelle assembly possible. The team further reduced drag by creating a streamline attachment for the tower and the nacelle, thus minimizing the pressure drag.

3.2 Foundation Objectives

There are two tasks targeted towards the foundation, these being the durability task and the structure weight task. The first objective is to create a foundation that would move no more than 6mm during wind tunnel testing. The second objective was to make the foundation as light as possible while still fulfilling the durability objective. Lastly, the foundation must be fully installed within the 15 minutes of allotted time.

Ultimately, the team prioritized durability as this was more crucial to the safe operation of the turbine. Multiple lightweight foundation designs were tested, but the team determined that these lightweight designs did not fulfill the durability objective.

4 Blade Design

4.1 Geometry & Airfoil Selection

In order to design and analyze blades, the team used a Matlab code based on Blade Element Momentum theory (BEM). This code was created by the team and output initial chord lengths and angles of twist at each blade section. The twist angles and chord lengths as a function of radial position can be seen in Figure 3:

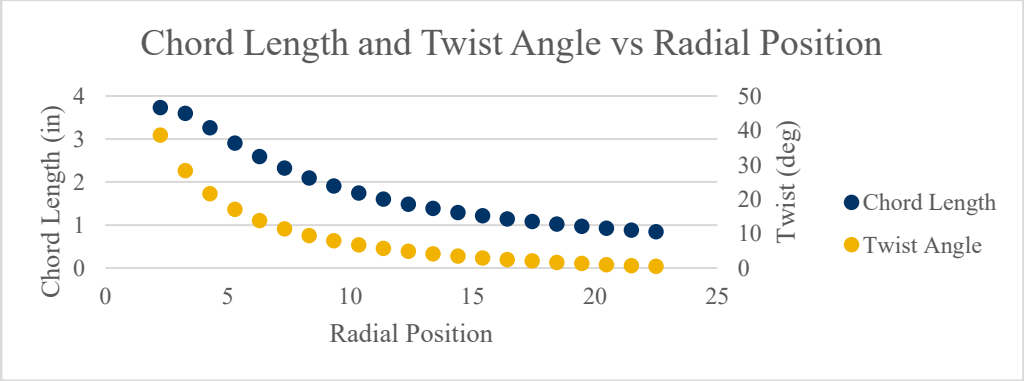


Figure 3: Chord Length & Twist vs Radial Position on the Blade

With these values, the Reynold's number range was calculated for the expected conditions at competition. The Reynold's number was used to evaluate various airfoils that were subsequently simulated using Q-Blade. This simulation data was used to estimate the Power Curve Performance Task score at competition. As a result of this process, the team settled on the GOE79 airfoil as it provided the best balance of manufacturability and performance [2].

4.2 Aerodynamic Analysis

Q-Blade simulations were used to estimate the Coefficient of Power, or Cp, of the blades at various tip speed ratios, or TSR's. As a result of these simulations, the team found a maximum Cp of approximately 0.44 at a TSR of 4.5. Additionally, due to the inclusion of an active pitching system in this year's turbine, Cp vs TSR curves were simulated for a variety of pitch angles relative to this maximum. These curves are overlayed in Figure 4 to visualize the change in performance for varying pitch angles and the ability to feather to turbine blades out of the wind. Similarly, the power curve from 5m/s to 22m/s was generated using simulations from Q-Blade. The rated power for the turbine is 54.3W as seen in Figure 5.

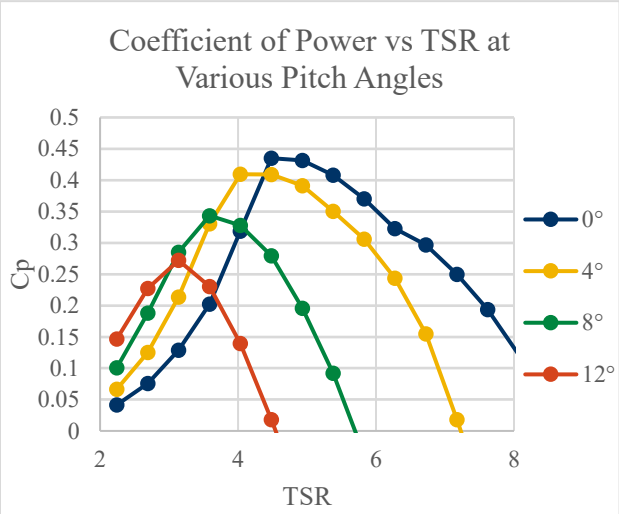


Figure 4: Power Coefficient vs Tip Speed Ratio at Various Pitch Angles

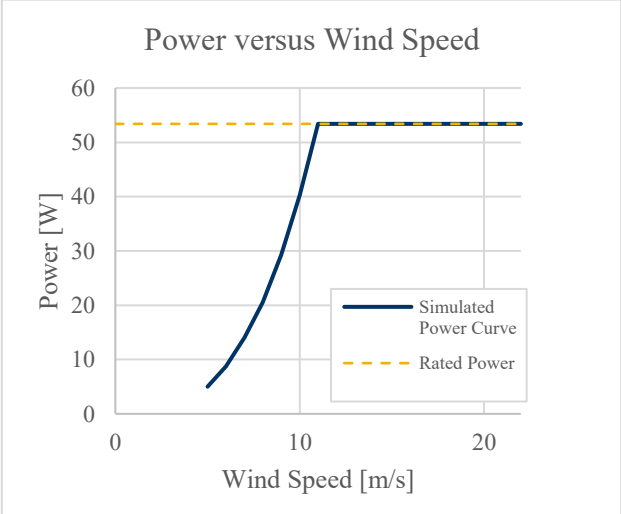


Figure 5: Power [W] vs Wind Speed [m/s]

4.3 Composite Manufacturing

After printing prototype blades, it was determined that fully 3D printed blades would not be suitable for the expected loads given the low percent thickness of the airfoil. After discussions with the composites sponsor, Gurit, the team decided to use BComp, a material similar to carbon fiber but sustainably made from flax seed. Without composite manufacturing experience, the team initially experimented with 3D printing split molds. However, due to the time commitment of designing and manufacturing new molds for every iteration of the blade design, the team decided to switch to vacuum bagging BComp around 3D printed cores. After countless attempts, the desired blade quality was eventually achieved through this method. The manufacturing process first involves hand laying-up the BComp around the cores, placing the blades in a sandwich of peel ply and breather fabric, and sealing the blades in a vacuum bag. Once the blades are removed, they are trimmed and additional coats of epoxy are applied to reach the desired surface finish.

The final blades have both a layer of unidirectional fabric and twill wrapped around a PLA core with a steel grommet inserted into the hub mounting point. The manufacturing process can be seen in Figure 6 with a final blade in Figure 7:



Figure 6: Blade Manufacturing Process



Figure 7: Final Blade

4.4 Blade and Hub Stress Analysis

Due to the complex nature of the composite blades, the team decided to do load calculations only on the mounting point and perform a series of tests on the rest of the blade structure. The load calculations were performed using the mass of the blade, location of the center of mass, and maximum angular velocity in order to find the maximum centripetal force. Using these calculations and the material properties provided by Gurit for the BComp fabric, the team estimated a factor of safety of 1.61.

In order to verify this factor of safety, the team mounted the entire shaft, hubs, and initial blades into a dynamometer and spun the blades until failure. The blades failed at 5306.1 rpm in the location expected, giving the blades a factor of safety of 1.3. As a result of this test, the team decided to alter the geometry of the blade by increasing the distance between the bottom of the blade and the mounting hole as well as imbedding a steel grommet to dissipate the centripetal load.



Figure 8: Blade Centripetal Force Testing Apparatus



Figure 9: Blade Centripetal Force Test Results

In addition to the centripetal test in the dynamometer, the team conducted a bending test. The blade bending test was completed by attaching a weight to the blade tip as seen in Figure 10. The calculated maximum bending stress was 255.02 kPa at 22 m/s, and the testing resulted in a bending stress of 1116.8 kPa before ending the test. This results in a factor of safety of at least 4.38 since blade failure was not reached.



Figure 10: Blade Bending Stress Testing Apparatus

The team also conducted separate hub tests in order to find a factor of safety for the hubs themselves. This was done by mounting weights at a known radius from the attachment point of the hubs and spinning them to a known angular velocity. Similar to the axial blade test, failure was not able to be reached. Due to limitations in the maximum dynamometer angular velocity, the hubs experienced a maximum of 721.2N of centripetal force, yielding a factor of safety of 12.1.

5 Foundation Design

5.1 Initial Axial Thrust and Tower Drag Calculations

When first prototyping foundation designs, the team needed an estimated of the loads the foundation must withstand in the conditions of a runaway event up to 22 m/s. The main sources of these forces were assumed to be the axial thrust of the turbine, the nacelle drag, and the drag on the tower as seen in Figure 11. These forces were estimated with the following equations:

$$T = \frac{1}{2}\rho A U^2[4a(1-a)] \quad \text{Eqn 1}$$

$$F_D = \frac{1}{2}\rho A U^2 C_D \quad \text{Eqn 2}$$

The axial force was estimated with equation 1, where T is the thrust force, ρ is the density of the air, A is the rotor area, U is the free stream velocity, and 'a' is the axial induction factor [2].

Operating at the Betz limit with 'a' = 1/3, sea level density $\rho = 1.23\frac{kg}{m^3}$, rotor area $A = \frac{\pi}{4}D^2$, and free stream velocity $U = 22$ m/s the maximum axial thrust force was calculated to be 42 N or 9.45 lbf. This procedure was done again using the power coefficient of the blades calculated through QBlade. The axial induction factor 'a' was then calculated to be 0.151, and thrust was solved for. MATLAB was used to create a plot of the estimated thrust forces from 0-22 m/s, shown in Figure 12. According to the QBlade limit, the maximum thrust force is 24 N, or 5.4 lbf.

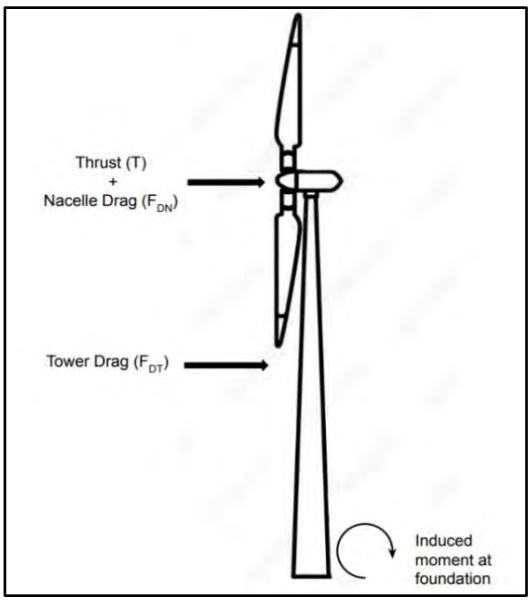


Figure 11: Nacelle and Tower Forces Diagram

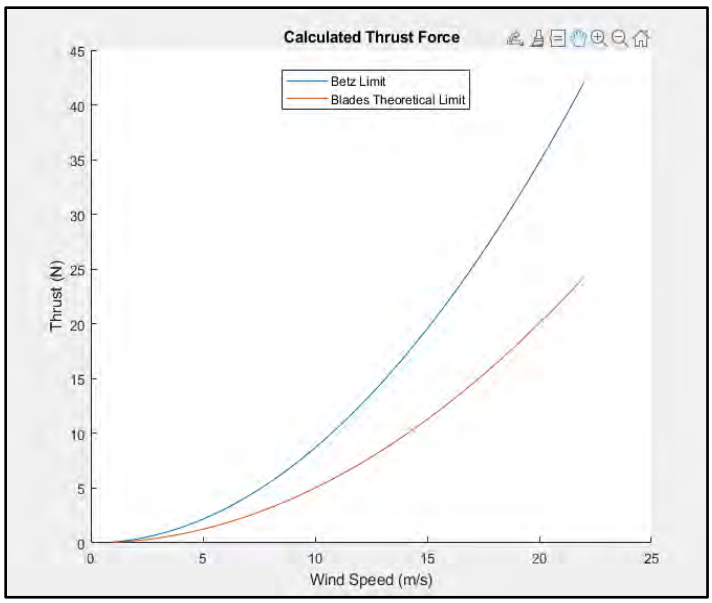


Figure 12: Thrust Force Testing Results

For the initial tower drag estimate, the team used equation 2, where C_D is the coefficient of drag, and A is the planform area of the cylinder. Initially, the tower was assumed to be a cylinder of 3.81 cm diameter with a height of 60 cm. At 22 m/s, the Reynolds number was calculated to be $5 * 10^4$, giving an estimated C_D of 1.1 [3]. Under these conditions, F_{DT} was estimated to be 7.5 N, or 1.7 lbf.

Lastly, the nacelle drag, or F_{DN}, was estimated. This was determined by modeling the nacelle as a simple cylinder of 10 cm diameter perpendicular to the wind, with a C_D of 1.2. Following equation 2 again, this gives a drag force of 2.8 N, or .63 lbf.

With these forces, the tipping moment at the foundation was calculated to determine the restoring moment needed to prevent the tipping of the foundation and turbine. Based on the estimated distance from the rotor center to the top of the sand as 1 m in the competition rules, the distance from the center of the tower would be approximately 0.7 m. By multiplying the forces with their respective lengths, the calculated maximum theoretical moment is 50 N*m, or 37 lbf*ft. Using the maximum Cp from Q-Blade, the maximum theoretical moment is 32 N*m, or 23.6 lbf*ft.

5.2 Axial Drag Reductions

After the initial forces were estimated, the team investigated ways to reduce these forces. Since the majority of the torque produced is from the thrust force of the rotor, the team looked at ways to reduce this thrust force. However, it was found that this would result in decreased performance in the power curve performance task. The team decided to prioritize decrease the drag on the nacelle and tower in order to improve the foundation durability without sacrificing power output.

To accomplish a reduction in drag on the tower, the team decided to create a streamline attachment to slide over the tower to reduce the pressure drag. The streamline chosen was an EPPLER 863 strut airfoil. This was chosen for two reasons. The first was due to the high percent thickness, allowing the full length of the airfoil to fit within the 15cm tower diameter requirement. A top view of this attachment can be seen in Figure 13. The second reason was the relatively low drag coefficient, minimizing the load on the foundation.

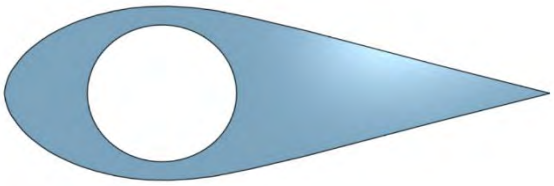


Figure 13: EPPLER 963 Airfoil Tower Attachment

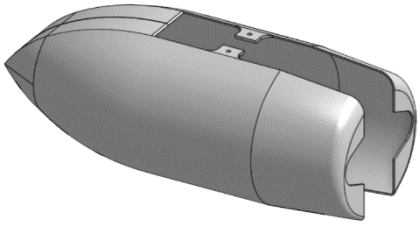


Figure 14: Streamlined Nacelle Covers

Similarly, the nacelle was also streamlined to reduce pressure drag. This was done through creating covers that tapered down to a point, mimicking the design of an airfoil, seen in Figure 14.

5.3 Load Cell Testing

To better determine the forces the foundation will be subject to, the team decided to devise a test to measure the horizontal drag forces. This was done through using a 10 kg load cell attached to the bottom of an extended tower that was designed to pivot about an axle. The turbine would then push against the load cell in the opposite direction of the incoming wind as seen in Figure 15. To calibrate the load cell, the team used a scale to pull at a known weight and inputted the value into the Arduino calibration code.

With this testing set up in combination with a cup anemometer, the team is able to estimate the drag forces on the turbine. After having done initial tests, the team noted that the maximum thrust output at approximately 15 m/s was on the order of 2 lbf, or 9 N. Referring to Figure 12 in section 5.1, this is slightly lower than the blades theoretical limit.

It should be noted that there are a few limitations with the current testing setup, mainly that the tower length above the pivot point is not identical to the competition tower length, and the drag on the tower below the pivot point will counteract the thrust force. Additionally, it was noted that the turbine created vibrations that are not easily replicable when testing the foundation.



Figure 15: Axial Thrust Force Testing Apparatus

5.4 Design Iterations

At the beginning of foundation testing, the team focused on the structure weight portion of testing. The first foundation prototype was a mesh box design intended to resist the predicted thrust force of 42 N. Due to the uncertainty of the sand properties, the team determined that it was essential to immediately begin testing procedures. After building the mesh prototype and testing apparatus similar to the one that will be present at the competition, foundation testing data could be collected. The mesh design resisted less than 4 N of force acting at the location of the hub and was therefore redesigned for a better performance.

The next design iteration made use of multiple “sand screws” that would be inserted into the ground and intended to maintain the stability of the foundation. 3D printed sand screws of various geometries were

created for testing purposes. After conducting similar testing to the mesh box, the team found that none of the sand screws designed were able to resist the estimated thrust loading.

The third design iteration was a steel box that would be inserted into the sand depth and then filled with sand to act as a weighted foundation. Multiple box geometries were created and tested including a box design with an angled backplate that was intended to make use of compressive forces in the sand. The highest amount of blade thrust force the box designs could resist was 11 N. The team tested the same steel box design and added 37.5 lbs of weights to the box. The weighted box resisted 42 Nm which had the best performance.

The design iteration process began with several lightweight structures that did not perform as well as anticipated. Due to potential improvements in the overall points scored at competition as well as preventing possible damage to the turbine, the priority shifted from weight reduction to durability.

The final design consists of a 25 x 25 cm 3/16 in thick steel plate with a 1.5 in steel tube welded to the center. Two threaded rods were then welded to the front half of the steel plate. Multiple 25 x 10 x 2.5cm steel blocks had holes drilled through them to allow them to fit over the threaded rods. A total of six blocks can be added, giving a final weight of 70 lbs, or 31.7 kg. Based on the maximum moment of 32 N*m calculated in Section 5.1, the factor of safety against tipping for this design is 1.84.

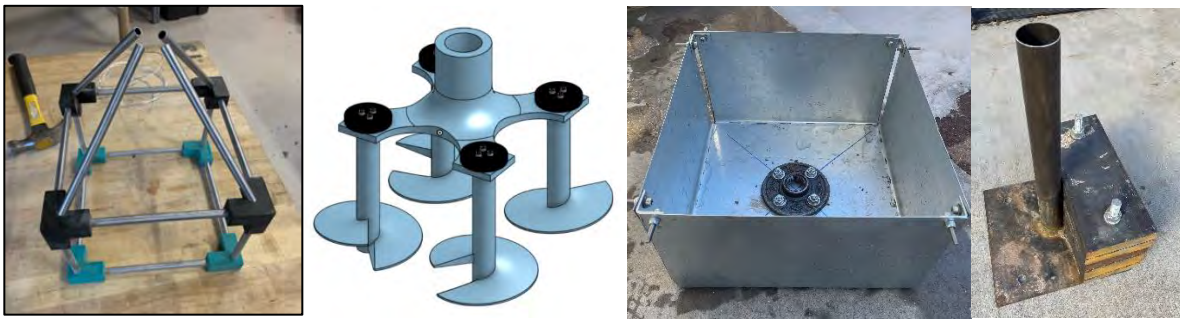


Figure 16: Foundation Design Iteration Method from Oldest (Left) to Most Current (Right)

5.5 Installation Procedure

The competition requires that the foundation design be installed into the testing facility without any of the team members' hands touching the water. For the installation process, the team has designed a square steel perimeter box (Figure 17) that slides into the sand. The steel perimeter box is dimensioned with an opening of 25 x 25cm that fits around the foundation and extrudes out of the water, allowing the team to hold onto it without touching the water. This installation tool also contains markings near the top of the waterline that depict how far into the sand the box should be installed.

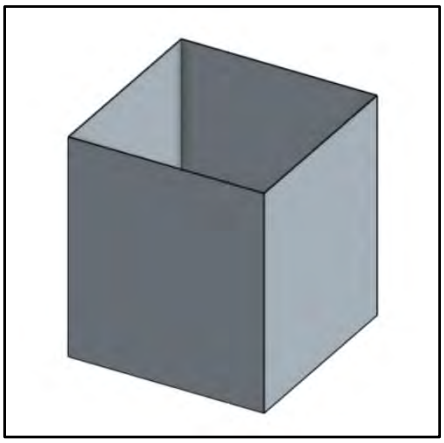


Figure 17: Installation Perimeter Box

The first step of installation is sliding the installation perimeter box into the sand until the waterline reaches the indicated marking. A long shovel is then used to dig out the sand within the box without touching the water. The sand removed from inside the box is simply dumped outside of the box. Once the team has dug out all the sand to the bottom of the perimeter box, a garden hoe is then used to remove any sand in the corners of the box. The garden hoe is

also used to pack down the sand at the bottom of the box and creates a flat surface for the foundation to rest. The foundation is then lifted by a team member and carefully dropped into the perimeter box until it is fully resting on the sand at the bottom. The perimeter box is then slid out of the sand and the excess sand surrounding the foundation is compacted. This completes the installation process.

5.6 Foundation Testing

The foundation was subjected to one test, a moment arm test. The foundation was installed as the team plans to do in competition. Then a fish scale was attached to the top of the tower, where the thrust force from the nacelle will act on the tower. The scale was then pulled until the tower moved more than 6 mm; the force needed to move the tower was recorded. The moment arm test was completed for every foundation design concept our team built.



Figure 18: Foundation Testing Setup

6 Mechanical Design

6.1 Nacelle

The nacelle is designed to provide mounting locations for both linear actuators, the generator, the shaft bearing, the linear bearings, the covers, and tower connection. The design went through two main iterations from the first to the second semester. The initial design consisted of a flat plate with slots to provide easy modification and design flexibility when designing the mounts for all subsystems. Once the team had decided on the overall nature of each subsystem, the nacelle went through a complete redesign.

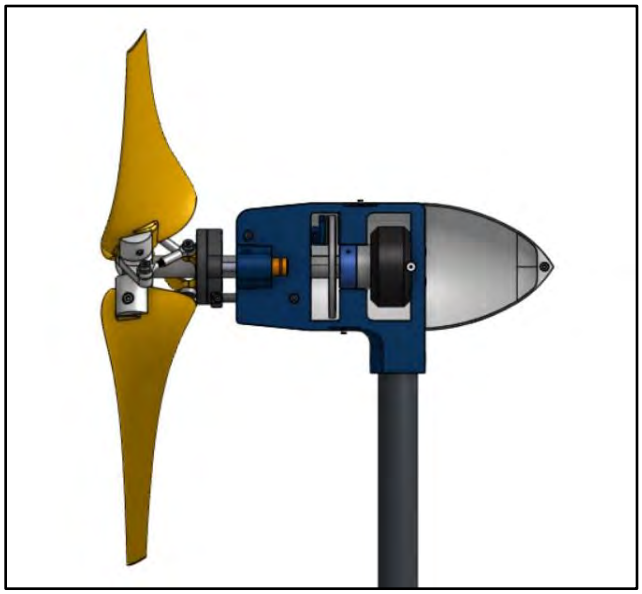


Figure 19: Wind Turbine Full CAD Model Internal View

This redesign was focused on reducing the size and part count of the turbine. Size reduction was prioritized in order to reduce the axial drag on the nacelle, and thus reduce the load on the foundation. The tower mount was also shifted towards the back of the nacelle in order to keep the mass of the turbine in front of the foundation's point of rotation. The current nacelle consists of only two 3D printed parts with various heat-set inserts used in order to provide reliable threads for subsystem attachment. The rear of the nacelle provides the mounting locations for the tower, generator, and stationary brake pad while the front holds the shaft bearing and linear bearings for the pitch system. Both actuators are imbedded within the front of the nacelle and various channels were designed to provide adequate cable management.

6.2 Pitching

The pitching system is designed to change the angle of all three blade simultaneously. The system will be used to prevent aerodynamic hysteresis and add redundancy to the braking system. The system is comprised of a linear actuator, a linear swash plate, three push rods, and three blade hubs. The blades are connected to the shaft via the hub pieces as seen in Figure 20, and these parts allow the blades to rotate around the bolt attaching the hub to the shaft. The push rods attach the hubs to the linear swash plate. The push rods are made up of two ball joints at each end of the rod, the ball joints allow the geometry of the system to change when pitching. The linear swash plate allows the inner disk to rotate with the rotation of shaft while holding the outside side steady in order to attach it to the linear actuator. The linear actuator is mounted to the nacelle and the piston rod is mounted to the linear swash plate. As the piston rod extends and retracts the blades all change angle in unison.

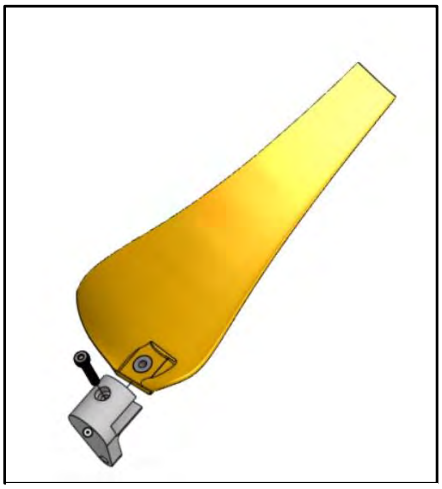


Figure 20: Blade and Hub Assembly

The entire system is controlled with a single linear actuator which means that the linear actuator chosen for the system must be able to withstand the force acting on it from the pitching moment. In order

to calculate the pitching moment created by the blades, the team had to first complete an analysis of the pitch mechanism geometry.

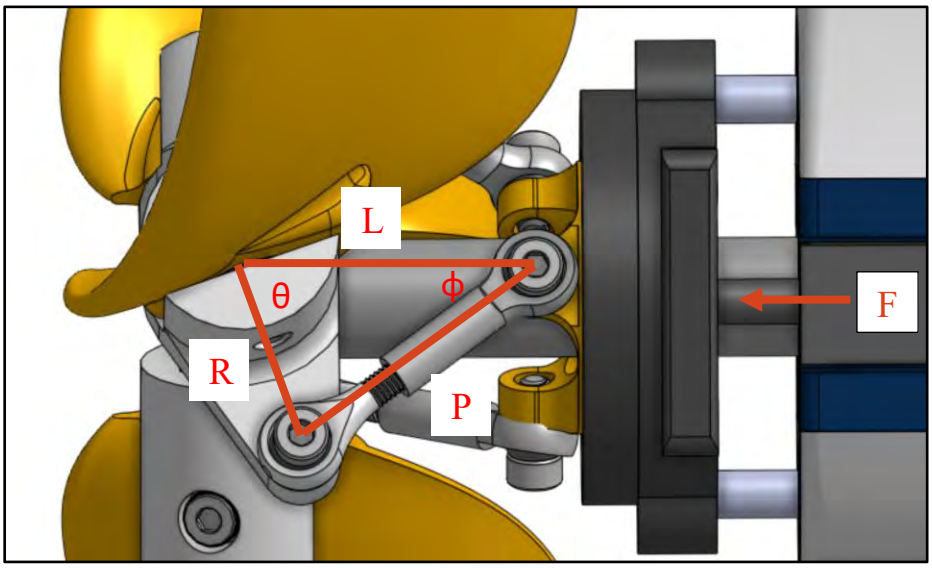


Figure 21: Pitching System Geometry

As seen in Figure 21, the pitch system has a constant hub length, R, and push rod length, P, but changes in length on the shaft, L, due to the change in the linear actuator piston rod length. The change in length causes the angles θ and φ to also change. The change in φ can be described using Equation 3. The total force can then be described using Equation 4, where M is the pitching moment for one blade. The force equation is specific to the geometry of the system. Once the previous two equations were developed, the total pitching moment for one blade was calculated elementwise using Equation 5.

$$\varphi = cos^{-1}\sqrt{1-(R/L)^2 \sin(\theta)^2} \qquad \text{Eqn 3}$$

$$F = \frac{3Mcos(\varphi)}{Rcos(90-\theta-\varphi)} \qquad \text{Eqn 4}$$

$$M = C_M(1/2)q_\infty {U_{rel}}^2 Ac \qquad \text{Eqn 5}$$

The variables in the Equation 5 are defined as follows: C_M is the moment coefficient of an airfoil at a specific Reynolds number, q_∞ is the dynamic pressure, U_{rel} is the wind speed relative to the blade, and A is the chord length, c, times the span, S. The geometry of the blade was gathered from the program QBlade, and the moment coefficient was gathered from Airfoil Toolbox [4] for a GOE79 airfoil. The team then calculated the relative velocity of the wind at each section of the blade, followed by calculating the pitching moment at each section of the blade. The air density was assumed to be standard air density at sea level. The following table shows the elementwise calculations for one blade:

Table 1: Blade Pitching Moment Analysis

	Blade Section	Chord Length (m)	Section Arean (m^2)	Local TSR	U relative (m/s)	Section Pitching Moment (Nm)
1	1	0.0491	4.9056e-04	0.5998	25.6540	0.0010
2	2	0.0523	5.2307e-04	0.8314	28.6103	0.0014
3	3	0.0511	5.1087e-04	1.0630	32.1073	0.0016
4	4	0.0480	4.8046e-04	1.2946	35.9879	0.0018
5	5	0.0445	4.4482e-04	1.5261	40.1410	0.0020
6	6	0.0410	4.0964e-04	1.7577	44.4902	0.0020
7	7	0.0377	3.7715e-04	1.9893	48.9834	0.0021
8	8	0.0348	3.4798e-04	2.2209	53.5844	0.0021
9	9	0.0322	3.2209e-04	2.4525	58.2676	0.0022
10	10	0.0299	2.9921e-04	2.6841	63.0148	0.0022
11	11	0.0279	2.7898e-04	2.9157	67.8124	0.0022
12	12	0.0261	2.6105e-04	3.1472	72.6505	0.0022
13	13	0.0245	2.4510e-04	3.3788	77.5215	0.0022
14	14	0.0231	2.3086e-04	3.6104	82.4196	0.0022
15	15	0.0218	2.1808e-04	3.8420	87.3402	0.0022
16	16	0.0207	2.0657e-04	4.0736	92.2798	0.0022
17	17	0.0196	1.9616e-04	4.3052	97.2353	0.0022
18	18	0.0187	1.8671e-04	4.5368	102.2046	0.0022
19	19	0.0178	1.7810e-04	4.7683	107.1856	0.0022
20	20	0.0170	1.7021e-04	4.9999	112.1769	0.0022
21	21	0.0163	1.6298e-04	5.2315	117.1771	0.0022

The summation of the pitching moment on each section of the blade was then used in the previous force equation with the system geometry to find the total force required for our linear actuator. Figure 22 describes the force required for the range of angles in our system.

The greatest force the linear actuator is required to hold is 11.17 N. The linear actuator being used is the PQ12-100-6-R Micro-Actuator. This linear actuator has a hold force of 50 N, giving the system a factor of safety of 4.48.

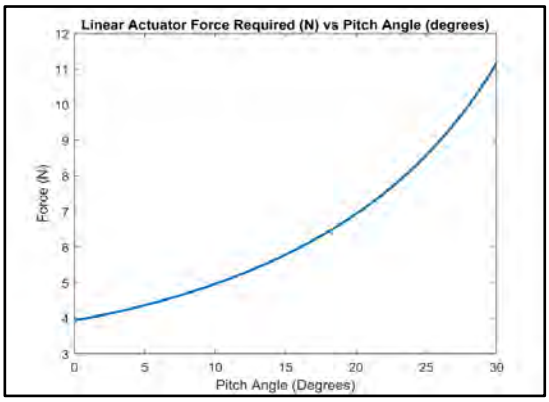


Figure 22: Linear Actuator Force Required vs Pitch

6.3 Brakes

The brakes use a linear actuator with a mounted brake pad to press against a sliding brake disc, compressing the disc with a secondary brake pad fixed to the nacelle. The actuator pad uses a 3D printed mount and both brake pads are made of neoprene rubber. The aluminum disc was manufactured using a CNC router. The chosen actuator is a micro linear servo capable of producing 50 N of force. The brake disc has a diameter of 7.2 cm giving the turbine a theoretical braking force of 3.6 N-m. The design was chosen by the equations for angular momentum and impulse.

The brake system also underwent two different tests: a static test and a dynamic test. The static test had the brake engaged and weight added to the radius of the disk brake. The weight on the radius of the disk brake created a moment on the system. Weight was added until the brake failed, in turn allowing the shaft to spin. While the static test did not show that the brake provided adequate force for the system, the dynamic car testing showed that the system sufficiently decelerated and could

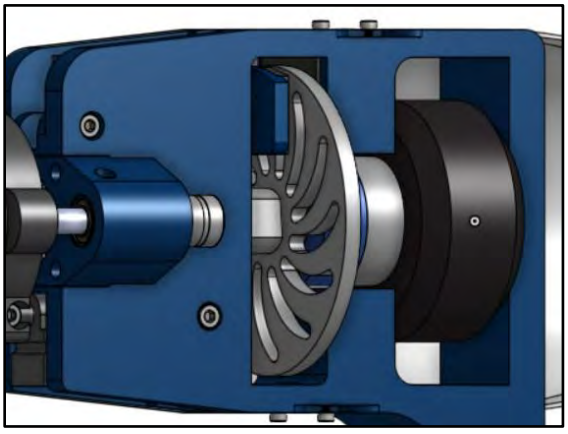


Figure 23: CAD Disc Brake Mechanism

withstand 22 m/s winds without brake failure. The team theorizes that this is due to rapidly decreasing the TSR of the blades and thus reducing the torque generated by the blades.



Figure 24: Static Brake Testing Apparatus

6.4 Tower and Yaw

The tower has been welded to a 0.5-inch-thick steel baseplate. In order to ensure that the weld can resist the forces acting on the tower, a load analysis was conducted to determine the minimum throat length of the weld necessary to maintain structural integrity. The forces acting on the tower were assumed to be equivalent to the axial thrust forces at the location of the nacelle (calculated previously as 42N). The force acting at the top of the tower, the diameter of the tower and the ultimate tensile strength of the welded material were used to estimate the specific weld size. The direct shear stress and bending tensile stress were calculated from Equations 6 and 7 and then combined in Equation 8 for a resultant stress at the weld location [5]. Eq. 9 was then used to find the minimum throat length to resist the estimated force.

$$\tau_s = \frac{Force}{Unit\ Throat\ Length} \quad \text{Eqn 6}$$

$$\tau_b = \frac{Moment * Y}{Unit\ Moment\ of\ Inertia} \quad \text{Eqn 7}$$

$$\tau_r = \sqrt{{\tau_s}^2 + {\tau_b}^2} \quad \text{Eqn 8}$$

$$throat = \frac{\tau_r}{Design\ Strength} \quad \text{Eqn 9}$$

From the above calculations it was determined that having a throat length of 3mm on for the weld will result in a factor of safety above 15. The team assessed this as adequate for maintaining the structural integrity of the tower and baseplate and moved forward with the weld design.

The yaw system is a simple bearing surface with a pin to prevent rotation after foundation installation. A loading force acting on the nacelle is expected to occur and cause stress at the location of the yaw. The team needed to assess the amount of force that could be placed on the yaw without causing the nacelle to fail. Through testing (Figure 25), the nacelle yaw was able to resist approximately 222 N of force. Compared to the expected thrust force acting on the nacelle of 42N, this is a minimum factor of safety of 5.



Figure 25: Nacelle Yaw Loading

7 Electrical System Design & Analysis

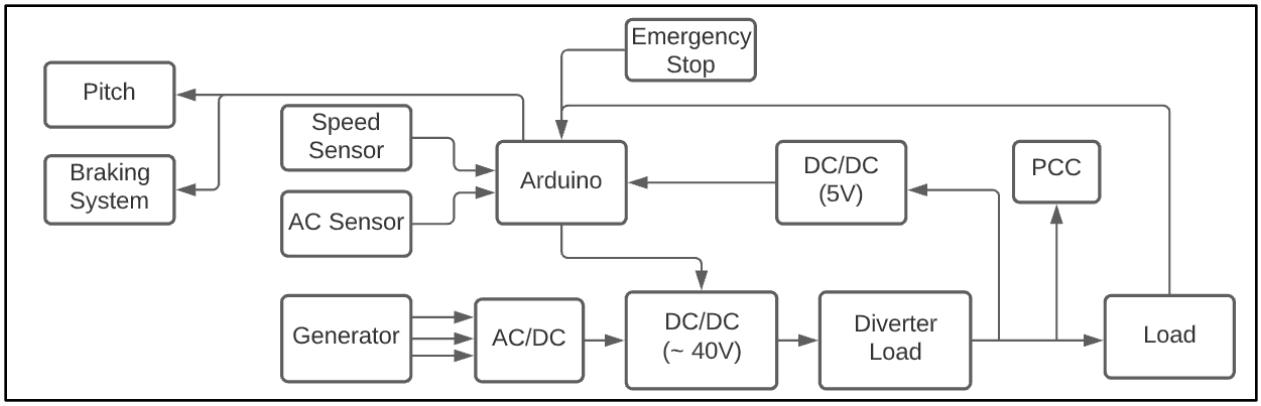


Figure 26: Electrical System Architecture

7.1 Generator

The selected generator for the electrical system was the MAD IPE 5012 160kV motor. The relatively low kv rating of the motor allows for the team to utilize a boost converter for all windspeeds expected at competition. The motor's higher efficiency than competitors at low RPMs made it an ideal candidate for selection in our design for the competition. Additionally, it only reaches about 54 °C after 5 minutes at maximum power output, which was significantly lower than that of its competitors [6].

7.2 AC/DC

A three-phase full wave bridge rectifier, Figure 27, is used to convert the three-phase output of the generator into a DC voltage. The DC voltage then goes through a capacitor of 10µF to help reduce the ripple created by the rectifier. This unit was purchased to help reduce the power losses compared to building one with 6 individual diodes.

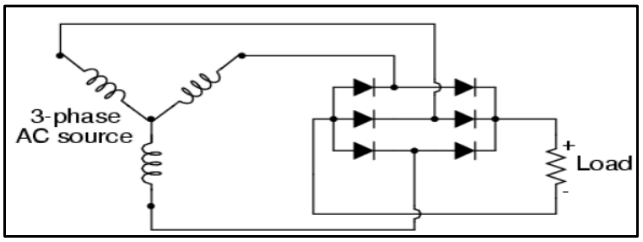


Figure 27: Three-Phase Full-Wave Bridge Rectifier

7.3 DC/DC Boost Converter

The main system is the DC/DC boost converter, Figure 26, this system consists of: 98.5µH inductor, N-channel power MOSFET, diode, and 100µF capacitor. The microcontroller in our system is the Arduino MEGA 2560 coded with MATLAB Simulink. The Arduino will take the output voltage from a voltage divider connected to the output of our system. Depending on the output voltage the duty cycle of the square wave going into the MOSFET will change from 20% to 60% as shown in Figure 28. This control in the duty cycle allows the voltage at the output to be controlled and limited to a maximum of 40 V.

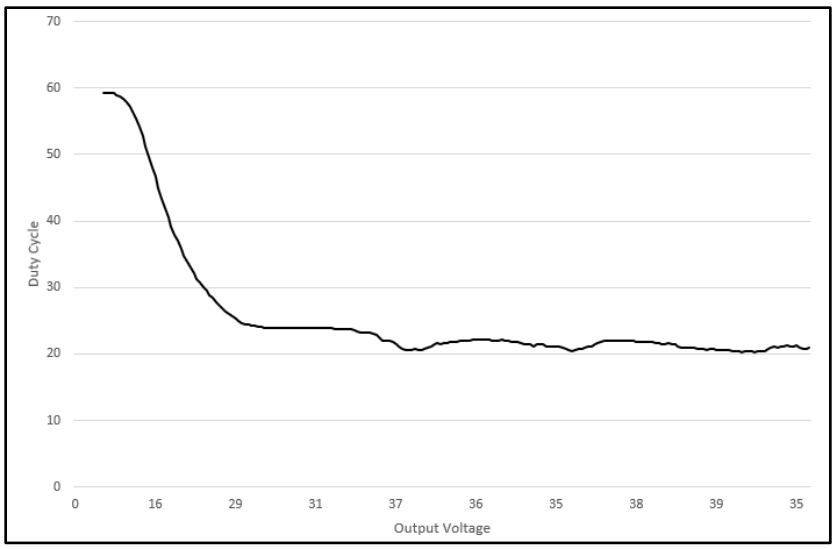


Figure 28: Duty cycle compared to Output Voltage

7.4 Diverter Load

Another important electrical system is the diverter load, Figure 26. The diverter load consists of twelve 10 Ω 100W rated resistors to make an equivalent resistance of 4Ω at 1200 W. This system is controlled by an N-channel power MOSFET used as a switch. The Arduino takes the output voltage and current sensor data to determine if a signal needs to be sent to the gate. If the current is zero, that indicates that the load is disconnected and the MOSFET will turn on, giving power to the diverter load. Within the Simulink code, power is also calculated. If output power reaches a certain value, in our case 40V to give the system some error before reaching the competition maximum of 48V in the case of a runaway or quick RPM boost, the MOSFET will turn on to not exceed that power output. Along with the DC/DC boost converter, this system will also regulate the system voltage when needed. It regulates the power of the system through the dissipation of heat into the large heat sink as seen in Figure 29.



Figure 29: Diversion Load

7.5 Printed Circuit Board

The system in Figure 26: Electrical System Architecture, is implemented onto a PCB. Wire connections are used for the generator, Arduino, diverter load, DC/DC buck converter, and load. The AC/DC Converter, DC/DC boost converter, and sensors are built onto the PCB. All the components on the PCB are through-hole compatible since through-hole components are easier to find higher rated devices for. The PCB is a 2-layer design with top traces shown in red and bottom traces shown in blue as seen in Figure 30. The traces are 1.02 mm equivalent to 18 AWG allowing the board to be rated for 10 Amperes. The board was purchased through JLC PCB.

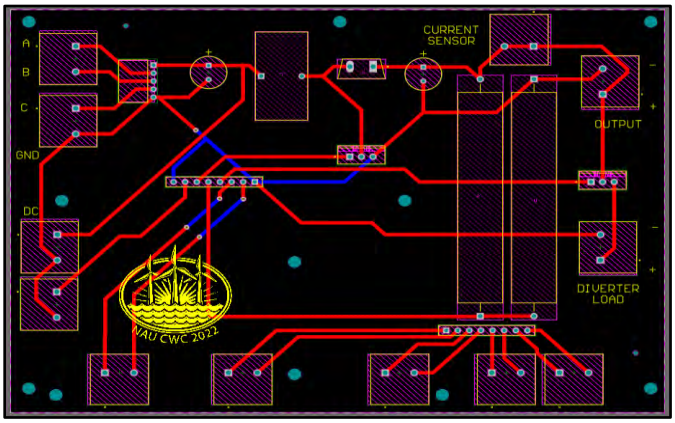


Figure 30: Electrical System Architecture

7.6 Load

The load for the system will be a power resistor capable of 200 W and around 2 Ω. When testing the system at different resistances such as: 15 Ω, 10 Ω, 4 Ω, and 2 Ω. It was found that at lower resistances the current drawn from the source and output current was much larger than when testing at higher resistances. Since the output current for our system can be a maximum of 10 A, the resistance of 2 Ω allows the most current: increasing our power output and efficiency.

8 Software Implementation and Testing

8.1 Software

The program that was used to control all electrical systems and the boosting of the boost converter was all done through MATLAB Simulink. Simulink allowed us to use block style programming and Arduino addon which helped make hardware uploading to the Arduino quite easy, this also helped make it easy to write the algorithms and was able keep everything clearly organized using subsystems for the various parts of the control system for the turbine shown in Figure 31. For testing, we

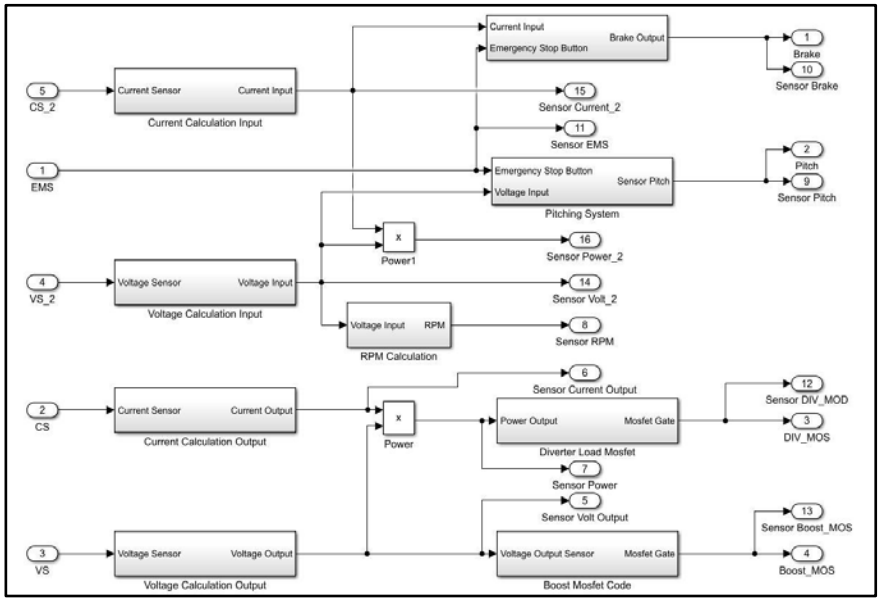


Figure 31: Main Control System Design

used sensor outputs that went to scopes in Simulink to help monitor the input and output data going to the Arduino. And we used another Arduino that read the actual pins going in and out of the main control Arduino and logged the data on an Excel spreadsheet.

9 Field Testing

9.1 Procedure

Before the completion of the full turbine testing, our team tested each subsystem individually. Each individual test allowed our team to gain a better understanding of what is to be expected in the full turbine test. The individual tests also provided our team with a factor of safety for each system, ensuring that each system will be strong enough before assembly. Each of the subsystem tests were completed multiple times to reduce random error with the exception of the tests that resulted in broken parts.



Figure 32: Car Testing Apparatus

Once the team completed individual tests for each subsystem and felt confident in the results gathered the team moved to full turbine testing. The full turbine test proved to be a challenge due to the wind tunnel at NAU not having a large enough test section for our turbine. As mentioned previously, our team designed and built an apparatus to mount our wind turbine on top of a car for testing as seen in Figure 32.

In preparation for car testing, our team assembled the entire turbine and mounted it to the testing apparatus, which was then mounted to the roof of a car. The wires for the motor and the two linear actuators were fed down the tower and into a window of the car. In the car, our team had all the electrical components, including our boost system, control system, and a PCC. A cup anemometer was also mounted in order to collect wind speed data. The PCC recorded the wind speed, voltage, and current of the turbine during each test. The pitch angle and the electrical resistance were changed independently, and values were recorded to compare the power output at various pitch angles and resistances. The axial drag induced on the foundation by the turbine was also tested in this system using the load cell discussed in section 5.3. The team then recorded the thrust force on the nacelle at wind speeds up to 22 m/s. The data provides an estimate for the moment that the turbine will experience at competition.

9.2 Results

During the car testing performed on the entire turbine system, the blades, pitch, brakes, and force acting on the foundation were assessed. Before car testing began, individual tests were conducted on the turbine subsystems to prove the durability and safety of each system. The following discussion determines the reliability and functionality of the designed wind turbine.

The primary form of testing conducted by the team was through car testing. The blade performance, pitch degree performance, and braking performance were all analyzed by this test. In addition to testing the individual subsystems, the overall functionality of the turbine was evaluated. All the subsystems were able to work in unison during car testing to generate power, resulting in a functional turbine. The pitch angle of the blades was changed to find the angle that would generate the greatest amount of power. The pitch angle for startup speeds and slow down speeds were also determined through car testing. It was determined that

the turbine could be completely stopped through the pitching mechanism. This reduces the rotation of the blades and allows for the disc brake system to act as an additional brake for safety purposes.

10 Changes from Last Year

This year's team was not involved with the design and construction of last year's turbine, so much of the current design is new. The four main subsystems that were inspired by previous years were the pitching, braking systems, and electrical system of last year and the composite blades from the 2014 team.

The pitching system from 2021 was designed around the traditional swash plate mechanism but was driven by a motor geared to a rack and pinion system. After discussions with the graduates of that team, it was found that they encountered difficulties in supplying enough force to counter the pitching moment of the blades with this design. Additionally, the design took up significant space inside the nacelle body. As a result, the team used the initial swash plate concept but redesigned with nacelle to accommodate a lead screw design initially, and eventually a linear actuator. The sliding disk brake was also inspired by last year, as well as the many other past teams from both NAU and other universities that utilized a similar system.

The electrical system took inspiration from the previous year's team with: the three-phase full wave bridge rectifier, DC/DC boost converter, and resistive load. The main changes for this year were: using MATLAB Simulink to code the Arduino MEGA 2560, designing the diverter load, designing the DC/DC boost converter, and designing a PCB for the system.

The manufacturing process of the blades was initially inspired by the 2014 team's split mold method. However, after initial prototype blades were made using this method, it was found that the process to re-manufacture the molds for new iterations of the blades was extremely time consuming. As a result, the team branched off into vacuum bagging composite material around a 3D printed core as this allowed for both rapid design iteration but also strong and rigid blades. This was an entirely new process for everyone on the team and took a significant amount of trial runs to reach the current state of the blades.

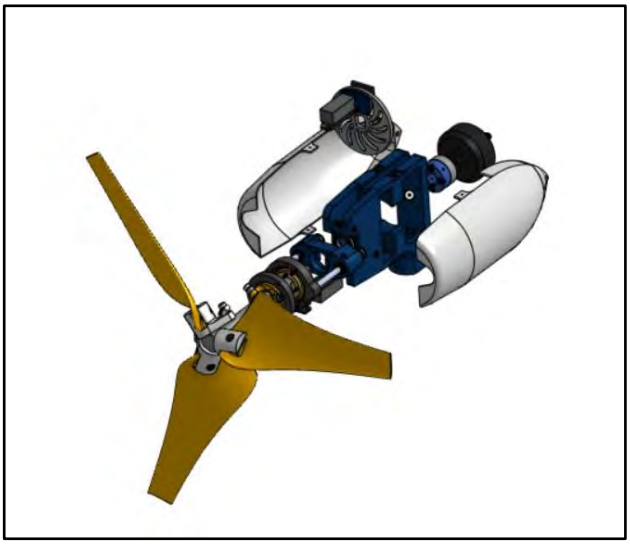


Figure 33: Turbine Exploded View



Figure 34: Assembled Turbine

11 References

[1] "U.S. Department of Energy Collegiate Wind Competition 2022," 14-Oct-2022. [Online]. Available: https://www.energy.gov/sites/prod/files/2020/10/f79/cwc-2021-rules-requirements.pdf. [Accessed: 29-Nov-2021].

[2] J. F. Manwell, J. G. McGowan, and A. L. Rogers, *Wind Energy explained*. Chichester: John Wiley, 2002.

[3] P. J. Pritchard, J. C. Leylegian, R. Bhaskaran, J. W. Mitchell, and R. W. Fox, *Fox and McDonald's introduction to Fluid Mechanics, 9th edition*. Wiley, 2015.

[4] "GOE79 (PFALZ 11) AIRFOIL," [Online]. Available: http://airfoiltools.com/airfoil/details?airfoil=goe79-il

[5] S. Ghosh, "Fillet weld strength calculation example for welded connection subjected to bending," *mechGuru*, 19-Oct-2019. [Online]. Available: https://mechguru.com/free-caculator/weld-strength-calculation-example-for-bending-moment-application/. [Accessed: 24-Apr-2022].

[6] "Amazon.com: Mad components 5012 IPE v3.0 160KV brushless ..." [Online]. Available: https://www.amazon.com/MAD-COMPONENTS-Multirotor-Quadcopter-Hexrcopter/dp/B08K482875. [Accessed: 25-Apr-2022].

12 Appendix/Photo Collection

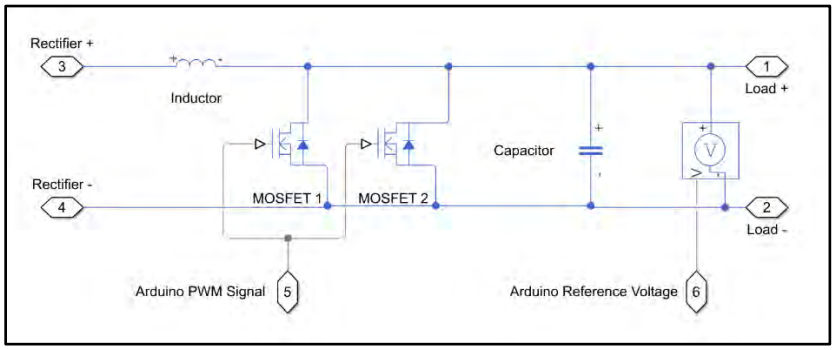


Figure A1: DC/DC Boost Converter

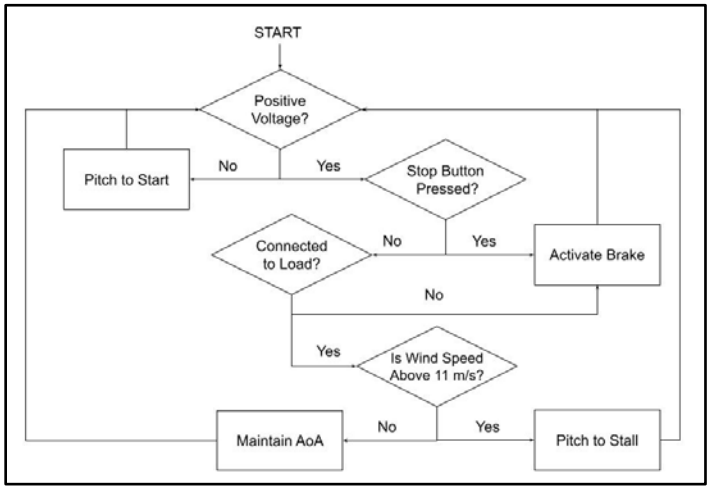


Figure A2: Control Flow Diagram

CU BOULDER WIND TEAM

2022 - 2023

TECHNICAL DESIGN FINAL REPORT

Prepared for Collegiate Wind Competition 2023

STUDENT LEAD:

Jeremiah Pare – Project Manager

jeremiah.pare@colorado.edu

TECHNICAL DESIGN TEAM:

Regan Barton – Environmental Engineer
Ariana Carmody – Financial Manager
Chris Holladay – Environmental Engineer
Will McConnell – Electromechanical Engineer
Lauren Mullen – Logistics Manager
Luis Munoz – Environmental Engineer
Rhett Nutter – Systems Engineer
Amanda Shields – Test Engineer
Ethan Smith – Electrical Lead
Ryan Stoltz – Manufacturing Engineer
Ryan Tasto – CAD Engineer
Heather Walker – Electromechanical Engineer

FACULTY ADVISOR:

Roark Lanning

roark.lanning@colorado.edu

TABLE OF CONTENTS

1. EXECUTIVE SUMMARY **2**

2. DESIGN OBJECTIVES **2**

3. NEW THIS YEAR **3**

4. ROTOR DESIGN **3**

4.1 Blades 3
4.2 Pitching System 6
4.3 Nacelle 8

5. STRUCTURE AND FOUNDATION DESIGN **10**

5.1 Tower 10
5.2 Foundation 10

6. ELECTRICAL DESIGN **11**

6.1 Electrical Diagram 11
6.2 Turbine PCB 12
6.3 Load PCB 12
6.4 Control Model Analysis 13
6.5 Software Architecture 13

7. FULL ASSEMBLY **14**

7.1 Final Turbine Assembly 14
7.2 Commissioning Checklist 15
7.2 Testing 16

8. LOOKING FORWARD FOR FUTURE CU WIND TEAMS **18**

REFERENCES **19**

1. EXECUTIVE SUMMARY

The University of Colorado Wind Competition Team has detailed the technical design of a small-scale wind turbine in this report. The turbine specifications follow the rules and regulations outlined by the U.S. Department of Energy (DOE) Collegiate Wind Competition (CWC). This is the third time the CU Wind Team will be participating at the Collegiate Wind Competition, and the second time competing in phase two. This year's team has been able to build on previous years' successes and learn from their failures. The main design goals for this year were consistency and robustness.

To meet these design goals, several areas of the design were prioritized. Namely, an in-depth blade analysis, an upgraded pitching system, increased focus on emergency stop, and the addition of an anemometer to simplify the control theory. Blade design had a slight oversight last year, and so the team started the design with an in-depth analysis of several airfoils and blade configurations. The idea was to design everything else around the blades. Using Qblade, the team analyzed over 30 different configurations and landed on the E216 blade design with a maximum C_L/C_D ratio of 43 and a maximum power coefficient of 0.54 at a tip-speed-ratio (TSR) of 3. After taking advice from the trials faced by the wind team last year, the team realized that designing a strong active pitching system would be critical to both the power generation and the emergency stop function. This active pitching system combines an original mechanical design with an optimized controls system to maximize consistent power generation at various wind speeds. The pitching system is also a critical piece in the emergency stop solution. Last year's team struggled with the emergency stop test during the competition, so this was a focus for the team. The emergency stop is accomplished using a triple redundancy system. When activated, the system will short the generator, pitch the blades to a negative angle, and a mechanical brake will be activated. To simplify the control theory, an anemometer, which will be mounted on the turbine tower, was added to the turbine design. The controls use this wind speed input to determine which control state to operate in. These additions and upgrades have helped to increase the robustness and consistency of the turbine's performance.

Other iterations in the turbine design include the foundation, simplified height adjustment, addition of a nacelle cover and the use of one microcontroller. The "offshore" turbine foundation builds on last year's suction bucket design but includes further optimization and manufacturing through thorough testing and prototyping. The team was able to hire a professional welder to manufacture the new suction bucket. The height adjustment piece was simplified to being a simple concentric steel insert with multiple configurations to adjust the height. Once the nacelle was fully assembled, a cover was designed, and 3-D printed to keep the enclosure secure and reduce drag on the components. To simplify the electronics, the team also opted to use a single microcontroller.

Overall, the turbine design has been upgraded from the previous years by consulting with industry experts, other team's final reports and team members from last year. Important lessons were learned through previous successes, failures, and rigorous testing. The team is confident the new design will perform as advertised during the competition. A large focus this year has been to create the CU Wind Team legacy both at the University of Colorado Boulder and in the CWC space.

2. DESIGN OBJECTIVES

Last year's team was the first CU team to compete in Phase Two of the CWC and their goal was to design mainly for functionality. The objective of this year's design was to design a small scale "offshore" wind turbine that will perform at competition robustly and consistently. This year, the team prioritized power generation optimization in order to make the highest performing and consistent small-scale wind turbine. This year's design focused heavily on the pitching system, blade design, emergency stop, and the controls systems. The team designed an original mechanical pitching system focusing on durability and creativity. Blade design included several iterations and explorations of different airfoils and chord lengths that were optimized to maximize the C_p value in Qblade. The emergency stop includes three different functions in order to ensure proper stoppage. The controls system was prioritized early in the academic year by

implementing more sensors, namely an anemometer, to simplify the control theory. With these additions, the team was able to make a fully functional, robust turbine that is more consistent in its performance than in previous years.

3. NEW THIS YEAR

Building on the previous year's design, the team determined early that the focus of the turbine design was to increase consistency and performance during testing, increase the design's robustness, and overall aesthetic. To begin improvements for this year's design, the team first discussed points of failure from last year as well as points of emphasis that team members felt passionate about improving. The previous year had issues with their pitching mechanism, mostly due to outsourcing the assembly from a toy helicopter that was built of many fragile plastic components. Additionally, they failed to properly perform the emergency stop function during the competition. Further sources of improvements are presented in the list below and explained in more detail in their corresponding sections:

- Iterated foundation design, early testing, outsourced welding
- Simplified height adjustment piece
- Extensive blade design analysis, including 30+ iterations
- Redesigned original pitching system to be more robust
- Wind speed sensor integration through a hot wire anemometer
- Constant resistance load instead of variable resistance
- Earlier emphasis on control theory
- Single microcontroller for simplicity
- Triple redundant emergency stop system
- Addition of nacelle cover for aerodynamics
- Emphasis on overall aesthetic of design
- Emphasis on team dynamics and culture

4. ROTOR DESIGN

4.1 Blades

The blades are designed to maximize power output while considering parameters that reflect the scale of the turbine and competition conditions. A horizontal axis wind turbine (HAWT) was chosen for the prototype design due to the high energy conversion efficiency compared to other turbines, resulting in a higher power output. Three blades were chosen for the turbine to increase stability and energy yield. Qblade simulations were used to finalize the blade design since the software effectively utilizes blade element momentum (BEM) theory to optimize the chord length and angle of twist at each cross section of the blade to yield the maximum power output possible. Multiple blade designs were considered by uploading various airfoils and applying parameters consistent with competition conditions to obtain accurate results.

Competition conditions input into Qblade included a range of wind speeds, rotor size, Reynolds number, and tip-speed-ratio (TSR). A wind speed of 8 m/s was used to determine the appropriate Reynolds number and TSR since this is the average of the critical wind speeds that the team will be tested at during the power curve test. A Reynold's number of approximately 50,000 was chosen based on air density, the average wind speed, the average chord length of the blade, and the kinematic viscosity of the air. The team also decided to design the blades around a constant TSR to maintain a consistent airflow angle over each blade element. A TSR of 3 was chosen due to the turbine's small rotor radius of 20 cm, average RPMs expected, and average wind speed expected in competition. Typically for 3 bladed, full-scale turbines, a TSR of 4-5 is chosen, but since the turbine is so small, a TSR of 3 was more suitable. This decision was confirmed by running simulations in Qblade, which proved that optimizing the blades to a TSR of 3 maximized the power output and C_p more than any other value (Figure 1). In addition, power output, C_p, speed, and torque data from QBlade provided information that helped the team determine generator

requirements. After deciding the correct parameters to design the blades around, the next step was to choose the appropriate airfoils.

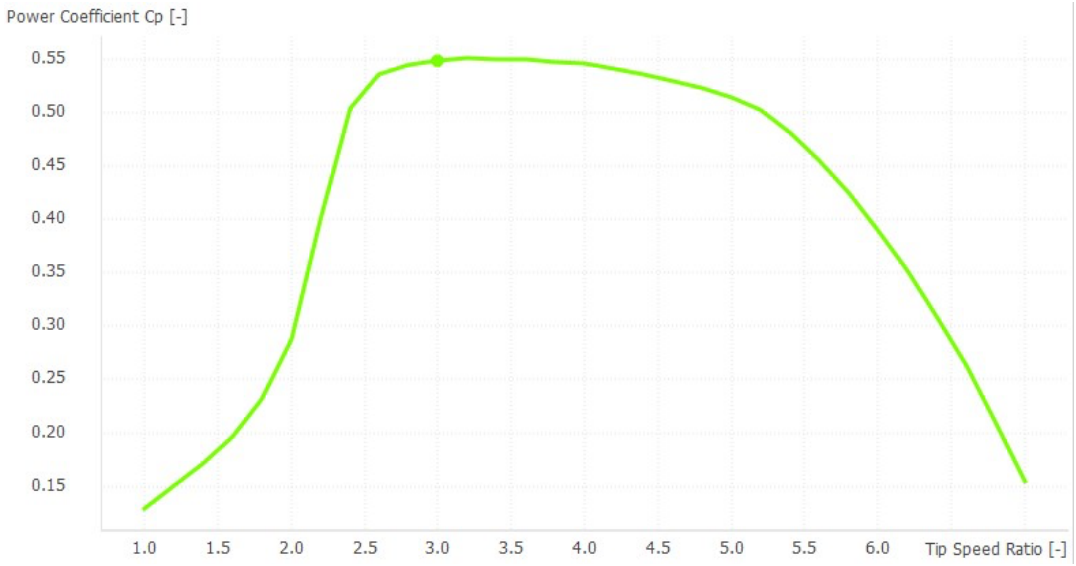


Figure 1: Cp-Lambda Curve for Final Blade Design

Four design goals were considered when designing the blades. The first design goal was to select airfoils with a thickness range between 10%-14% since the blade must be structurally sound yet still aerodynamically favorable. The second design goal was to pick airfoils with high C_L/C_D ratios since more lift creates more torque, which results in a larger power output. The third design goal was to only use one airfoil throughout the whole blade since using two or more airfoils of different thicknesses for such a small turbine can cause a disturbance at the transition [3], which noticeably increases drag. The last design goal is to pick blades that maximize the power output since this is the critical component for the power curve test in the competition. The airfoils considered for the final design were all downloaded from airfoiltools.com, which allowed us to sort through thousands of airfoils by applying the "Max Cl/Cd @ RE = 50,000" filter and inputting the desired range of thickness airfoil. Approximately 20 of the top airfoils on this list were uploaded into Qblade and were analyzed for maximum power production. The top performing airfoils included the E216, GOE79, Wortmann FX-160 126, and SG6042. The top three blade designs meeting each of the design goals were chosen and a decision matrix was created that weighed the importance of each goal and then scored each blade design for how well it met the design goal (Figure 2). The blade that scored the best was made of the E216 airfoil throughout the whole blade. The E216 blade design had a maximum C_L/C_D ratio of 43 and a maximum power coefficient of 0.54 at a TSR of 3.

			Score (1-3)	
Design Goal	**Weight (1-5)**	**Wortmann FX-60 126 & SG6042**	**E216**	**GOE79**
Structurally Sound (Thickness ≥ 10%)	5	3	2	1
High Cl/Cd	4	2	3	3
1 Airfoil	3	1	3	3
Power Output	5	2	2	1
	Total:	**36**	**41**	**31**

Figure 2: Blade Decision Matrix

To manufacture the blades, the team used a SLS Formlabs Fuse 1+ printer and printed the blades in Nylon 12 material because of its high strength and smooth surface finish (Figure 3). Nylon 12 was ideal for the blades because it is impact resistant and can withstand fatigue during high frequency cyclic loading. Bending and centripetal force tests were conducted to ensure that the blades did not break or detach from the rotor when subject to the maximum wind speeds of 22 m/s.



Figure 3: Rendering of Final Blade Design

Blade Deflection Test

The maximal normal load a blade is expected to experience at 22 m/s was calculated using Qblade to be 17 N. Additionally, a deflection test was performed to ensure the blade does not fracture or deflect enough to hinder the turbine's performance. For this test, the bushing was connected to the blade via a shoulder bolt, and a table clamp secured the bushing to the table with the rest of the blade hanging over the edge (Figure 4). The team tied a rope to the tip of the blade and connected a force gauge to the other end, slowly increasing the force until failure occurred. The blade failed at the root once the blade was subjected to 34.1 N (2" deflection), giving us a F.O.S. of 2.01. Because the F.O.S. was greater than 2, the team concluded that the blade design was strong enough to avoid failure at maximum wind speeds.

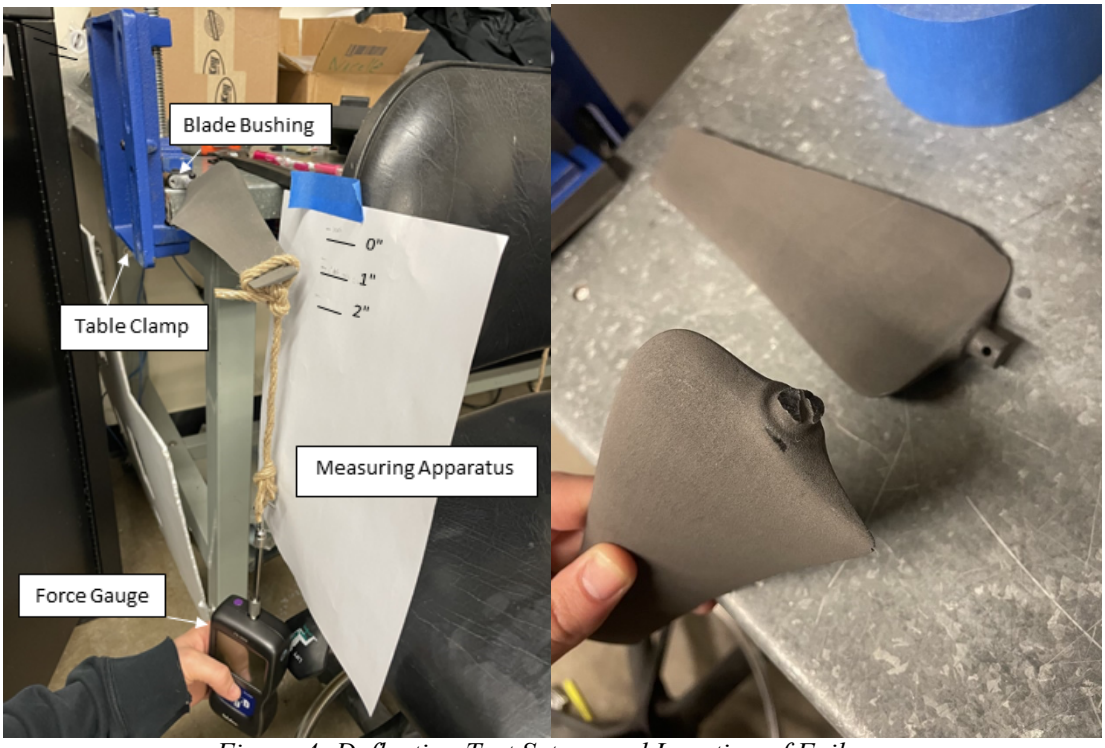


Figure 4: Deflection Test Set-up and Location of Failure

Centripetal Force Test

The purpose of the centripetal force test was to simulate maximum wind speeds of 22 m/s to confirm the blades and rotor assembly are strong enough to withstand all testing conditions. The highest expected

RPMs is less than 2000, but the team tested up to 2500 RPMs to take a conservative approach in case pitching fails. For this test, the team fully assembled the turbine and enclosed the rotor in a wooden box for safety purposes (Figure 5). The team used a battery to increment the RPMs by 200 up to a maximum of 2500. The team decided that if failure occurred before the turbine reaches 2500 RPMs, the design would have to be modified accordingly. The results concluded that the design is robust enough to withstand maximum wind speeds even if pitching fails since there was no failure from the blades or rotor at 2500 RPMs. This test discovered that the actuator screws loosen at high RPMs, but the team remedied this issue by applying Loctite to the thread.



Figure 5: Centripetal Force Test

Static Performance Analysis

A static performance analysis was conducted based on data collected from the area encompassing the proposed leasing blocks off the coast of Louisiana at a hub height of 1 meter. Specifically, the projected power curve of the turbine, including losses, was compared to the wind speed frequency histogram data collected in the project development portion of the competition to calculate the annual power production of the turbine. Using this analysis, the calculated annual energy production (AEP) was 44 kWh.

4.2 Pitching System

In order to both maximize the power during the power curve test and minimize the power during the emergency stop, the thrust produced by the blades needed to be controllable which was achieved through an active pitching system (Figure 6). Based on the previous team's performance, a robust yet simplistic design was the main objective which is why a custom metal subassembly was chosen. The active pitching centers around a swash plate design since the entire plate can translate linearly while each side of the plate has independent rotation. This allows for a device that is fixed to both the swash plate and the nacelle to translate the swash plate, while the other side can independently spin with the shaft. The linear movement of the swash plate is transferred through ball joint push rods that rotate L-shaped bushings upon which the blades attach to. Due to concerns of the push rods binding from becoming out of phase with the hub and swash plate, a splined shaft with broached hubs was chosen. The tight clearances between the broach and shaft minimize backlash and allow for smooth sliding of the swash plate.

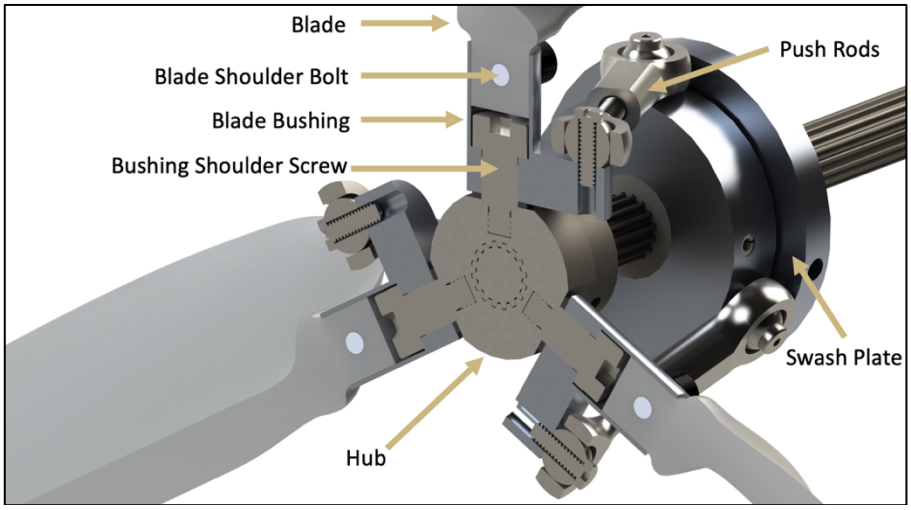


Figure 6: Pitching System Render with Cross Section of Hub

The linear translation of the swash plate is controlled by two linear actuators. In selecting a linear actuator, the back drive force, stroke length, and voltage were considered. To achieve both zero thrust for the emergency stop and maximum thrust, 100 degrees of pitching rotation is needed. Using the geometry shown in Figure 7, the change in length of b to achieve 100 degrees of rotation of θ was found to be 2.3 cm. Since the actuators need to hold their position even without power being supplied, the back drive force is crucial. The force on the actuator would be a function of the moment created by the blades and the geometry of the push rods. Using the coefficient of moment, C_m , from QBlade, The moment from the blades, M, was calculated using Equation 1 and the force on each actuator was then calculated using Equation 2 to be 35 N.

$$M = \frac{1}{2} C_m \rho_{air} \int_0^R (U_{wind}{}^2 + (r\omega)^2) c^2 dr \quad \textbf{Equation 1.} \qquad F_A = \frac{3M\cos\alpha}{2\sin\gamma\alpha} \quad \textbf{Equation 2.}$$

To minimize the power drawn from the generator during operation, a voltage of 5V was chosen. Based on the above parameters, the Actuonix L16-50-150-6-R was chosen.

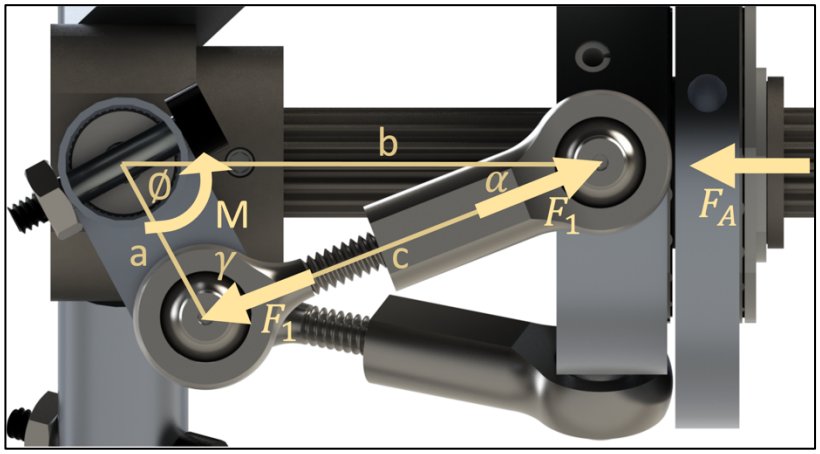


Figure 7: Pitching System Geometry and Forces

Due to the high centripetal forces that will be exerted on the blades and attachment pieces from the predicted 1600 RPM, the shear forces on the tapped holes in the hub were analyzed. Using the center of mass of the blade and bushing, the centripetal force calculated provided a safety factor of 3.1 which was verified during centripetal force testing where the rotor got up to a max speed of 2500 RPM without failure.



$$F_{cent} = M_{blade}\omega^2 r_{blade} + M_{attachment}\omega^2 r_{attachmennt} \quad \textbf{Eq. 3} \qquad \tau_s = \frac{F_{cent}}{A_s} \quad \textbf{Eq. 4}$$

Figure 8: Centripetal Force Diagram

With last year's teams running into issues with binding of the pitching system during competition, The team wanted to start testing the design from the very beginning to prevent a critical system from failing. To check for initial design issues that could lead to binding, a prototype was built using off the shelf components and SLA prints for custom components shown in Figure 9. No issues were discovered in the prototype, so manufacturing of the design was moved forward.

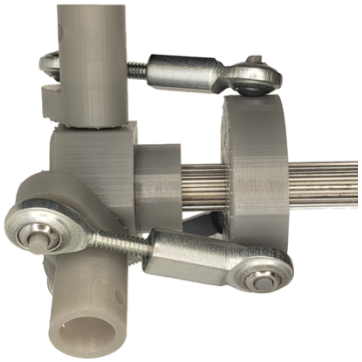


Figure 9: Pitching Prototype

Most of the components were custom and required in house manufacturing using lathes and mills. Due to the complexity of the blade bushings, they were made on a CNC mill. All components were made from 6061 aluminum besides the shaft, hub, and swash plate sleeve which were made from 1015 steel due to its higher strength and higher wear resistance. During manufacturing, one issue that came up was the manufacturability of the swash plate sleeve which required changing from a set screw collar to a retaining ring to assemble the swash plate.

4.3 Nacelle

The nacelle houses the electronics and mountings for the rotor which is fastened onto a baseplate and surrounded by the nacelle cover (Figure 10). The nacelle cover was printed from nylon 12 and comes in two halves that fit around the base plate and is fastened together with bolts.

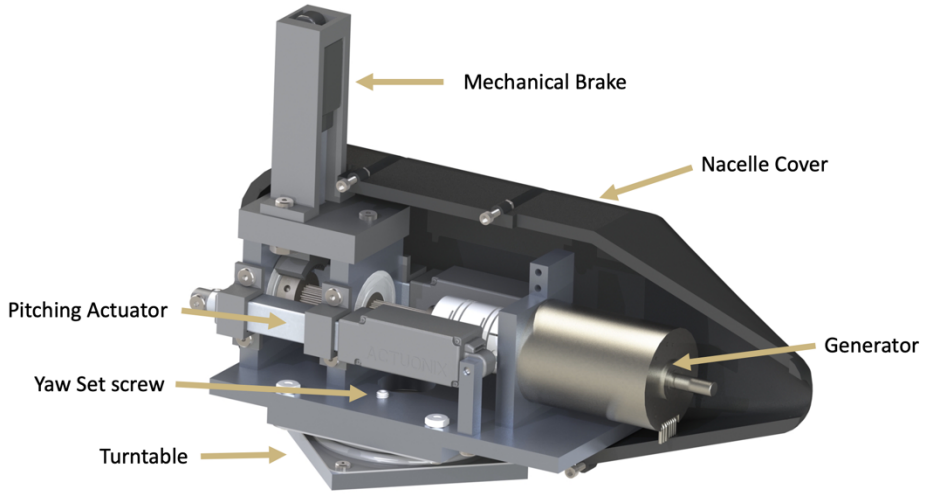
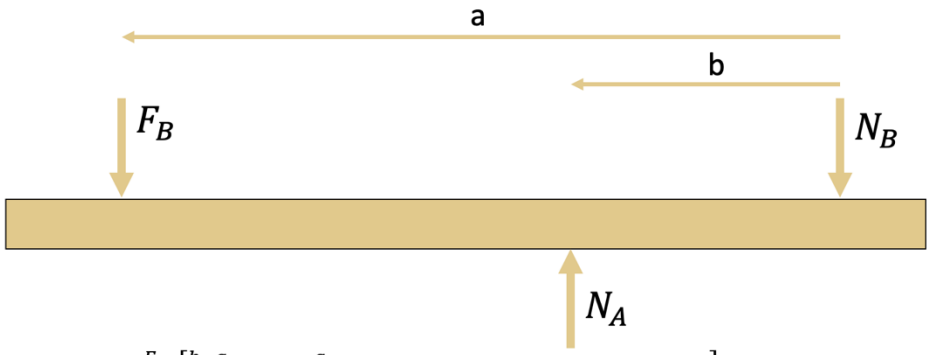


Figure 10: Nacelle Rendering

The shaft is supported by two custom pillow blocks which were milled, and press fit with ball bearings. Using predicted radial loads and rotational speeds, the basic life cycle was analyzed and found to be acceptable for the applications. Due to the use of a splined shaft, broached adaptors were needed between the inner bore of the bearing and splined shaft which were then press fit into the bearing inner bore. When trying to minimize binding in the pitching system, the deflection in the shaft needed to be minimal. With a shaft diameter of 0.79 cm, the maximum deflection was analyzed as a simply supported beam shown in Figure 11 and found to be 0.018mm which results in a safety factor of 3 for the allowed deflection of 0.005mm.



$$y = \frac{F_B}{6EI}\left[\frac{b-a}{b}\langle x\rangle^3 + \frac{a}{b}\langle x-b\rangle^3 - \langle x-a\rangle^3 + b(a-b)x\right] \quad \textbf{Eq. 5}$$

$$I = \frac{1}{4}\pi\left(\frac{D}{2}\right)^4 \quad \textbf{Eq. 6}$$

F_B= Weight of Rotor
$N_A = N_B = Bearing\ support\ forces$
D= minor diameter of spline shaft
E= Modulus of Elasticity

Figure 11: Deflection Diagram of Shaft

Initially, the yaw system was an active system utilizing a tail fin that aligned the rotor with the predominant wind direction, but during testing there was excessive amounts of wobble. This led the team to pivot to a passive system that is manually aligned in the tunnel and then set in place with two set screws.

The nacelle also houses the mechanical brake which will be utilized as a backup during the emergency stop test. It consists of a linear actuator that is mounted above the shaft with a neoprene rubber pad attached on the end. When needed, the actuator presses against the shaft creating a friction force to slow the spinning. The back drive force of the actuator is 25 N so at a minimum when unpowered will provide a braking torque of 0.19 Nm.

5. STRUCTURE AND FOUNDATION DESIGN

The structure consists of everything below the nacelle and includes the tower, tower plugs, anemometer mount and sensor, base flange, stub, nominal tube, height adjustment piece and the foundation. The purpose of the structure is to support the turbines weight and to maintain stability during the durability test.

5.1 Tower

The tower is made from 1.5" outer diameter, 1/8” thick 6061 aluminum tubing and is sized such that the rotor hub is at the center of the wind tunnel. The tower connects to the nacelle and base plate via tower plugs which are custom concentric aluminum inserts. The tubing allows for all electrical wires to pass down through the tower and out the foundation. Attached to the tower tubing is the anemometer sensor which is located just below the swept area of the rotor and mounted via a 3D printed mount and hose clamp (Figure 12). A hole in the tubing allows for the wiring to pass down to the turbine PCB. The tower attaches to the base flange which sits on the provided competition stub and below the stub is a nominal steel tubing with the required 1.5” outer diameter. This nominal tube then attaches to the height adjustment piece, a concentric steel insert with 3 threaded holes and 5 different configurations, 0.25” apart. This redesigned height adjustment piece was chosen for its lightweight and simple design (Figure 12). The bottom half of the height adjustment piece connects to the foundation’s upright post. The tower is designed to have clearance for all electrical cables to pass down from the nacelle and out the height adjustment piece.

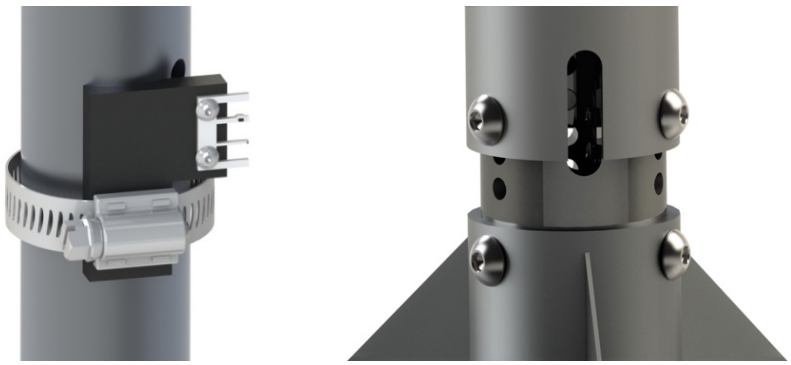


Figure 12: Anemometer Mount and Height Adjustment Piece

5.2 Foundation

The foundation design selected for the turbine model is a single monopile suction bucket caisson commonly used in industry. The design selection was based on the success of last year’s foundation and an extensive literature review. The mechanism that drives the foundation design is a pressure differential between the inside and the outside of the suction bucket [2]. The suction force is created during installation by drilling three holes on the top face of the foundation, allowing water to escape from the inside of the caisson as it penetrates the sand. Once the top face is flush with the sand, the holes are sealed with bolts that create a water-tight seal. After fully tightening the bolts, the pressure differential between the inside of the suction bucket and the outside drives the foundation into the seabed, creating a stable support for the turbine. Through the research conducted, the team discovered that the mathematical model for suction buckets relies heavily on empirical data collected from testing, so the team conducted prototype testing to determine the feasibility of the foundation design.

Multiple prototype designs were created and tested by subjecting them to the expected forces from the competition’s maximum wind speeds. The team underwent three stages of prototype testing, constructing suction buckets from varied materials and subjecting them to static loading under conditions identical to competition testing parameters, modeled in Figure 13. The prototype testing confirmed that the suction bucket design is stable during testing, and the volume of the suction bucket was directly correlated to its

stability indicating bigger is better. When testing the final design, the foundation achieves a safety factor of 2.1 with a weight of 4.1 pounds.

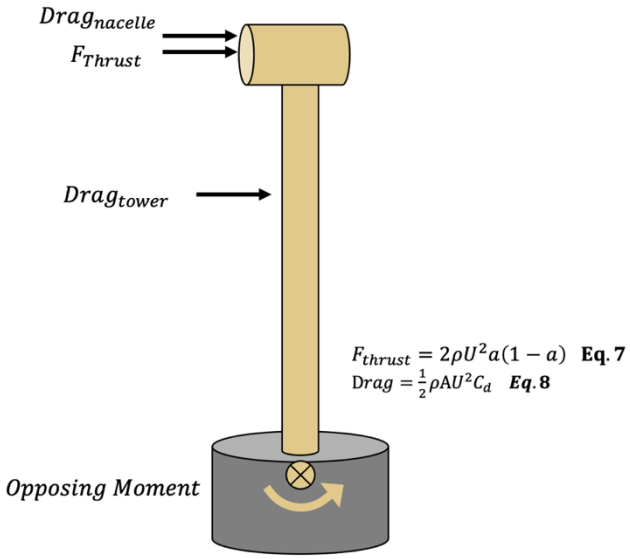


Figure 13: Engineering Diagram of Foundation

The team constructed the foundation using 0.036" 4130 alloy steel, which was welded together by a professional welder to form the thin-walled pressure vessel. From prototyping, the team concluded that a large volume would produce the most stable design, and so the dimensions of the suction bucket were designed near the maximum allowed constraints. The diameter is 28 cm, and the height is 18 cm, leaving a 2 cm buffer on both the height and area to account for any deformation during welding. Designing towards the maximum depth also maximized the surface area in contact with the sand which further increases stability by allowing for more frictional forces to be applied to the foundation that help restrict the movement of the foundation. To ensure that the welded joints between the upright tube and the top face are stable enough to withstand the dynamic loading of the wind, the suction bucket has three welded support gussets that connect the top face of the foundation to the upright tube that connects to the bottom of the transition stub. Welding strength calculations indicated the requirement for extra support to prevent any joint degradation in the upright tube [4].

6. ELECTRICAL DESIGN

The electrical design for the turbine is comprised of the electrical components within the nacelle and two custom printed circuit boards (PCBs), one for the turbine side and one for the load side. The nacelle components include a Maxon EC-i 40 three phase brushless DC motor and three Actuonix linear actuators [1]. The motor serves as the turbine generator by converting the rotational energy from the shaft into electrical AC power. Additionally, the electrical system uses the hall effect sensors on the motor to measure the RPMs of the turbine shaft. Two of the linear actuators within the nacelle are used to pitch the blades back and forth depending on the wind speed, while the third one is used as the mechanical braking mechanism. Each actuator requires a 5-volt input to operate effectively. Finally, both PCBs were designed using Altium Designer and manufactured by JLCPCB. Each of them contains several components that are critical to the functionality of the turbine.

6.1 Electrical Diagram

Figure 14 below shows the general layout of the electrical system. The left side of the diagram shows the turbine side electronics, while the right side shows the load side.

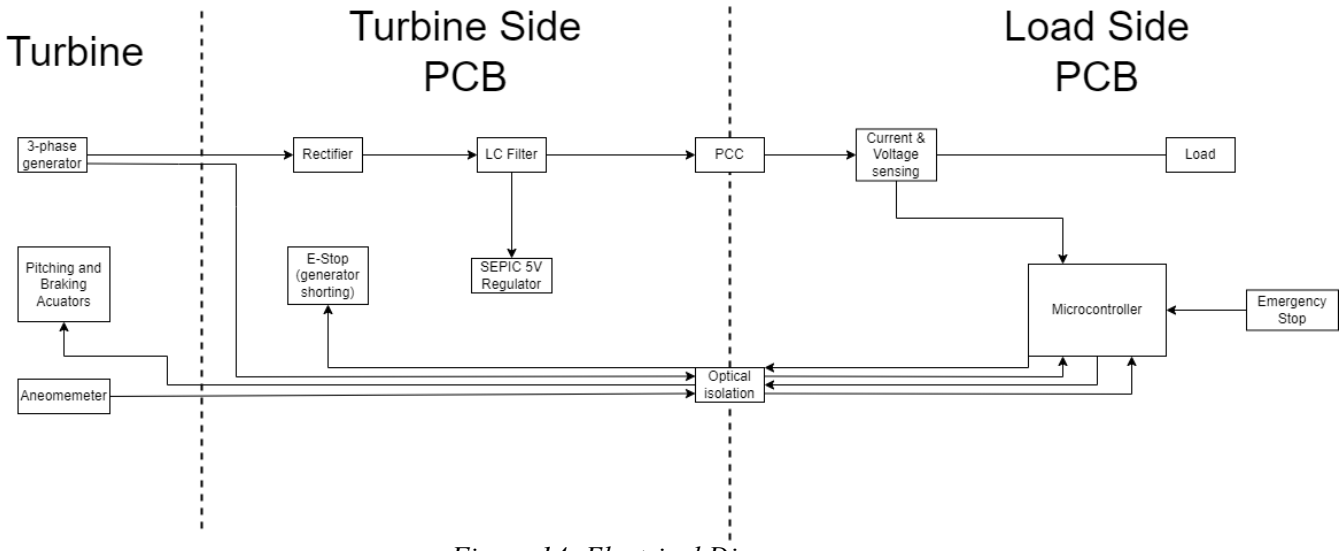


Figure 14: Electrical Diagram

6.2 Turbine PCB

The turbine side PCB shown in Figure 15 can be broken down into five key components. The first is a three-phase rectifier that converts three-phase AC power from the generator into DC power (1). Next is an LC filter that smooths out current and voltage ripples (2). Through testing, the team determined that the voltage that leaves this filter is less than 35 volts for all expected speeds of the rotor. The third component of the PCB consists of the three emergency-stop solid state relays, which act as switches to short the three phases of the motor (3). The fourth component on the turbine PCB is a single-ended primary-inductor converter (SEPIC), which bucks or boosts the power generated by the turbine to a consistent five volts (4). The five-volt output is then used to power the linear actuators and various sensors throughout the system. The final component on this PCB is the "brain" side of the anemometer (the sensor side is mounted on the turbine tower), which is used to amplify the wind speed analog values so the microcontroller can easily read and interpret the sensor's data (5). The three-phase rectifier, LC filter and SEPIC were initially simulated using LTSpice and then tested on a breadboard before being implemented into the PCB design.

6.3 Load PCB

The load side PCB shown in Figure 15 has seven main components. First, the voltage sensor, which is a voltage divider circuit that scales the voltage down to values that the microcontroller can read. Second, is a SparkFun current sensor that monitors the amount of current traveling through the PCC (1 & 2). The current sensor and voltage sensor are vital to the system because the readings are used to measure the power travelling through the PCC. The next components are the digital and analog optical isolators, which are used to ensure that power does not cross through the signal wires to the turbine side electronics (3). The largest component is the SparkFun Reboard Turbo microcontroller, which manages the input and output signals of the system (4). The actual turbine load, a metal-oxide semiconductor field-effect transistor (MOSFET) operating in the ohmic region, has a large heat sink attached to dissipate the heat it produces (5). Additionally, the load side has a boost converter (6* - underneath) to boost the input voltage from five to 28 volts to power the turbine side SEPIC during startup. Finally, there is a relay that can be turned on during turbine start-up to send power to the turbine side PCB (7).

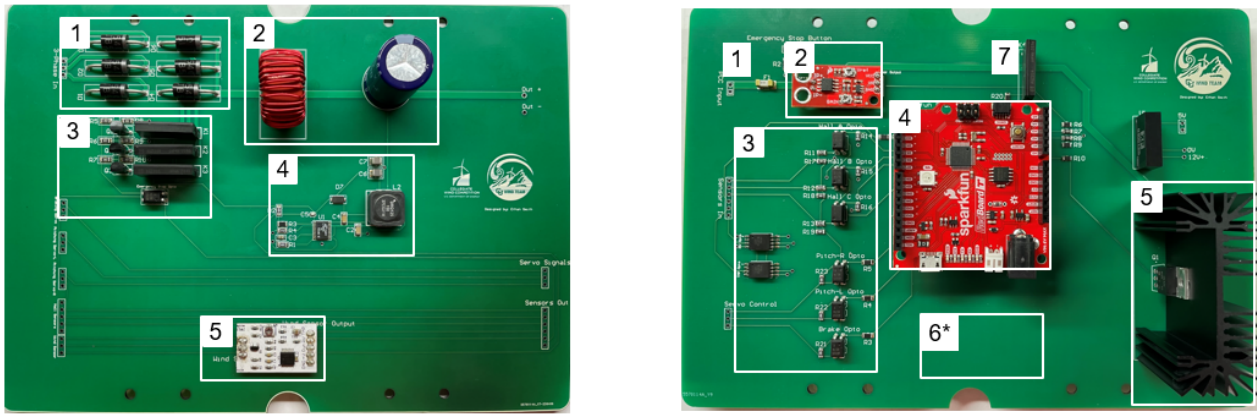


Figure 15: Turbine PCB (left) and Load PCB (right)

6.4 Control Model Analysis

There are five main control states for turbine operation shown in Figure 16. The control system, which is run on the microcontroller, switches between the control states depending on the wind speed and the emergency stop condition. The wind speed is measured using a hot wire anemometer that is mounted to the front of the wind turbine tower. This speed determines when the controls switch between the first four states. To determine if the emergency stop is triggered, the microcontroller reads the voltage from the emergency stop button circuit to decide if the button is actuated. Additionally, the controls use a current sensor and hall effect sensor to determine if the load is disconnected. If the current sensor reads zero current and the speed of the rotor shaft is above a threshold level, then the microcontroller knows that the load is disconnected, and engages the emergency stop.

There are different functions that occur during each separate control state. In the first control state, the power relay is actuated so that power is transferred from the load side to the turbine side. Additionally, the load MOSFET is turned off and the blades are pitched to the optimal cut-in angle. In the second control state, the load is turned on and the blades are pitched to maximize the power output of the turbine. For the third control state, the blades are pitched to maintain a constant power output and rotor speed. In the fourth control state, the blades are pitched back in order to limit the torque on the rotor. This pitching position will produce a low rotor speed, so there will still be a positive power output of the turbine. Finally, the last control state pitches the blades back to produce zero thrust and, if necessary, engages the mechanical brake and generator shorting relays.

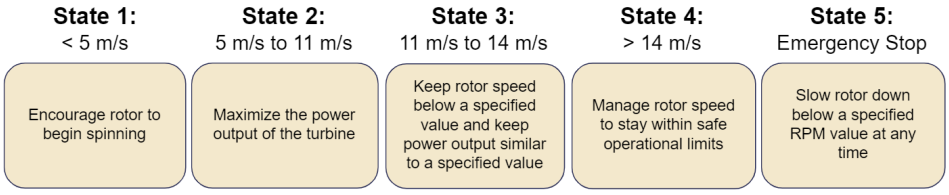


Figure 16: Turbine Control State Goals

6.5 Software Architecture

To control the turbine actions, the team decided to use Arduino to program the SparkFun Redboard Turbo microcontroller. This controller will act as the DAQ for all the sensors in the system and adjust all control surfaces accordingly.

The inputs to the software through the microcontroller are signals from the anemometer, current sensor, voltage sensor, and hall effect sensor (for readings of the generator shaft speed). The anemometer, current sensor, and voltage sensor all output analog voltage signals that are discretized by the microcontroller. The

software uses the 12-bit value from the sensors as well as calibration equations to calculate accurate values of wind speed, current, and voltage. The hall effect sensor works in a different way in that it outputs digital pulses to the microcontroller that signify each rotation of the generator shaft. The Arduino code measures the time between pulses and converts this value into rotations per minute of the rotor.

The output signals from the microcontroller affect the functions of the pitching actuators, the braking actuator, the power relay, the generator shorting relays, and the load MOSFET. To control the position of the actuators, the software outputs a pulse width modulation (PWM) signal to set the distance of the linear actuator arms. The relays are controlled with a digital voltage signal that sets the state of the relay. Finally, the load MOSFET is controlled with an analog voltage signal that comes from the software as a 10-bit value. This analog signal sets the resistance of the load because the MOSFET operates in the ohmic region.

The team decided to use maximum power point tracking (MPPT) Arduino code in order to pitch the blades during state 2 (power performance). The design was inspired by the concepts of proportional-integral-derivative (PID) control, but it uses a feedback control system that was made specifically to match the requirements of the competition and the components of the assembly. This code fuses blade pitch adjustments in order to maximize the power output of the turbine. The system waits for the wind speed to stabilize before beginning the MPPT code to prevent any confusion during changing tunnel wind speeds. This stability is evaluated using a record keeping system that tracks when recent measurements deviate from a moving average by a specified figure. After determining a constant wind speed from the anemometer, the pitch is set to an estimated ideal position that was attained from testing. Then, the code performs a pitch adjustment and evaluates the power change from the adjustment. By comparing the original and new power values, the system determines the direction to move the actuators to increase power (if not already at a maximum power point). The code then moves the actuators incrementally in the chosen direction, taking readings after each adjustment and keeping a short record of recent measurements. The system constantly searches these records for a displayed peak in the output power. When a peak like this is found, the system stops and moves to that pitch position, thus finding the maximum power point at said wind speed. This process repeats while the wind speeds are between the designated speeds for state two.

For state 3, the team has implemented code in order to maintain a constant rotor speed and power output. The main function of this code is to monitor the power output from the turbine and to adjust the pitching accordingly. The software constantly compares the instantaneous power output to the power output determined at 11 m/s. The power output at 11 m/s will be measured through testing and will be stored as a variable in the control code. If the instantaneous power is higher than the set value, then the controls pitch the blades away from the wind, which will lower the rotor speed and power output of the turbine. If the instantaneous power is lower than the set value, then the controls pitch the blades in the direction that will increase the rotor speed and power output of the turbine.

7. FULL ASSEMBLY

7.1 Final Turbine Assembly

After subsystem testing was completed, the team worked collectively to integrate all of the components into a fully assembled turbine shown in Figure 17. The turntable driving the yaw system was implemented between two plates connecting the tower and nacelle. The nacelle base plate was connected to the turntable using bolts and served as a ground to secure the pillow blocks and pitching actuators. The rotor shaft was fit into the pillow blocks, secured with set screws, and attached to the motor using a flexible shaft coupler. The swash plate and the hub were then added to the shaft and fastened to the linear actuators. The blades were attached to the rotor using a shoulder bolt that attaches the blade bushing to the blade. The entire nacelle was then fastened to the tower using bolts. The structure team verified that the height adjustment piece fit in the upright tube of the foundation and was able to achieve the correct heights prior to testing. Once the foundation was securely connected to the height adjustment, the team attached

the transition stub to the top of the height adjustment component. The tower was then attached to the top of the transition piece, with the nacelle already fastened, completing a full assembly for final testing.



Figure 17: Full Turbine Assembly

The team was divided into three subsections to make sure design, manufacturing, and testing of each subsystem was completed on time and with distinction. The three sub teams were structure, rotor, and electrical. These sub teams met biweekly while the entire team met once weekly to discuss updates and make sure the team fully agreed with design and testing decisions. The team emphasized respect and community this year as team dynamics played a significant role in fostering a positive work environment and increasing overall productivity. Weekly progress updates and feedback sessions proved to be extremely effective in creating a sense of community and group accomplishment.

7.2 Commissioning Checklist

In order to properly set up the wind turbine in the competition wind tunnel and ensure that it will work, a structured installation procedure with diagnostic checks must be followed. This will guide the team in setting-up for competition testing and in debugging any potential issues. The team divided the checklist into two parts: one for the installation of the turbine with the foundation and one for the controls testing to ensure that the turbine functions properly. Testing in the practice wind tunnel will be conducted to recalibrate sensors, run through control architecture, verify expected speed and power, troubleshoot electrical issues, and observe and remedy any problems that might arise during testing.

Installation:

- ❑ Install the foundation
    - ❑ Unscrew the three bolts on the foundation

        - ❑ Put the foundation in the water and push it all the way into the sand
        - ❑ Ensure that the foundation is level using a bubble level
        - ❑ Tighten the three bolts on the foundation using the extended socket wrench
    - ❑ Place the cables in the slot in the top of the foundation
        - ❑ Make sure that there is sufficient length of cable on each side of the foundation
    - ❑ Attach the height adjustment piece and adjust it if necessary
    - ❑ Run the cable through the competition stub piece and attach the stub piece to the foundation
    - ❑ Place pre-assembled turbine through wind tunnel turbine door and attach the cable connector pieces
    - ❑ Tighten stub assembly wing nuts to secure turbine
    - ❑ Align the yaw mechanism with the wind direction and tighten the set screws
    - ❑ Attach cables to the PCBs outside of the tunnel
    - ❑ Attach the required cables to the PCC
    - ❑ Plug the load side into the wall power supply

Controls Testing:

- ❑ Ensure that the anemometer readings match the wind speed set by the competition
    - ❑ If they do not match, adjust the zero-wind speed in the code to recalibrate the sensor
- ❑ With the tunnel wind speed at 11 m/s, record the power output of the turbine and set this value in the control code so the code has an accurate value for the control of rated power portion of the testing
- ❑ With the wind tunnel at a high speed, test that the emergency stop mechanisms will actuate and slow the rotor speed sufficiently when the emergency stop button is pressed and when the load is disconnected

7.2 Testing

Testing of the four critical subsystems was completed as early and often as possible before integrating each subassembly into a full system. The four subsystems included the foundation, blades, rotor system, and power & controls. One of the largest challenges the team faced was not having access to a wind tunnel large enough to fit the rotor inside the testing chamber. To solve this issue, the team created a homemade wind tunnel by designing a diffuser to attach to the end of a leaf blower and adding a vinyl enclosure to the diffuser to act as a controlled testing chamber.

During the early stages of full system testing, the team determined what load resistance should be used at different generator shaft speeds. According to theoretical calculations, to maximize the power output at the PCC, the load resistance should be equivalent to the internal resistance of the generator windings. The motor spec sheet lists a constant value for this, meaning that the load resistance should be set to that value, but the team wanted to complete testing to ensure that this was the case. After testing the power outputs at different shaft speeds and load resistance values, the team determined that the best value for the load resistance was 0.45 Ω at all rotor speeds.

In addition to load resistance, the team also wanted to determine the pitch angles for different wind speeds. For states one, four, and five, the pitch angles determined through testing are coded in as set values. For states two and three, the code uses these pitch angles as starting pitch angles before beginning the MPPT and constant power output algorithms. The team determined the cut-in wind speed of the turbine to be 4.8 m/s at a pitch angle of 10 degrees. The optimal pitch at 11 m/s was determined to be 40 degrees since this is the angle at which power was maximized. The team is utilizing the few weeks until the competition to determine the optimal pitch angles at the rest of the wind speeds, which will yield the actual power curve of the turbine. Once final testing is completed, the actual power curve will be compared to the theoretical power, which was determined through running simulations in Qblade (Figure 18).

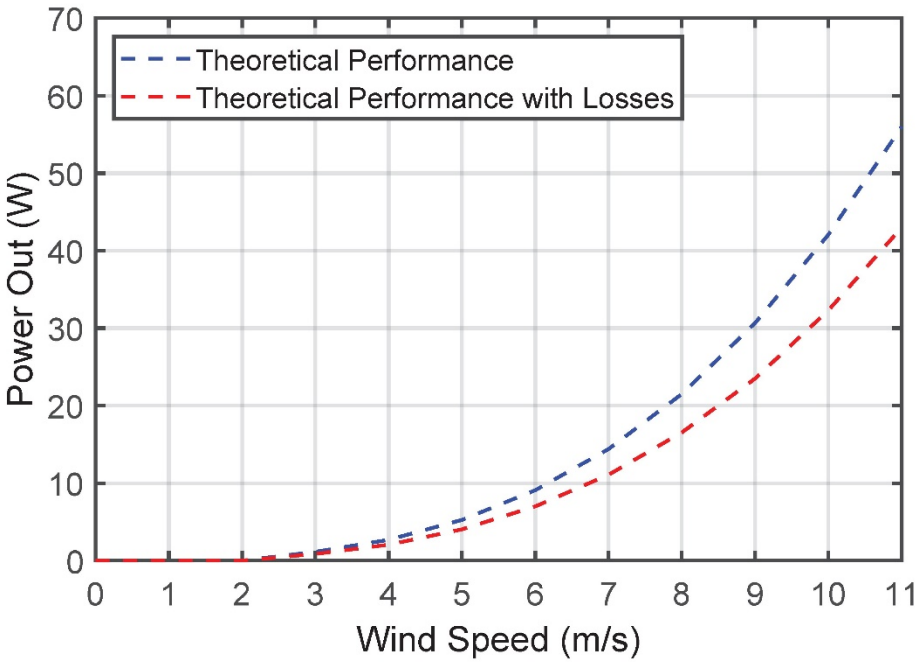


Figure 18: Theoretical power curve before and after theoretical losses (Prandtl tip losses, 3D correction, drag correction)

The team designed a system that would use active pitching, generator shorting, and a mechanical brake in conjunction to significantly reduce the rotor speed to the competition standards. Initial testing of the emergency stop system included pitching the blades at a negative angle in front of the homemade wind tunnel to observe the effectiveness of active pitching on rotor speed. Additionally, the team shorted each phase of the generator, and tested the back-drive force of the brake actuator. During wind tunnel testing, the team observed the most significant results from active pitching, as the hall effect sensors from the generator showed a dramatic decrease in RPMs. At a maximum wind speed of 22 m/s, pitching the blades brought the rotor to a complete stop within approximately five seconds of being engaged, proving to be very effective as the primary emergency stop mechanism (Figure 19). To test the generator shorting, the team used a motor driver to spin the motor and then shorted each phase while monitoring voltage output. During this test the team observed a voltage spike which could potentially exceed competition limits across the PCC. For this reason, the generator shorting will no longer be included in the emergency stop system. To test the efficiency of the mechanical brake, the team engaged the braking actuator, which has a neoprene brake pad mounted to it, against the rotor shaft while it was spinning at various speeds and measured the decrease in RPMs using the hall effect sensors. This test proved that the mechanical brake did not perform as effectively as the negative pitching at wind speeds over 10 m/s. For this reason, the decided to use negative pitching as the main mechanism for the emergency stop system and the mechanical brake as a secondary option.

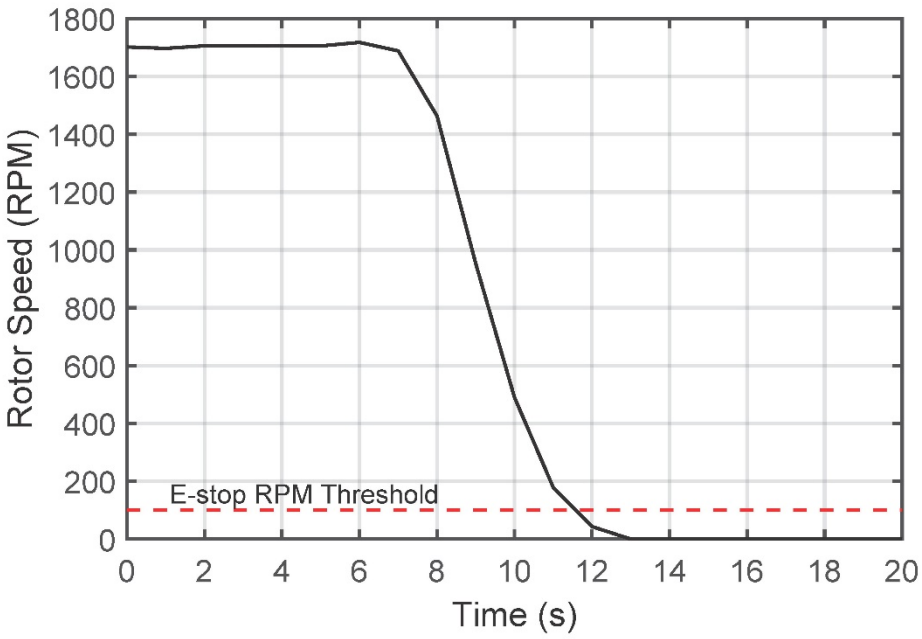


Figure 19: RPM vs Time for Emergency Stop

8. LOOKING FORWARD FOR FUTURE CU WIND TEAMS

Since CU is still relatively new to the CWC and the wind team competes as a single-year senior design team, there is a focus is to organize the team's data such that it's easily accessible for next year's team. The importance of clear documentation will make this transition seamless for the following years. Other ideas are being considered to make the team span across multiple years. The creation of a club has helped, but ways to hold members accountable and motivated need to be further clarified.

Furthermore, CU will dedicate an entire sub team next year to the development of a wind tunnel so proper testing can be conducted. This was one of the biggest challenges this year as a lack of consistent wind speeds required us to get creative to conduct full systems testing. Further development of testing capabilities would improve the team's turbine design significantly and help prioritize early testing and the optimization of the controls systems.

REFERENCES

[1] Kafader, U. (2022). *Maxon motors as generators – maxon support*. https://support.maxongroup.com/hc/en-us/articles/360004496254-maxon-Motors-as-Generators

[2] Liu, M., Yang, M., & Wang, H. (2014). Bearing behavior of wide-shallow bucket foundation for offshore wind turbines in drained silty sand. *Ocean Engineering*, 82, 169–179. https://doi-org.colorado.idm.oclc.org/10.1016/j.oceaneng.2014.02.034

[3] Sessarego, M., Wood, D. Multi-dimensional optimization of small wind turbine blades. *Renewables* 2, 9 (2015). https://doi.org/10.1186/s40807-015-0009-x

[4] Ward, J. (2021, September 8). *Tips for welding thin gauge sheet metal*. SNIPS RSS. https://www.snipsmag.com/articles/94455-tips-for-welding-thin-gauge-sheet-metal#:~:text=0.023%20should%20be%20fine%20unless,requires%20less%20heat%20to%20melt.

Turbine Design Report

Wildcat Wind Power
Kansas State University



2022 | 2023

Officer Team
Brianna Wagoner | President
Andy Freshnock | Vice President
Jacob Lowe | Mechanical Team Co Lead
Rebecca Semple | Mechanical Team Co Lead
Michael Brosseit | Electrical Team Co Lead
David Pierson | Electrical Team Co Lead
Israel Barraza | Siting Team Co Lead
Jakob Long | Siting Team Co Lead
Kent Deterding | Secretary
Macie Sexten | Treasurer

Contact
barrazab@ksu.edu
Carl R. Ice College of Engineering
1046 Rathbone Hall
1701B Platt St., Manhattan, KS 66506
785 532 560

Mechanical Team
Jose Rodriguez
Josh Meurer
Jacob Ronnekamp
Phillip Shirkey

Electrical Team
Cameron Million
Sidney Wagner
Parker Dawdy
David Ochner

Siting Team
Nick Saia
Rory Jenkins
Chase Classcock
Levi Francis

Contents

Executive Summary 2
Design Objectives 3
Knowledge From Past Competitions 3
Technical Design 4
Foundation and Tower 4
Nacelle and Yaw 5
Active Pitch 6
Blade Design 6
Generator Selection 9
Turbine Side 10
Load Side 11
Electrical Systems Manufacturing 14
Software 15
State Machine Operation 16
Final Turbine Assembly 19
Assembly and Commissioning Checklist 20
References i

Executive Summary

Wildcat Wind Power at Kansas State University aimed to tackle the electrical, mechanical, and aerodynamic challenges set forth by the 2023 Collegiate Wind Competition. To this end, our team designed and fabricated a small-scale wind turbine system to be tested in a wind tunnel with a sea simulation tank. Our turbine, anchored to the simulation seabed, is designed to handle wind speeds up to 22m/s in a safe and reliable manner. This document takes an elemental approach to the design, construction, and testing process of our scaled offshore wind turbine system. Coupling mechanical and electrical control elements has allowed our team to assemble a system capable of meeting the requirements of the competition. Our final turbine for competition is pictured in Figure 1 below.



Figure 1: Full Turbine System (left) and 3D Exploded Assembly (right)

A strong foundation to anchor our turbine to the simulation seabed was of utmost priority. An octagonal prism that could be screwed into the sand was fabricated from plate and sheet steel. Moving upwards, at the top of the turbine assembly sits our 3D printed nacelle which houses our linear actuator and generator. This linear actuator powers the active pitch mechanism which provides our three blades over 100° of rotation for RPM control purposes. After over 45 design iterations, the optimal 3D printed blades were selected. The brushless DC generator, coupled to the rotor, converts rotational energy into electrical energy to be measured by the competition. Passive yaw allows our turbine to orient into the airflow through an acrylic tailfin mounted to the rear of the nacelle.

Our electrical system facilitates turbine operation as well as dissipates and controls power produced by the turbine. A Teensy 4.1 microcontroller mounted to our load-side board controls the system with information from sensors on both the load and turbine-side boards. For load optimization and power regulation, our team uses a DAC controlled, current sinking MOSFET load. To regulate RPM, our linear actuator is powered by a 7.4V buck converter and controlled by optically isolated, full-duplex serial communication with the load-side microcontroller. RPM is measured with the frequency of an optically isolated Hall-effect signal from the turbine-side board, and load voltage and current is measured with an INA260 IV sensor located on the load-side board.

Design Objectives

First and foremost, our team believes that the competition constraints and safety requirements should primarily inform our system's design objectives. After that, we believe the next most important objectives are those informed by the four turbine tasks.

- *Competition Safety and Technical Requirements*

Our turbine must fulfil certain safety and technical requirements laid out in the *Safety and Technical Inspection Sheet* to be deemed safe for competition. These requirements serve as a baseline for all design decisions.

- *Power Curve Performance Task Design Objective*

Efficiency of key power generation components is the main design consideration of this task. Due to the heavy emphasis on power generation in this task, the generator selection and blade design process are driven by the desire to maximize power during tested windspeeds.

- *Control of Rated Power and Rotor Speed Task Design Objective*

This task requires designing control mechanisms to precisely regulate both RPM and power during high wind speeds. The regulation of RPM is largely dependent on mechanical design while regulation of power is largely dependent on electrical design.

- *Safety Task Design Objective*

To complete the objective, our turbine must be able to rapidly shut down upon an open e-stop switch or a PCC discontinuity. Mechanical systems aim to physically shut down and reduce our turbine's RPM. Electrical systems must navigate the signal processing to initiate a shut down.

- *Durability and Foundation Success Tasks Design Objective*

The task requires mitigating mechanical stress under demanding tunnel conditions. Regulating RPM is necessary to keep rotor components within their operational limits. The foundation has stability at the forefront of design considerations. Weight is a secondary design consideration when feasible.

Knowledge From Past Competitions

Our team utilized knowledge gained from last year's competition for the design process of this year's system. A full list of ideas and designs utilized from previous years is as follows:

- *Foundation*

A box-shaped foundation design was very stable for us during last year's competition. This design was modified to conform to the no-excavation rule of this year's competition. A solid steel base plate with sheet metal walls remained the same for this year's competition.

- *Tower*

Our team entirely reused our aluminum tower from previous competitions. Utilizing a recycled tower allowed our team to focus manufacturing efforts elsewhere.

- *Active Pitch*

Last year, our team successfully designed and built an active pitch system. Because it was able to regulate RPM, the fundamental design mostly remained the same.

- *Sensors and Circuits*

The diode bridge rectifier, Pololu buck/boost converter, and LC filter on the turbine-side board remained mostly the same. Basic code and circuitry for interacting with our linear actuator, IV sensor, and Hall-Effect sensor from last year was also reused. Because of past effectiveness, our team saw no need to explore new designs.

- *Operational Modes*

Although this year's software structure is entirely new, many concepts from previous experience were used in the design process. This experience was especially useful during the design of our state machine. An understanding of how and when to transition between states enabled a more efficient design process.

Technical Design

Foundation and Tower

To design an anchor capable of keeping our entire turbine assembly stable while minimizing weight, our team took from past experience. Past competitions showed that the most effective anchors were ones that utilized the weight of the sand to their advantage. This led our team to again design a steel plate bottom anchor with side walls. However, to comply with the no-excavation rule, our team sought to create a screw out of the base plate of the foundation instead of manually filling the foundation with a shovel. For easy screw installation, a circular design was selected for the base plate. An early prototype of the foundation was made from a trashcan with slits cut in bottom to allow it to burrow into the seabed [Figure 2]. Proof of concept testing was conducted with the prototype, and it was decided to move forward with this design.

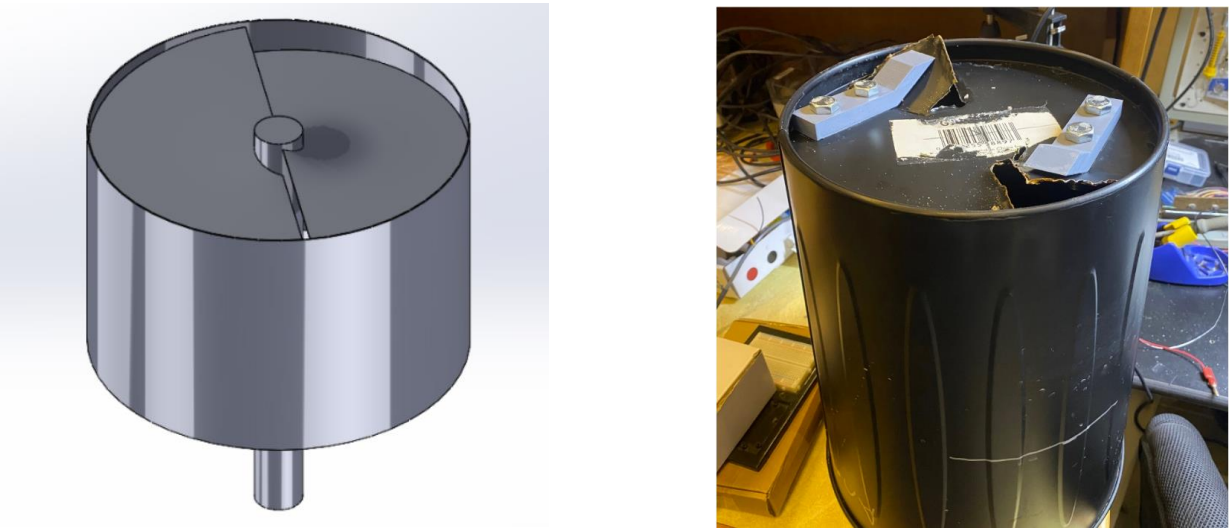


Figure 2: Initial Foundation Design 3D Rendering (Left) and Prototype (Right)

For easier manufacturing, it was decided that an octagonal base plate design was optimal. A waterjet was used to cut the perimeter of the baseplate and square spurs [Figure 3]. The spurs were then bent into place using a hydraulic press. After the baseplate was made, a 1.5" OD steel tube was metal inert gas (MIG) welded to the center of the baseplate to allow for the competition stub connection. Sheet metal was then bent and riveted to the baseplate to form the side walls of the anchor.

A T-shaped installation tool was manufactured from two steel tubes to provide leverage for rotating the foundation into the sand [Figure 3]. A 3D printed part mounts the two tubes perpendicular to one another. The installation tool slides over the foundation center tube and locks on using a retaining bolt.

To test our manufactured foundation, a recycled 35-gallon drum was cut in half to form a testing tank. This tank was then filled with sand and water to the competition specifications. Because we are unable to test the turbine in our wind tunnel while attached to the foundation, the completed foundation was tested separately in the tank using a spring scale, which determined it was stable to a torque of 34 Nm [Figure 3]. Calculations found the maximum torque our foundation will experience is 15 Nm. The weight of our final manufactured foundation is 6.94lbs.

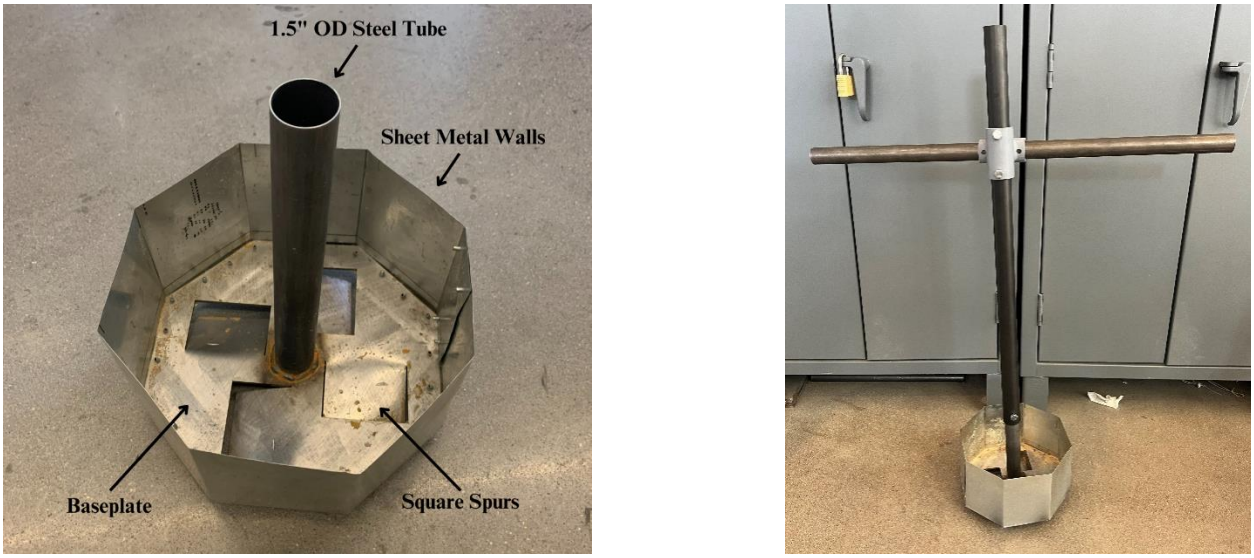


Figure 3: Manufactured Foundation (Left) and Installation Tool (Right)

Our aluminum tower, reused from last year, connects the competition stub piece to the nacelle. The tower features a press-fit bearing at the top to enable passive yaw.

Nacelle and Yaw

The geometry of the linear actuator, active pitch system, and generator primarily governed the 3D printed nacelle design. Our original nacelle design held two linear actuators on either side of the generator. To reduce power consumption, a single linear actuator design was adopted. Originally, we tested with the single linear actuator on the horizontal axis, but this placement resulted in a consistent yaw to one side. To prevent this, the linear actuator was moved to sit directly below the generator. This placement fixed the yawing issue and allowed for a narrower nacelle design [Figure 4].

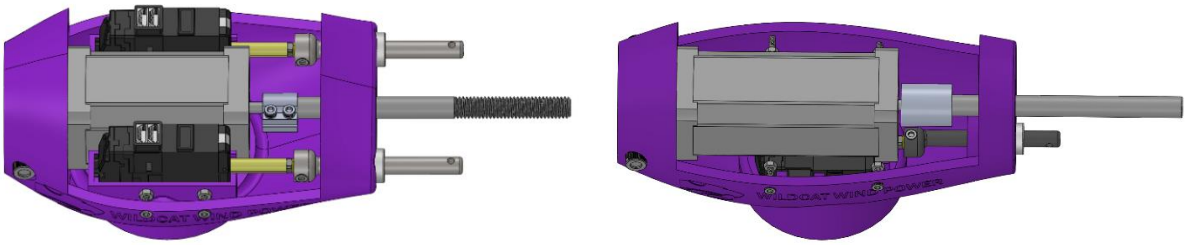
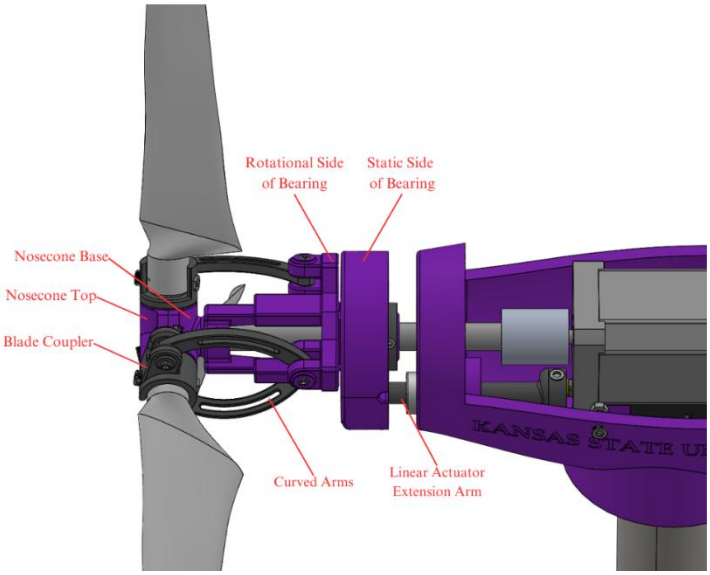


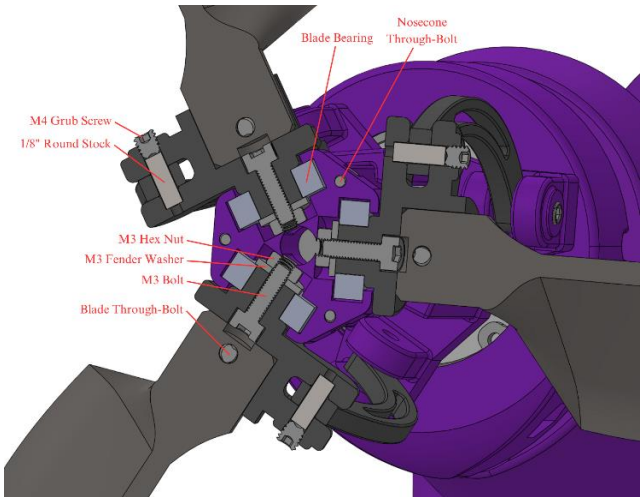
Figure 4: Dual Linear Actuator Nacelle Design (Left) and Single Linear Actuator Nacelle Design (Right)

The yaw system is comprised of two laser cut acrylic fins attached to the back of the nacelle and a press-fit bearing between the nacelle and turbine tower. The fins are connected to the nacelle with an angled 3D printed piece. These components allow for simple, passive yawing.

Active Pitch

The single linear actuator located within the nacelle controls the active pitch system. An extension arm allows the linear actuator to apply force to the static side of a bearing concentric with the rotating shaft. The static side of the bearing works to move the rotational side of the bearing horizontally as it rotates with the nosecone. Each of the three blades are secured to the nosecone via a blade coupler and bearing. The blade coupler is inserted into the bearing and secured with a M4 bolt. The two-piece nosecone encloses the bearings leaving the blades free to rotate. Three curved arms connect the blade couplers to the rotational side of the bearing. This connection allows the linear actuator to pitch the blades over 100 degrees. Aside from off-the-shelf bearing and pin joints, all individual components of the assembly were 3D-printed. The linear actuator to drive the system is a Progressive Automations PA-12 7.4V model which provides very high precision linear motion and performs well at all windspeeds. The active pitch has been tested up to 5,500 RPM but is regulated to 2,900 RPM during operation. A labelled SolidWorks model of the full final design, along with a diagram of the blade coupling and connection, is shown in Figure .





Blade Design

Our team chose to remain with a three bladed design for this year, as three bladed designs have a high theoretical maximum coefficient of performance (Cp), approximately 50%, compared the ultimate maximum Betz law, 59.3% [1]. A four bladed design was briefly considered as it has a higher max Cp, but three blades is inherently more stable and easier to balance. Additionally, a 4 bladed turbine would require more slender blades that would be more prone to bending.

The blades are optimized for a tip speed ratio (TSR) of six which offers the highest coefficient of power for a three bladed turbine. The chord lengths of the blades are calculated based on the TSR, induction factors, and coefficient of lift produced by the airfoils that make up the cross sections of the blade.

For the Power Curve Task, the blades are optimized for a low wind speed of 4 m/s. This ensures that the turbine can produce power at the lowest windspeed of the task, 5m/s. The chord length calculations and the airfoil selection are completed with Airfoilbook 5, a python program our team developed this year. The new code is based in blade element momentum theory (BEM) and quickly calculates axial and tangential induction factors to determine optimum chord lengths as well as inflow angles and velocities. The inflow velocities and chord lengths are then used to determine the Reynolds number and Mach speed of the airflow at each section of the blades. The performance of each airfoil is analyzed by sending the Reynolds and Mach speed to Xfoil 6.99 and running a polar analysis to find the coefficients of lift and drag for a range of attack angles. Multiple instances of Xfoil are processed at once using parallelization which allows it to analyze all 1600 airfoils available in University of Illinois Urbana-Champaign (UIUC) airfoil database in less than 20 minutes. The airfoil that produces the design coefficient of lift with the lowest coefficient of drag is selected for the blade. Finally, the blade twist is calculated with inflow angle and optimum angle of attack for each blade section.

The Selig-Donovan and Selig-Giguere airfoil families were used because they were designed for wind turbines at low Reynolds number airflow. The chosen airfoil for our turbine blade was the SD2030. The last step before manufacturing is analyzing the blades performance in the newly released Qblade CE, to take advantage of Qblade's more precise BEM analysis and produce the coefficient of power vs TSR graph seen below [Figure 6].

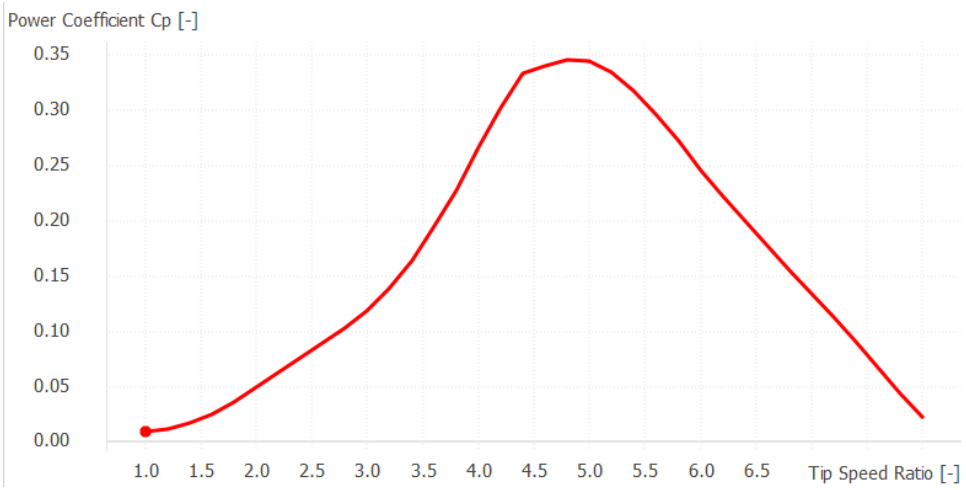


Figure 6: Cp vs. λ (TSR) with DTU Poly BEM, Prandtl Tip Loss, and 3D Correction

Satisfied with the performance, the blades are modeled in SOLIDWORKS and printed using an ultraviolet (UV) resin Liquid Crystal Display printer which has a much higher resolution than traditional FDM printers [Figure 7]. This is useful for accurately producing the airfoil geometry needed for a high-performance turbine blade. Once the blades are printed, all uncured resin is removed with isopropyl alcohol and the blades are cured for an additional 3 minutes under a UV lamp. This step increases the tensile strength of the resin to 49 MPa. Utilizing the QFEM tool in QBlade CE allows us to calculate the stress our blades will undergo is 2.06 MPa under static loading conditions. The additional curing process, while increasing tensile strength, also increases the brittleness of the blades. Initial blades had very fragile trailing edges that were prone to chipping during assembly. Chipping was prevented by making the trailing edge a minimum thickness of 0.15mm which is the cause of the squared-off trailing edge.

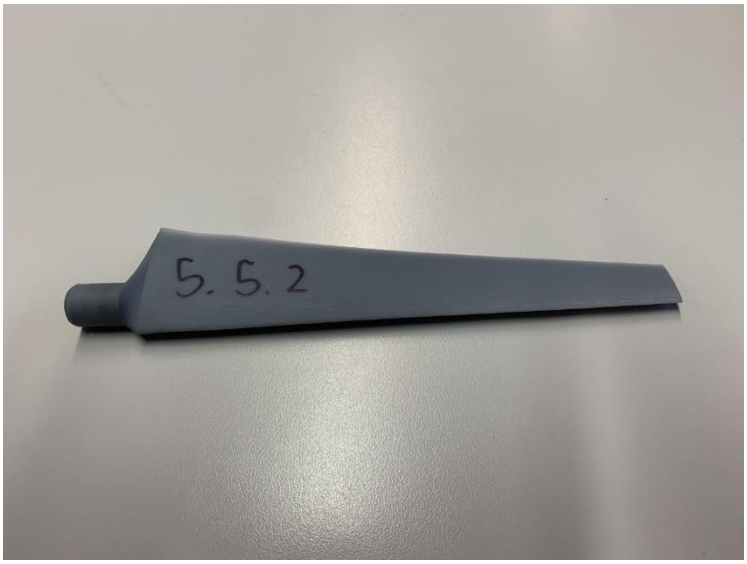
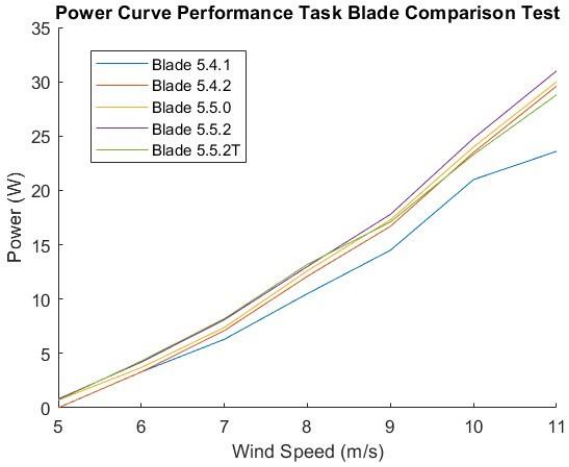


Figure 7: Final competition blade design (5.5.2)

After finalizing our design, we tested in the wind tunnel to confirm our simulation results. We tweaked the airfoil selection process to improve the blades between prototypes. The following graph and chart show the comparison of power output at various wind speeds for several different iterations of our blades. We calculated our Power Curve Performance Task score for each blade to get an accurate grasp on the blades expected competition results. Our highest score was 37.16 with blade design 5.5.2, surpassing the team's past competition performance [Figure 8].



Blade Power Curve Performance Task Scores	
Blade Name	**Score**
5.4.1	**29.49**
5.4.2	**33.48**
5.5.0	**35.31**
5.5.2	**37.16**
5.5.2T	**36.44**

Figure 8: Power Curve Performance Task blade comparison test results

Generator Selection

To select our generator, our team conducted testing to determine a suitable fit for our system. Performance during the *Power Curve Performance Task* was the most important selection criteria. Our team selected two brushless DC generators with differing rated power and RPM to test. Upon testing, a 48V 6000RPM generator scored 25.57 on a *Power Curve Performance Task*, while a 24V 4000RPM generator only scored 22.15 [Figure 9]. Our team selected the DB42C01 48V 6000RPM brushless DC

generator for our turbine. While the selected generator has a rated voltage of 48V, during testing, the voltage never exceeded 12V. Additional voltage regulation to stay under the competition limit of 48V will not be necessary due to our generator choice. The selected generator also boasts a built in Hall-Effect sensor which our team uses to measure RPM of the turbine. The built in Hall-Effect sensor reduces the needed space inside of the nacelle by eliminating the need for an external RPM measurement device.

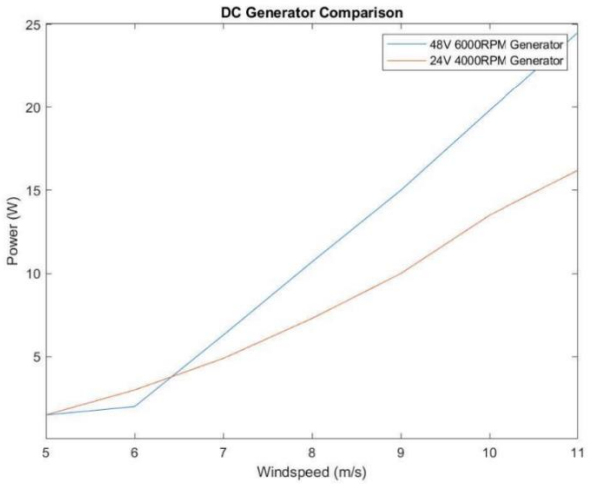


Figure 9: Generator Testing Power Curve

Turbine Side

The turbine-side printed circuit board (PCB) was designed with power efficiency and simplicity in mind. The board contains circuitry for a rectifier, a low pass filter, PCC disconnect detection, linear actuator communication, and a Hall-Effect sensor. The board also has buck and buck/boost converters to power said circuitry and an idle power consumption of approximately 0.7W. A one-line diagram outlining our electrical system's main power paths can be seen in Figure 10.

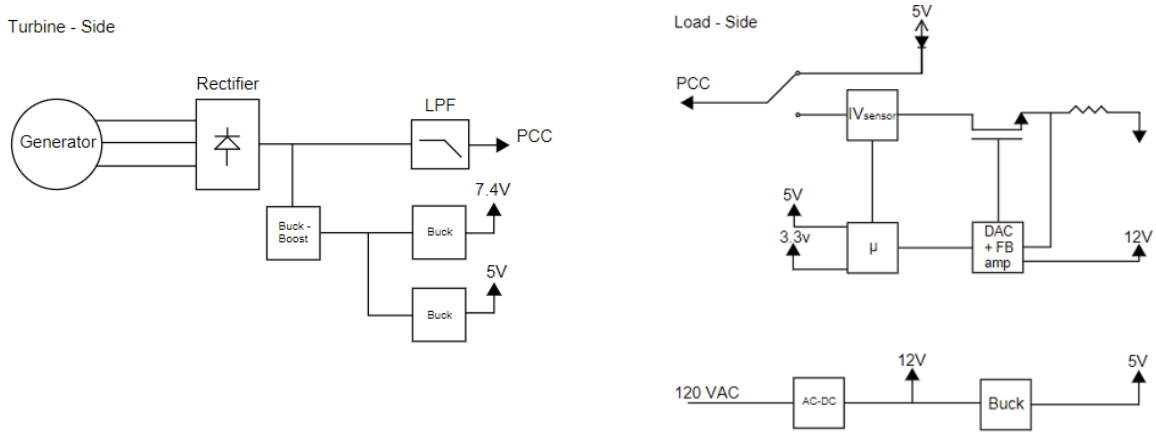


Figure 10: Electrical System One-Line Schematic

The turbine-side board contains 9V, 7.4V, and 5V power rails. The 5V rail powers optical isolation circuitry, the hall effect sensor, and a half to full-duplex converter IC for the linear actuator. The 7.4V rail powers the linear actuators. The 9V rail acts as an input to parallel buck converters whose outputs

are the 7.4V and 5V rails. The 9V rail is created by a wide input range (2.9-30V) Pololu DC to DC buck/boost converter.

Initially, our active rectifier displayed potential during breadboard testing. However, once the design was integrated into our final PCB, it failed to operate correctly and consumed more power than a conventional diode bridge rectifier. Nevertheless, we were able to convert our system into a three-phase diode bridge rectifier design, as we had anticipated the possibility of a failure of this kind and designed this part of our board to be adaptable.

Our rectified voltage is filtered through two bypass capacitors and a series inductor to reduce voltage and current ripple at the PCC. During testing, we verified through our data acquisition system that our power fluctuation remained below what is acceptable during the *Power Curve Performance Task*.

This year, we sought to simplify our method of detecting a PCC disconnection. In previous years, we've used an IV sensor IC on the turbine side board in order to know the exact voltage on the turbine side of the PCC. This year, we reduced the complexity down to a simple Schmitt-trigger comparator circuit that would be driven high or low when the PCC voltage went above or below a certain volage. However, during testing, we realized that even a comparator was unnecessarily complicated. Since the comparator only had power when the turbine-side board had power, the input threshold voltage became irrelevant. Instead, we decided to ground one channel of an inverting buffer which drives an optocoupler connected to the load-side microcontroller. When the turbine-side voltage is high, the buffer is on and the microcontroller sees a logic low, otherwise, the buffer is off and a pull-up resistor on the optocoupler output creates a logic high.

Our generator's Hall effect sensor requires 5V to be powered and has three output signals, one for each phase of the generator. Since only the frequency and not the relative phase of the output signal is relevant to our RPM calculation, any one of these three could be used. The sensor output is open drain and uses a 4.7kΩ pull-up resistor. The signal is optically isolated and sent to the system's microcontroller where the frequency is measured and multiplied by a constant factor which converts it to the generator shaft RPM.

During a PCC disconnect safety state, for the linear actuators to fully pitch the blades before power is lost, a large amount of capacitance was added to the 9V and 7.4V rails. The 9V rail contains 40 and 15mF, 10V capacitors. The 7.4V rail also has a 40mF, 10V capacitor attached to it. The LC filter contains 2200 and 3300uF capacitors both rated for 25V. This totals 6.46J of energy storage on the turbine-side board.

Load Side

Our load-side PCB contains a controlled current sink MOSFET load, a load IV sensor, a PCC relay, opto-isolators for communication with the turbine-side board, and a Teensy 4.1 microcontroller which runs our entire electrical system's state machine. The load-side PCB is powered by 120VAC and has an idle power consumption of approximately 3.3W, the majority of which is consumed by the enclosure's exhaust fan.

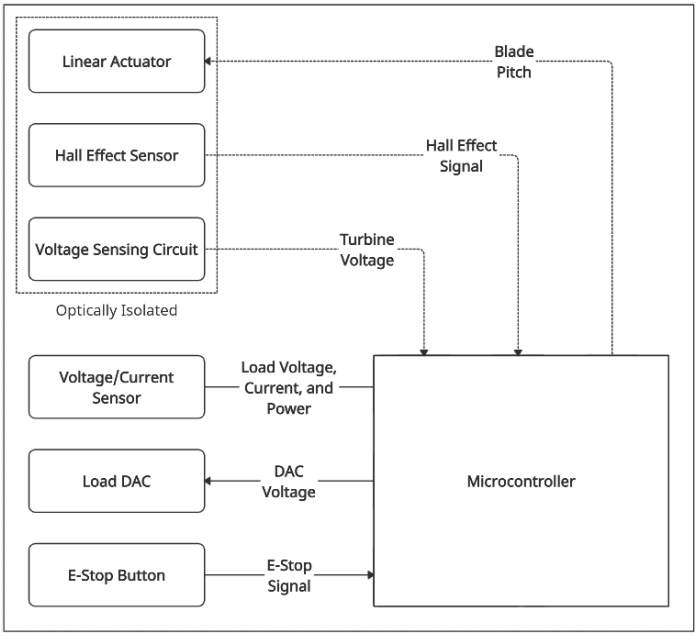


Figure 11: Load-Side Block Diagram

Our team made the decision to use a singular microcontroller on the load-side board instead of a microcontroller located on either side of the PCC. For one, we believed it was most logical to have our central processing unit located on a board which would always have consistent power during testing. Additionally, last year, communicating with another microcontroller on the turbine-side board proved difficult during conditions of low or unstable turbine power. While an undervoltage-lockout circuit would most likely help prevent microcontroller brownouts, this could mean that our turbine-side electronics would be entirely inoperative during low power conditions. The team decided that turbine-side ICs would interface directly with the load-side microcontroller over optically isolated channels instead of with an on-board microcontroller.

Early in the first semester, our team decided to protype a load architecture which would primarily control load current. While our team had great success with a variable resistance load last year, our variable current design sought to improve the load by increasing the absolute range of load impedances, increasing the precision of impedances that the load can take on, and decreasing the complexity of accompanying circuitry. Figure 12 shows a schematic of the principal design.

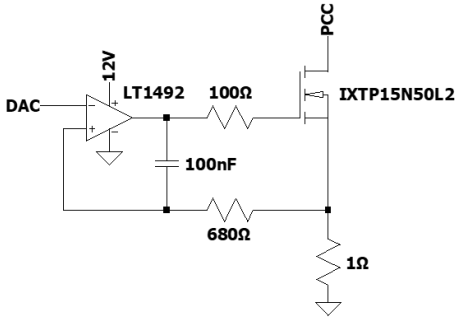


Figure 12: Fundamental Load Schematic

In theory, once the DAC voltage is set, negative feedback to the Op-Amp will adjust the MOSFET gate voltage in order to maintain a constant voltage across the source resistor. This results in a constant

current through MOSFET and source resistor. The maximum allowable current is approximately equal to the maximum DAC voltage divided by the value of the resistance to ground attached at the source of the MOSFET (1Ω in Figure 12). The load N-FET was chosen partially because of its high current rating, but mostly because it was intended to operate in its linear region, which is necessary for the design. The passive values in the feedback path were found through trial and error after the protype was breadboarded. Until the optimal passive values were found, the load would usually experience large and slow oscillations in current. The final protype, however, experienced current oscillations of less than 10mA when connected to a constant load voltage and constant DAC voltage. After seeing benchtop success, a variation of the design was added to the final schematic, which can be seen in Figure 13.

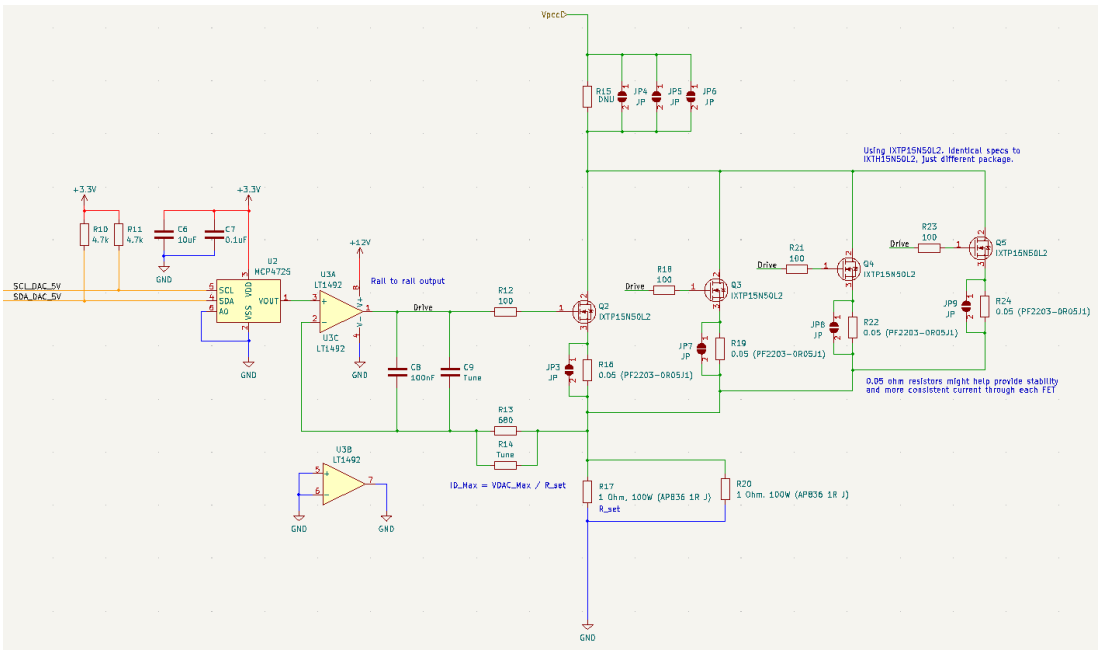


Figure 13: Final Load Schematic

The largest change between the final design and prototype was the number of MOSFETs used. By putting three additional MOSFETs in parallel, the power dissipated by each one is quartered. In making this change, we wanted to prepare for the possibility of performance changes as well. We added additional through-hole footprints in parallel with the passive feedback components critical to reducing oscillation in case those values needed tuning. We also added additional spots for resistors on the drains and sources which would further reduce the amount of power dissipated across each FET and possibly help alleviate current imbalances between the FETs. Testing of the design with a benchtop power supply was primarily successful without the need of additional tuning passives or resistors.

However, when the new load was finally tested with a turbine in our wind tunnel, we encountered some unexpected results. Last year, we saw our generator respond well to a specific resistance during the *Power Curve Performance Task*. So, this year, we hypothesized that the same would be true for a specific current. When trying to pull constant current from the generator at a fixed wind speed, the turbine would oscillate greatly in RPM shortly before the RPM fell to near-zero due to overloading. We tried to remedy this issue by instead writing a perturb and observe algorithm which would attempt to continuously respond to the generator and find an optimal current. This algorithm sometimes kept the turbine running for longer, but still resulted in large RPM and power oscillations. Our postulation is that

any control algorithm which attempted to find an optimal current ended up overloading the generator whenever there was a decrease in generator voltage due to transience or mechanical noise. If the system tried to maintain current during a voltage drop, the equivalent resistance of the load would be decreased, which resulted in a positive feedback loop further decreasing the RPM and generator voltage. To fix this issue, a resistance-based algorithm was developed. This program aimed to make our load look more like a resistor than a current sinking load by maintaining a voltage to current ratio. This adjustment showed immediate improvement to our system.

All power produced by our turbine is dissipated in the form of heat. Both the power MOSFETs and resistors of our load have aluminum heatsinks fastened to their TO-220 package. Our heat sink system can dissipate over 200W of power at room temperature. To maintain stable temperature inside the box, an exhaust system has been designed. A 19 CFM exhaust fan coupled with a filtered air inlet provide ample heat rejection for the system while maintaining NEMA1 standards.

In our load power path is an INA260 current and voltage sensor IC. This chip is located right before our MOSFET load and informs our microcontroller of the current through and voltage across our load over an I2C bus. This information allows us to perform the current and voltage ratio matching described above in order to make our load appear more like a resistor. It also informs our system during the *Control of Rated Power and Rotor Speed Task* by calculating power with voltage and current data.

The load-side of the PCC is connected to the common pin of a relay controlled by the microcontroller. The normally closed path of the relay connects to the IV sensor and MOSFET load previously described. The normally open path, however, is connected to the load-side board's 5V rail though a diode. The microcontroller can flip this relay to the normally open path in order to provide power to the turbine-side board when initializing cut-in pitch or exiting safety states. The diode protects the 5V rail in the event the path is connected when the generator is producing a higher voltage. The only rework performed on this section of the board was the addition of a current limiting resistor in series with the diode. When powering the turbine-side electronics through this path without the current limiting resistor, the 5V rail would momentarily sag and brownout the microcontroller.

Optical isolation circuitry for communication between the load and turbine-side board appears on the load-side PCB [Figure 14]. Isolation is done with two-channel, high-speed optocouplers. To ensure adequate current, the recommended inverting buffer ICs drive the LED side of the optocouplers. This provides two logic inversions, meaning that the output of the optocouplers is the same logic as the input of the buffers. The load-side board contains isolated ground and 5V rail planes that connect to the turbine-side board, meaning certain ICs will only be powered and operational when the turbine-side board has power.

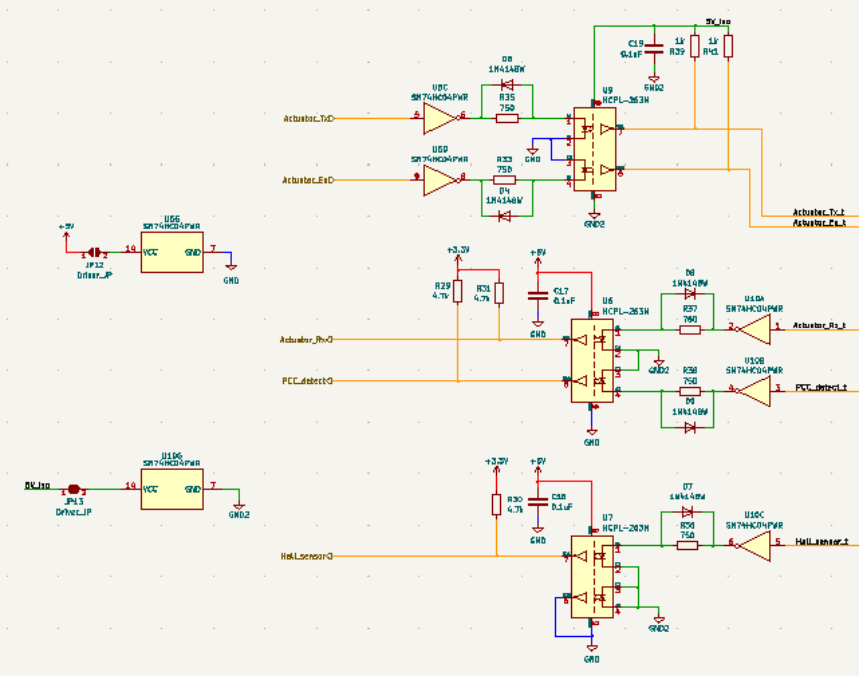


Figure 14: Optical Isolation Schematic

We decided that our emergency stop switch should be located on the load-side board because it always has power. If it was located on the turbine-side board, we would only be able to use the emergency stop when the turbine-side board had enough power to facilitate communication. A 470 Ω pull-up resistor connected to the microcontroller and competition provided switch enables emergency stop signal detection. When closed, there will be approximately 7mA through the switch, and the microcontroller will read a logic low. When open, the current through the switch will naturally be 0A, and the microcontroller will read a logic high, causing the turbine to shut down.

The load-side board contains 12V, 5V, and 3.3V rails. The 12V rail comes from our AC to DC converter which has a 120VAC wall-plug input. The 12V rail is used by the MOSFET load gate driver Op-Amp, exhaust fan, and 5V buck converter. The 3.3V rail is provided by an integrated LDO on the Teensy 4.1 microcontroller. ICs throughout the load board utilize the 3.3V and 5V rails.

Electrical Systems Manufacturing

PCBs for both the turbine and load-side are manufactured by JLCPCB and contain a combination of surface mount and through-hole components. The assembly process begins with the placement of surface mount parts onto the boards. This is accomplished by securing footprint stencils onto the boards, applying solder paste across the stencils, removing the stencils, placing the components onto the boards, and then baking the boards in a reflow oven. After the boards have cooled down, each chip is inspected under a microscope to ensure that reflow is adequate. In some cases, minor additional rework is required to reposition chips or remove solder beads that may be shorting neighboring pins. The remaining through-hole components are manually soldered in place.

To protect our PCBs with NEMA1 standards, we have chosen to use polycarbonate enclosures due to their malleability [Figure 15]. Our team has utilized drill and rotary tools to create holes for the installation of cable passthroughs and a heat rejection system. Our enclosure manufacturing process ensures that each PCB can be easily removed during the subassembly testing.

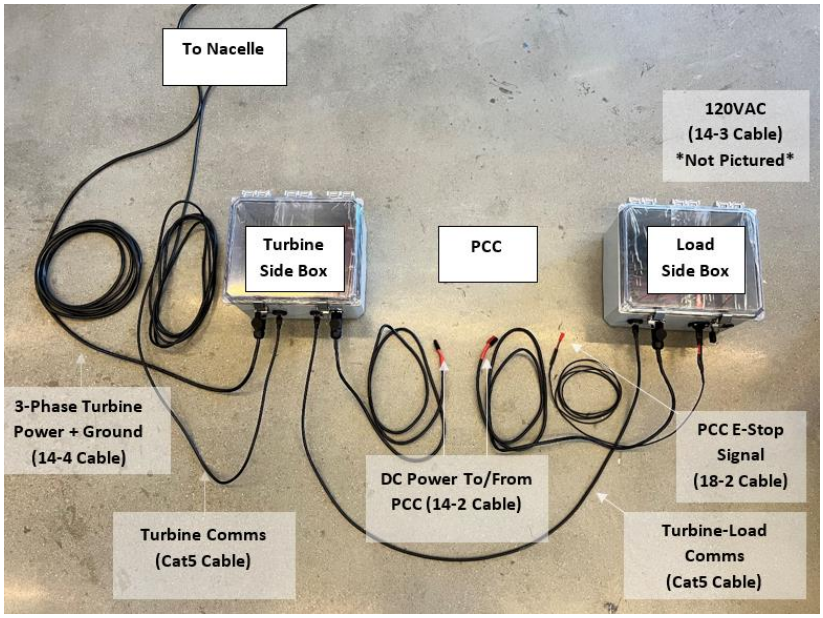


Figure 15: System Cable Map

Software

Software development for our team this year started with smaller code blocks for individual electrical subsystems. While prototyping, code blocks for our linear actuator, MOSFET load DAC, IV sensor, and Hall-Effect sensor were made. For the Teensy to communicate with our linear actuator, MOSFET load DAC, and IV sensor, each part required a library provided by the manufacturer. Once these were downloaded, test code was run to confirm that each part was operational. The Hall-Effect sensor code, however, was entirely original because we simply count and take a moving average of the sensor's output frequency to calculate generator RPM. Each of these parts required some minimal amount of additional electrical hardware in order to test operation. The linear actuator code was tested with our team's old turbine-side board because it was populated with a necessary half to full-duplex digital communication buffer IC. The MOSFET load DAC code was tested with a small breakout board manufactured by Adafruit which was populated with the desired DAC. The IV and Hall-Effect sensor code was also tested with the team's old electronics which contained the desired ICs and necessary pull-up resistors.

After electrical subsystem software was developed, software components could be integrated together. Components were brought together in Arduino IDE utilizing GitHub as a repository. This phase of the software development process corresponded with the completion of our team's PCB fabrication. This allowed all the electrical subsystems to be controlled by a single Teensy 4.1 microcontroller which facilitated the integration of subsystem code.

After confirming that individual software components did not negatively interfere with each other, a full program for competition was developed. This program development began with the building of user interface in the form of the Arduino serial monitor. This interface displays all microcontroller data and allows the user to change variables in the software. This interface allows our team to view and gather data for testing purposes. Finally, the state machine to run our system was built.

State Machine Operation

Our team's turbine operates using a state machine control model with states designed for individual turbine testing tasks [Figure 16]. Separating each turbine testing task into a state allowed for a more efficient design process. These states were first tested individually before the transitions and state

machine were tested. From our experience, transitions between states are the most crucial part of the system.

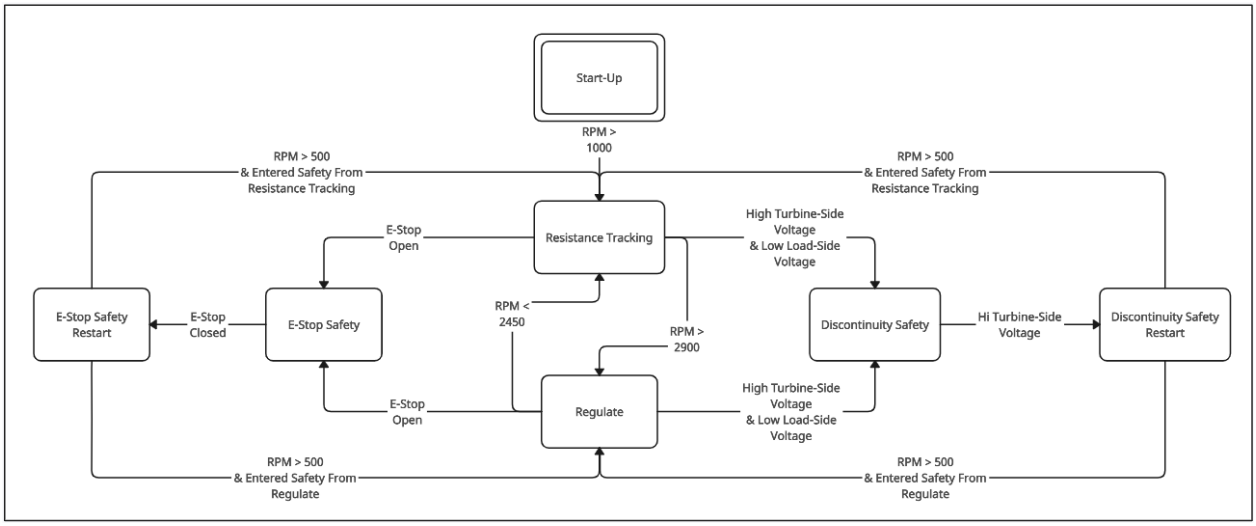


Figure 16: State Diagram

- ***Start-Up State***

The Start-Up state is the default state of the system and is only operated during windspeeds below 5 m/s. This state sets the pitch of the blades to the optimal cut-in pitch and allows no current to flow into our load. These two conditions maximize RPM which helps the generator overcome static friction. Once our turbine has surpassed 1000 RPM, it will transition to the Resistance Tracking state.

- ***Resistance Tracking State***

Our system remains in the Resistance Tracking State during the entirety of the *Power Curve Performance Task*. During this state, our blade angle and effective load resistance are set to fixed values that produced the best *Power Curve Performance Task* score recorded during testing.

- ***Regulate State***

The Regulate State is where the system operates during both the *Control of Rated Power and Rotor Speed Task* and the *Durability and Foundation Success Tasks*. RPM of our turbine is used to determine when to enter and leave the state. Our system remains in this state from 11m/s to 22m/s. This state uses blade pitch as the primary regulation mechanism and effective load resistance as a secondary control mechanism. The setpoints that our team regulates to are the maximum RPM and Power at 10.5 m/s. To regulate RPM, our system utilizes blade pitch and a dynamic step-size algorithm. The algorithm analyzes the difference between our desired RPM and the current RPM to determine how large an adjustment is needed. Once the adjustment is made, there is a settling time to allow for the change to take effect and the process is repeated. Fine power regulation is controlled by our MOSFET load. This regulation is also a dynamic step-size algorithm very similar to the RPM regulation algorithm. As the wind speed increases, our blades feather more and our load increases its effective resistance. This minimizes mechanical and electrical stress on our system. Successful operation of this state can be seen from the data presented in Figure 17.

- ***E-Stop Safety State***

The E-Stop Safety State allows our system to shut down during the e-stop portion of the *Safety Task*. This state is entered upon the opening of the e-stop button contacts. Immediately upon entering the

state, power is provided to the turbine-side board through the PCC and the blades are fully feathered to halt rotation. Next, our system waits for the e-stop button to close.

- *E-Stop Safety Restart*

This state allows our system to smoothly come back up to speed when exiting the E-Stop Safety state upon the signal that the button has closed. Once the state is entered, the blades are pitched to their operational angle and the system is allowed time to spin up. Once sufficient RPM is achieved, the state machine returns to the state the system was in when the e-stop button was pressed.

- *Discontinuity Safety State*

The Discontinuity Safety State allows our turbine to shut down during the discontinuity portion of the *Safety Task*. Entrance to this state is signaled by a high voltage on the turbine-side board and a low voltage on the load-side board. This signals that there is a discontinuity at the PCC. Upon entering the state, the blades are fully feathered. The power necessary for this action is supplied by capacitors on the turbine-side board. After a waiting period to ensure the capacitors have discharged, our load-side board attempts to supply power to the turbine-side board. A reconnection has occurred when the power is successfully supplied to the turbine-side board and a high voltage on the turbine-side is seen. Once a reconnection has occurred, the system transitions to the Discontinuity Safety Restart state.

- *Discontinuity Safety Restart State*

The Discontinuity Safety Restart State transitions from a discontinuity safety task back to normal operation. Upon entrance to the state, the blades are pitched to their operational pitch which allows the system to gain speed. Once the system is at operating speed, the state machine is returned to the state the system was in when the disconnect occurred.

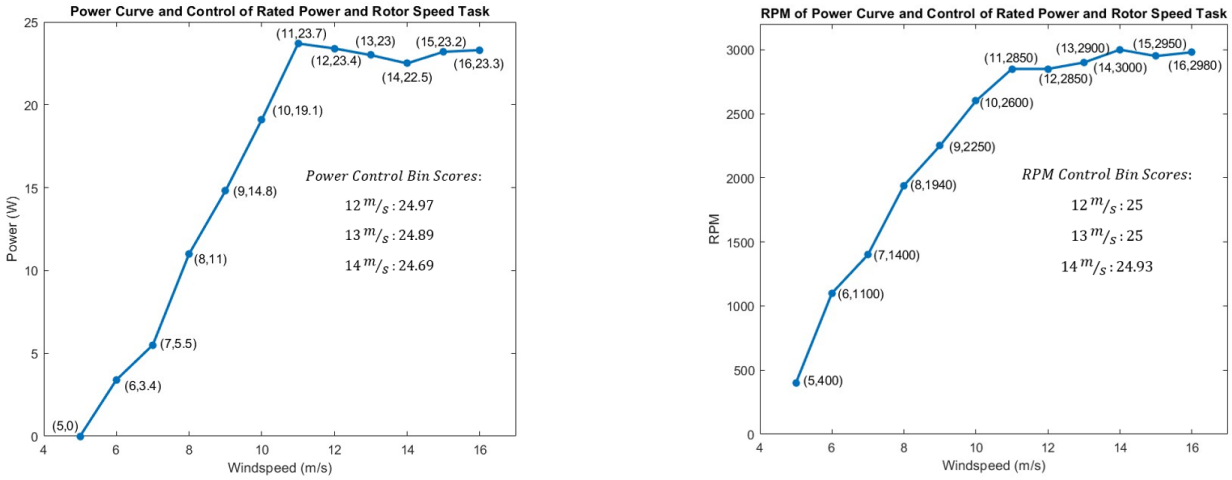


Figure 17: Power Curve and Control of Rated Power and Rotor Speed Task Test Results

Final Turbine Assembly

In an effort to minimize installation time at the wind tunnel, all subsystems that can be assembled will be assembled prior to our provided installation time. The nacelle assembly is the primary component that can be fully constructed before installation. This assembly process includes: mounting the generator inside the nacelle, fastening the active pitch mechanism to the generator, attaching the tailfin, and closing the hatch atop the nacelle. The foundation, electronics, and combined nacelle assembly will require installation during our allotted installation time. These systems were designed for ease of installation as time is an important aspect of the process. After our foundation is installed, the rest of the on-site assembly process takes no more the five minutes. To ensure proper installation on-site, our team has developed an assembly and commissioning checklist seen below.

Assembly and Commissioning Checklist

Assembly and Commissioning Step	Initiating Team Member Initials	Verifying Team Member Initials
Attach the foundation installation tool to the top of the foundation tubing with set screw	JM	JL
Feed the turbine power and the communication cables through the foundation tubing	JM	JL
Set the foundation into the tank and turn the tool clockwise until the foundation is level with the top of the tank	JM	JL
Check foundation for level	JM	JL
Unscrew the set screw, remove the foundation installation tool	JM	JL
Ask the judges to move the tank under the tunnel and install the stub	JL	MB
Feed the turbine power and the communication cables through the turbine tower	DP	MB
Place the tower on the stub, tighten the wingnuts to secure the tower to the foundation	RS	JL
Connect the communication and the power cable from the nacelle to their corresponding cables	DP	MB
Carefully feed the cables back into the tower and place the nacelle on the press-fit bearing at the top, the nacelle should push down firmly and sit flush with the bottom of the bearing	DP	MB
Orient the nacelle in the upwind direction	JL	RS
Connect the power and communication cables from the turbine to the turbine control box	DP	MB
Connect the DC power cable for the turbine-side box to the PCC	DP	MB
Connect the communications cable from the turbine control box to the load side box	DP	MB
Connect the DC power cable from the PCC to the load-side box	DP	MB
Connect the power cable from the load side box to 120VAC	DP	MB
Connect the emergency stop cable from the load-side box the PCC	DP	MB
Ensure the heat rejection fan is running in the load-side box	DP	MB
Verify active pitch system has actuated to cut-in pitch	DP	JL

References

[1] J. Burton, N. Jenkins, and D. Sharpe, "Wind Energy Handbook," Chichester, West Sussex, UK: John Wiley & Sons, Ltd, 2001.

The Pennsylvania State University

Wind Energy Club

Technical Design Report

Submitted to the 2023 U.S. Department of Energy Collegiate Wind Competition
May 4, 2023

Aerodynamic Design Team

Shana Hartwick	**Director**
Alex Scheffler-Murry	**Lead**
Austin DiSciullo	**Lead**
Diana Deleon	Member
Jue Huang	Member
Lauren Myers	Member
Jason Oh	Member
Daniel Romero	Member
Kathryn Sharp	Member
Rochelle Xavier	Member

Generator Design Team

Conner Burger	**Director, VP**
Kan Petyim	Member
Armend Berisha	Member
Ryan Manning	Member
Aditya Ghadigaonkar	Member
Luke Price	Member

Foundation Design Team

Eric Sarbacker	**Director**
Matthew Reagan	Member
Liam Cassidy	Member

Electrical Design Team

Satyam Patel	**President**
Rahul Shekar	**Co-Lead**
Hamdan Almarzooqi	**Co-Lead**
Alan Arechiga	Member
Caroline Brustoloni	Member
Ethan Farrow	Member
CJ Young	Member
Anum Jan	Member
Ian Lin	Member
Folayemi Omogboyega	Member
Blake Wall	Member
Erik Long	Member
Maddi Waehner	Member
Megan Wolff	Member

Software Design Team

Brian Truong	**Director**
Jiaming Wang	**Lead**
Mark Young	Member
Parth Kshirsagar	Member
Yashas Anapindi	Member

Academic Advisors

Dr. Susan W. Stewart
Dr. Mark A. Miller

COLLEGIATE WIND COMPETITION
U.S. DEPARTMENT OF ENERGY

Table of Contents

ABSTRACT 2

AERODYNAMICS DESIGN 3

Blade Design, Manufacturing, & Analysis 3

Rotor Hub 4

Collective Blade Pitch System 4

Nacelle Design, Manufacturing, & Analysis 5

Passive Yaw System 5

GENERATOR DESIGN 6

FOUNDATION DESIGN 8

THE SAND SCREW EGG CRATE 8

INSTALLATION 8

TESTING 8

ELECTRICAL DESIGN 9

Rectification 9

Regulation 10

PCC Over-voltage Protection 11

Load System 11

Variable Load 11

Startup Power Source 11

Electromechanical Relay Protection 11

SOFTWARE DESIGN 13

State Machine 13

Variable Load Control 14

Power Curve Task 14

Deep Dive into States 15

TURBINE TESTING 17

COMMISSIONING CHECKLIST 17

ANNUAL ENERGY PRODUCTION 19

DESIGN CHANGES TABLE 20

ABSTRACT

This report outlines the design of a fixed-bottom offshore wind turbine developed by the Penn State Wind Energy Club for the 2023 Collegiate Wind Competition. The team had maintained a conservative approach to design changes from the 2019 to 2022 competition year - focusing on incremental improvements to inadequate subsystems while maintaining other systems at satisfactory level. However, following lackluster performance in the 2022 competition, the team has completely overhauled the wind turbine for the 2023 competition. This newly designed wind turbine is shown in Figure 1, and Figure 2.

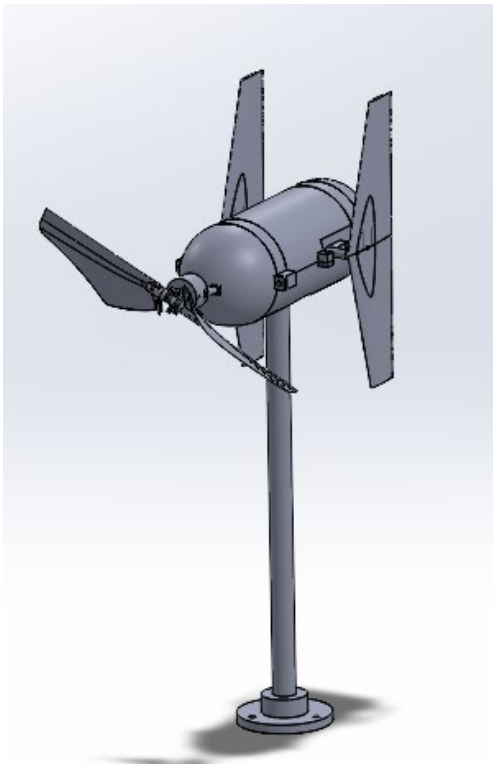


Figure 1 CAD Rendering of the Assembled Turbine

The primary design objective was to redesign every subsystem of the turbine focusing on safety, reliability, and efficiency. The turbine is composed of five subsystems: aerodynamics, generator, foundation, electronics, and software. In redesigning each subsystem, the team reviewed the weak points of previous iterations while developing new ideas around the 2023 rules and regulations.



Figure 2 Assembled Turbine

The turbine utilizes a two-blade rotor to operate the nine-phase, three-stage axial flux permanent magnet generator. The nacelle encloses the generator, and it follows a “soda bottle” shape to house two linear actuators that operate the pitching mechanism. The nacelle also encloses an onboard rectifier to convert AC power produced by the generator directly to DC. A hall effect sensor is embedded within the generator to monitor turbine RPM. In addition, a pitot tube pressure differential sensor is also mounted to measure airspeed.

A turbine-side power-and signal modulation box is used to regulate power produced by the turbine to operate all the turbine peripherals. Power produced by the turbine is across the Point of Common-Coupling (PCC) where it is consumed by the 10 Ω – 160 Ω variable load. Two microcontrollers are housed in the load box which operates the control code that operates the wind turbine. The control system can shut down the turbine when it detects a PCC disconnect, or when the Emergency Stop button is depressed. The control also runs various algorithms that manipulate pitch angle and load resistance depending on the operational state.

AERODYNAMICS DESIGN

The aerodynamic subsystem's design objective was primarily focused on streamlining the turbine nacelle while improving the component packaging and improving overall reliability and performance. While the two bladed designs have remained the same this year, nearly all other components of the nacelle and blades have been either updated or remanufactured using new materials.

Blade Design, Manufacturing, & Analysis

The design of the blades attempted to optimize the rotor power output while considering the small scale of the competition rotor. Since the blade radius was constrained to 45-cm, the rotor aerodynamics are quite different than large, commercial wind turbines. The rotor's design goal was to maximize the glide ratio, or ratio of lift to drag forces, $\frac{C_l}{C_d}$. The airfoil chosen to achieve this is the Ma 409, shown in Figure 3. Drag generally decreases and the stall point of an airfoil increases as the scale or Reynolds number, Re, of an airfoil becomes larger. Increasing the Re is most easily accomplished by increasing the chord length along the rotor blade. However, only increasing chord length causes the rotor solidity, or ratio of blade area to rotor swept area, to increase as well. This has the effect of reducing the point of maximum rotor efficiency in the power coefficient, $C_{p,max}$onsequently, the aerodynamics team reduced the number of blades from three to two in order to keep the rotor solidity approximately constant.

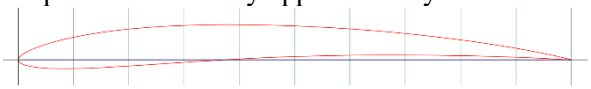


Figure 3 Ma 409 airfoil.

This year the Aerodynamics team focused on fixing structural and integration challenges from prior years instead of redesigning the aerodynamic shape of the blades. One aspect of this was identifying a stronger blade material. Figure 4 shows three blades—moving from left to right—from 2021, 2022, and 2023, respectively. The 2021 blade was made of Nylon 12. The Nylon 12 blades not as rigid as expected, primarily due to issues with the blade CAD model which was fixed in later years. The 2022 blade was fabricated using Accura 60 and an updated CAD model, making for a blade with much higher stiffness. The Accura 60 blades had a smoother surface finish due to the stereolithography 3D printing process used to fabricate them. The Accura 60 blades were however very brittle near the trailing edge, which made transportation and handling difficult. Online fabrication service Xometry manufactured both the Nylon 12 and Accura 60 blades. The 2023 blades were fabricated using a different stereolithographic 3D printing material called Rigid 10K, and were fabricated by the Penn State Applied Research Laboratory (ARL). ARL recommended Rigid 10K because they often print research-quality rotorcraft blades with the material. The team ultimately chose Rigid 10K because of the material's stiffness. Rigid 10K can withstand significant loads without bending [1]. Wind turbine blade stiffness is important because blade deformation can cause an unstable power output [2].

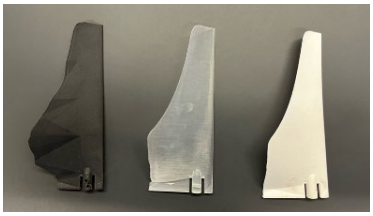


Figure 4 Blade evolution from left to right.

To validate the blade material choice, the team conducted a finite element analysis (FEA) on blade geometries using Rigid 10K's material properties from the manufacturer (Formlabs) in SOLIDWORKS, using the von Mises stress criterion to map the stress levels. The FEA was then compared to past FEA for Nylon 12 and Accura 60. The figures below represent the FEA results, with warmer colors indicating higher stress (red highest) and cooler color indicating lower stress (blue lowest).

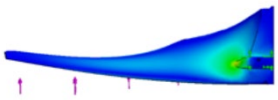


Figure 5 Stress results for Nylon 12

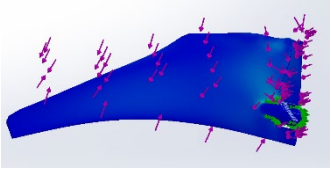


Figure 6 Stress results for Accura 60

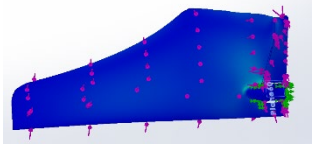


Figure 7 Stress results for Rigid 10K

The FEA results indicate that Rigid 10K experiences lower peak stress as compared to Nylon 12. In Figure 5, there is a point of high stress near the root, which is indicated in green. In comparison, the FEA using Rigid 10K, shown in Figure 7, experiences less stress at the same region due to lower deflections and greater stiffness. When comparing the Accura 60 and Rigid 10K (Figures 6 and 7), the amount of stress experienced appears relatively similar. However, the stress results show a larger deflection for Accura 60 as compared to Rigid 10K. The estimated deflection value for the Accura 60 was 58.27 mm compared to Rigid 10K's lower 17.52 mm. To investigate the blade deflections further, another SOLIDWORKS simulation was created where different loads were applied to determine the tip deflection.

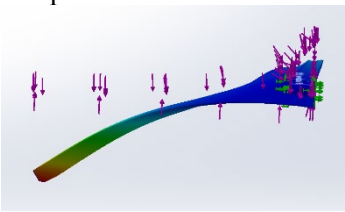


Figure 8 Deflection results for Accura 60

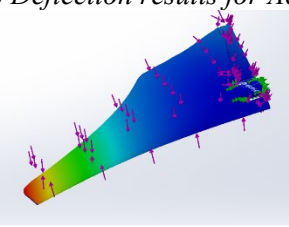


Figure 9 Deflection results for Rigid 10K

Figures 8 and 9 suggest that the Accura 60 experiences a larger deflection than Rigid 10K. An experimental test was conducted to confirm this simulation result. The blade deflection test was conducted by sliding a clamp onto the blade. The blade was weight applied at the midspan because the team had 3-D printed clamping blocks to use at this location. The clamp had a hook to which loads could be applied. The hook was loaded in 8.896-N increments until the total weight equaled 31.138-N which was the maximum that could be applied with this method.

Figure 10 verifies the SOLIDWORKS simulation. The Accura 60 material experiences more deflection than the Rigid 10K material. The culmination of the blade analysis supports the team's decision to proceed with Rigid 10K as the blades' final material.

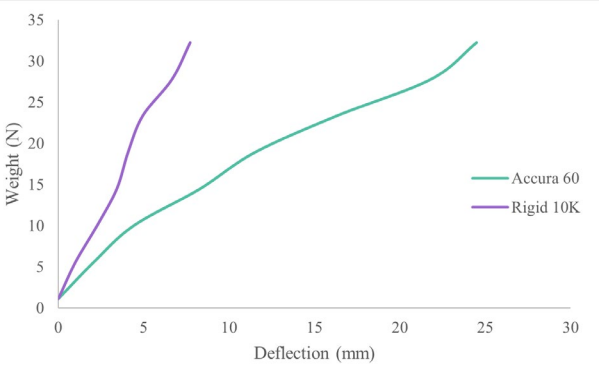


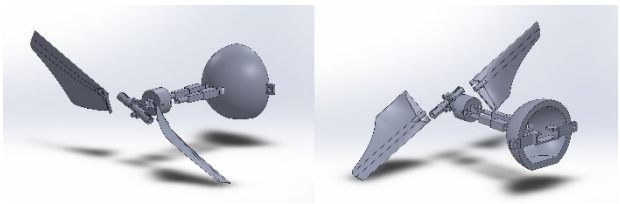
Figure 10 Weight versus deflection

Rotor Hub

The turbine uses an Align 700 rotor hub—a repurposed RC helicopter tail rotor. The rotor hub was strength tested during the 2021 competition year. To conduct the strength testing, a block with a rod on one end was clamped to an I-beam that was attached to a strongback on the wall of the Aerospace Engineering's structures lab. The rod emulated the drive shaft and the rotor hub was attached to it in the same way as the competition turbine. A bolt was then fixed to the rotor hub piece. A chain was attached to the bolt and applied an upward force on the rotor hub. The SolidWorks model estimated that the rotor hub should withstand an estimated 110 N on each side to fully support the blades at their maximum speed. The rotor hub was tested up to 890 N with only minimal damage to the screw, making the test successful with a safety factor of 8.09. Since the current rotor has not been damaged in the past two years, the team did not retest the rotor hub's strength due to its high factor of safety.

Collective Blade Pitch System

The rotor hub pitch mechanism is actuated by two parallel linear actuators to simultaneously pitch the blades. The previous pitch mechanism used six different pieces to connect the rotor and the linear actuators. The pitch mechanism—shown in Figure 11—was redesigned to use one circular cuff to connect the rotor and linear actuators. The linear actuators connect on either side of the circular cuff. Reducing the pitch mechanism from six pieces to one piece simplified the design while ensuring that the system does not create an undesirable bending moment when operating.



(a) Front *(b) Back*

Figure 11 Exploded View of Pitch System

Nacelle Design, Manufacturing, & Analysis

The past nacelle design included a rectangular body with a rounded lid, which resembled a mailbox. The nacelle was designed to *only* house the generator, leaving little room for electronics or other hardware. This year, the team decided to focus on completely redesigning the nacelle to create a more streamlined turbine shape and integrate the electronics and hardware in a more functional package.

The redesigned nacelle consists of four main components: the nosecone, midsection, lid, and tailcone, shown in Figure 12. Figure 13 shows a SOLIDWORKS flow visualization simulation, verifying that the new nacelle design is more streamlined than the mailbox-shaped nacelle.

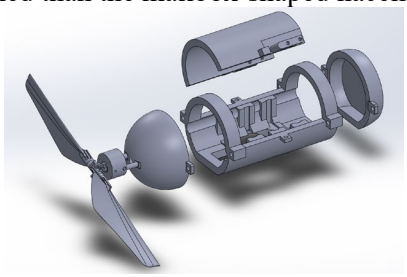


Figure 12 Exploded view of nacelle

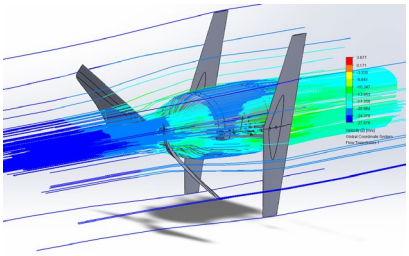


Figure 13 Flow visualization

A new design requires a new loading analysis. In a similar method to the blade analysis, SOLIDWORKS was used to model the forces that the nacelle will experience. Figure 14 shows that the nacelle sees the largest force at the front of the nosecone and at the leading edges of the tail fins. Because of the high forces generated on the nosecone of the nacelle, a simulation predicting the stresses that the nosecone will experience individually was generated and is presented in Figure 15.

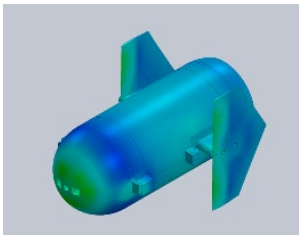


Figure 14 Pressure distribution

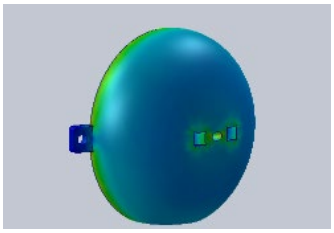


Figure 15 Stress Diagram for Nacelle Nose Cone

Figure 15 predicts that the highest areas of stress will be where the linear actuators for the pitching mechanism and the rotor axle turbine are located. To strengthen the nosecone and the rest of the nacelle, the nacelle's wall thickness was made to be 1.26-cm.

Passive Yaw System

The passive yaw system on the nacelle is much different than designs in prior years. Moving the linear actuators for the pitch mechanism inside the nacelle caused the nacelle's overall length to increase, leaving no room for a vertical stabilizer on the back of the nacelle. Mounting a fin on the top and bottom would limit the vertical stabilizer's length. Consequently, the new passive yaw system design includes two tailfins on either side of the nacelle lid, as shown in Figure 13. The tailfins are mounted as far back on the nacelle body as possible to maximize the restoring moment that the tailfins will exert as the turbine attempts to yaw during operation. Analysis of several symmetrical NACA series airfoils showed that the NACA-0009, shown in Figure 16, had several positive attributes including the greatest lift-curve slope of the symmetrical airfoils studied, the widest range of angles of attack before stall, and the smallest profile drag coefficient. Thus, the NACA-0009 is the most effective at producing a restoring moment to align the turbine with the oncoming wind and was chosen for the new tailfins.

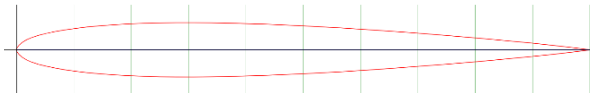


Figure 16 NACA-0009 airfoil

GENERATOR DESIGN

The generator converts mechanical energy produced by the blades into electrical energy. Electromagnetic generators translate rotational kinetic energy to a spinning rotor with embedded magnets or conductive coils. Permanent magnets produce magnetic fields with opposite directions on each face as illustrated in Figure 17. The north pole of a permanent magnet emits a positive magnetic field leaving the surface, and the south pole of a permanent magnet emits a negative magnetic field.

Due to the rotation, the magnetic flux passing through the conductive coils is continuously changing. As described by Faraday's Law (Eq.1), changes in magnetic flux will induce an EMF. Lenz's Law dictates that the induced current will produce a magnetic field in the opposite direction of the inducing magnetic field.

$$E_b = -N\left(\frac{d\Phi}{dt}\right) \quad (1)\ \textit{Lenz's Law}$$

There are two primary types of Electromagnetic Generator Designs: Axial Flux Generator [AFG], and Radial Flux Generator [RFG]. Magnetic flux changes in the direction parallel to the axis of rotation in an AFG. The magnetic flux changes in the direction perpendicular to the axis of rotation in an RFG as illustrated in Figure 17.

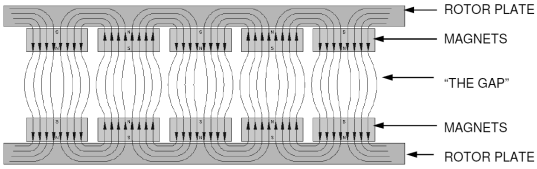


Figure 17: Flux Lines Traced Through an Axial Flux Dual-Rotor Permanent-Magnet Generator Source: Adapted from [5]

The team chose an axial flux design due to its manufacturability, adjustability, and efficiency. RFGs utilize enveloping cylinders to hold the stator and rotor in place. These parts can be difficult to fabricate through additive manufacturing; however, the disk stator and rotor designs of AFGs are much easier to produce with 3D printing. RFGs need new stator/rotors to adjust airgaps. The airgaps in AFGs can be adjusted by sliding the rotor/stator along the axle. The path of magnetic flux in an AFG is relatively short compared to the RFG, and therefore has a lower price to performance ratio in comparison to RFGs [6].

To design an axial flux generator, a major parameter to determine is the number of poles. Each magnet in the rotors creates a pole for the generator. To have an efficient generator a ratio of four poles to three stators coils must be maintained [6]. Our design specifically includes eight poles and six coils per stator. The AC output frequency of the generator is dependent on the turbine's rotational speed and number of poles as show in Eq. 2. However, since the output is rectified to DC the AC frequency is irrelevant.

The strength and dimensions of the magnets used also play a critical role in the electrical output of the generator. The magnets used are N52 grade cylindrical magnets with a diameter of 0.5 in and a height of 0.1875 in with a remnant magnetic field strength of 1.48 Tesla. The field strength reaching the surface of the stator is a strong function of air gap. The airgap is important since magnetic field strength decreases as the distance from the magnet increases as seen in Figure 17. Given the team's smallest achievable air gap of 1.8 mm the stator surface magnetic field strength is 4.296 Tesla.

The max magnetic flux is used to find the number of turns needed in each coil and is found by multiplying the surface magnetic field strength by the magnets' circular surface area as seen in Eq. 3. Eq. 4 shows the relationship between the number of coils and the generator parameters. Using this relationship, the team created a MATLAB calculator to determine the number of turns needed per coil to be 276.

Poles and Rotational Speed

$$P = \frac{120\, f_{nom}}{n_{nom}} \quad (2)$$

Flux Max from Magnetic Field Intensity

$$\phi_{max} = B_{mg} * A3)$$

Number of Turns Calculation

$$N_c = \frac{\sqrt{2}E_f}{q*2\pi*\kappa_w\phi_{max}*n*\frac{p}{120}}4)$$

Where:

E_f	electro-magnetic force (V)
k_w	$Winding\ Coefficient$ (0.95)
n	generator RPM
p	number of pole pairs
q	number of coils per phase

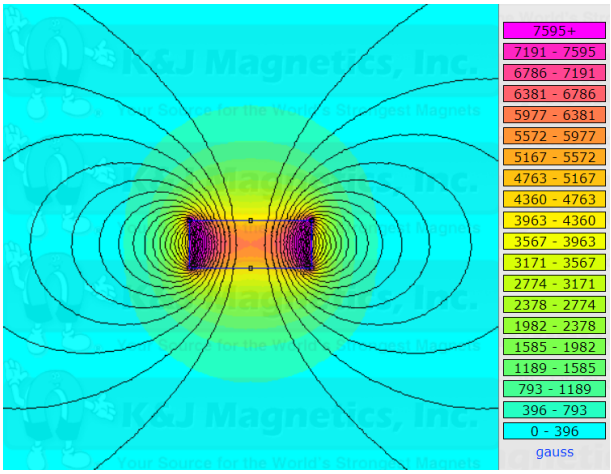


Figure 18 Magnetic Field Map of Magnets Used in Rotor Source: Adapted From [7]

The key features that needed improvement from last year's design are size, weight, and rotor clearances. To reduce size and weight the three generator stages were moved closer with virtually no gap between each stage which also allowed for the aluminum carriage to be shortened, reducing weight. To further reduce weight a much thinner carriage was used again replacing aluminum with the lighter 3D printed nacelle. To create better rotor clearances, new rotors with a smaller tolerance of the shaft hole were used to keep the rotors perpendicular to its surface. The final dimension was determined by 3D printing circular holes with various diameters and testing their fitment on the shaft. This allowed the team to achieve the 1.8 mm airgap described above. The final generator design is seen in Figure 19 and Figure 20.

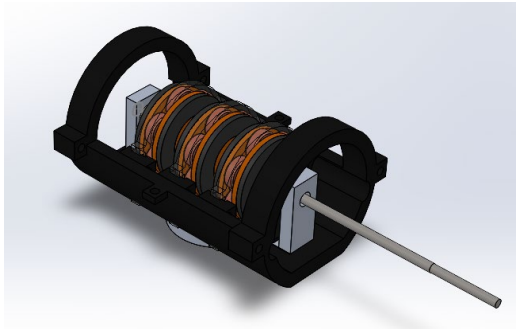


Figure 19 Generator SolidWorks

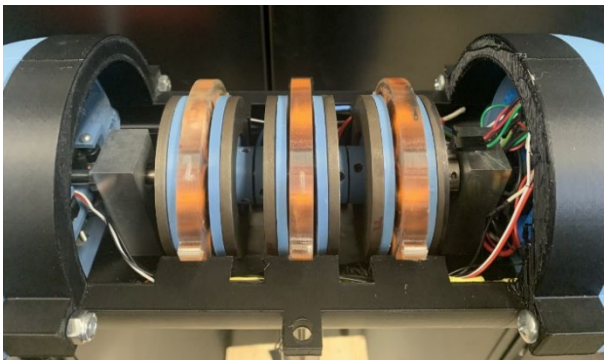


Figure 20 Physical Generator

Performance

To measure the generator's performance the team used a dynamometer and connected the generator's input shaft to the device. The dynamometer allows for the rpm to be changed while a variable load allows for various loading conditions to be tested. The team completed runs varying the rpm while keeping load constant for each run. The results of this testing are displayed in Figure 21. These results reveal that at lower loads more power is produced, but the higher loads allow for greater speeds. The team capped the testing speed at 2000 rpm since this rpm caused the dynamometer to reach its input power maximum. Comparing the results to last year's generator we find slight increases in power due to the smaller airgap. The generator also ran much smoother than the previous design with less vibration due to the tighter stator holders and rotor tolerances.

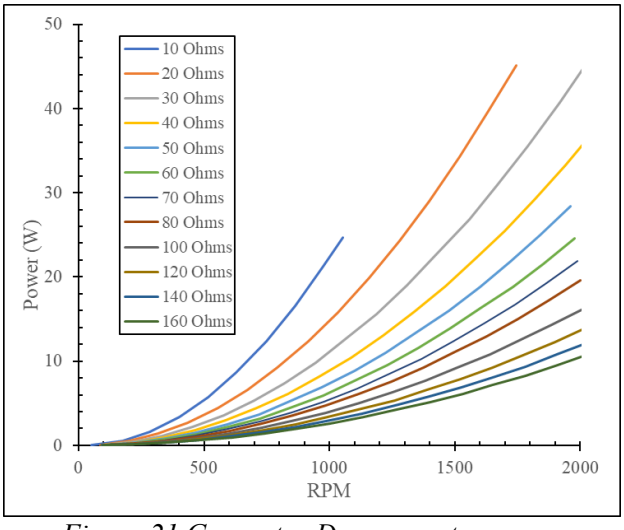


Figure 21 Generator Dynamometer Performance Curves

Foundation Design

The fixed offshore turbine foundation is the newest challenge to the Collegiate Wind Competition. The team discarded the previously attempted suction caisson design, and instead of researching other commercially used offshore foundations, gathered inspiration from previously successful foundations as they directly account for the same installation scenario. The most effective designs were similar to the suction caisson or used anchors.

The Sand Screw Egg Crate

The design for the foundation is based on egg crate paneling, which is commonly used in lighting. This design was chosen due to its ability to be easily designed, manufactured, and tested. The egg crate panels were designed such that there are two different configurations within the foundation, as shown in Figure 22. Typically, only configuration A would be necessary, but configuration B allows for two sides of the egg crate to support all adjoining sides. Thus, two configuration A panels were bolted to the top plate of the foundation, preventing any other paneling from falling out. Additionally, two B panels were bolted as well for stability and to maintain symmetry.

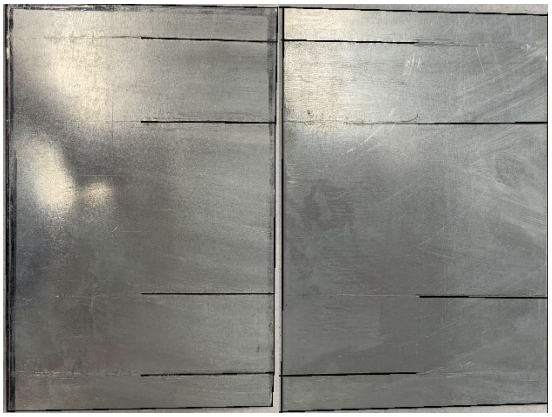


Figure 22 Egg crate panel configuration A (left) and B (right)

The foundation is critical to the turbine operation and must support all mechanical and aerodynamic loads imposed by the turbine system. This task was assessed by first understanding that the largest risk to the turbine's stability is the 11.5 lbs. of thrust force caused by the blades. Accounting for the 4 ft. moment arm from the top of the sand to the centerline of the turbine, the maximum load of the turbine is 46 ft-lbs. of torque can be expected at 25 m/s. As an added precaution against any time-dependent weakening of the foundation, the team decided on a safety factor of 2 for the moment resistant capacity.

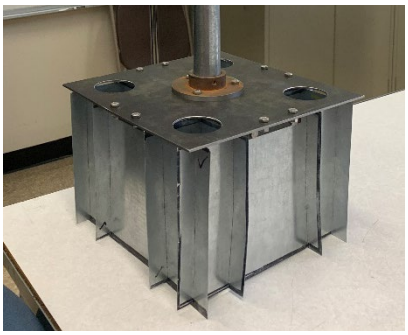


Figure 23 Fully Built Foundation

To retain the spirit of commercialized installation, the foundation design was developed such that it could be installed facing any direction and that the turbine could resist winds from any direction. The foundation is designed to hold four screws as this choice provides the aforementioned safety factor but could be modified slightly to account for more screws, and thus more stability to ensure safety during emergency scenarios that occur during high wind speeds.

Installation

The current foundation design prioritizes a fast installation time. First an orbital hand sander is used to vibrate the egg crate into the sand, then the anchors are drilled into the sand using an impact drill. The installation of the anchors adds additional resistance to tipping, but also aids in packing the sand within the foundation.

Testing

The foundation was tested in all aspects of operation for the competition: weight, installation, and durability. The weight of 5.2 kg was measured using a scale. Practiced installations of the foundation in a simulation sand box were done and total installation took on average: 10.42 minutes.

Durability was tested more thoroughly as it was considered the highest priority for the competition turbine. Experiments were done via a series of tip over tests to examine the capabilities of the foundation design, where a moment would be applied until the foundation failed. To apply a moment to the foundation, a weight was attached to a string that ran over a pulley and connected to a moment arm. Failure is determined either when the

tower shifted greater than 10mm or 15º. The test setup can be seen in Figure 24. Different combinations of anchors and walls were tested to empirically model the strength of the various configurations.

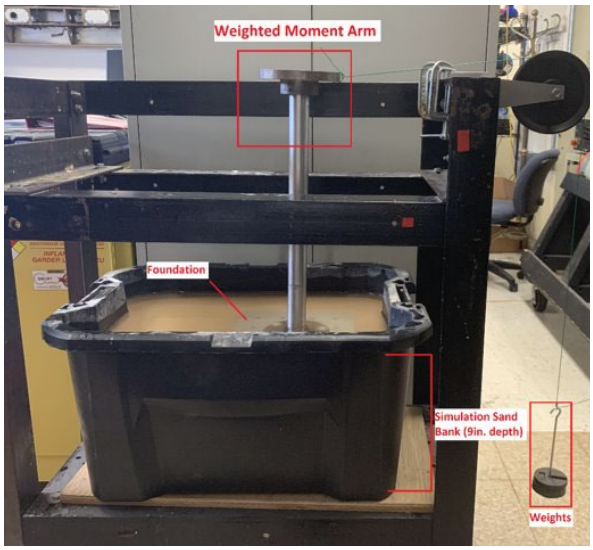


Figure 24 Foundation Testing Rig

The sole testing of anchors determined that the anchors near the tail of the turbine had little to no effect on the tip-over moment resistance of the foundation. The anchors were symmetric in strength fore and aft, perpendicular to the direction of wind, and their moment-resistive force can be described using Eq. 5.

$$R(x) = (R_{max} - R_{min})e^{\left(-\frac{\pi}{2}*x^2\right)} + R_{\min}$$

where x is the distance in inches from the centerline of the foundation tower. $R(x) = 0$ for negative values of x.

The sole testing of walls revealed a similar pattern of diminishing returns. Overall, the moment resistive strength of the walls and anchors combines additively, resulting in a total strength of 96 ft-lbs, giving this foundation design an overall safety factor of 2.1.

Electrical Design

The turbine electronics convert and optimize power while controlling various subsystems for safe and efficient operation. The entire electrical system was redesigned from previous competition years to promote efficiency and reliability. The turbine electronics are subdivided into four primary segments: rectification, regulation, over-voltage protection, and variable load. The analysis of the turbine control system will conclude with an overview of the assembled hardware. A single-line diagram of the power system can be found in Figure 25.

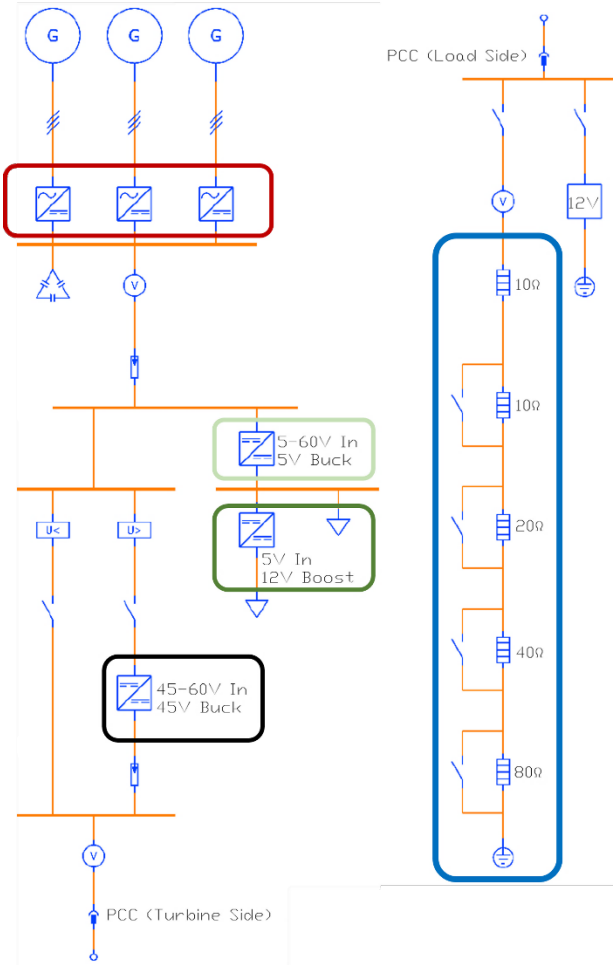


Figure 25 Single Line Diagram (SLD)

Rectification

The generator produces three staggered stages of 3-phase AC power that must be converted to DC power. In previous competition years, the rectification of the nine total AC phases occurred in the turbine electronics box.

In 2022, the team used an 18-24 pin connector to interface the nacelle/tower with the signal modulation circuit box because various sensors were being integrated into the nacelle. It is not feasible to route this many power and signal cables through the tower. Therefore, the team has now moved rectification to the nacelle, which means that we have reduced the number of power connector pins from 9 to 1.

The team has designed an ideal rectifier that uses controller ICs to trigger MOSFETs as switching elements rather than traditional diodes. However, due to the complexity of the circuit, it had to be converted into surface mount components to fit within the size constraints of the nacelle. Because of this, the team went with traditional diode bridge rectifiers this year but plans to introduce ideal rectification in the 2024 competition turbine.

The team is using three FUS45-0045B three-phase bridge rectifiers (boxed in red in Figure 25) because of their low forward voltage drop of 0.55V. To reduce rectification voltage ripple, the team calculated the minimum filtering capacitance using Eq. 6, where N is the generator RPM, P is the number of rotor poles, I is the rectified current, and V_{p-p} is the rectified peak-to-peak voltage ripple.

$$C = \frac{I}{2fV_{p-p}} \; where \; f = \frac{NP}{120} \quad (6)$$

The minimum capacitance was determined to be 1800 µF based on generator RPM values ranging from 0 to 2000 RPM with a desired voltage ripple of 0.1 Vp-p. By mitigating voltage ripple, the turbine will be outputting a cleaner DC voltage thus boosting the power curve score.

Regulation

Certain turbine actuators and sensors require regulated voltage for normal functionality. The power system utilized two primary switching converters boxed in light and dark green within Figure 25. A wide input buck converter operates at an input voltage ranging from 5 to 60 V_{DC}. This converter (shown in light green in Figure 25) converts rectified voltage from the generator to 5 V_{DC} out. 5 V_{DC} is required to power the turbine's two Actuonix L12 actuators, and the A3144 hall effect sensor. A 5V to 12V boost converter (shown in dark green in Figure 25) is connected to the output of the buck converter. It is necessary to have 12V power the turbine's MPXV7002DP pressure differential sensor and two SPDT electromechanical relays. Figure 26 illustrates the schematic of the 5 V_{DC} buck converter based on a TL2575-05 IC. A schematic of the 12 V_{DC} boost converter based on the LM2577-12 IC is found in Figure 27. The maximum current of the buck and boost circuits is 1.2 A_{DC}. Since the primary purpose of the regulation circuits is to power microcontrollers, sensors, and actuators, it will never come close to the maximum current limit.

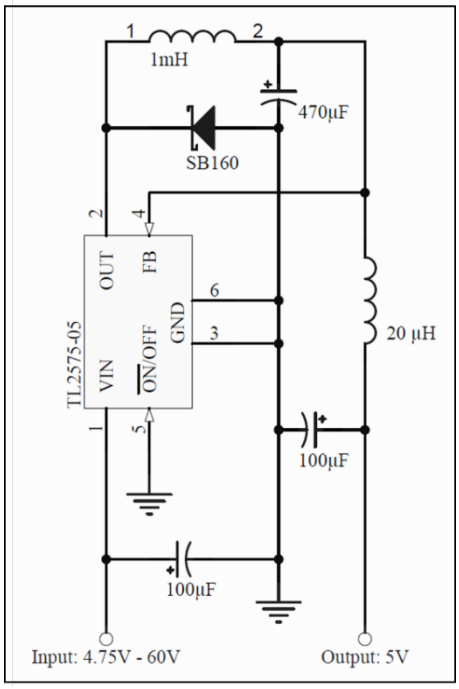


Figure 26 5 V_{DC} Buck Converter

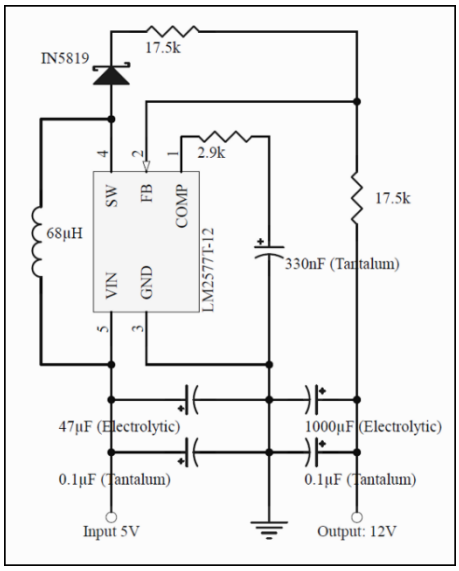


Figure 27 12 V_{DC} Boost Converter

Components for each of the switching converter circuits were chosen with reference to data sheets and predicted performance parameters. Although switching converters are more expensive and complex in comparison to linear regulators, the team chose switching converters due to their high efficiency. As configured, the buck and boost converters in the power system operate at roughly 90% conversion efficiency while linear regulators operate at most 60% efficiency. Switching regulators

also can handle wider input voltage ranges. Buck and boost converters have a high degree of switching noise. To mitigate noise, LC filters are used to smooth out voltage ripples.

PCC Over-voltage Protection

In certain operating conditions, the generator may produce more than 48 V_{DC}. To prevent the PCC voltage from ever exceeding 48 V_{DC}, a third high voltage switching buck circuit based on the LM2576HV is used to limit the turbine's output voltage to 45 V_{DC}. To avoid switching power loss, the over voltage buck circuit will only activate when the PCC voltage sensor reads a value exceeding 45 V_{DC}. Under most operation conditions, the turbine side SPDT relay sends power from the rectifier directly to the PCC thus bypassing the over voltage buck circuit. When the PCC voltage exceeds 45 V_{DC}, the SPDT relay turns on and sends power into the over voltage buck circuit. The turbine power system is designed to withstand at least 60 V_{DC}. If the turbine ever detects generator voltage exceeding 60V, the turbine will shut down. The 45V buck is boxed in black within Figure 25. The schematic of the buck circuit is shown below in Figure 28.

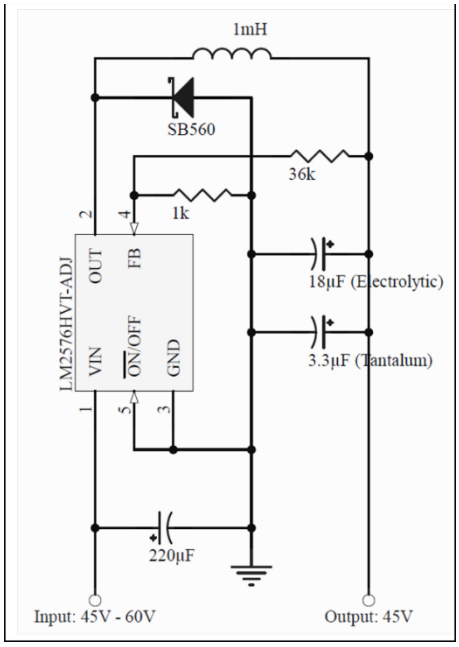


Figure 28 Over Voltage Buck Converter

Load System

As shown in the right side of the SLD (Figure 25). The primary purpose of the load is to power the turbine during startup and dissipate power during normal operation. The load system also houses two microcontroller boards: Arduino Mega 2560 operated by the ATmega2560 chip, and the Arduino Micro operated by the ATmega32U4 chip. The Arduino Mega conducts most of the computation for the control system while the Arduino Micro runs the RPM calculation software.

Variable Load

The variable load is a binary composition of 10 Ω, 20 Ω, 40 Ω, and 80 Ω power resistors in series with a non-controllable 10 Ω resistor as shown in Figure 25 (boxed in blue). SPST relays are connected in parallel to each resistor. When a relay is turned on, current is shorted around the resistor turning it off. This enables the control system to adjust the turbine's load resistance from 10 Ω to 160 Ω in 10 Ω increments.

The team initially tested the variable load with traditional electromechanical relays due to their low cost and availability. The electromechanical relays were prone to failure, and they had a high-power draw. Because of this, searched for solid-state alternatives and chose the newly released IXYS CPC1705Y phototransistor-based solid-state relay. These highly efficient SPST relay ICs utilize p-type optical FETs (normally closed logic) which simplifies the load control software.

When the turbine switches load resistances, there may be millisecond periods where all the controllable resistors are turned off. In these cases, the turbine's load resistance will be 10 Ω because a non-controllable 10 Ω power resistor is always in series with the variable load. This safety feature prevents the turbine load from ever shorting out, which may cause excessive current that could potentially damage the generator or electronics.

Startup Power Source

During startup, the turbine may not be producing enough power to drive all the peripherals. In this condition, the SPDT electromechanical relay sends power from the 12 V_{DC} supply in the load across the PCC into the Turbine. Once the turbine is producing sufficient power, the relay switches on, and power from the generator is sent into the load.

Electromechanical Relay Protection

Within the power system the SPDT relay plays a critical role in directing power in the turbine and in the load. If one SPDT relay fails, the turbine is

unable to function. At the same time, electromechanical SPDT relays are one of the most unreliable parts in the power system. Voltage swings, contact damage, or even physical shock due to travel or drops can break electromechanical relays. Due to the functionality of SPDT relays, there are not many solid-state replacements for SPDT relays. Figure 29 illustrates the SPDT electromechanical relay protection circuit used in both the turbine and load boxes.

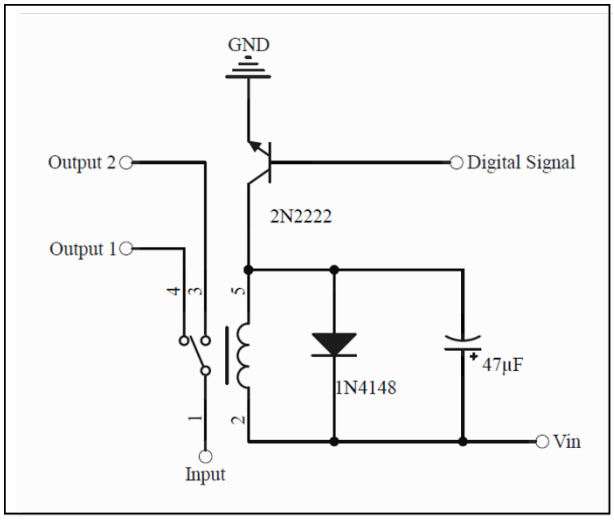


Figure 29 Relay Driving and Protection Circuit

The circuit drives the relay with the 2N2222 BJT which applies just the minimum current to switch on the relay coils. This will prevent over-voltage swings that occur when a relay is switched on and off that can burn out the coil within the relay.

Both the turbine and load circuit boards include custom made sockets to quickly replace the electromechanical relay if it fails. These sockets are made of Dupont female header pins as shown in Figure 30.

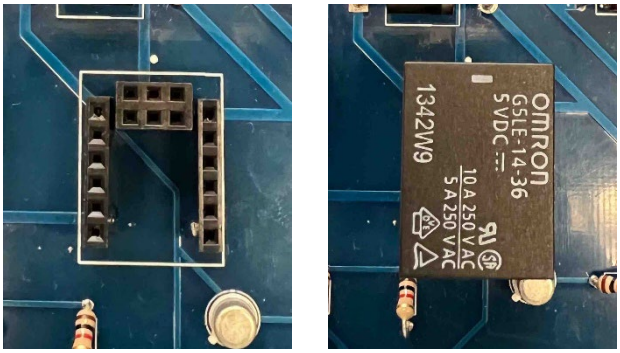


Figure 30 Custom Socket (On Left), Relay Placed into Socket (On Right)

Hardware Overview

The rectification electronics are housed within the Nacelle as shown in Figure 31. A more explicit view of the rectification board can be seen in Figure 32. Nine phases of power from the generator input into the board. The board also supplies GND, 5V, and 12V for the sensors installed inside the nacelle.

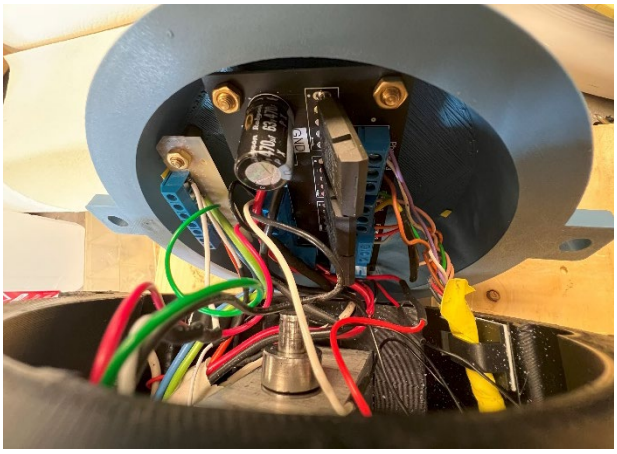


Figure 31 Rectification Board Mounted inside the Nacelle



Figure 32 Rectification Board

A turbine-side Power and Signal Modulation Box houses all the regulators as shown in Figure 33. It also acts as the bus facilitating communication between the load box, and the sensors mounted in the nacelle. The power and signal modulation circuit board can be seen in Figure 34.

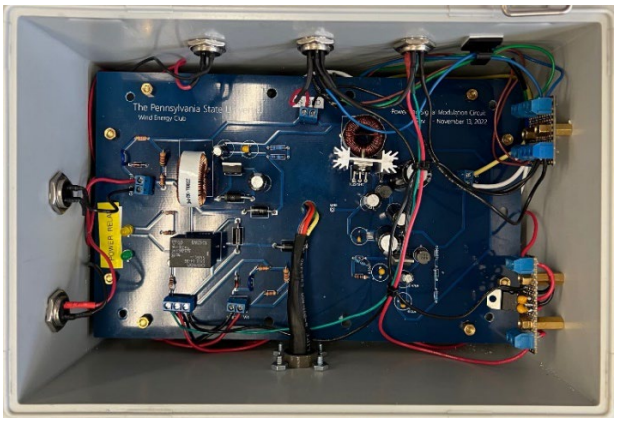


Figure 33 Turbine-Side Power and Signal Modulation Box

The 5V Buck converter is boxed in green, the 12V boost converter is boxed in yellow, the 45V buck converter is boxed in white, and finally the SPDT relay is boxed in red.

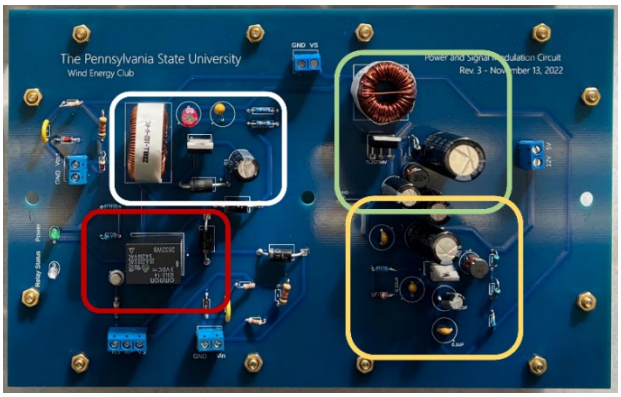


Figure 34 Power and Signal Modulation Board

A Point of Common Coupling (PCC) terminated by Anderson Power Pole connectors facilitates power transmission from the turbine-side Power and Signal Modulation Box to the Load Box. The Load box (shown in Figure 36) houses the variable load circuit and the two microcontrollers.



Figure 35 Variable Load Board

The solid state relays interfacing with the variable load are boxed in white, and the SPDT relay is boxed in red within Figure 35. The load box also uses fans to actively cool the power resistors mounted in the load box.

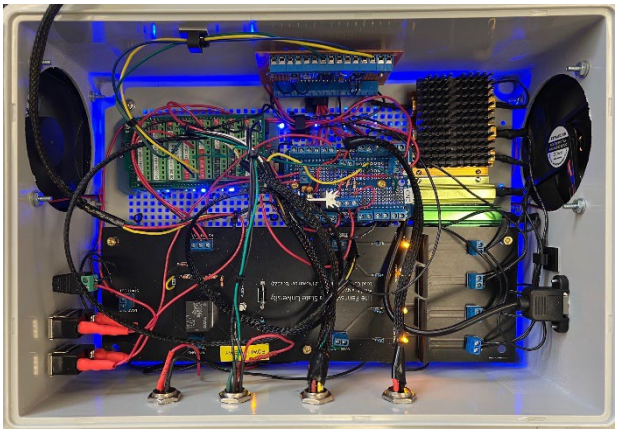


Figure 36 Load Box

Software Design

The objective of the turbine's software is to maintain safety for the turbine while also producing the most power based on the incoming wind speed. The team completely redesigned the turbine control code to address several of the shortcomings experienced during the 2022 competition. There were a lot of shortcomings in last year's code with inefficient data acquisitions and failure to pass safety tasks. For this year, we have implemented many improvements including an efficient codebase, and data collection with visualization capabilities.

State Machine

At the beginning of the semester, the team evaluated several different code architectures. The two major options under consideration were multithreading or state machines. We ultimately decided to design our code as one state machine for its simplicity and efficiency. Due to the nature of embedded systems—which have limited resources—state machines have a much lower memory usage compared to multithreading. State machines can also avoid the overhead of thread management, which requires significantly more resources for memory and processing power to manage and switch between threads. Threading can also create unpredictable execution flow due to thread scheduling and synchronization. State machines allow us to define a clear set of states and transitions between them, giving us predictability and the ability to debug easily.

Each hardware component on the turbine is represented as a module in software. Each module then has a function that represents tasks it should run

during that state. The states are startup, looping, and stop. Using the incoming sensors' values, we determine the state the turbine should be in at any given time. By making each module independent of another, this prevents unintended interactions between the different modules and contributes to a more understandable and maintainable codebase.

Variable Load Control

The load resistance system is created with four resistors of 10, 20, 40, and 80 ohms to generate 16 different possible load resistance through different combinations of each resistor, with an additional 10-ohm resistor to ensure the circuit is not shorted. Given a value to set the system to, we subtract the value by 10 then divide it by 10 to receive a number between 0 - 15. We can then convert this number into its binary representation and set each representing resistor to the value of the binary digit where 1 means on and 0 means off.RPM Sensor

We cannot accurately track RPM on the Arduino Mega that hosts the control code due to the time required to loop through all its processes. The RPM code must loop fast enough to measure the speed of the spinning turbine. Unfortunately, Arduinos can only execute one program at a time, so we implemented an Arduino Micro to separately run the RPM code. The Micro sends data to the Mega through the TX and RX pins using serial communication, while the Mega retrieves the RPM value prompted by the control code.

RPM Sensor

We utilize a hall effect sensor to measure the rotational speed of the generator by detecting changes in a magnetic field caused by the presence of magnets attached to a metal ring in the generator. These magnets are placed near the circumference of the metal ring at opposite ends. When the magnets pass the sensor, they create a magnetic field that causes a voltage drop across the sensor. The frequency of these voltage changes corresponds to the RPM of the generator.

The code that calculates the RPM records the time when it detects a magnet. It saves these times into an array of a size divisible by two; every two magnet detections correspond to one full rotation of the generator. We then take the array and find the latest and earliest times and calculate the difference between the two. Lastly, we use a proportions formula to find the RPM and send this value to the Arduino Mega. Figure 37 compares sensor produced RPM data to dynamometer readouts. The sensor performs very close to the ideal curve shown in green.

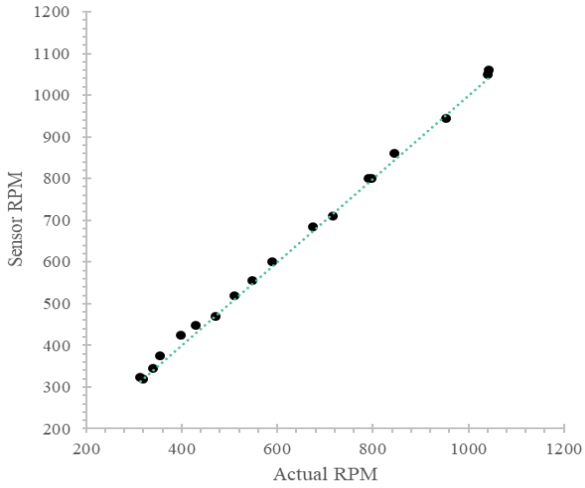


Figure 37 RPM Sensor Performance

Power Curve Task

Power captured by the rotor is obtained via Eq. 7:

$$P_{rotor} = 0.5\rho A v_{wind}^3 C_p \quad (7)$$

where the rotor power coefficient, C_p, is a function of tip speed ratio, λ, and the blade pitch angle, β. A variable load controls the generator's rotational speed, ω_{rotor}, allowing the team to adjust λ because $\lambda = \frac{\omega_{\text{rotor}} R_{\text{rotor}}}{v_{\text{wind}}}$. Controlling λ through the variable load and β with the pitching mechanism, the control system maximizes C_p at any wind speed through a maximum power point tracking (MPPT) algorithm. The turbine's MPPT incremental conductance algorithm measures changes in current, δI, and voltage, δV, to predict how changes in λ or β impact the C_p.

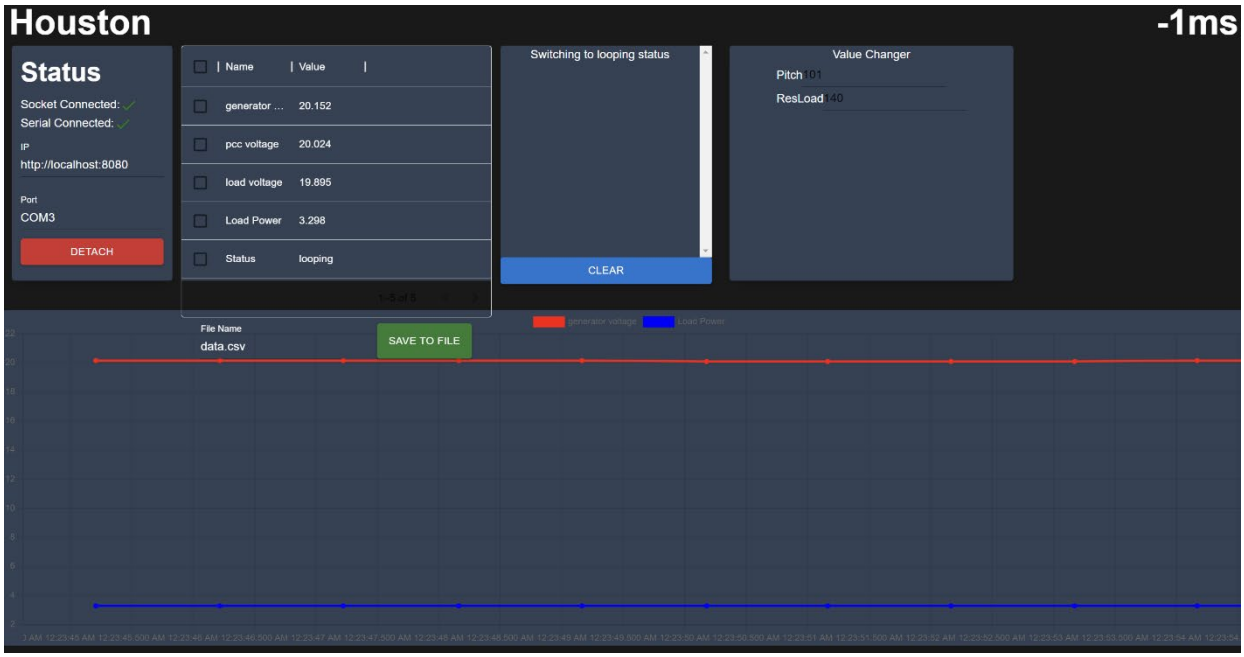


Figure 38 Houston Data Collection

Data Collection Hub

The data collection hub, otherwise known as Houston, is our internal tool for acquiring data and setting parameters on the operating turbine. With Houston, we can display, graph, and save data coming from the Arduino Mega. Houston also allows for live variable tuning during runtime. For example, we can adjust pitch angle to test power production without reuploading code for each test, saving significant testing time. This tool runs on any computer and is very user-friendly. It allows other sub-teams such as Aerodynamics and Electronics to test without having the Software team on hand to individually set testing points. Houston can also automatically save all the experiment data to a .csv file, allowing the other teams to test and acquire data without needing extensive programming experience.

Deep Dive into States

Startup Mode – In startup, we will initialize sensors, the wind turbine will pitch to its starting angle, and check for PCC disconnect or emergency stop. If either is detected, it will move to stop. If not, it will keep repeating these operations until we detect over 9 volts in the generator, then it will move to the looping state.

Looping – In looping, the wind turbine will detect if we are in power curve, rotor speed control, or durability test base on the wind speed. The wind turbine will then try to find the best pitch angle and load resistance to accomplish the needed goal. To learn how we do this, please refer to the interpolation section. If the load voltage ever exceeds 45 volts, power is redirected through the 45-volt buck circuit to reduce the output voltage to meet competition standards. On top of this, the turbine is also constantly checking if the emergency stop has been pressed or if there is a PCC disconnect. If either an

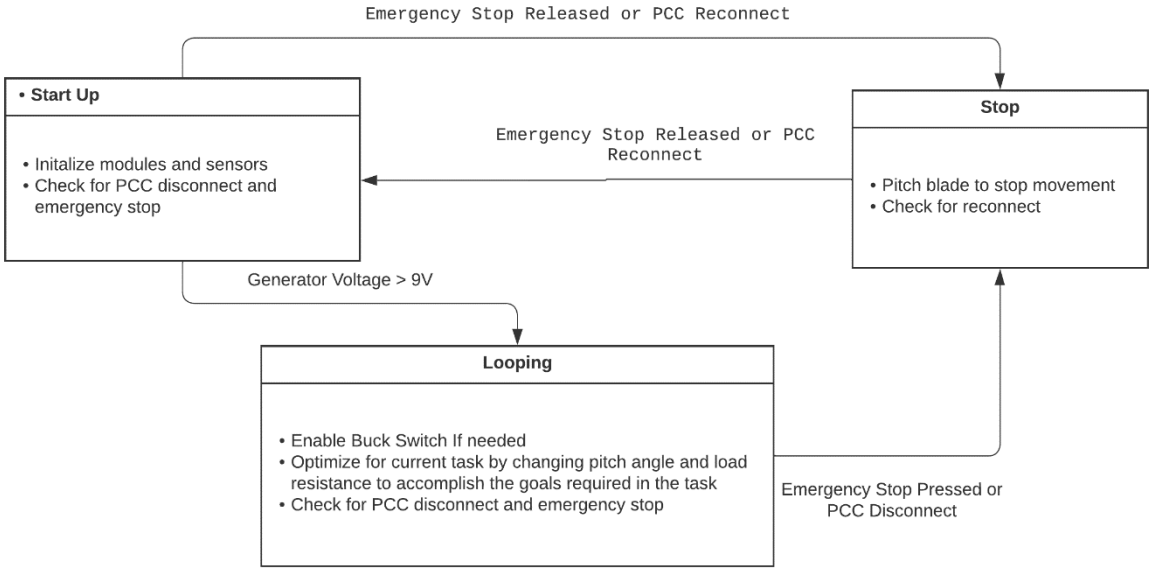


Figure 39 Emergency Stop/PCC Disconnect

emergency stop or PCC disconnect has been detected, we move to the stop switch.

Stop – In stop, the turbine will pitch to a predetermined angle that we know will stop the blades from spinning and maintain it. It will also check if we can move back to startup. If the stop state was caused by the emergency stop button, it will simply move back to startup once the button has been released. If it is a PCC disconnect, then we first wait for the voltage in the PCC to drop below a certain threshold. This means we have truly stopped the blades and prevented false startups. Then we wait for the PCC voltage to go above a threshold to move to the startup state.

Interpolation

Interpolation – If a data set is nonlinear, then a linear regression would obviously be a poor choice. Not only would it be inaccurate, but there would also be points of discontinuity. However, by using cubic spline interpolation, a smooth curve can be generated between each pair of points. Overall, this would create a continuous curve that provides a smooth estimate of data while minimizing the error between the curve and the data points. It is also very light on computation since the cubic spline function is generated beforehand, so the actual interpolation during runtime is simply a few multiplications.

TURBINE TESTING

XTURB-PSU Simulation models produced the data illustrated in Figure 40. At start-up and low wind speeds, high pitch angles must be used to achieve the most optimal C_P (power coefficient). As the wind speed increases, pitch angles must be reduced to achieve the highest C_P. The most optimal rotor power coefficient is achieved at a pitch angle of 1.5 degrees and a TSR of 4.1.

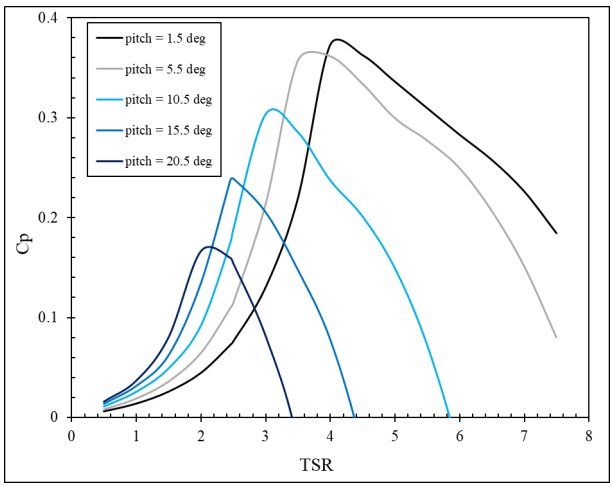


Figure 40 C_p versus λ

The team was only able to reserve one week of wind tunnel testing prior to the submission of the deliverable. It was soon discovered that the pitching mechanism was configured to pitch from 0° to -8°; however, the airfoils were only designed to function optimally in positive pitch range from 1.5° to 55°. Because of this, sub-optimal power curves were obtained through testing as shown in Figure 41 and Figure 42. The team has readjusted the pitching mechanism so that it can now pitch through 0° to 50°, so that proper experimental Cp/λ curves will be ready for the Q/A session.

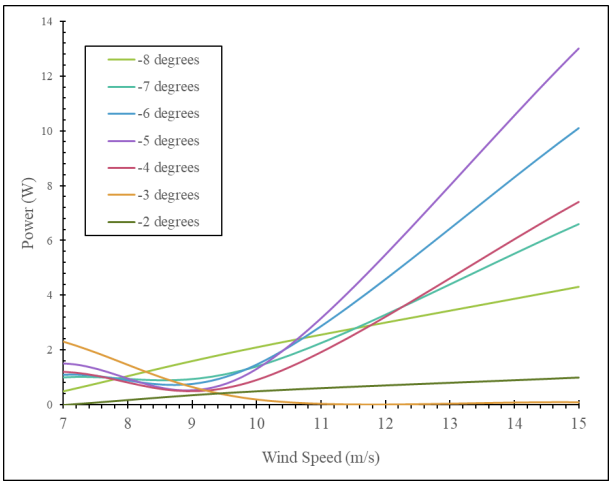


Figure 41Power Output with Negative Pitch at 80 Ω

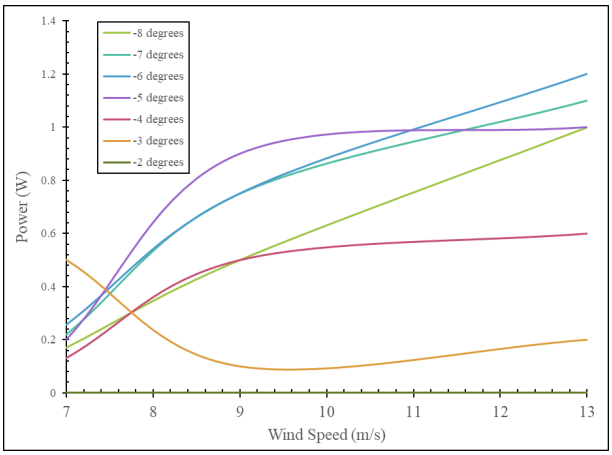


Figure 42 Power Output with Negative Pitch at 120 Ω

COMMISSIONING CHECKLIST

Table 1 displays a checklist utilized to confirm that the turbine is free from any damage, assembled accurately, and functioning normally.

Table 1: Commissioning Checklist

Turbine Testing Verification Procedure	Team Lead #1 Certification	Team Lead #2 Certification
Generator Subsystem Verification Steps		
Check for damage or cracks to the generator stators		
Confirm 3-Phases are connected to each of the three stages		
Tighten the set screws on the rotors		
Confirm airgap between every rotor and stator		
Verify signal and power cables are not in contact with the rotors		
Aerodynamic Subsystem Verification Steps		
Verify the servos are attached properly to the nacelle		
Tighten all fasteners in the pitch mechanism		
Confirm that the mechanism is not locked up		
make sure the 7-pin connector cable is connected properly to the electronics/sensors in nacelle		
Check blade for structural integrity		
Attach blades to pitching mechanism		
Attach nacelle lid to the nacelle middle piece		
Electronics Subsystem Verification Steps		
attach the 7-line cable to the turbine box		
Connect communication cables between load and turbine box		
Connect E-stop out wire to the emergency stop button		
Connect PCC cables from both load and turbine box to wind tunnels connectors		
Plug in the 12v input on the load box and flip the switches on		
Check all indication lights for power (Relay, Arduino, Load)		
Foundation Subsystem Verification Steps		
Ensure foundation walls are unbent		
Ensure foundation walls are slotted together fully		
Tighten angle brackets to walls with washer		
Tighten walls to top plate		
Pull wires through foundation tower		
Secure foundation tower to top plate		
Final Verification Steps		
Connect 7-line cable from nacelle to 7-line cable from foundation power		
Line up flange holes with studs on transition piece and place turbine on top		
Ensure the turbine is facing the correct direction		

ANNUAL ENERGY PRODUCTION

A Weibull distribution was applied to the simulated turbine power curve to estimate annual energy production. Figure 43 shows the input power curve used based on XTURB-PSU simulation data. Figure 44 illustrates the output annual energy production for average annual wind speeds ranging from 3 m/s to 8m/s.

The scale factor of the Weibull distribution (λ) is determined through Eq. 8:

$$\lambda = \frac{\bar{u}}{\left(\frac{\sqrt{\pi}}{2}\right)} \qquad (8)$$

Where, $\bar{u}$ is the annual average wind speed and the shape factor, k, is set to 2 (Rayleigh distribution). The Weibull values as set by these parameters were multiplied by the wattage of the power curve and the number of hours in a year. The sum of these values provided the energy production for a particular annual average wind speed condition as shown in Figure 44.

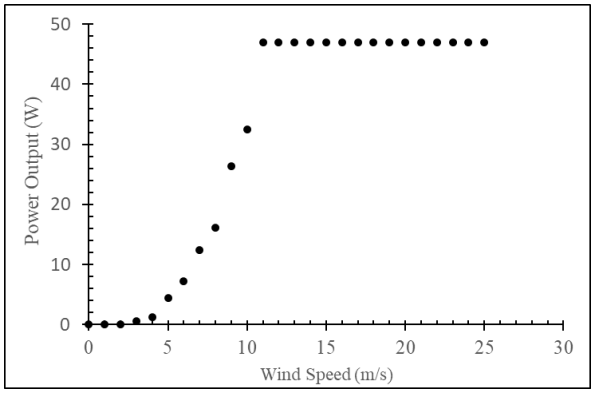


Figure 43 Turbine Power Curve

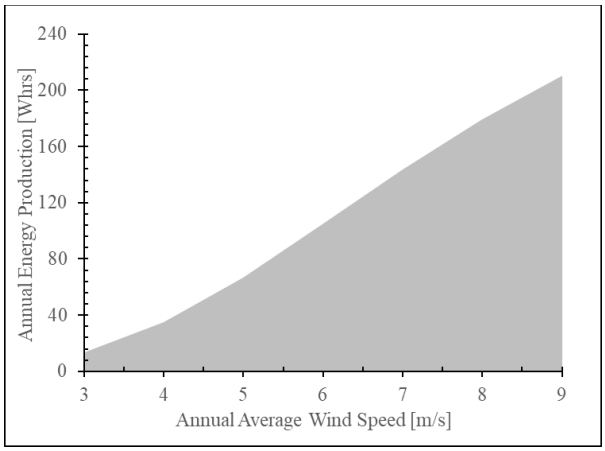


Figure 44 Annual Energy Production vs Annual Average Wind Speed

DESIGN CHANGES TABLE

AEROSPACE SUBSYSTEM	
Nacelle	A new bottle-shaped nacelle was designed for the 2023 competition year
Blades	New blade material (Rigid 10K) Same blade design as 2021
Pitching Mechanism	A new linear actuator-based pitching mechanism was designed and moved to the inside of the Nacelle
Fins	New "Tie-fighter" like blades were designed for the turbine
GENERATOR SUBSYSTEM	
Rotors	New rotors were designed and built to replace the old rotors from 2018
Stators	The same stator design from 2018 is still being used in the 2023 competition
ELECTRICAL SUBSYSTEM	
Rectifier Board	A new rectifier board was designed and mounted to the nacelle
Turbine box	A new turbine box was designed and built with a custom power and signal modulation circuit board
ELECTRICAL SUBSYSTEM CONTINUED	
Load Box	A new turbine box was designed and built with a custom variable load circuit board
FOUNDATION SUBSYSTEM	
Foundation	The entire foundation sand screw egg foundation is newly designed and built
SOFTWARE SUBSYSTEM	
Turbine Code	The entire turbine code was written from scratch
Houston DAQ	The Houston Data Collection hub was newly designed for the 2023 competition



References

[1] “Rigid 10K,” *RIGID 10K MATERIAL PROPERTIES DATA*. [Online]. Available: https://asset.dynamism.com/media/catalog/product/pdf/Formlabs_Rigid_10K_TDS.pdf. [Accessed: 04-May-2023].

[2] C. Chen, T. Wang, and L. Wang, “Sensitivity study of the influence of blade sectional stiffness parameters on the aeroelastic response of wind turbines,” *Frontiers*, 21-Jun-2021. [Online]. Available: https://www.frontiersin.org/articles/10.3389/fenrg.2021.707082/full. [Accessed: 04-May-2023].

[3] “Linear Regulator and switching regulator (what is the difference between linear and switching regulators?),” *ROHM*. [Online]. Available: https://www.rohm.com/electronics-basics/dc-dc-converters/linear-vs-switching-regulators. [Accessed: 04-May-2023].

[4] “Magnetism Basics,” *How magnets work*. [Online]. Available: https://ece.northeastern.edu/fac-ece/nian/mom/work.html. [Accessed: 10-Feb-2022].

[5] S. Fahey, “Basic Principles Of The Homemade Axial Flux Alternator Basic Principles Of The Homemade Axial Flux Alternator,” Dec. 2016.

[6] K. C. Latoufis, G. M. Messinis, P. C. Kotsampopoulos, and N. D. Hatziargyriou, “Axial Flux Permanent Magnet Generator design for low cost manufacturing of small wind turbines,” *Wind Engineering*, vol. 36, no. 4, pp. 411–431, 2012.

[7] “The K&J Magnetic Field Calculator,” *K&J Magnetics*. [Online]. Available: https://www.kjmagnetics.com/fieldcalculatorold.asp. [Accessed: 04-May-2023].

California State University – Maritime Academy Wind Team

2024 Collegiate Wind Competition
Final Turbine Design Report

Faculty Advisor *– Dr. Thomas Nordenholz | TNordenholz@csum.edu*

Project Manager *– Jasen Nicolas | JNicolas56@csum.edu*
Connection Creation Lead *– Vonne Ng-Bader | Vng-Bader63@csum.edu*
Project Development Lead *– Matthew Rizzi | MRizzi49@csum.edu*

Blades *– Victor Mashevsky*
Mechanical *– Tobias Afdahl & Lucas Kennedy*
Generator *– Nathan Witte & Dayton Huffaker*
Foundation *– Vonne Ng-Bader & Kent Suzuki*
Instrumentation & Electronics *– Nathan Witte, Cyrus Khaleeli, & Jasen Nicolas*

A Very Special Thanks To:

Dr. Tom Oppenheim | Mr. Steffan Long | Mr. Michael Kazek | Mr. Michael Strange | Mr. David Grover
Ms. Samantha Koekemoer | Mr. Guy Sanchez | Dr. Zachary Nosker | Mr. Tom Clyatt | Mr. Josh Short

Many Thanks To Our Sponsors:

Table of Contents

Executive Summary **2**
Chapter 1: Turbine Design **2**
1.1 Blades 2
1.1.1 Airfoil Selection 2
1.1.2 Optimized Blade Geometry 3
1.1.3 Static Performance Analysis 3
1.1.4 Manufacturing/Material 3
1.1.5 Mechanical Loads Analysis 3
1.2 Mechanical Design 4
1.2.1 Pitch Overview 4
1.2.2 Pitch Assembly 4
1.2.3 Actuation Linkage 5
1.2.4 Blade Connection 6
1.2.5 Stress Calculations 6
1.2.6 Nacelle and Tower Assembly 6
1.3 Foundation 7
1.3.1 Foundation Integrity Analysis 7
1.3.2 Manufacturing Process 7
1.3.3 Durability/Load Testing 8
1.3.4 Foundation Design Iterations 8
1.4 Generator 8
1.4.1 Overview 8
1.4.2 Rotor Design 8
1.4.3 Stator Design 9
1.4.4 Operating Voltage/Performance Testing 9
1.5 Electrical and Instrumentation 9
1.5.1 Turbine Side Electronics 9
1.5.2 Load Side Electronics 10
1.5.3 Instrumentation 10
1.6 Software 11
1.6.1 Individual Component Development 11
1.6.2 Integration of Components 11
1.6.3 State Machine 12
Chapter 2: Full Turbine Assembly **13**
2.1 Full Turbine Integration 13
2.2 Distributed Team Environment 14
Chapter 3: Turbine Testing Results **14**
3.1 Wind Tunnel Testing 14
3.2 Field Testing 14
3.3 Annual Energy Production 14
Chapter 4: Influence of Previous Design **15**
Chapter 5: Commissioning Checklist **15**
Bibliography **16**

Executive Summary

Cal Maritime's turbine design is a three-bladed, controllable pitch, horizontal-axis turbine fixed to a custom-built radial flux generator. AC power from the generator is rectified to DC power, through a 3-phase full-bridge passive rectifier and is connected to our variable resistive load. Our turbine structure will be supported and anchored into sand by a bucket-type foundation.

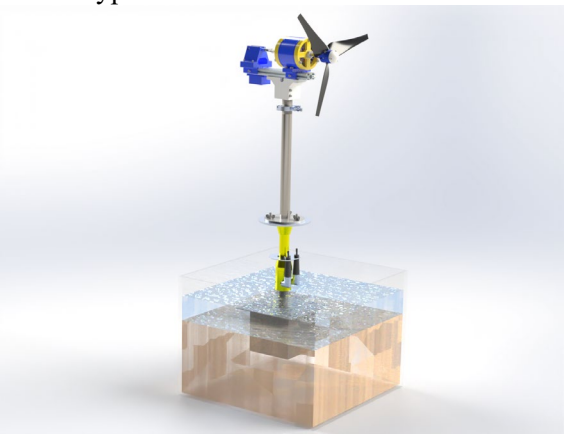


Figure 1: Full Design Render

Our primary objective in the 2024 Collegiate Wind Competition was to create a simple and robust design to maximize effectiveness at completing competition tasks while complying with design constraints. To achieve this objective, we maximize power at wind speeds from 5 to 11 m/s, maintain our rated power and rotor speed at wind speeds from 12 to 14 m/s, conduct shutdown and restart scenarios, and withstand wind speeds up to 22 m/s.

For blades, the airfoil we chose is the A18 which is thinner than the airfoils used by previous years, to maximize aerodynamic efficiency. To offset our thinner design, we manufactured our blades out CF-PLA which is more rigid than materials used in previous years. To further maximize power, we built a custom radial flux permanent magnet generator to eliminate cogging, and a variable resistive load to reach maximum power at wind speeds from 5 to 11 m/s through a perturb and observe maximum power point tracking (MPPT) algorithm.

We developed a new type of controllable pitch mechanism which is used to pitch the blades in safety shutdown and restart scenarios as well as being used in conjunction with the variable load system to modulate power and RPM at wind speeds above 11 m/s. Our pitch system design uses a concentric shaft, with a scotch-yoke mechanism to pitch the blades.

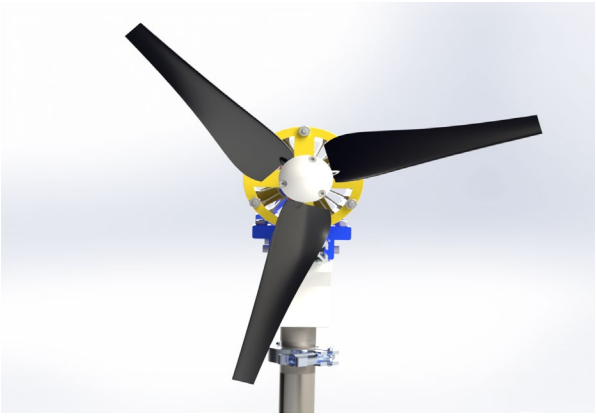


Figure 2: Full Render Front View

To maintain simplicity and ensure proper functionality of the system throughout the entire testing period, a single microcontroller is used on the load side. The system collects measurements from our RPM, windspeed, voltage, and current sensors, and outputs signals to the load and the linear actuator.

Finally, similar to our 2023 counterparts, we ensured that the blades, mechanical systems, and the foundation were properly sized to withstand the loads of the following operating conditions. The first state considered is maximum power at 11 m/s, just before the rotor pitches to shed power. We expect the maximum thrust from the blades in this scenario. The second state is runaway, which captures forces at 14 m/s and 4500 RPM just before we feather our blades. This state will primarily affect the blades as they endure extreme bending moments and radial forces. This shaft speed was determined by disconnecting the load at 14 m/s. The final state under consideration is the durability state, where the wind speed is at 22 m/s and our turbine is below 300 RPM. In this scenario, the maximum aerodynamic drag and maximum total force is experienced by the foundation.

Chapter 1: Turbine Design

1.1 Blades

1.1.1 Airfoil Selection

The focus for blade design this year was maximizing aerodynamic efficiency given the low Reynolds number flow. A thin airfoil would be ideal for this purpose, but airfoils that are too thin quickly approach material stiffness limitations. After iterative testing, the final airfoil chosen was the Archer A18 with a thickness to chord ratio of 7.3% and a peak glide ratio (C_L/C_D) of 48.6 at our expected Reynolds number of 60,000. The A18

airfoil has sharp peaks in its C_L/C_D vs angle of attack (AoA) graph. Although this behavior is undesirable, our rotor maintains a relatively broad power curve, which lends itself to smooth controllability, with near maximum power between a tip speed ratio (TSR) of 3.8 and a TSR of 5, as shown in Figure 3, which corresponds to 1800 to 2500 RPM. Overall, we decided that the trade-off was worth it for better efficiency.

1.1.2 Optimized Blade Geometry

Unlike previous Cal Maritime teams, we used the A18 airfoil along the entire span of the blades instead of blending in a thicker airfoil near the root because research indicates that using multiple airfoils of different thicknesses on a single blade disrupts the smooth transition of flow, increasing drag [5]. Additionally, the blades have a high factor of safety despite the thinner airfoil, as shown in section 1.1.5. The blade geometry optimization and simulation were conducted using Qblade CE version 2.0.6.4. To maximize power, we used the Schmitz optimization method–which is derived from Blade Element Momentum (BEM) theory–to create an optimal chord (c) and twist (θ) distribution. Schmitz optimization requires a design TSR, so a TSR of 4.2 was chosen; both because iterative testing in Qblade showed that it was optimal, and because it is backed by empirical research findings [6]. Since Reynolds number can vary over the span of the blade, from about 40,000 at the root to 60,000 at the tip for the rated wind speed, and because the optimal angle of attack shifts with Reynolds number, the multi-polar blade design function was used, which automatically adjusts the AoA of each section in accordance with the local Reynolds number [1].

1.1.3 Static Performance Analysis

The overall rotor performance was quantified using Qblade, which we used to calculate the non-dimensional coefficient of power (C_P). This was the metric used to compare blade geometries in the design phase. Our final design achieved a max C_p of 0.4. The static performance graph shown in Figure 3 correlates well with real world testing.

1.1.4 Manufacturing/Material

To allow easier manipulation of the blade design in CAD, we developed a plugin for Fusion 360 that takes the blade details from Qblade as well as the airfoil shape and creates a smooth solid body that is much easier to work with, allowing us to integrate the blade root into the blade with ease. Like previous years, the blades were FDM 3D printed at 100% infill, which has the benefit of easy manufacturing and rapid prototyping. We noticed that stiffer materials increased performance by reducing blade deflection, so the material we settled on is carbon fiber filled PLA, with 15% micro carbon strands by weight, and a tensile strength of 48 MPa [2]. This material was chosen for its increased rigidity over regular PLA. Rigidity is measured using the flexural modulus, which is 3200MPa for standard PLA compared to 6320MPa for the CF-PLA [2].

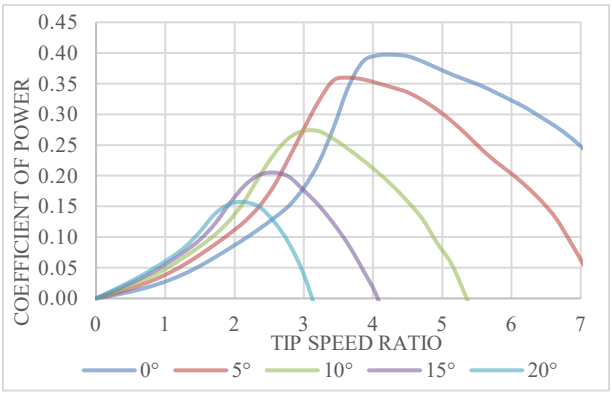


Figure 3: Power Performance Curves

1.1.5 Mechanical Loads Analysis

1.1.5.1 Blade Span

Operating State	Radial Load (N)	Stress (MPa)	Deflection (mm)	Pitching Moment (N-m)	FS
Runaway	270	2.85	0.15	0.06	19
Rated Power	120	1.28	0.09	0.05	43

Table 1: Blade Load Analysis Results

Our mechanical load analysis was conducted using a similar method to the 2023 Cal Maritime team. The wind and radial loads along the span of the blade were modeled as a rotating cantilever beam, with neglected twist. Based on an MIT aerodynamics lecture, we compensated for the area properties of the airfoil-shaped cross section [3]. The blade is subjected to distributed wind loading on the flapwise side, which is calculated by Qblade, and radial loading, which creates stress at the root of the blade and creates a restoring moment that helps the blade resist deflection in an effect known as centrifugal stiffening. To model the deflection of the blades accounting for centrifugal stiffening, we used an iterative solver developed in MATLAB by the 2023 Cal Maritime team, which accounts for centrifugal stiffening with a fourth order differential equation in terms of the centrifugal force, distributed wind

loading, and internal forces as a function of radius [4]. The calculation was done at the rated power state at 11 m/s and 2300 RPM as well as a worst-case runaway state at 14 m/s and 4500 RPM, which occurs momentarily if the load is disconnected at 14 m/s before the blades pitch back. The results of the analysis are compiled in Table 1.

1.1.5.2 Root Connection

To integrate the blade root connection tightly with the mechanical pitch system and maximize swept area for the blades, we redesigned the blade root compared to our Phase II design. The new design consists of a threaded heat set insert mounted directly to the root of the blade, as well as an indexing tab which interfaces with the pitch system to fix the angle of the blade, see Figure 10 for detail. Because the interaction of the heat set inserts and the base plastic is difficult to model, we decided to verify the integrity of the root via direct experimentation. As shown in Table 1, the maximum load we expect the root to be subjected to is 270 N or 60 lbf. We attached a section of blade to a static load testing jig and loaded it with 180 lbs of weights, as shown in Figure 4. The root held up perfectly, which gives us a factor of safety of at least 3 for the blade root. Note that maximum stress occurs at the root of blade, so that is the connection we tested. The ability of the root connection to withstand the expected pitching moment was also tested by connecting the blades to a mock hub and applying load with a force meter at a known moment arm. The root did not deflect when 10x the expected moment was applied.



Figure 4: Blade Root Test

1.2 Mechanical Design

Our design goals with pitch control are to have a robust system with 90˚ of blade rotation. The system is used for the safety tasks to stop the turbine and to regulate the turbine's speed and power during the control power and RPM task.

1.2.1 Pitch Overview

The pitching mechanism we chose is inspired by a controllable pitch propeller used on some ships to control the speed of the vessel. Our miniaturized system is made up of two main subassemblies: the hub in the front, and the actuation linkage in the rear of the turbine, as shown in Figure 5.

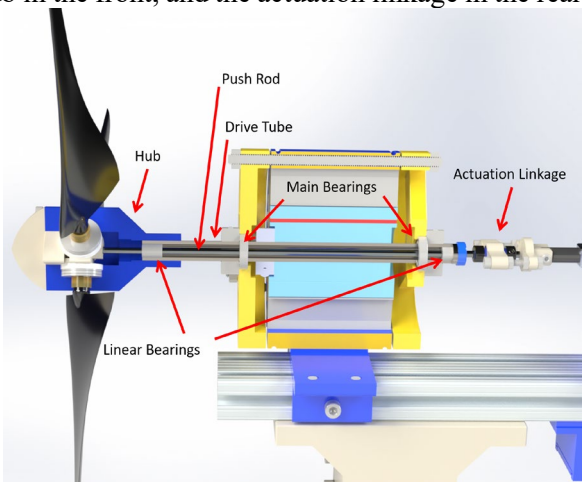


Figure 5: Pitch Mechanism Overview

The generator's main shaft is the drive tube, supported by the main bearings at either end of the generator. This allows us to run a pushrod through the center of the generator, supported by linear bearings on the ends of the drive tube. On the rear of the generator, this pushrod is attached to the actuator linkage, and allows the actuator to move the pushrod, rotating the blades. This movement is provided by the Actuonix L12-30 linear actuator. In the hub on the left side of Figure 5, the pushrod is connected to the control crosshead, which is a triangular shaped block with a transverse groove at its midpoint, as shown in Figure 6. The crosshead is the translating link of the scotch yoke mechanism, which when translated linearly causes the blades to rotate. Each of the three blades is mounted to a blade controller that holds the blade into the hub. The blade controller is made up of a disc, pin, and a post as shown in Figure 10. The pin is located at the edge of the disc, and rides in the groove of the crosshead with a tight tolerance. As the crosshead moves, the blade controller is rotated by the action of the pin-groove arrangement, as seen in Figure 7. Subsequently, the blade controller posts and blades are rotated in a collective fashion.

1.2.2 Pitch Assembly

The hub shown in Figure 6 is made up of two casings which serve as the structure for the scotch yoke mechanism. Each of these casings have three semicircular indents which fit the blade controllers and provide support surfaces. Each blade and blade controller set is provided with a PTFE sleeve bearing to reduce friction. Each blade controller also has a needle thrust bearing, which allows it to rotate freely

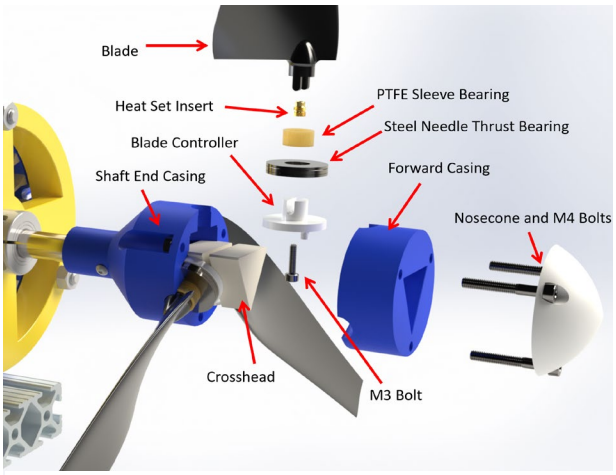


Figure 7: Turbine Hub Exploded View

while absorbing the centrifugal load from the blades. The crosshead is housed in the center and its corners interact with the casing so that the drive tube and push rod rotate together. The hub casings and crosshead are made of 3D printed PETG which is strong and has low surface friction. We chose to machine the blade controllers out of acetal Delrin for its high strength and low friction.

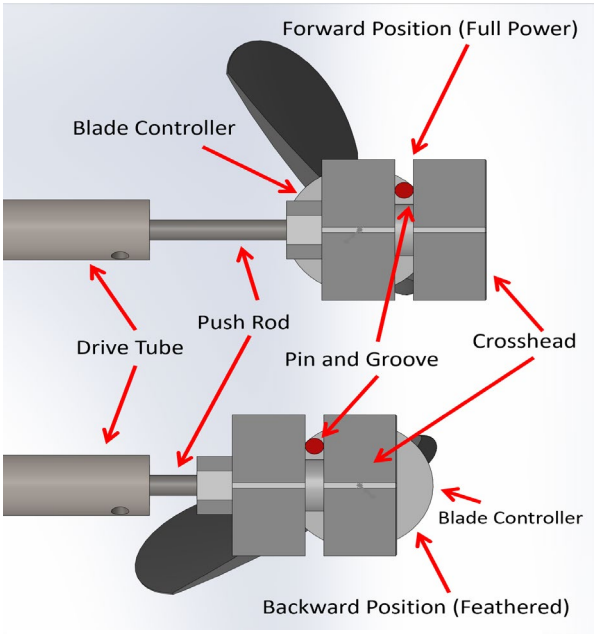


Figure 8: Hub Motion Diagram

The system is set up so that the forward position of the crosshead sets the blades in their full power position, and pulling backward feathers the blades. While the blades are in the full power position, the controller pin angle θ is 45˚ forward relative to the plane of blade rotation. The controller and pin can rotate back to -45˚ to feather the blades. This arrangement allows for a 90˚ range of motion and

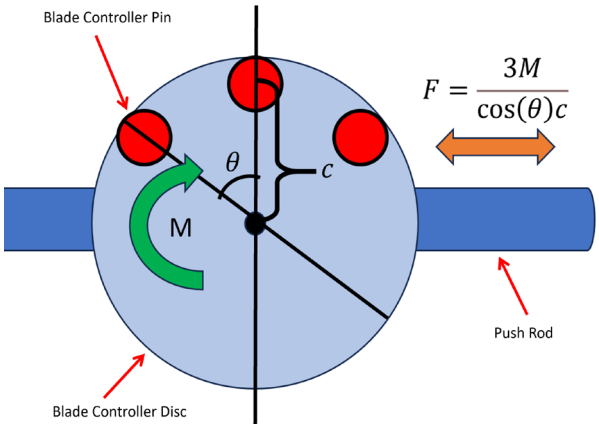


Figure 6: Blade Controller Analysis

reduces the chance that the pin binds up the system by getting stuck. Using the applied moment (M) of the blades from Table 1 of 0.06 Nm at rated speed, we calculated the force (F) against the push rod to be 23.3 N (See Figure 8). This prompted us to select the Actuonix L12 actuator with a 210:1 gear ratio, which has a maximum force output of 80 N and a back drive force of 45 N [10]. Additionally, based on the geometry and the resolution of the L12 of 0.2 mm, we estimate the system to have 1.05˚ of angle control resolution of the blades.

1.2.3 Actuation Linkage

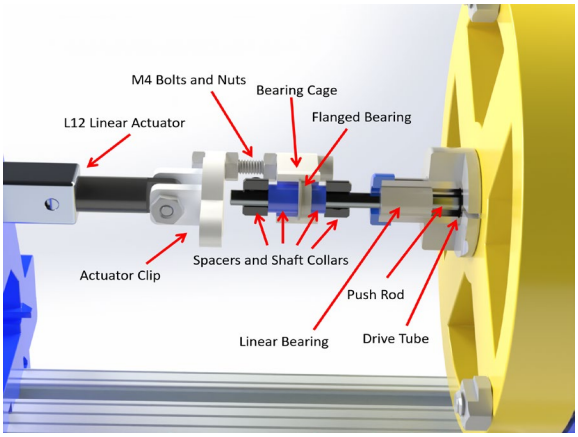


Figure 9: Actuation Linkage

The linear actuator at the back of the turbine controls the motion of the crosshead. The crosshead and actuator are connected by a pushrod which runs through the generator and to the linkage. The pushrod linkage consists of a flanged bearing, seated within a bearing cage. The bearing cage is bolted to the linear actuator. Movements from the actuator are transferred through the bearing cage to the outer race of the bearing. The inner race of the bearing is provided with spacers and shaft collars on either side

to transfer the movement to the pushrod, and subsequently the crosshead in the hub.

1.2.4 Blade Connection

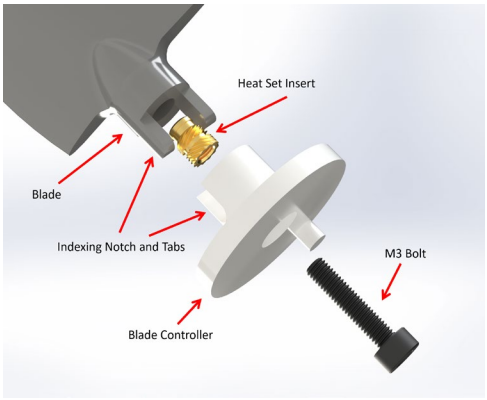


Figure 10: Blade Root Connection

The blade root connection needs to securely mount the blade and index it correctly so we can have accurate control of the blade angle, as shown in Figure 10. This was accomplished by creating a notch and tabs in the blade and blade controller, respectively. The blade controller has a counterbored hole in the bottom, through which an M3 bolt is inserted and screwed into the heat set insert at the bottom of the blade. The counterbore allows the blade controller to still have a flat surface which rides on the crosshead.

1.2.5 Stress Calculations

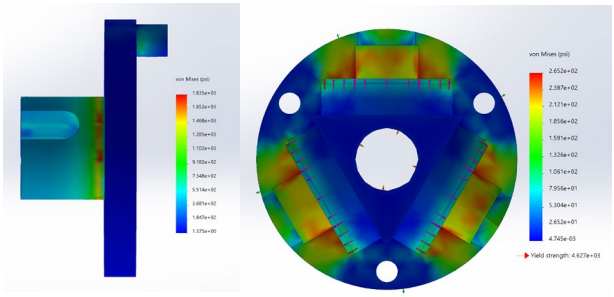


Figure 11: Axial Load on Blade Controller and Hub Casing Radial Loading

The part that brought up the most concern with loading in this design was the blade controller. It is subjected both to the axial load from the centrifugal force of the blades as the rotor spins, as well as the moment exerted by the blades on their axis. The blade controller must withstand both of these forces to keep the blade held in its position in the casing and hold its angle relative to the shaft. Referring to Table 1, the centrifugal force of the blade in the runaway state is 270 N, or about 60 lbf. This causes the highest stress we see in the form of an axial load concentrated at the base of the blade controller's post, as seen in Figure 11. The maximum stress is 1840 psi and the acetal Delrin has a yield strength of 9500 psi [7], giving a safety factor of 5. Additionally, the moment from the blades is being exerted onto the pin of the blade controller. From Table 1, the moment of 0.06 Nm from the blades induces a maximum stress of 734.9 psi, so the pin of the blade controller has a safety factor of 13. The hub casings also experience the same 270 N (60 lbf) in each of the three blade controller indents. The maximum stress induced is 265 psi which is dwarfed by PETG's yield strength of 4,627 psi [9]. The casings have a safety factor of 17.

1.2.6 Nacelle and Tower Assembly

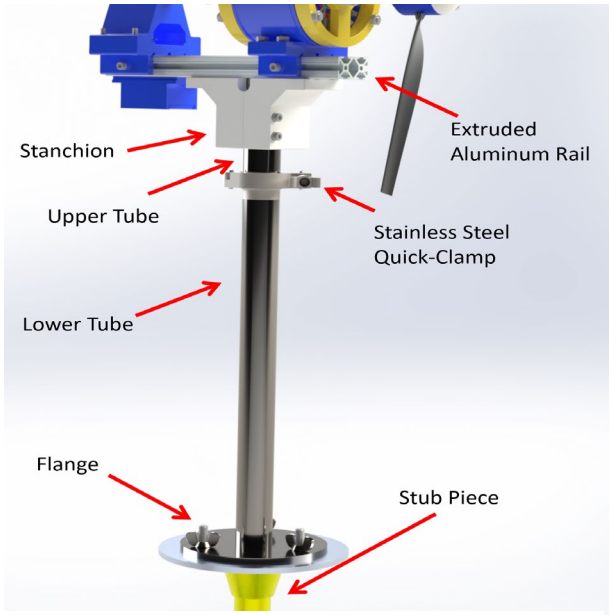


Figure 12: Nacelle and Tower Assembly

As shown in Figure 12, the nacelle features our blades, pitch system, generator, mounting rail, stanchion, and upper tube. The blade and pitch system are secured to the generator and linear actuator assembly, which are both fastened to an extruded aluminum rail, allowing for ease of installation and modularity to the design. A stanchion, adjustable along the bottom length of the rail, secures the upper tube by compressing around it using two bolts and nuts. The upper tube features a male fitting, located just below the stanchion.

Also shown in Figure 12, the tower features the lower tube with a female fitting at the top and a flange at the bottom, attaching the entire assembly to the competition-provided stub piece. The male and female fittings are secured using a quick-clamp,

enabling us to quickly install and remove the nacelle and/or tower without interfering with the foundation. The stanchion and the quick-clamp allow us to easily yaw the nacelle to align the turbine with the wind direction.

1.3 Foundation

In the past two years, we used a quadpod design but during last year's competition, one of the legs sheared off due to a weld failure. To address this issue, we created a bucket-type design that distributes forces over a larger surface area, rather than concentrating loads. It utilizes compression and friction forces to keep the structure in place, while maximizing use of the overall volume.



Figure 14: Bucket Foundation Prototype

1.3.1 Foundation Integrity Analysis

1.3.1.1 Turbine Expected Loads

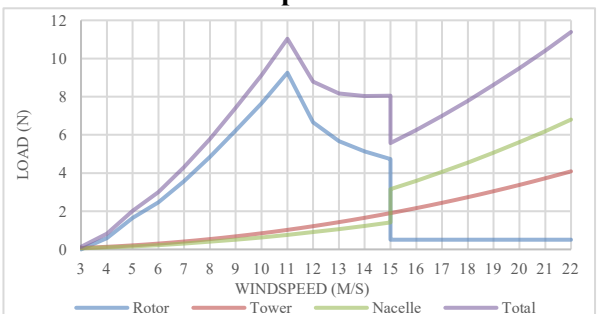


Figure 15: Expected Turbine Loads with Pitch

As seen in Figure 14, the main sources of load being applied to the turbine are thrust from the rotor and drag from the tower and nacelle. The data for the thrust generated by the rotor is derived from a QBlade simulation. Once the wind speed exceeds 11 m/s, the thrust force of the rotor decreases due to the feathering of the blades. After 15 m/s, the thrust from the blades drops due to feathering, but the load on the nacelle increases due to the loss of the axial induction factor from the rotor. For the tower and nacelle drag calculations, the tower was modeled as a vertical cylinder, and the nacelle was assumed to have a high drag coefficient of 1.4 due to its complex geometry. These assumptions give a conservative estimate of drag. To increase our confidence, we also simulated the expected loads if the blades fail to pitch, shown in Figure 15. For this situation, the load that's being applied on the rotor continues to

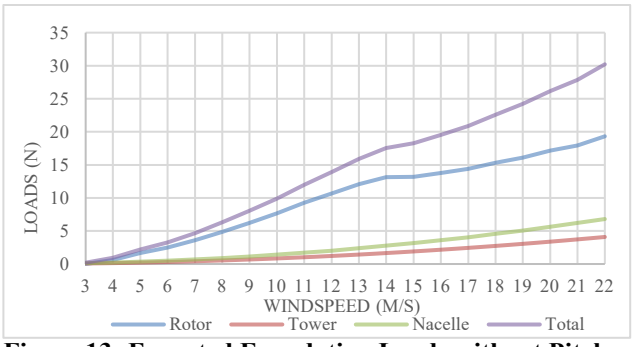


Figure 13: Expected Foundation Loads without Pitch

increase as wind speed increases. For this worst-case scenario, the expected load is 30 N at 22 m/s.

1.3.1.2 Free Body Diagram

Every component of the turbine induces an overturning moment on the foundation. When the force from the nacelle, tower, and rotor is being applied, the foundation overcomes the moment by utilizing a combination of soil interactions as shown in Figure 16. The sand is compacted by the top plate adding to the compression forces on the side walls. Inside the bucket the weight of the sand acts as a deadweight holding the foundation in place. With a combination of these factors, the foundation can be secured in the sand with minimal horizontal displacement.

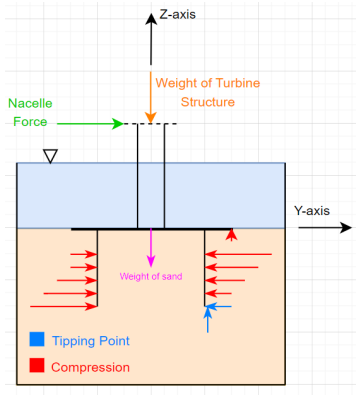


Figure 16: Foundation Free-Body Diagram

1.3.2 Manufacturing Process

The foundation was manufactured by laser cutting and bending sheet metal into a square shape to create the side walls. After bending, seams of two side walls were TIG welded. Since the weld was on a wall face, there is no concern of the weld failing. Shown in Figure 17, the side walls have a width of 20.32 cm (W_S) and depth of 16.51 cm (D), and the dimensions are the same for all sides. The top plate was then laser cut and welded on the top of the side walls. The top plate has dimensions of 25.4 cm by 25.4 cm (W_T). All dimensions are in accordance with the competition rules.

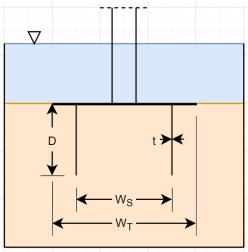


Figure 17: Side Profile of Bucket Foundation

1.3.3 Durability/Load Testing

To simulate the expected loads on the foundation, we used a force meter as a substitute for the drag forces. After placing the foundation into the test area, we inserted a 95 cm tall connection piece to simulate where the turbine drag forces will be applied. To simulate the "failed displacement" condition, we placed a piece of tape 25 mm away from the foundation piece, as shown in Figure 18. Next, we pull on the connection piece with the force gage from the appropriate height to simulate all the forces on the turbine. Once the foundation touches the tape, we make note of how much load it could withstand before displacing. By doing multiple tests, we can get an accurate idea of what load the foundation can consistently withstand and can guarantee that it will hold up to repeated installations.



Figure 18: Foundation Load Testing

1.3.4 Foundation Design Iterations

Multiple iterations of the foundation design were manufactured, varying the thickness of the side walls and the top plate. The experimental data in Table 2 showed that thinner wall designs could withstand less load. The decision had to be made whether we prioritize structure weight over durability, and we decided that the durability and the load it could withstand will take precedence, in order to ensure a passing score for the Durability Task.

Comparing the nacelle load data in Figure 14 to the collected data in Table 2, the maximum expected load of 14 N is dwarfed by the observed capability of 62 N for the 0.075" design. The factor of safety of 4 meets our goal of ensuring a passing score for the durability task. It even covers the maximum expected load in the worst-case scenario where the blades don't pitch back at all, shown in Figure 15, with a factor of safety of 2.1.

Table 2 Foundation Test Results

Wall Thickness	Trial 1	Trial 2	Trial 3	Trial 4	Average
0.060"	53 N	53.5 N	44.5 N	44.5 N	47.7 N
0.075"	35 N	50 N	67 N	63 N	62 N

To determine how much the sand in the bucket affects foundation performance, a test was conducted which consisted of digging a hole in the tank of sand, placing the foundation in the hole, packing the outer walls with sand, then measuring the force required to displace the foundation. This was to measure how much the compression forces, shown in Figure 16 contribute to the overall durability. The results shown in Table 3 suggest that the force the sand is applying onto the inner walls contributes to half of the total load it would otherwise withstand.

Table 3 Foundation Test Results without Sand

Wall Thickness	Trial 1	Trial 2	Trial 3	Trial 4	Average
0.060"	24 N	25 N	28 N	26 N	25.75 N
0.075"	35 N	38 N	41 N	36 N	37.5 N

1.4 Generator

1.4.1 Overview

The generator we decided on is a custom-built three-phase permanent magnet generator. A custom-built generator was chosen because of the team's experience building them for previous projects, to reduce cogging torque compared to off-the-shelf options, and to manipulate power output characteristics. The generator consists of two primary parts: the stator and the rotor. Each part was designed using SolidWorks and 3D printed in PLA.

1.4.2 Rotor Design

The rotor has eight magnetic poles, with eight additional smaller magnets oriented perpendicular to the main magnets, creating a Halbach array.



Figure 19 Finished Rotor

The purpose of the Halbach array is to focus the magnetic flux of the main magnets outward towards the coils. This effect was confirmed in the QuickField magnetic flux simulation software, shown in Figure 20. This increase in magnetic flux improves the power for a given rotor without increasing the number of poles. In addition, the use of smaller Halbach magnets also allowed us to fit more magnets on the outer edge of the rotor, further increasing the magnetic flux density.

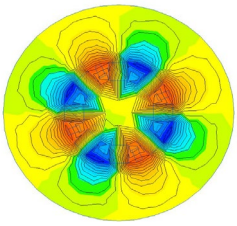


Figure 20: 8-pole Halbach Magnetic

The other focus of the rotor design was the structural integrity of the rotor and the magnets. We found upon analyzing the rotor itself, using SolidWorks

FEA, that the epoxy would be the weakest link. Knowing this we verified that the magnets would be held in by the epoxy. Using rotational kinematics, we found that the stress on the epoxy would not exceed 251 psi, which has a safety factor of 13 with the bond strength of 3300 psi [8].

1.4.3 Stator Design

Table 4 Stator Details

Generator Details	V1	V2	V3
# of Coils	9	24	24
# turns per coil	100	24	18
AWG	22	22	20
Max Power Curve Voltage	26	30	33

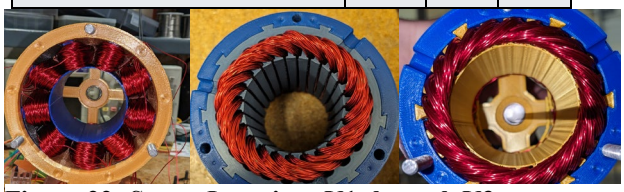


Figure 22: Stator Iterations V1 through V3

When designing the stator, we focused on ease of assembly, and modularity of the stators. This was done so an iterative approach could be used to find the highest-performing stator. The configurations, shown in Figure 21, were designed and built to be tested and compared. V1 (left) was built with 9 concentrated windings and was based on generators we have seen from previous Cal Maritime teams. V2 (middle) and V3 (right) both used distributed windings which allows for tighter packing of coils. All generators are wired in Delta, because in Wye, the voltages exceeded 48 V. Wiring in Delta reduces voltage of the generator by a factor of $\sqrt{3}$.

1.4.4 Operating Voltage/Performance Testing

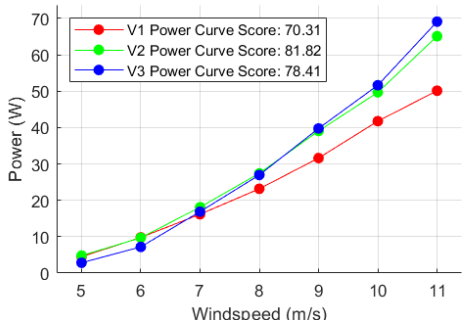


Figure 23: Generator Comparison Power Curve

All three stators were tested in a mock power curve test. The tests were conducted sequentially with all other equipment and conditions remaining the same. As shown in Figure 22, the V2 stator scored the highest, despite not having the highest peak power. V2 also fell in the middle of the pack for voltage as shown in Table 4. Due to the higher score and desirable voltage at peak power, the V2 stator was selected.

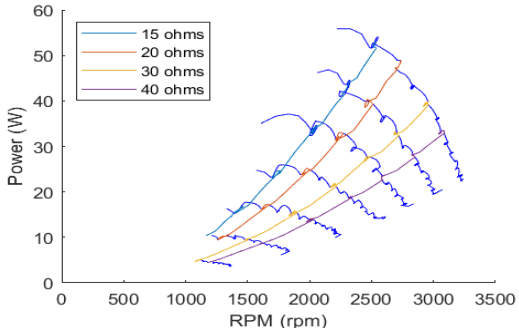


Figure 21: Generator Resistance Sweep

In addition to the power curve testing, we also established a range of optimal resistances shown in Figure 23. This generator model shows the response to certain electrical conditions and informed the electrical system design.

1.5 Electrical and Instrumentation

The electrical system is made up of the generator itself, the turbine box, and the load box. The turbine box includes the rectifier, peripheral instruments, and their necessary power converters. The load box contains our variable resistive load, microcontroller, and backfeed system. Power flows from the generator to the turbine box, through the PCC, and to the load box. Data is communicated via an I2C network that is optically isolated between the turbine and load boxes.

1.5.1 Turbine Side Electronics

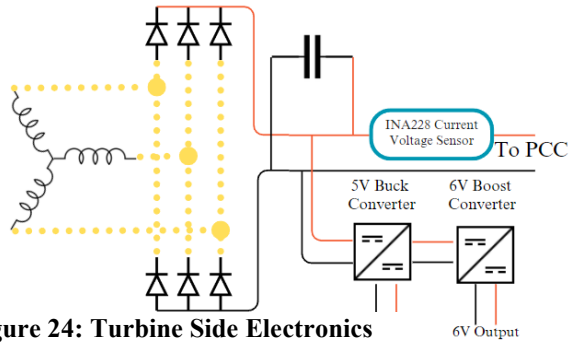


Figure 24: Turbine Side Electronics

The turbine side electronics, shown in Figure 24, link the generator to the PCC. The generator produces 3-phase AC, which we need convert to a stable DC output for the PCC. The off-the-shelf passive 3-phase full bridge rectifier we selected uses six diodes to convert the AC power created in our generator to a DC source. Although the rectifier

outputs DC, it still has ripple from the sinusoidal input, so we include a capacitor on the turbine side high voltage bus to smooth the output to the PCC. Additionally, the capacitor acts as energy storage for the load disconnect task.

All turbine side equipment is powered via a 5 V buck converter for the instrumentation and a 6 V boost converter for the linear actuator. These converters draw power from the turbine side high voltage bus. Typically, this bus is powered by the generator through the rectifier. However, when the generator is not supplying the required voltage to power the turbine side electronics, power is backfed from the load side of the electrical system.

With the current design, voltage stays below the 48 VDC limit due to the generator configuration. To further ensure the voltage limit is not exceeded, we will be implementing a voltage regulating circuit. This circuit uses a comparator op-amp to control two MOSFETs to engage or bypass an off-the-shelf 45 VDC regulator.

1.5.2 Load Side Electronics

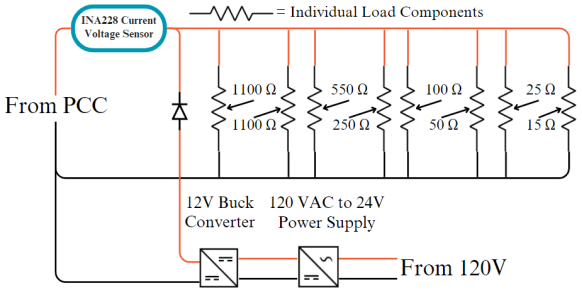


Figure 25: Load Side Electronics

The load side takes the power coming through the PCC and provides the load where the power is dissipated. To achieve maximum power for every given operating condition, we vary the resistance being applied to the generator.

1.5.2.1 Resistive Load

Our variable resistive load design mimics a parallel decade box. The nine individual load components contain different power resistors, each in series with an N-type MOSFET, as shown in Figure 26. Each individual load component is controlled by a microcontroller pin, and they are placed in parallel with each other, as shown in Figure 25.

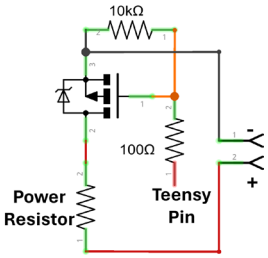


Figure 26: Individual Load Component

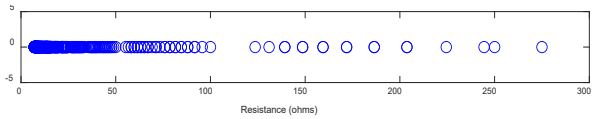


Figure 27: All Possible Load Resistances

Figure 27 shows how switching different power resistors on and off with their respective MOSFETs allows a wide range of resistances to be created. We use logic level MOSFETs, meaning they can be easily driven directly by the 3.3 V digital pins of the Teensy 4.1. This working design is incredibly reliable and has been used for all turbine tests to ensure reliability.

1.5.2.2 Backfeed

Additionally, we use the wall power on the load side to provide a stable power source to the turbine side when it loses power. 120 VAC wall power is converted to 24 VDC, for the load side fans, and is then stepped down to 12 VDC for the backfeed, shown in Figure 25. This power is then passed through a standard diode and into the positive side of our load side high voltage bus. The use of a diode allows for passive transfer from wall-supplied power to generator-supplied power, keeping our turbine side of the system online in all conditions except an extended load disconnect.

1.5.3 Instrumentation

Measuring operating conditions of the system is the primary basis of control for the entire turbine. The instrumentation system includes various sensors to collect data. Using this data, the software will determine how to use the controllable outputs to change the turbine operating conditions.

1.5.3.1 Turbine Instrumentation

The turbine has three devices mounted locally: sensors to measure RPM and wind speed, and a controllable linear actuator to manipulate the blade angle. The RPM sensor is mounted on the generator casing to detect changes in magnetic flux from the rotor. It is a hall effect sensor that measures the change in polarity of the magnetic field as the rotor spins. A high (5 V) or low (0 V) signal is sensed depending on the polarity of the magnet passing the sensor [11]. Wind speed is measured using a pitot tube and a differential pressure sensor [12]. The local wind speed can be found using the difference of pressures and a basic form of Bernoulli's equation. The linear actuator takes a 0-5 V analog input, which is correlated to a position setpoint that the PID loop seeks to achieve [10].

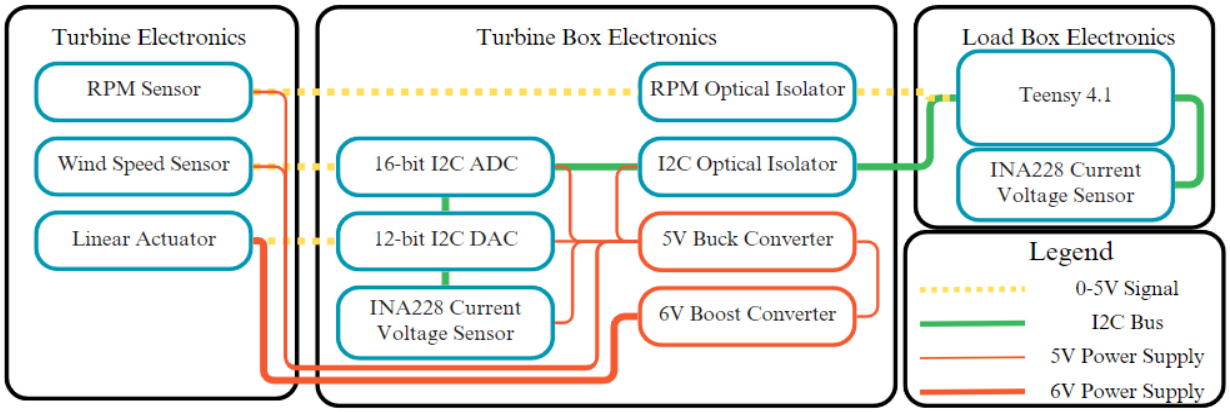


Figure 28: Instrumentation Wiring Diagram

1.5.3.2 Turbine Box Instrumentation

The turbine box includes the instrumentation required to communicate with the turbine instrumentation, measure the power on the turbine side, and send the information to the load box. We use a 16-bit I2C analog to digital converter (ADC) to read the wind speed sensor 0-5 V signal [13]. A 12-bit I2C digital to analog converter (DAC) sends a 0-5 V signal to the linear actuator [14]. Voltage, current, and power are measured via an INA228 20-bit I2C power monitor [15]. All I2C devices are chained together to the optically isolated I2C turbine box to load box connection. Our system has two bidirectional optical isolators, one for passing the digital RPM signal to the microcontroller and the other for the general I2C communication network, which includes the rest of the instrumentation [16]. These optical isolators allow data to be transferred with both sides electrically isolated. This prevents any power flow between the load box and turbine box through the data connections.

1.5.3.3 Load Box Instrumentation

The load box includes the Teensy 4.1 microcontroller and an additional INA228 power monitor. The Teensy 4.1 acts as the brains of the entire turbine and communicates with the turbine side via the optically isolated I2C bus shown in green [17].

1.6 Software

1.6.1 Individual Component Development

After completing a control system design of what sensors and controllable outputs we wanted to incorporate, the software for each component was developed. Many of the components we used, especially the ones from Adafruit, came with pre-written Arduino libraries. These libraries could be used to easily get data from each sensor individually for component verification and testing.

We also developed code for some of our custom components, like our RPM sensor. The RPM sensor, as mentioned in section 1.5.3, is a simple hall effect sensor. We can measure the time it takes for the polarity to switch 10 times, and multiply by a factor related to the number of poles to get the RPM.

Another sensor that required extra work was the wind speed sensor. We chose to calibrate the wind speed sensor against traditional manometers, to ensure the pressure difference measurements were accurate. From here we could implement Bernoulli's equation which transformed the delta pressure measurement to a wind speed measurement.

1.6.1.1 Load Control Code

As described in section 1.5.2.1, we can vary our resistance by switching different MOSFETs on and off. To choose which switches should be open to achieve a desired resistance we used a lookup table generated in MATLAB. The lookup table consists of all possible resistances available, and what combination of switches is needed to achieve it. We can then choose the nearest possible resistance to what we need and activate the necessary MOSFETs to achieve the desired load.

1.6.2 Integration of Components

After developing individual codes for all our instrumentation, we created a library for the entire turbine control system to streamline the program that the microcontroller would be running. The library has functions to pull data from each sensor and manipulate each controllable output. The library uses the work we had done individually on each sensor, but without needing to repeat the code each time, which made implementation into a state machine easier and more readable.

1.6.2.1 Integration Testing

Once the individual code and the electrical wiring was developed, we first wrote code that allowed manual control of the linear actuator and resistance, while recording all the sensor data. This helped us to work out many of the integration bugs before moving on to a system that could control itself through each task.

1.6.3 State Machine

Our final turbine code builds off everything we wrote before and compiles it all into one state machine-based control system. The state machine includes a state for each task in the competition testing, and the transitions determine which state the machine should be in at any set of conditions, as shown in Figure 29.

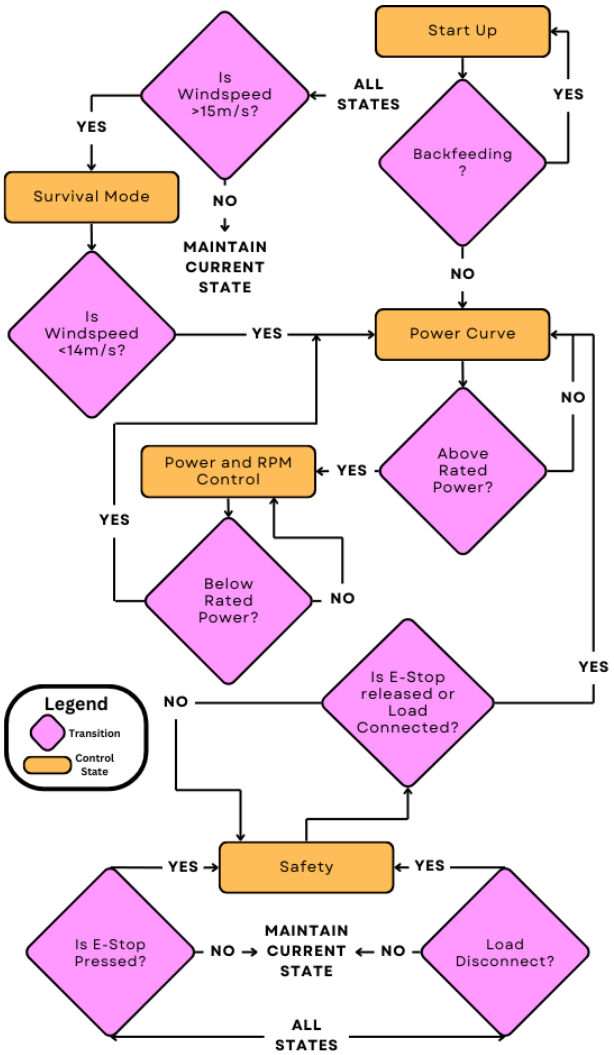


Figure 30: State Machine Flow Chart

1.6.3.1 Start Up

The Start Up state is where the turbine begins testing. The goal of the Start Up state is to improve the cut in speed of the turbine and overcome the backfeed voltage. If the blades are not spinning the pitch is set to a blade angle of 9° which was found in testing to decrease the cut in speed from 3 m/s to 2 m/s. Once the turbine is above 100 RPM the pitch will be set to 0° to maximize the RPM and power. Once the turbine is spinning at 1000 RPM, it will generate more than 12 V which is enough to overcome the backfeed voltage. This will cause the turbine side voltage to increase beyond 12 V, which when measured will make the turbine transition to the Power Curve state.

1.6.3.2 Power Curve State

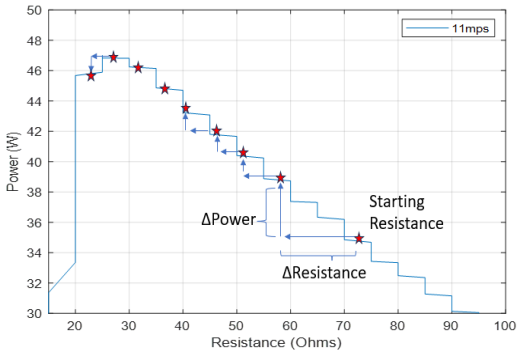


Figure 29: Perturb and Observe Algorithm

The goal of the Power Curve State is to maximize the power by altering the resistance of the load. This is accomplished using a perturb and observe algorithm, which relies on measurement of the change in power to determine the direction of the next change in resistance. Figure 30 contains data we took at various resistances and shows how our algorithm would respond to its starting resistance of 72 ohms. The resistance step size is dependent on the current resistance value, meaning that for higher resistance values the step size will be larger. This is done to decrease the settling time and works well because changes at higher resistances have smaller effects on power and RPM. The direction of each step is determined by whether the power increased or decreased with the last change in resistance. For example, when the resistance passes over the peak of the curve shown in Figure 30, the power will decrease causing the direction of the next resistance step to be positive. These steps are taken every 2.5 seconds, to allow for the turbine to reach a new steady state power, as shown in Figure 31. The Power Curve state is used from when the turbine

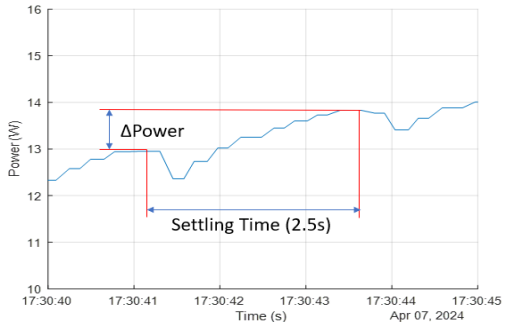


Figure 31: Power Curve Settling Time

transitions out of the Start Up state until the turbine reaches its rated power for more than 10 seconds. Once this occurs the turbine will set the current power and RPM reading as the rated power and transition to the Power and RPM Control state.

1.6.3.3 Power and RPM Control Task.

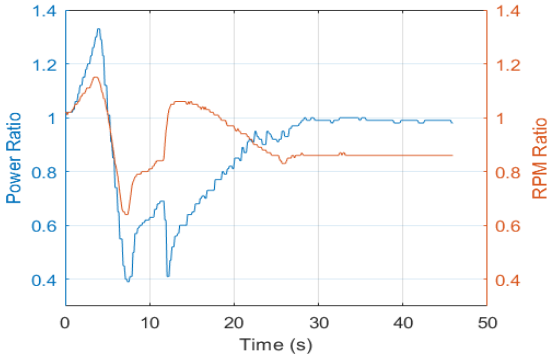


Figure 32: Control Power and RPM Task Test Data

The Power and RPM Control state seeks to maintain the power and RPM that was measured when the state began. To accomplish this, the program has two controllable outputs: pitch and resistance. In testing we found that pitch control is useful for shedding power at higher wind speeds, but with our accuracy capabilities getting fine power control with only pitch was a challenge. For that reason, we use pitch control to reduce the RPM to between -15% and +8% of the rated RPM. Then the resistance control takes over is used to finely adjust the power until it is ±8%. These guidelines help to decrease the settling time by widening the acceptable power and RPM windows, while still ensuring Power and RPM Control Task scores above 48 points. Figure 32 shows data from a test in which the wind speed was increased from 11 m/s to 13 m/s, the settling time was about 20 seconds, and the final score was 50 out of 50.

1.6.3.4 Safety Stop and Load Disconnect

Both the Safety Stop and Load Disconnect Tasks are accomplished by the same Safety state. Any state can transition to the Safety state at any time. This state can be activated by either detecting the E-stop being pressed or detecting a load disconnect. To detect the E-stop being pressed we send one lead to ground and the other to a pulled-up microcontroller pin, which reads whether the pin is high or low. This arrangement is designed for a normally closed E-stop switch. In order to detect a load disconnect, we compare the load and turbine side voltage. If the load side drops to 12 V (which is held by the passive backfeed), while the turbine side stays where it was, a load disconnect is triggered. For the E-stop and load disconnect situations the blades are commanded to feather. Both the E-stop and load disconnect have been tested from 5-15 m/s in our wind tunnel as shown in Figure 33. We feel this is representative of the full operating conditions, as above 15 m/s we plan on having the blades feathered for the survival task.

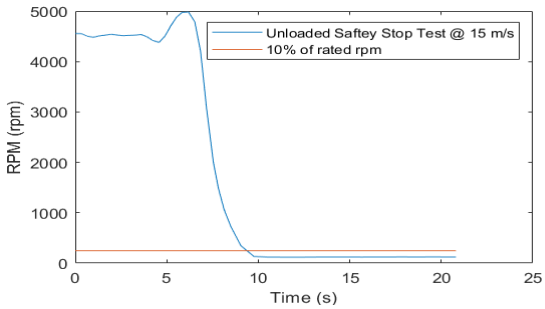


Figure 33: Safety Stop Task Test @ 15 m/s

1.6.3.5 Survival Task

Any state, except the Safety state, can transfer to the Survival state if the wind speed exceeds 15 m/s. At this point in testing, power generation is no longer required. To reduce the rotor thrust, the blades are feathered, reducing the load that is put on the foundation above the cutoff wind speed.

Chapter 2: Full Turbine Assembly

2.1 Full Turbine Integration

Our turbine consists of three main components: the nacelle, the tower, and the foundation. The nacelle features our blades, pitch system, generator, mounting rail, stanchion, and the upper tube with a male fitting at the bottom. The nacelle is secured to the tower via mating the respective fitting and fastening a quick-clamp. The tower assembly, with its flange, mates with the competition provided stub piece with wing nuts. Yaw adjustment is possible at the stanchion and quick-clamp. The stub piece mates with the foundation. Finally, to connect the electrical

system to the turbine, the power and signal wires run through the tower, stub piece, and foundation.

2.2 Distributed Team Environment

This competition is our members' senior capstone project. We delegated our team members into subteams based on interests and previous experience. Our team meets weekly to ensure all subteams are up to date on the progress of the entire turbine and all design changes maintain compatibility with other sub-systems. Each subteam is primarily made of two members with each having one lead. Initially, as a whole team, we decided on bigger design choices such as horizontal axis versus vertical axis, variable or fixed pitch. Then, given these major decisions, each subteam did research on their design. These designs were pitched to the whole team and were chosen based on feasibility and effectiveness at achieving our design objectives. From that point forward each subteam has prototyped their designs while ensuring compatibility with other subteams. As we moved into Phase III of the competition, next year's team began attending our weekly meetings and we have been integrating them into the testing and analysis process to ensure the longevity of the team in future competitions.

Chapter 3: Turbine Testing Results

3.1 Wind Tunnel Testing

With our wind tunnel built from our alumni, we were able to conduct testing up to 14 m/s allowing us to successfully test most competition testing tasks including: Power Curve, Rated Power and Rotor Speed, and Safety Shutdown.

The results of our Power Curve task test can be seen in Figure 34, where we scored a total of 81.82 points. We believe it is highly possible our actual wind speed is higher than our measurements, leading to higher power than might be possible. With this caveat, we were able to determine the rated characteristics of our turbine. Our Rated Power and Rotor Speed are 63.45 W and 2500 RPM.

The results of our Rated Power and Rotor Speed task test can be seen in Figure 35, concluding that we are able to maintain power within a 3% band and rotor speed lower than our rated characteristics. This results in a score of 50 points in this task. Finally, we were able to test the Safety Shutdown Task up to 14 m/s, where we were able to successfully able to shut down and restart in both the E-Stop and Load Disconnect scenarios, netting us full points.

3.2 Field Testing

To ensure that our that our foundation can support the rest of our turbine assembly at wind speeds up to 22 m/s, as previously stated, we performed a conservative theoretical analysis to predict the maximum amount of force experienced by the full turbine and then conducted a pull test. In the worst-case scenario, where our blades do not feather past 15 m/s, our foundation must be able to withstand 30 N. Through our pull tests previously explained, our final foundation design was able to withstand 62 N which resulted in a safety factor of 2.

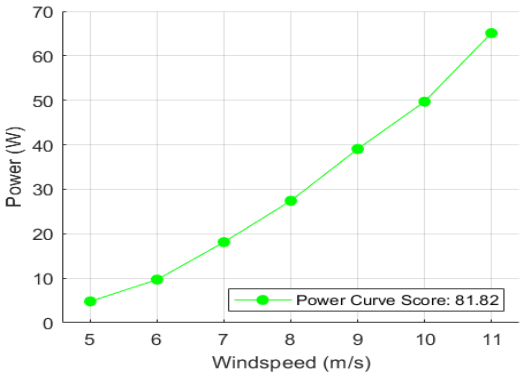


Figure 35: Power Curve Test Data

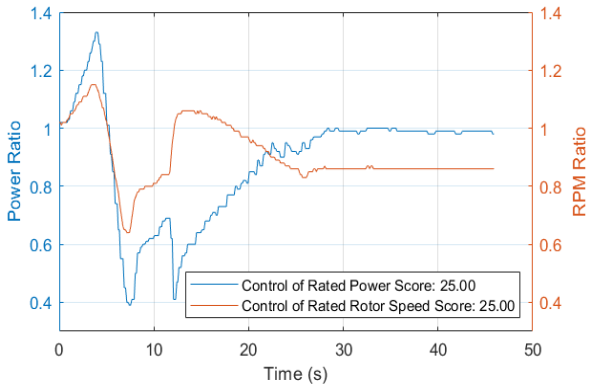


Figure 34: Control Task Test Data

To ensure that the tower assembly and the nacelle are also able to withstand wind speeds up to 22 m/s we are developing a mount that is able to secure the turbine to a truck bed. Additionally, through this test setup we will be able to verify safety shutdown and restart procedures at wind speeds higher than our wind tunnel outputs.

3.3 Annual Energy Production

We used power output results for our V2 generator, shown in Figure 35, as well as the average wind speed in Vallejo, CA of 3.9 m/s and the Rayleigh probability distribution for wind speeds to calculate our expected AEP of 39,835 Wh.

Chapter 4: Influence of Previous Design

Our previous years' designs and performance assisted in identifying key factors to maintain and improve upon creating a strong foundation for us to build upon. After determining these fundamental design decisions, each subteam (blades, mechanical, generator, instrumentation, controls & electrical, and foundation) virtually redesigned everything to ensure functionality through a simplistic and robust design.

Previous Designs	Influence on Current Design
Safety Task Accomplished by Feathering Blades	Created new, robust pitch system to ensure completeness of safety task
Custom Built Generator	Eliminates cogging torque, allowing for high power generation at lower wind speeds
Turbine State considerations for Mechanical Loading	Similar states with updated characteristics of current turbine assembly
Force Analysis of Full Turbine Assembly up to 22 m/s	Similar calculations with updated dimensions and characteristics of current turbine assembly.

Chapter 5: Commissioning Checklist

Before Installation into the wind tunnel and the commissioning begins, we will ensure that:

1) Nacelle is Built (Blades, Pitch, Generator, Linear Actuator Assembly connected and secured to the aluminum rail, which is connected to the stanchion and the upper tube), and Individual Parts have been inspected
2) Foundation has been installed and placed under the tunnel with the stub piece connected
3) Power and Signal Connection have been fed through foundation and stub piece

After these steps have been conducted and verified, commissioning will commence with all Installation Commissiong Tasks being conducted and/or verified by a team lead. Each Task will then be conducted and/or verified again by a different Team Lead.

Installation Commissioning Task	Certification #1	Certification #2
Inside of Tunnel Tasks		
Feed Power and Signal Cables through Tower		
Secure Turbine Tower to the stub piece		
Mount Nacelle to Tower		
Connect Power and Signal Cables to Nacelle		
Orient Rotor Axis In-line with Wind Direction		
Inspect Integrity of Blades (Cracks, Surface Inconsistencies, etc.)		
Verify Components are Secured to Frame (push/pull test)		
Ensure Expected Smooth Rotation of Rotor		
Visually Verify Proper Range and Operation of Pitch Assembly		
Outside of Tunnel Tasks		
Verify Power and Signal Cable Connections with Multimeter Continuity Test		
Connect Wall Power to Receptacle on Load Side Box and Close Switch		
Connect Power and Signal Cables to Turbine Side and Load Side Control Boxes and the PCC Respectively		
Connect E-Stop Out Wire to PCC Connection		
Verify All Sensors and Communication Devices Power Indication Lights		
Upload Manual Control Program		
Increase Windspeed to 5 m/s and Verify Proper Operation of Pitch System, Various Sensors, and Positive Power		
Upload Competition Turbine Testing program		

Bibliography

[1] "Blade Design Overview — QBlade Documentation 2.0.6.4 documentation." Available: https://docs.qblade.org/src/user/blade/blade.html.

[2] 3DXTech, "Technical Data Sheet: CarbonX™ CF-PLA 3D Printing Filament" Available: https://www.3dxtech.com/wp-content/uploads/2021/03/PLA_CF-TDS-v03.pdf.

[3] "spl10b.pdf | Unified Engineering I, II, III, & IV | Aeronautics and Astronautics," MIT *OpenCourseWare*. Available: https://ocw.mit.edu/courses/16-01-unified-engineering-i-ii-iii-iv-fall-2005-spring-2006/resources/spl10b/

[4] J. Nelson *et al*., " Cal Maritime Collegiate Wind Technical Design Report 2023," California State University Maritime Academy, 2023.

[5] M. Sessarego and D. Wood, "Multi-dimensional optimization of small wind turbine blades," Renewables, vol. 2, no. 1, p. 9, Dec. 2015, doi: 10.1186/s40807-015-0009-x. Available: https://jrenewables.springeropen.com/articles/10.1186/s40807-015-0009-x.

[6] Ragheb, M. "Optimal rotor tip speed ratio." Lecture notes of Course no. NPRE 475, 2014. Available: http://users.wpi.edu/~cfurlong/me3320/DProject/Ragheb_OptTipSpeedRatio2014.pdf.

[7] Rapiddirect, "Acetal vs Delrin: What Are Their Differences," rapiddirect. Accessed: Apr. 13, 2024. [Online]. Available: https://www.rapiddirect.com/blog/acetal-vs-delrin-what-are-their-differences/

[8] "Gorilla Epoxy," *Gorilla Glue*. Available: https://www.gorillatough.com/product/gorilla-epoxy/.

[9] "PolyLite™ PETG," Polymaker US. Accessed: Apr. 15, 2024. [Online]. Available: https://us.polymaker.com/products/polylite-petg.

[10] Actuonix Motion Devices, Inc, "Miniature Linear Motion Series · L12" 2019. Available: https://www.actuonix.com/assets/images/datasheets/ActuonixL12Datasheet.pdf.

[11] Melexis, "Hall Latch – High Sensitivity", US1881, January 2006. https://www.sparkfun.com/datasheets/Components/General/Hall-US1881EUA.pdf

[12] Sensirion, "Differential Pressure Sensor with Analog Output", SDP8xx-Analog, March 2018. https://sensirion.com/media/documents/68DF0025/6167E542/Sensirion_Differential_Pressure_Datasheet_SDP8xx_Analog.pdf

[13] Texas Instruments, "Ultra-Small, Low-Power, 16-Bit Analog-to-Digital Converter with Internal Reference", SBAS444B, May 2009, Revised October 2009. https://cdn-shop.adafruit.com/datasheets/ads1115.pdf

[14] Microchip, "12-Bit Digital-to-Analog Converter with EEPROM Memory in SOT-23-6", MCP4725, 2009. https://cdn-shop.adafruit.com/datasheets/mcp4725.pdf

[15] Texas Instruments, "INA228 85-V, 20-Bit, Ultra-Precise Power/Energy/Charge Monitor With I 2C Interface", SLYS012A, January 2021, Revised May 2022. https://www.ti.com/lit/ds/slys021a/slys021a.pdf?ts=1713330686996

[16] Texas Instruments, "ISO154x Low-Power Bidirectional I2C Isolators", SLLSEB6E, July 2012–Revised April 2019. https://cdn-learn.adafruit.com/assets/assets/000/099/320/original/iso1540.pdf?1612894897

[17] PJRC, "Teensy 4.1 Development Board", Revised March 2023. https://www.pjrc.com/store/teensy41.html

CU Boulder Wind Team

2023-2024

Turbine Design Final Report

April 18th, 2024

Student Lead:

Elyse DeBarros
Elyse.DeBarros@colorado.edu

Kaity Plutt – *Turbine Design and Testing Lead*
Aria Mundy – *Financial Manager*
Carver Lindley – *CAD Engineer*
Dane Robinson – *Electromechanical Engineer*
Donggyu Jang – *Turbine and Wind Farm Engineer*
Liam West – *CC Lead & Turbine Engineer*
Loren Peterson – *Electromechanical Lead*
Megan Finnigan – *Test Engineer*
Preston Brumley – *Controls Engineer*
Stewart Rojec – *Electrical Engineer*
Tim Herwig – *Logistics Manager*

Faculty Advisor:

Roark Lanning
Roark.Lanning@colorado.edu

Table of Contents

Executive Summary 2

Design Overview 2

Design Objective 2

Components from Prior Competition 3

Changes from Prior Competition 3

Static Performance Analysis 3

Annual Energy Generation 4

Engineering Diagrams of Mechanical Systems & Load Analysis 4

Emergency Stop 4

Pitching System 5

Blade and Rotor Analysis 6

Nacelle and Yaw Sub-System 8

Tower Design 8

Foundation Engineering Diagram 9

Electrical Subsystem 10

Electrical System Overview and One-Line Diagram 10

Generator Selection 11

Control States and Operational Modes 12

Software Architecture 13

Final Assembly 13

Assembly and Commissioning Checklist 13

Installation 13

Commissioning 14

Testing 14

Foundation Stability Test 14

Emergency Brake Test 14

Rotor Spin Test 15

Load Test 15

Wind Tunnel System Integration Testing 15

Executive Summary

As part of the 2024 Collegiate Wind Competition (CWC) sponsored by the Department of Energy and the National Renewable Energy Laboratory, this year's CU Boulder Wind Team has designed a small-scale prototype offshore wind turbine capable of withstanding wind speeds up to 22 m/s. The turbine will compete in a set of six tasks to evaluate its performance in conditions that model real-world scenarios and will be scored based on its ability to function safely and reliably while fulfilling requirements put forth by the CWC. This report details the technical design of this wind turbine, including the design goals, mechanical loading analysis, aerodynamics, electrical design, software architecture, and testing progress made by the team.



Figure 1. Full turbine assembly and CAD model

This year's turbine utilizes a suction caisson as the anchoring system. The stub piece will slide smoothly over the top tube of the foundation. A ¼-inch base plate serves as an interface between the stub piece and tower, which is held in place by a collar placed on the exterior of the aluminum tube. This year's team opted to use manual yaw, which features a yaw collar connected to the nacelle base plate and is aligned by hand with the prominent wind direction, held in place with two set screws. The nacelle includes a mechanical brake fashioned after a bicycle disc brake, the generator, the drive shaft and its supports, and a place to ground the base plate. A new triple Miter gear pitching system has been implemented with a custom-made clamshell gearbox to house the gears and blade shafts, which hold the blades in place and are secured with shoulder bolts. The pitching system is powered by a Pololu gearmotor and uses a slip ring to transmit signals and power to the rotating motor. A main drive shaft transfers power from the mechanical power in the wind harnessed by the blades to the generator.

The electrical system consists of one PCB on each side of the Point of Common Coupling (PCC). A brushless DC motor is used as the generator, which powers each turbine side system. The turbine's primary load is a MOSFET and a sense resistor for feedback current control. The load PCB also houses an Arduino Uno microcontroller, which sends optocoupled signals for pitching, braking, and load control while receiving information about rotor speed, motor positioning, and power.

Design Overview

Design Objective

The fourth University of Colorado Collegiate Wind Competition team's goal was to design, manufacture and test a small-scale offshore wind turbine that will perform safely and efficiently during the turbine testing competition tasks. The 22-23 CU CWC team performed well in the durability,

foundation success and foundation weight tasks, but struggled to earn points in the power curve and control of rated power and rotor speed tasks. For this reason, our team's focus has centered around improving the pitching, electrical, and controls systems, to convey signals more reliably and mitigate problems that last year's team experienced. We also focused on simplifying our emergency stop system for reliability and repeatability.

Components from Prior Competition

There are two design aspects from last year's turbine that were analyzed, tested, and proven to be the best option to meet the team's design goals. They include the following components:

Suction Caisson Foundation

The team's suction caisson design earned 88 of a possible 90 points in last year's CWC for the foundation success and foundation weight tasks. The 2024 CU CWC team conducted calculations to further optimize the size of the suction caisson. We considered passive and active earth pressures and suction forces to counter the overturning moment from nacelle drag and thrust and drag on the blades. We manufactured and tested a new suction caisson without last year's height adjustment piece. Additionally, the team conducted testing with the foundation system to ensure it could sustain the maximum theoretical expected forces. These results are discussed in more detail below.

Maxon 488607 Generator

The team evaluated 8 generators. They were first compared in a MATLAB model that used generator specifications to predict the efficiency of power generation. The two top-performing generators from the model were then compared in physical testing (further explained below). The Maxon EC-i40 488607 generator was chosen based on its performance in both theoretical modelling and physical testing.

Changes from Prior Competition

New design changes include a complete overhaul of the pitching system to include a triple Miter gear assembly inspired by the Cal Maritime design from 2023, removal of the height adjustment piece from the foundation assembly, a modification to the base collar so it surrounds the exterior of the tower tube, the implementation of a manual yaw system, a redesign of the mechanical brake fashioned after a bicycle disc brake, a complete redesign of the turbine and load electrical systems, and a modified control scheme.

Static Performance Analysis

The turbine blades must capture the maximum amount of energy in the wind during the power curve task, while remaining lightweight and fitting within the designated tolerances. The angle of twist of the blade was optimized to enable power production at low wind speeds, and a literature review advised a Tip Speed Ratio (TSR) of 7 [1].

The majority of the team's blade optimization and calculations were conducted in QBlade, a simulation software that analyzes wind turbine blade performance and aerodynamics in a variety of conditions. QBlade's algorithms are based on the Blade Element Momentum (BEM) Theory, which is central to proper blade analysis.

The preliminary design process for the turbine blade's airfoils considered benchmarking other teams, and optimizing airfoils based on their glide ratio (C_L/C_d) at relevant Reynolds numbers (between 60,000-265,000) as well as maximizing thickness as a percent, to at least 10% of the chord length. Airfoils were selected from the Airfoil Tools Database. In QBlade, the blade cord lengths and twist angles were optimized with the Betz law and our selected TSR (lambda). We chose the SG 6042 air foil. We designed multiple blades with a TSR of 4 and 7, which perform best in the literature [1]. We plan to test which TSR will be the most optimal in the weeks before competition, using the UCAR Wind Tunnel discussed in the Testing section.

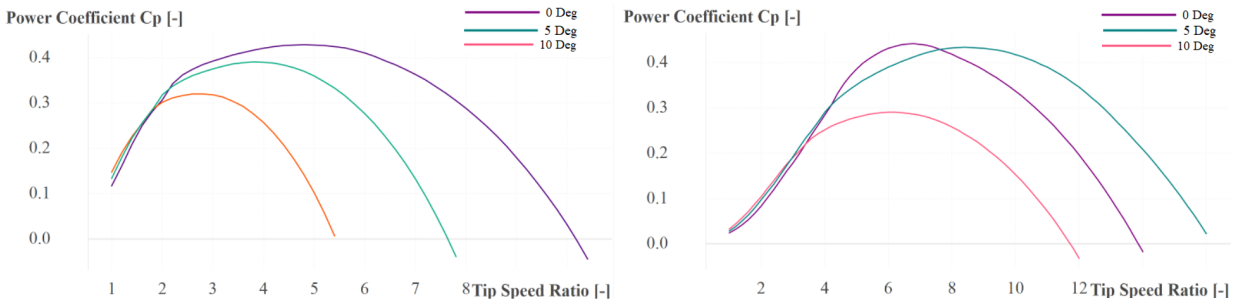


Figure 2. A graph showing the Coefficient of Power (Cp) vs Tip Speed Ratio at 8 m/s. Optimization for TSR 4 (left) and TSR 7 (right).

The max coefficient of power (C_p) QBlade anticipates is 0.43 for the blade design optimized at a TSR of 7, shown on the right, and 0.43 for design optimized at TSR 4, shown on the left. Both values are less than the Betz limit of 0.593. The use of Qblade's Prandtl Tip Loss and 3D Correction adjusted the solutions to be more accurate and put them in a range we expect to see in testing.

Annual Energy Generation

Using the 2012 wind speed data from the Wind Toolkit for Boulder, Colorado with an adjusted a hub height of 95 cm (as mandated by competition specifications), the annual energy generation was estimated to be 35.4 MWh, assuming a blade length of 22.5 cm. This is enough energy to supply a house with electricity for 42.5 months, power 71 refrigerators nonstop for a year, or drive an electric car 127,440 miles [2].

Engineering Diagrams of Mechanical Systems & Load Analysis

Emergency Stop

A modified braking mechanism will allow the turbine to perform better during the emergency stop task. Last year's design featured a triple redundancy emergency stop system that employed a mechanical brake, shorting the generator, and negative pitching. This year's turbine utilizes a simple mechanical brake inspired by a disc brake on a bicycle. The system consists of a custom disc rotor mounted to the back-shaft of the generator, and a custom brake caliper assembly with off-the-shelf bike brake pads. We are using a linear actuator with a 1:375 gear ratio to deliver a pushing force of 200 N to the generator. We calculated the maximum possible braking force using common friction coefficients of off-the-shelf bike brake pads and the given actuator force. Multiplying by the radius of the rotor gives us a braking torque of 3.18 N-m. We then considered the overall moment of inertia of all rotor and driveshaft components and found that this e-brake design could decelerate from 2800 RPM to 0 RPM in about 0.5 seconds, 20 times faster than the required 10 seconds.

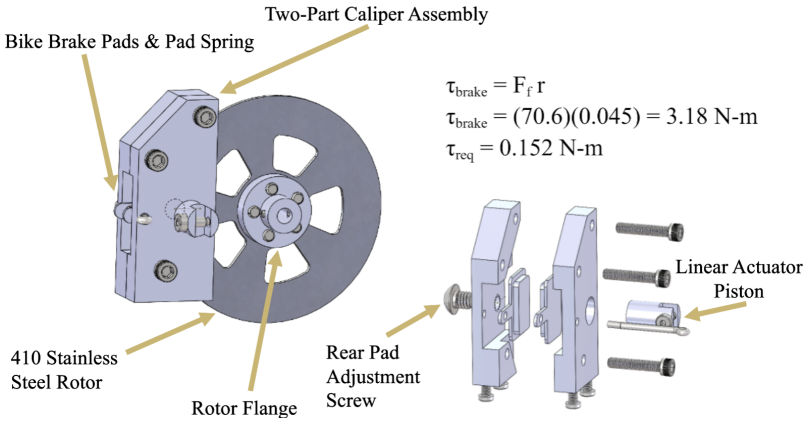


Figure 3. Emergency stop design and factor of safety calculations.

Pitching System

To improve our performance in the power curve and control of rated power and rotor speed tasks, we redesigned the turbine's pitching system from a swash plate design to a miter gearbox design. Our miter gearbox redesign features a robust system that can accurately pitch with minimal power draw and reduces the risk of binding by eliminating all metal-on-metal sliding interfaces. It utilizes a 6V DC 499:1 gearmotor that is mounted directly to the driveshaft inside a hollow aluminum housing component. An integrated 48 CPR quadrature encoder sends signals back to the Arduino which uses proportional feedback to control the angular position of the gearmotor's output shaft.

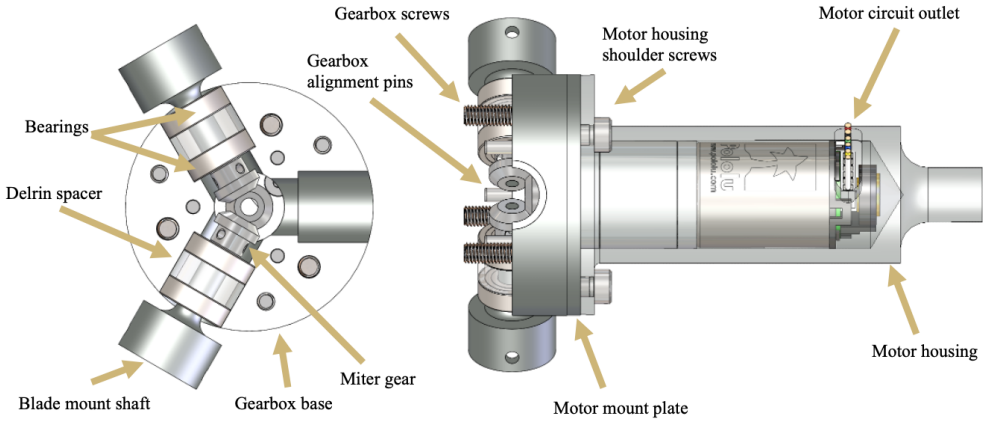


Figure 4. Internals of the miter gearbox pitching assembly

A central drive gear is mounted directly to the gearmotor shaft and meshes with the 3 blade gears with a 1:1 ratio. Each blade gear is attached to a blade mount shaft, which means that 1 degree of angular actuation of the drive gear corresponds to 1 degree of blade pitch. Equation 1 was used to determine the anticipated maximum torque each blade would experience. We assumed a windspeed of $U_\infty = 22$ m/s, a rotational velocity of $\omega = 2800$ rpm, and used a moment coefficient pulled from QBlade of $C_m = 0.15$. The blade torque was then multiplied by 3 to find the max torque on the drive gear to be 0.15 N-m. The chosen gearmotor is rated to provide torque up to 0.49 N-m.

$$T_{blade} = \frac{C_m \rho}{2} \int_0^R (U_\infty^2 + (r\omega)^2) * L_c^2 dr \quad (1)$$

Our miter gear selection was informed by using a modified Lewis equation, shown in Eq.2, and the previously calculated max torque value of 0.15 N-m. We decided to use a 10 mm pitch diameter, 20 tooth, 20° pressure angle, 1045 steel gear manufactured by Misumi. We used a conservative tensile yield strength of 310 MPa for the 1045 steel material (typical range of 310-450 MPa).

$$\sigma_{tooth} = \frac{2T_p}{dFmJ} * \frac{K_a K_m K_s}{K_v K_x} \quad (2)$$

Even under the most extreme anticipated shock loading scenarios, this gear will theoretically hold a tooth shear safety factor of 3.9. The gearbox itself is a clamshell design machined from 7075-T6 Aluminum, which allows us to open it entirely for any assembly, adjustments, or maintenance, while still being stiff enough to hold the precise miter gear mesh in place even under maximum stress conditions.

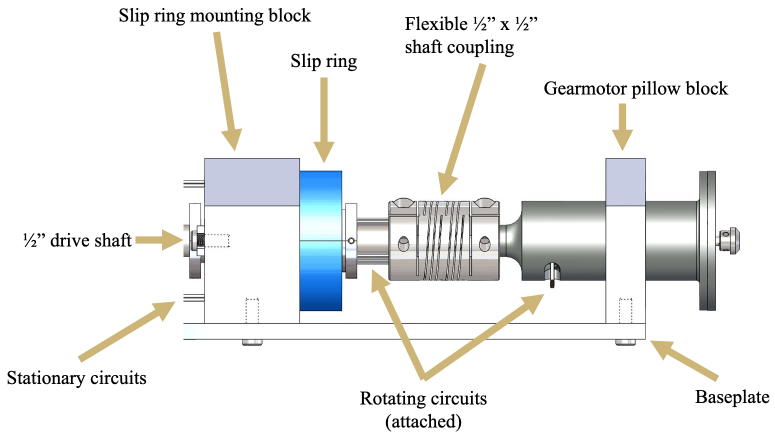


Figure 5 Rotor drive shaft layout.

Since the gearmotor itself is spinning with the rotor, we utilized a high-speed through-bore slip ring, rated for continual use up to 5000 RPM, that allows us to send power and signal between the gearmotor and the Turbine PCB. However, during testing we discovered that the slip ring adversely affects the signal quality from the pitching encoder, and we decided to include a Schmitt trigger on the Load PCB to ensure clean, crisp square waves are reaching the Arduino.

Blade and Rotor Analysis

Beyond the optimization of the blades' power output, we needed to ensure their structural integrity. Figure 6 shows the free body diagram for all forces acting on the spinning blade using simplified Blade Element Momentum theory [3]. This analysis was conducted in three dimensions using cylindrical coordinates. The forces acting on the blade include centripetal, drag, lift and acceleration from emergency stop. It also includes internal reaction forces acting on the root of the blade (reactions forces were solved in 3d but only 1d is shown in Figure 6 for clarity). The internal reactions include shear (V), normal (N) and bending/moment (M). A MATLAB model was created to calculate all forces on the blade root, assuming a rotational velocity of 2800 RPM and an emergency stop deceleration of 3.18 N-m.

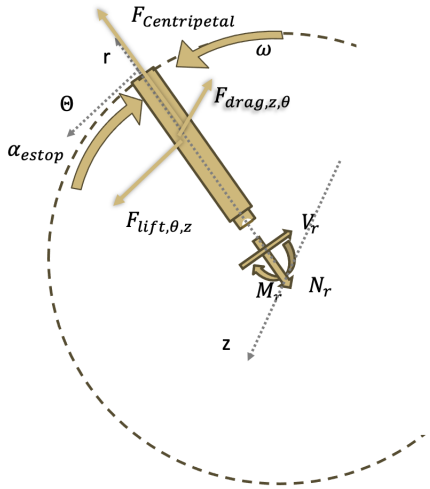


Figure 6. A free body diagram of one blade for structural analysis.

The failure modes we were concerned about were bending failure at the root of blade and through-hole tear-out. Our analysis considered stress concentrations from the through hole in the blade root, using

the Peterson stress concentration charts [3]. The model we created was parameterized first for the diameter of the blade root. We also explored using two different 3D printed materials. Next, we parameterized for the mounting through hole considering the associated stress concentration.

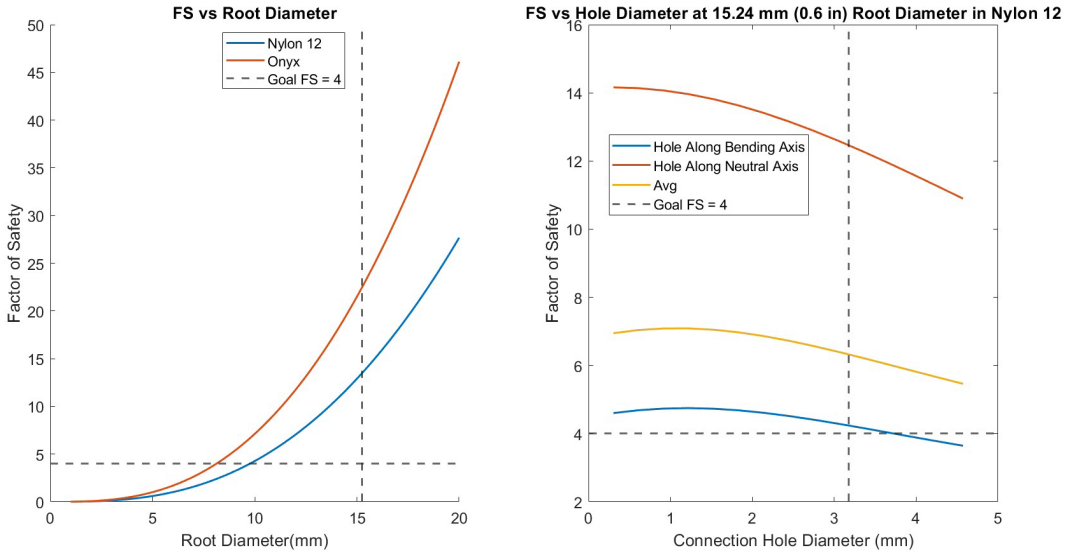


Figure 7. (Left) Blade root diameter vs factor of safety. (Right) Assuming chosen root diameter from right, parametrized for through hole diameter and through hole orientation.

The blade root is one of the failure points we are most concerned about, and it is difficult to precisely model the loading conditions a blade will undergo during testing. For this reason, we chose to design the blade root with a conservative factor of safety (FS) of 4. We chose to manufacture the blades by 3d printing them in Nylon 12 using a FormLabs Fuse1 SLS printer (blue on the left in Figure 7). While Nylon 12 has a smaller ultimate yeild strength than ONYX, an SLS print is perferable over an FDM print because FDM prints introduce anisntropic materials propeties that would be undesirable. We decided we were able to compensate for the weaker material with a thicker diamter section. We chose a diameter of 15.24mm for the blade root and a 3.98mm (5/32”) through hole for connecting to the rotor.

We translated the load calculations from the blades into an analysis of the connection shaft (blade shaft) between the blade and pitching system.

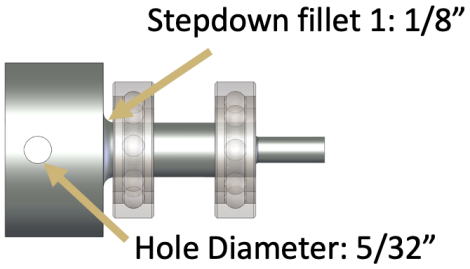


Figure 8. Blade shaft key dimensions.

We were concerned about hole tear out and failure at each of the two steps of this component due to stress concentrations. We integrated this analysis into the MATLAB model mentioned above and designed the connection within similarly conservative safety factors: hole tear out FS: 4.25, failure at stepdown 1 FS: 4.75, failure at stepdown 2 FS: 15.15.

Nacelle and Yaw Sub-System

The yaw system must align the turbine rotor with the predominant wind direction, despite the bolt orientation of the stub piece being unknown. Installation must be quick and provide stable alignment throughout turbine testing. This year's team chose to use a simple yaw collar with two set screws to manually align the nacelle with the wind direction. A mechanical analysis is shown below, assuming a maximum of a 5-degree misalignment with the wind direction from visual inspection.

When deciding on a manual yaw system, we were first concerned with potential power losses from misalignment. We explored the equation for the power generated by a wind turbine. If the turbine can only harness the fraction of wind energy perpendicular to the swept area, swept area A would be replaced by the projection of the swept area when there is a yaw misalignment of angle θ. This projection is an ellipse with an area of A*cos(θ). Then, the power equation is given by:

$$P = \frac{1}{2} C_p \rho A v^3$$

We can expect that the actual power produced from misalignment could be less than the expected value because our airfoils will no longer behave ideally. However, at a small misalignment, the non-idealities would be small, and the equation above should be valid. Therefore, the expected power output from a 5° misalignment would be about 99.6%, meaning we expect less than 1% power loss.

Secondly, we needed to ensure the yaw setscrews would be able to withstand uneven loading due to potential maximum 5° misalignment. We simplified the distributed loadings on the blades from the wind to point loads at the tips and neglected the forces on the nacelle. We used the blade loading MATLAB model mentioned above, assuming a wind speed of 22 m/s, and found the maximum force in the downwind direction to be a distributed load of 24 N across the blades, increasing towards the outer tip.

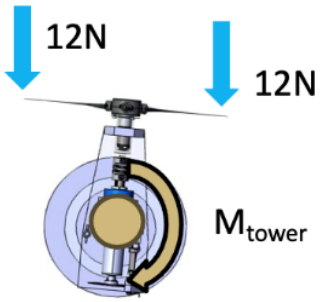


Figure 9. A top-down free body diagram of the turbine and the forces on the blades with a 5° misalignment.

At a 5° misalignment, the difference in the moment arm from the center of the tower is 0.044 m. The torque would be 0.06 N*m. We decided to use ¼" 20 hex head cone head set screws to lock the yaw collar rotation on the tower. Based on tabulated results from safety socket [4]. we found that a ¼" diameter set screw can give us a holding torque of 85 N-m. The FS for torque on yaw is 2833.

Tower Design

The turbine tower is responsible for supporting the weight of the nacelle and rotor subassemblies as well as any nacelle drag and thrust from the rotor. We wanted to check buckling and bending failure. A moment due to a maximum misalignment in the yaw system of 5 degrees was also included in calculations, as shown below.

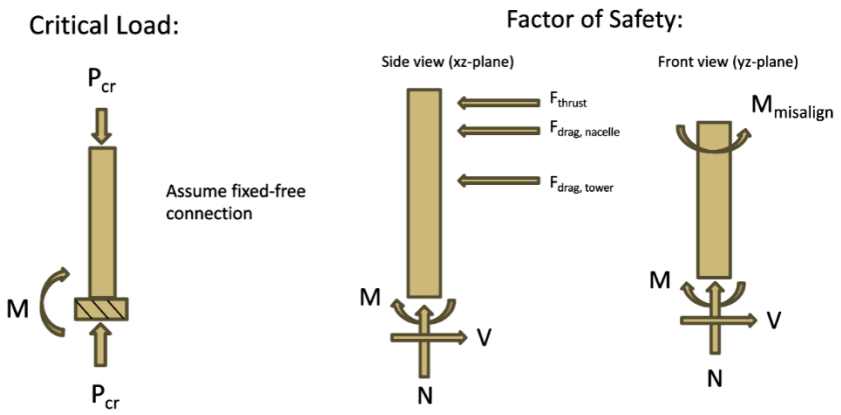


*Figure **10**. Static analyses of the tower.*

Based on these calculations, it would require 24,500 N of force to cause buckling in the tower tube, which is much greater than the expected load of 44.5 N from the weight of the nacelle and rotor assemblies. The expected shear force caused by thrust and drag forces is 23.3 N. Combining the effects of the vertical weight forces of the rotor and nacelle and the horizontal forces from thrust, the net stress is 4.702 kPa. Comparing this with a yield strength of 265 MPa for Aluminum 6061-T6 gives a very comfortable safety factor of about 50.

The team modified the tower base collar and yaw mechanism so that both lie on the exterior of the tower to allow for a minimum of 1 inch of clearance for electrical connectors.

Foundation Engineering Diagram

The foundation must provide stable anchorage for the turbine, remain within dimensional limitations, and comply with the no-excavation rule. Per competition requirements, it must also withstand rotor forces at wind speeds up to 22 m/s. Calculations based on QBlade outputs quantify the horizontal force at the rotor height to be 36 N, which applies a moment of 34.2 N-m on the foundation. Several foundation designs were considered to meet these requirements. As mentioned in the prior competition section, we chose a suction caisson as the final design because it is lightweight, easy to install, and strong enough to meet the functional requirements, as discussed below.

We conducted a civil engineering analysis to assess the stability of the suction caisson design in the context of varying earth pressures. Research showed that this analysis could focus solely on evaluating the passive earth pressure's impact on the rotating bucket's stability, with negligible consideration for active and at-rest earth pressures [5]. This simplified approach involved defining passive earth pressures using specific equations accounting for lateral and vertical stresses applied to the caisson, as shown in Figure 11. Moreover, a static analysis was performed to ensure that soil and suction forces could effectively counteract potential rotation. The resultant forces from these pressures were calculated to confirm that the resisting moment exceeded the overturning moment, considering assumptions regarding force distribution and acting angles. It was assumed that both inner and outer earth pressures act on half of the total bucket surface area either above or below the axis of rotation. Additionally, it was assumed that resultant forces acted in the midplane.

The team developed a MATLAB script to analyze different suction bucket geometries, mainly focusing on different length-to-depth (L/D) ratios of the suction cylinder to identify configurations offering adequate resistance against turbine loads while minimizing weight. The turbine's estimated maximum drag and thrust forces were calculated to be 26.35 N-m, and we decided on designing in a minimum safety factor of 3 to ensure stability against overturning forces. This analysis led to the identification of an optimal design with a diameter of 28.58 cm, a length of 17.17cm, and an L/D ratio of 0.60. The resulting weight of this design, when constructed from 0.813mm thick 4130 steel, totals only 1.39 kg.

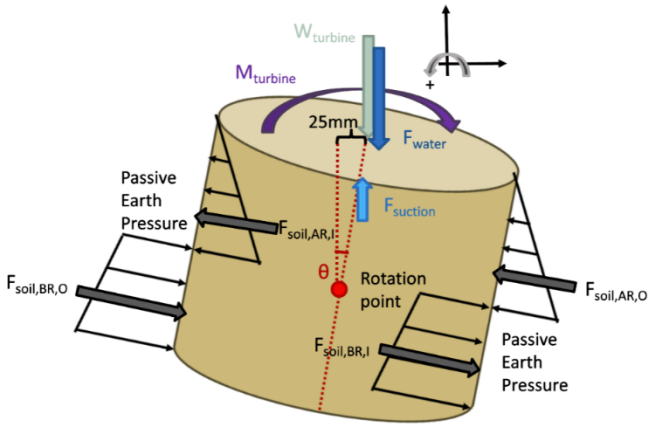


Figure 11. Civil engineering analysis of the suction caisson anchoring system

While the static analysis of this design works out great, the use of such thin sheet metal results in an inherently weak welded connection between the foundation top tube and the suction caisson. To ensure this joint would not fail under maximum stresses, a set of 3 triangular gussets was added to the design, adding strength while contributing negligible additional weight.

Electrical Subsystem

Electrical System Overview and One-Line Diagram

The electrical system is divided into 3 sections to best comply with the competition's isolation requirements. The first is the nacelle, which houses the electronics that need to be physically close to the rotor to operate the turbine. These components include the pitching actuator, brake actuator, and generator. The nacelle also houses a cable assembly that arranges the incoming and outgoing signals and power lines into just 3 connectors for ease of assembly and compliance with competition requirements. The signals transmitted from the nacelle to the next section, the Turbine PCB, are shown in Figure 12.

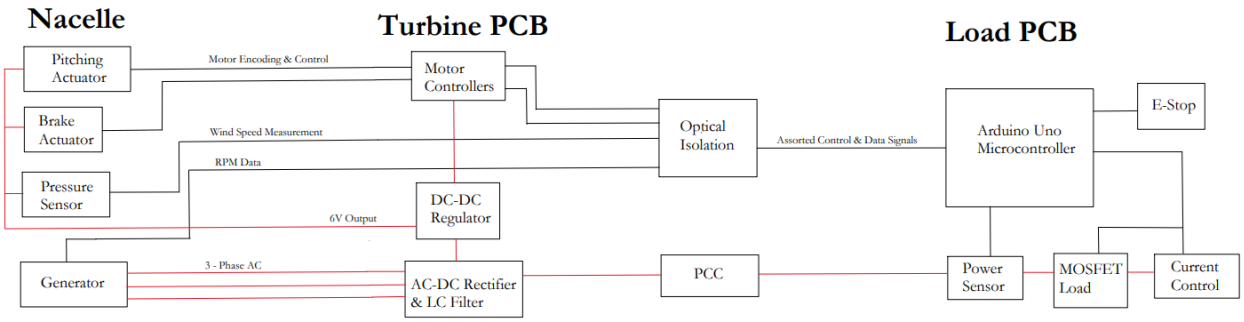


Figure 12. Electrical One-Line Diagram

The Turbine PCB houses turbine power conditioning, a buck-boost converter, pitching & brake motor control, and necessary optical isolation circuitry. Since the entire turbine must be self-powered, active rectification is not possible. Thus, the 3-phase AC power from the generator is rectified using an array of 6 diodes, then filtered using an LC stage before reaching the PCC terminal. To power the nacelle peripherals and the rest of the turbine board, a buck-boost DC-DC converter is connected in parallel with the PCC. Since efficiency is of utmost importance, an off-the-shelf converter is used instead of a custom one. We selected the Pololu S18V20F6 for its wide input range and DC output of 6V, which is within specification to power all the turbine components. The pitching motor is controlled with a Toshiba TB6612FNG motor driver, selected for its versatility and input voltage. The brake control is done with Pulse-Width Modulation from the microcontroller, but still requires some circuitry on this board to ensure

functionality. Since the brake must be powered by the turbine, and the brake is used to stop the rotor in an emergency stop condition, energy storage must be added to the turbine board to disengage the brake when to fulfill the automatic restart requirements. To accomplish this, a separate 6V line is used for the brake, and the brake 6V bus includes an 88 mF capacitor bank that can be discharged through a high current gain optocoupler. The other capacitors on the turbine board are a 22 µF decoupling capacitor and the 1 mF filter capacitor. Our total energy storage is calculated below:

$$E = \frac{1}{2}CV^2 = \frac{1}{2}(88 * 10^{-3} * 6.3^2 + 10^{-3} * 50^2 + 22 * 10^{-6} * 10^2) = 2.997\,J$$

The last section of the electrical design is the Load PCB, which includes our microcontroller, load control circuit, and optical isolation. The microcontroller we selected is an Arduino Uno R3, which is ideal for this application since the control software is relatively simple and not storage intensive, and it has enough GPIO pins to facilitate all necessary communication, including an I^2C bus. It is powered by a 12 V input from a wall AC converter, which is also used by the current control circuit, and provides the 5 V bus for the rest of our components. For our load, we decided to use an N-channel enhancement MOSFET because they have a large power dissipation capacity and a highly variable impedance depending on the gate voltage. This gives us higher control over the behavior of the generator, since the resistance at its terminals controls the torque required to spin the rotor. The MOSFET is combined in series with a current sense resistor, whose voltage drop can be compared to a reference input from the microcontroller with an op-amp. This allows us to precisely control the current through the load and algorithmically maximize the generator's power output. Increasing the current through the load beyond the maximum power point will also decrease the generator's produced voltage, allowing us to constrain the power line to be within 0-32 V, which is our circuit's designed operating range.

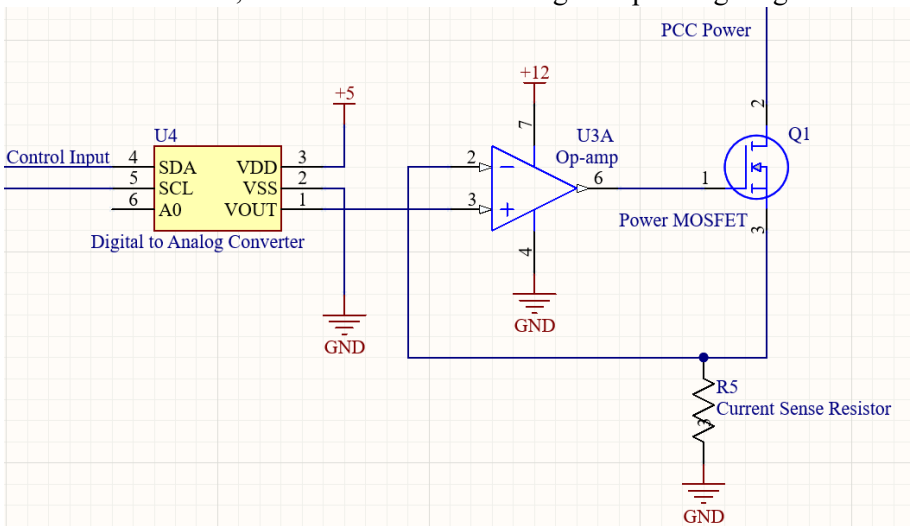


Figure 13. Load Control Circuit Schematic

Signals are optically isolated throughout the electrical system to comply with competition requirements. We used an active high topology for our optocouplers, which means the signals are isolated on the side of the PCC where they're received. The load board receives the generator's Hall sensor and pitching encoder signals, and sends pitching control, brake control, and buck-boost control signals to the turbine board to be optocoupled using turbine power.

Generator Selection

The team decided to use an off-the-shelf brushless DC motor to generate electricity from the rotation of the turbine. Although a brushless motor generates AC, the efficiency loss of a rectifier and filter circuit is less than that of brushes. Additionally, the team did not have the necessary resources and manpower to build a custom generator from scratch. After researching 8 generators, the team decided to use the Maxon EC-i40 488607. Generators were compared using a model that assumed a fixed mechanical power input at

each wind speed and then found a theoretical optimal load for electrical power generation. The model gave estimates for power generation, torque, angular velocity, voltage, and current for each wind speed. The expected power generation at each wind speed was adjusted with tournament weighting and then summed to give a generator score. The Maxon EC-i40 488607 had the second-highest generator score and large factors of safety for maximum angular velocity, torque, voltage, and current predicted by the model. Images of the efficiency curves and power generation for each of the 8 generators are shown in Figure 14.

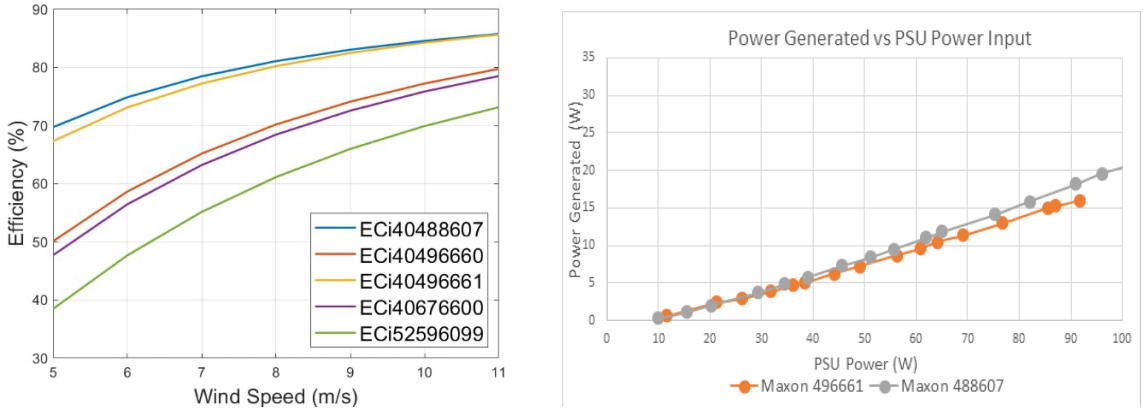


Figure 14. Modeled generator efficiency curves (left) and power generation from testing (right)

To confirm the generator choice, the team produced power curves for 2 generators. To do this, a driving motor was used to spin a shaft connected to the generator being tested and the power output corresponding to each RPM (as measured with a tachometer) was measured. This test was performed on both the Maxon EC-i40 40488607 and 40496661 models, and it was found that the Maxon EC-i40 488607 operated more efficiently leading to its selection in the final turbine design.

Control States and Operational Modes

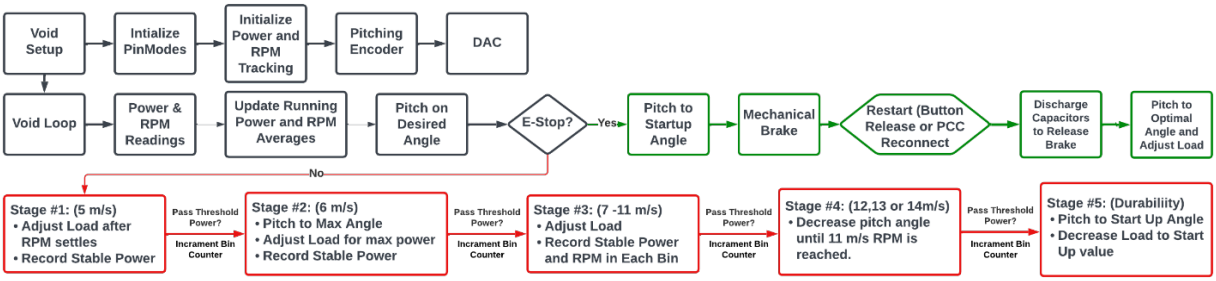


Figure 15. Diagram depicting the full turbine control algorithm and stages.

The full turbine control algorithm includes a wide variety of component setups, functions and initializations. This all happens prior to the main algorithm loop which iterates based on E-Stop conditions and sensor readings. In terms of operational modes of the turbine, there are a total of four main stages based on the logistics of the competition testing. Each stage depends on whether an E-Stop condition has been met and the wind speed. The wind speed is determined by a counter sequence based on the power increments determined at each respective speed.

For the first stage from 0-5 m/s, the load resistance will be reduced to assist in startup and the blades will maintain a pitch position for cut-in at low wind speed. We do not predict having enough power to pitch at 5m/s. Once the wind speed increases to 6m/s, our controls allow the rotor to accelerate and once there is enough power to pitch. Then the blades will pitch in increments to a 50° angle, this serves to maximize RPM. The controls algorithm will then incrementally introduce load until maximum power is reached. In the 7-11 m/s bins, the system will only adjust load to maximize power. The maximum stable

power and RPM at 11 m/s are saved. For control of rated power and RPM, the rotor is given time to spin to a higher power and RPM than the 11m/s max. Then it will pitch to less aggressive angles until the 11m/s RPM is reached. In the case of an E-Stop condition at any point in these stages, the turbine will revert to optimal startup conditions (pitch and load) and apply the mechanical brake until the turbine reaches a reduction to 10% of its maximum RPMs, as stated in the rules. To automatically restart, the brake will be released with energy from the capacitor bank mentioned above. Then it will pitch to 50° and re-introduce load as per the bin in which e-stop was activated.

Software Architecture

When it comes to the development of the software, the foundation was primarily constructed based on the compatibility of the components with an Arduino Uno. With this, individual control files for each component were generated. Each of these then underwent minimum communications tests to verify their functionality and capabilities. Once full-scale functionality for each component was achieved, we integrated the full system.

To begin with full system integration, the software was developed in a piece-by-piece fashion to verify compatibility on a smaller scale. With this, different variations of compatibility were verified when it came to the load, hall effect sensor, pitching system and braking system. Once these were all verified to be compatible and functional with one another, the software from each component was able to be combined into one final file.

To test this full system integration, the full turbine was then placed into a wind tunnel where it was able to simulate testing conditions expected at competition. From this testing, we then modified the software architecture based on the data findings and generated the respective power increment stages. These modifications allowed for finding proper pitching angles, load resistance values and respective power increments for each respective stage/wind speed.

Regarding data acquisition, the Arduino Uno was utilized in unison with PuTTY to act as a data acquisition machine. When it comes to data recording, the turbine can send data regarding current, voltage and RPM. With these data recordings, functions were then implemented within the full system controls to acquire wind speed and power values.

Final Assembly

The wind turbine was divided into 4 subsystems: the foundation; the structure, comprised of the tower, yaw mechanism; and the nacelle, containing the rotor system (blades and pitching system), the nacelle baseplate, generator mount, pillow blocks supporting the rotor and driveshaft, and emergency brake; and the electrical and controls systems, including the PCBs, harnesses and cabling and control algorithms.

The distributed team environment was managed through ample communication both in-person and online, weekly meetings, and trial and error. Team members chose which subsystem they'd like to work on in the early weeks of the project. Everyone oversaw part of a subsystem, such as blade design, electromechanical integration, and the suction caisson. Maintaining communication between team members was key to ensuring designs could be properly integrated and that a variety of design failure points were considered.

Assembly and Commissioning Checklist

Installation

- Run commissioning code on the nacelle system to set startup pitch angle.
- Run the cables through the top of the foundation and out through the slot. Ensure there is at least 14 inches (0.3556 m) of cable on the tower side, and 106 inches (2.69 m) on the PCC side. Hold ends together to keep dry.
- Install the foundation.
    - Unscrew the three bolts on the foundation so they are engaged with only 1-2 threads.
    - Put the foundation in the water and push it all the way into the sand.
    - Ensure the foundation is level using the provided bubble level.

    - Tighten the three bolts on the foundation using the extended socket wrench.
- Run the cable through the competition stub piece and attach the stub piece to the foundation.
- Place the pre-assembled turbine through the wind tunnel door and attach the cable connectors.
- Tighten stub assembly wing nuts.
- Align the yaw mechanism with the wind direction and tighten the set screws.
- Attach the cables to the PCBs outside of the tunnel.
- Plug the load side into the wall power supply.

Commissioning

- With the tunnel wind speed at 11 m/s, record the power output of the turbine and set this value in the control code to calibrate the control of rated power portion of testing.
- Still at 11 m/s, test that the emergency stop mechanisms will actuate and slow the rotor speed sufficiently under both emergency stop conditions.

Testing

Foundation Stability Test

The foundation stability test procedure involved installing our foundation in the competition-specified sand and water configuration, and ultimately sought to quantify the maximum load that can be applied at the turbine's nacelle before displacing the turbine at the vertical location of the bottom of the wind tunnel by a maximum of 25 mm. The foundation assembly was able to support a maximum load of 66.75 Newtons before displacing 25 mm. To make a conservative estimate of the maximum horizontal force the turbine will experience during competition testing, the power of the wind at 22 m/s was calculated to result in a maximum force of 36 N at the rotor, yielding a factor of safety of 1.89.



Figure 16. Experimental setup of the structural stability test. The foundation is mounted to competition testing specifications in the metal horse trough on the right side of the image.

Emergency Brake Test

To test the functionality of the braking mechanism, a flywheel designed to replicate the expected moment of inertia of the rotor components was attached to a drive train, which was also connected to the disc brake system and a gear that meshed with a driving motor. The driving motor was used to spin the shaft up to maximum speeds of 2200 rpm. The brake was able to bring the system to a full stop in under 2 seconds.

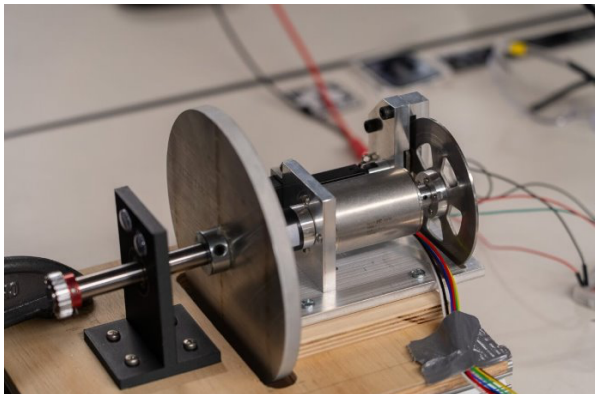


Figure 17. Mechanical brake test setup.

Rotor Spin Test

Mechanical failure is most likely to occur at the rotor, either due to fracture of a blade or failure at the point of interconnection of the blade shaft. Last year's team also reported difficulties with the blades loosening within their blade shafts after repeated testing, so the team would like to see if design modifications have resolved this issue. This testing was particularly important to complete prior to testing in the wind tunnel to ensure there would be no turbine debris that could damage the tunnel or harm the team. We drove the rotor from the generator side of the drive shaft to rotational velocities ranging from 600 to 3200 RPM. Between each test we visually inspected all rotor components. Then we spun the rotor to 3200 RPM and actively pitched 90 degrees. Finally, we spun the rotor at 3200 RPM for 20 minutes. In all cases there was no damage, failure, or signs of fatigue.

Load Test

To ensure our ability to manage and maximize the power being generated by the turbine, we tested the MOSFET load with feedback current control detailed above on a protoboard. We combined a protoboard rectifier and filter with the same driving motor test setup to simulate the wind spinning the generator and set up the current control circuit to be controlled manually through the Arduino IDE serial monitor. The test itself involved externally measuring the current through the load at various generator speeds and various current settings to determine how well the circuit keeps current constant at various RPM and how accurately it could set the current through the load. We found that the regulation worked spectacularly, and the measured current showed very little fluctuation (<1%) with high fluctuations of more than 15 V of input voltage. The accuracy of the current setting against the actual measured current had a margin of error, but this error was very linear, staying constant at about 20 mA difference between the set and measured current. There is only a slight increase in the discrepancy at very low currents and at a very low voltage to current ratio where the op-amp is at max output and the MOSFET is at its minimum resistance. This result gave us confidence in our design since the circuit only needs to be able to regulate current relative to power rather than at an absolute value.

Wind Tunnel System Integration Testing

Previous CU teams have not had access to a competition specification wind tunnel for testing. This year, we have had access to a wind tunnel from the University Corporation for Atmospheric Research (UCAR), and we also have a team of fourth-year mechanical engineering students nearing completion of a wind tunnel on campus that meets CWC testing specifications. So far, wind tunnel testing has been used to integrate the electrical and mechanical systems and simulate the expected conditions of competitions. Data points relating wind speed, load, and pitch angle have helped characterize the expected behavior of the full system, thus informing controls protocols and identifying issues to resolve prior to competition.

References

[1] M. Ragheb, "Optimal Rotor Tip Speed Ratio," Worcester Polytechnic Institute, 2014. [Online]. Available: users.wpi.edu/~cfurlong/me3320/DProject/Ragheb_OptTipSpeedRatio2014.pdf. [Accessed 28 Nov 2023].

[2] B. Nussey, "What can you do with a megawatt-hour?," Accessed: . [Online]. Available: https://www.freeingenergy.com/what-is-a-megawatt-hour-of-electricity-and-what-can-you-do-with-it/. [Accessed 18 Apr. 2024].

[3] P. J. Moriarty and A. C. Hansen, "AeroDyn Theory Manual," *NREL,* 2005.

[4] S. Socket. [Online]. Available: https://www.safetysocket.com/wp-content/themes/epca/files/parts/bd/Products/setscrewtorque.htm .

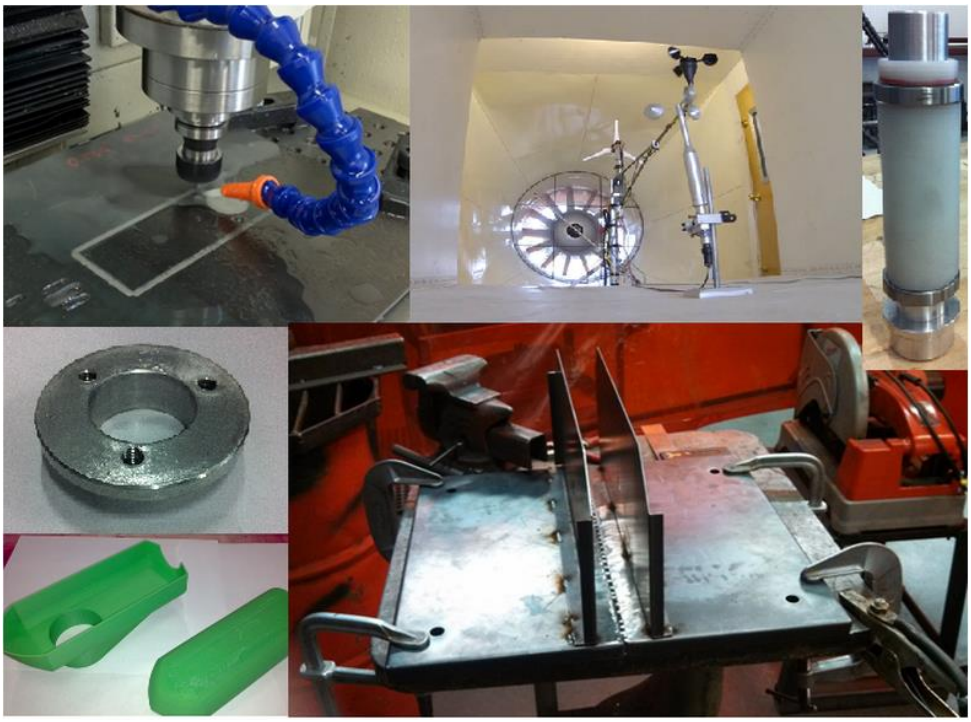
[5] B. Liu, Y. Zhang, Z. Ma, K. Andersen, H. Jostad, D. Liu and A. Pei, "Design considerations of suction caisson foundations for offshore wind turbines in Southern China," *Applied Ocean Research,* vol. 104, 2020.

[6] National Renewable Energy Laboratory (NREL), [Online]. Available: https://wrdb.nrel.gov/data-viewer.

[7] N. R. E. L. (NREL). [Online]. Available: https://wrdb.nrel.gov/data-viewer.

[8] W. D. e. a. Pilkey, Peterson’s Stress Concentration Factors, Wiley, 2020.

Northern Arizona University



Wind Turbine Technical Design Report

The Collegiate Wind Competition

Sponsored by the Department of Energy

Submitted towards partial fulfillment of the requirements for

The Design Review Subcontest

NORTHERN ARIZONA UNIVERSITY

FLAGSTAFF

Table of Contents

1.0 Design Objective 3

2.0 Design Overview 3

2.1 Blades 3

2.2 Hub Design 5

2.3 Nosecone 5

2.4 Yawing System 6

2.5 Integrated Nacelle Design 6

2.6 Mainframe 7

2.7 Base 8

2.8 Tower 8

2.9 Battery 9

2.10 Electronic Controls 9

3.0 Design Team 11

4.0 Modeling and Testing 12

4.1 Rotor/Blade Design Modeling 12

4.2 Blade and Hub Design Modeling 13

4.3 Tower Design Modeling 14

4.4 Nacelle Flow Modeling 15

4.5 Base Design Modeling 15

5.0 Engineering Diagrams 15

6.0 Engineering Specifications 16

6.1 Technical Specifications 17

6.3 Turbine Component Dimensions 18

6.4 Power Curve Specifications 19

7. 0 References 19

8.0 Appendices 20

8.1 Appendix A: Team Member Roles 20

List of Tables

Table 1: Tower Analyses Summary 14
Table 2: Technical Specifications 17
Table 3: Major Turbine Component Dimensions 18

List of Figures

Figure 1: Blade Profile 4
Figure 2: Manufactured hub 5
Figure 3: Nosecone Design 5
Figure 4: Yawing System 6
Figure 5: Rapid Prototyped Nacelle 6
Figure 6: Mainframe and Bracket 7
Figure 7: Base 8
Figure 8: Guy Wire Fixture 8
Figure 9: Schottky Three Phase Bridge Rectifier 10
Figure 10: Top Level Algorithm Diagram of the MSP430 code 11
Figure 11: Testbench setup with Motorsolver Dyno Kit equipment 12
Figure 12: Blade Mold Design 13
Figure 13: Turbine Assembly 16
Figure 14: Initial Rotor Power Curve 19

1.0 Design Objective

The business team has developed a need for a transportable energy source to be used in disaster relief situations. To satisfy this need the project goal is to develop a durable, portable wind turbine to be used in post disaster scenarios. This would allow people to continue using their phones, laptops, and other small electronics after the onset of major disasters and allow people to gather in locations containing disaster relief turbines, enabling them to communicate for emergency aid. In disaster relief situations, the turbines can also be used to power small electrical components such as cell phones.

The design objective of the turbine is to be lightweight and transportable by a maximum of three persons. The turbine base is designed to act as a sturdy base when the turbine is in use and as a platform for which small electronics can be placed while being charged. The base can be fixed into the ground with several different fixtures which allows it to be used on a variety of different terrains. The aerodynamic tower design, discussed later in the report, differentiates the turbine from those currently on the market. The top of the tower utilizes a symmetrical airfoil shape to lessen the turbulence of the airflow around the tower.

2.0 Design Overview

The downwind, horizontal axis wind turbine is designed to fulfill competition requirements. The system makes use of a passive yawing system and three blades which provide a balance between torque production and RPM/power production. This turbine is designed to coincide with the business plan and has been fabricated with lightweight, durable materials to ensure the product's portability. All design analysis can be found in the Rendering Document.

2.1 Blades

Working with such a small rotor diameter, the Reynolds number of a wind turbine blade is extremely low. This made it very hard to model an accurate blade shape because not much data exists for wind turbines with such low Reynolds numbers. This created the challenge of designing a single surface airfoil that would operate at extremely low Reynolds numbers. Testing was completed in an open circuit

subsonic wind tunnel to obtain lift and drag data of a flat plate at low Reynolds numbers and determine the stall characteristics. A flat plate, having a chord length of 0.5 inches and a length of ten inches, was designed with a slight camber for testing. Data is recorded for the normal and axial forces acting on the thin airfoil while wind velocity was steadily increasing. This data is recorded automatically in a LabVIEW program, then the total lift and drag force of the thin airfoil was calculated using the normal and axial forces and the angle of attack.

This information provided the knowledge to be able to run a code utilizing the Blade Element Momentum (BEM) theory to obtain an optimized blade shape [1]. This blade shape contains a certain twist and chord length that was optimized using the BEM code generated. A slight camber is also applied to the airfoil so that the blades will obtain enough torque to get started. The final airfoils are the S834 and CP-080-050-GN (single surface airfoil), which are used in the final design. From these two airfoils, the blade design was optimized using two different software packages and the Blade Elemental Momentum (BEM) theory. Initially two, three, four, and six bladed systems were considered for competition; however, a three bladed system was chosen for the final design because of its ability to cut in at low wind speeds and run at high rpms. The two programs used, BLADED and FAST, determined the forces that are acting on certain blade sections. The final blade profile is shown in Figure 1 and was analyzed using BEM, FAST, and BLADED.

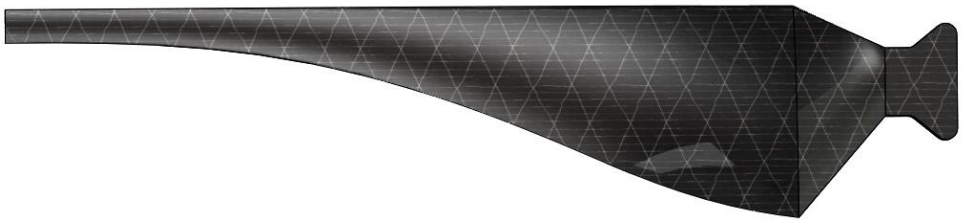


Figure 1: Blade Profile

The final blade shape is designed around the operating Reynolds number from wind speeds varying from 2-17 m/s. In low wind speeds,

the team used a single surface airfoil design to improve the turbine efficiency by having the blades cut-in sooner and produce more power.

2.2 Hub Design



Figure 2: Manufactured hub

The blade root was designed to fit exactly into the hub shown in Figure 2. The three slots in the hub are where each blade root will fit and will be held in place with a hub plate and bolt. The borehole of the hub will be connected to the drivetrain using a collet. The hub design used Aluminum stock, which is cheap, strong, and easy to manufacture.

2.3 Nosecone

To minimize the effects of vortices that shed off of the rotor, a nosecone is included to provide an aerodynamic structure to the design. This nosecone is a simple design which can be clipped onto the hub and is easy to assemble and cheap to manufacture. This design is a simple hemispherical shape that lets the air flow smoothly over the back of the turbine. This design is shown in Figure 3**.**

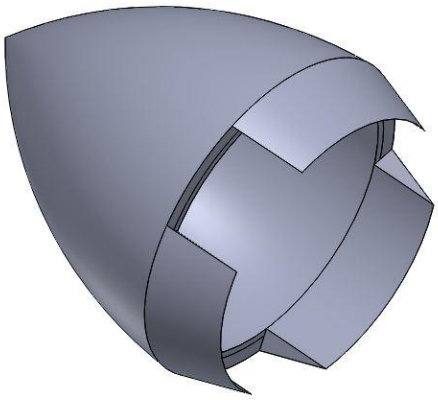


Figure 3: Nosecone Design

2.4 Yawing System

The turbine utilizes a passive yawing system which allows the blades to be directed into the wind. The yawing system design consists of two single row, deep groove ball bearings, a three phase slip ring, a threaded base plug, a yaw sleeve, an upper yaw plug, and a yaw shaft. A sectional view of the yawing system can be seen in Section 1 of the Rendering Document. This image shows how all of the components in this system fit together. The yaw shaft is threaded into a plug at the base of the system. The two bearings and plastic bearing spacers sit on the shaft and an aluminum sleeve fits over the top with a plug press fit into the top. Figure 4 shows the yawing system with the mainframe, slip ring, and generator attached.

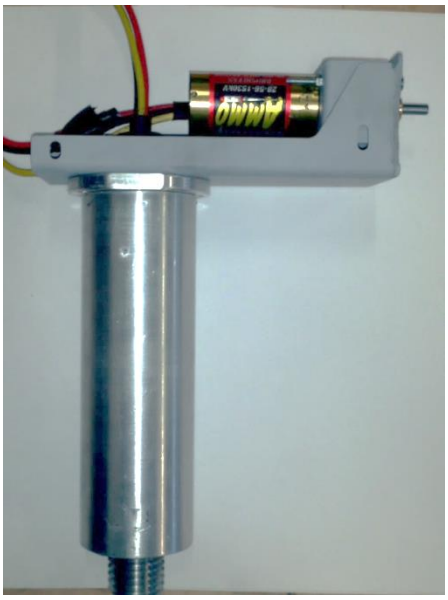


Figure 4: Yawing System

2.5 Integrated Nacelle Design

A fared tower section encases the yawing system and allows for less turbulent wind flow across the turbine tower. This minimizes vortex shedding as wind flows over the trailing edge of the tower, reducing inefficiencies as the turbine blades pass behind the tower. This aerodynamic casing has been integrated into the nacelle design to create a sleek and aesthetically appealing design.



Figure 5: Rapid Prototyped Nacelle

The nacelle sits above the fared tower section and was designed around the dimensions of the mainframe and the hub. The nacelle is only slightly larger than the hub to lessen inefficiencies as air flows over the nacelle and to the blades. A removable door has been built into the top half of the nacelle to ensure that components can be properly placed and to allow components to

be fully inspectable. The integrated nacelle design has been rapid prototyped using ABS and Ultem plastic. Ultem was used due ease of access of material and will not be used in the market turbine. Figure 5 shows the nacelle just after it was rapid prototyped. The two bottom components were secured together with JB weld and a coat of paint was applied to the whole nacelle (not shown).

2.6 Mainframe

The mainframe is designed to withstand all loading and act as a completely rigid structure while being small enough to fit behind the shadow of the hub. The mainframe has been constructed from 16 gauge sheet metal and cut to shape using a CNC milling machine. FEA proved 16 gauge sheet metal to be sufficient to withstand the necessary loads, this analysis can be seen in Section 2 of the Rendering Document. The piece was then bent into shape to provide structural rigidity. This component was then painted with a cold-galvanizing compound to prevent corrosion. This design makes use of two components to make accessing the generator simple and to allow the mainframe to be used for a direct drive system and a system which utilizes a gearbox. The generator is first mounted onto a bracket which can then be mounted onto to the mainframe. These two components can be seen in Figure 6. The mainframe supports the provided Great Planes Ammo GPMG 5225 motor, a three phase slip ring, the nacelle structure, and provides mounting for the passive yaw system. This system is bolted to the yaw plug located at the top of the yawing system and fastened to the nacelle.

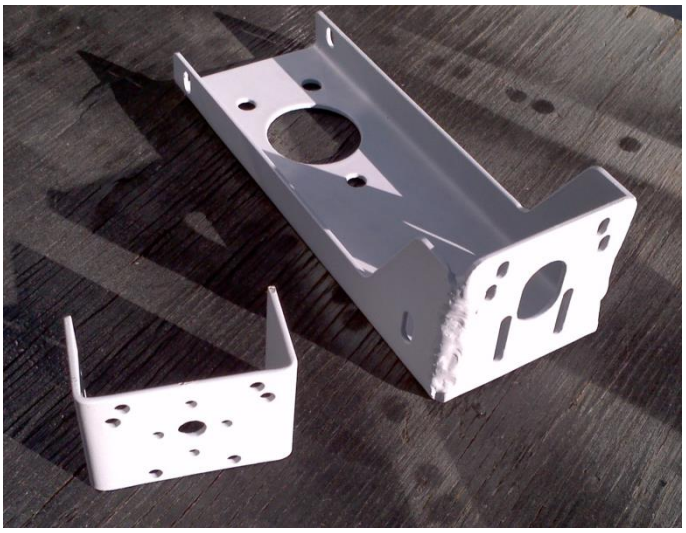


Figure 6: Mainframe and Bracket

2.7 Base

The base has been constructed from 16 gauge sheet metal and has a footprint of roughly 20 inches by 18 inches with a height of 9 inches. There are four holes on the base plates to allow for anchors to be driven into the ground to stabilize the base while the tower is being raised. A hole was placed in the two vertical sections of the base to allow a 3/4" bolt to be placed through the holes to act as a pivot point when raising the tower. The base has also been painted with a cold-galvanizing compound to prevent corrosion. The turbine base can be seen in Figure 7. A shelf was placed on the base where a weatherproof enclosure sits and contains the electrical components. This structure also acts as a convenient place for the user to place their electronics while they are being charged.

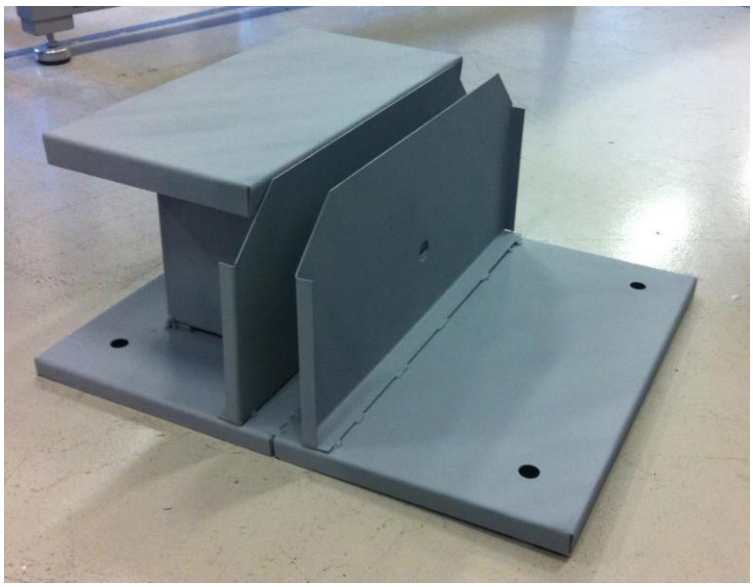


Figure 7: Base

2.8 Tower

The turbine tower consists of three 6 ft. long threaded 6061 aluminum alloy sections and a single 3 ft. section at the top of the tower. Each section is held together with a threaded fitting with the exception of the first and final sections. The first section, located at the base of the tower, is held in place with a bolt which securely fixes it to the base and allows the tower to rotate around the bolt. The tower rotation allows for the tower to be erected simply while the base remains fixed. The

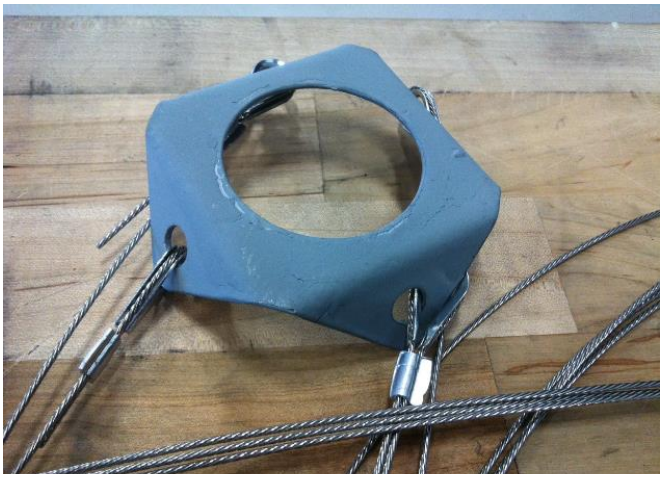


Figure 8: Guy Wire Fixture

final section, located at the top of the tower, has a threaded plug press fit into the top where the yaw shaft threads into the tower. A guy wire fixture sits on the final tower couple and can be seen in Figure 8. This fixture is where the guy wires are attached to the tower and is angled at the ideal guy wire angle of 60^{o} with respect to the ground. A cold-galvanizing compound covers the guy wire fixture to prevent corrosion.

2.9 Battery

Although not required for the competition, the battery bank is a key component of the business plan. The UB12120 12 V 10 Ah battery was selected to demonstrate the battery bank application for the competition. This battery was selected based on storage, temperature, humidity, extreme weather conditions and time of the year data. It will be used in Midwest and Coastal areas during hurricane and tornado seasons. From these areas, the turbine system is expected to obtain up to 25 Wh at optimum wind speed with 2 days of autonomy. It is also designed to operate between 30 ^{o}F – 75 ^{o}F with humidity accounted for. It is a 12 V system battery that can be connected to the power output to store unused power for later use.

2.10 Electronic Controls

For the controller design, the team began searching for a rectifier to convert the AC power from the wind turbine into DC to charge electronic devices. Some rectifiers were considered for low forward voltage drop. It was determined that the Schottky three phase bridge rectifier with peak reverse voltage of 45 V and max current output of 45 A provided the best results, shown in Figure 9. The Schottky diodes in this rectifier together have a very low forward voltage drop (less than 0.65 V) and can switch at extremely fast rates.

In order to regulate the output voltage to 5 V into the grid, the team designed a boost converter circuit that could withstand 20 V and 15 A, since previous generator tests results showed that this was an obtainable range. Three iterations of these circuit designs were made as well as revisions of them by implementing them on homemade printed circuit boards. This custom process started with using photo paper and a laser jet printer to print out the basic design. Next, the team cleaned the clad board and cut it to dimensions, which is noted on Table 3. A household iron was used to iron the ink into the clad board. Once the ink was sealed on the board, the team put it into a bath of muriatic acid. This created a reverse of the PCB and left the ink where it was. Finally, it was bathed in acetone to remove the ink, which gave the team their final PCB layout. After that, they were able to drill the mounting holes for the electrical components. This design can be found on the final Printed Circuit Board (PCB) schematic, shown in Section 4 of the Rendering Document.



Figure 9: Schottky Three Phase Bridge Rectifier

The final PCB schematic, shown in Section 4 of the Rendering Document, has the MSP430 as the microcontroller. This was determined as best suited for this application due to its interrupt capabilities and extensive low power mode options. A top level diagram of its operation is shown in Figure 10. Several iterations have been made to create a final design that is determined to be capable in handling the electrical brake of the wind turbine. This design has three phase power flow into the PCB from the motor where it is then loaded onto resistors. Brakes are handled by the MSP430 using bipolar junction transistors (BJT's) for each phase of the circuit. These transistors are useful for handling high AC current, which helps to control the motor's desired frequency. The outgoing three phase power will then flow through the slip rings and to the components.

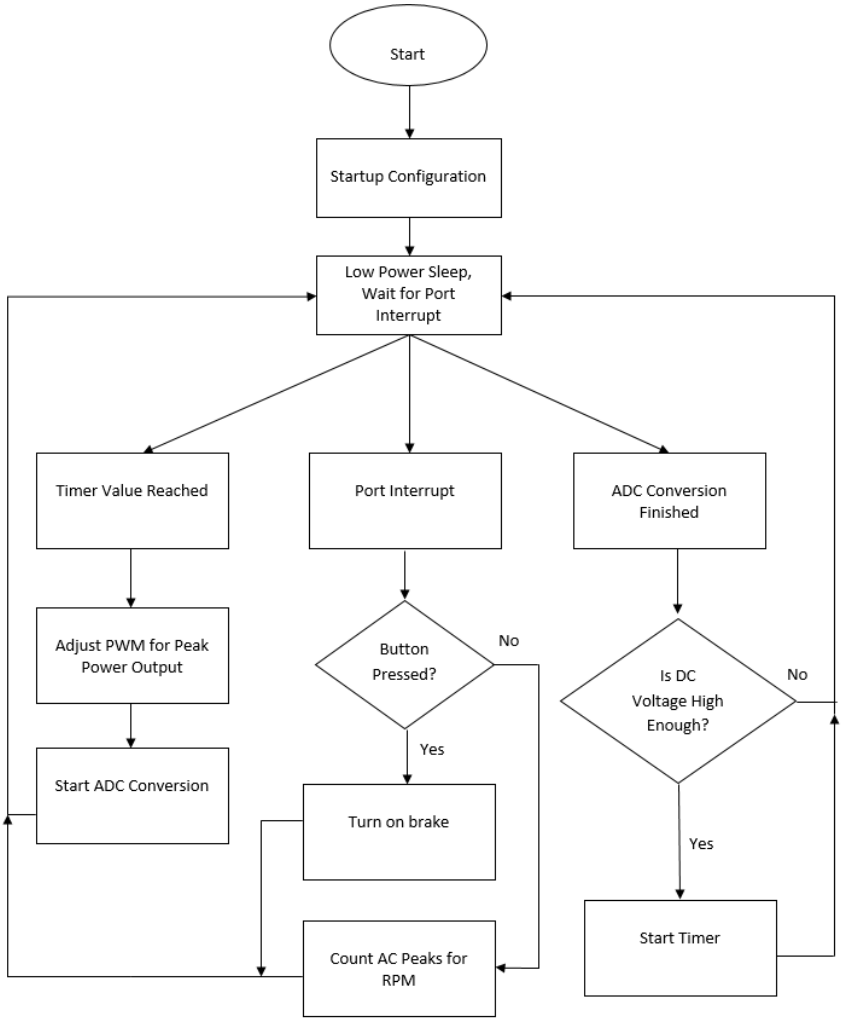


Figure 10: Top Level Algorithm Diagram of the MSP430 code

3.0 Design Team

The NAU team consists of five different sub-teams that all have a wide range of experience and talents. There are three engineering teams in charge of designing and constructing the overall turbine, a business team dedicated to creating the business plan, and a wind market issues team which collaborates for the Market Issues Presentation. The three engineering teams consist of a blade and hub design team, a balance of system and testing team, and a controls and charging team. The business team is full of business and market plan specialists that have created a business plan and will present the turbine market and company at competition. There is also a market issues team that will work on

completing the Market Issues Presentation. A complete list of all the engineering team members and their project roles is shown in Appendix A.

4.0 Modeling and Testing

Motor testing was completed using testing procedures designed specifically to measure the AC voltage, AC current, DC voltage and DC power waveforms from the motor. A testbench and dSPACE ControlDesk software were used to control the permanent-magnet DC (PMDC) motor and MATLAB software to produce desired plots. Figure 11 shows the equipment used for motor testing. In this set-up, an armature voltage can be applied to the PMDC motor and allow the user to acquire information. This was used to obtain the motor's rotational speed and carefully regulate the motor in order to maintain a current below 4.5 A, as this is the maximum operating current for this setup.

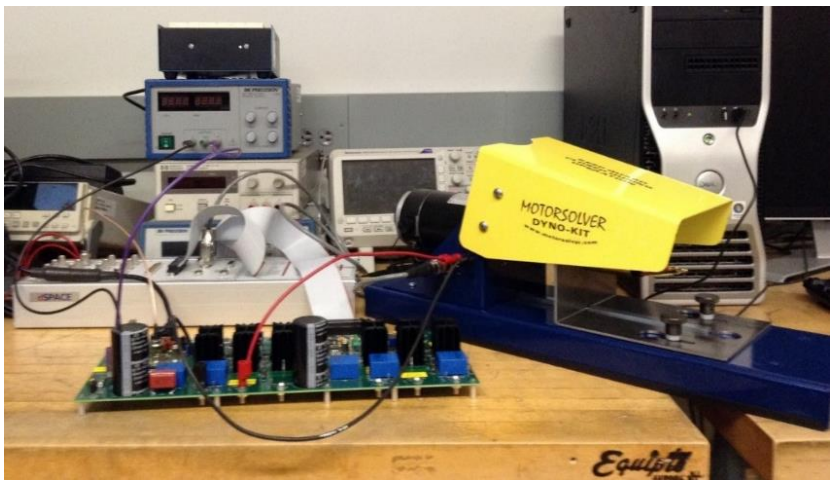


Figure 11: Testbench setup with Motorsolver Dyno Kit equipment

4.1 Rotor/Blade Design Modeling

The blade's Reynolds number was on the order of 10^4 which is extremely low for finding lift and drag on an airfoil. Leading the team to design a 3 bladed design which has a very long chord length and fits perfectly within the constraints of the competition rules and regulations. The chord length and twist of the blade root elements were exaggerated to provide the optimal amount of lift to get the blades to cut-in. The main objective of the blade design was to take up as much rotor plane area as possible to get as much power out of the wind as possible. The stresses on the blades and hub are included in the rendering document which was found using ANSYS Workbench FEA software.

Manufacturing of the blade design incorporated a mold that was completed in SolidWorks. This mold is made up of two sections that have been rapid prototyped to be able to form the very thin shape of the blade profile. These two halves come together to make a single blade. One-half of the mold can be seen in Figure 12.

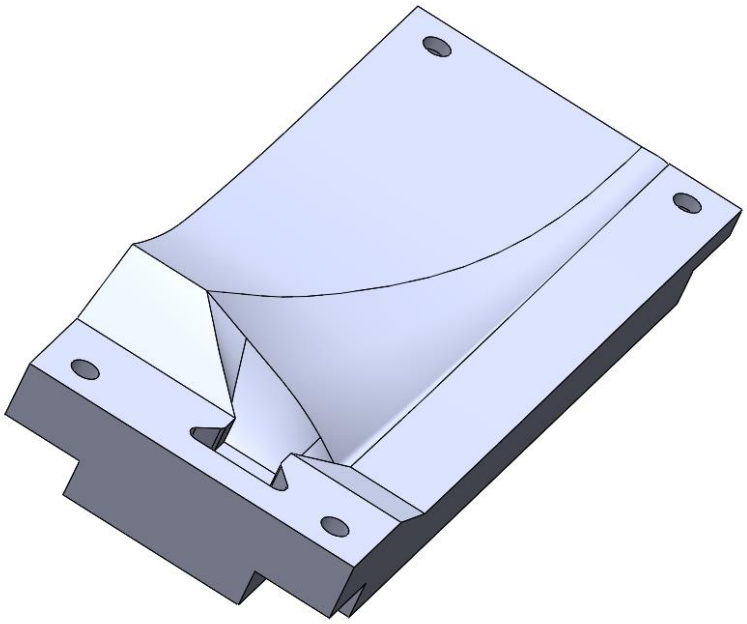


Figure 12: Blade Mold Design

An extremely thin and strong design was needed to ensure that the blades could be made as thin as possible. Various iterations of the blade design were rapid prototyped to see how the design would look and perform in the wind tunnel. The team sought out the design of carbon fiber blades, over 3D printing, so that the blades could meet the dimensional criteria the team needed. The blade profile could not be rapid prototyped because the blades were so thin and that the machine could not generate the blade tip. A mold was designed in order to create the exact geometry that was needed.

4.2 Blade and Hub Design Modeling

The team iterated through many blade designs which were all modeled through FEA software. The teams FEA expert was able to accurately determine the factors of safety and other stress concentrations that occurred on the blades. Using the ANSYS Workbench, the team applied directions of forces, material properties, and geometry of the designed blade and hub for the rotor. Through this analysis

the team was able to inspect each blade element through a fine mesh that was modeled. For the hub, the highest stress concentrations were located at the edge of the blade root slots. This was because of the radial force that the blades will reach from the maximum RPM. For the blades, the team was concerned about the flapwise bending moment forces acting on the blades. These forces proved to show very slight deflections of 5 millimeters at the tip and factors of safety of 1.5. The described FEA modeling of the blades and hub is shown in Section 2 of the Rendering Document.

4.3 Tower Design Modeling

Analysis initially completed on the tower showed that the tower exhibited fairly large deflections at the desired height and diameter. To minimize deflection, guy wires are used to stabilize the tower. In order to determine the optimal position to reduce buckling deflections, the resultant tension force was placed at a series of heights initially aligning with tower segment, or 6ft (1.83m), increments. This analysis found that the ideal guy wire location was at 14ft (4.27m). Bending analysis was completed assuming the highest stress scenario would be when the tower is raised with a maximum nacelle weight of 60N. Section 2 of the rendering document shows the tower deflection due to a buckling stress from the weight of the components up tower.

Table 1 provides a summary of the results obtained from the analyses done. Using the values for maximum stress, obtained using finite element analysis on the tower design with guy wires, the minimum factor of safety was found to be 4.2, occurring while raising the tower.

Table 1: Tower Analyses Summary

Analyses With Guy Wire Supports for Max Load	
Top Load from Turbine Weight	60 N
Wind Load	100 N
Tower Height	6 m
Maximum Bending Stress	55 MPa
Bending Factor of Safety	4.2
Maximum Buckling Stress	0.4 MPa
Buckling Factor of Safety	180

4.4 Nacelle Flow Modeling

Research conducted on faired tower sections for downwind turbines showed that implementing this design could reduce vortex sheading and decrease loads on the blades. Further analysis was completed using Solidworks Fluid Flow Simulation to determine an ideal taper angle. Several iterations of this analysis was completed with differing taper angles to determine which angle would work best at the rated wind speed of 12 m/s. Based on the results of the velocity flow profile and flow trajectory plots shown in Section 3 of the Rendering Document, a 12 degree taper angle was found to be the best for angle for this application. Flow simulations were also done at the cut in and cut out wind speeds of 4 m/s and 17 m/s for the chosen taper angle in order to verify results.

4.5 Base Design Modeling

To ensure that the material of the base would be sufficient to withstand the forces it was exposed to, analysis was done on the assembled base design in SolidWorks. The individual components of the base were made out of 16 gauge metal in SolidWorks and were assembled as a single assembly using welds. The main force that the base must withstand takes place at the pivot point on the base where the tower bolts to the base. Therefore, the force exerted by the tower under operating conditions was placed there to analyze the Von Mises stress and the displacement. From the FEA analysis seen in Section 2 of the Rendering Document, it can be seen that the greatest Von Mises stress is 2.24MPa and the greatest deflection is 1.82×10^{-2}mm. From this data, it was found that 16 gauge sheet metal was sufficient for the design of the base.

5.0 Engineering Diagrams

An image of the current design configuration is shown in Section 1 of the Rendering Document. This design displays the complete rotor design, nacelle and other major turbine components in Figure 13. The assembled figure shows that all of the turbine components have the proper connections. The hub is connected to the drivetrain through a series of shafts and bolts. The drivetrain and electrical components sit on the mainframe and transmit power down tower via slip rings. The slip ring sits on the

yaw shaft which is enclosed by the integrated nacelle and the yawing system is attached to the tower with a threaded fixture.

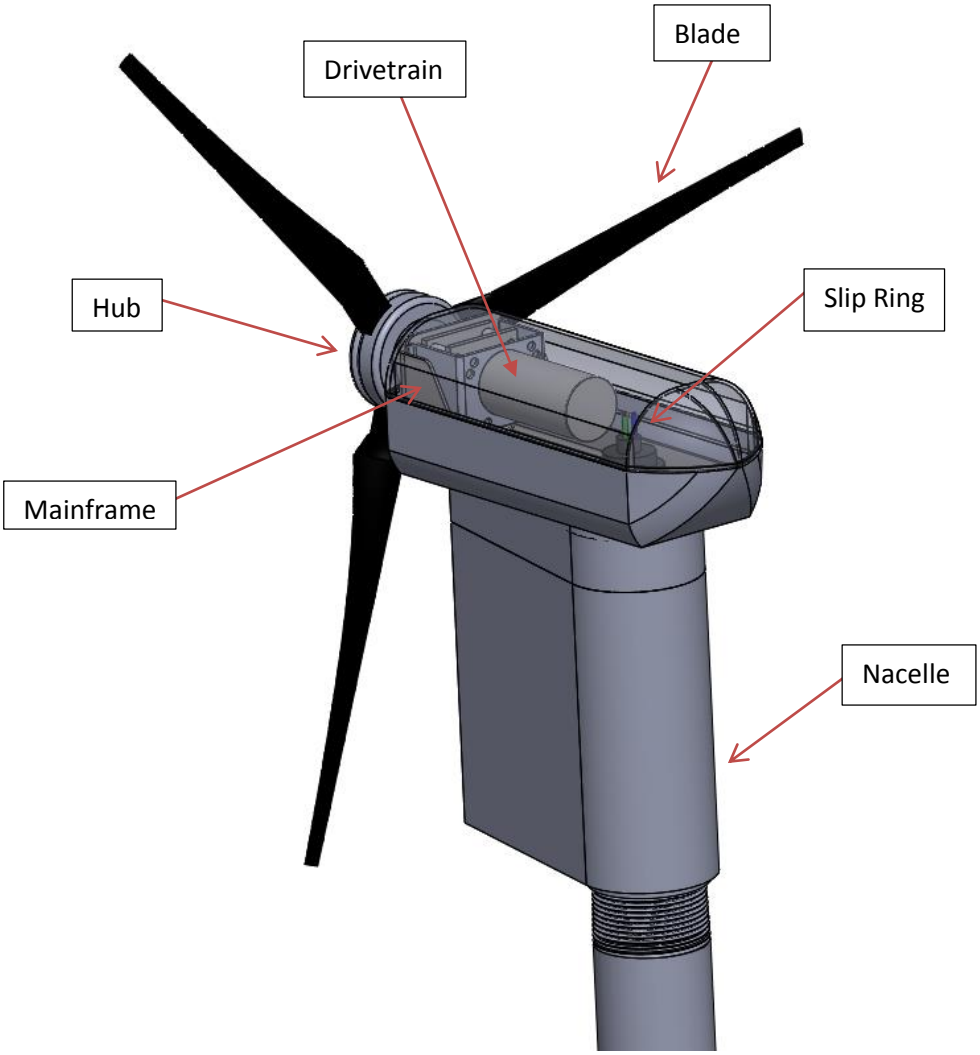


Figure 13: Turbine Assembly

6.0 Engineering Specifications

This section includes the mechanical and electrical engineering specifications of the current turbine design. The technical specifications of the turbine system can be seen in Table 2. Dimensions of major turbine components are detailed in Table 3 of this section.

6.1 Technical Specifications

Table 2 lists the technical specifications of the wind turbine system. Two blade options were considered for design, both of which are listed in the blades row of the technical specifications table.

Table 2: Technical Specifications

Temperature Rating	5 to 122^{o}F (-15 to 50 ^{o}C)
Swept Area	962.1 in² (6221 cm²)
Rotor Diameter	17.5 in (44.5 cm)
Design Power	14 W at 20 m/s
Weight	35.3 Ib (16 kg)
Shipping Dimensions	20”x18”x10”
Tip Speed Ratio	Outboard TSR of 7, Inboard decreases to 5.5
Turbine Controller	MSP430 16-bit microcontroller
Blades	(3) Carbon Fiber Composite (3) Polycarbonate Composite
Motor	Permanent Magnet Brushless In-Runner
Battery	12 V 10 Ah Lead Acid AGM
Airfoil Sections	Single Surface AirfoilS834 and CP-080-050-GN

6.3 Turbine Component Dimensions

Table 3 displays the dimensions of major turbine components.

Table 3: Major Turbine Component Dimensions

	Specifications	Value	Units
Blade Design	Rotor diameter	17.9	in
	Hub diameter	2	in
Yawing System	Yaw Shaft Outer Diameter	2.12	in
Tower	Outer Tower Diameter	1.89	in
	First three tower section lengths	6	ft ea.
	Final tower section length	3	ft
	Assembled tower height	21	ft
Mainframe	Length	6	in
	Width	2.3	in
	Maximum height	2	in
PCB	Length	4.45	in
	Width	5.1	in
	Maximum height	1.5	in
Battery	Length	5.94	in
	Width	3.88	in
	Maximum height	3.78	in

6.4 Power Curve Specifications

The following graph, shown in Figure 14, displays the power curve for the turbine design that was completed using NREL's FAST program to model the turbine design. This data uses the required dimensions of the blade shapes and also the mass of the design, plotting a power curve from a cut-in wind speed of around 5 m/s and a cut-out wind speed of 20 m/s. The calculated rated power is approximately 65 W at a rated wind speed of approximately 12m/s.

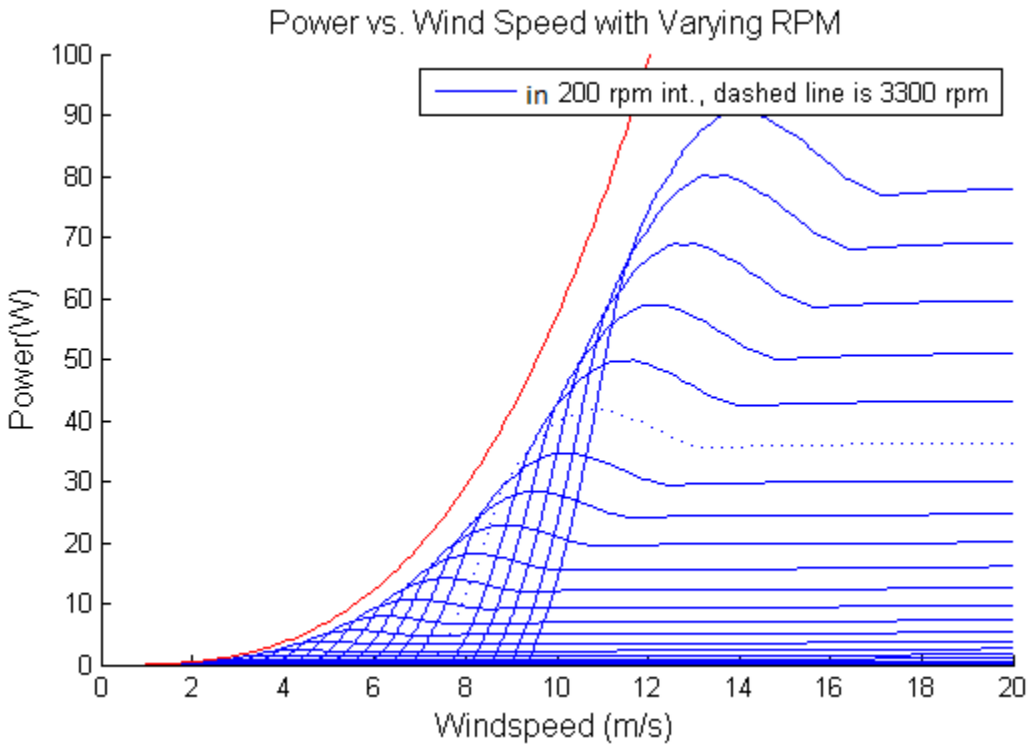


Figure 14: Initial Rotor Power Curve

7. 0 References

[1] J.F Manwell, J.G. McGowan, A.L. Rogers, 2009 Wind Energy Explained: Theory, Design and Application 2nd Edition. Wiley Publications. Chapter 3, Section 3.9 pg. 131-13.

8.0 Appendices

8.1 Appendix A: Team Member Roles

Name	Project Role	Responsibilities
Andrew Hoffman	Project Manager	Team leader, MATLAB, Circuit Analysis and Finances
Carlos Tarango	Secretary	Spreadsheets, presentations, and PSpice
Ian Mason	Assistant Technical Lead	Wind Turbine Interface (MSP430 integrated circuit)
Jared Parks	Technical Lead	Wind Turbine Interface, electrical aspects of the wind turbine
Jonathan Pepper	Treasurer	Constructing PCB layouts
Mariflor Caronan	Rules/Regulation Expert	Coordinating info with team members on rules and regulations updates
Nathan Croswell	Technical Lead	Make sure everything is completed. FAST Program Leader
Devon Martindale	Project Manager	Directs team to stay on task. Compile Deliverables. FAST secondary lead
Gabriel O'Reilly	Machine Design Tech	Shaft Design Leader and Machine Design Leader
Norman Khoo	FEA/Stress Analysis Lead	COSMOS, SolidWorks, ANSYS FEA analysis leader
Chris Feyen	Hub Design Lead	Hub Designer and Secondary SolidWorks leader.
Kenneth Saxer	Computer Coding Lead	Software, BEM and SolidWorks Leader
Chris Bozorth	Technical Lead	Ensures technical aspects of the project are completed correctly.
Melissa Head	Project Manager	Facilitates communication between engineering and business students.
Kyle Yates	Inventory Control Lead	Ensures all turbine components fit together and are feasible to manufacture
Anna Manning	Software Lead	Ensures the design and analysis of turbine components in software are correct. SolidWorks leader
Charles Burge	Aerodynamic Specialist	Makes certain turbine components are aerodynamic
Ashley Jerome	Report and Presentation Lead	Edits documents and ensures that all necessary information is included.

Final Written Report

Submitted to:
U.S. Department of Energy

Submitted toward fulfillment of the
2016 Collegiate Wind Competition

Due: *May 1st, 2016*
Submitted: *April 30th, 2016*

From:

Northern Arizona University
Collegiate Wind Competition Team

Flagstaff, AZ 86011

Principal Investigator: Karin Wadsack (Karin.Wadsack@nau.edu)
NAU Student Team Lead: Michael Wertz (mcw233@nau.edu)

Team comprised of:

3 Faculty Mentors
18 Undergraduate Engineering Students
16 Undergraduate Business Students

Engineering Team Members

Last	First	Major
Alkandari	Anas	ME
Allen	Randon	EE
Alramadhan	Hashim	ME
Bauer	Jessica	ME
Ceniceros	Nathan	ME
Clark	Norman	ME
Cook	Jeremy	ME
Evans	Michael	EE
Holaas	Korey	EE
Melton	James	ME
Muente	Scott	ME
Pellerin	Brock	EE
Richard	Tyler	ME
Robinson	Jess	EE
Sabol	Zachary	EE
Schatz	Ryan	ME
Wertz	Michael	ME
Worrell	Brayden	EE

Business Team Members

Last	First
Alajlan	Budur
Baxter	Luke
Begay	Thomas
Bryniarski	Randall
Campbell	Connor
Carneal	Heather
Coil	Michael
Deheer	Nathan
DeSerio	Adam
Grizzle	Dakota
Lambright	Carl
Lyndsay	Kyle
McWhirter	Nathan
Rittenhouse	Heather
Skorich	Blake
Thompson	Kyle

Technical Advisors

Last	First
Acker	Tom
Chopin	Marc
Taylor	Ross
Wadsack	Karin
Willy	David
Yaramasu	Venkata

Photo/Videographer

Last	First
Kirkov	Kiril

Sponsors

Institution Name
U.S. Department of Energy
National Renewable Energy Laboratory
Northern Arizona University
NovaKintetics AeroSystems

Table of Contents

Executive Summary 5
1 Business Plan 6
1.1 Business Overview 6
1.2 Market Opportunity 6
1.2.1 Direct Competitors 6
1.2.2 Significant Competitors 6
1.2.3 Value Proposition 6
1.2.4 Carbon Tax in India 7
1.2.5 Target Companies 7
1.2.6 Pricing 7
1.2.7 Levelized Cost of Energy 8
1.2.8 Standards in Wind 8
1.2.9 Key Success Factors 8
1.2.10 Barriers to Entry 9
1.2.11 Intellectual Property 9
1.3 Management Team 9
1.4 Deployment and Operations 10
1.4.1 Business Model 10
1.4.2 Partnerships 10
1.4.3 Turbine Design Compatibility with Target Market 10
1.4.4 Business Risks 11

1.5 Financial Analysis 11
2 Technical Design 12
2.1 Design Objective 12
2.2 Final Designs 13
2.3 Static Performance Analysis 14
2.3.1 Blade Design 14
2.3.2 Generator Selection 16
2.4 Stress/Load Analysis 17
2.4.1 Blade FEA 17
2.4.2 Interface FEA 18
2.4.3 Hub FEA 18
2.4.4 Expected loads and FOS Summary 19
2.5 Electrical Analysis 20
2.5.1 Rectifier 20
2.5.2 DC-DC Converter 21
2.6 Control Model Analysis 21
2.6.1 Control State Definition 21
2.6.2 Control Model Design 22
2.7 Documentation of Software 22
2.7.1 Control Model Program 22
2.7.2 Bonus Load Program 22
2.7.3 Initial Blade Design (BEM) 22
2.8 Results of Testing 22
2.8.1 Generator 22
2.8.2 Brakes 23
2.8.3 Control Program 24
2.8.4 DC-DC Converter 24
2.8.5 Blades 25
2.9 Engineering Diagrams 25
2.9.1 Rectifier Schematic 25
2.9.2 DC-DC Converter Schematic 26
2.9.3 AC & DC Brake Schematic 26
3 Deployment Strategy 27
3.1 Identify Site and Dataset 27
3.1.1 Stakeholder Identification and Communication 28
3.2 Timeline & Lifecycle 29
3.3 Installation and Maintenance 29
3.3.1 Installation 29
3.3.2 Maintenance 30
3.4 Reliability and risk management 30
3.4.1 Electrical Reliability 30
3.4.2 Mechanical Reliability 31
3.4.3 Financial Reliability 31
4 References 32
Appendix A - Business Financials 34
Appendix B – Engineering Diagrams 36

Table of Figures

Figure 1-1: 4 Major Indian Telecom Tower Companies & # of Owned Towers 7
Figure 1-2: TES company structure and management roles 9
Figure 1-3: Initial Company Responsibility Breakdown 10
Figure 2-1: Final Designs 13
Figure 2-2: De-rated Power Curves w/ Control States 16
Figure 2-3: Coefficient of Power Curves at Different Wind Speeds 16
Figure 2-4: Blade FEA Results 17
Figure 2-5: Interface FEA Results 18
Figure 2-6: Hub FEA results 19
Figure 2-7: Rectifier DC Output Without a Capacitor 20
Figure 2-8: Dynamometer test of SunnySky 23
Figure 2-9: Brake Prototypes 23
Figure 2-10: Rectifier Schematic 26
Figure 2-11: DC-DC Converter Schematic 26
Figure 2-12: Brake Used for Turbine Shutdown 27
Figure 3-1: India Wind Power Density Map (W/sq. m) [15] 28
Figure 3-2: Deployment Timeline 29
Figure 2-8: Control State Flow Chart 39

Table of Tables

Table 1-1: Cost Comparison between Diesel Generator & TES's Wind Turbine 8
Table 2-1: NAU design constraints/considerations 13
Table 2-2: Final Design Theoretical Properties 14
Table 2-3: Reynolds Number Operation Ranges for Each Turbine 14
Table 2-4: Tunnel Blade Design Properties (TSR – 4 Max Cp **– 0.32)** 15
Table 2-5: Deployment Blade Design Properties (TSR – 6, Max Cp **– 0.42)** 15
Table 2-6: Resistive torque requirements at 95% confidence 17
Table 2-7: Tunnel Turbine expected loads and FOS at 24 m/s winds 19
Table 2-8: Deployment Turbine expected loads and FOS at 25 m/s winds 20
Table 2-9**:** Rectifier Input and Output Voltages 20
Table 2-10: DC-DC Converter Simulation Results 21
Table 2-11: **Open Circuit** Brake System Test Results 24
Table 2-12: Boost Converter Bench Test Results 25

Executive Summary

Telecom Energy Solutions (TES) has identified a targeted market for the development and operations of their small scale wind turbine. The identified market was the telecommunication industry in India, where currently 400,000 telecommunication towers are in service, with an expected 3% annual increase. To maintain the electrical demanded of the telecommunication industry (2.5kW/h), diesel generators are used. To compete with the diesel generators, TES has performed a cost comparison over 10 years to see if the wind turbine is a liable solution. From this cost comparison, it was determined that the diesel generator would cost the company an estimated $86,724.00 whereas the turbine would only cost $10,000. From the financial analysis it is seen that the TES turbine can indeed compete with the diesel generator, in terms of pricing.

From the identified market, a deployment turbine was designed to meet the specified power needed. To meet the power needed a wind resource assessment was performed. The implementation of the wind resource assessment allowed an understanding of the wind speeds seen at the telecom sites. From this information, a marketable wind turbine was created and produced 4 kW at a wind speed of 11 m/s.

To solidify the marketable turbine design, a proof of concept was implemented by creating a scaled down version. The proof of concept (tunnel turbine) used a scale factor of 1/10 and 1/6 for the length of the blade (span) and width of the blade (chord) respectively. These scale factors kept the two turbines linked mathematically and allowed for preliminary testing. A wind tunnel test was then implemented and showed that the tunnel turbine was capable of reaching 23 W at 11m/s.

The validation of working turbines has allowed TES to further develop a deployment strategy for the telecommunication industry. The steps that have been established are as follow: identification of the telecom consumer, sell turbine by underlying key opportunities, begin manufacturing of main turbine components, pre-assemble priority components (generator and yaw), ship to consumer and begin installation.

1 Business Plan

1.1 Business Overview

Telecom Energy Solutions Inc. (TES) offers small wind turbines to provide a more reliable, clean source of energy to telecommunication towers. The small wind industry is growing internationally, with an increase in interest aiming to provide more efficient and earth-friendly energy solutions [1]. TES provides wind turbines that are attached to telecom towers in order to generate electricity for the tower and decrease the need for costly, polluting diesel fuel. TES has determined that India will be our first target market. India's telecom industry is growing at a very rapid pace. The telecom towers have very unreliable connections to the power grid so they have to have a backup power sources in order to provide continuous reliable cell service to their customers. Also, India has passed regulations that require the telecom tower operators to greatly decrease their emissions [2]. TES will initially partner with GTL, a telecom tower maintenance company, and will work into the market through offering proof-of-concept test turbines in exchange for contracts to purchase. Overall, it is TES's vision to offer a power source to India's telecom towers that is lower cost than diesel generation, reliable over the long term, and friendlier with the environment.

1.2 Market Opportunity

TES has determined that India will be the first target market. There are over 400,000 telecom towers currently installed, and that number is expected to grow by 3% annually [3]. It is estimated that 80% to 90% of these turbines are on grid and the telecom towers that are connected to the grid have unreliable connections [4]. Thus the towers have to have a backup power source in order to continue providing cell service to their customers. Diesel generators are used to fill this role, but produce harmful emissions. It is also estimated that as much as 80% of the diesel fuel is stolen out of the generators before it is even used by the towers [5]. In addition, India has passed regulations that require the telecom towers to greatly decrease their emissions produced by these generators [2]. Wind turbines provide an excellent solution for these problems. As such, TES has determined that we will establish our first office in Mumbai, India because it has the most streamlined governmental regulations for starting a new business in India.

1.2.1 Direct Competitors

Xzeres is a direct competitor of TES. They own the Skystream 3.7, an off-grid small-wind turbine that can power telecommunication towers. The Skystream systems are located in Australia, Africa, Europe, Asia and North America. Xzeres sells and installs the Skystream turbines directly to customers through physical stores and online [6]. Their turbines are estimated to cost between $17,000 and $20,000 per unit (turbine and installed cost). In comparison, TES will offer our product at $4,000, which will be much less expensive for customers.

1.2.2 Significant Competitors

Whisper, Bergey Wind Power, Windside, and Aeolos Wind Turbines are all potential significant competitors in the small wind industry. They all offer products that can easily be fitted to power telecom towers. In addition, they all have an international presence.

1.2.3 Value Proposition

TES's offer of reliable, renewable energy for the telecom industry stands apart from the competition because we are working with telecom maintenance companies who already have a trusted relationship with the tower companies. TES's turbines are a low-cost solution for the telecom companies. It is

estimated that these companies spend over $1.5 billion per year in diesel fuel. There is also a significant, and recently increasing, tax on top of the base cost of diesel fuel.

To break into the market we are providing five wind turbines to our potential partner companies for proof of concept before they have to purchase the turbines. TES's turbines also have many technical factors that set them apart from the competition. The yaw system has a vibration isolator that makes the whole turbine more stable, especially in high wind speeds, and prevents damage to towers. The blades have a high in-board angle of twist that allows for low cut-in wind speed. Also, the turbine has a coefficient of performance (Cp) of 0.42 at rated wind speeds that allows for extremely efficient power generation. Lastly, the braking system stops the turbine from producing power when necessary to reduce potential operational issues at very high wind speeds. A tail furling is also included into the design to increase high wind speed survivability (see **Section 2**).

1.2.4 Carbon Tax in India

Because the turbine converts the wind's kinetic energy into electrical power, this product produces 'green' energy, emitting no pollution and using no water. The use of wind energy will reduce carbon dioxide emissions for the telecom tower owners. As the typical Indian telecom tower runs a generator an average of 10 hours/day, it uses 24 liters of fuel in a day. In a year, this results in 8,760 liters of fuel being consumed, amounting to approximately 23 tons of CO_2 [7]. India does not currently have an official carbon tax, but plans to institute one in its signed commitment for the United Nations Paris Accords climate agreement in December 2015. In its commitment, India suggested that a reasonable carbon tax would be $35/ton, but argued that it already has an "implicit" carbon tax of $64/ton on diesel fuel due to high Value-Added Taxes. India has gone from having heavy government subsidies for diesel fuel to having high taxation on fuel, in part as an environmental strategy. At a $35/ton tax rate for carbon, the annual tax, assuming running a diesel generator for an average of ten hours a day, would be $805 per tower. In a year, across the entire Indian telecom industry, this works out to $201,125,000 that would be spent on carbon taxes alone, not including the base cost of the diesel itself. Implementation of a wind turbine will significantly decrease the cost of having to keep diesel generators fueled and reduce the expenditures on carbon taxes. It will also protect the tower owners against the risk of future increases in carbon taxes as India strives to meet its national and international environmental commitments.

1.2.5 Target Companies

TES plans on using the partnership with GTL to target the four companies that own telecom towers. These companies have a combined 154,000 towers that can benefit from wind turbine power **(Figure 1-1)**. Most of these towers are currently connected to the unreliable grid in India with backup diesel generators.

Indus	Reliance Infartel	QTIL	Bharti Infratel
•80,000	•31,000	•23,000	•20,0000

Figure 1-1: 4 Major Indian Telecom Tower Companies & # of Owned Towers

1.2.6 Pricing

TES will offer the wind turbine at $4,000 uninstalled. This is an attractive offer for the telecom towers because they will greatly decrease their need for costly diesel fuel. As stated above, it is estimated that

telecom companies spend over $1.5 billion a year on diesel fuel for telecom towers plus the heavy diesel fuel tax. Our competition, Xzeres, estimates that the cost of installing and purchasing their wind turbine is between $17,000 and $20,000. Our product is estimated to be much less in cost to the telecom towers with the turbine and installation.

1.2.7 Levelized Cost of Energy

As mentioned, telecom towers in India generally run on generators, using them on average for a total of about 10 hours a day. These generators use 2.4 liters of diesel fuel an hour to make electricity. The current price of diesel fuel in India is $0.80/liter. Assuming a 3kW generator is using 2.4 liters of fuel per hour to make 3 kWh of electricity, the cost per kWh is $0.64. The sale price of the turbine is $4000. We are estimating the average labor, materials and logistics of installation at a cost of $1200, which we believe is a high estimate. We have calculated the lifetime maintenance of the turbine to be $4800. This assumes a day of labor a month for a technician to check the tower during a regular fueling visit, which is a conservative approach, and uses the average annual materials costs for maintenance for a turbine of this size according to the United States National Renewable Energy Laboratory [8]. Thus, the total lifetime system cost to our customer is $10,000. Using the System Advisory Model (SAM), specifications for our turbine, and wind data from near Mumbai, India, we calculated our annual expected generation to be 9760 kWh and a resulting levelized cost of energy of $0.0642. This model accounts for some degradation of the turbine, as the simple "cost per kWh" shown below by dividing the turbine performance by lifetime costs yields a per-kWh cost of $0.0512. **Table 1-1** below outlines these values.

Table 1-1: Cost Comparison between Diesel Generator & TES's Wind Turbine

Diesel		**Wind turbine**	
Cost per liter	$0.80	Sale cost	$4,000
Liters of fuel/hour	2.4	Lifetime annual maintenance	$4,800
Kwh/hour	3	Installation	$1,200
Cost per kWh	$0.6400	Total lifetime cost	$10,000
		Annual kWh	9760
		Cost per kWh	0.0512
		Cost per kWh calculated by SAM	0.0642

1.2.8 Standards in Wind

There are internationally accepted standards, the IEC 61400-2, that regulate the size, safety, reliability, power performance, and sound levels of small wind turbines. Tests must be run to determine that the wind turbine will meet all of these regulations and an accredited certification must be awarded in order to operate in the small wind industry [2]. However, this certification is not required to sell turbines in India. We will begin selling our turbine in India submitting it for review and certification. We are seeking this certification in order to gain more trust in the Indian wind market.

1.2.9 Key Success Factors

There are several factors that make companies in the wind industry successful. Firstly, companies have to be able to successfully negotiate with regulatory agencies in the countries in which they have turbines. In most countries, the wind industry is highly regulated and companies need to be able to negotiate or comply with the regulations. However, this is favorable to TES because the regulations in India are not very strict. Secondly, companies have to pass on any increases in cost to their customers. The capital investments in this industry are relatively high so it is important that businesses pass on any extra costs to their customers so they do not lose their margins. We will combat this barrier by

controlling our costs through manufacturing in China to keep our part cost low. Thirdly, turbines should operate at the full capacity as much as they can. Wind turbines only generate energy when wind is available, so it is important that idle time is minimized as much as possible. TES's turbine will interface directly with the battery energy storage system on the telecom tower, offsetting the need for diesel fuel whenever the wind is not blowing. Lastly, the debt and profit management is extremely important in this industry. Because it takes a very large amount of capital to build wind turbines it is important that the debt accumulated and borrowing interest rates are tightly managed [4]. TES will pay very close attention to the cash flows to ensure that the available funds are managed well.

1.2.10 Barriers to Entry

This industry has very high barriers to entry. There is a high initial cost when producing wind turbines. The turbines themselves are very expensive to produce and companies typically produce, at least in the beginning of the business, their turbines before they have payment from their customers. TES will be producing five turbines that will be given to a telecom company for proof of concept with the condition that if after three months the turbines are successful then they will purchase the five turbines and 100 more in the first year. In addition, there is a very large amount of expertise needed when entering this industry. TES will have two full time engineers once the operations begin to continue with the product development. This will allow our product to continue to improve. These are the biggest barriers to entry in the wind industry.

1.2.11 Intellectual Property

TES has decided not to file for a patent because of the lack of enforcement of patents in India. The US Chamber of Commerce's Global Intellectual Property Center released an International Intellectual Property Index in 2012 and 2014 wherein India was the worst of twenty-five countries for enforcing intellectual property.

1.3 Management Team

Figure 1-2 shows the breakdown of the planned company structure.

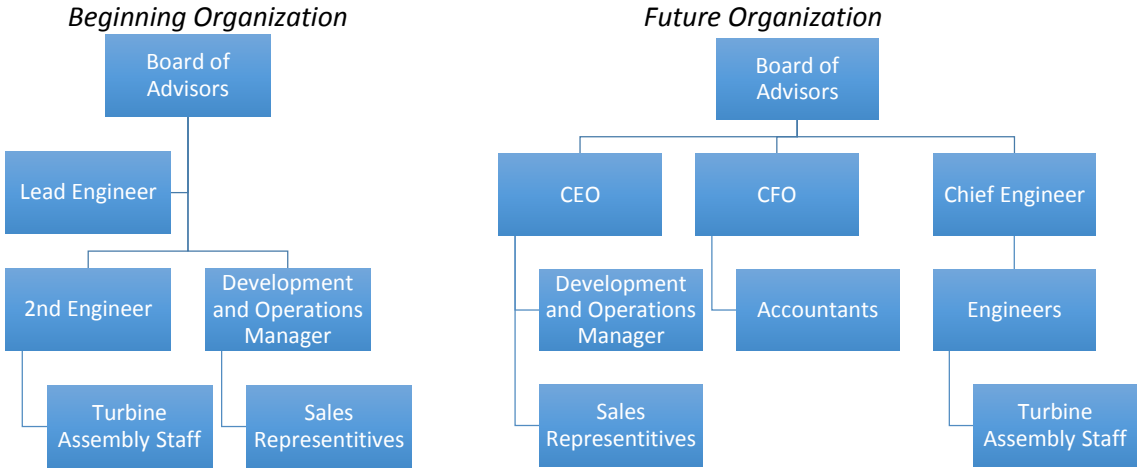


Figure 1-2: TES company structure and management roles

Initially, TES will have a board of advisors made up of individuals with legal, international business, and small wind industry expertise. The lead engineer, a Professional Engineer, will report to the Board of Advisors and oversee the activity of the 2nd Engineer and the Development and Operations Manager.

The 2nd Engineer will be in charge of overseeing the Turbine Assembly Staff to ensure that the turbines have a high quality of assembly. The Development and Operations manager will be in charge of TES's growth and expansion. This manager will also oversee the Sales Representatives, who will be working directly with current and potential customers. The 2nd Engineer and the Development and Operations Manager will visit China on a rotating basis to ensure that the manufacturing is being performed at the highest quality.

1.4 Deployment and Operations

1.4.1 Business Model

TES will outsource the manufacturing of the wind turbine parts to China. These parts will then be shipped to India where they will be assembled by our assembly team. As mentioned above, TES will initially partner with GTL, but will also target a number of other telecom tower maintenance companies. By partnering with GTL, we will be able to gain access into a market that is difficult to get into. They have built a trust relationship with the tower owners and they know more about the actual telecom towers themselves, making them the perfect company to partner with. GTL will be doing the installing of the turbines, as well as the maintenance. TES will receive $4,000 per wind turbine, depending on the company sold to as stated above, and GTL will charge the customers for the installation cost.

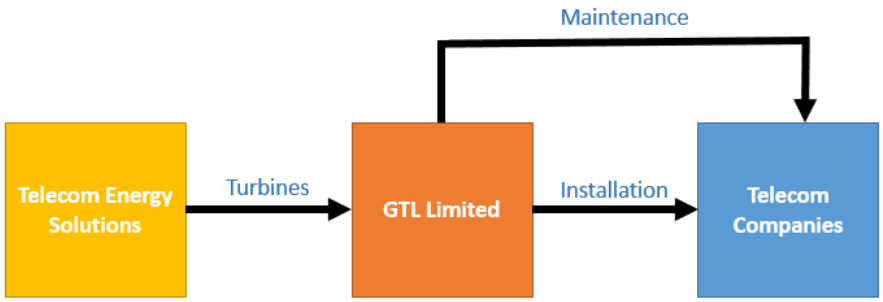


Figure 1-3: Initial Company Responsibility Breakdown

1.4.2 Partnerships

TES will partner with Indian telecom maintenance companies or telecom tower companies. These companies will not only serve as initial customers, but they will provide their employees to attend training at our facility to learn how to perform installation and maintenance for the turbine. Strong partnership with our clients will enable us to troubleshoot installations and streamline processes. The tower maintenance companies and owners have an incentive to provide quality installations and to alert us to any issues that arise. We will provide technical support and seek their advice on system design improvements. Potential future partners include emerging battery technology companies, such as Fluidics, which is a company based in Phoenix, Arizona. This would be a partnership leveraged to help supply stored energy from the wind turbine in the event that TES wants to expand its business model to supply more of the whole energy system.

1.4.3 Turbine Design Compatibility with Target Market

The installation will utilize a pulley system for lifting the wind turbine to the telecom tower, significantly minimizing installation costs. This strategy works well for the target market because using cranes is logistically and cost prohibitive. In addition, using trained partners takes advantage of the low cost of

labor and the incentive mentioned above to perform a high quality installation. The telecom tower must be able to withstand additional loads from the wind turbine. Loads from the wind turbine will be distributed but will still be considerable. Only telecom towers that can withstand the additional load will be considered as potential sales targets. The required power to run a telecom tower averages 2.52 kW [7], and our company's wind turbine will provide 3 kW. Thus, the system will be suitable to run a telecom tower sufficiently.

In terms of research and development for our company, a few turbines will set-up with anemometry in various location in India. The data from the turbines, as well as feedback from the customers, will fuel our research and development for new products.

1.4.4 Business Risks

1. Exchange Rate Risk
2. Cash Flow (Liquidity) Risk
3. Commodity Price Risk
4. Increasing Competition
5. Regulatory Risk

ETC will face an exchange rate risk when supplying its row materials from china. According to Apoorv Srivastava, "The Reserve Bank of India (RBI) would intervene to halt any rupee decline, whereas exporters were of the view that the Rupee has always been overrated and that there is no way that it shall appreciate from the present value. This traditional mindset has kept companies away from hedging their exposures" [9]. Like any startup company, TES will have a cash flow risk, which is the risk of not having enough money to meet financial demands. TES will overcome this risk by diligently budgeting and keeping up with current costs. Additionally, TES will run the risk that the price of an input for the turbine will increase. This risk will also be diminished through thorough budgeting and by sustaining relationships with suppliers. Although there is the risk that competition might increase in the future, the relationships TES builds with the telecom companies and tower owners will give the company an advantage. Switching costs should also protect TES from any competition taking business opportunities. There is also a risk the India will increase regulations for manufacturing, turbines, or companies in general. If there is an increase, TES will abide with all new regulations.

1.5 Financial Analysis

(See Appendix A for statements)

In quarter one, we will begin operations of manufacturing and setting up a business in India simultaneously. It takes approximately 57 days to officially set up our business in India. It costs approximately $500 to set up a business in India. We will not be able to sell any product until we go through this process, but with manufacturing and shipping as well as the assembly we will be ready to sell products around the same time that the business process will be complete. TES will give 5 turbines at the beginning of quarter 2 for proof of concept to a leading telecom provider, installed through GTL, with stipulation that they purchase the turbines at the end of quarter 2. Also in the contract will be a stipulation that they purchase 50 more units in each of quarters 3 and 4. Each turbine will be sold for $4,000. The manufacturing cost for the parts of the turbine is $1340 (per turbine). We will purchase materials in quarters 1 and 3 to maximize the use of space in our 20ft X20ft shipping container. In quarter 4, purchases will be made for the first quarter of year 2 sales. TES will have 3 employees in quarter 1 working 20 days. These 3 employees will begin working full time in quarter 2. TES will have 5

assembly employees in quarter 3 and quarter 4 to keep up with growing demand. Assembly employees will have a wage of $10.70 per day. TES will purchase some power tools and 1 forklift in quarter 1. We will also expect to replace some broken equipment in quarter 2-4 as well as supply gas for our forklift, so we will allot $50 per quarter to cover these costs. TES will have three sales representatives who will receive 5% commission on sales made, up to $2000 each per month. TES will also employ 2 engineers. The lead engineer will make $65,000/year and the second engineer will make $55,000/year. The Development and Operations Manager will make $60,000 and is responsible for finding new markets. Rent and utilities are based off typical rent for a 10,000 sq. ft. warehouse in Mumbai. TES does expect to have a very minimal negative cash flow in year one.

TES is estimating revenue will go up to $800,000 by the end of year two due to an increasing number of sales. Because of the increase in sales, we will order the supplies in quarter four of the first year to meet the demand in the second year. Due to increase in demand, the company is planning to increase the purchases from suppliers to $285,450. By the end of the third year, sales are estimated to increase to $1 million. The purchases from suppliers will increases as well and will cost $351,080. The wages expense for the company is going up to $15,997 in the third year because two additional workers will be added to meet the increase in demand. TES estimated the sales to be $1,200,000 by the end of year four. The supplier's purchases will go up to $419,464 to meet the anticipated demand. The wages expenses will go up to $27,820 because two more workers will be hired to meet the demand.

TES will experience higher costs in year one due to startup expenses. These expenses will be a sunk cost and are required in order to see income growth. Even with the initial startup costs, TES is projected to make a profit in the first year of operation. The performance will then increase each consecutive year for the following four years. Expenses will remain variable to the number of units sold, meaning that expenses will increase at the same rate as sales. Because of this, TES estimates increasing net revenue (after tax expense) amounting in $400,823 by year five. TES expects a tax rate of 33% for companies that operate in India [10]. As long as TES sales continue to increase while keeping costs at a consistent rate, the company should see expanding profits throughout its future.

2 Technical Design

2.1 Design Objective

Two turbines were designed to encompass all competition requirements. The first design was the deployment turbine, which focused on product development for a start-up company with a focus on the Indian telecommunication market. Secondly, the tunnel turbine design focused on the wind tunnel tests to be performed at the 2016 competition. The tunnel turbine can be considered a proof of concept prototype for the deployment turbine. Although different in many respects, the two turbine designs are aerodynamically linked through scalar factors, as discussed in **Section 2.2.1**. **Table 2-1** shows technical constraints and requirements for both designs as specified by the Department of Energy (DOE) or identified by market research [11].

Table 2-1: NAU design constraints/considerations

Wind Tunnel Turbine Design	Deployment Turbine Design
• Max wind speed of 18 m/s • Generate 10W between 5 to 11 m/s • Supply a Load System • Rotor dimensions cannot exceed 45 cm cubed • Rotor center within 2.54 cm of the wind tunnel centerline • Mountable at a specified location within the wind tunnel • Base plate constructed of material no thicker than ½ inch • Turbines must fit through the turbine door assembled • Maximum output voltage 48VDC at PCC • No batteries of any type or excessively large capacitors • Provide wiring and connectors for PCC and kill-switch • Verify zero energy at the start of the test • Bulk energy storage is safe and reliable • Power fluctuation ± 10% for any 5 second interval • RPM and power control • Cut in wind speed of 5 m/s or less • Turbine performs different wind regimes	• Rated wind speed 11m/s • Generate 3 kw between 7-11m/s • Cut-in wind speed less than 4 m/s • Cut-out wind speed 28 m/s • Max survivable wind speed 45 m/s or greater • Project site evaluation • Project site selection • Environmental suitability • Economic opportunities • Geographic requirements • Relative wind resource required for unit operation • Business feasibility • Target market power and resource overlaps • Stakeholder identification and communication • Deployment timeline • Project life cycle • Installation and maintenance • Reliability and risk management • Technical and environmental suitability

2.2 Final Designs

Using these specified design criteria and the analyses in the sections below, final turbine designs were developed for both aspects of the competition (**Figure 2-1**).

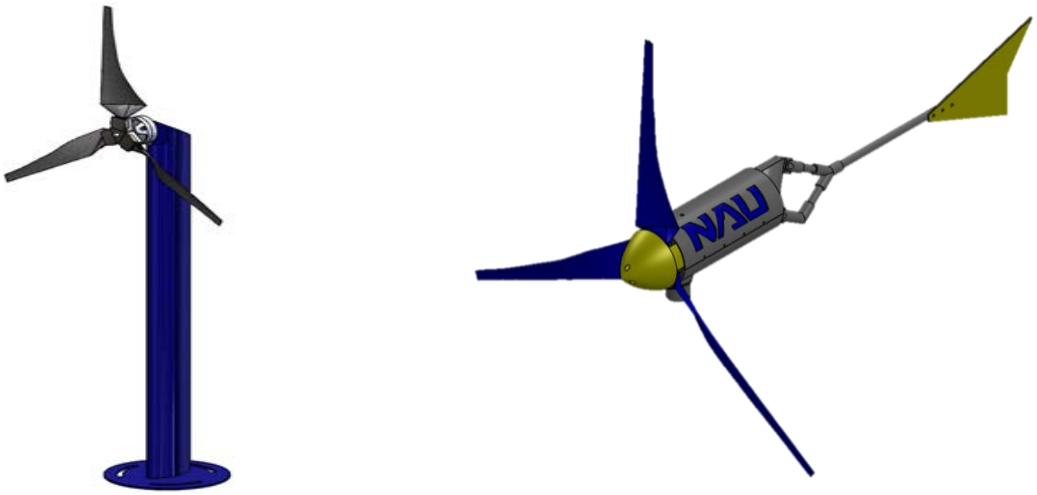


Figure 2-1: Final Designs A) Tunnel Turbine and B) Deployment Turbine

These turbines were designed for different purposes, and as such have different properties. The analyses involved creating these individual designs, as well the design link between the two are contained tin the following section. **Table 2-2** provides an outline of the performance aspects of the final designs. Note that the tunnel turbine does not have a design cut-out speed but is rather designed to handle up to 18 m/s winds, the max possible in testing at the CWC. Also, the cut-in speed of the turbine was determined analytically for this table and had some error associated with it due to an uncertainty in the resistive torque from the generator. The cut-in speed found in testing can be seen in **Section 2.8.5**.

Table 2-2: Final Design Theoretical Properties

	Tunnel Turbine	**Deployment Turbine**
Rated Speed	11 m/s	11 m/s
Rated Output	23.16 W	4 kW (3 kW used for financial analyses)
Cut-in Speed	5.7 m/s	3.6 m/s
Cut-out Speed	N/A	25 m/s

2.3 Static Performance Analysis

Performance of the two turbines was analyzed on an iterative basis allowing for optimization of the performance to meet the design constraints (**Table 2-1**). Specifically, two components critical to turbine performance were fully examined, the blade and generator (refer to **Section 2.4** for FEA analysis on these and other critical components).

2.3.1 Blade Design

The blade design began with the use of a MATLAB [12] code utilizing the blade element momentum theory (BEM) [13]. After this code yielded an initial blade shape based on aerodynamic performance, the design went through multiple iterations to improve aerodynamic start-up (cut-in), design for manufacturability (DFM), and design for structural loading (FEA).

In order to improve start-up and structural performance QBlade was used and checked against hand calculations. A Reynolds number operation range was determined for each turbine at different wind speeds and systematically applied to the corresponding design in QBlade (**Table 2-3)**. Looking at the cut-out range, the tunnel and deployment values are roughly related by a factor of ten, whereas the rated range is roughly rated by a factor of six. The range seen in each data bin represents the differing Reynolds numbers seen along the length of the blade. Based on these values, airfoils were selected with similar lift to drag properties for the respective turbines.

Table 2-3: Reynolds Number Operation Ranges for Each Turbine

	Tunnel	**Deployment**
Start-up	18,200-21,500	70,000-90,000
Rated	40,000-47,700	255,000-336,000
Cut-out	65,500-78,000	615,000-892,000

Through the iterations, various airfoils, chord lengths, and attack angles were analyzed via QBlade for their performance characteristics. The final design properties can be seen in **Table 2-4** and **Table 2-5** for the tunnel and deployment turbines respectively. Note that the M3 attached to each airfoil denotes an iteration in altering the basic NACA 4402 airfoil. The NACA 4402 and SG6043 were chosen due to their optimal performance at the given Reynolds number ranges. In three iterations (M1, M2, and M3),

thickness was continuously added to this airfoil at 29.1% of the chord length to improve the overall structural rigidity (as analyzed in **Section 2.4.1**) without detracting from aerodynamic performance.

*Table 2-4: Tunnel Blade Design Properties (TSR – 4 Max C_p **– 0.32)***

Blade Section	Position (m)	Chord (m)	Twist (º)	Airfoil
1	0	0.0555	45	NACA 4402-M3
2	0.019	0.045	35	NACA 4402-M3
3	0.038	0.0375	25	NACA 4402-M3
4	0.057	0.03	17.22	NACA 4402-M3
5	0.076	0.024	13.04	NACA 4402-M3
6	0.095	0.021	10.12	NACA 4402-M3
7	0.144	0.018	7.88	NACA 4402-M3
8	0.133	0.015	6.37	NACA 4402-M3
9	0.152	0.0135	5.09	NACA 4402-M3
10	0.17	0.012	4.06	NACA 4402-M3

*Table 2-5: Deployment Blade Design Properties (TSR – 6, Max C_p **– 0.42)***

Blade Section	Position (m)	Chord (m)	Twist (º)	Airfoil
1	0	0.333	42	SG6043
2	0.19	0.27	35	SG6043
3	0.38	0.225	25	SG6043
4	0.57	0.18	17.22	SG6043
5	0.76	0.144	13.04	SG6043
6	0.95	0.126	10.12	SG6043
7	1.44	0.108	7.88	SG6043
8	1.33	0.09	6.37	SG6043
9	1.52	0.081	5.09	SG6043
10	1.7	0.072	4.06	SG6043

The design link between these two turbines is that the position of each blade section of the deployment design is scaled by a factor of 10, whereas the chord length is scaled by 6 when compared to that of the tunnel turbine. The twist angles were kept the same other than the in-board blade element angle, which was changed to reflect the change in resistive torque of the larger size turbine. Also, the airfoils were changed between the designs for the same reason, their ability to perform efficiently within the respective operational Reynolds number range. This results in the deployment turbine having roughly a 10% greater coefficient of performance at all wind speeds when compared to the tunnel turbine at the same speeds.

With these design parameters in place, power curves were generated using QBlade to show the theoretical power output by the turbine. These power curves are de-rated, meaning they account for the efficiency based energy losses through various mechanical and electrical components. **Figure 2-2 A** & **B** show the de-rated power curves for the tunnel and deployment turbines respectively. Note that the legend shows the electrical control states of the turbines, which will be discussed in **Section 2.6**.

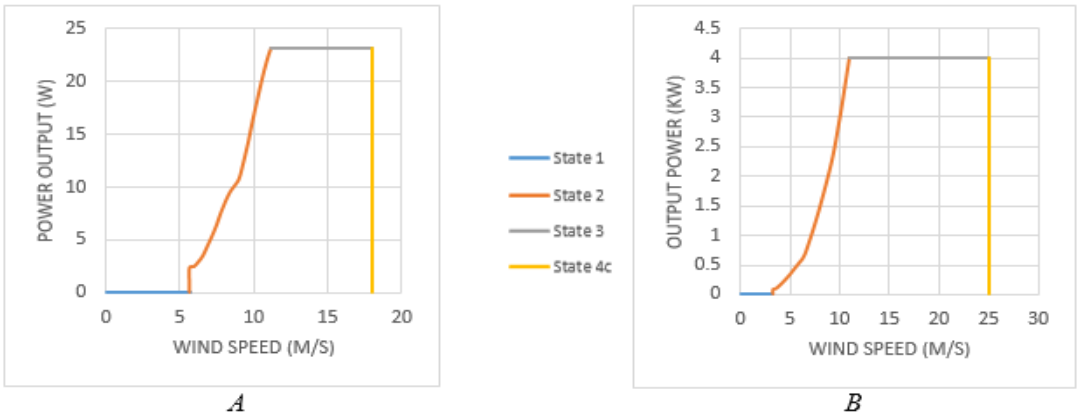


Figure 2-2: De-rated Power Curves w/ Control States for A) Tunnel Turbine & B) Deployment Turbines

Related to these power curves, coefficient of power (Cp) versus tip speed ratio (TSR) plots were also created. This relationship is used to find an optimum efficiency and operating TSR of the blades based on the speed of the blade tip for different wind speeds. **Figure 2-3 A** & **B** depict theses curves for each turbine.

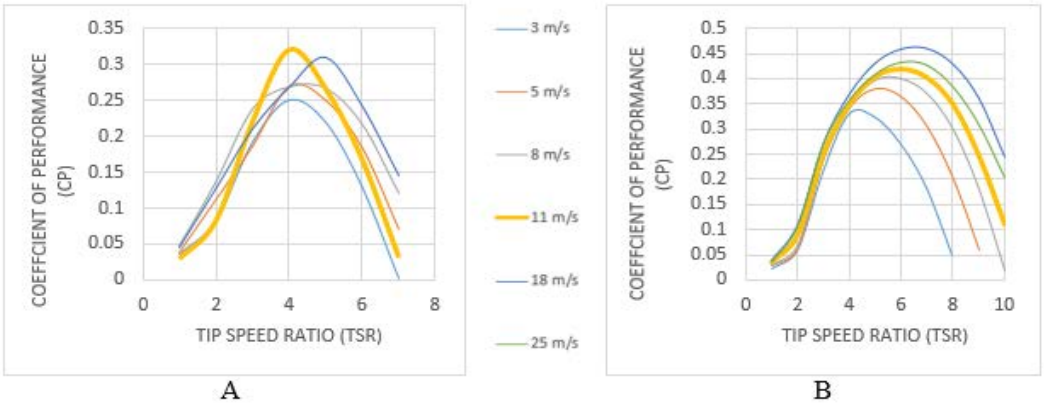


Figure 2-3: Coefficient of Power Curves at Different Wind Speeds for A) Tunnel Turbine & B) Deployment Turbine

2.3.2 Generator Selection

Early in the design process, it was decided that a generator would be selected rather than designed. The generator selection process was based on matching the power and RPM characteristics of the rotor as well as the power, voltage, and current of the power electronics and load. During selection, several generators were considered for the tunnel turbine, but only two passed the initial screening criteria stated above, the Sunnysky X4108s and Turnigy 4114. The deciding factor between the generators was the amount of force required to overcome the resistive torque, which is the sum of the electrical cogging torque and the torque required to overcome friction in the bearings. **Table 2-6** contains the resistive torques for each generator considered. Note that the uncertainty changes between the generators due to the tighter bin of data collected for the Sunnysky compared to the Turnigy.

Table 2-6: Resistive torque requirements at 95% confidence

Generator	Resistive Torque
Sunny Sky X4108s	0.019 N-m ± 0.002 N-m
Turnigy 4114	0.040 N-m ± 0.005 N-m

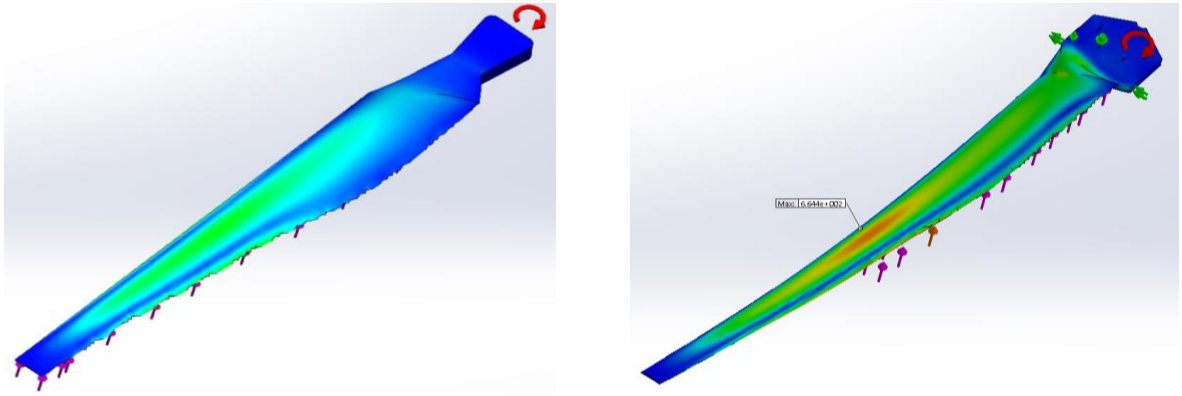
2.4 Stress/Load Analysis

Critical components involved in the construction of the turbine have been analyzed for stress and displacement characteristics, including the blades, interface, and hub. This analysis was primarily done using finite element analysis (FEA) through SOLIDWORKS [14]. The results gathered were used to make both material specifications changes and design refinements for each component.

2.4.1 Blade FEA

Of the critical components analyzed, the blade was most likely to fail due to its thin profile and high applied centrifugal and thrust forces. In setting up the FEA model for the blades, the thrust force was calculated per annulus of the rotor and applied correspondingly. A centrifugal force was also applied to the blade to represent the rotation of the rotor. The initial FEA on the tunnel blade showed that the overall profile thickness was too thin to survive high wind speeds. Thus approximately 3 iterations were used to find the proper airfoil thicknesses. Small increases in the airfoil iterations were implemented (M1, M2, M3), which led to the final design (M3) discussed in **Section 2.3.1**. **Figure 2-4 A** shows the resulting analysis of the final tunnel turbine blade at a 24 m/s winds, which resulted in a factor of safety of 1.60.

Similar to the tunnel blade, the deployment blade was also relatively thin and saw high applied forces. However, in the case of this blade rather than altering the thickness of the original airfoil (the NACA 4402), a different airfoil was selected with a greater thickness (the SG6063). The FEA forces and conditions used for analyzing this blade was identical to the tunnel design, but had a great increase in the applied forces due to the much larger size of the blade. **Figure 2-4 B** shows the resulting final analysis with a resulting factor of safety of 1.04 Note that the thrust forces applied to the blade were exaggerated, adding in an additional factor of safety. The applied thrust force is assuming the blades are flat plates rather than a curved surface.



A
Min FOS – 1.60

B
Min FOS – 1.04

Figure 2-4: Blade FEA Results for A) Tunnel Blade at 24 m/s and B) Deployment Blade at 25 m/s winds

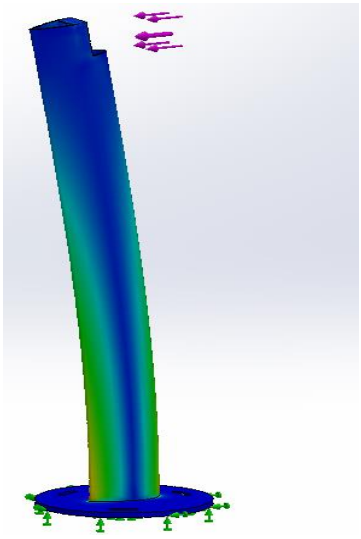
Note that the 24 m/s wind speed was used in the tunnel turbine analysis because it was the max speed producible by the tunnel available to NAU for initial testing.

2.4.2 Interface FEA

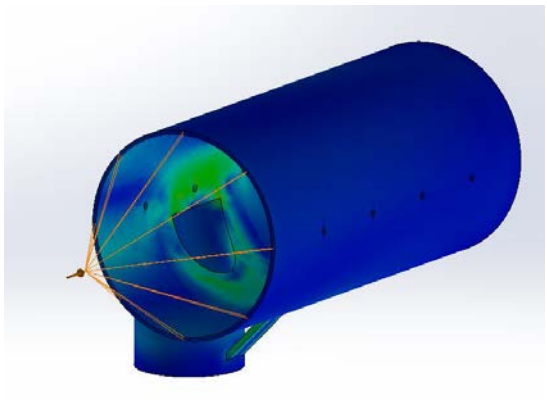
In terms of the interface, it varied for both of the designs. For the tunnel turbine the interface and tower were combined into a single structure. However, the deployment turbine used a nacelle which is turn is connected to a tower via a yawing mechanism.

The tower design for the tunnel turbine was structurally sound with the first iteration, and thus further design iterations were only used to account for different generator mounting methods. When developing the FEA model, the sum of the thrust forces seen by the rotor was applied to the generator mounting position. **Figure 2-5 A** shows the results of the stress analysis, with a resulting factor of safety of 18.2.

For the deployment turbine's nacelle, a basic cylindrical structure was selected due to its easy of manufacturing with pipe or tubing. Similar to the tunnel tower, the sum of the thrust force seen by the rotor was applied to the front of the nacelle. For analysis purposes, the nacelle was restricted from rotation due to the incorporated furling design. **Figure 2-5 B** shows the results of this analysis, with a resulting minimum factor of safety of 3.6.



A
Min FOS – 18.20



B
Min FOS – 3.60

Figure 2-5: Interface FEA Results for A) Tunnel Tower at 24 m/s and B) Deployment Nacelle at 25 m/s winds

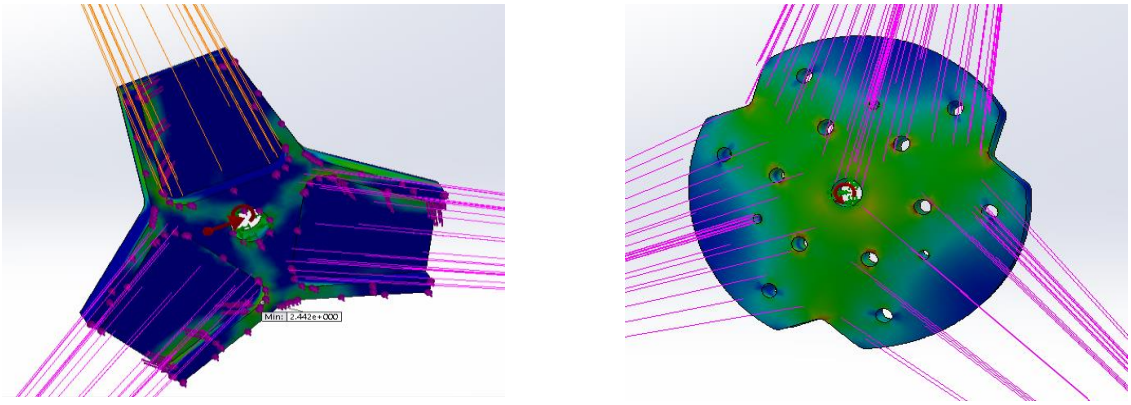
2.4.3 Hub FEA

Like other critical components, the hub for both turbines went through several iterations. While the tunnel hub iterated to address weight and structural rigidity, the deployment hub iterated to address different types of blade mounting systems and structural rigidity to meet CWC testing constraints.

The tunnel hub iterations attempted to reduce overall weight of the part in order to improve turbine start-up. Similar to the blade FEA model, the thrust and centrifugal forces seen by the blades were

applied to the hub. **Figure 2-6 A** shows the analysis results, where the minimum factor of safety was 2.95.

Alternatively, the deployment hub was iterated for different blade mounting configurations, leading to the final design. The last iteration altered the thickness of the plate and the material selected for structural rigidity considerations. **Figure 2-6 B** shows the FEA results for the final hub deployment hub design, which had a minimum factor of safety of 1.30.



A
Min FOS – 2.95

B
Min FOS – 1.30

Figure 2-6: Hub FEA results for A) Tunnel at 24 m/s and B) Deployment at 25 m/s winds

2.4.4 Expected loads and FOS Summary

Similar analyses were performed on the remaining loaded components to verify their ability to withstand the applied forces. **Table 2-7** and **Table 2-8** contain the analytical results from the stress analyses performed on the tunnel and deployment turbines respectively.

Table 2-7: Tunnel Turbine expected loads and FOS at 24 m/s winds

Component	Material	Minimum Factor of Safety	Expected Loads	Load Description
Blade ***(Fig. 2-3 A)***	Carbon fiber	1.93	16.9 N, 545.45 rad/s	Thrust, centrifugal forces
Tower ***(Fig. 2-4 A)***	Chromoly Steel	18.2	16.9 N	Thrust force
Hub ***(Fig. 2-5 A)***	6061-T6 Aluminum	2.95	16.9, 545.45 rad/s	Thrust, centrifugal forces
Thrust Washer	Aluminum Alloy	1.73	16.9 N, 545.45 rad/s	Thrust, centrifugal forces
Hub Adaptor	Aluminum Alloy	1.7	16.9 N, 545.45 rad/s	Thrust, centrifugal forces

Table 2-8: Deployment Turbine expected loads and FOS at 25 m/s winds

Component	Material	Minimum Factor of Safety	Expected Loads	Load Description
Blade ***(Fig. 2-3 B)***	S-2 Glass Fiber	1.04	2.5 kN, 150 rad/s	Thrust, centrifugal forces
Nacelle ***(Fig. 2-4 B)***	6061 Aluminum	3.6	2.5	Thrust force
Hub ***(Fig. 2-5 A)***	Plain Carbon Steel	1.30	2.5 kN, 150 rad/s	Thrust, centrifugal forces

2.5 Electrical Analysis

2.5.1 Rectifier

Testing the DC-DC converter required control programming that is capable of providing the correct duty cycle at the correct frequency to the switching transistors. By using a bench testing analysis, the outputs were compared to the theoretical calculations and adjusted in the circuit for proper boosting.

The Rectifier is a Shottky Three Phase Bridge, comprised of 6 diodes. Two diodes are necessary for each of the three phases, as this is a passive rectification system. The voltage drop is the change in voltage between the input AC voltage and the output DC voltage. **Table 2-9** shows the voltages, voltage drops, and the average voltage drop.

Table 2-9: Rectifier Input and Output Voltages

Input AC (line-to-line)	Input AC (rms)	Output DC	AC-DC Voltage Drop
3.8	5.4	4.2	1.2
4.4	6.2	5.2	1.0
4.8	6.8	5.4	1.4
5.1	7.2	5.9	1.2
6.5	9.2	8.0	1.2
7.2	10.2	8.7	1.5
		Average Drop:	1.25 V

A heat sink for the rectifier was added to avoid damage to the components and efficiency losses. A capacitor was also added to smooth out the voltage ripple. **Figure 2-7** shows an oscilloscope waveform of the rectifier output. Note the small ripple: without a capacitor, this would be much more erratic and harmful to the circuit.

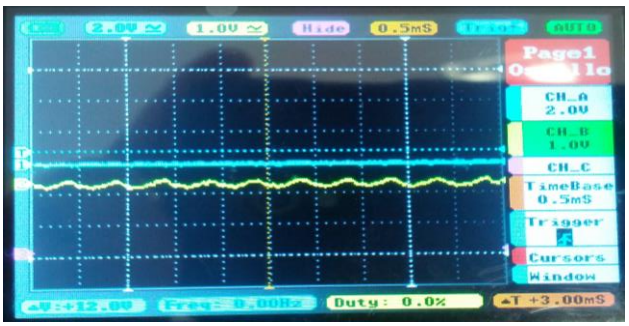


Figure 2-7: Rectifier DC Output w/ a Capacitor ($\Delta x = 0.5\ ms, \Delta y = 1V$)

2.5.2 DC-DC Converter

Initial testing of the DC-DC converter was conducted digitally using PSpice. This analysis allowed for component values previously calculated by hand to be confirmed before final testing. The simulations initially used R_{load} = 0.256 Ω, which represented the equivalent resistance of the 6V lead-acid battery that was to be employed as the load. However, through multiple iterations of the simulation values it became clear that such a low resistance would not facilitate the more important output voltage requirements, especially at low input power that would be seen near the cut-in wind speed. Upon changing the load resistance to 1 Ω, the simulations then showed that for the calculated values of capacitance, inductance, and switching frequency the output voltage could be attained and thus led to a new load design. **Table 2-10** shows the final results.

Table 2-10: DC-DC Converter Simulation Results with f_{sw}=150kHz, R_{load}=1.0Ω, L=78µH, and C=300µF

V_{in} (V)	D_1	$V_{out,min}$	$V_{out,\ max}$	ΔV_{out}
1	0.9	7.55	7.7	0.15
2	0.81	7.6	7.73	0.13
3	0.745	7.44	7.56	0.12
4	0.68	7.46	7.57	0.11
5	0.627	7.68	7.79	0.11
6	0.582	7.63	7.73	0.1
7	0.552	7.9	8.01	0.11
8	0.51	7.53	7.61	0.08
9	0.48	7.51	7.59	0.08
10	0.461	7.82	7.89	0.07

2.6 Control Model Analysis

2.6.1 Control State Definition

Based on the turbine power curve, there are 4 main states that need to be controlled for operation, as seen in **Appendix B**, **Figure B4**.

State one is labeled as waiting. In this state the system is simply waiting for the turbine to cut-in and start generating power.

State two is labeled as optimizing output power. This state optimizes the generation of the turbine during the ramp up to rated output. The goal within state two is to reach the rated output power of the turbine as quickly as possible. When the turbine exceeds the rated power, the system moves from state two into state three.

State three is labeled as modulating the output power. Once the generation meets rated output, this state forces the turbine to stay within a specific generation range near output despite any increasing wind speeds. In order to do this a pulse width modulation (PWM) controller driven by a feedback loop off of the turbine's output is utilized.

Last is **state four**, which has three sub-states, 4A, 4B, and 4C. In state 4A the system is generating power until a kill switch is engaged, which causes the turbine to brake. State 4B engages the brake if the load is disconnected from the turbine. Lastly, state 4C brakes the turbine at the specified cut-out speed (this is specific to the deployment system). States 3 and 4 are needed in order to safely run the turbine without exceeding rated values or running the turbine in unsafe conditions.

2.6.2 Control Model Design

In order to emulate the states of the turbine describe above, a flow chart was created to address the basic operation of the coding and control components, as seen in **Appendix B**, **Figure B4**.

2.7 Documentation of Software

2.7.1 Control Model Program

For software used, a control program was implemented by using an Arduino Zero microcontroller. The microcontroller was used to control the four different states seen in the turbine (refer to **Appendix B**, **Figure B4** for control model flow chart).

This program is used to handle each individual state the turbine goes through, from state 1 to state 4. In states 2 and 3, the Arduino Zero is used to generate a PWM that directly controls the DC-DC converter.

In state 4, two conditions need to be met in order to pass the safety test of the competition, the first being brake by load disconnect and the second being brake when a specific input is provided by an outside source. In order to sense the load, an Arduino Zero micro-controller is used to sense a specific voltage drop from the current flow from the turbine. However when the load is disconnected the flow of current will stop, resulting in a voltage reading of 0. To overcome the other form of braking, normally closed relays are used to brake the turbine.

2.7.2 Bonus Load Program

The program being used within the bonus challenge reads values off a secondary shunt located in the bonus load, as specified within state 4. The value being read is the voltage being produced by the turbine from the point of common coupling (PCC). As the turbine's RPM and power production increases, the Arduino will read the power at the PCC and display the power level in small increments (using LED lights) until the turbines rated power is produced.

2.7.3 Initial Blade Design (BEM)

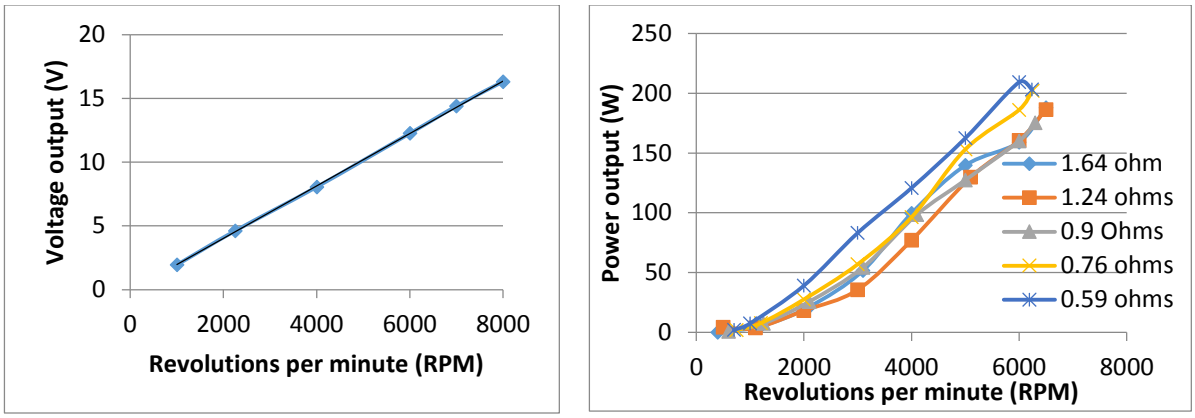
The blade element momentum theory [13] was used for the design of the blades through the use of MATLAB [12]. This theory entailed two steps: the use of Betz' optimum rotor design with wake rotation, and the BEM code. From the Betz' optimum rotor design, tip speed ratios, rotor radii, and number of blade sections were used as input values. These input values yielded optimal chord lengths, which were in turn used in the BEM to find the angle of twist needed for each blade section.

2.8 Results of Testing

To design a tunnel turbine that would operate successfully, testing was performed on each component in the design using a wind tunnel testing apparatus. The systems tested include: generator, brakes, DC-DC converter, blades, and control systems.

2.8.1 Generator

After the generator selection, 2 tests were performed. Test 1 used a dynamometer to find the RPMs, voltage, current, and power whereas test 2 used a level arm to find the cogging torque. **Figure 2-8 A** shows the voltage produced by the generator whereas **Figure 2-8 B** shows the power out of the generator. Note that both of these plots were derived from the results of test 1.



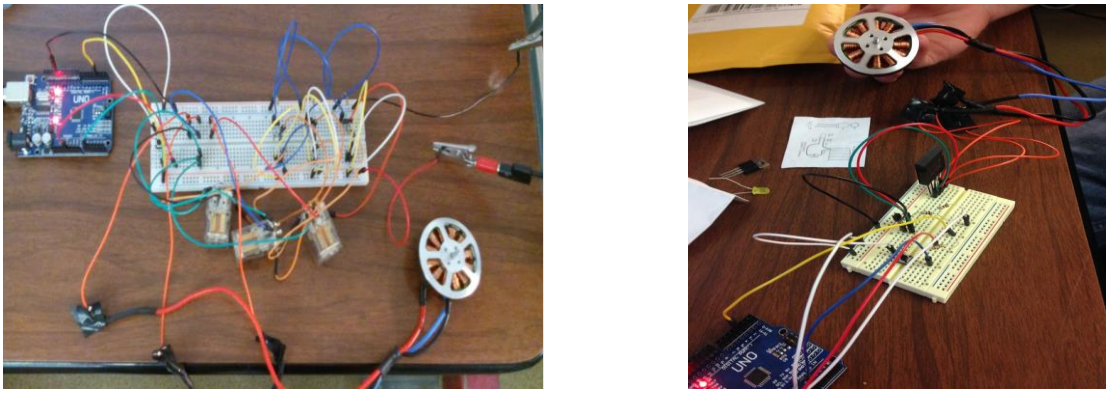
A B

Figure 2-8: Dynamometer test of SunnySky for A) Open Circuit Output & B) Loading Power Output

Similarly, for the turbine test, an open circuit voltage test (Voc) was conducted, as well as loaded circuit tests to determine the power output at various RPM. The current flow was calculated by measuring the DC voltage drop across a shunt.

2.8.2 Brakes

Before construction of the actual AC and DC brakes to be used in the wind tunnel, prototyping was done with a breadboard, Arduino Uno, and Mystery brushless test motor. Each brake system was tested for proof-of-concept by rotating the motor by hand, and observing increased rotational resistance when braking. **Figures 2-9 A** and **B** display these prototypes.



A **B**

Figure 2-9: Brake Prototypes A) AC Brake B) DC Brake

The dynamic AC and DC brake system was tested for functionality at wind speeds ranging from 5 to 20 m/s. An anemometer was used to measure wind speed, and AC and DC open-circuit voltages were monitored for safety reasons. A successful instance of braking was decided by visually observing the reduction in RPM after braking. If this reduction was significant enough to eliminate the blur seen in fast-moving blades, the braking instance was deemed successful. Although the brakes were capable of activating at all wind speeds up to 20 m/s, successful turbine shutdown was only observed from all wind speeds up to and including 12 m/s, after which the brakes were not able to significantly reduce RPM. Wind speeds above 15 m/s were not recorded for this reason. **Table 2-11** displays these results.

*Table 2-11: **Open Circuit** Brake System Test Results*

Wind Speed (m/s)	AC Voltage from Turbine (V)	DC Voltage from Turbine (V)	Brake?
5.1	0	0	N/A
5.6	2.78	3.65	Yes
6.9	3.9	5.35	Yes
8.6	5.2	6.8	Yes
9.9	6.1	8.3	Yes
11.7	7.3	9.8	Yes
12.7	8.1	11	Yes
13.9	8.9	12	No
15.1	9.9	13.3	No

2.8.3 Control Program

In order to check the viability and functionality of the control systems, the corresponding electrical systems that needed to be controlled were tested with the proper coding. This allowed for the individual systems to be actuated individually to verify that they were being controlled properly. Thus, this testing was done in tandem with the other electrical components (refer to **Sections 2.8.2** and **2.8.4** for bench testing procedures).

2.8.4 DC-DC Converter

Initial bench testing was conducted using an off the shelf boost converter that was purchased online. The boost converter is rated for input voltages between 3 and 35 volts, 9 amperes input current, 6 amperes output current, and an overall output power rating of 65 watts. The purpose of this testing was to not only create a benchmark upon which future prototypes would be compared against, but to also confirm that the off the shelf converter would serve as a suitable backup. The converter was subjected to steady state testing using a DC power supply to simulate the input power from the rectifier, a 10 Ω power resistor connected to the output leads to simulate the load, and a digital multimeter (DMM) to measure the voltage drop across the resistor. Proper performance of the converter was confirmed by first supplying it with 4 volts from the DC power supply and then adjusting the potentiometer that controls the output voltage so that the converter output 8 volts. The input voltage was then reduced to just below its minimum input voltage rating to confirm the minimum input voltage required for proper operation. The input voltage was then stepped up by 0.5 volt increments and output measurements were taken each step along the way, as can be seen in **Table 2-12.** The outcome of this testing confirmed that without further adjustments to the potentiometer, the off the shelf boost converter successfully regulated the output voltage within the range of expected input voltages and thus would make a suitable backup.

Table 2-12: Boost Converter Bench Test Results

I_{in}	V_{in}	V_{out}
0.22	3	2.68
1.61	3.5	7.99
1.34	4	8
1.17	4.5	8
1.04	5	8.01
0.94	5.5	8.02
0.85	6	8.02
0.77	6.5	8.02
0.72	7	8.02
0.68	7.5	8.03
0.63	8	8.03
0.57	8.5	8.08
0.61	9	8.58
0.62	9.5	9.08
0.62	10	9.58

A similar test was conducted in a local wind tunnel by connecting the converter to peripheral devices and using an additional DMM on the input in order to compare it with the output.

2.8.5 Blades

The blades were tested for their cut-in speed. This was done by starting the wind tunnel at the slowest speed possible and slowly ramping up until the blades started to spin and a positive voltage and amperage were read from the generator. Wind speed was measure via the use of an anemometer.

Testing performed in the wind tunnel has shown that the aerodynamic start-up required to surpass the resistive torque (of the generator) was between 3.5 and 5 m/s.

2.9 Engineering Diagrams

The engineering diagrams for the competition and deployment turbines can be seen in **Appendix B Figures B1** and **B2**. They show an exploded view of the turbines with the necessary components required for the mechanical assemblies. The electrical one-line operation diagram can be seen in **Appendix B, Figure B3**.

2.9.1 Rectifier Schematic

A three-phase, passive diode bridge turns the AC waveform into a fairly stable DC voltage with current. A capacitor helps smooth out the DC voltage even further for ease-of-control on the DC/DC Converter's side. The team chose the passive design because it would be easier to implement, and the downsides of the increased voltage drop were not significant enough to harm electrical efficiency. In addition, if the team had extra time, they could go back and design their own active rectifier to replace it. **Figure 2-10** helps illustrate the design, and also shows the pin numbers of the rectifier.

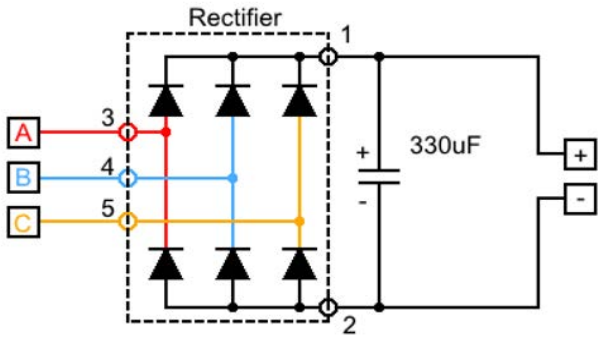


Figure 2-10: Rectifier Schematic

2.9.2 DC-DC Converter Schematic

Figure 2-11 shows a PSpice schematic representing the DC-DC converter. The control signal provided by the Arduino is represented here by a saw tooth carrier signal operating at the appropriate switching frequency compared to a control voltage, thus resulting in a pulse-width modulated signal that controls the switching of the transistor. The transistor is modeled by an ideal switch to simplify the simulation, but is also configured to represent the appropriate $R_{ds,on}$ resistance of the NMOS transistor used in the physical circuit. The inductors and capacitors are configured to represent the actual component configuration that was assembled on the prototyping board.

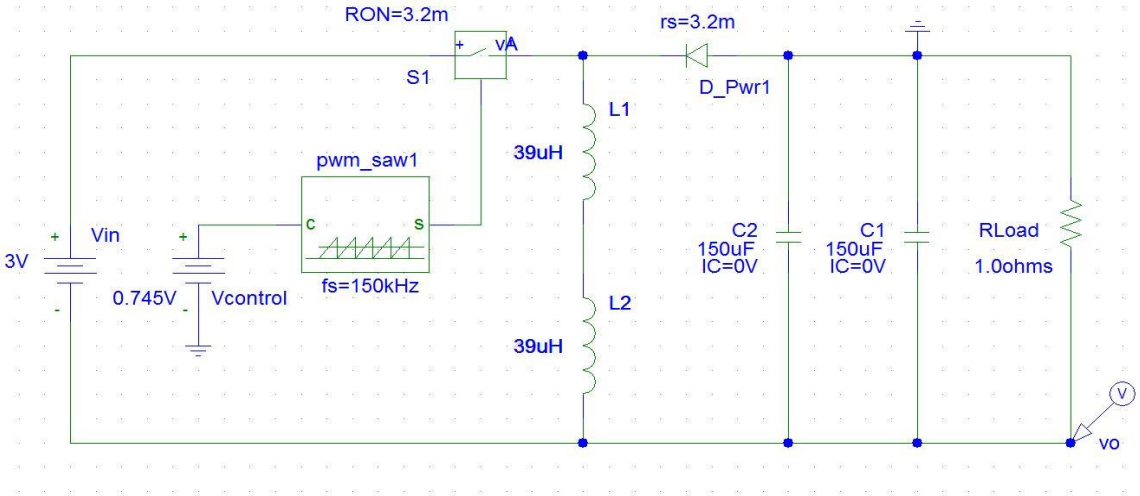


Figure 2-11: DC-DC Converter Schematic

2.9.3 AC & DC Brake Schematic

Figure 2-12 illustrates a simplified version of the AC and DC brake system. The AC brake consists of three, wye-connected relays. Upon loss of power or a low output signal, the relays will connect each of the generator output leads together. This action will dynamically brake the turbine through the use of feedback current being forced into the generator. In addition, a DC brake was added to strengthen the braking power of the AC brake. This system used similar principles to dynamically brake the turbine on the DC side. As a result, the DC brake fed back remaining current – not captured by the AC brake – back into the turbine, initiating turbine shutdown.

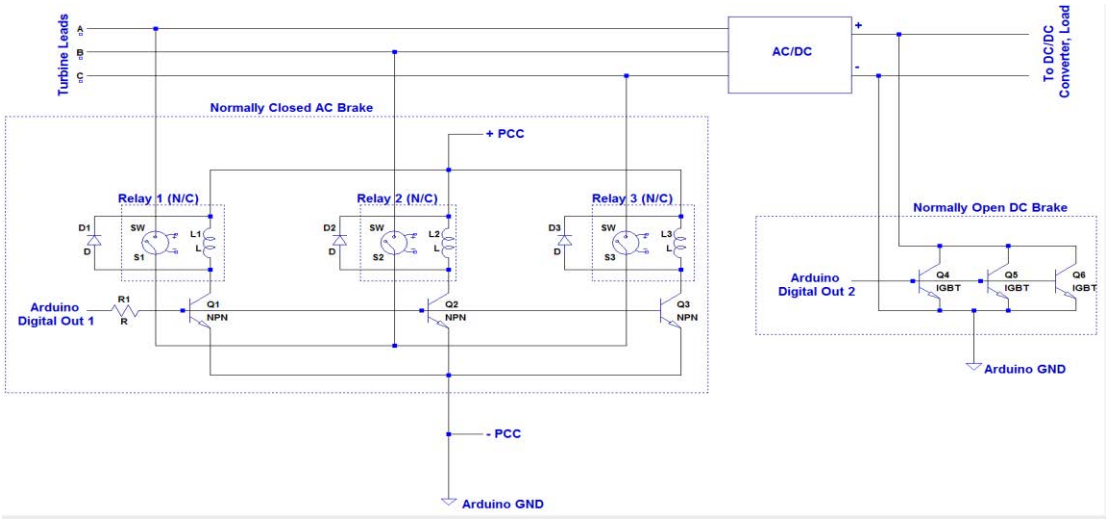


Figure 2-12: Brake Used for Turbine Shutdown

3 Deployment Strategy

Considerations in this section are specifically related to the business plan and the deployment turbine design.

3.1 Identify Site and Dataset

The wind resource is a key consideration since the resource itself drives the turbine's production. Obtaining wind resource data in a region is a crucial step in the site identification and validation process. This allows our company to have a complete understanding of how much electricity the turbine will produce at a specific site. For wind farm development, this data would be as detailed as 5-minute averages of the wind speed collected over the span of 1-3 years. However, finding this data can be difficult, and in many cases it does not exist at all for the site in question. In our case, wind resource maps and publicly available wind measurements will be used. This includes airport wind speed data nearest to the site being considered, as well as other wind resource data sets for the region and data collected at existing telecom towers. Selected sites are analyzed to determine whether or not they possess a wind resource necessary to financially benefit the customer. Sites that have average annual wind speeds ranging from five to fifteen meter per seconds are preferred. Our company engineers will manage a wind data repository and continually refine a wind map of relevant telecom tower sites in India, similar to that seen in **Figure 3-1**. Based on this figure, our turbine could produce at least 1.26 kW regularly in a majority of India (minimum of 100 W/sq. m).

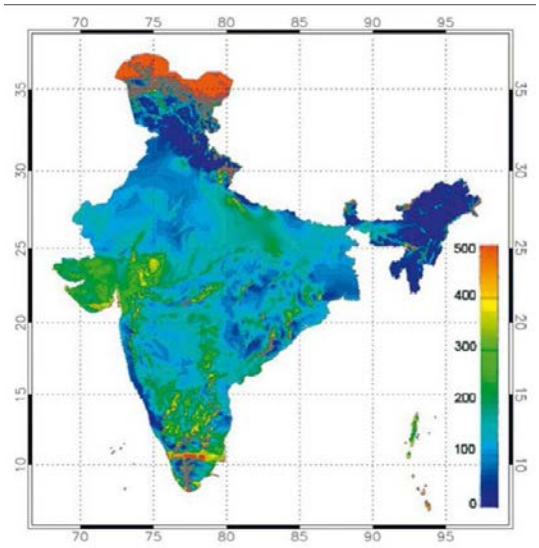


Figure 3-1: India Wind Power Density Map (W/sq. m) [15]

The telecom tower must be able to withstand an additional 4.39 kN horizontal loading force during wind speeds of thirty meters per second at the top of the tower. This is equivalent to 987.31 pounds of force. This translates to larger loads toward the bottom of the tower, strictly dependent on the height of the tower. A FEA evaluation will be done on each tower to determine whether or not it will be able to sustain the additional force. The owner of the tower will provide information such as structural information and any CAD files that will help with the analysis. If the owner does not have these files from the manufacturer of the tower, the tower company will be contacted to obtain the information needed. All this documentation will be saved for future reference for research and development.

3.1.1 Stakeholder Identification and Communication

Determining compatibility with the telecommunication infrastructure is done with an examination of the electrical load and structural stresses of the telecom tower. A typical cell tower's power is determined by the number of base transceiver stations housed. The power needed ranges from 1 kW to 8.5 kW, and more than 80% of these configurations have a demand less than 3.5 kW [7]. To accommodate this range of power, the deployment turbine is designed for these power conditions, as stated in **Section 2.1**. To ensure the selected tower can handle the additional structural stress from the thrust load on the turbine, TES will perform an analysis of the client's tower. This will ensure that the tower can support the turbine and its thrust load at maximum wind speeds.

Indus Towers has the largest market share of the telecom industry in India with 80,000 telecom towers in operation. Targeting Indus is beneficial because of their market saturation in India, making Indus a major stakeholder. Other companies we will target include Bharti Infratel, BSNL, Reliance Infratel, Viom Networks, and of course GTL, as identified in **Section 1.2.5**. Initial contact and sale pitches will be conducted by email, phone, and through visits in person to demonstrate the turbine and its financial rewards. We will also explore opportunities to exhibit through trade shows and to share information about our company through the Indian ministry of telecommunications itself.

Long-term customer communication will occur on an annual basis, as TES will check in with customers to see how turbines are performing. This will be an important aspect of both building customer relations as well as helping TES with research and development for future products. Should a customer request more frequent contact after the initial sale, TES will be happy to oblige. Communication in terms of

maintenance and warranty will occur on a monthly basis with maintenance companies to ensure proper handling and care of the turbine.

Lastly, TES will hold training sessions for turbine maintenance and tower companies on how to properly maintain the turbine on an annual basis or as needed during start-up. How to install the turbine with the provided pulley system, basic troubleshooting, and the maintenance procedures involved with turbine upkeep will be covered in this training.

3.2 Timeline & Lifecycle

In order to spark interest in the product, TES will offer five turbines, free of charge, to several of the tower companies. This will accompany a negotiation with the customer that if the turbines meets their needs, the customer must buy the five turbines following initial testing and an additional 100 within six months.

After making the deal, TES will notify the manufacturer to ship more turbine components to the warehouse to supply the number of turbines the customer ordered. The manufacturers are located in China and the warehouse is located in India, so shipping time is allotted for. Once the parts arrive at the warehouse, they will be assembled into larger components that are ready for installation. Finally, the components will be delivered to the customer, and final assembly will occur at the respective tower. **Figure 3-2** shows the whole process with projected time allotments.

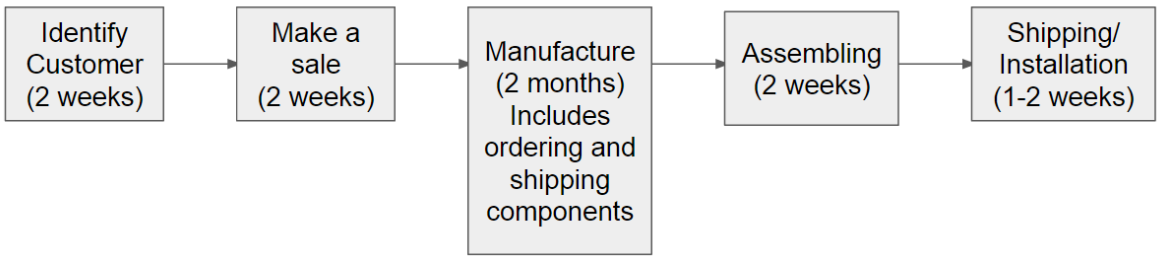


Figure 3-2: Deployment Timeline

It is projected that after installation, with proper maintenance, the turbine will have a lifespan of approximately 20 years. In order to ensure that any manufacturing or assembly defects are taken care of, the turbine will have a limited parts and labor warranty for the first two years of operation. Proper maintenance, as discussed in **Section 3.3**, is described as an annual full service, and monthly inspection.

3.3 Installation and Maintenance

Once the site and tower have been approved for the turbine, it will be shipped from the manufacturing facility to the site with a team of installation experts from our company if the customer asked for installation service. If not, then TES the will ship the parts to the customer for installation.

3.3.1 Installation

The installation team will carry seven items with them to the site, including:

- 3 blades & Hub
- Nacelle
- Tail vane
- Tower mounting adaptor
- Battery
- Electrical control components

The facility will receive the turbine parts from the manufacturer, or the installation team will deliver the parts and install the system on the tower. In both cases, the installation will be performed with a pulley system and a winch, allowing for a very low-cost installation that can be performed by a small team. Four people minimum are required for installing the turbine. One person will operate the winch. Two people will climb the tower and set the pulley system to lift and install the turbine on the tower. The last two people will assemble the turbine on the ground, one of whom can also operate the winch. For safety, installation should not occur during high winds or extreme weather conditions. A safety belt must be worn by the individual who is climbing the tower at all times. Every activity during the installation must be recorded in a logbook and any damages must be reported to TES and the tower company. All workers must be familiar with safety rules before any work can begin. After installation, the team will ensure that the turbine is working properly before leaving the site.

Installation Steps:

- Attach the nacelle to the tower mounting adaptor
- Attach the tail vane to the back of the nacelle
- Attached blades to the hub
- Connect the hub to the generator shaft; insert the shaft key, then attach the nose cone
- Set the turbine in a location where it can be easily picked by the winch, then hoist it into place
- Connect stub tower to telecomm tower
- Connect the system to the battery and other electronics
- Run the turbine and make sure it is working before leaving the location

3.3.2 Maintenance

Our partner companies will be trained in proper maintenance procedures for our turbine, and our engineers will be available to consult as needed on maintenance issues. Full maintenance should be performed annually and after any severe weather conditions. The GTL maintenance team will have the same safety rules as the installation team.

3.3.2.1 Annual Maintenance

It is recommended that technicians who are trained in turbine installation perform a monthly check of all turbine systems, accompanying or taking the place of other tower employees who are visiting the tower to refuel or for other purposes. Annual maintenance is recommended for turbine safety and longevity. It includes inspecting electrical wiring, torqueing all bolts for structural safety, lubricating all bearing, and performing visual inspections on the hub, blades, and the generator to ensure all are functioning properly. It is also recommended that the client inspect each turbine after a severe weather event in the same way the annual maintenance is performed.

3.4 Reliability and risk management

Even with proper maintenance and installation, it is important to recognize that any wind turbine has a set of associated risks. A number of business risks were addressed in **Section 1.4.4**. In this section we examine the electrical, mechanical, financial reliability that mitigate some of these risks.

3.4.1 Electrical Reliability

The generator is the main electrical component, and is a 3 kW permanent magnet generator (PMG) manufactured by Henry D [16]. The PMG is designed to satisfy the load requirements of the tower without much overload, prolonging the system life. The turbine will optimize the working condition of the actuators by adjusting the controller. By doing so, the extreme loads on the actuator can be avoided

and thus the system life span will be increased. The health rate of the motor is used as additional control input to modify the controller properties according to the motor state and thus to extend the motor lifetime.

3.4.2 Mechanical Reliability

The blade design has a factor of safety of 1.04, as discussed in **Section 2.4.1**, which make them able to withstand a direct wind speed up to 25 m/s when spinning, or 60 m/s when not spinning. In addition, turbine also features a tail vane and nacelle with a gravity driven furling design. This causes the turbine to rotate out of the wind at 30 m/s, protecting the blades from extreme wind speeds. When the wind drops below 30 m/s, the tail vane, which furls upward at a compound angle, is forced back into position by its own weight, swinging the turbine back into the wind. Also, in order to protect the tower from any vibration damage, the yaw system design incorporates eight vibration isolators to dampen any potential threats.

3.4.3 Financial Reliability

Since up to 90% of the telecommunication towers in India rely on diesel generators, our turbine will offer reliable electricity at a competitive price. The uninstalled turbine cost is $4,000, while the fuel costs for running the diesel generator alone is $7,000 per year based on the calculations shown in **Section 1.2.7**. The turbine lifetime maintenance costs are minimal, and the turbine installation cost is minimized by using a pulley system instead of a crane or lift.

In conclusion, this turbine makes great financial sense for application on telecommunication towers in India where a wind resource is available. By utilizing the existing tower infrastructure, the initial cost of the turbine is minimized, maximizing the savings seen by the customer.

4 References

[1] H. Joshi, "Indian Tower Industry: The Future is Data," [Online]. Available: https://www2.deloitte.com/content/dam/Deloitte/in/Documents/technology-media-telecommunications/in-tmt-indian-tower-industry-noexp.pdf. [Accessed 1 March 2016].

[2] "Small Wind Turbine Standard," 15 January 2014. [Online]. Available: http://www.renewableuk.com/en/utilities/document-summary.cfm?docid=97D39F8A-0760-45C5-8D9D6B8E7F2302FD. [Accessed 7 March 2016].

[3] M. Bhawan and L. N. Marg, "Annual Report 2013-2014," December 2014. [Online]. Available: http://www.trai.gov.in/WriteReadData/UserFiles/Documents/AnuualReports/TRAI-Annual-Report-(English)=01042015.pdf. [Accessed 27 February 2016].

[4] Greentech Media, "Beyond the Electrical Grid: India's Off-Grid Solar Opportunity," 08 November 2011. [Online]. Available: http://www.greentechmedia.com/articles/read/beyond-grid-electricity-india . [Accessed 29 April 2016].

[5] R. Taylor, Interviewee, *Insight into The Small Wind Industry.* [Interview]. 6 April 2016.

[6] Xzeres, "Telecom," [Online]. Available: http://www.windenergy.com/markets/telecommunication. [Accessed 27 February 2016].

[7] Intelligent Energy, "The True Cost of Providing Energy to Telecom Towers in India," January 2012. [Online]. Available: : http://www.gsma.com/membership/wp-content/uploads/2013/01/true-cost-providing-energy-telecom-towers-india.pdf. [Accessed December 2015].

[8] National Renewable Energy Labratory, "Distributed Generation Renewable Energy Estimate of Costs," February 2016. [Online]. Available: http://www.nrel.gov/analysis/tech_lcoe_re_cost_est.html. [Accessed 30 March 2016].

[9] D. Diment, "Competitive Landscape," July 2015. [Online]. Available: http://clients1.ibisworld.com/reports/us/industry/competitivelandscape.aspx?entid=1913#MSC. [Accessed 14 May 2016].

[10] S. Apoorv, "Foreign Exchange Risk Management in India," FICCI Blog, 1 February 2013. [Online]. [Accessed 24 April 2016].

[11] Ernst & Young LLP, "Doing Business in India," November 2013. [Online]. Available: http://www.ey.com/Publication/vwLUAssets/India_-_Doing_Business/$FILE/Doing%20Business%20in%20India.pdf. [Accessed 26 April 2016].

[12] U.S. Department of Energy, "CWC Rules and Regulations," 8 February 2016. [Online]. Available: http://energy.gov/sites/prod/files/2016/02/f29/CWC%20Rules%20and%20Regulations%20Manual_Rev3_160203.pdf. [Accessed 30 April 2016].

[13] *MATLAB and Statistics Toolbox Release 2015b,* Natick, MA: The MathWorks Inc. .

[14] J. Manwell, J. McGowan and A. L. Rogers, Wind Energy Explained: Theory, Design, and Application, Wiley, 2009.

[15] *SolidWorks 2015-2016,* Dassault Systemes.

[16] India Wind Turbine Manufacturers Association, "Wind Resource Map," [Online]. Available: http://www.indianwindpower.com/news_views.php#tab3. [Accessed 26 April 2016].

[17] "alibaba.com," Qingdao HenryD Wind Power Equipment Co. Ltd, [Online]. Available: http://hldwtg.en.alibaba.com. [Accessed 25 February 2016].

Appendix A - Business Financials

Cash Flow Year 1

	Quarter 1	Quarter 2	Quarter 3	Quarter 4
Sales	$0	$0	$220,000	$200,000
Total Collections	$0	$0	$220,000	$200,000
Cash Disbursements				
Purchases	$73,708	$0	$67,007	$67,007
Assembly Wages	$642	$2,087	$3,478	$3,478
Assembly Machinery	$500	$50	$50	$50
Cost to Start Up in India	$500	$0	$0	$0
Shipping	$500	$0	$500	$500
Import Cost (to India)	$1,462	$0	$1,462	$1,462
Sales Representatives	$0	$0	$11,000	$12,000
Salaries	$45,000	$45,000	$45,000	$45,000
Building Rent	$5,409	$5,409	$5,409	$5,409
Utilities	$1,200	$1,200	$1,200	$1,200
System analysis and software testing	$0	$500	$500	$500
Solidworks Subscription	$2,746	$2,746	$2,746	$2,746
Total Disbursements	$131,667	$56,992	$138,352	$139,352
Beginning Cash Balance	$0	-$131,667	-$188,658	-$107,010
Add: Inflows	$0	$0	$220,000	$200,000
Subtract: Outflows	-$131,667	-$56,992	-$138,352	-$139,352
Ending Cash Balance	-$131,667	-$188,658	-$107,010	-$46,361

Cash Flow Years 2-5

	Year 2	Year 3	Year 4	Year 5
Sales	$800,000	$1,000,000	$1,200,000	$1,400,000
Total Collections	$800,000	$1,000,000	$1,200,000	$1,400,000
Cash Disbursements				
Purchases	$285,450	$351,080	$419,464	$485,131
Assembly Wages	$13,910	$15,997	$27,820	$27,820
Assembly Machinery	$200	$200	$200	$200
Shipping	$4,500	$4,500	$4,500	$4,500
Import Cost (to India)	$8,772	$8,772	$8,772	$8,772
Sales Representatives	$72,000	$72,000	$72,000	$72,000
Salaries	$180,000	$180,000	$180,000	$180,000
Building Rent	$21,636	$21,636	$21,636	$21,636
Utilities	$4,800	$4,800	$4,800	$4,800
System analysis and software testing	$2,000	$2,000	$2,000	$2,000
Solidworks Software	$10,980	$10,980	$10,980	$10,980
Total Disbursements	$604,248	$671,965	$752,172	$817,839
Beginning Cash Balance	-$46,361	$149,391	$477,426	$925,255
Add: Inflows	$800,000	$1,000,000	$1,200,000	$1,400,000
Subtract: Outflows	-$604,248	-$671,965	-$752,172	-$817,839
Ending Cash Balance	$149,391	$477,426	$925,255	$1,507,416

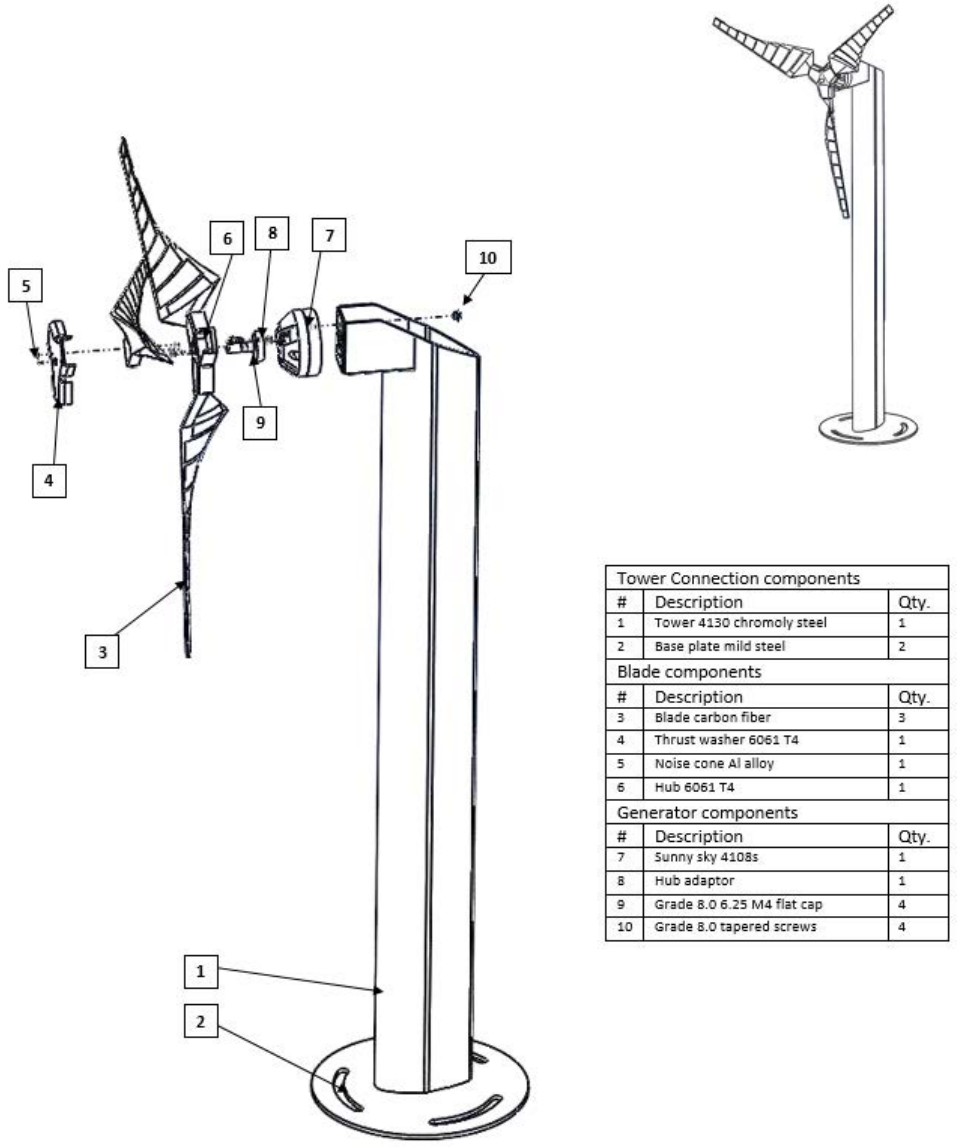
Income Statement Year 1- 5

	Forecast Period				
	Year 1	Year 2	Year 3	Year 4	Year 5
Sales	$420,000	$800,000	$1,000,000	$1,200,000	$1,400,000
Cost of Goods Sold	$140,715	$268,028	$335,035	$402,042	$469,049
Gross Profit	**$279,285**	**$531,972**	**$664,965**	**$797,958**	**$930,951**
Operating Expenses					
Assembly Wages	$9,684	$13,910	$15,997	$27,820	$27,820
Assembly Machinery	$650	$200	$200	$200	$200
Cost to Start Up in India	$500	$0	$0	$0	$0
Shipping	$1,500	$4,500	$4,500	$4,500	$4,500
Import Cost (to India)	$4,386	$8,772	$8,772	$8,772	$8,772
Sales Representatives	$23,000	$72,000	$72,000	$72,000	$72,000
Salaries	$180,000	$180,000	$180,000	$180,000	$180,000
Building Rent	$21,636	$21,636	$21,636	$21,636	$21,636
Utilities	$4,800	$4,800	$4,800	$4,800	$4,800
System analysis and software testing	$1,500	$2,000	$2,000	$2,000	$2,000
Solidworks Software	$10,984	$10,980	$10,980	$10,980	$10,980
Total Expenses	$258,640	$318,798	$320,885	$332,708	$332,708
Net Income Before Taxes	**$20,646**	**$213,174**	**$344,081**	**$465,250**	**$598,243**
Tax Expense (33%)	$6,813	$70,347	$113,547	$153,533	$197,420
Income after Tax Expense	$13,833	$142,827	$230,534	$311,718	$400,823

Balance Sheet

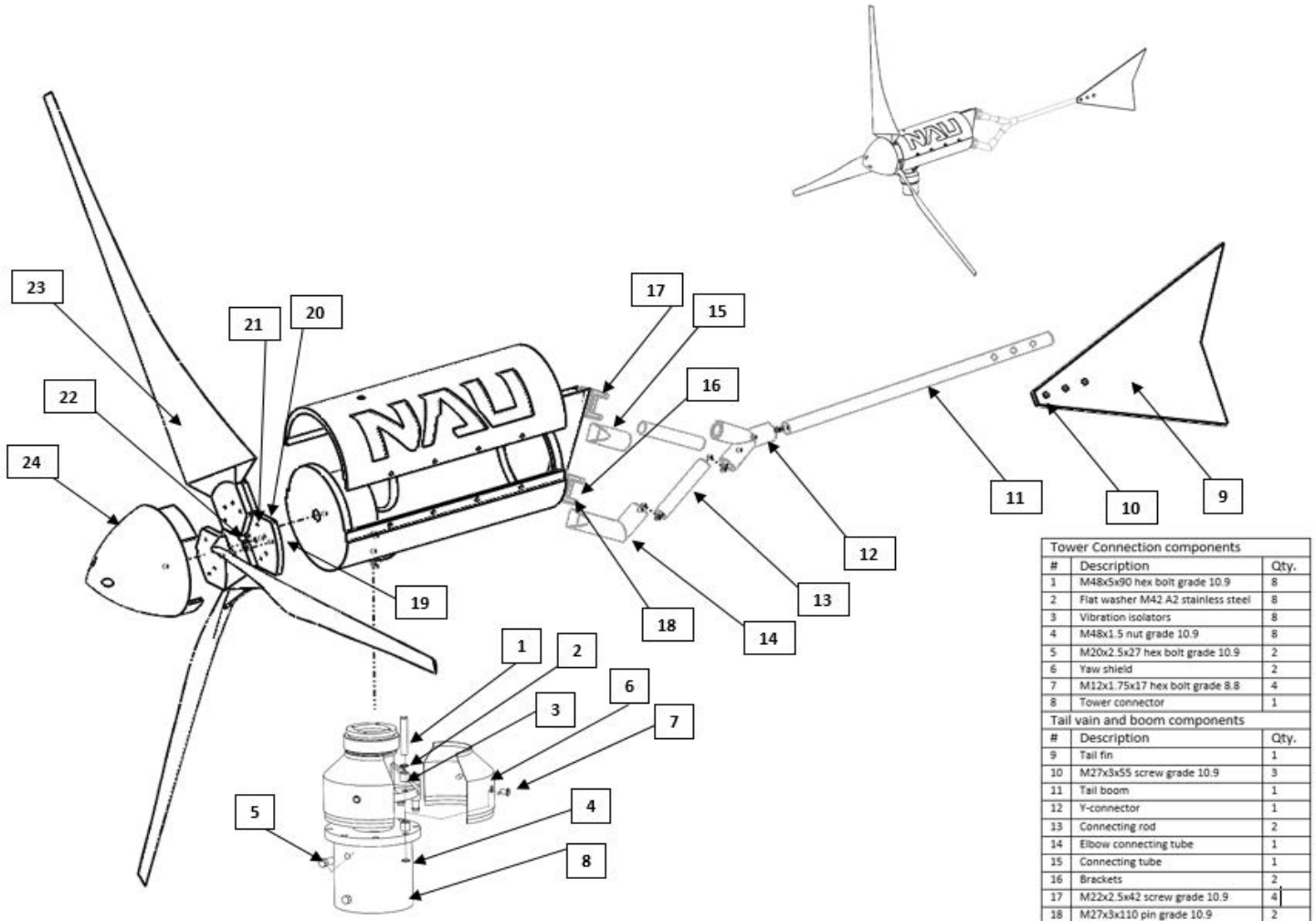
Pro Forma Balance Sheet	
Assets	Year 1
Cash	-$46,361
Inventory	$207,722
Total current assets	$161,361
Equipment	$650
Net Fixed Assets	$650
Total Assets	**$162,011**
Liabilities	$0
Total current liabilities	$0
External Funds Needed	$162,011
Total Liabilities	**$162,011**

Appendix B – Engineering Diagrams



Tower Connection components		
#	Description	Qty.
1	Tower 4130 chromoly steel	1
2	Base plate mild steel	2
Blade components		
#	Description	Qty.
3	Blade carbon fiber	3
4	Thrust washer 6061 T4	1
5	Noise cone Al alloy	1
6	Hub 6061 T4	1
Generator components		
#	Description	Qty.
7	Sunny sky 4108s	1
8	Hub adaptor	1
9	Grade 8.0 6.25 M4 flat cap	4
10	Grade 8.0 tapered screws	4

Figure B1: Exploded view - Tunnel Turbine



Tower Connection components		
#	Description	Qty.
1	M48x5x90 hex bolt grade 10.9	8
2	Flat washer M42 A2 stainless steel	8
3	Vibration isolators	8
4	M48x1.5 nut grade 10.9	8
5	M20x2.5x27 hex bolt grade 10.9	2
6	Yaw shield	2
7	M12x1.75x17 hex bolt grade 8.8	4
8	Tower connector	1
Tail vain and boom components		
#	Description	Qty.
9	Tail fin	1
10	M27x3x55 screw grade 10.9	3
11	Tail boom	1
12	Y-connector	1
13	Connecting rod	2
14	Elbow connecting tube	1
15	Connecting tube	1
16	Brackets	2
17	M22x2.5x42 screw grade 10.9	4
18	M27x3x110 pin grade 10.9	2
Blade components		
#	Description	Qty.
19	M12x1.75x56 screw grade 10.9	12
20	M20x2.50x72 screw grade 10.9	3
21	Hub plate	1
22	M16x2 nut grade 10.9	1
23	Blade	3
24	Noise cone	1

Figure B2: Exploded view – Deployment Turbine

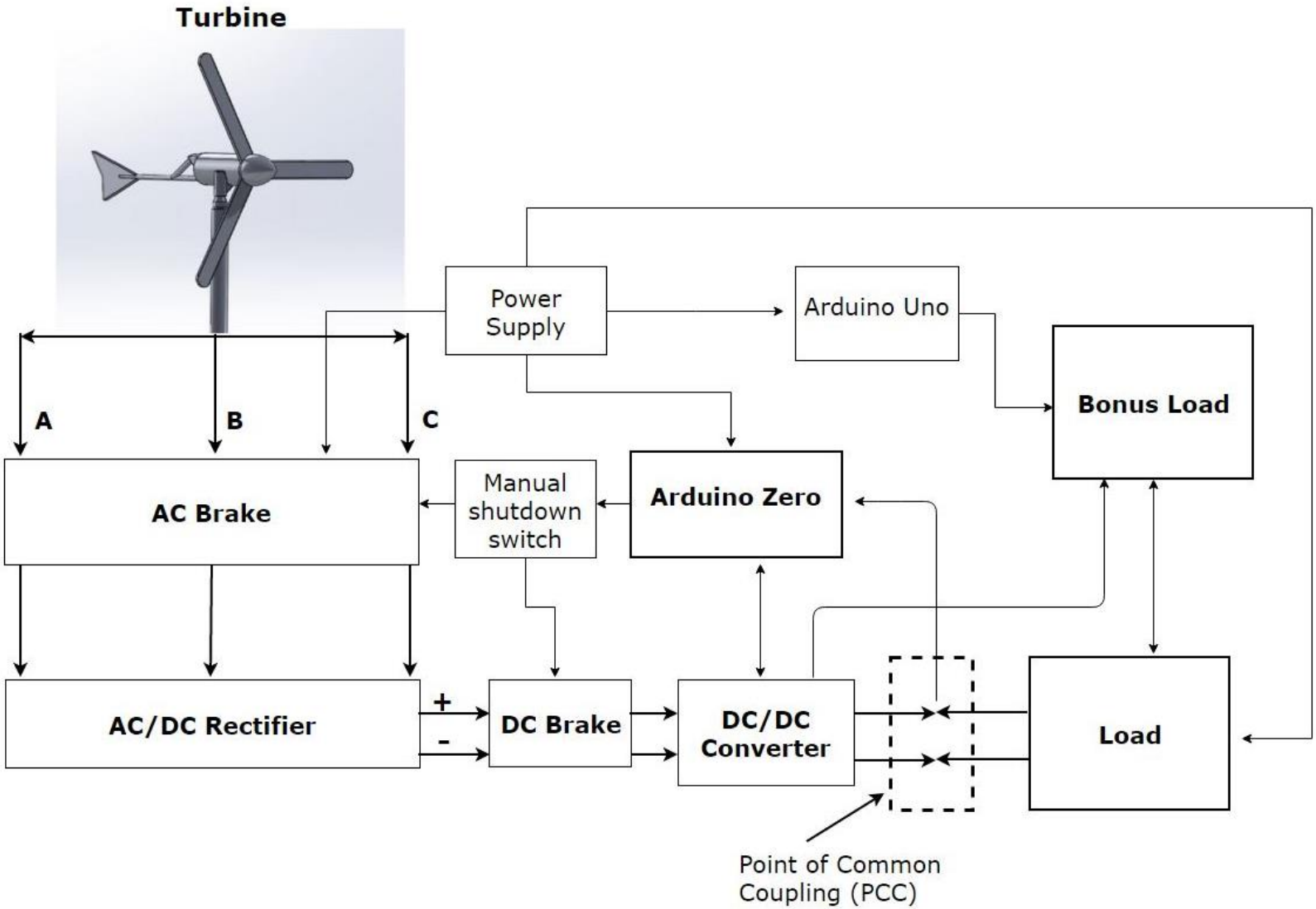


Figure B3: Electrical One line diagram

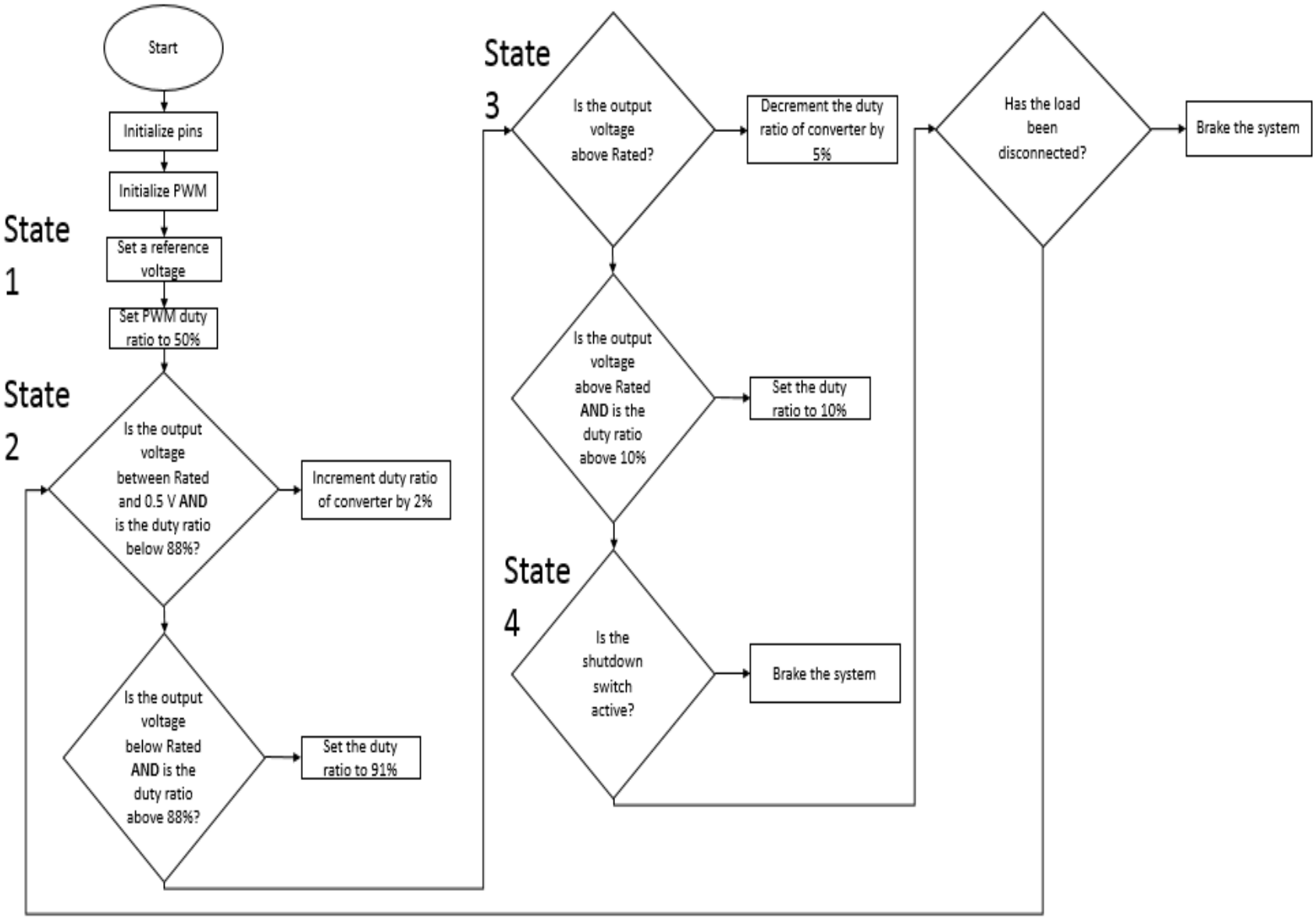


Figure B4: Control State Flow Chart

Northern Arizona University

Wind Turbine Technical Report
Submitted to: US Department of Energy
April 5, 2017



Collegiate Wind Competition Team

Mechanical Engineering Team:

Melissa Hoover (Project Manager)
Jesus Bravo (Blade Design)
Joshua Danny (Brake Design)
Chase Donnell (Tower Design)
Brent McFarlane (Budget Liaison)
Rafeal Vera Jr. (Design & Manufacturing Lead)

Electrical Engineering Team:

Mary Koehler (Project Manager)
Jialin Min (Client Liaison)
Victor Rinaldi (Development Manager)
Yakun Qie (Resource Investigator)

Faculty Mentors:

David Willy (Co-PI and Mechanical Technical Advisor)
Karin Wadsack (Principle Investigator)
Venkata Yaramasu (Electrical Technical Advisor)

Table of Contents

1 Executive Summary 1
2 Technical Design 2
2.1 Design Objective 2
2.2 Static Performance and Aerodynamics Analysis 3
2.3 Mechanical Loads 4
2.3.1 Rotor Dynamics 4
2.3.2 Blade Analysis 5
2.3.3 Main Shaft Analysis 5
2.3.4 Mechanical Brake Dynamics 6
2.3.5 Mainframe 7
2.3.6 Tower 7
2.3.7 Results and Factor of Safety Summary 8
2.4 Design for Varying Wind Direction 9
2.4.1 Bearing Selection 9
2.4.2 Tail Vane Design Analysis 9
2.4.3 Tail Vane Dimensions 9
2.4.4 Force Analysis 9
2.4.5 Yaw System Design Conclusion 10
2.5 Electrical Design 11
2.6 Electrical Analysis 11
2.7 Controls Analysis and Software Documentation 12
2.8 Testing 15
2.8.1 Testing Results 15
2.8.2 Testing Plans 15
3 References 16
4 Appendix A: Exploded View-Mainframe Tower, Tail, and Yaw System 17
5 Appendix B: Exploded View-Hub, Brakes, Drivetrain 18
6 Appendix C: Shaft Analysis MATLAB Program, DE-Gerber Failure Criteria 19
7 Appendix D: Equations 20
8 Appendix E: Assumptions and Material Properties 21

List of Tables

Table 1: Blade Design Elements 3
Table 2: Rotor Dynamics Calculated Values 5
Table 3: Drivetrain Factors of Safety 8
Table 4: Expected Loads and F.O.S. 9
Table 6: Wind Moment Results 10

List of Figures

Figure 1: 2017 Tunnel Turbine Designs: A) 2016 B) 2017 2
Figure 2: Power Output vs Wind Speed 4
Figure 3: Cp vs Tip Speed Ratio 4
Figure 4: Blade FEA Results: A) Deformation B) Stress 5
Figure 5: Main-Shaft Dimensions (mm) 6
Figure 6: Drivetrain Configuration 6
Figure 7: SOLIDWORKS FEA: A) Stress Distribution B) Deflection Analysis 7
Figure 8: Supporting Tower: A) Stress Distribution B) Deflection Analysis 8
Figure 9: Yaw System Design 10
Figure 10: Power Converter Topology 12
Figure 11: Boost Converter Topology 12
Figure 12: High Level block diagram for ABC/αß control 13
Figure 13: Electrical One-Line Diagram 14
Figure 14: Control State Flow Chart 14
Figure 15: Mechanical Braking System 15

1 Executive Summary

Team NAU has accepted the challenge to design a small-scale wind turbine to compete in the US Department of Energy Collegiate Wind Competition (CWC). This year, the team iterated upon Team NAU's 2016 design, with a focus on components including high performance blades, an originally designed DC-DC Boost Converter, and both yawing and braking systems. Analysis software, tools, and design processes from the previous year were utilized; however, the final product was used as a benchmark to improve upon.

The design constraints were derived from the competition rules and include size, power, and safety requirements. Some of the requirements exclusive to this year's competition include yaw rates up to 180 degrees per second, braking on command and when disconnected from the load, and cut-in speed between 2.5 and 5 m/s. These became the starting point for Team NAU's CWC17 turbine design and the emphasis for the redesign of the previous system. After the focus was identified, the team began analysis on individual subsystems to complete these tasks. The electrical team began research into boost converter designs by simulating power converters, power transformations and various boost converter designs. The team then designed a test bench, which included a purchased vertical Permanent Magnet Synchronous Generator (PMSG) wind turbine, diode bridge rectifier, off-the-shelf DC-DC Boost Converter and load to test components and boost converter designs. The mechanical team iterated over the requirements and began their comprehensive design. The first component designed was the blades. The blade performance was evaluated using Q-Blade, in which airfoils, twist, and chord length could be manipulated and simulations could be run to find the approximate cut-in speed and power output using the blade design. The next subcomponent was the mechanical braking system. The goal of the brake design is to reduce the rotor RPMs to less than 10% of full performance at that wind speed, and if possible, to zero RPMs with the capability of rapid start up. Team NAU chose a brake design that utilizes a carbon fiber disc brake with aluminum calipers controlled by a solenoid linear actuator. The final subcomponent designed was the yawing system for varying wind direction. The team decided to equip the turbine with a two-bearing and tail vane yawing system. The tail vane utilizes the normal force provided by the wind to orient itself parallel to wind flow, and the bearings located within the tower allow the mainframe to rotate about its axis.

The following report gives further explanation and documentation of Team NAU's design for the 2017 Collegiate Wind Competition. Analyses included are static performance and aerodynamics, mechanical load and safety factors, design for varying wind direction, electrical design and simulation, controls and software, and field-testing. Special acknowledgements to ***W.L. Gore and Associates*** for their financial donating as well as Michael and Justin Clifton at ***ARE Telecom and Wind*** for providing testing facilities.

2 Technical Design

2.1 Design Objective

The design objective for Team NAU for the 2017 Collegiate Wind Competition (CWC) was to iterate upon Team NAU's design for the 2016 competition. Last year's design included carbon fiber blades and a simply designed drive system with no yaw system. Additional competition tasks were added for this year's competition, which include safety tasks that require the turbine to stop on command and when disconnected from the load as well as durability tasks that require the turbine to remain oriented in the direction of yawed wind flow. These competition tasks defined the technical design requirements for the iterated turbine design. A few of the major requirements include: high power output, low cut-in speed, durability, safety, yawing, braking, minimal deployment time, and compact size. Team NAU's 2016 tunnel turbine design can be compared to the iterated 2017 tunnel turbine design in **Figure 1**. Full Exploded views of Team NAU's 2017 design can be found in Appendices A and B. The full list of technical design constraints for this year's design is listed below:

- Maximum wind speed of 18 m/s
- Yaw rates up to 180°/s
- Generate 10W between 5 to 11 m/s
- Supply a Load System
- Rotor dimensions less than 45 cm^3
- Non-rotor turbine parts fit within 15 cm diameter cylinder
- Rotor center within 2.54 cm of tunnel centerline
- Mountable within wind tunnel
- Base plate no thicker than ½ inch
- Turbine fits through the turbine door
- Maximum output voltage 48VDC at PCC
- No batteries
- Wiring and connectors for PCC and kill-switch
- Zero energy at the start of the test
- Bulk energy storage is safe
- Power fluctuation ± 10% for any 5s interval
- Cut-in speed less than 5 m/s



A **B**

***Figure 1**: 2017 Tunnel Turbine Designs: **A**) 2016 **B**) 2017*

2.2 Static Performance and Aerodynamics Analysis

Blades were designed to have low cut-in speed, to have high power output, and to be structurally sound based on a four-blade rotor. Blade shape was originally designed using Blade Element Momentum theory (BEM) and MATLAB. BEM requires inputs of Reynolds numbers, blade length, number of blade elements, tip speed ratio, and wind speed.

The Reynolds numbers for the blades were relatively low compared to those for industrial blades, so thin airfoils with high camber were chosen. Reynolds numbers for cut-in and rated speeds were 4,000-17,000 and 8,000-33,000 respectively. NACA airfoils were created to fit the requirements on thin airfoils with high cambers, and the airfoils tested were NACA 4402, 4605, 6715, 4404, 3408, 9422, 9620, also S1223 and Miley M06-13-128. These airfoils allow for lower cut-in speeds and higher power outputs for the small-scale blades. Analyses were ran for each airfoil using the blade analysis program Q-Blade, for the different Reynolds numbers along the chord length of the blade element. The resulting lift and drag ratios associated with different angles of attack were evaluated to select the airfoils with the ideal angles of attack. The final selected airfoils were NACA 4404, NACA 4605, and NACA 3408. Thinner airfoils were selected at first, but after 3D printing prototype blades it was apparent that the airfoils needed to be thicker to be more structurally sound. After airfoils selection, blade analysis was conducted on Q-Blade.

Blade chord length, twist, and airfoils were used in the blade analysis in Q-Blade; chord lengths and twists were gathered from the BEM calculations. 77 iterations were performed in Q-Blade that adjusted chord length, twist, and placement of the selected airfoils until a blade was created that met cut in and power requirements. The final blade properties are listed in **Table 1**. Although the team is concentrating efforts into the four-blade system, the team has also designed a simple three-blade rotor using only the NACA 4402 airfoil throughout the blade for contingency; however, the primary analysis focuses on a four-blade rotor design.

***Table 1**: Blade Design Elements*

Current Blade Design			
Blade Position (mm)	**Chord (mm)**	**Twist (degrees)**	**Airfoils**
0	90	55	NACA 4404
19	76	47	NACA 4404
38	62	43	NACA 4404
57	55	37	NACA 4404
76	42	25	NACA 4605
86	37	17	NACA 4605
95	32	10	NACA 4605
114	29	6	NACA 3408
133	25	4	NACA 3408
144	24	2	NACA 3408
152	23	0	NACA 3408
170	20	-4	NACA 3408

Q-Blade analysis shows that the turbine will produce 17 watts of power at a wind speed of 10 m/s and a maximum power output of around 125 watts for higher wind speeds. However, this does not reflect actual power generation as the electronic and the mechanical losses are not accounted for in Q-Blade analysis. Cut-in speed is estimated at 3 m/s by comparing the output torque of the blades and the cogging torque of the generator. Figure 2 shows power output vs wind speed and Figure 3 shows coefficient of

performance vs tip speed ratio. Coefficient of power helps display how much of the available wind power the turbine is extracting, showing that the blades are working efficiently.

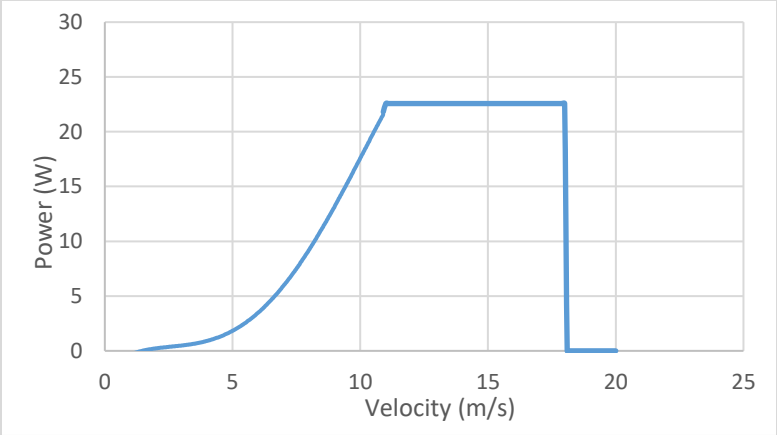


***Figure 2**: Power Output vs Wind Speed*

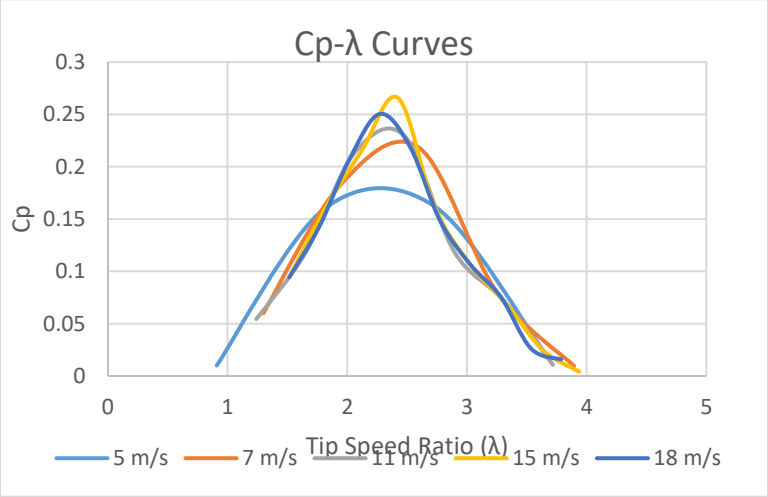


***Figure 3**: Cp vs Tip Speed Ratio*

2.3 Mechanical Loads

The effect of wind loads imposed on critical components such as the blades, main shaft, braking surfaces, support tower, and mainframe were analyzed for failure due to stress. A combination of SOLIDWORKS finite element analysis (FEA) and manual analysis were employed to refine each component for durability.

2.3.1 Rotor Dynamics

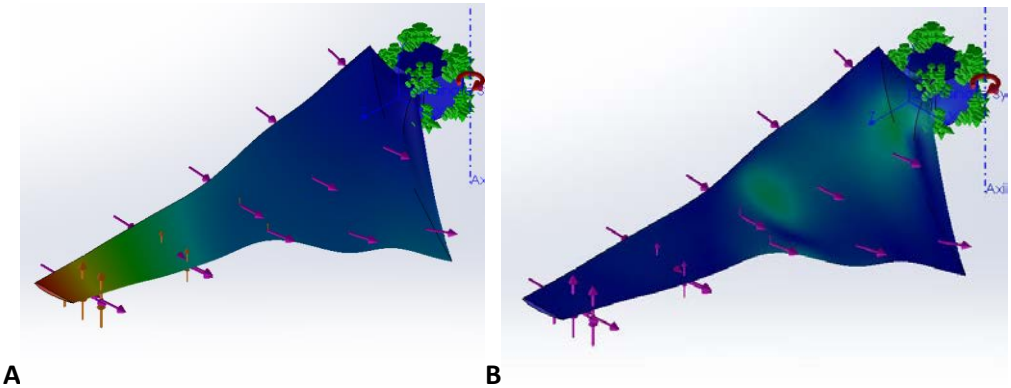
The blade rotor design consists of two separate configurations: three-blade and four-blade rotors. The rotors have similar designs and consist of a thrust washer and a hub which is mounted onto the main-shaft. The resultant rotor force from the four-blade rotor, F_R, generated by the centrifugal forces was used to estimate reactions for the drivetrain assembly. Centrifugal forces were also incorporated into the blade stress analysis. Direct thrust forces were incorporated into blade, mainframe, and supporting tower analyses but were assumed negligible on other non-rotor components due to compressive loading. Rotor torque was calculated for an ideal rotor using a conservative Coefficient of Performance of 0.500 and the Tip Speed Ratio of four. The resulting values for these analyses are listed in **Table 2**.

***Table 2**: Rotor Dynamics Calculated Values*

Property	**Calculated Value**
Actual Total Hub Mass	m_{HB} = *0.180 kg*
Analysis Total Hub Mass	m_{HB} = *0.305 kg*
Wind Speed	v_w= *18 m/s*
Estimated Maximum RPM	*n =6000 RPM's*
Estimated Maximum Torque	*Q = 0.200 N-m*
Thrust Force	F_T = *20 N*
Resultant Rotor Force	F_{Ry} = *3 N*

2.3.2 Blade Analysis

Blades were analyzed for yielding and deformation. The blades are manufactured using VEROCLEAR 3D printing filament that has an approximate yield stress of 50 MPa. Due to material flexibility, SOLIDWORKS FEA was used to determine stress factors of safety and deflections. The results of these analyses are shown in Figure 4. Forces considered include: centrifugal force, braking torque, and thrust force due to wind. Each blade was analyzed at a rotational speed of 6000 RPM with a torque of 0.250 Nm and a total thrust force of 20 N acting as a distributed load throughout each blade with majority of thrust applied at the blade tips. Four blade iterations were made to increase the factor of safety, clearance between mainframe components, and printing quality. The final blade design employs a thick blade root that decreases localized stress and deflections. The final blade design has a factor of safety of 1.35 and a maximum deflection of 6mm.



A **B**

***Figure 4**: Blade FEA Results: **A**) Deformation **B**) Stress*

2.3.3 Main Shaft Analysis

The resultant rotor force, F_R, was used to estimate reactions. The main shaft was modeled as a simply supported shaft with reaction forces at the rotor, bearing, and brake. The resulting reactions were 3N at the rotor, 5N at the main bearing, and 2N at the generator.

Since the reaction at the generator location was small, the bearing load at the generator was modeled at the end of the main-shaft assembly. The resulting torque was amplified by a compensation factor of two that accounts for rotational inertia. A shaft with initial estimated dimensions was iterated based on fatigue and static loading calculations using the DE-Gerber Failure Criteria shown in Appendix C. A MATLAB program was used to quickly calculate the shaft factors of safety for fatigue and static yielding, n_f and n_y. The material for the driveshaft is 7075-T651 Aluminum. Critical locations were identified where large stress concentrators were present. The main-shaft dimensions for the final iteration with final reactions are shown in Figure 5.

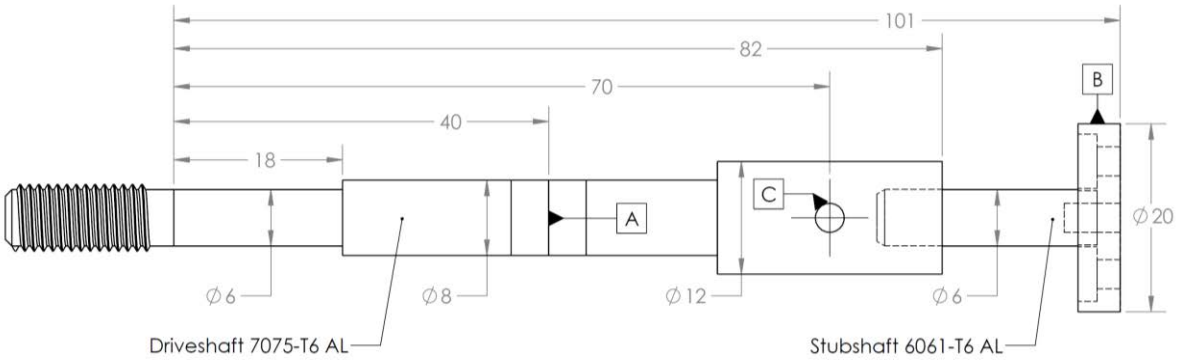


***Figure 5**: Main-Shaft Dimensions (mm)*

The bearing supporting the main-shaft at A has a maximum dynamic load rating of 2550N, is flange mounted and is self-aligning to +/- 5 degrees to account for shaft misalignment during assembly. The maximum dynamic load for each of the two bearings inside the SunnySky x4108s-380kV generator is 714N.

To facilitate manufacturing and to have a high level of concentricity, the final main-shaft design incorporates a two-piece assembly consisting of a stub shaft and driveshaft. The stub shaft is made of 6061-T6 Anodized Aluminum and is threaded into the driveshaft. Torque is transferred between the driveshaft and stub shaft through a jam nut. The flange on the stub shaft is attached to the generator with screws using the generator's factory mounting recommendations. A through hole at location C transfers torque from the driveshaft to the brake hub via steel torque screw. The final dimensions and factors of safety of the main-shaft assembly satisfy the goal of providing a lightweight, strong, and easy to assemble means of torque transfer.

2.3.4 Mechanical Brake Dynamics

The driving constraint for the driveshaft was to incorporate a powerful and reliable mechanical braking system. Other design constraints included: mass, failsafe capabilities, generator magnetism, and size. A carbon fiber brake disk with aluminum friction brake pads was selected to satisfy these constraints. The material combination decreases the rotational mass of the driveshaft, allows for large braking pressures, eliminates ferrous brake debris, and reduces the brake system size. Material properties are listed in Appendix E. Torque is transferred from the main-shaft to a 6061-T6 Aluminum brake hub through a torque screw. Torque is transferred from the brake hub to the brake disk through a hexagonal interface. The layout of the brake and drivetrain configuration is shown in **Figure 6**.

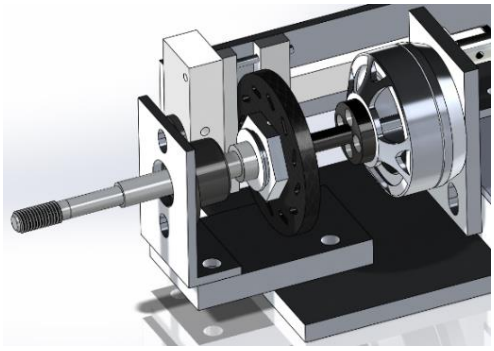


***Figure 6**: Drivetrain Configuration*

Using the equations found in Appendix D, brake force was estimated to be 55 N. However, the force is applied gradually using a spring to prevent shock to the blades. Brake force is adjusted by substituting

different springs with an actual applied force between 20 to 30 N. The maximum interface pressure between the brake disk and pads is 0.1837 MPa. To increase braking capacity and add modulation for RPM control, the dynamic brake from the previous turbine system is used in conjunction with the mechanical brake system to achieve satisfactory requirements.

2.3.5 Mainframe

The mainframe was designed to provide a rigid mounting platform for critical components to facilitate assembly. The mainframe consists of a 6061-T6 aluminum base plate and a 6061-T6 aluminum bearing flange that are welded together. A static SOLIDWORKS FEA analysis was performed with a distributed thrust load of 20N on each component face that is normal to wind direction. Results for stress distribution and deflection are shown in **Figure 7**. The resulting maximum stress was 9.16 MPa and the maximum deflection was 0.097 mm.

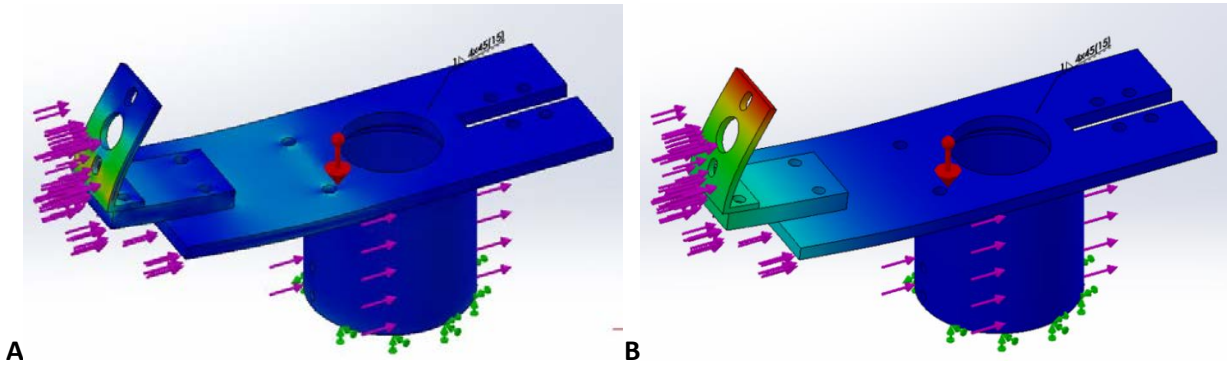


***Figure 7**: SOLIDWORKS FEA: **A**) Stress Distribution **B**) Deflection Analysis*

All mechanical turbine components are bolted onto mainframe. Interfaces between the mainframe and directly attached components compress thin rubber gaskets to reduce vibrations. Components mounted on the mainframe are aluminum to achieve an ideal weight distribution for yawing, with a center of gravity located above the center of rotation.

Yaw bearings are mounted inside the bearing flange with a near clearance fit for ease of assembly. The inner race of the bearings are mounted to the top of the supporting tower with an intermediate fit.

2.3.6 Tower

The tower must withstand the combined mechanical and thrust loads form the turbine components. The tower shaft was machined from A513 thick-walled mild steel tubing. The robust design accounted for freedom for machining steps for bearing mounting during the design phase. The tower shaft was welded to a A513 mild steel base plate. Thrust forces and gravitational loads were used to analyze stress at the weld and deformation at the upper section. Since the weld is much stronger than the material itself, the yield strength of A513 mild steel is used to calculate a conservative factor of safety. The stress distribution and deflections of the tower are shown in Figure 8. The maximum stress at the weld is 6.50 MPa and the maximum deflection of the tower is 0.075 mm.

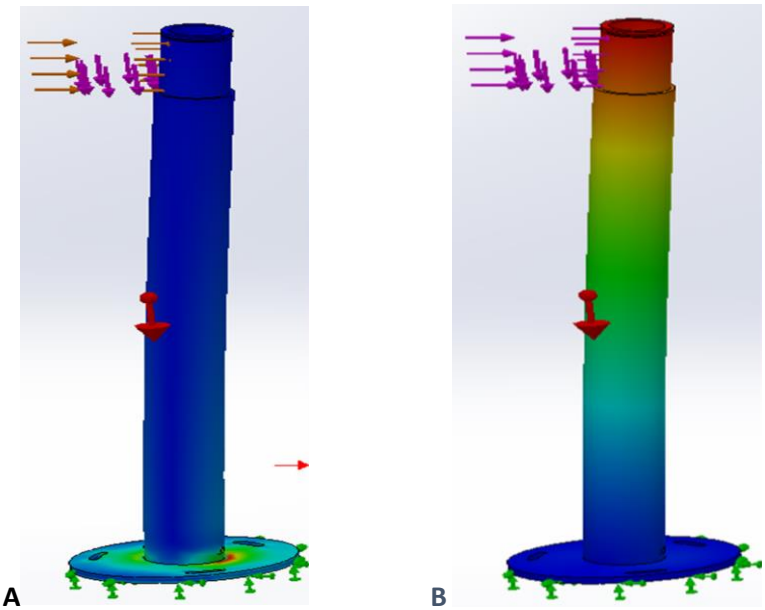


***Figure 8**: Supporting Tower: **A**) Stress Distribution **B**) Deflection Analysis*

2.3.7 Results and Factor of Safety Summary

Essential turbine components were analyzed for excessive stress and deformation to ensure the durability of the turbine. The resulting factors of safety (F.O.S.) for fatigue, static, and bearing dynamic loads for critical displacements along the drivetrain shaft as well as the alternating bending moments ($\mathrm{M_a}$) and mean torque ($\mathrm{T_m}$) at each of these locations are listed in Table 3 with reference to the main-shaft in Figure 5 with the datum at the left end of the main-shaft. The expected loads and factors of safety for crucial components are listed in Table 4.

***Table 3**: Drivetrain Factors of Safety*

Displacement	**18 mm**	**40 mm**	**70 mm**	**80 mm**
Dynamic Loads	M_a= 54.0 N-mm T_m = 375 N-mm	M_a= 120 N-mm T_m = 375 N-mm	M_a= 62.0 N-mm T_m = 375 N-mm	M_a= 38.0 N-mm T_m T_m= 375 N-mm
Fatigue F.O.S., n_f	n_f = 24.91	n_f = 46.05	n_f = 96.79	n_f = 13.44
Static F.O.S., n_y	n_y = 27.45	n_y = 61.66	n_y = 102.05	n_y = 13.39
Bearing Dynamic F.O.S.		n_A = 510		n_B = 714

***Table 4**: Expected Loads and F.O.S.*

Component	Material	Minimum FOS	Expected Loads	Load Description
Blades	VEROCLEAR 3D Filament	1.35	F_T = 20 N ω = 628 rad/s	Thrust Force, Centrifugal Force Brake Torque
Main-Shaft	7075-T6 and 6061-T6 Aluminum	13.39	R_{Ay} = 5 N M_a= 120 N-mm T_m = 375 N-mm	Max Reaction Force, Bending Moment, Mean Torque
Brake Assembly	6061-T6 Aluminum and Carbon Fiber Composite	13.60	F_B = 55N T_B = 375 N-mm p_{max} = 0.183 MPa	Braking Force, Braking Torque, Max Interface Pressure
Mainframe	6061-T6 Aluminum	30.00	$F_{T,D}$ = 20 N	Distributed Thrust Force
Tower	A513 Mild Steel	85.67	$F_{T,D}$ = 20 N F_M = 20 N	Distributed Thrust, Gravitational Load

2.4 Design for Varying Wind Direction

The turbine utilizes a passive yaw design to reduce the complexity of the system. This section covers aspects of the yaw design including bearing selection and loading as well as tail vane dimensioning and force analysis. Once these key factors were determined, they were evaluated to design an effective yawing system.

2.4.1 Bearing Selection

Bearing selection was dependent on the axial load due to the mass of the components that the bearings support. The mass of the upper turbine assembly was calculated by combining the mass of every component that is mounted to the mainframe. The total supported mass (hardware estimations included) is approximately 2 kilograms with a resultant force of 20N. From the selected bearing specification sheet, each bearing can withstand a static loading of 10.8 kN [8] and an axial load of one-fourth of the static loading value [9]. The maximum axial loading of each bearing becomes 2.7 kN. At this rating each yaw bearings has a factor of safety greater than two hundred.

2.4.2 Tail Vane Design Analysis

A main component for the passive yaw system is the tail vane that utilizes wind force to rotate the turbine about its axis until it is parallel with the wind. The analysis in this section determines the optimal tail vane design for successful tracking. The material selected for the tail vane was acrylic plexiglass. This material was chosen because of its durability, ease of manufacturing, and density required to balance the turbine's center of mass.

2.4.3 Tail Vane Dimensions

The surface area of the tail vane needed to be large enough to generate normal pressure adequate for the yawing moment required for wind tracking. The necessary surface area was calculated by multiplying two times the blade length squared, then dividing by 40 [1]. Using this formula, the necessary tail surface area was determined to be 32.4 cm^2.

2.4.4 Force Analysis

A force analysis was completed to determine if the selected tail vane design was sufficient to yaw the turbine into the wind. The two deep groove ball bearings in the tower create frictional resistance that the yawing moment must overcome. The combined frictional moment for both bearings was 0.001 N-m. The

frictional moment of the bearings was compared to the yawing moment, which was calculated using the force of the wind. To replicate a worst-case scenario, a wind speed of 2.5m/s was used to evaluate the yaw performance at the lower limit of the cut in speed.

Wind does not always contact the tail vane perpendicularly, but rather at an angle (Θ) which is defined as the yaw error. The cosine of this angle yields the component of the wind normal to the tail vane. Multiplying this by the force of the wind and the length of the moment arm gives the yaw moment. To maximize turbine performance, a maximum yaw error of 5° was desired, establishing the angle, Θ, used in this calculation.

After estimating the required surface area using a triangular model, it was determined that the area was not adequate to generate sufficient force to yaw the turbine efficiently. The surface area was then increased to 320 cm^2 and the new the factor of safety (F.O.S.) increased to above five. Using these values, the wind force was calculated to be 0.25 N. The final tail vane design was modified for aesthetics to replicate the shape of an axe blade to resemble Northern Arizona University's Logo. Although not triangular, the final shape provides the similar surface area of 290 cm^2 with comparable results. Table 5 shows the results of the wind force on different tail vane sizes with the final design denoted in blue.

***Table 5**: Wind Moment Results*

Tail Vane Size (cm^2)	Wind Force (N)	Yaw Moment (N-m)	Bearing Resistance (N-m)	F.O.S.
40	0.03	0.0007	0.001	0.7
320	0.25	0.0055	0.001	5.5
290	0.22	0.0050	0.001	5.0

2.4.5 Yaw System Design Conclusion

The yaw system analysis ensures the design of a reliable yaw for the turbine system. The final design yields better results than the initial surface area analysis used to find the minimum area required to rotate the turbine. The required surface area was increased to provide a larger force for a more reliable yaw. The tail vane design and yawing components are shown in **Figure 9**.

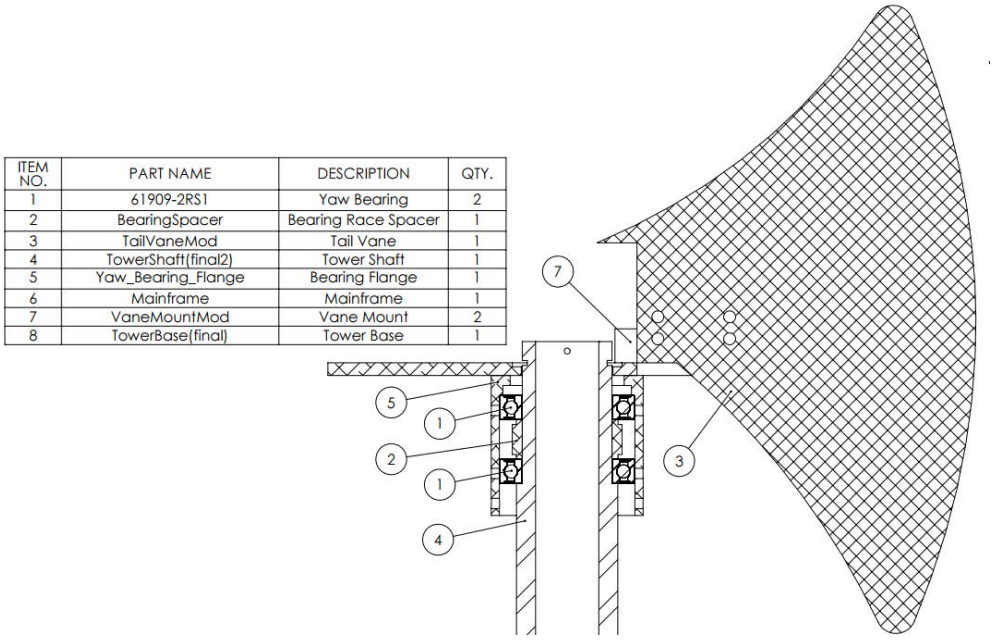


***Figure 9**: Yaw System Design*

2.5 Electrical Design

To test various off-the-shelf diode bridge rectifiers and boost converters, the Electrical team built a test bench to be used until the Mechanical team completed the working prototype of the wind turbine. A low power 75 W vertical wind turbine was purchased and mounted to a secure base. The three phase power wires were connected to a bread board for easy connection to various diode bridge rectifiers, boost converter designs, and a voltage regulated resistive load at 6V, 9V or 12V.

Two diode bridge rectifiers were tested with the test bench. One was made with six Schottky diodes and the second was IXYS FUS45 three phase AC-DC Rectifier. Six diodes were used because two diodes are required for passive rectification for each phase. Upon testing with the purchased wind turbine, the IXYS rectifier experienced smaller losses and preformed more efficiently than the other rectifier by 0.5 – 1V. The IXYS was then used to develop a separate rectifier board, which included a smoothing capacitor, bleed off resistor and heat sink. The heat sink was added to increase heat dissipation from the rectifier, increase efficiency, and avoid damage to components from excessive heat. It was then soldered to a printed circuit board (pcb) in preparation for future components.

Two off-the-shelf boost converters and one boost/buck converter was purchased and tested with the test bench to evaluate performance and observe difference in parts utilized in the design and research topologies. All three boost converters operated similarly and none of them performed better than the others with various load values. These boost converters were used as models for the final original design developed by the team. The parts used in these models were researched thoroughly and similar parts were purchased for the design.

Five Arduino Micro boards were purchased and programmed to control the regulated switching component of the original boost converter designed by the team. The microcontroller is passed in voltage and current levels from the boost converter and uses an OTSR Maximum Power Point Tracking algorithm to determine the reference variables needed to calculate the duty cycle of the switching component. The PID controllers needed to produce the reference current variable and duty cycle were programmed using Arduino's PID and PID Tuning libraries.

2.6 Electrical Analysis

Electrical Analyses were completed to confirm that the power circuit and its components met the expectations and requirements of the client.

The Arduino Micro microcontroller was programmed with the switch control algorithm with various switching frequencies to test the reliability of the microcontroller and confirm the effects on the circuit output. The MOSFET switching components were chosen over IGBTs because of their small current tail, optimizing performance in low-power applications. In the circuit testing stage, a MOSFET transistor replaced the boost converter diode to increase efficiency. Upon analysis, this synchronous boost converter configuration only increased efficiency by roughly 2%, but caused latency in the changes in the microcontroller duty cycle. The synchronous boost converter design was discarded. Silicon Carbide (SiC) Schottky Diodes were selected for the boost converter diode because of their low forward voltage and forward current. The forward voltage was measured to confirm the catalog ratings. No further relevant analysis was conducted. To minimize power dissipation in the circuit, the boost converter inductor value was minimized and the capacitor value was maximized within the bounds calculated by the team.

The final power circuit solution with the rectifier-board, OTSR controlled boost converter, and voltage regulated resistive load was tested along a spectrum of off-the-shelf turbine outputs and yielded an efficient and smooth power curve. The final circuit topology can be observed in Figure 10.

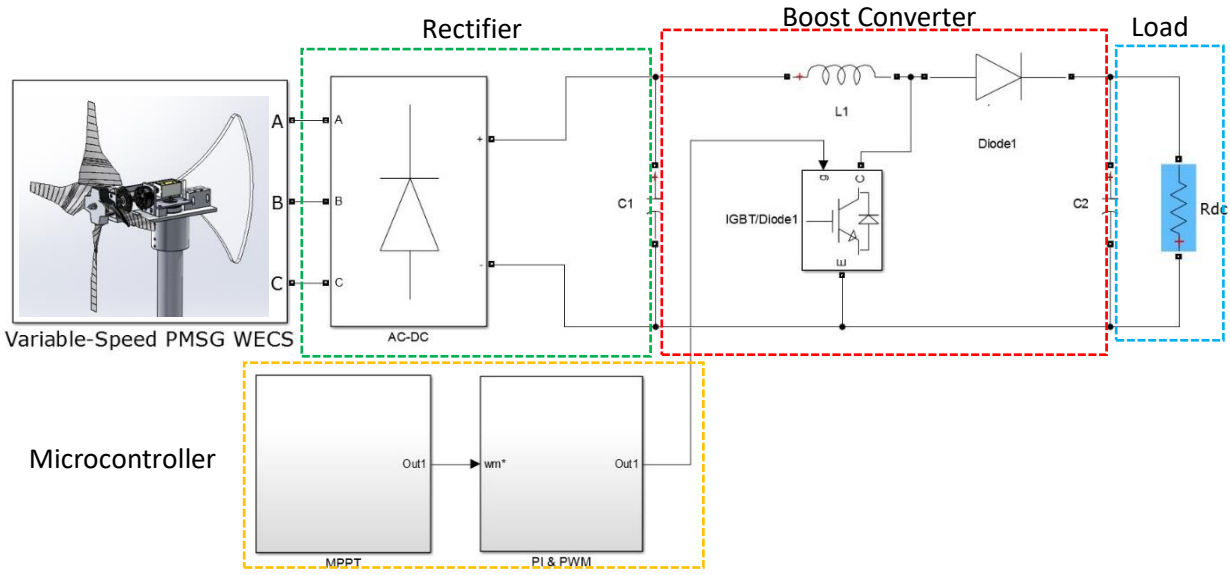


Figure 10: Power Converter Topology

2.7 Controls Analysis and Software Documentation

Simulations of various boost converters, diode bridge rectifiers, and control schemes were conducted using MATLAB's Simulink software. The simulations included multiple PI controllers as well as capacitor and inductor values to gain an overall understanding of the basic turbine, rectifier, boost converter and load design. The first simulation was comprised of a variable speed permanent magnet synchronous generator, a six-diode diode bridge rectifier, and a boost converter with an IGBT that is controlled with optimal tip speed ratio control. The circuit was connected to a resistive load to focus on the individual circuit elements and PI controller tuning. The overall boost converter topology, including smoothing capacitors, can be seen in Figure 11.

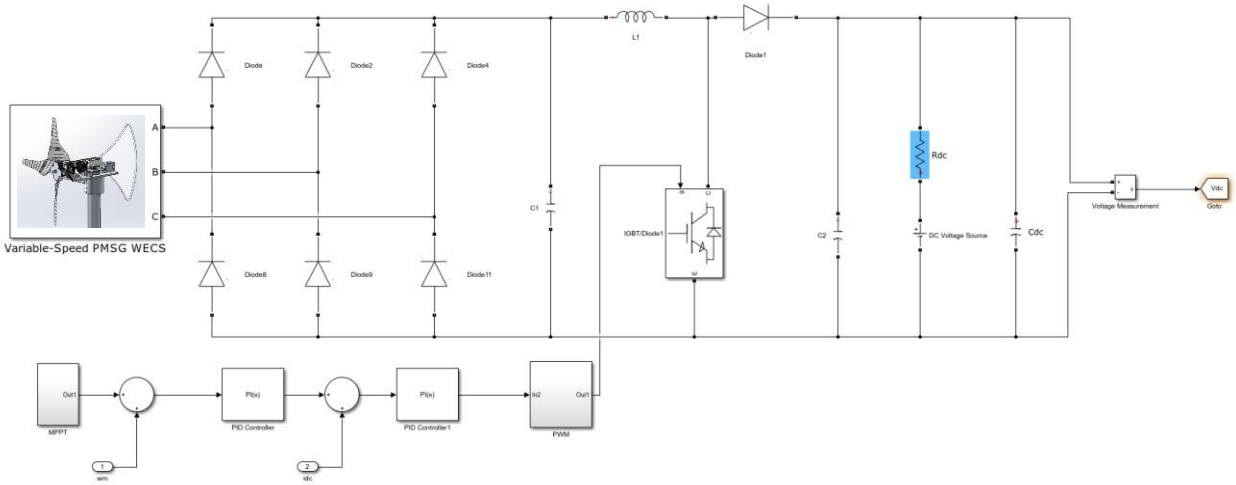


Figure 11: Boost Converter Topology

After completing the first simulation and thoroughly testing it, two simulations were developed for ABC/αß and ABC/dq control to invert the DC-DC Converter output for regulated grid-controlled power. The ABC/αß and ABC/dq control simulations were connected to a DC power supply, a two-level voltage source converter and an RL load. These conditions were chosen because of their simplicity both in construction as well as within the simulation. **The only difference between the two simulations was the calculation block for the conversion from one reference frame to the other; the two were otherwise identical.** The topology was tested for the observed current from the load to the reference current, the three-phase voltage, natural voltage and line-to-line voltage. The low-level block diagram can be seen in Figure 12.

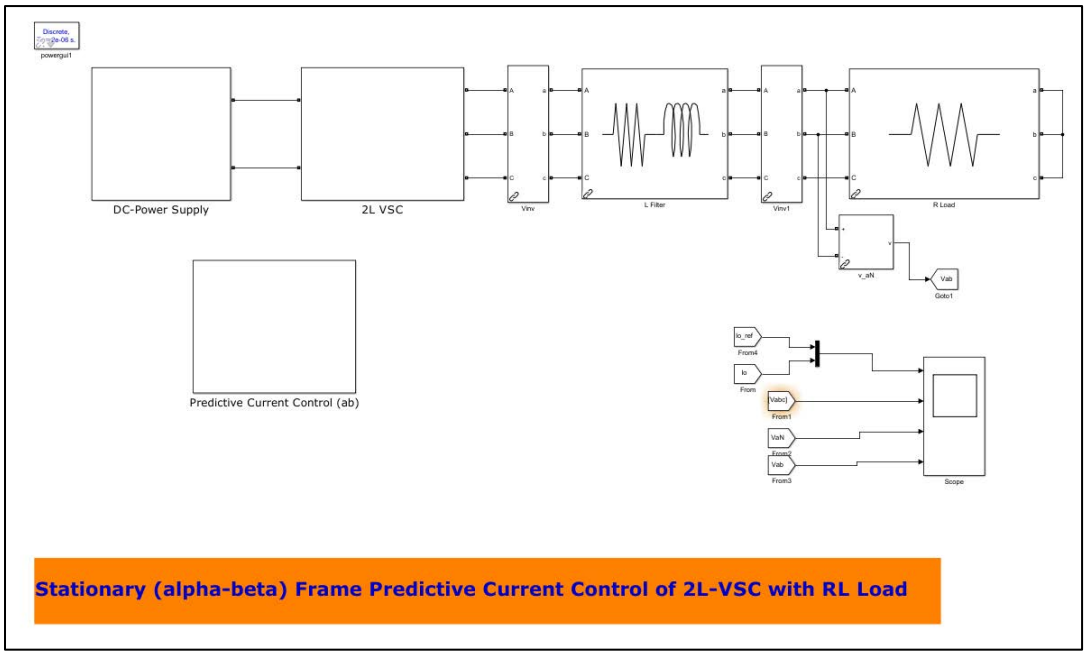


Figure 12: High Level block diagram for ABC/αß control

A similar circuit was constructed for the standalone application at the competition. The design for this circuit includes electrical and mechanical brakes and dependencies and connections for the system and its controllers. The electrical one-line diagram seen in Figure 13 contains these components and displays their purpose regarding the entire system.

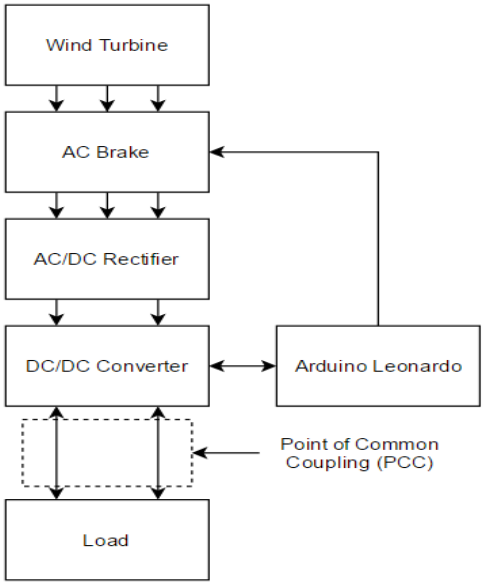


Figure 13: Electrical One-Line Diagram

Following integrated testing of purchased components, the microcontroller was programmed to determine the variable duty cycle for the switching component. The microcontroller algorithm Proportional Integral (PI) controllers and pulse width modulation (PWM) is summarized in Figure 14.

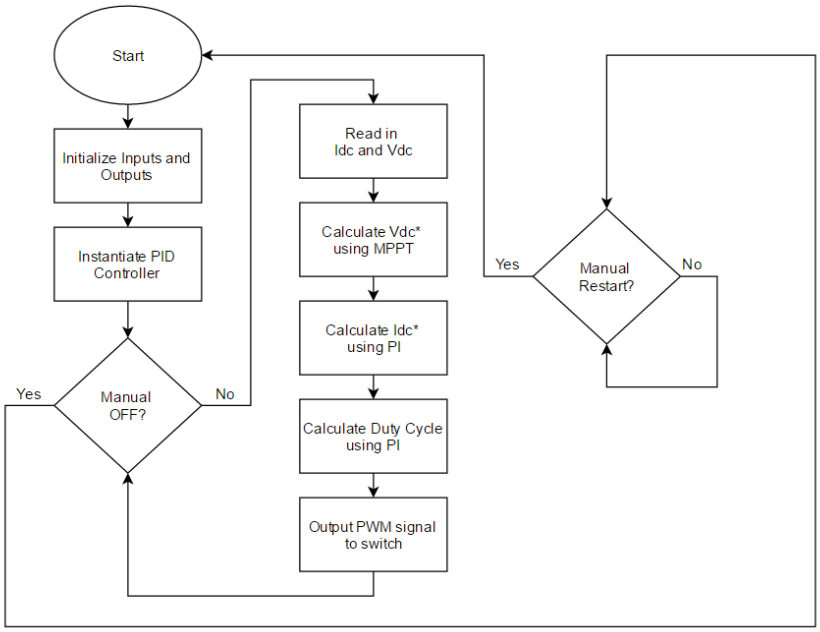


Figure 14: Control State Flow Chart

Development of a three-channel boost converter simulation was attempted; however, it was rejected when the team began development of the single-channel boost converter due to budget and time constraints. If the team is unable to produce a working DC-DC converter, the team will default to one of the purchased off-the-shelf converters for use during the competition.

2.8 Testing

2.8.1 Testing Results

The mechanical brakes were tested on a pass fail basis for functionality. The tests consisted of observing the successful actuation of the brakes by switch and actuation by disconnection from the load. Figure **15** shows the breadboard that was used for prototyping, with a latching solenoid and Arduino Nano. The latching solenoid has a permanent magnet to counteract the force of the return spring to keep the brake caliper in an open position. Once released the return spring provides the force to brake the turbine effectively. The spring constants of different springs were analyzed on how much counteractive force they can provide to the turbine assembly. The Arduino Nano is used to measure voltage drop across a shunt resistor and relate the value to the current drop once the turbine is disconnected from the load and signal the turbine to brake. The AC brakes will be used alongside the solenoid to provide the braking force to control the rpms of the driveshaft.

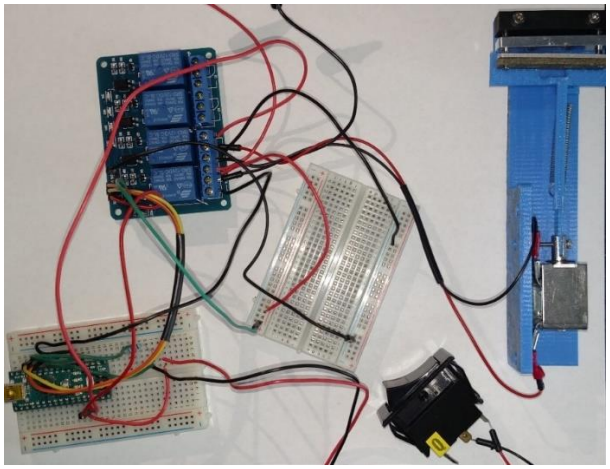


***Figure 15**: Mechanical Braking System*

2.8.2 Testing Plans

Future field testing at the wind tunnel will be split into three major tests to evaluate the three critical mechanical components of the turbine: yaw, blades, and brakes. The objective is to evaluate each subsystem based on the established design criteria.

The blades will be tested by measuring cut-in speed, power output, and structural integrity. Blades will be tested for power output performance by generating and recording power curves for wind speeds from 5m/s to 11m/s increasing by 1m/s. Wind speeds from 1-5m/s will be tested to determine when the turbine begins to generate power. The power performance of the blades will solidify the operating voltage of the turbine with test values of 6V, 9V or 12V.

The brakes will be tested for actuation and braking time at various wind speeds. The mechanical brakes will first be empirically tested on a pass/fail basis based on successful actuation of the brakes by switch and disconnection from the load. The second test will be to determine the braking time intervals at different wind speeds up to 18m/s.

The yaw system will be tested at varying angles to determine if the system can efficiently rotate the turbine into the direction of the wind. The yaw system will be tested for wind tracking response time for the wind turbine to fully orient itself into the wind. The yaw system and tower will be evaluated at integral wind speeds up to 18 m/s to determine if the turbine performs safely for any wind speed and maximum vibrational loads.

3 References

[1] J. Manwell, *Wind Energy Explained*. New York: John Wiley 2001

[2] Michael Ching Kwei Kang, "Wind Turbine Blade Automatic Pitch Control using Centrifugal Force," U.S. Patent 20120141267 A1, Abbrev. June 7 2012

[3] R. Budynas and J Nisbett, *Shigley's Mechanical Engineering Design 10th Edition.* New York: McGraw-Hill 2015

[4] Oak Ridge National Laboratory, "Basic Properties of Reference Crossply Carbon-Fiber Composite," Lockheed Marting, February 2000, [Online]. Available: http://web.ornl.gov/~webworks/cpr/v823/rpt/106099.pdf

[5] ASM International, "Contact Fatigue", Transportation.org, [Online] Available: http://highways.transportation.org/documents/sec06-lts-5trev.pdf

[6] MatWeb Material Property Data, "ASTM A36 Steel Bar", [Online] Available: http://www.matweb.com/search/datasheet.aspx?matguid=d1844977c5c8440cb9a3a967f8909c3a&ckck=1

[7] J. Schon, "Coefficient of Friction for Aluminum in Contact with Carbon Fiber Epoxy Composite", February 2004, [Online] Available: http://www.sciencedirect.com/science/article/pii/S0301679X03002305

[8] "Deep groove ball bearings 61909"Internet: http://www.skf.com/us/products/bearings-units-housings/ball-bearings/deep-groove-ball-bearings/deep-groove-ball-bearings/index.html?designation=61909, [Nov. 18, 2016].

[9] "Bearing Loads" Internet: http://www.skf.com/group/products/bearings-units-housings/engineered-products/insocoat-bearings/insocoat-deep-groove-ball-bearings/loads/index.html, [Nov. 18, 2016].

[10] "SUNNYSKY." Internet: http://www.hobby-wing.com/sunnysky-x4108s-multicopter-brushless-motor.html, 2006 [Nov. 18, 2016].

[11] "Cheap Slip Rings." Internet: http://www.dxsoul.com/product/wind-turbine-6-wire-5a-per-circuit-electrical-slip-ring-for-wind-power-generation-system-901390064#specifications-detailinfo, 2006 [Nov. 18, 2016].

[12] "1/5 Baja 5B Disc Brake." Internet: http://www.dollarhobbyz.com/collections/disc-brake-parts/products/hpi-1-5-baja-5b-disc-brake-set-aluminum-rear-upper-plate, [Nov. 18, 2016].

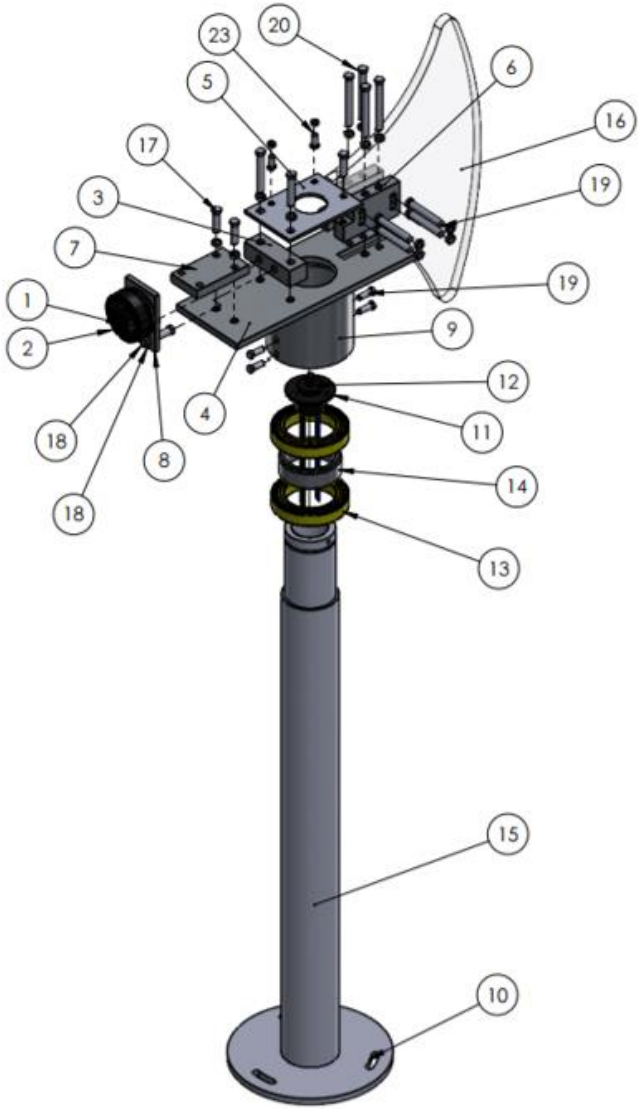
[13] D. Wood, Small wind turbines, 1st ed. New York: Springer, 2011, pp. 145-166.

[14] "Estimating the frictional moment", Skf.com, 2016. [Online]. Available: http://www.skf.com/us/products/bearings-units-housings/ball-bearings/principles/friction/estimating-frictional-moment/index.html. [Accessed: 13- Nov- 2016].

[15] "Wind Velocity and Wind Load", Engineeringtoolbox.com, 2016. [Online]. Available: http://www.engineeringtoolbox.com/wind-load-d_1775.html. [Accessed: 17- Nov- 2016].

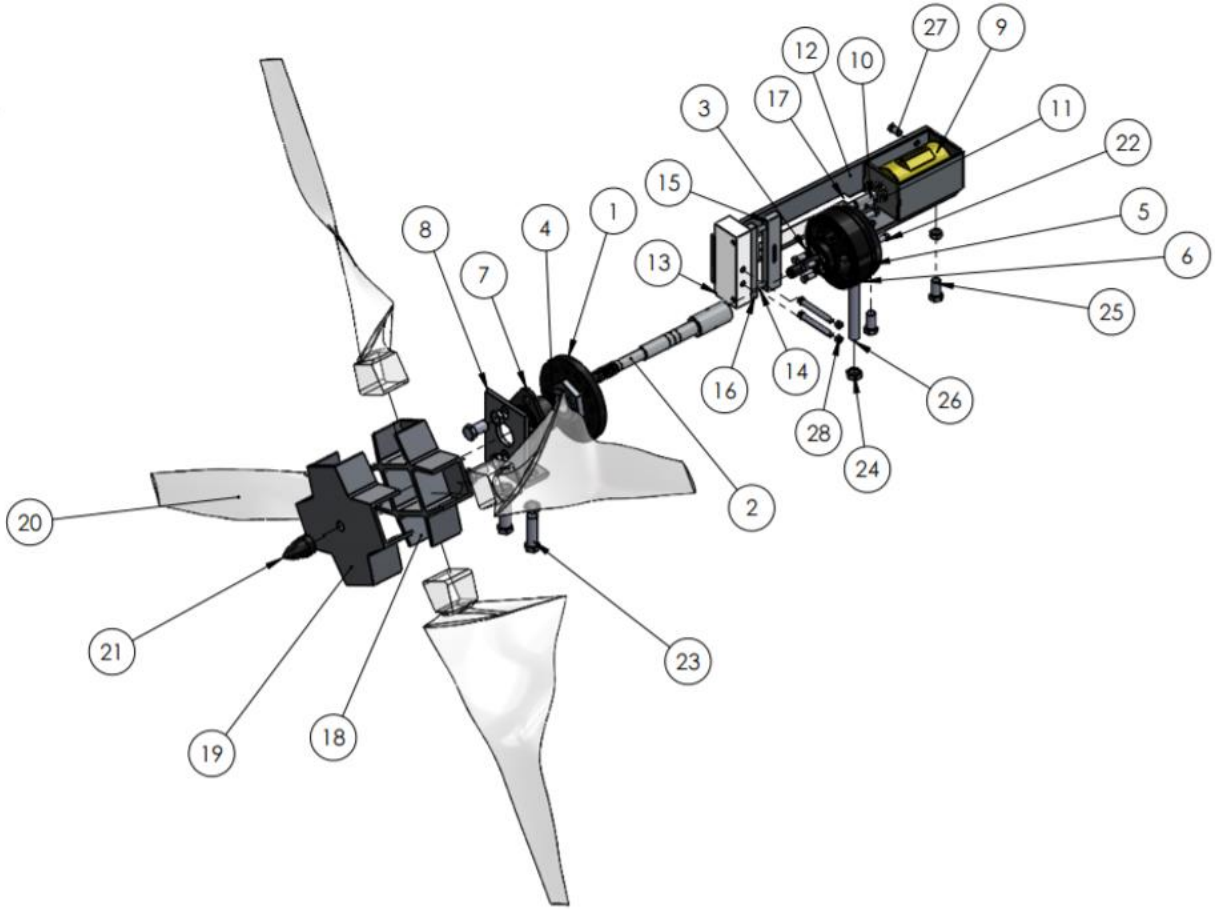
4 Appendix A: Exploded View-Mainframe, Tower, Tail, and Yaw System

ITEM NO.	PART NUMBER	QTY.
1	Motor Stator	1
2	Motor Rotor	1
3	Block	1
4	Mainframe	1
5	Mount	1
6	Vane Mount	2
7	Riser Block	1
8	Motor Plate	1
9	Yaw Bearing Flange	1
10	Tower Base	1
11	Slip Stator	1
12	Slip Rotor	1
13	Yaw Bearing	2
14	Bearing Spacer	1
15	Tower Shaft	1
16	Tail Vane	1
17	M6x1.0 (20mmx 5, 30mmx1, 40mmx9)	15
18	M6x1.0 Nut	14
19	M5x1.0 (10mmx2, 15mmx6)	8
20	M5x1.0 Nut	2



5 Appendix B: Exploded View-Hub, Brakes, Drivetrain

ITEM NO.	PART NAME	QTY.
1	BrakeRotor	1
2	Drive Shaft	1
3	Stub Shaft	1
4	Brake Hub	1
5	Motor Stator	1
6	Moter Rotor	1
7	Flange Mount, Self Align, Needle Roller Bearing	1
8	Bearing Plate	1
9	Solenoid	1
10	Plunger	1
11	Spring	1
12	Mount 2	1
13	Caliper	1
14	Pin	2
15	Shoe 2	1
16	Shoe 1	1
17	Arm	1
18	Hub Base	1
19	Hub Top	1
20	Blades	4
21	Nosecone	1
22	M3x0.8	12
23	M6x1.0 (10mm x 2, 20mmx 2, 40mm x 1)	5
24	M6x1.0Nut	5
25	M5x1.0 10mm	2
26	M5x1.0 Nut	2
28	M3x0.8 Nut	2



6 Appendix C: Shaft Analysis MATLAB Program, DE-Gerber Failure Criteria

```
%% Rafeal Vera Jr. Last Updated 3-28-17
%% This program is used to solve for the factors of safety for fatigue using
%the DE-Gerber failure criteria and also checks for static loading factor of safety
%use in conjunction with Shigley's Mechanical Engineering Design
%% User Inputs
diameters = input('Enter the diameter at location of interest in mm:\n'); %Diameter of
interest
Sut = input('Enter material ultimate tensile strength in MPA for shaft (pg 1048+)\n')
; %tensile strength input
Sy = input('Enter material yield strength in MPa\n'); %yield strength input for factor
of safety
%% Material Yield Stresses
Sep = Sut * .5; % Se' for Sut less than 200 kpsi or 1400 MPa
a = (4.51);  % Surface mod constant for CD or machined steel or aluminum 4.51 for MPa
2.7 for Kpsi
b = -0.265; % Surface mod constant for CD or machined steel or aluminum
ka = a * ((Sut)^b); %surface mod factor
kb = (1.24) * (diameters^-0.107);  % for inches :(0.879) * (diameters^-0.);
%kc = 1; %Because loading is in bending
Se = ka*kb*Sep;
% rod = .15; % fillet radius vs diameter ratio    larger means safer
%% Dynamic Loads
Momenta = input('Enter the alternating bending moment (Ma) at location of interest in
N-mm\n');
Torquem = input('Enter the Mean Torque (Tm) at location of interest in N-mm\n'); %Mean
Torque Through Shaft
%% Stress Geometry and Material Factors
kt  = input('Select an Kt Bend from(A-15-9) pg 1036 \n'); %kt = 2.14 and kts = 3.0 for
keyway groove
kts = input('Select an Kts tors from(A-15-8) pg 1038 \n');
q = input('Enter a value for q (notch sens) from handout or pg 303 \n'); % your gonna
need Sut
qs = input('Enter a value for qs (shear notch sense) from handout or pg 304 \n');
%% Stress Concentration Modification
kf = 1 + (q * (kt-1 )); %kt = 2.14 and kts = 3.0 for keyway groove
kfs = 1 + (qs * (kts-1 )); %surface/stress concentrator modification factors
%% De-Gerber Criteria
A = sqrt(4*((kf*Momenta)^2));
B = sqrt(3*((kfs*Torquem)^2));

ns = 1/(((8*A)/(pi*Se*diameters^3))*(1+(1+[(2*B*Se)/(A*Sut)]^2)^(1/2))); %DE-Gerber
Failure Theory: fatigue
sigprimax = sqrt (( ((32*kf*Momenta)/ (pi * diameters^3))^(2) + (3*(((16*kfs*Torquem)/
(pi * diameters^3)))^(2)) ));
ny = Sy / sigprimax;  %factor of saftey for static yield failure
nd = 1.1;
newdiameter = ( (8*nd*sqrt(4*(kf*Momenta)^2))/(pi*Se))
*(1+[1+[(2*Se*sqrt(3*(kfs*Torquem)^2))/(Sut*sqrt(4*(kf*Momenta)^2))]^2]^(1/2))^(1/3);

fprintf('Factor of saftey for fatigue is : %.4f \n' ,ns);
fprintf('Factor of saftey for yield is : %.4f \n' ,ny);
fprintf('The new diamter should be : %.4f \n' ,newdiameter);
```

7 Appendix D: Equations

Dynamics Equations:

Newton's Second Law: $F = ma_n$

Normal Acceleration: $a_n = (R_o - R_i)\omega^2$

Revolutions per Minute: $n = \frac{60\ U\ \lambda}{\pi\ D}$

Angular Velocity: $\omega = \frac{2\pi\ RPM}{60}$

Torque Coefficient: $C_Q = \frac{C_p}{\lambda}$

Rotor Torque: $Q = C_Q \frac{1}{2}\ \rho\pi R^2 U^2$ [1]

Fatigue and Yield Equations:

DE-Gerber Failure Criteria: $$\frac{1}{n_f} = \frac{8A}{\pi d^3 S_e}\left\{1 + \left[1 + \left(\frac{2BS_e}{AS_{ut}}\right)^2\right]^{1/2}\right\}$$

Where: $A = \sqrt{4(K_f M_a)^2}$ *and* $B = \sqrt{3(K_{fs} T_m)^2}$

Von Misses Static Yield Criteria: $n_y = \frac{S_y}{\sigma'_{max}}$

Loading is Fully Reversed therefore: $M_m, T_a = 0$

S_e , S_y , σ'_{max} *and* S_{ut} *are calculated using material properties and modification factors from Shigley's [3] and are omitted in this report*

Uniform Pressure Criteria (Brake) Equations:

Braking Force, New Brakes: $F = \frac{1}{2}(\theta_2 - \theta_1) p_a (r_o^2 - r_i^2)$

Resistive Torque: $Q = \frac{1}{3}(\theta_2 - \theta_1) f p_a (r_o^3 - r_i^3)$

8 Appendix E: Assumptions and Material Properties

Dynamics Assumptions:

Angular Velocity is Constant ω = constant, Tangential Acceleration is zero, $a_t = 0$

Blade Radius, Hub Radius and Total Rotor Diameter, R_B = .20 m, R_H = .02 m and D = .44 m

PLA Blade and Aluminum Hub Mass, m_B = 0.022 kg/blade, m_H = 0.022 kg/arm

Golden, Colorado Air Density, $\rho = 1.324\ kg/m^3$

Tip Speed Ratio, λ = 4 (for maximum torque)

Average Coefficient of Performance, $C_p = 0.500$ (for maximum torque)

Brake Assumptions

Theta is Brake Pad Span in Radians: θ_1*= 0.523 and* θ_2*= 2.617*

Inner and Outer Brake Pad Radii are: r_i*= 14 mm and* r_o*= 22 mm*

The Pads are assumed to be Annular (Curved)

Material Properties:

6061-T6 Aluminum: S_{ut}= 310 MPa ,S_y= 276 MPa

7075-T6 Aluminum: S_{ut}= 593 MPa, S_y= 542 MPa

VEROCLEAR 3D Filament: S_y= 50MPa

Brake Pads are T6-6061 Aluminum with Max Contact Pressure of: 241MPa [5]

The Brake Disk is Carbon Fiber ($\pm$45° fiber orientation) with Max Contact Pressure of: 163 MPa [4]

Max Contact Pressure of Steel (for Estimation Purposes) is: 152MPa [6]

Max Contact Pressure of Carbon Graphite on Steel (for Estimation Purposes) is: 2.10 MPa [3]

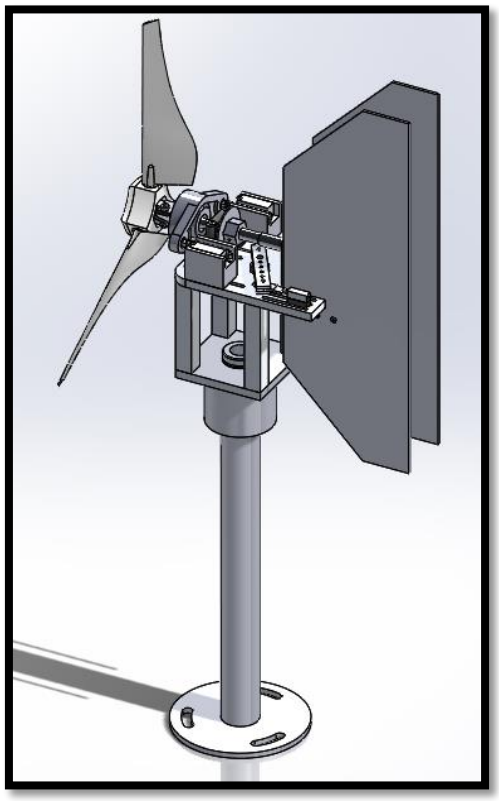
Coefficient of Friction of CF-AL Ranges from: f=0.23-0.68, Estimated at f= 0.37 [7]

Estimated Max Pressure for CF-AL Interface: 2.50 MPa

NAU Collegiate Wind Competition 2017-2018

Final Report





Project Sponsor: U.S. Department of Energy & National Renewable Energy Laboratory

Faculty Advisors:

Karin Wadsack, Principal Director, School of Earth Science and Environmental Sustainability

David Willy, Co-investigator, Mechanical Engineering

Denise Linda Parris, Ph.D., Franke College of Business

Capstone Instructor: Sarah Oman, Ph.D.

Founding Business Team Members	
Jordan Parker - Finance Lead	Shawn Malkou - Marketing Lead
Diana Carlson - Management Lead	Tyler Brown - Information Systems Lead
Founding Engineering Team Members	
Leo Segura De Niz - Project Lead	Alex Dahlmann - Tunnel Team Lead
Anthony Cheslic - Market Team Lead	Devon Hardy - Tunnel Team Mechanical Design Lead
Alana Benson - Siting Lead	Tristan Scott - Tunnel Team Electrical Design Lead
Craig Collins - Blade Development	Aaron DeLuca - Tunnel Team Electrical Design
Michael Vogelsang - Market Conceptual Design	Dakota Sallaway - Tunnel Team Mechanical Design
Mitchell Green - Market Conceptual Design	Benjamin Macleod - Tunnel Team Mechanical Design
Kory Joe - Tunnel Team Mechanical Design	Spencer McMahon - Tunnel Team Mechanical Design
Jacob Peterson - Tunnel Team Mechanical Design	Qian Zhao - Tunnel Team Electrical Design
Evan Heiland - Tunnel Team Electrical Design	Soud Alsahli - Tunnel Team Mechanical Design

EXECUTIVE SUMMARY

An electric vehicle (EV) is only as clean as the source that powers it. While EVs do not emit tailpipe emissions, there are emissions associated with the source of electricity used to power them. By 2040, there will be 530 million EVs worldwide. With the EV market on the rise there are concerns about the increased demand for nonrenewable energy for charging these vehicles.

To help offset this problem, CleanerGrid is a wind farm developer who provides EV charging station companies an alternative source of energy to offer their end consumers. Power produced by CleanerGrid's wind farms is sent to the grid and distributed. The business generates revenue by establishing Power Purchase Agreements (PPAs) with EV charging station companies and selling excess energy to the grid. The amount of energy used by the client is determined monthly and CleanerGrid will receive payment based on the amount used.

CleanerGrid's secondary focus is to develop vehicle to grid (V2G) technology. Three years after CleanerGrid begins operations, a V2G technology license will be sold as a secondary source of revenue.

CleanerGrid is looking to obtain a $170 million loan with a 5% interest for 20 years, which will cover the cost for the turbines, installation, and business capital costs for the start-up of the business and the first wind farm.

CleanerGrid's wind farms will be composed of 28 turbines with rated power of 3.5 MW each. A prototype 3.5 MW wind turbine was designed to assess feasibility of the concept. The designed market turbine features a hybrid concrete-steel tower, 70-meter blades, and a 120-meter tower. A test scale turbine was designed and tested to operate is various wind conditions with a passive yaw and active blade pitching system for optimum performance. Turbine performance and FEA analysis was completed for both systems. Appropriate factors of safety were selected to ensure a reliable design. Mechanical and electrical systems of the test turbine were tested proving a safe and dependable design.

Table of Contents

1. BUSINESS PLAN 5
1.1 Business Overview 5
1.2 Market Opportunity 6
1.2.1 Market Growth 6
1.2.2 Power Purchase Agreements (PPA) 7
1.2.3 Business Competition 8
1.3 Management Team 8
1.3.1 Founding Team 8
1.3.2 Full-time 8
1.4 Development and Operations 9
1.4.1 Vehicle to Grid (V2G) Research and Development 10
1.5 Financial Analysis 10
1.5.1 Start-up Financing 10
1.5.2 Depreciation 10
1.5.3 Income Statement 10
1.5.4 Sales and Revenue 10
1.5.5 Operating and Administration Expenses 11
1.5.6 Net Income 11
1.5.7 Balance Sheet 11
1.5.8 Cash Flow 11
1.6 Risk Mitigation 11
2. TECHNICAL DESIGN 12
2.1. Market Turbine 12
2.1.1. Deviations from Test Turbine 12
2.2. Tunnel Turbine 13
2.2.1. Static Performance Analysis 13
2.2.2. Mechanical Loads Analysis 13
2.2.3. Yaw System 17
2.2.4. Electrical Analysis 17
2.2.5. Software Description 18
2.2.6. Testing Results 18
3. APPENDIX A: BUSINESS FINANCIALS 22
4. APPENDIX B: TUNNEL TURBINE DRAWINGS 25

1. BUSINESS PLAN

1.1 Business Overview

CleanerGrid develops wind farms to provide a clean energy solution for the $75.7 billion Electric Vehicle (EV) market, expected to grow to $127.7 billion dollars by 2020 [1]. The business makes money by selling wind energy to charging stations companies through Power Purchase Agreements (PPAs) and selling excess energy to utility companies. CleanerGrid's purpose is to offer an alternative source of energy. Cleanergird will do this by encouraging consumers to educate themselves about renewable energy, drive investment in renewable energy to protect the environment and improve green infrastructure within the EV market. The vision is to be the primary renewable energy provider within the electric vehicle market.

Table 1: EV Energy Usage per Year

Value	Description
30	kwh (to charge 100 miles)
0.3	kwh/mile
12,000	average miles traveled per year
3,600	kwh/year/EV

As of 2017, in the U.S. there were 16,000 charging stations that received their power from the grid [2]. Roughly 5 million charging stations will be necessary to support the estimated 7 million EVs by 2025 [3]. In 2017, 4,015 billion kilowatt-hours (kWh) were produced in the United States. Of this production, the electricity generation portfolio consisted of 63% fossil fuels, 20% nuclear, and 17% renewable [4]. Based on the assumptions and calculations in Table 1, each EV consumes 3600 kWh per vehicle per year; 7 million EVs would require roughly 25.2 billion kWh to charge each EV per year [5]. This results in two unintentional impacts: 1) increased demand for non-renewable energy to charge EVs, and 2) potential destabilization of the grid.

Based on the electricity generation portfolio, the large percentage dedicated to fossil fuels implies that it is the familiar and reliable choice [6]. The second impact, destabilization of the grid, will warrant a change in the electrical infrastructure. Mark Parker, a Supervisor of Customer Design at Salt River Project (SRP), explained that a fast EV charging station requires large equipment that results in overbuilding and underutilization due to the fluctuation of charging demand. A building that SRP normally powers, is constantly drawing power for 9-12 hours, and in some cases up to 24 hours. This allows the meter to run more constant; whereas, charging station meters only run when vehicles are charging. These charging stations experience a huge inrush of current when the consumer plugs in. This results in a voltage drop in the grid. Without proper implementation of capacitors on the system, nearby buildings may experience flickering lights or appliances burning out because the voltage on the system is not high enough to sustain it.

Increasing competition is driving EV charging companies to find innovative ways to capture more EV drivers to utilize their charging stations. After conducting primary market research and speaking to the President of Blink Charging Co., the team found that charging station companies are interested in providing a renewable energy option to meet their consumer demand. CleanerGrid will be able to satisfy this end user demand by creating PPAs with charging station companies.

A survey conducted by CarMax and CleanTechnica found 38% of the 2,300 EV owners purchase EVs to limit their impact on the environment, but our assumption is that their EV is only as clean as the source that powers it [7]. Currently, there is a need for awareness of the benefits, affordability, and accessibility of renewable energy. EV charging station companies have an interest in supplying clean energy to their users. Furthermore, utility companies have observed a demand for clean energy options from their users.

Many utility companies are diversifying their portfolio to include renewable energy sources to meet the customer demand. According to the utility company, "SRP has established a goal that by 2020, SRP will meet a target of 20 percent of its expected retail energy requirements with sustainable resources. Among them are a diversified resource mix of wind, geothermal, large hydro and low-impact hydro, and solar [8]." The increasing demand for energy results in the increasing use of non-renewable energy due to its familiarity. Utility companies can meet their sustainability goals by purchasing excess power that is not sold to the primary EV market, from CleanerGrid.

The want and need for renewable resources is intensifying and the solution is CleanerGrid. The first wind farm project will begin in June of 2018 in West Texas. The wind farm will be composed of 28 turbines, each with a rated power of 3.5 MW. The farm is expected to operate at 45% capacity producing a total of 386 Gigawatt-hours over a one-year period. Revenue will be generated by selling clean energy to charging station companies through PPAs, and excess power to utility companies. CleanerGrid and the customer will sign a PPA that specifies the rate for electricity over the span of the contract.

CleanerGrid has a secondary focus on developing a reliable vehicle to grid (V2G) connection to help stabilize the grid. Research and development will begin in June 2018 and V2G technology will be released in 2021. This technology will allow bidirectional power flow, thus allowing the vehicle to discharge the energy stored in the battery, adding value to the parked vehicle. EV owners will then have an asset in their vehicle, which due to its storage capacity can be used to support grids of varying scales. V2G can also be associated with distributed generation systems to promote the integration of renewable energy in the grid.

In 2022, CleanerGrid will expand, at the same location, to increase the production of energy by building a second 98 MW power plant with utility scale wind turbines. The expansion will be completed in 2023; this expansion will allow CleanerGrid to produce 772.6 Gigawatt-hours per year to meet current and prospective charging station companies' demand.

1.2 Market Opportunity

CleanerGrid conducted primary research by fielding a survey to EV owners and received 430 respondents. The survey found 63% of EV owners want to be environmentally friendly; however, they have not considered the source of the electricity that fuels their vehicles.

1.2.1 Market Growth

According to the U.S. Department of Energy (DOE), "EVs, while operating in all electric mode, do not produce tailpipe emissions. However, there are emissions associated with much of electricity production in the United States [9]." The DOE states that 3.7 pounds of CO_2 equivalent is generated per mile driven in an EV based on its power source [9]. The primary purpose of an EV is to reduce pollution and greenhouse gases. In today's marketplace, the goals of EVs regarding environmental improvements are not being met to its full potential. According to the International Energy Agency, "Renewables only account for 26% of electricity consumption of EVs while it's expected to rise to 30% by 2022 [10]." CleanerGrid is looking to work towards increasing this growth rate.

The EV market is growing at an astonishing rate, and Bloomberg predicts by 2040 there will be 530 million EV's worldwide [11]. Based on driving and energy consumption averages, over 2.1 million GWh is needed to power these electric vehicles per year. CleanerGrid will capitalize on this rapid growth by being the first wind developer focused on powering EVs. According to Bloomberg's New Energy

Finance's annual long-term forecast of the world's electric vehicle market, the EV market is growing steadily and will continue to grow [11]. The Federal (up to $7,500) and State incentives for consumers to purchase EV's are encouraging growth. Every state has its own incentive programs for EV purchases and as the market grows, the infrastructure needs to grow with it. CleanerGrid will be assisting with the growing infrastructure by building an initial 98 MW wind farm and continuing to expand with market growth. According to our primary market research, 63% of respondents are interested in a renewable source of energy as an option to charge their vehicles. CleanerGrid is the solution to this problem by partnering with EV companies to offer a green charging option to the end user.

In addition to sourcing more renewable energy for EVs, CleanerGrid is expecting to release new technologies (such as the vehicle-to-grid technology by 2021 to car part manufacturers). About 85% of respondents surveyed showed interest in being able have green energy sourced to their home. This is just another reason that opens more opportunities in the industry for CleanerGrid to grow. CleanerGrid doesn't want to stop at providing clean energy to just car charging stations, we plan to expand across the entire grid.

1.2.2 Power Purchase Agreements (PPA)

CleanerGrid will have PPAs with charging station companies to provide their stations with renewable energy. Blink, one of the largest charging station providers in the United States, has already agreed to working with us on a PPA. PPAs allow for CleanerGrid to generate and sell electricity to these clients for a locked rate over the course of the next 20 years. We have decided to sell our renewable wind power at premium rate of $0.06 per kWh per PPA agreement.

Our clients can then charge end consumers a premium for charging their vehicles with renewable energy. Whether it be in monthly memberships or pay as they go, the end goal of powering consumers' EVs with green energy can be accomplished through PPAs with us. According to our own market research, 79% of users surveyed said they would be willing to pay at least $0.05 or more per kWh to charge their EV with renewable energy, reference Figure 1. Some respondents even made it clear that they'd be willing to pay upwards of $0.75 extra per kWh for clean charging. Based on our survey results it will be beneficial for EV charging station companies to partner with us via a PPA.

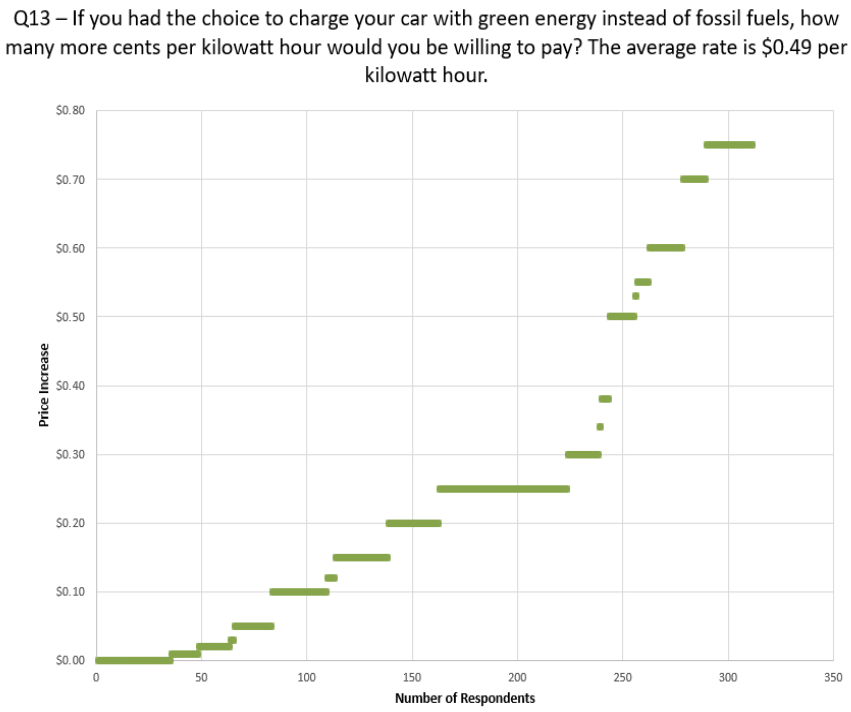


Figure 1: Survey Results for Market Opportunity

1.2.3 Business Competition

CleanerGrid will not have any direct competition upon entry to the market. No charging company in the market place is offering its consumers 100% renewable energy. The only two indirect competitors are clean energy providers and traditional electricity providers.

Renewable energy developers and providers, such as industry leader NextEra, build wind farms to power numerous different projects. NextEra and related companies do not source clean energy directly to EVs. The direct competition expected in this specific field that the end consumers will be presented with are: to power their vehicles with premium clean energy or to purchase cheaper, environmentally damaging energy to power their EV. CleanerGrid provides a logical solution to help create a cleaner environment while powering the ever growing EV market.

With the V2G market, car companies such as Nissan and Renault (with the help of energy supplier companies) are in the early development stages of V2G technology. According to Ovo, one of the United Kingdom's largest energy suppliers, EV owners would need to purchase and install a special charger in their home [12]. CleanerGrid strives to develop a user friendly (plug and play) experience that is far more enticing to end users.

1.3 Management Team

1.3.1 Founding Team

Founding members have committed to work 10 hours per week for one year without compensation for a combined total of 10% equity in the company, with no payment until year 2026. The founding members will identify three full-time employees to take over the business model. The founding team will spend their time overseeing operations and assisting the full-time employees as needed.

1.3.2 Full-time

CleanerGrid will work with the board of advisors to fill three full-time positions to run our wind farm(s) and lead the V2G research. In 2019, the company will on-board one engineer and in 2020 will on-board two additional engineers to assist with the research and development for V2G. Below is a list of necessary employees for the future success of CleanerGrid with desired/acquired expertise.

Chief Executive Officer:

- Entrepreneur
- Visionary
- Renewable energy expert
- Great knowledge of EV's
- Knows how to establish partnerships

Chief Operating Officer:

- Great understanding of the grid
- Wind turbine experience
- Visionary
- EV knowledge
- V2G knowledge
- Engineer background

Lead Project Developer:

- Leadership skills
- Experience overseeing contractors on projects
- Project Management experience
- Wind turbine knowledge

Board of Directors

Our board will consist of 5 members each with one or two of the expertise listed below:

- EV expert
- Financial law operations
- Wind/renewable energy
- Lead engineer experience

Board of Advisors

Our board of advisors will consist of three professional connections. These individuals have agreed to be available to give advice as necessary and to help hire our CEO and COO. The board members will receive a combined total of 2% equity in our company with no payment until 2026.

Ross Taylor

- Numerous years of experience in the wind industry
- Has installed complex wind turbines
- Experience installing turbines all around the world

Andy Kinard

- President of Blink Charging stations
- Extensive EV experience
- 15 years of experience working in the energy sector
- Renewable energy experience

Jake Styacich

- Strategic Communications and Policy Associate at EDTA
- EV policy expert
- Experience working with numerous EV companies
- Always up to date on new EV information

1.4 Development and Operations

Each 98 MW wind farm will be composed of off-the-shelf 3.5 MW wind turbines; therefore, CleanerGrid will not be responsible for any turbine manufacturing. CleanerGrid's technical team will focus its early efforts on site planning and site development. Once the first site is developed and CleanerGrid can afford it, research and development operations will be focused around the vehicle-to-grid integration (V2G). For these operations, CleanerGrid will be hiring full time technical employees.

CleanerGrid's service distribution will operate on a business-to-business (B2B) basis. The company will generate energy by use of 98 MW wind farms and sell the energy to EV charging station companies and excess energy to the grid. Technical constraints to implementation include areas of the country where we

can't easily deliver electricity from our initial wind farm in West Texas due to existing infrastructure. This technical constraint is not a concern for CleanerGrid because we will be using virtual PPAs to sell our energy.

1.4.1 Vehicle to Grid (V2G) Research and Development

The wind farm will work in conjunction with a vehicle-to-grid (V2G) charging system to operate in an islanded mode. The system will rely on using electric vehicles plugged into charging stations or specialized outlets as a form of battery storage that can hold power and then return it to the grid when told to via a signal from the power company. To study the application of a V2G system on a microgrid, a preprogrammed example of a V2G microgrid in Simulink was examined [13].

1.5 Financial Analysis

CleanerGrid made assumptions for portions of the financial statements based upon a financial model run through the System Advisory Model (SAM) [14].

1.5.1 Start-up Financing

CleanerGrid will be seeking a $170 million government backed loan in 2018. American Wind Energy Association (AWEA), explains that the "cost of the wind turbine is the single largest cost component, and can make up 70% or more of the entire cost of a land-based wind project. The cost of installation, such as construction, makes up the remaining capital costs [15]." Therefore, the amount of the loan will cover the turbine costs, development, installation, and business capital costs. The interest on the loan is 5% with a term of 20 years. This results in yearly payment of $13,463,088. We acquire a second loan in 2022 with the same terms and conditions.

1.5.2 Depreciation

The company has decided to use a mixed allocation strategy for depreciation. The reason for this strategy was determined by the diverse assets that CleanerGrid owns. The depreciation allocation is as follows: 90 percent to 5-year MACRS, 1.5 percent to 15 year MACRS, 2.5 percent to 15 year straight line, and 3 percent to 20 year straight line. Note that the depreciation allocation sums to 97 percent. The remaining 3 percent are due to non-depreciable assets.

1.5.3 Income Statement

Reference Appendix A, Table A.1.

1.5.4 Sales and Revenue

Sales is separated into two categories: sales (EV) and sales (grid). A portion of the actual energy produced is allocated to sales in each category. Our sales assumption (EV) is determined by the amount of kWh needed for users who choose to purchase wind energy while charging publicly. Then, sales (grid) is determined by the difference of the production of actual kWh and sales allocated to EV. The wind farm will be constructed in 2018; therefore, 2019 will be the first year revenue is captured.

In 2021, the V2G technology will be sold to automakers through licensing. An assumption was made that 15% of EV purchases would have the option of the V2G technology incorporated in the vehicle. CleanerGrid valued the V2G technology license at $435 per vehicle which results in roughly $42.8 million at 15% of sales for 2021.

1.5.5 Operating and Administration Expenses

Expenses for CleanerGrid are based by year and have a direct correlation with the increase of revenue streams (Expansion and V2G).

1.5.6 Net Income

CleanerGrid will experience a positive net income in the year 2021. Net income will consider federal and state taxes along with the production tax credit. After the year 2021, the net income will increase then decrease in 2023 due to the expansion. Net income will increase thereafter.

1.5.7 Balance Sheet

CleanerGrid projected financial balance sheets for 2018 to 2025, reference Appendix A, Table A.2. Development and expansion capital is a current asset necessary for contracting, land fees, excavation, and closing costs. Other assets include bond issuance, bonuses and reserve accounts. The property, plant and equipment (PP&E) is made up of turbines, depreciation and equipment. The cost per turbine was $1,200 per kW. This cost comes to $4,200,000 per turbine. Since we have 28 turbines this results in the total cost being $117.6 million. Equipment accounts for business technology including computers, software and software updates, and technology improvements.

Liabilities are made up of current and long-term liabilities. Current liabilities are comprised of loans payable, accounts payable, and accrued wages. Long-term liabilities accounts for our long-term debt.

Owners' equity is comprised of retained earnings and additional capital expenditures. Retained earnings becomes positive in 2021 and can be reinvested to pay off debt or for research and development. Money allocated to additional capital expenditures is used for upgrades in our assets and other reinvestments into the business. This equity is not recognized until 2024 because the company's focus was in expansion and development.

1.5.8 Cash Flow

Positive net cash is first observed in 2023. This is because the total cash flow from operations outweighs the total cash flow from investing and financing. Reference Appendix A, Table A.3 for CleanerGrid's cash flow.

1.6 Risk Mitigation

The largest risk factor is the capital cost associated with building a wind farm. To mitigate this risk, we have formed PPAs with EV charging companies before construction begins to guarantee revenue upon completion.

CleanerGrid will reduce environmental impacts by continuously performing the due diligence to satisfy environmental, ecological, and societal assessments.

We are taking grid demand into consideration, by doing this we are ensuring our excess power does not go to waste. The business will adjust prices accordingly based on the grid demand. To mitigate this risk, we will be continually seeking EV companies to sign PPA's with, which will lower our excess energy available.

2. TECHNICAL DESIGN

2.1. Market Turbine

The business plan uses an off-the-shelf 3.5 MW turbine. The engineering team designed a model turbine like what would be purchased for the business plan. A model of the market team turbine was created in SolidWorks and a top-level design of the electrical system was created using Simulink, reference Figure 2. A large view of the SolidWorks model can be seen in the cover page of this report. Parameters resulting from the design of the market turbine are summarized in Table 2.

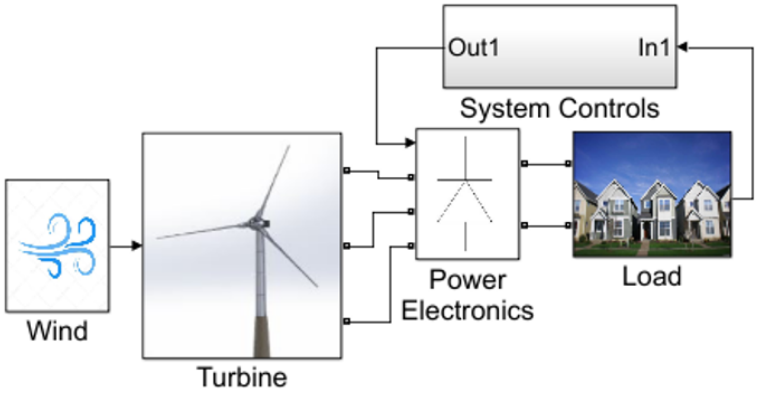


Figure 2: Market Turbine Electrical System Overview

2.1.1. Deviations from Test Turbine

The differences between the Tunnel and Market turbines are listed in Table 2.

Table 1: Tunnel and Market Turbine Comparison

Characteristic	Tunnel Turbine	Market Turbine
Average Reynolds Number	25,000	1,130,000
Number of Blades	3	3
Blade Airfoils	NACA 4410 NACA 5408 NACA 6308	S811 S810 S809
Cut in Speed	3 m/s (expected)	2 m/s
Rated Output Speed	10 m/s	10 m/s
Rated Power Output	26 W (expected)	3.9 MW
Cut out Speed	20 m/s	20 m/s
Rotor Diameter	44.5 cm	150 m
Tower Height	60.25 cm	120 m
Yaw System	Passive	Active
Pitching System	Active	Active
Maximum Power Coefficient (C_p)	0.22	0.39
Generator	Permanent Magnet Synchronous Generator	Permanent Magnet Synchronous Generator

2.2. Tunnel Turbine

The design objective of the turbine is to produce 26 W of power at wind speeds of 10 m/s. The turbine combines the following subsystems to meet the design requirements in the rules and regulations document: blades, hub, shaft, yaw, tower, nacelle, and brake. Figure 3 depicts the designed mechanical system. Reference Appendix B, Figure B.1 for an assembly drawing of the tunnel turbine.

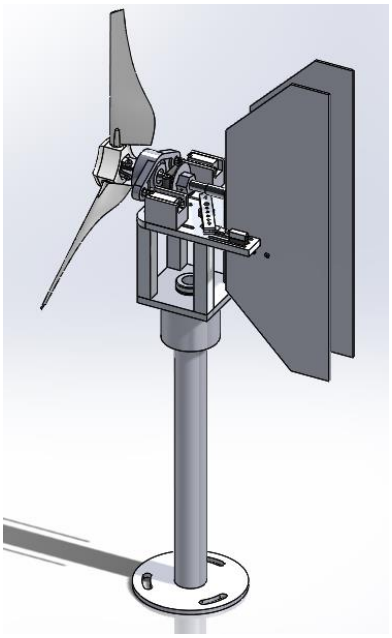


Figure 3: SolidWorks Model of Tunnel Turbine

2.2.1. Static Performance Analysis

The tunnel turbine blades were designed using MATLAB, analyzed in Qblade, and modeled in SolidWorks. The design tip speed ratio is 4.5, and associated power coefficient is 0.242. Figure 4 shows the power coefficient curve vs. the tip speed ratio. Figure 5 shows the power curve with a rated wind speed of 12 m/s.

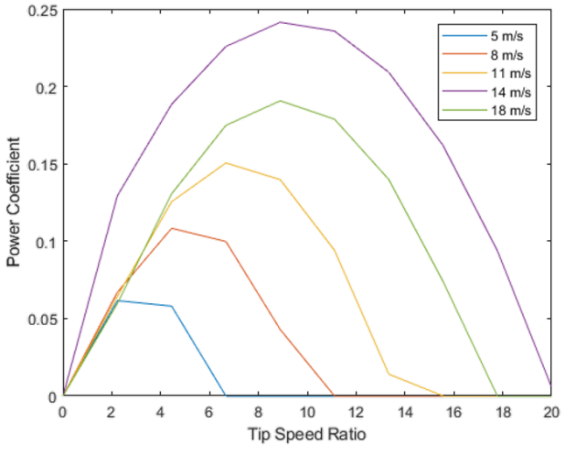


Figure 4: Power Coefficient vs. Tip-Speed Ratio

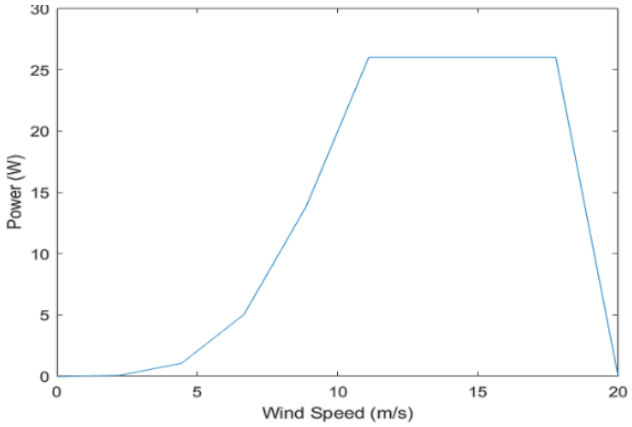


Figure 5: Power Curve

2.2.2. Mechanical Loads Analysis

Mechanical subsystems were analyzed using a multitude of software including SolidWorks, MATLAB, and Qblade, Table 3 summarizes factors of safety for mechanical components.

Table 3: Factors of Safety (FOS) for Mechanical Components

System	Material (s)	Loads Description	Loads Applied for analysis	Minimum FOS
Tower Shaft	4130 Alloy Steel	Distributed Drag Force, Targeted Thrust Force	F_D = 9 N Th = 37.5 N	8
Baseplate/ Tower Weld	4130/A36 Alloy Steels	Distributed Drag Force, Targeted Thrust Force	F_D = 9 N Th = 37.5 N	8.35
Blades	ULTEM 9085	Lift, Drag, Centrifugal	F_L 30N FD = 5N w = 650 rad/s	2.5
Hub	ABS 3D Filament, 6061 T6 Aluminum	Thrust Force, Centrifugal Force, Braking Torque	Th = 37.5 N w = 650 rad/s FB = 2210 kpa	2.75
Brakes	Zinc Coated Steel Disk, Rigid Molded Asbestos Pads	Applied Pad Pressure, Pad Force	p_a = 2210 kPa F = 1080.8 N	88.7
Nacelle	6061 T6 Aluminum	Targeted Thrust Force	Th =37.5N	149.3
Shaft	7075-T6 Aluminum	Rotor Torque Rotor Weight Brake Torque	T_R = 3 N-m WR = 4 N TB = 12.5 N-m	2.99

2.2.2.1. Blade Analysis

The thrust from the turbine was calculated from the maximum wind velocity, the density of air, and the rotor plane area. The maximum bending deflection and maximum stress were analyzed in SolidWorks. These forces were applied with the centrifugal forces from the rotation of the blades, the lift and drag forces associated with the blades. The lift and drag from each blade was found using coefficients of lift and drag from X-foil, the dynamic pressure, and the platform area of the blade. The load and factor of safety values are shown in Table 3.

2.2.2.2. Hub Analysis

The active pitching hub experiences dynamic thrust, torque loading and centrifugal tensile loading from the blade actuation and mounting. The hub material was selected through a MATLAB code that calculates maximum forces, and verified using SolidWorks FEA, as shown in Figure 6. The final materials, loads, and factor of safety are shown in Table 3.

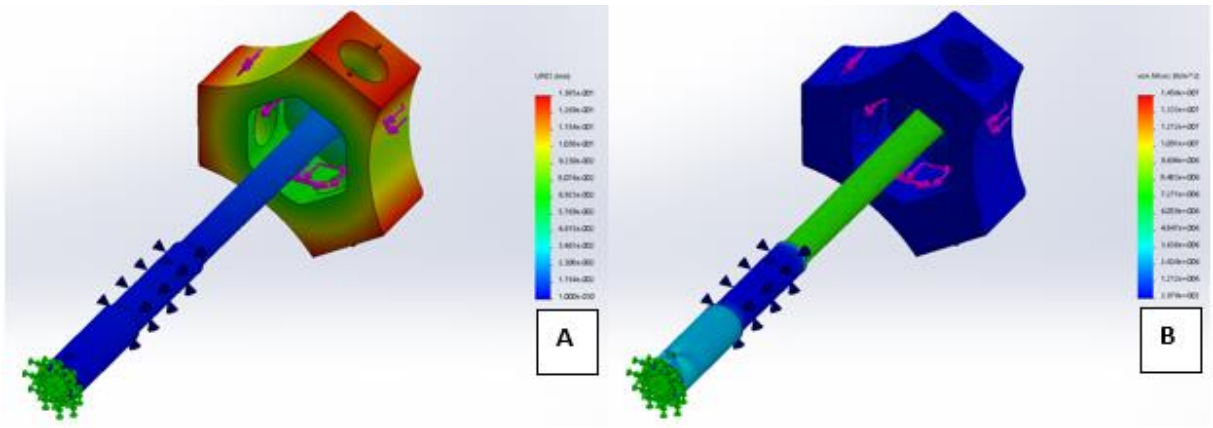


Figure 6: SolidWorks FEA: Hub displacement (A) and von Mises Stress (B).

2.2.2.3. Shaft Analysis

The shaft is directly-driven and simply supported. It handles dynamic forces at the rotor, shaft bearing, disk brake, and generator. The design was analyzed using DE-Gerber Failure Criterion in a MATLAB code, and verified in SolidWorks FEA. The material used was chosen because of its high tensile strength. Connections and expected load values are shown in Table 4.

Table 4: Shaft Connection Types and Expected Forces

Component	Connection Type	Expected Dynamic Loads
Rotor	M10x½ thread	T_R = 3 N-m W_R = 3.9 N
Shaft Bearing	Mounted	$F_{R,Be}$ = -114 N
Disk Brake	Hexagonal Radial Pin	T_B = 12.5 N-m W_B = 0.2 N
Generator	Set Screw	$F_{R,G}$ = 110 N

The rotor's expected torque on the shaft was multiplied by 2 to account for rotational inertia. The generator is assumed to provide a reactive force (similar to the shaft bearing), because the reactive torque from the connection is small. The final materials, loads, and factor of safety are shown in Table 3. Reference Appendix B, Figure B.2 for a SolidWorks drawing of the designed shaft.

2.2.2.4. Disk Brake System Analysis

The disk brake applies torque to the shaft to regulate its rotational speed. The components of the disk brake assembly were chosen because of their availability. The force the brake pad applies to the rotor disk via the linear actuator lever arm was found through a static analysis; reference Figure 7 for representation of the brake system. The brake pad and actuator are on opposite ends of the beam so when the actuator pulls on the beam, the pad is pushed onto the disk centered on the spinning shaft. The instantaneous torque applied to the shaft is adequate for stopping the shaft while being structurally stable. The materials, loads, and factors of safety can be seen in Table 3.

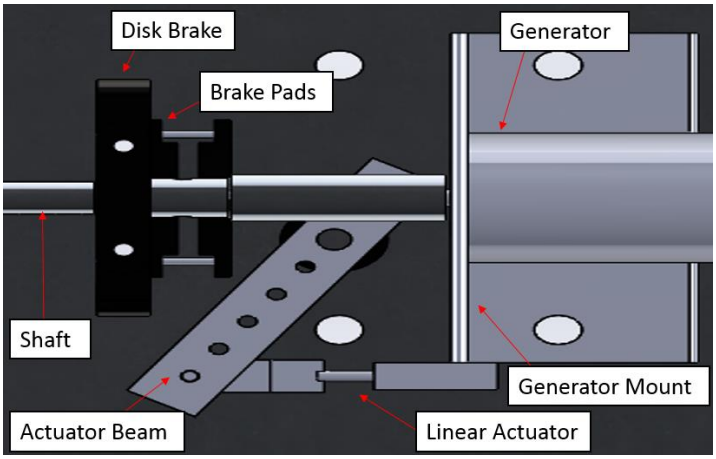


Figure 7: Disk Brake Assembly

2.2.2.5. Nacelle Analysis

The Nacelle supports each of the mechanical components of the wind turbine while maintaining structural integrity; reference Figure 8 for FEA analysis on this sub system. A two-plate approach was taken to fit a slip ring correctly and allow for proper rotation about the tower's axis without the electrical components tangling. The mechanical components attached to the nacelle are bolted with washers and spacers to align the shaft axis with the horizontal midplane inside the wind tunnel. The top plate is placed off center to allow the hub and plane of the blades to be closer to the tower's axis. This will cause the center of gravity to be closer to the tower's axis, creating a smaller moment for the yaw to correct. The final materials, loads, and factor of safety are shown in Table 3. Reference Appendix B, Figure B.3 for a SolidWorks drawing of the upper nacelle subsystem.

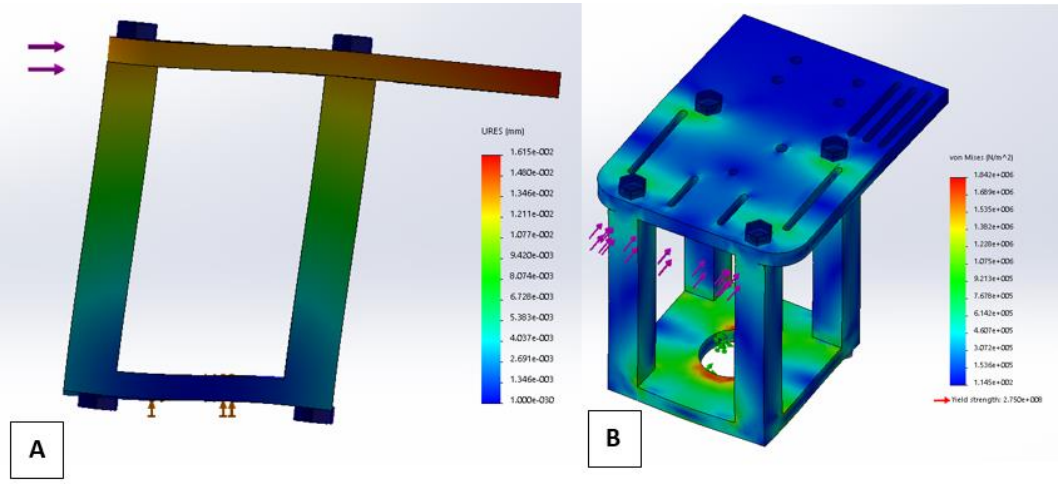


Figure 8: SolidWorks FEA: Nacelle displacement (A) and von Mises Stress (B).

2.2.2.6. Tower Analysis

The tower experiences a combined load of thrust, drag and gravitational forces. It was designed using a MATLAB code that solved for the outer diameter of the tower. All other factors, including the factor of

safety, were held constant and tested for potential materials. The baseplate to tower shaft connection was designed and confirmed in SolidWorks FEA, reference Figure 9. The tower shaft was designed for assembly with shelves for the baseplate connection and a bearing area for yawing. The materials, loads, and factor of safety are shown in Table 3.

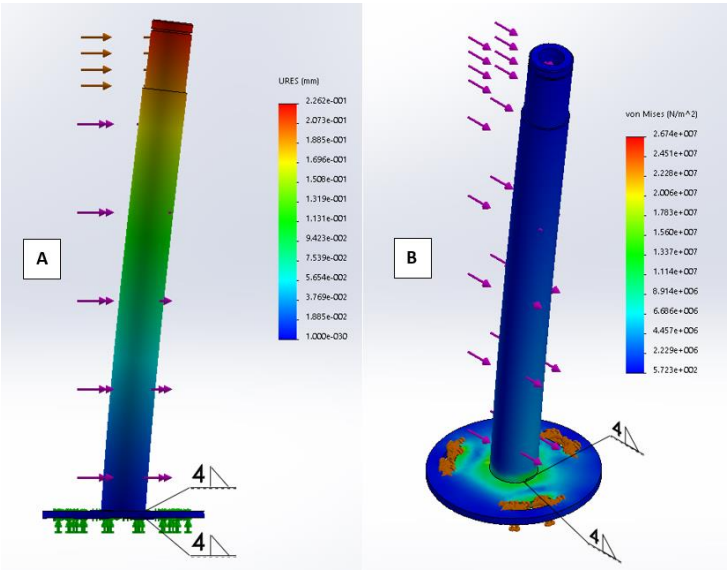


Figure 9: SolidWorks FEA: Tower Displacement (A) and von Mises Stress (B).

2.2.3. Yaw System

The Passive Yaw system is made from two bearings press fitted on the tower with an outer sleeve that is connected to the lower nacelle; reference Figure 10. The Yaw fins are made from ⅛" aluminum sheet metal. The tail boom length vs. rotor diameter ratio is not within the recommended range so this will be a source of yaw error. This dimension is limited by the size constraint noted in the competition. The yaw is a two-fin system because the tail boom length is shorter than recommended.

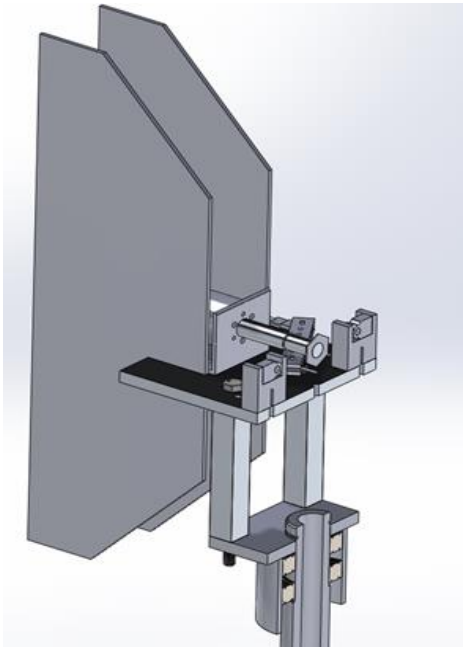


Figure 10: Section View of Bearing Sleeve Yaw system.

2.2.4. Electrical Analysis

The electrical system changes the three-phase input from the generator into a single signal for a passive rectifier. The rectifier is connected to a dump load and two separate boost converters. Reference Appendix B, Figure B.4 for the electrical topology of the boost converter. The dump load activates when the generator produces too much power for the system to handle. The buck/boost circuit is connected to the supercapacitor storage element, allowing for bi-directional power flow during the durability task. The main DC-DC converter in the system is a three-channel interleaved synchronous boost converter. The boost converter outputs a constant 5V by altering the duty cycle accordingly. After the primary boost

converter is the point of common coupling and load. To control the pitching and braking mechanisms, linear actuators are connected to relays controlled by the Arduino. Throughout the system are 2 voltage sensors (using voltage dividers) and 1 current sensor continuously sending data to the Arduino for proper control of the electrical system. Figure 11 depicts a full schematic of the electrical system for the tunnel turbine.

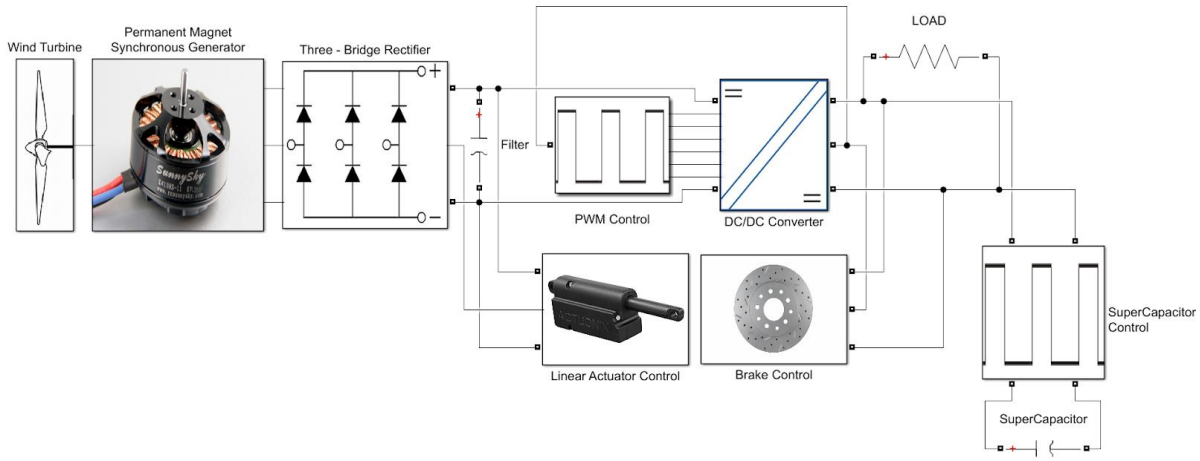


Figure 11: Tunnel Turbine Electrical System

2.2.5. Software Description

An Arduino Due performs all the control theory. This includes the control theory for the brakes, active pitching, hub, and boost converter. The boost converter is controlled using a voltage-oriented control algorithm that compares the output voltages and adjusts the duty cycle of the three PWM signals. All three channels have gating signals that are phase shifted by 120 degrees. A current sensor helps determine whether there is a shutoff of power in the system. The brakes are controlled by a solenoid that activates on two conditions, first when the button pressed, second when there is a cut off in power from the PCC. The hub is controlled by a linear actuator that activates depending on the voltage being sensed from the voltage divider.

2.2.6. Testing Results

2.2.6.1. Electrical Testing Procedures

Generator

The generator testing is performed using a dynamometer to monitor the voltage and current being produced by the generator. We use this to generate curves of voltage and current vs time and see what values we are putting out at important wind speeds, as well as what the maximum values are.

Arduino

For the Arduino testing, we first test just the code for the actuators and boost converter to determine whether it is working as intended. For the boost converter, the duty cycle must be adjustable to maintain a constant output voltage given a range of different input voltages. For the linear actuators, they must be able to extend, and contract based on the input values.

Linear Actuators

To test the linear Actuators, they are hooked up to the power supply of the Arduino to ensure that the 5V from the Arduino is adequate to power them. A code is then generated to extend and contract the actuators to ensure that they are actuating properly.

Boost Converters

For these 2 converters, we test them both individually by providing an input voltage from a voltage source and monitor the output voltage to confirm that they are putting out the correct values. We then cascade them in the same way that they are arranged in the circuit to ensure that the overall output is the 7V needed to safely power the Arduino.

Entire Electrical System

For the whole system test, the turbine is placed in the wind tunnel and subjected to a range of wind speeds to simulate the conditions it will be under during the competition. The current and voltage are monitored at several key points in the system to determine whether or not the system is working properly. These points are after the generator, after the rectifier, going into the Arduino, after the boost converter, and at the PCC. These measurements are taken using a multimeter or with the built-in voltage and current sensors within the circuit. Monitoring current and voltage at these points allows us to quickly isolate the component that is causing a problem if the system isn't working properly and determine what is wrong with it. It also ensures that these values are at safe levels and are not endangering certain components within our system.

During the test, the 2 main things we are looking for from the system as a whole are the power curve and the constant 5V output. The first test is a continuous ramping of the wind speed, which should give a power curve that ramps up with the wind speed and then eventually stabilizes and starts to decay at high wind speeds. This simulates the first test that will be performed at the competition. The second test is a simulation of the durability test at the competition, where the turbine is subjected to a range of wind speeds that fluctuate up and down and is expected to maintain a constant 5V output by charging and discharging the super capacitor. An equivalent durability task circuit model was created and is shown in Appendix B, Figure B.5.

2.2.6.2. Mechanical Testing Procedures

Blades

To begin testing the blades, the team sets them in a fixed position to test the overall strength. The wind tunnel is set to the maximum velocity of 20 m/s that the turbine will experience while testing and at the competition. The following procedure for the blades allow them to spin about the shafts axis to determine the blades' capabilities to handle angular forces at the maximum velocity.

Hub

The hub's testing procedures begins with placing the blades at the optimum performance setting. Linear actuators are used to offset the blades at a setting that allows for more torque by targeting a distance away from the hub for the actuators to be mounted. Once the targeted distance for the linear actuators is found, the wind tunnel is turned on and both the optimum performance setting and the higher torque setting are tested at the maximum wind speed. After the hub is tested at the two performance settings, the actuators are tasked with rotating the blades between the two settings at the maximum wind speed. This determines

the hub's capabilities of pitching the blades with the highest stress factors.

Tower/Baseplate/Nacelle

The components are tested throughout each testing procedure and experience minimum to maximum forces during each test. The structural components of the turbine are visually measured while the wind tunnel is in operation.

Brake

Testing the brake requires the wind tunnel to be set to the maximum velocity that the turbine will experience at the competition. This wind speed produces the maximum torsional forces on the shaft, which requires the brake to perform better than at lower wind speeds. The brake is applied in small increments to avoid damage to the brake as well as the other components of the turbine. The brake is only required to reach a rotational speed that is below 10% of the average RPM that the turbine produces. The average RPM is based on five separate wind speed settings during testing. The rotational speed is measured during the braking test to determine if the rotors are under this 10% limit if the brakes are unable to stop the rotor completely.

Yaw

The yaw test is begun by setting the turbine at a 10° offset from direction of the wind. The wind tunnel is then turned on with an increasing velocity until the yaw corrects the direction of the turbine. This process is repeated by increasing the angle offset by increments of 10° until a 180° offset is tested, or until the yaw no longer corrects the turbines direction.

Shaft

The shaft is the last mechanical component to be fully tested. Once each of the other components are tested, the wind tunnel is turned on while slowly increasing the wind speed, and the shaft's ability to withstand forces while each of the previous tests are performed simultaneously. The combined test incorporates the hub pitching and rotating the blades from the high torque setting to the optimum performance setting, while the brakes attempt to slow down the rotor once the maximum wind speed is reached.

3. REFERENCES

[1] Cision PR Newswire, "The global market for electric vehicle (EV) will grow from $75.7 billion in 2017 to around $127.7 billion by 2022 with a compound annual growth rate (CAGR) of 11.0% for the period of 2017-2022".

[2] USA Today, "Number of electric vehicle charging points to rise significantly in 2018".

[3] A. C. a. K. Schefter, "Plug-in Electric Vehicle Sales Forecast Through 2025 and the Charging Infrastructure Required," *Edison Electric Institute*, 2017.

[4] U.S. Energy Information Administration, "What is U.S. electricity generation by energy source?," 2018.

[5] T. Moloughney, "How Much Does It Cost To Charge An Electric Car?," *Plug In America.*

[6] U.S. Energy Information Administration, "Renewable Energy Explained," 2017.

[7] Carmax, "2017 Hybrid & Electric Cars Survey Results," 2017.

[8] SRP, "2035 Sustainability Goals Delivering today, shaping tomorrow".

[9] U.S. Department of Energy, "Emissions from Hybrid and Plug-In Electric Vehicles," *Fuels and Vehicles.*

[10] International Energy Agency, "Renewables 2017".

[11] Bloomberg New Energy Finance, "Electric Vehicle Outlook 2017," 2017.

[12] The Guardian, "Electric car owners 'can drive for free by letting energy firms use battery'".

[13] MathWorks, "24-hour Simulation of a Vehicle-to-Grid (V2G) System".

[14] National Renewable Energy Laboratory (NREL), "System Advisory Model (SAM)".

[15] American Wind Energy Association, "The Cost of Wind Energy in the U.S".

3. APPENDIX A: BUSINESS FINANCIALS

Table A.1: CleanerGrid's Income Statement

Year	2018	2019	2020	2021	2022	2023	2024	2025
Production: Actual KWh		**386,316,000**	**386,316,000**	**386,316,000**	**386,316,000**	**772,632,000**	**772,632,000**	**772,632,000**
Sales (EV)	$0	$1,729,878	$3,700,332	$6,940,632	$12,019,961	$19,669,389	$30,852,205	$46,831,698
Sales (Grid)	$0	$7,149,694	$6,570,139	$5,490,039	$3,796,929	$9,050,703	$5,323,098	$0
V2G	$0	$0	$0	$42,873,948	$42,873,948	$42,873,948	$42,873,948	$42,873,948
Revenue	$0	$8,879,572	$10,270,471	$55,304,619	$58,690,839	$71,594,040	$79,049,251	$89,705,646
Operating Expenses								
Marketing	$0	$50,000	$100,000	$200,000	$200,000	$200,000	$200,000	$200,000
Research & Development	$500,000	$100,000	$100,000	$500,000	$100,000	$100,000	$100,000	$100,000
Leasing of Land (Turbines)	$224,000	$224,000	$224,000	$224,000	$224,000	$448,000	$448,000	$448,000
Operation & Maintanance	$0	$2,576,003	$2,640,403	$2,706,414	$2,774,074	$5,686,852	$11,658,046	$23,898,993
Utilities	$6,000	$6,000	$6,000	$6,000	$6,000	$6,000	$6,000	$6,000
Rent Expense (Building)	$20,000	$20,000	$20,000	$20,000	$20,000	$20,000	$20,000	$20,000
Insurance	$815,217	$835,597	$856,487	$877,900	$899,847	$1,844,686	$3,781,607	$7,752,295
Depreciation	$0	$32,114,384	$32,114,384	$31,219,199	$19,022,576	$51,116,617	$41,967,498	$31,932,969
Total Operating Expenses	$1,565,217	$35,925,985	$36,061,275	$35,753,512	$23,246,497	$59,422,155	$58,181,151	$64,358,257
Administrative Expenses								
Supplies	$17,700	$4,000	$4,000	$4,000	$4,000	$4,000	$4,000	$4,000
Professional Fees (Legal, contracting, etc)	$8,150,000	$1,630,000	$1,630,000	$1,630,000	$8,150,000	$1,630,000	$8,150,000	$1,630,000
Salary	$180,000	$210,000	$270,000	$270,000	$270,000	$270,000	$270,000	$270,000
Total Adminstrative Expenses	$8,347,700	$1,844,000	$1,904,000	$1,904,000	$8,424,000	$1,904,000	$8,424,000	$1,904,000
Operating Income	-$9,912,917	-$28,890,413	-$27,694,803	$17,647,107	$27,020,342	$10,267,885	$12,444,101	$23,443,389
Non-Operating Expenses								
Interest Expense	$8,384,668	$8,124,846	$7,851,731	$7,564,642	$7,262,866	$6,945,651	$6,612,206	$6,261,701
Total Non-Operating Income	$8,384,668	$8,124,846	$7,851,731	$7,564,642	$7,262,866	$6,945,651	$6,612,206	$6,261,701
EBT	-$18,297,585	-$37,015,258	-$35,546,534	$10,082,465	$19,757,476	$3,322,235	$5,831,895	$17,181,688
Rate (State and Federal)	**0.22**	**0.22**	**0.22**	**0.22**	**0.22**	**0.22**	**0.22**	**0.22**
Income Tax (State and Federal)	$ -	$ -	$ -	$2,218,142	$4,346,645	$730,892	$1,283,017	$3,779,971
Production Tax Credit ($/KWh)	**$0.014018**	**$0.014228**	**$0.014442**	**$0.014658**	**$0.014878**	**$0.015101**	**$0.015328**	**$0.015558**
Production Tax Credit	$0	$5,496,608	$5,579,057	$5,662,743	$5,747,684	$11,667,800	$11,842,817	$12,020,459
Net Income	-$18,297,585	-$31,518,650	-$29,967,476	$13,527,066	$21,158,515	$14,259,143	$16,391,694	$25,422,175

Table A.2: CleanerGrid's Balance Sheet

Year	2018	2019	2020	2021	2022	2023	2024	2025
Assets								
Current Assets:								
Cash	$ -	$ 8,139,608	$ 10,154,563	$ 51,551,774	$ 58,408,654	$ 70,518,774	$ 78,427,984	$ 88,817,613
Accounts Receivable	$ -	$ 739,964	$ 855,873	$ 4,608,718	$ 4,890,903	$ 5,966,170	$ 6,587,438	$ 7,475,470
Prepaid land lease	$ 224,000	$ 224,000	$ 224,000	$ 224,000	$ 224,000	$ 448,000	$ 448,000	$ 448,000
Development/Expansion Capital	$ 43,958,332	$ -	$ -	$ -	$ 40,510,103	$ -	$ -	$ -
Other assets	$ -	$ 36,281,675	$ 22,494,186	$ 7,067,822	$ -	$ 22,930,825	$ -	$ -
Total Current Assets	$ 44,182,332	$ 45,385,247	$ 33,728,622	$ 63,452,314	$ 104,033,660	$ 99,863,769	$ 85,463,421	$ 96,741,084
Property, Plant, & Equipment								
Turbines	$ 117,600,000	$ 117,600,000	$ 117,600,000	$ 117,600,000	$ 235,200,000	$ 235,200,000	$ 235,200,000	$ 235,200,000
Less depreciation	$ -	$ 32,114,384	$ 32,114,384	$ 31,219,199	$ 19,022,576	$ 51,116,617	$ 41,967,498	$ 31,932,969
Equipment	$ 13,000	$ 13,000	$ 13,000	$ 13,000	$ 13,000	$ 13,000	$ 13,000	$ 13,000
Total PP&E	$ 117,613,000	$ 85,498,616	$ 85,498,616	$ 86,393,801	$ 216,190,424	$ 184,096,383	$ 193,245,502	$ 203,280,031
Total Assets	$ 161,795,332	$ 130,883,863	$ 119,227,238	$ 149,846,115	$ 320,224,084	$ 283,960,152	$ 278,708,923	$ 300,021,115
Liabilities								
Current Liabilities:								
Loan Payable (First Loan)	$ 13,463,088	$ 13,463,088	$ 13,463,088	$ 13,463,088	$ 13,463,088	$ 13,463,088	$ 13,463,088	$ 13,463,088
Loan Payable (Second loan)	$ -	$ -	$ -	$ -	$ 13,463,088	$ 13,463,088	$ 13,463,088	$ 13,463,088
Accounts Payable	$ 9,912,917	$ 5,655,601	$ 5,850,891	$ 6,438,313	$ 12,647,921	$ 10,209,538	$ 24,637,653	$ 34,329,288
Accrued Wages	$ 180,000	$ 210,000	$ 270,000	$ 270,000	$ 270,000	$ 270,000	$ 270,000	$ 270,000
Total Current Liabilities	$ 23,556,005	$ 19,328,689	$ 19,583,979	$ 20,171,401	$ 39,844,097	$ 37,405,714	$ 51,833,829	$ 61,525,464
Long-term Liabilities:								
Long-term debt (First loan)	$ 156,536,912	$ 143,073,824	$ 129,610,736	$ 116,147,648	$ 102,684,560	$ 89,221,472	$ 75,758,384	$ 62,295,296
Long-term debt (Second loan)	$ -	$ -	$ -	$ -	$ 156,536,912	$ 143,073,824	$ 129,610,736	$ 116,147,648
Total Long-term Debt	$ 156,536,912	$ 143,073,824	$ 129,610,736	$ 116,147,648	$ 259,221,472	$ 232,295,296	$ 205,369,120	$ 178,442,944
Owner's Equity								
Retained Earnings	$ (18,297,585)	$ (31,518,650)	$ (29,967,476)	$ 13,527,066	$ 21,158,515	$ 14,259,143	$ 16,391,694	$ 25,422,175
Additional Captial Expenditures	$ -	$ -	$ -	$ -	$ -	$ -	$ 5,114,280	$ 34,630,532
Total Owners' Equity	$ (18,297,585)	$ (31,518,650)	$ (29,967,476)	$ 13,527,066	$ 21,158,515	$ 14,259,143	$ 21,505,974	$ 60,052,707
Total Liabilities & Owners' Equity	$ 161,795,332	$ 130,883,863	$ 119,227,238	$ 149,846,115	$ 320,224,084	$ 283,960,152	$ 278,708,923	$ 300,021,115

Table A.3: CleanerGrid's Cash Flow

Cash Flow From Operations	2018	2019	2020	2021	2022	2023	2024	2025
Net Income	-$18,297,585	-$31,518,650	-$29,967,476	$13,527,066	$21,158,515	$14,259,143	$16,391,694	$25,422,175
Account Receivable Increase	$0	-$739,964	-$855,873	-$4,608,718	-$4,890,903	-$5,966,170	-$6,587,438	-$7,475,470
Prepaid Expenses increase	-$224,000	-$224,000	-$224,000	-$224,000	-$224,000	-$448,000	-$448,000	-$448,000
Plus Depreciation	$0	$32,114,384	$32,114,384	$31,219,199	$19,022,576	$51,116,617	$41,967,498	$31,932,969
Accounts Payable Increase	$9,912,917	$5,655,601	$5,850,891	$6,438,313	$12,647,921	$10,209,538	$24,637,653	$34,329,288
Total Cash Flow From Operations	**-$8,608,668**	**$5,287,370**	**$6,917,926**	**$46,351,860**	**$47,714,109**	**$69,171,127**	**$75,961,408**	**$83,760,962**
Cash Flow From Investing								
Turbines	$117,600,000	$0	$0	$0	$117,600,000	$0	$0	$0
Purchase of equipment	$17,700	$4,000	$4,000	$4,000	$4,000	$4,000	$4,000	$4,000
Total Cash Flow From Investing	**$117,617,700**	**$4,000**	**$4,000**	**$4,000**	**$117,604,000**	**$4,000**	**$4,000**	**$4,000**
Cash Flow From Financing								
Repayment of First Loan	$13,463,088	$13,463,088	$13,463,088	$13,463,088	$13,463,088	$13,463,088	$13,463,088	$13,463,088
Repayment of Second Loan	$0	$0	$0	$0	$13,463,088	$13,463,088	$13,463,088	$13,463,088
Total Cash Flow From Financing	$13,463,088	$13,463,088	$13,463,088	$13,463,088	$26,926,176	$26,926,176	$26,926,176	$26,926,176
Net Cash	-$139,689,456	-$8,179,718	-$6,549,162	$32,884,772	-$96,816,067	$42,240,951	$49,031,232	$56,830,786

4. APPENDIX B: TUNNEL TURBINE DRAWINGS

Figure B.1: Tunnel Turbine Final Assembly

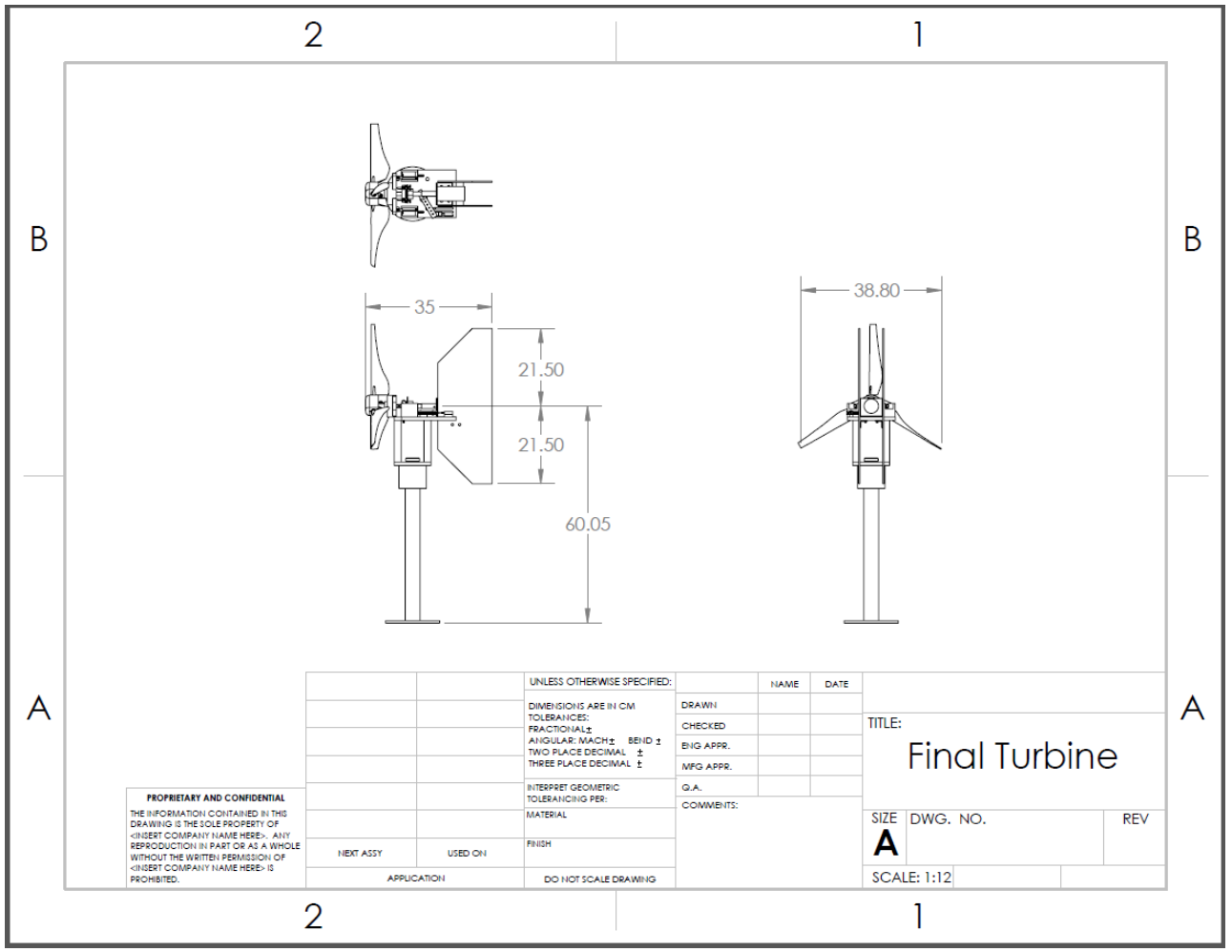


Figure B.2: Tunnel Turbine Shaft

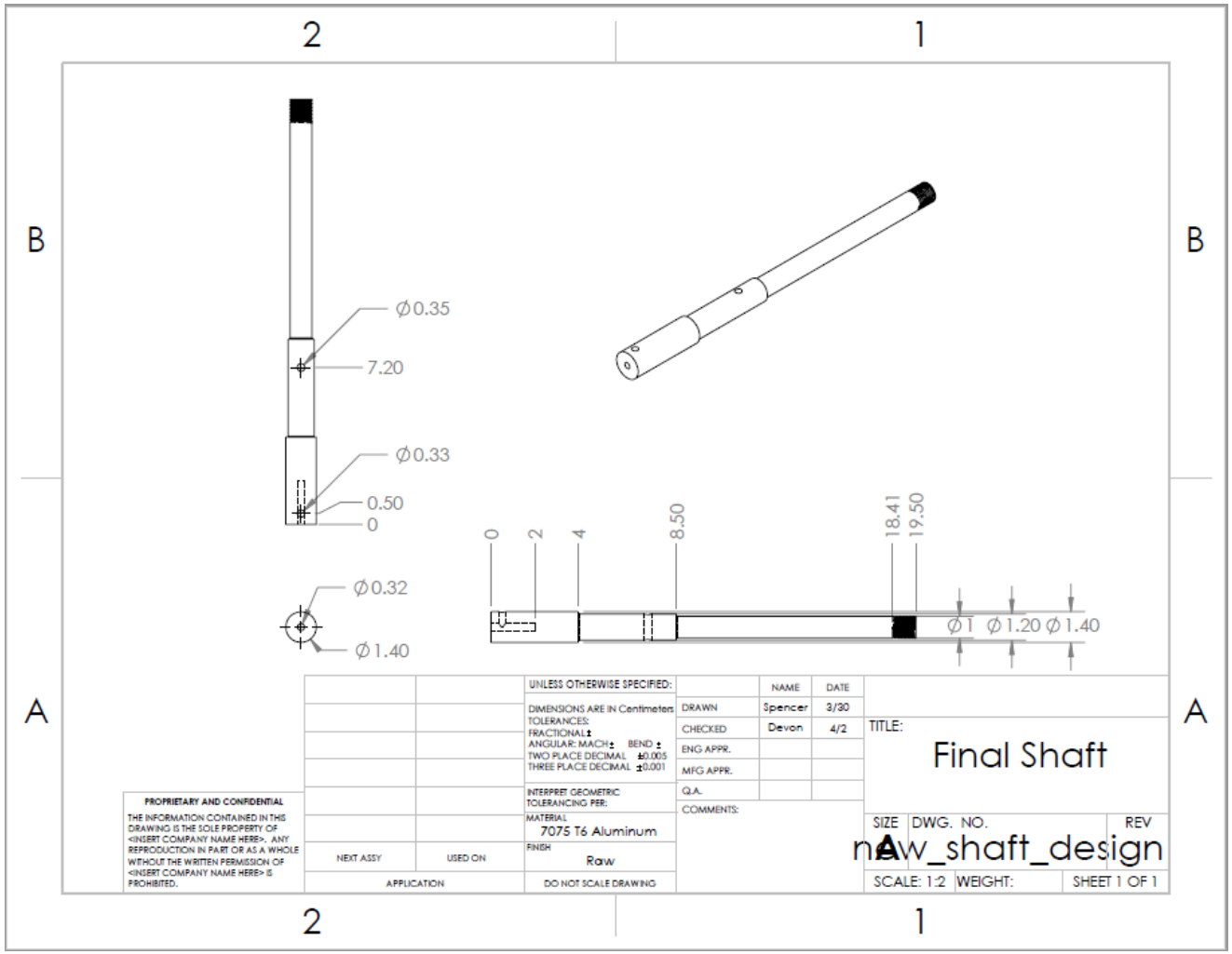


Figure B.3: Tunnel Turbine Upper Nacelle

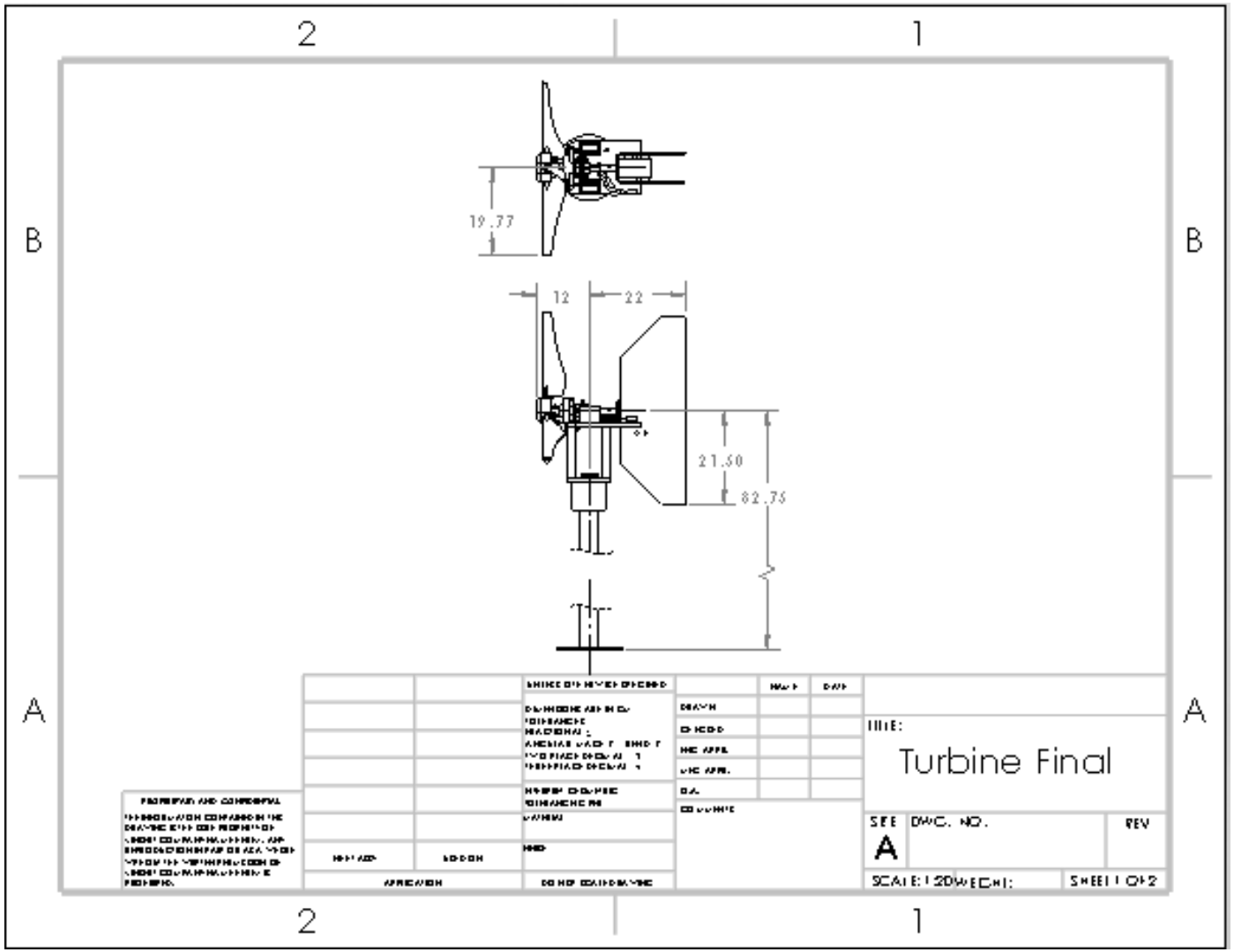


Figure B.4: Tunnel Turbine Electrical Topology for Boost Converter

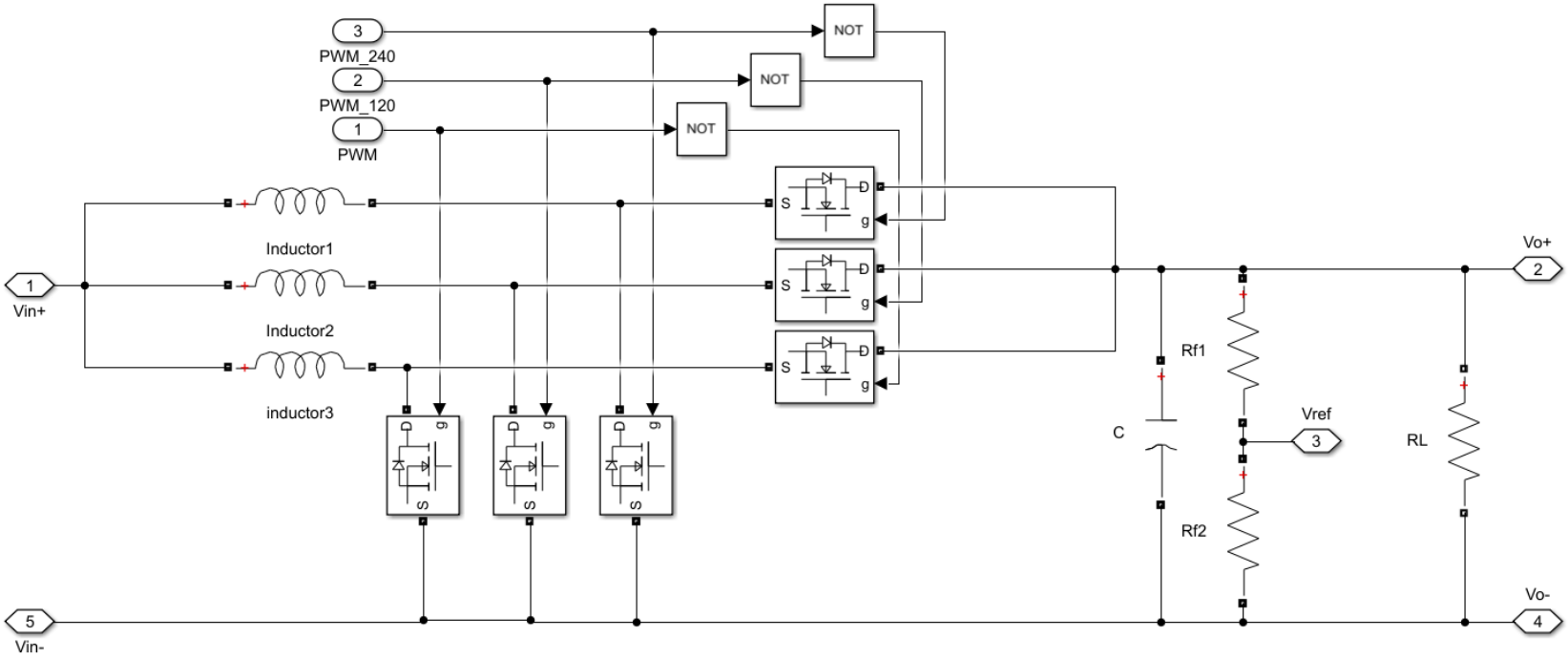
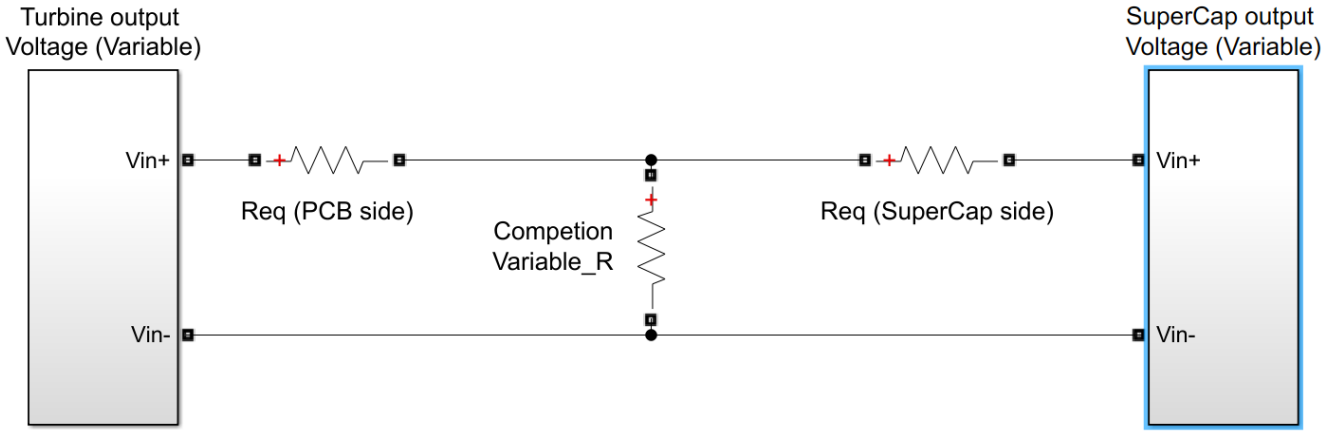


Figure B.5: Durability Test Equivalent Circuit Model



NORTHERN ARIZONA UNIVERSITY

College of Engineering, Informatics, and Applied Sciences

Tunnel Turbine Technical Report

Submission Date: April 20, 2019



Collegiate Wind Competition 2019

Mechanical Design Tunnel Team:

Riley Sinek (rps62@nau.edu) - Blade & Pitching Design
Tanner Lehr (tdl73@nau.edu) - Brake, Nacelle, & Tower Design
Naser Alrashidi (nea63@nau.edu) - Shaft Design
Faisal Alrashidi (fea26@nau.edu) - Yaw-Tail Design

Electrical Design Tunnel Team:

Abdallah Alsharrah (ana326@nau.edu) - Buck Converter
Juntong Liu (jl2986@nau.edu) - Simulations & Modeling
Chris Taylor (cmt348@nau.edu) - Rectifier & Boost Converter

Faculty Mentors:

David Willy (David.Willy@nau.edu) - PI and Mechanical Technical Advisor
Venkata Yaramasu (Venkata.Yaramasu@nau.edu) - Electrical Technical Advisor

Executive Summary

Team NAU is competing for the sixth time in the Department of Energy Collegiate Wind Competition. The 2019 team iterated on the previous year's designs with a focus on an active pitching mechanism which has yet to be successfully completed by any previous NAU team. The design constraints were derived from the competition rules and include size, power, and safety requirements.

The turbine designed by Team NAU in 2019 is a three-bladed upwind horizontal axis wind turbine that features an active pitching mechanism, passive yawing system, open nacelle with up-tower slip ring and rectifier, and buck and boost converter. In this document, the team summarized their efforts in completing the turbine design which included simulations done to evaluate the performance of the turbine, mechanical loads, and electric systems. The turbine endured thorough bench testing done for each component of the system to ensure success during full scale testing. The details of the team's yearlong effort to complete the mechanical and electrical aspects of the design are highlighted within this document. The mechanical engineer's comprehensive explanation of the technical design includes analysis of each component used for the final design of the wind turbine. A separate team of electrical engineers headed the design and production of the electrical systems for the wind turbine. The design process for the three converters is described and images of the final products are provided. A full electrical analysis was conducted to ensure cooperation between the components and verify functionality for competition. The controls and software analysis were used to determine which software would be used for the design of the turbine. Bench testing on all mechanical and electrical components demonstrated that the prototypes would perform during competition. Once all individual aspects of the design were tested, the components were connected and tested as a full system. Team NAU is still conducting testing as competition approaches. With competition quickly approaching, Team NAU is working diligently to complete all necessary testing before showcasing our complete design.

Contents

1 Technical Design 1
1.1 Static Performance Analysis 1
1.2 Mechanical Loads Analysis 1
1.2.1 Blades 2
1.2.2 Hub 2
1.2.3 Shaft 3
1.2.4 Brakes 3
1.2.5 Nacelle 4
1.2.6 Tower 4
1.2.7 Yaw System 5
2 Electrical Design 6
2.1 AC/DC Rectifier 7
2.2 DC/DC Boost Converter 8
2.3 DC/DC Buck Converter 9
3 Electrical Analysis 10
4 Controls Analysis and Software Documentation 10
5 Testing 10
5.1 Generator 10
5.2 Arduino 11
5.3 Linear Actuators 11
5.4 Rectifier 11
5.5 Boost Converter 12
5.6 Buck Converter 12
5.7 Entire Electrical System 12
5.8 Mechanical Testing Procedures 12
5.9 Future Testing 13
6 References 14
Appendix A 15

List of Tables

Table 1-1: Blade Geometry 1
Table 2-1: AC/DC Rectifier 7
Table 2-2: DC/DC Boost Converter 9
Table 2-3: DC/DC Buck Converter 9
Table 5-1: Brake Testing Results 12

List of Figures

Figure 1-1: Blade FEA results 2
Figure 1-2: Hub Claws FEA Results 2
Figure 1-3: Hub FEA Results 3
Figure 1-4: Shaft FEA Results 3
Figure 1-5: Brake Configuration 4
Figure 1-6: Nacelle FEA results 4
Figure 1-7: Tower FEA Results 5
Figure 1-8: Yaw Bearing Assembly 5
Figure 1-9: Tail FEA Analysis 6
Figure 2-1: AC/DC Rectifier 6
Figure 2-2: Buck Converter 6
Figure 2-3: Boost Converter 7
Figure 2-4: Rectifier 8
Figure 2-5: DC/DC Boost Converter One Line Diagram 8
Figure 2-6: DC/DC Boost Converter 9
Figure 5-1: Generator Power Capabilities vs. Blades' Theoretical Output 11
Figure 5-2: Rectifier Testing 12

1 Technical Design

The design objective for Team NAU in the 2019 competition was to optimize components of the wind turbine by iterating upon last year's design. The disassembly of Team NAU's previous turbine provided strong insight to the design of this year's tunnel turbine. Between faculty advising and competition rules [1], the team was able to compile a list of **Design Objectives**:

- Wind speeds up to 20 m/s
- Yaw rates up to 180°/s
- Rotor axis 60±3cm above flange
- 45-by-45-by-45 cm^3 volume cube
- Modular design
- Increased Rotor Solidity
- Integrated parts
- Reliable braking design
- Active pitching mechanism

1.1 Static Performance Analysis

The geometry of the blades was determined using the blade element momentum (BEM) theory to optimize the characteristics for discretized elements of the blade. BEM receives tip-speed ratio, blade length, ideal angle of attack, and number of blades [2]. The code was built to iterate using this theory used the inputs to determine the shape of the blade, including chord length, angle of relative wind, and twist at each section of the blade. Using a tip-speed ratio of 5, a blade length of 17cm, and an ideal attack angle of 5°, the results for blade geometry were determined and could then be exported to Q-Blade for simulations. The results that were exported to Q-Blade for the final iteration are shown in Table 1-1.

Table 1-1: Blade Geometry

Radius from root(cm)	chord(cm)	Rel. Wind direction(°)	Twist(°)
0.5	7.5	54.42	49.42
2.3	7.167	37.03	32.03
4.17	6.493	26.14	21.14
6	5.35	19.69	14.69
7.83	4.42	15.64	10.64
9.67	3.73	12.92	7.92
11.5	3.21	10.98	5.98
13.33	2.81	9.54	4.54
15.167	2.5	8.42	3.42
17	2.24	7.54	2.54

The Reynold's number for the blade geometry was calculated along the length of the blade for two primary scenarios. These scenarios were the start-up and operating conditions for the blade. The Reynold's numbers were used with resources from *airfoiltools.com* [3] to determine the airfoils that would be implemented into the blade. The team elected to incorporate three airfoils throughout the length of the blades, each having a high camber to achieve ideal lift characteristics within the low Reynold's number operating environment for the blades.

After completing the airfoil selection process, the blade geometry and airfoils were used in Q-Blade to create a 3D model to complete analysis on. The Q-Blade results showed that the turbine should output approximately 40W at an anticipated rated wind speed of 11m/s [4].

1.2 Mechanical Loads Analysis

Team NAU performed thorough Finite Element Analysis (FEA) in SolidWorks on each component of the design to achieve a safe and reliable design. As advised, the turbine was built to anticipate the failure of certain components, and therefore the turbine was designed for quick maintenance when necessary.

1.2.1 Blades

The blades were assumed to be stressed under thrust and centrifugal forces. The thrust calculation performed found that the blades achieved a thrust force of 25N. The centrifugal force of the blades was applied at an angular velocity of 5500rpm. The combined forces were applied to the blade using nylon 101 as the selected material in SolidWorks, as a substitute for the chosen carbon-fiber reinforced nylon filament. The material was chosen because it had similar strength characteristics to the filament selected by the team, aside from the modulus of elasticity. As the simulation results show in Figure 1-1, the current minimum **factor of safety is .785** due to a small stress concentration point near the blade root, circled in red in Figure 1-1. To address this concern, the team layered the printed blades with an epoxy coating, which is anticipated to increase the strength of the blades at each point. Due to the higher elastic modulus in the reinforced nylon, the team does not expect the blade to deflect to the degree that the simulation currently shows.

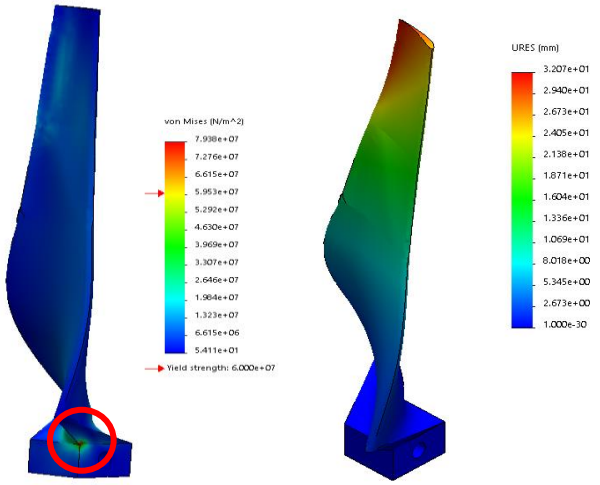


Figure 1-1: Blade FEA results

1.2.2 Hub

Each component of the hub was manufactured out of 6061 aluminum, and the FEA simulations were performed on the same material. For the hub claws, the primary force applied was the effective centrifugal force from the blades. The FEA results showed promising safety for the hub claws along with minimal deflection during operation. The minimum **factor of safety** for the claws was found to be **1.32**. The results for the claw are shown in Figure 1-2.

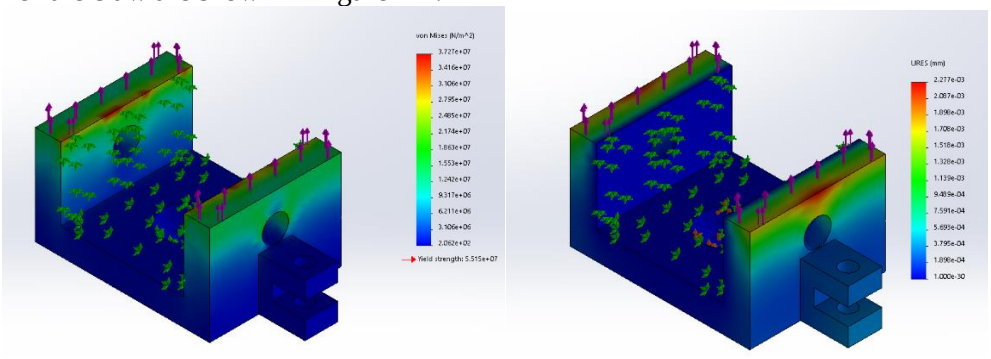


Figure 1-2: Hub Claws FEA Results

Furthermore, FEA stress and deflection analyses were completed on the main hub to determine the safety of the design. Between the claw and blade, it was estimated that the hub should withstand a maximum force of 300lbs. in the direction of each blade. The **factor of safety** of the design was found to be **1.17** for

the hub at maximum rotor angular velocity. The results of the stress and deformation simulations are shown in Figure 1-3 below.

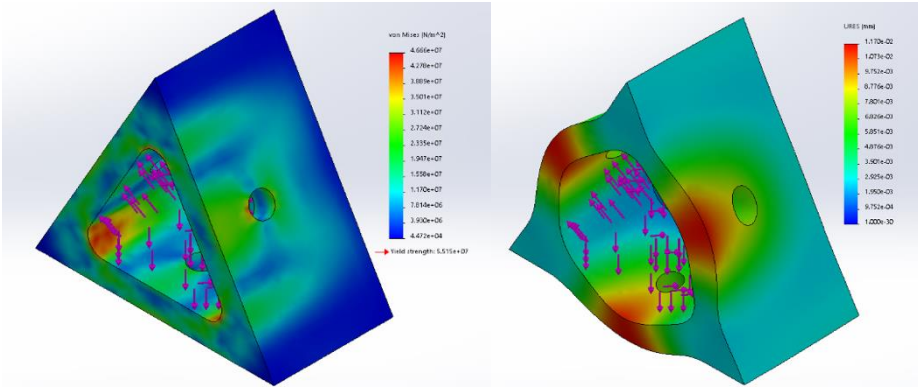


Figure 1-3: Hub FEA Results

1.2.3 Shaft

The main forces that will be seen along the shaft will be torque from the rotor and generator. Since the maximum angular velocity produced from the blades will be 5500rpm with a resulting torque of 3N-m. In order to show that the shaft design is safe enough, SolidWorks FEA was used to find out how much stress could be applied. After 5N-m of torque was applied across the shaft, it showed that the maximum stress of 351 MPa would be on the turned down section near the generator. This is most likely because it is a small diameter for a small length across the shaft. The FEA results for the shaft are shown in Figure 1-4.

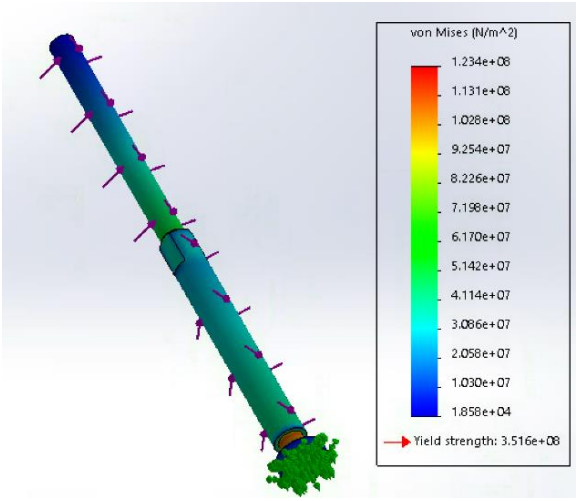


Figure 1-4: Shaft FEA Results

1.2.4 Brakes

To have a good braking system, the design was iterated on multiple times to ensure that the brakes would be reliable. The main constraints that drove the design were size, consistency, and being able to incorporate a bearing block into the design. The brake pads are standard disc brakes for a mountain bike. This was incorporated with a 6061-T6 aluminum disc, which was machined in-house. The brake pads and rotor disc were selected due to how well they work on high end mountain bikes. To incorporate this design into the turbine, a brake caliper with a bearing block was designed to hold everything in place. This was also machined out of 6061-T6 aluminum to ensure safety from the torque applied by the brake. The configuration of the brakes is shown below in Figure 1-5.

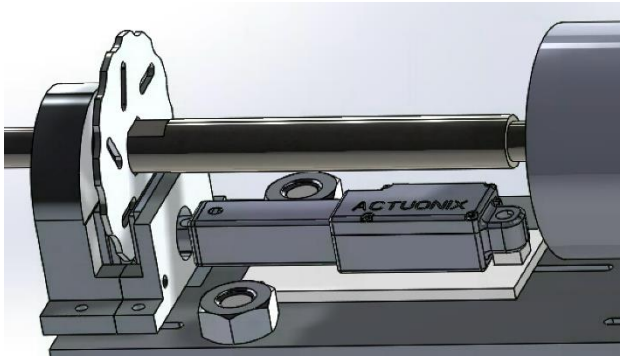


Figure 1-5: Brake Configuration

The brake force that can be applied by the linear actuator is 22N. When considering the diameter of the disc rotor and the area of the brake pads the clamping force can be estimated at 530N [5]. To ensure that the disc rotor would not sheer when that amount of pressure is applied, the actuator will gradually clamp down onto the rotor.

1.2.5 Nacelle

The nacelle was designed to house all mechanical components, as well as some electrical components. To make sure the design would be able to hold up during testing, it was machined out of 6061-T6 aluminum. A force of 35N was applied due to drag from the wind as well as the thrust force from the rotor (23N) in SolidWorks FEA. The maximum stress that is resulted from the wind and thrust is 55 MPa, which can be seen below in Figure 1-6.

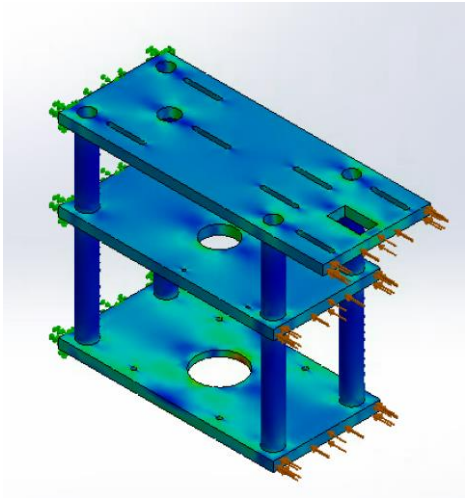


Figure 1-6: Nacelle FEA results

All the mechanical and electrical components that are mounted to the frame are using nylon insert locking nuts, star washers, and Loctite to ensure that nothing comes loose during testing.

1.2.6 Tower

During testing the tower must be able to withstand loads coming from the wind and the mechanical thrust from the blades. To ensure that the tower would be able to withstand those forces, 1018 steel was chosen. The same material was chosen for the baseplate. This would guarantee that the strength of the weldment would be equivalent on both the tower and base plate. The wind and thrust forces that are expected in the tunnel were used to calculate the yield stress, deflection, and factor of safety (shown in Figure 1-7). These results are as followed: 5.5MPa, .07mm, **46.5 factor of safety**.

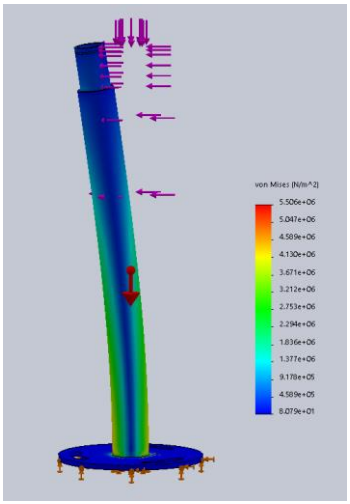


Figure 1-7: Tower FEA Results

1.2.7 Yaw System

For the competition, the yaw system is a passive system that allows the turbine to turn into the direction of the wind. For this design, a tail vane is needed to cooperate with a bearing assembly at the top of the tower.

1.2.7.1 Yaw Bearing Design

When designing the yaw bearing assembly, the main criteria was that it needed to be able to yaw at least 180°/s when in the wind tunnel. This allows for a complete change in wind direction that the turbine must adjust to. To accommodate this, two bearings with a low friction factor were used to ensure that the turbine can turn adequately. Alongside the two bearings, there is a spacer in between them to ensure the races of the bearings are not interfering with one another. An aluminum sleeve is attached to the nacelle and used as a cover for the bearings, allowing the nacelle to spin while still being supported by the tower. A figure of the design can be seen in Figure 1-8.

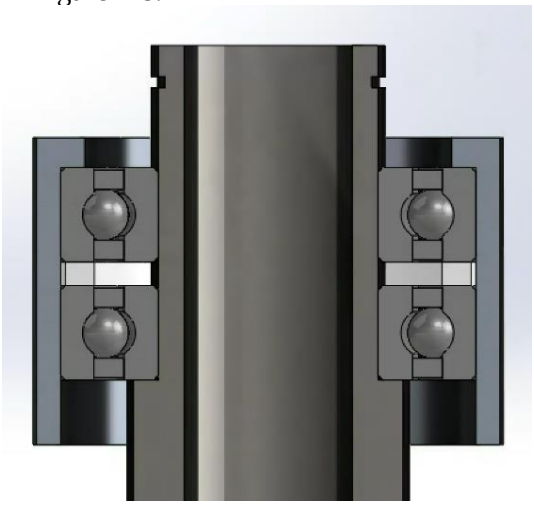


Figure 1-8: Yaw Bearing Assembly

1.2.7.2 Tail Vane Design

In order to maximize how fast the turbine can turn into the wind, it is necessary to have a tail vane with a large surface area. From this it was determined that the surface area needs to be 49cm^2. The FEA and geometry of the tail is shown in Figure 1-9.

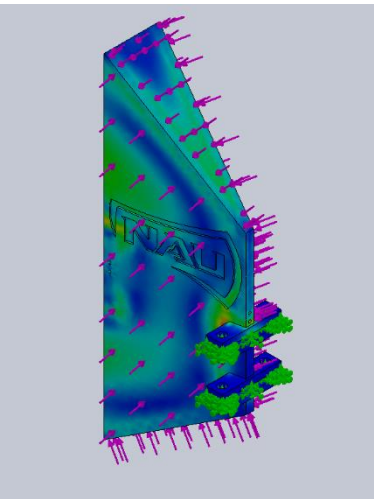


Figure 1-9: Tail FEA Analysis

2 Electrical Design

The first step in designing the converters was creating a model of each converter in Simulink. The models allowed a wide range of test voltages using different components. The simulations gave a clear picture of what components would be needed to build each converter. Below, the rectifier, buck converter, and boost converter are shown in Figure 2-1, Figure 2-2, and Figure 2-3, respectively.

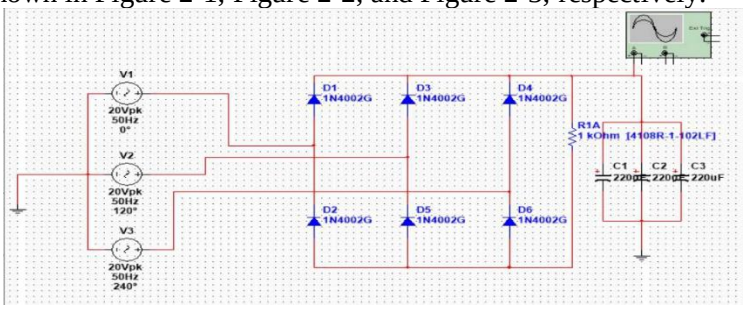


Figure 2-1: AC/DC Rectifier

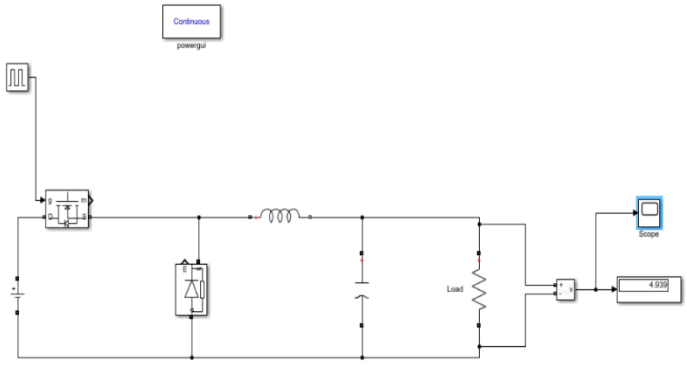


Figure 2-2: Buck Converter

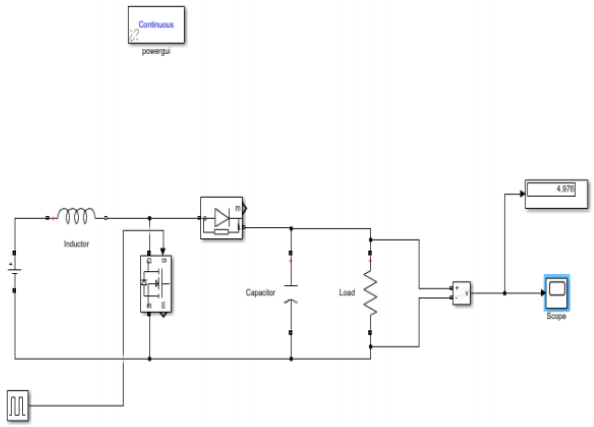


Figure 2-3: Boost Converter

Following the simulations, research was conducted to determine which components would operate under high voltage and current conditions. The components were arranged on a breadboard following the simulation diagram and tested with low voltages to verify the functionality of the circuit. The electronics were then soldered onto perf boards for higher voltage testing. The final product was soldered onto a printed circuit board for clean finish and easy replication.

2.1 AC/DC Rectifier

This passive converter consists of six high current Schottky Rectifiers, a capacitor to smooth the output signal, and a resistor to drain the capacitor when not in use. The six diodes are needed to make a three-phase rectifier. Two diodes are required for passive rectification for each phase. The rectifier works entirely passively, and all the components are soldered onto a small perf board that will be mounted up-tower to the nacelle behind the blades. The DC output from this converter will be directly connected to the input of the boost converter. In total, 5 rectifiers will be built before competition to have ready in case any components burn out during testing. While it was recommended to use a heatsink with the diodes, the team made a design decision to mount the rectifier up-tower to cool the diodes convectively. The diodes are designed to withstand up to 130 °C. During testing, the diodes never exceeded 100 °C. Although the diodes may not work at maximum efficiency at higher temperatures, the team decided a smaller, more compact rectifier would best suit the design. The specifications for the rectifier are shown below in Table 2-1, and the built rectifier is shown in Figure 2-4.

Table 2-1: AC/DC Rectifier

Component	Description
Prototype Board	Double sided PCB used for prototyping and soldering components.
TO-220AC Schottky Diodes	15V, 20A Diodes used for rectification.
Capacitor 220uF/35 v	Capacitor used for smoothing the signal after rectification
1K Ohm Resistor	Resistor used for draining the capacitor when disconnected

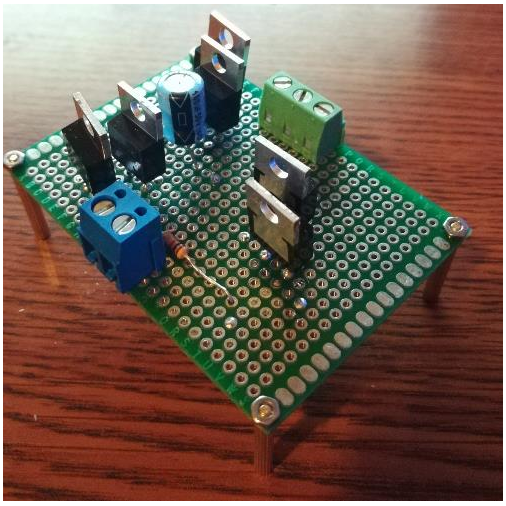


Figure 2-4: Rectifier

2.2 DC/DC Boost Converter

Testing showed that the generator and rectifier produced up to 5V while operating under 1000 RPM. The boost converter is designed to accept an input voltage between 1 and 5 volts and boost that to a voltage higher than 5V. The duty cycle is controlled through the Arduino and will always boost the voltage above 5V but never exceed 25V. The board depicted below as Figure 2-5 has a buck and a boost converter. The relays are used to switch between the converters depending on the input voltage. When under 5V the input goes to the boost converter and when over 5V the buck converter receives the input voltage. The screen displays the input voltage, output voltage, and which converter the input voltage is going to. The screen will most likely be removed before competition which is why there are also LEDs to determine which mode the circuit is operating in. The DC/DC Boost Converter specs are summarized in Table 2-2, while the constructed converter is shown in Figure 2-6 [6].

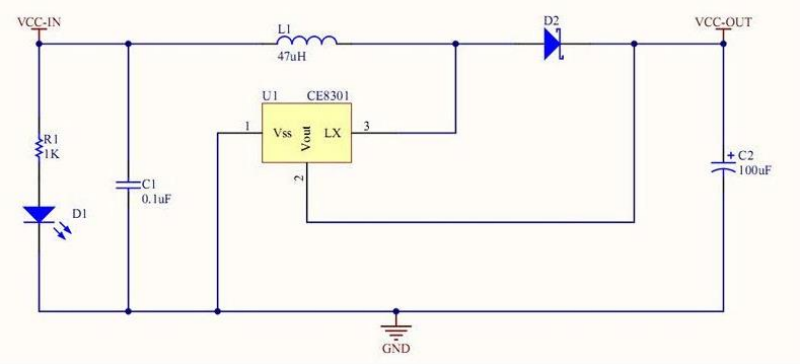


Figure 2-5: DC/DC Boost Converter One Line Diagram

Table 2-2: DC/DC Boost Converter

Comment	Description	Designator	Footprint	LibRef	Quantity
0.1uF	Capacitor	C1	0805	CAP	1
100uF	Polarized Capacitor (Surface Mount)	C2	CAP_6_5	Cap Pol3	1
LED	Typical INFRARED GaAs LED	D1	LED-0805	LED	1
	Schottky Diode	D2	SS14	D Schottky	1
47uH	Inductor	L1	INDUCTOR_6_5	Inductor	1
1K	Semiconductor Resistor	R1	0805	RES	1
CE8301		U1	SOT89L	CE8301	1

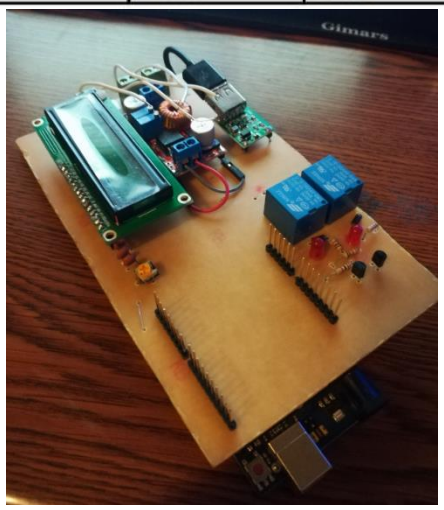


Figure 2-6: DC/DC Boost Converter

2.3 DC/DC Buck Converter

The buck converter accepts an input voltage between 5 and 25 volts. The Arduino adjusts the duty cycle to always produce a 5V output. The components for the buck converter are built to withstand up to 20A. The team experimented with many different components and were not able to get the desired results. For this reason, a pre-built buck converter was purchased and modified to suit the needs of competition. The modifications for the buck converter limited the current going into the converter with resistors and current limiting diodes. The specs for the pre-built buck converter are shown in Table 2-3 [7].

Table 2-3: DC/DC Buck Converter

Component	Description
XL4015	DC/ DC 180-KHz Buck Converter, 5 A/36 V
M7	SMD version of 1N4148 Diode
HSN3631A S	Numeric Three-Digit LED Display,
LM317	Adjustable Voltage Regulator
SS54	Schottky Diode 40 V/5 A
47 uH/5 A	Power Inductor
50K MT	Multi-Turn Preset Potentiometer 50K
LED	Indicator light
Capacitor 220uF/35 v	Capacitor used for smoothing the signal
Capacitor 100uF/50 v	Capacitor used for smoothing the signal

3 Electrical Analysis

The first component of power electronics in contact with the generator is the AC/DC rectifier. The generator is activated by spinning the blades of the turbine which will produce wild, three-phase AC voltage. This variable voltage will go directly into a passive rectifier designed to produce a steady DC voltage. The Schottky Rectifiers are designed to withstand up to 200V and 15A. While testing the rectifier on a closed circuit, the voltage never reached greater than 20V and 11A at maximum expected angular velocities. The Schottky Rectifiers reach temperatures up to 75 °C while in use. To avoid mounting a heat sink to the converter, the rectifier will be mounted up-tower directly behind the blades making use of air flow as effective convection medium. The rectified DC voltage is smoothed through a capacitor and deposited into the DC/DC boost converter. The boost converter is designed to accept an input voltage between 1 and 5 volts and output a voltage greater than 5V. The boost converter will be active while the generator is spinning under 1000rpm. Once the input voltage is greater than 5V, a relay is used to send the input voltage into the buck converter. The DC/DC buck converter is designed to accept an input voltage between 5 and 25 volts. The buck converter is controlled through an Arduino Uno that adjusts the duty cycle to produce a constant 5V output.

4 Controls Analysis and Software Documentation

The electrical engineering team started by creating simulations of the converters that would be designed for competition. Using Simulink, the three converters were designed and analyzed for what components would need to be purchased for the building of the converters. Once the parts were purchased and the circuit was built, the electrical engineers coded the Arduino Uno to produce the expected output from the system. There are two Arduino Uno's used throughout the entire system. The first Arduino is used to control the brakes and active pitching mechanism. The second Arduino is used to control the buck and boost converters which adjusts the duty cycle of the converters to produce the correct output. The brakes are controlled by a linear servo that actuates under two conditions, when the button is pressed or when there is a loss of power from the PCC. The pitching mechanism is controlled by an Arduino that activates two actuators based on voltage sensed from the voltage divider.

5 Testing

Team NAU performed bench testing throughout the design process to ensure that each subsystem would operate efficiently when integrated into a full-scale test.

5.1 Generator

The generator was tested alongside an AC/DC rectifier. A dynamometer was used to apply rotation to the generator and the rectifier received the input voltage from the three-phase generator. The generator had a known KV rating which was tested through an open circuit. By applying an increasing rotational speed to the generator, the KV rating was verified. During this test, the input voltage and amperage were recorded.

The team initially gathered data to ensure that the motor would provide ideal power characteristics using a commercial rectifier. After applying loads to the generator/rectifier set-up, power calculations were carried out to verify that the generator would not limit the team's capability of producing power. The plots of theoretical power output from the blades and bench testing are shown in Figure 5-1. Also shown in the figure is the first iteration of handcrafted rectifier to compare with the commercial rectifier originally tested.

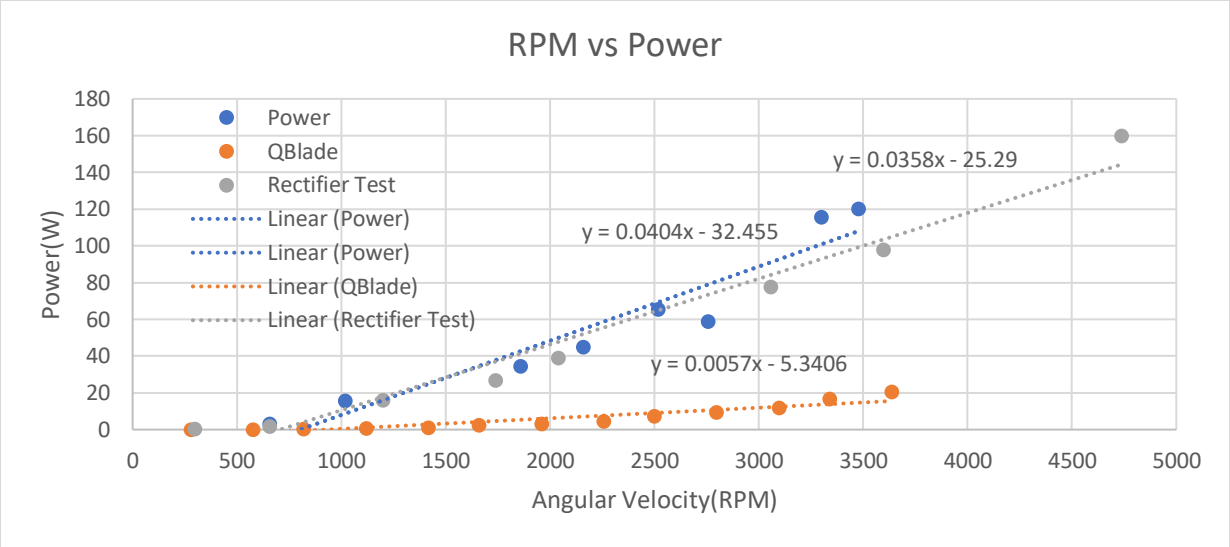


Figure 5-1: Generator Power Capabilities vs. Blades' Theoretical Output

5.2 Arduino

Arduino coding was the primary medium for Team NAU's coding. Arduino was used in the power electronics algorithms and linear actuation for the active pitching mechanism and braking system.

5.3 Linear Actuators

A total of three linear actuators were used in the design with Arduino to perform the desired tasks in a simple way. One actuator was used for the brake system, and two are used in the active pitching mechanism with a modified remote control (RC) helicopter swashplate. For bench testing the pitching mechanism, the team wired the two actuators with a breadboard, Arduino, and input signal via button press. This bench testing is completed to ensure that the two actuators are extending and retracting simultaneously without binding the swashplate while the hub rotates. After completing bench testing with a button press, the algorithm was modified to pitch the blades automatically by using logic statements that could be easily modified for full-scale testing. For the operation of the turbine, the Arduino Uno board is programmed to pitch based on a voltage reading from the rectifier. This voltage will allow the algorithm to quantify the angular speed of the rotor and adjust the blades' pitch angles appropriately. One Arduino Uno board will be used for both pitching and braking systems. Per competition requirements, the turbine's brake system operates via button press and from the discharge of a capacitor when the turbine is disconnected from the PCC.

5.4 Rectifier

The rectifier was tested on both an open and closed circuit by using a dynamometer. The open-circuit test determined the maximum voltage expected, while the closed-circuit test verified the components could maintain functionality with increased amperage. The custom-built rectifier was tested against a pre-built rectifier and the results were nearly identical. The dynamometer testing set-up is shown in Figure 5-2.

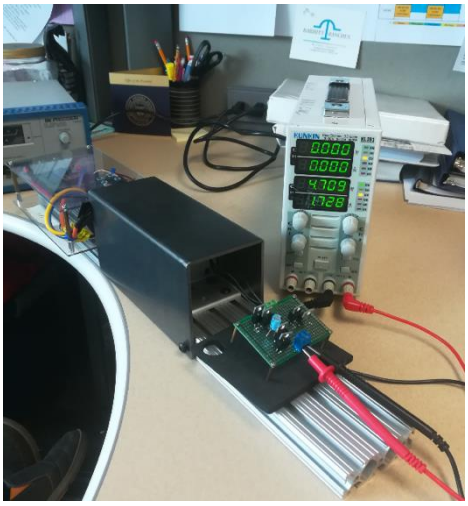


Figure 5-2: Rectifier Testing

5.5 Boost Converter

The components of the boost converter were first tested using a breadboard with a low input voltage. The Arduino was used to measure the output voltage and adjust the duty cycle depending on the input voltage. The components were then soldered onto a perf board for higher voltage testing. The Arduino code was adjusted to always boost the input signal above 5V but never exceed 25V. Using a DC power supply, the boost converter was tested at a multitude of input voltages and the outputs were recorded.

5.6 Buck Converter

The testing procedure for the buck converter was identical to the boost converter. The Arduino regulated the duty cycle to always produce an output of 5V with an input between 5 and 25 volts. The buck converter was tested between its operating input range and the output was verified to always be 5V.

5.7 Entire Electrical System

The entire electrical system was tested using the dynamometer. The generator was hooked up to the rectifier. The output of the rectifier went into the boost converter. The output of the boost converter then went into the buck converter. The converter outputs were measured and recorded using a multimeter.

5.8 Mechanical Testing Procedures

The brakes have been bench tested using Arduino and all machined parts. To make sure the linear actuators can be tested repeatedly and produce the same results, there were 10 tests completed to show how much force it could apply. The results can be seen in Table 5-1 below.

Table 5-1: Brake Testing Results

Linear Actuator (g)	Linear Actuator (N)
2090	20.482
2044	20.0312
2130	20.874
2295	22.491
2122	20.7956
2262	22.1676
2291	22.4518
2390	23.422
2243	21.9814
2260	22.148

The actuator was tested using a kitchen scale that read out in grams which could then be converted into Newtons. This averaged out to be 21.68N which is just below the rated force of 22N. The braking actuator was proven by the test results to be good enough for full-system integration. This year's team made the braking system a priority to capitalize on previous team's mistakes. This was due to the brakes not disengaging from the caliper completely when the releasing clamping force. This year's design can repeatedly actuate a consistent distance without lack of disengagement.

5.9 Future Testing

Team NAU is currently manufacturing a mounting surface for a Subaru roof rack to complete field testing. At the time of submission for this report, the team was unable to complete any tests in a controlled environment due to the anticipated wind tunnel being out of commission. During testing that will take place following the submission of this document, the team will be simulating a competition run via car-mounted tests outside of city limits to ensure safety. The team is also creating a stand for an anemometer to verify the wind speeds being applied to the turbine to allow the team to tune the electronics properly. The electrical components' wires will be run into the vehicle for testing and control of the braking mechanism. After ensuring that the turbine will be capable of performing the mandatory tasks at low winds, further testing will be done at higher wind speeds to evaluate the durability of the design.

6 References

[1] C. W. Competition, "Rules and Regulations document," National Renewable Energy Laboratory, Boulder, Colorado, 2019.

[2] J. Manwell, *Wind Energy Explained*, West Sussex, United Kingdom: John Wiley & Sons Ltd., 2002.

[3] "Airfoil Tools," 2019. [Online]. Available: http://airfoiltools.com/. [Accessed January 2019].

[4] TU Berlin, *QBlade*, 2019.

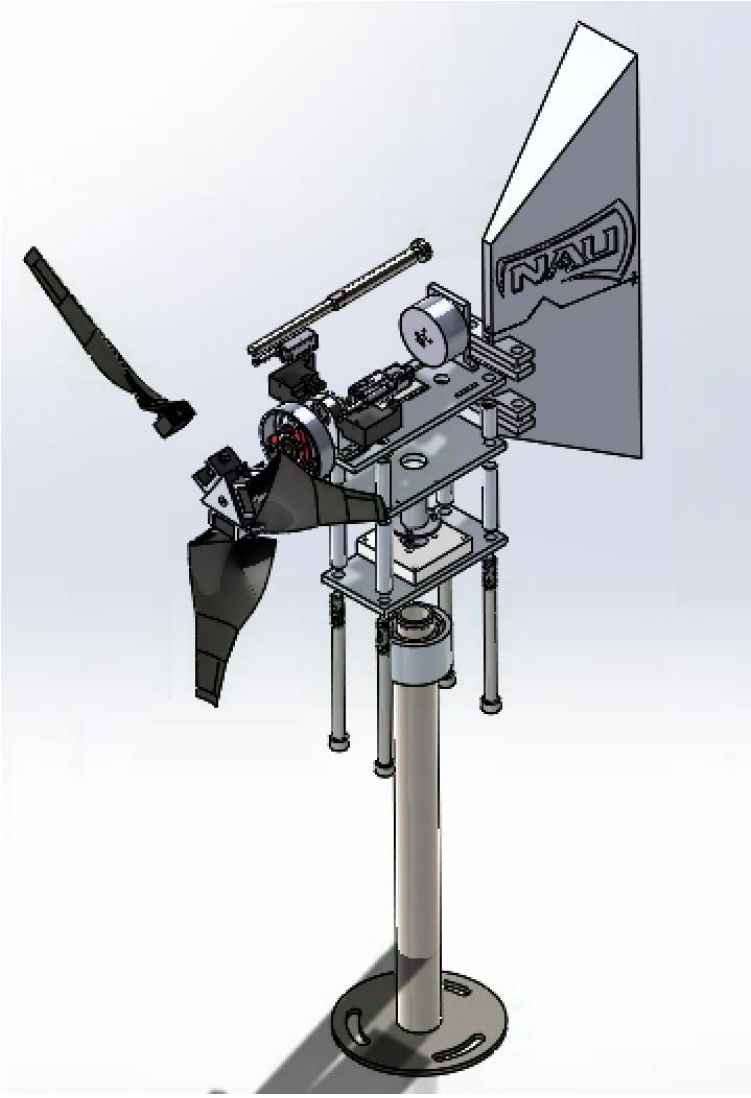
[5] J. Kang and H. Lee, "The Development of Rotor Brakes for Wind Turbines," *Internation Journal of Applied Engineering Research*, vol. 12, 2017.

[6] J. Bauer, "Arduino DC/DC boost converter design circuit with control loop," 24 May 2016. [Online]. [Accessed 17 January 2019].

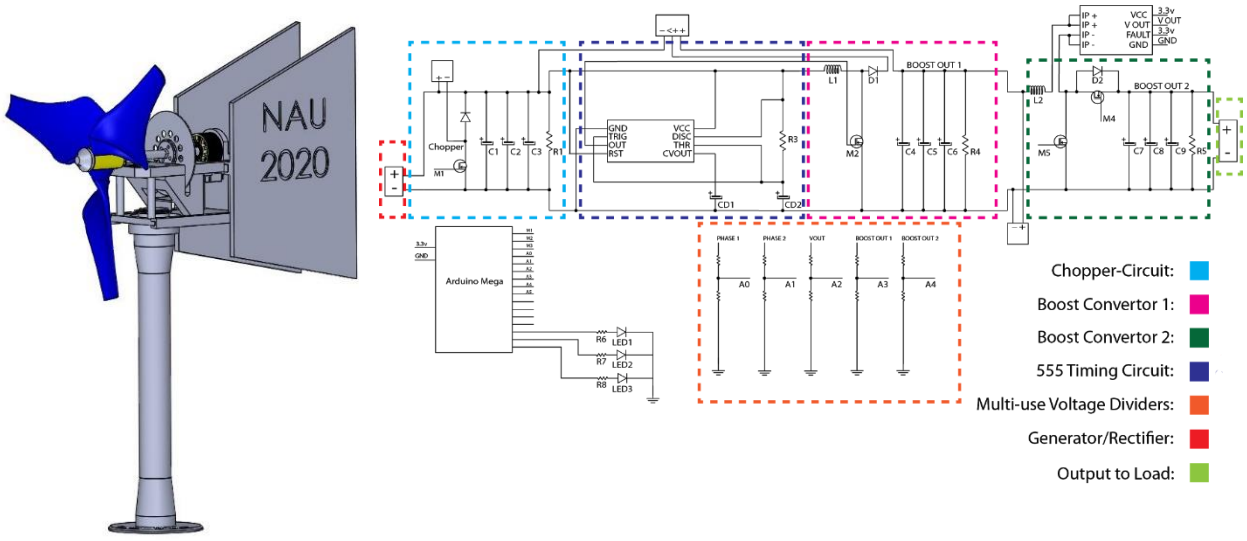
[7] A. Negi, "DC/DC Buck Converter Circuit," Circuit Digest, 13 September 2017. [Online]. [Accessed 17 January 2019].

Appendix A

Appendix A-1: Exploded View



CWC20 NAU Technical Design Report



Student Authors:

Member	Role	Contact
Lucas Duncan	ME Team Lead	ldd55@nau.edu
Calum Eikenberry	EE Auxiliary Team Lead	cje223@nau.edu
Nigel Grey	EE DC-DC Convertor Team Lead	ng474@nau.edu
Ethan Maltaverne	ME budget liaison/ Motor specialist	epm49@nau.edu
Daniel Massaglia	ME Manufacturing Member	dm976@nau.edu
Marina McCue	ME Aerodynamics Lead	marina_mccue@nau.edu
Matt Mennell	ME Manufacturing Lead	mlm636@nau.edu
Sean Veden	ME Brake Design Lead	jfv32@nau.edu

Project Sponsor: U.S. Department of Energy, National Renewable Energy Laboratory, W.L. Gore

Principle Investigator/Faculty Advisor: David Willy

Co-Principle Investigator/Faculty Advisor: Dr. Venkata Yaramasu

Capstone Instructor: Dr. David Trevas, Dr. Kyle Winfree

Table of Contents

Executive Summary (Sean) 4
1. Design Requirements (Ethan) 5
2. Static Performance Analysis (Marina) 6
3. Mechanical Loads Analysis 8
3.1. Blade Analysis (Marina) 8
3.2. Shaft Analysis (Matt) 9
3.3. Brake Analysis (Sean) 9
3.4. Nacelle Analysis (Daniel) 10
3.5. Tower Analysis (Daniel) 11
4. Yaw System (Lucas & Marina) 12
5. Electrical Analysis (Calum & Nigel) 12
6. Software Description, System Control (Calum & Nigel) 14
7. Testing Results 15
7.1. Electrical Testing Procedure (Calum & Nigel) 15
7.2. Mechanical Testing Procedure 16
7.2.1. Blades & Hub (Lucas & Matt) 16
7.2.2. Tower/Baseplate/Nacelle (Daniel) 16
7.2.3. Brake (Sean) 17
7.2.4. Yaw (Lucas, Marina & Matt) 17
7.2.5. Shaft (Lucas, Marina & Matt) 17
References 18

List of Table

Table 1: Design Requirements [1] 5
Table 2: Wind Turbine Blade Geometry 6
Table 3: Mechanical Component Factor of Safety (FOS) 8
Table 4: Runaway Wind Speeds and Braking System Factor of Safety 10
Table 5: Rotor Strength Test Results 16

List of Figures

Figure 1: Full Assembly 4
Figure 2: Coefficient of Power versus Tip Speed Ratio 7
Figure 3: Aerodynamic Power Curve 7
Figure 4: Annual Energy Production 8
Figure 5: Wind Turbine Blade Finite Element Analysis 9
Figure 6: Shaft 9
Figure 7: Brake Assembly 10
Figure 8: Tower Stress Analysis 11
Figure 9: Von Mises Tower Analysis 11
Figure 10: Yaw 12
Figure 11: Greater-than-one-line Diagram 12
Figure 12: Simulink Duty Cycle Output 13
Figure 13: Final PCB Design 13
Figure 14: PI-Controlled Synchronous Boost Converter Schematic 14
Figure 15: PI-Controller Arduino Program 14
Figure 16: Control Module Flowcharts 15
Figure 17: Rotor Strength Test Enclosure 16
Figure 18: Blades in Enclosure 16
Figure 19: Actuator Slider Testing 17

Executive Summary (Sean)

The Northern Arizona University (NAU) Collegiate Wind Competition (CWC) 2020 turbine team completed a design for a small-scale wind turbine. The turbine is a three-blade design with a passive yaw, dynamic and mechanical braking, and a closed-loop controlled synchronous boost converter electrical subsystem. The parts used in this turbine were either commercially available or manufactured by the team. The design team was split into three: one mechanical engineering team and two electrical engineering teams. The mechanical engineering team was tasked with designing the aerodynamic, structural, and mechanical parts of the turbine. The electrical DC-DC converter team was tasked with the design and simulation of the converter topology. The electrical auxiliary team was tasked with converting the DC-DC team's design into a printed circuit board (PCB) and complimenting it with low forward-voltage component selections. To aid in the design process, the team used computer programs such as MATLAB-Simulink, QBlade, Arduino IDE, and SolidWorks. Once the parts were designed, testing was completed to ensure the design worked as expected. The testing procedures are described within this document.

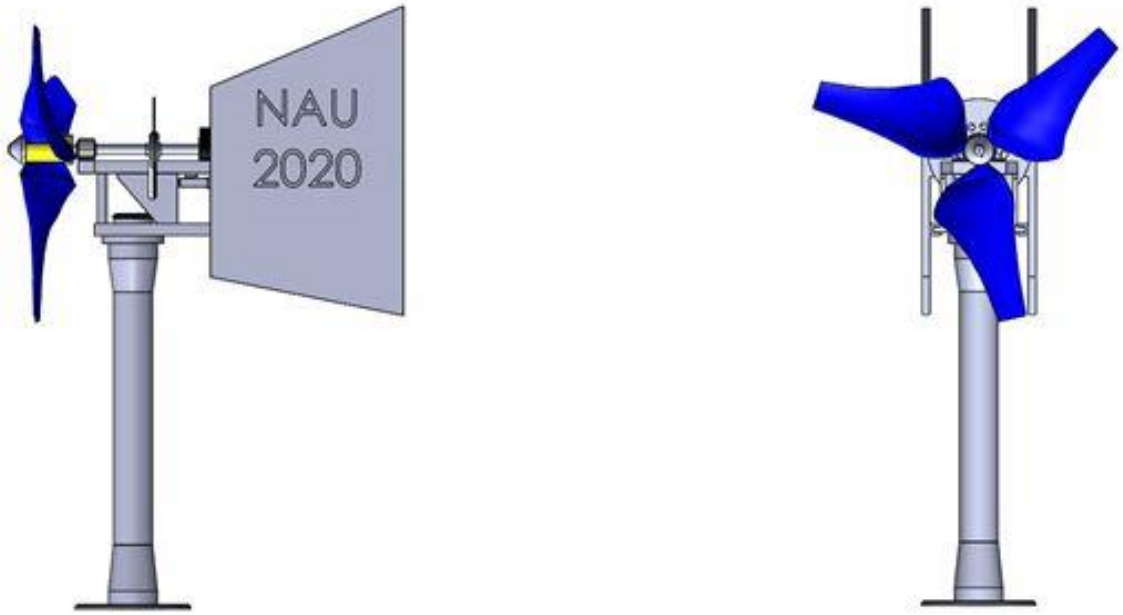


Figure 1: Full Assembly

1. Design Requirements (Ethan)

Table 1: Design Requirements [1]

Electrical Engineering Requirements	Mechanical Engineering Requirements
Voltage must be direct current (DC) and less than 48 V at any point in the system	Withstand wind speeds up to 22 m/s during operation and up to 25 m/s during braking
No capacitors greater than 10 J of energy storage may be used on the turbine side of the system	Yaw rate of 180 °/s
Capacitors and inductors may not be used as bulk energy storage on the turbine side of PCC	Cut-in between 2.5 m/s and 5 m/s wind speeds
All external wired connections must be optically isolated	+/- 10 % maximum average power
Team load must run on a maximum of 120 VAC	Control rated power between 12 m/s and 18 m/s wind speeds
Electrical systems are tied to ground at 100 kΩ or lower resistor	Braking system activated when an emergency stop button is pressed, disconnected from PCC, or subjected to wind speeds greater than 22 m/s

Our design revolved primarily around the predetermined engineering requirements. This gave the team a direction for which to start searching for hardware. The first mechanical engineering requirement was the ability to withstand 25m/s wind speed. This led us to develop a ridged tower to minimize deflection. A 2-in wide tower tube stock with a wall thickness of 0.5-in was selected to be lathed to the proper fitment for the receiving bearing chosen for the lower nacelle. the yaw rate restriction drove us to balance and center all internal nacelle parts to further enable the influence of the yaw that was yet to be developed. The earliest possible cut-in speed was one of our top priorities in blade development. The target was cut in at 2.5 m/s. this meant both blade development and motor selection had to be focused on this characteristic. After the cogging torque testing of 3 motors, we were able to find a motor with power rating above 100 W at 4,000 RPM and the least resistive torque of any motor tested. blades were reiteratively altered to find the most aggressive blade without compromising the performance in the windspeeds up to 25 m/s.

Our brake system would need to have several times the braking forces of previous models due to the runaway test. This led our design to utilize a 135 mm disk and an 80 N actuator to accomplish a total braking force of 5.4Nm. The team produced a reverse mounted drop-down brake system that allowed the brake disk to intrude into the lower nacelle cabin area, ultimately solving this performance issue.

Throughout this project appropriate mounting and dimensioning was found to be one of the most crucial aspects of development. With our extremely compact design most components found themselves within 3 mm of each other. This constraint pushed us to develop the multipurpose rail system implemented into the upper nacelle plate. This system utilizes the limited space of the nacelle and maintains assembly simplicity and reducing required hardware.

2. Static Performance Analysis (Marina)

The wind turbine blades were first designed using MATLAB, analyzed and modified using QBlade, and then rendered using SolidWorks. The MATLAB code assumed an ideal rotor with wake rotation and calculated chord length and twist angle from a design tip speed ratio of 1.5, angle of attack of 16 degrees, rotor radius of 20.6 cm, hub radius of 1.9 cm, and 3 blades. This information, along with selected airfoils, were inputted into QBlade and the power performance was analyzed. Chord length and twist angle were exaggerated, and different airfoils were analyzed until desirable characteristics were achieved. The final blade geometry is located below in Table 2. Figure 2 displays the coefficient of power versus tip speed ratio for angular velocities ranging from 0 to 3500 RPM, with a maximum coefficient of power of 0.3 at the design tip speed ratio.

Table 2: Wind Turbine Blade Geometry

Local Rotor Radius (cm)	Chord Length (cm)	Twist Angle (Degrees)
1.7	10.0	45
3.4	10.8	27
5.2	11.2	18
6.9	9.1	13
8.6	7.6	9.0
10.3	6.5	6.5
12.0	5.6	4.7
13.7	4.9	3.3
15.5	4.5	2.2
17.2	4.0	1.3
18.9	3.7	0.6
20.6	3.4	0

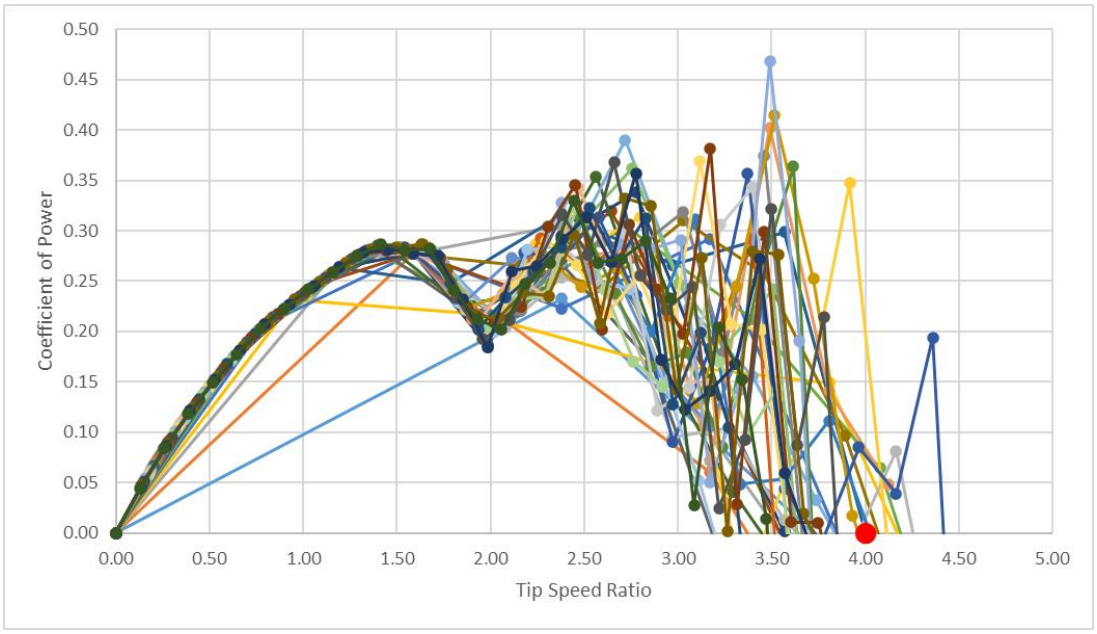


Figure 2: Coefficient of Power versus Tip Speed Ratio

The wind turbine cuts-in at 2.0 m/s and produces a rated power of 28 W at 11 m/s, shown in the power curve below in Figure 3. Using the power curve and a Rayleigh probability distribution, the annual energy production was calculated and is displayed in Figure 4.

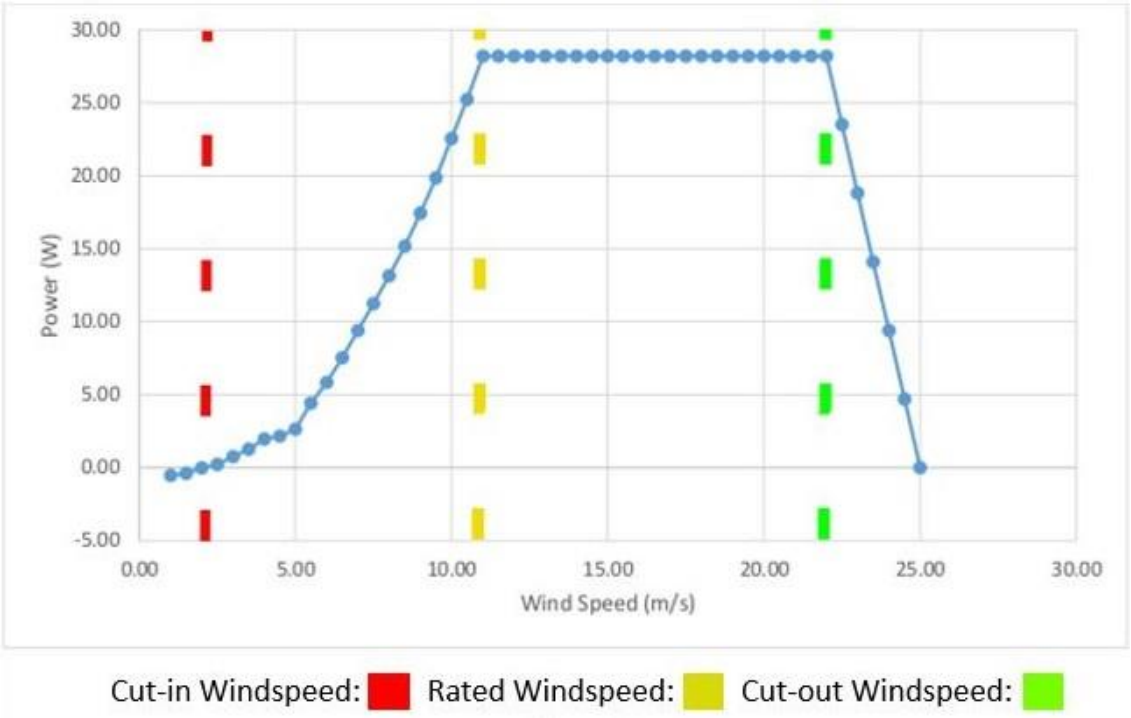


Figure 3: Aerodynamic Power Curve

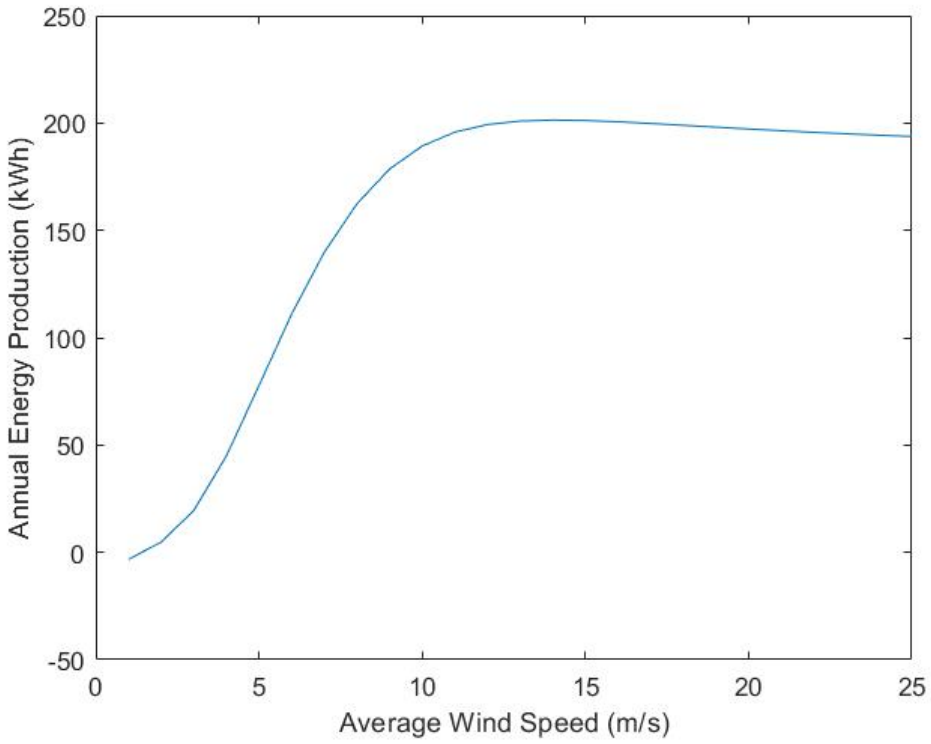


Figure 4: Annual Energy Production

3. Mechanical Loads Analysis

Table 3: Mechanical Component Factor of Safety (FOS)

System	Material(s)	Load Description	Loads Applied	Minimum FOS
Blades	Polycarbonate	Thrust, Centrifugal	$T = 17.0\ N$ $\Omega = 4341\ RPM$	2.74

3.1. Blade Analysis (Marina)

The final wind turbine blade finite element analysis was conducted using SolidWorks, shown below in Figure 5. The centrifugal load was determined from the runaway rotor speed, which was calculated using the tip speed ratio where the coefficient of power is zero (see the red dot from Figure 2) about 4.0, rotor radius of 20.6 cm, and maximum wind speed of 25 m/s. The thrust force was calculated using air density for standard atmospheric conditions 1.225 $\mathrm{kg/m^3}$, area of the rotor plane, maximum wind speed, and ideal axial induction factor of one third. In the next iteration of the FEA, the lift and drag force would be calculated to determine the resultant force along each section of the blade. This would then be used in lieu of the estimated thrust force.

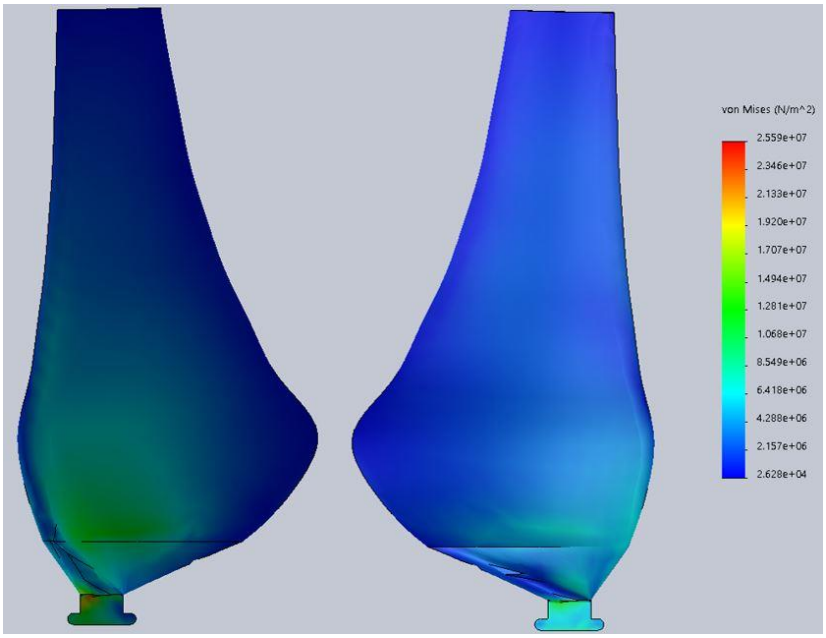


Figure 5: Wind Turbine Blade Finite Element Analysis

3.2. Shaft Analysis (Matt)

The shaft design, in Figure 6, relies on dimensions such as length and cross-sectional areas as well as the maximum centripetal forces experienced. These forces can be determined by the startup torque and during hard braking. The chosen design includes a short section of the shaft which is has a larger diameter and milled to have a key shape in order to lock the disc in rotation. One end of the shaft is attached to a coupler to the motor shaft. The other end of the shaft is turned down over two inches with an inch of threads cut out. This allows the hub to slide onto the shaft and lock rotation when the hub nose screws on to clamp the hub in place. The shaft is locked in place through the motor mount while support for the weight of the hub and blades on one end and reduced friction is helped with the use of a pillow block bearing mounted to the top nacelle. Due to incompletion of manufacturing of final shaft no physical testing was taken but through calculations a factor of safety of 2.1 was determined.

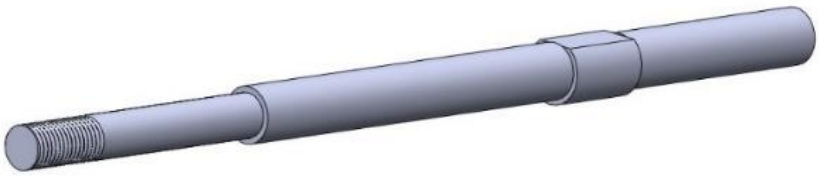


Figure 6: Shaft

3.3. Brake Analysis (Sean)

Figure 7 above shows the brake assembly within the upper level nacelle plate and provides a label of parts shown. The slider and the rail system used is made of polycarbonate and is 3D printed. The braking slider and stopper behind the disk have a slot where a brake pad is pressed into each. The braking slider is fastened to the linear actuator to clamp the brake disk when the actuator is extended. The linear actuator

shown is controlled using an Arduino microcontroller and a linear actuator control board. The control board allowed for less coding and allows for fine tuning of the actuator speed and stroke length.

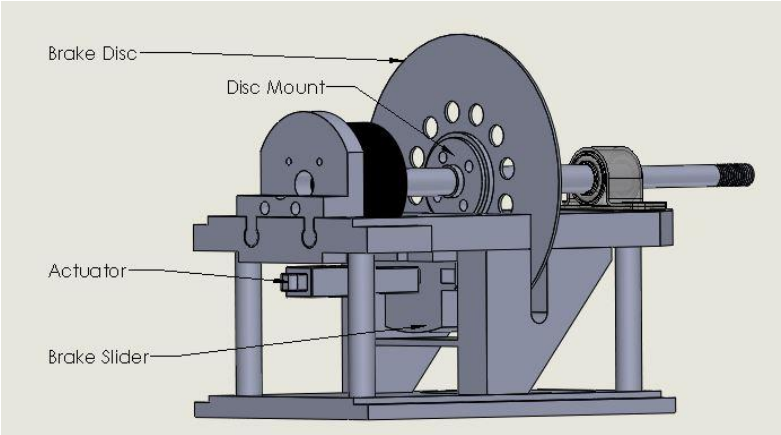


Figure 7: Brake Assembly

Based the on analysis of the blades, the torque that must be overcome to stop the rotation of the blades is shown in Table 4 below. This table outlines the torque produced by the blades at runaway wind speeds and the factor of safety the braking system.

Table 4: Runaway Wind Speeds and Braking System Factor of Safety

Wind Speed [m/s]	Torque of Blades [N-m]	Factor of Safety
18	2.5	2
22	4	1.35
25	5	1.08

The brake disk is 67.5 mm in radius and the linear actuator produces 80 Newtons which means the torque of the braking system is 5.4 N-m. The design decision to make the disk 135 mm in diameter was to ensure that the sub-system could achieve a FOS of 2 at runaway speeds. Since runaway speed testing begins at 18 m/s, the design will need to actuate at the beginning of the speed ramp up for the safety of the turbine. If testing was able to have been completed the team may have found that this design was over engineered and in that case the size of the disk could be modified. The 80N actuator was chosen based on estimated values of tip speed ratio and power produced by the blades at runaway speeds. These values led to back of the envelope calculations that told the team that an 80N actuator would be the safest option. The L12P actuator used produces the maximum force sold in the micro size. For this reason, the only viable option to modify the torque of the braking system was to change the brake disk size. This design can stop the turbine with the use of a push button and with speed sensors that actuate the braking system when runaway wind speeds are sensed.

3.4. Nacelle Analysis (Daniel)

The nacelle is comprised of two sections including a lower and upper plate. The lower plate, made of aluminum manufactured in the NAU machine shop, lets wiring from the generator and brake assembly run down the tower while not binding when the turbine experiences direction change. The upper nacelle

plate is produced from the Rapid Lab using polycarbonate material. It is made up of two sections that bolt to the bottom plate which are both designed to fasten the nacelle cover and yaw in place.

The top nacelle plate serves multiple purposes. Starting with the bottom of the top plate, an actuator mounts for the brake to linearly push a brake pad against the brake rotor housed within the nacelle. Moving to the upper face, a single pillow block with a pressed bearing provides support to the drive shaft. In addition to this block, the generator itself helps provide support through a coupler where the shaft ends. The generator mounts to a motor mount which utilizes a rail system to mount into the upper nacelle.

3.5. Tower Analysis (Daniel)

Using steel tube stock to manufacture, the tower of the turbine was designed on SolidWorks and used in a stress and displacement analysis. In order to machine the tube stock to a desired shape, a 2-inch outer diameter with a half inch wall thickness was utilized for ideal dimensions. It is important to make sure that the tower design could withstand the forces it would experience in the wind tunnel. Shown in **Error! Reference source not found.** and Figure 9, the von Mises stress distribution and stress analysis across the chosen tower design. The importance of these stresses relates to where a part can fail due to fatigue or yielding. Using mild steel, the amount of stress that the tower is miniscule in respect to what it would take to yield the steel. Computing a factor of safety of 116, the towers wall thickness could be decreased from 1/4th of an inch to 1/8th of an inch and still have a large factor of safety.

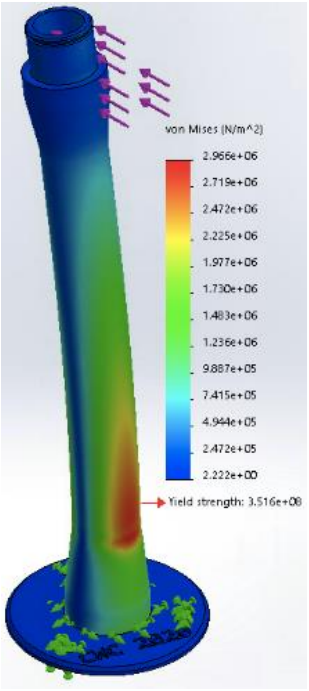


Figure 9: Von Mises Tower Analysis

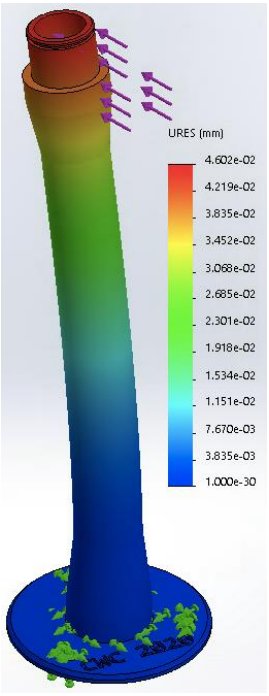


Figure 8: Tower Stress Analysis

Error! Reference source not found. illustrates that the yield strength of the tower is 3.5e8 Pa, and the maximum stress that the tower would experience at maximum wind load was estimated to be 3e6 Pa. Using mild steel for material selection, it can be concluded that this material and dimensions have more than enough strength to withstand the expected forces.

4. Yaw System (Lucas & Marina)

The Yaw of the turbine helps keep the rotor plane perpendicular to air flow as it sits on a ball bearing. This design utilizes two tails to increase the surface area which decreases the amount of force needed to hold the nacelle in an ideal position. Attached rails with fasteners to secure the yaw to the nacelle.

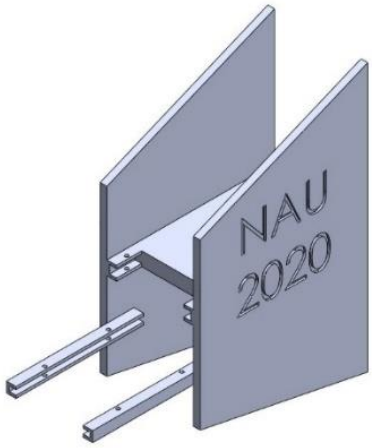


Figure 10: Yaw

5. Electrical Analysis (Calum & Nigel)

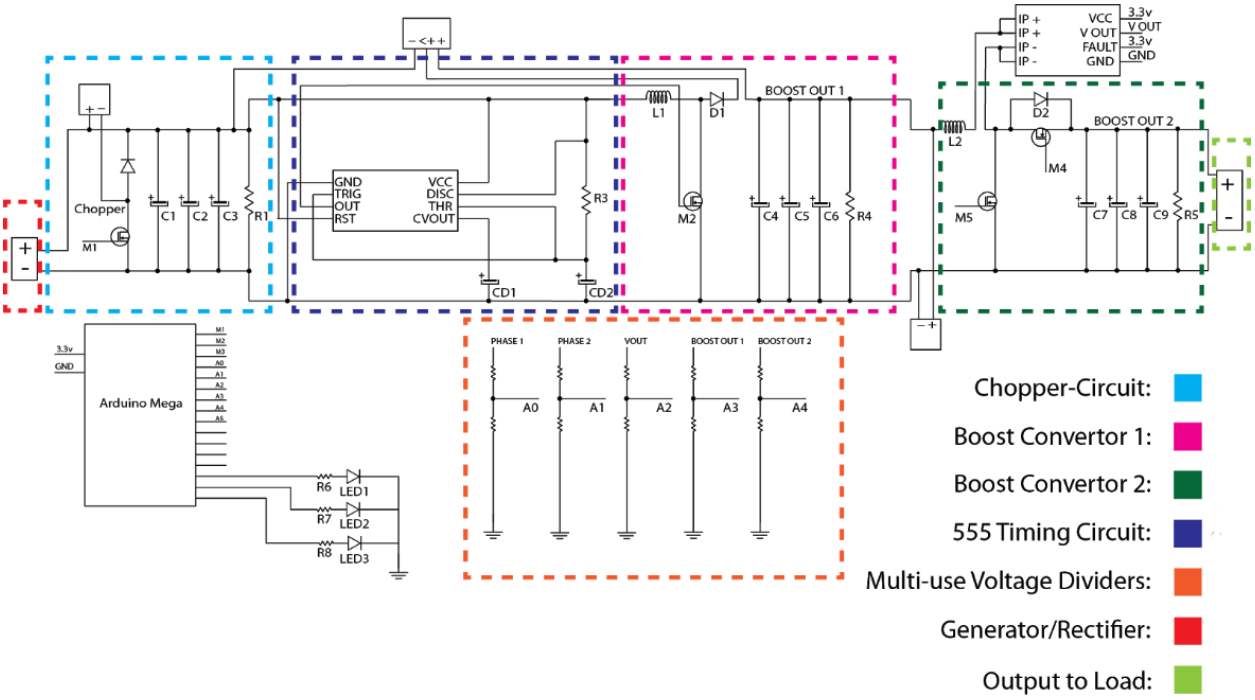


Figure 11: Greater-than-one-line Diagram

The electrical analysis and sub-system design processes were delegated to two sub-teams: the DC-DC team and the Auxiliary team.

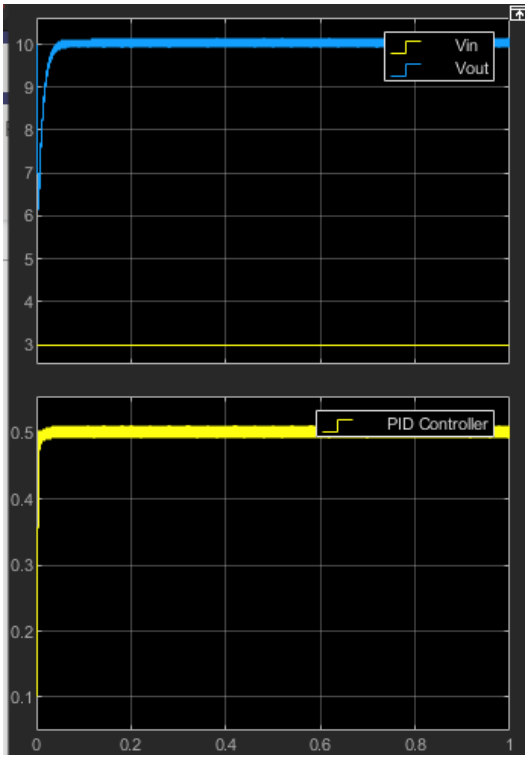


Figure 12: Simulink Duty Cycle Output

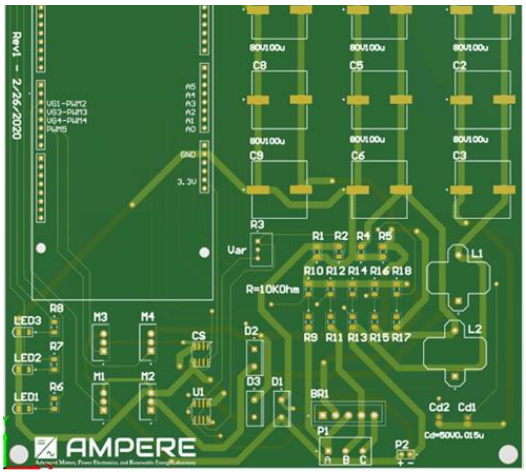


Figure 13: Final PCB Design

The **DC-DC team** primarily worked to design, simulate, and build a three-stage boost convertor system that utilized a synchronous boost converter topology (two complementary MOSEFTs) in place of a standard MOSFET and diode combination (***see Figure 11***). The goal of the design was to maximize power generation at low wind speeds, while minimizing the total voltage drop of the system (***see Figure 11***). Most testing for the synchronous topology was done with a MATLAB-Simulink PID simulation that returned exactly a 3.3x voltage output with little ripple current (***see Figure 12***). This operation was repeated with breadboarding to similar results. Difficulty was expected upon implementing this design within the overall circuit due to several parallel processes running independently on the Arduino, and so an optional diode was implemented to provide a non-synchronous topology option.

The **Auxiliary team** worked in parallel with the DC-DC team to optimize all electrical components (i.e. rectifier, auxiliary component wiring, generator) to best complement the low cut-in design and synchronous topology. In addition, the Auxiliary team spearheaded the printed circuit board (PCB) design and construction (***see Figure 13***), which integrated the entire power/control system from Figure 13 into one circuit. Furthermore, the team tested multiple control algorithm's functionality with an Arduino Uno which provided successful operations of necessary breaking functions. until hard programming was deemed unnecessary due to the ability to flash programs directly from MATLAB-Simulink.

Altium Designer was utilized by the Auxiliary team to create a 6" by 6", single-sided PCB (***see Figure 13)*** with all discrete components mounted to it (excluding braking chopper chassis mount resistor and packaged boost convertor for initial microcontroller power source). The design of this PCB included LEDs to allow visual verification that each stage (rectifier, first boost converter, second boost converter) was on, flush-mounted spacing for the Arduino Mega, additional footprints for parallel capacitors for quick changes in signal rectification after each convertor, and the maximum separation of control components/routing from power components/routing as to minimize signal interference. The control components lay along the bottom-left of the board and the power components across the top-right to center-right.

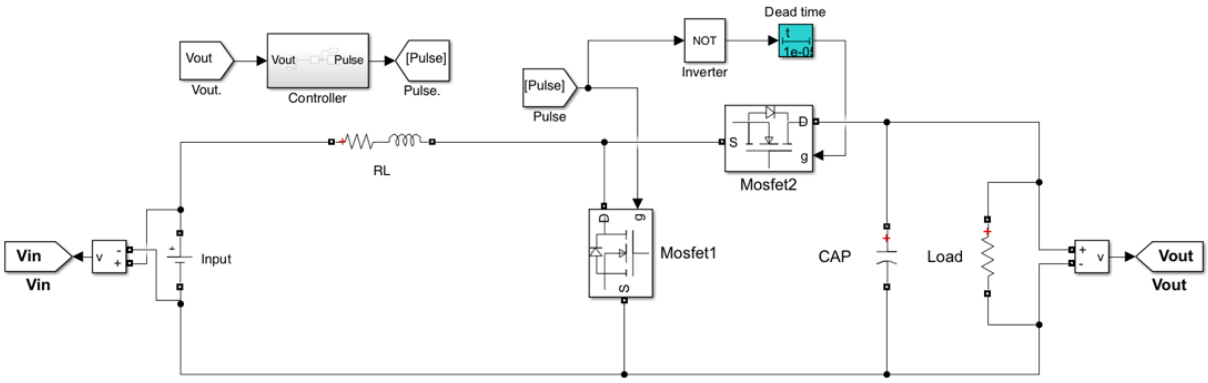


Figure 14: PI-Controlled Synchronous Boost Converter Schematic

The intended load attached at the end of the schematic diagram (***see Figure 11***) was to be a fixed resistance load with a 300W power rating and 10 Ohm resistance. Upon further testing the team would home in on the optimal resistance/power rating.

6. Software Description, System Control (Calum & Nigel)

MATLAB Simulink was used for circuit and closed-loop control simulations (***see Figure 14***). Simulink also allowed for a block-programming style that easily modularized the numerous electrical and mechanical turbine control algorithms and allowed a direct export to the Arduino Mega microcontroller (***see Figure 15***).

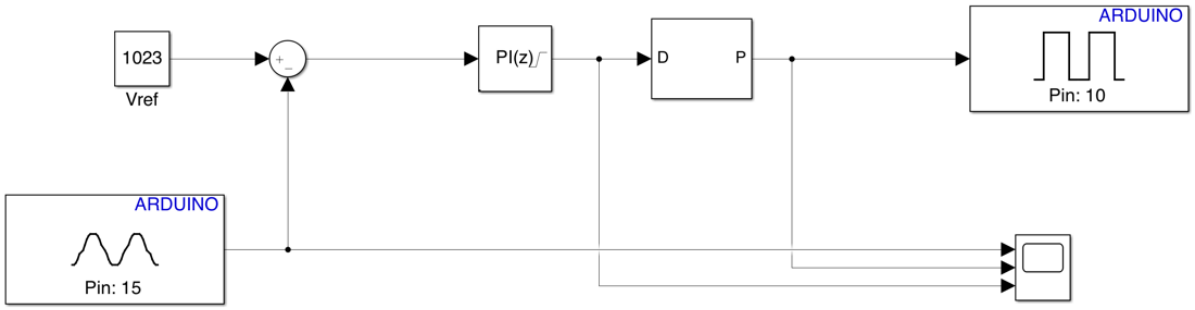


Figure 15: PI-Controller Arduino Program

All control modules (***see Figure 16***), were to be modeled within the Simulink environment and then exported directly to the microcontroller (same style of programming implemented in Figure 14) to reduce timing complications and optimize the controller's multithreading capability.

Control Module Descriptions:

1. Dump-Load Circuit: when an overspeed event occurs, route the rectified signal through an external resistor to ground via the ***"Chopper Circuit"*** in Figure 11. This control module is active only during the ***"Durability Task Power Dump"*** region (***see Figure 16)***.
2. Phase 1-2 Voltage Measurement: calculate the turbine rpm via phase 1 and 2 x-axis crossing point difference. This module occurs as soon as the microcontroller is powered on as to detect the point in time to trigger the system brake for the ***"Initiate Brake"*** region (***see Figure 16***).

3. PI Controller: utilizes proportional integral calculation to control second stage boost converter duty-cycle.
4. Current Sensor Measurement: used to detect and signal if load is disconnected. This module is active as soon as the "System Cut-In Region" is reached and detects the ***"Disconnect from Load"*** region (***see Figure 16***).
5. Stage 2, 3, & 4 Voltage Measurements: voltage divider circuits used to detect electrical potential at each key stage; trigger LEDs to provide visual feedback. This is also utilized to detect the ***"Disconnect from Load"*** region (***see Figure 16***).
6. Actuator Signal: provides PWM signal for mechanical braking control and is utilized during the ***"Initiate Brake"*** region (***see Figure 16***).

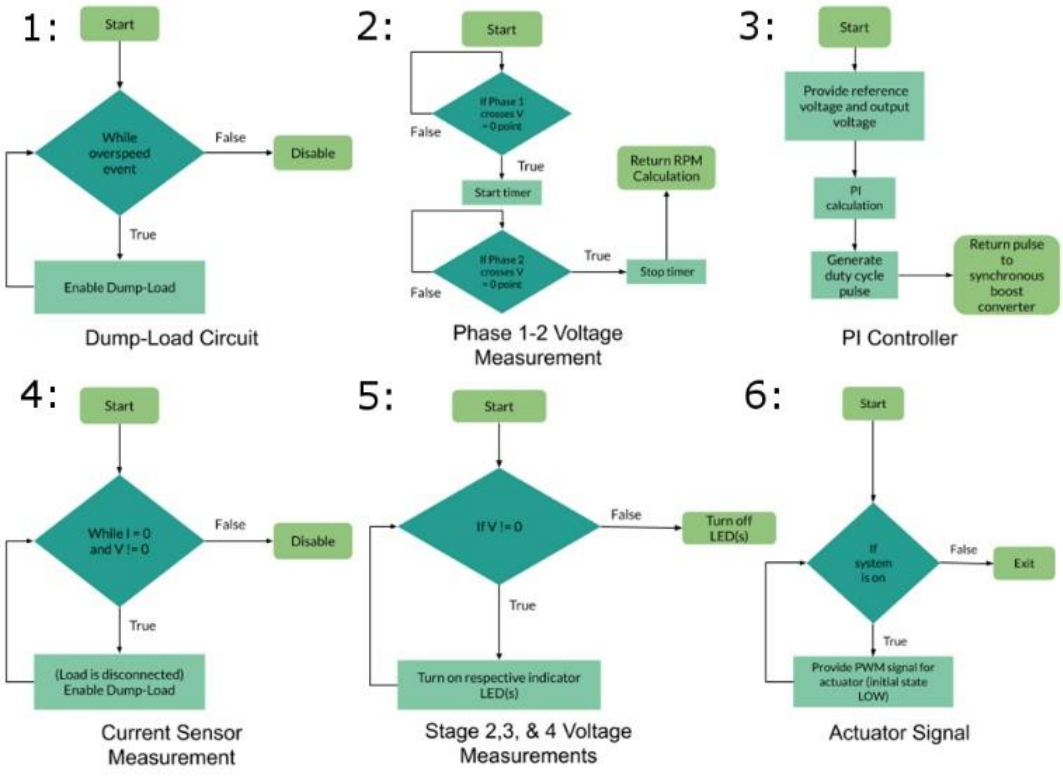


Figure 16: Control Module Flowcharts

7. Testing Results

7.1. Electrical Testing Procedure (Calum & Nigel)

Testing and power quality measurements of the PCB with all soldered components was to take place immediately after receiving of the PCB from the manufacturer if the project were able to continue. LEDs were integrated after each stage of conversion within the circuit to provide visual feedback to the tester, and an oscilloscope would be used to provide exact measurements per the CWC2020 rules and requirements. The design (***see Figure 11)*** featured the ability to change the capacitance values to decrease noise and increase signal integrity. Due to the modular capacitance and closed-loop control, additional filtering techniques would not likely be needed. The generator output would be tracked with the use of a dynamometer throughout this testing.

7.2. Mechanical Testing Procedure

The testing procedures for the turbine have come to a stop, but in the following sections each major sub-system testing procedures that have been done will be discussed. The findings during these tests will be gone over and how it aided in the team's design decisions. Also discussed below is the testing procedures that would have taken place if the times would allow.

7.2.1. Blades & Hub (Lucas & Matt)

The blades and hub subsystem were tested early during the semester. Members of the team assembled a safety container out of wood and Plexiglass, shown in Figure 18. Attached to the back of the box was a rail system which fastened a motor in place to turn a shaft up to 3300 rpm, shown in Figure 17. The box is equipped with two self-aligning flange bearings which helped smooth un-concentric rotation. The rotor testing taken concluded with two sets of broken blades which had different density values. It was found that the area where the blades formed into a key for the hub was the weakest point. This led to a redesign of the hub and blades to fix the failure point and another rotor strength test was conducted, which was successful. The results of the rotor strength test are displayed below in Table 5.



Figure 17: Rotor Strength Test Enclosure



Figure 18: Blades in Enclosure

Table 5: Rotor Strength Test Results

Rotor Iteration	Material	Fill	Failure
1st	ABS	10%	Yes, 2200 RPM
1st	ABS	20%	Yes, 3000 RPM
2nd	ABS	100%	No

7.2.2. Tower/Baseplate/Nacelle (Daniel)

Improper design relating to these systems of the turbine can cause catastrophic failure within operation. Failures can include the tower disconnecting from the baseplate due to faulty welds, improper bearing fitment resulting in a low preforming yaw, and overall shearing of the tower due to shear forces. Shown above (**See Figure 8**)**,** the tower analysis gave reassurance that a final design could withstand possible forces up to ten times the maximum amount of yield stress experienced. Once the tower and baseplate are manufactured, testing by mounting the turbine to a car to simulate wind would determine if the math

behind the design was correct. Forces experienced can be estimated with a known temperature and speed of travel.

7.2.3. Brake (Sean)



Figure 19: Actuator Slider Testing

The braking system for the turbine was one aspect of the assembly that was behind schedule. Due to this, the testing of the sub-system was not completed before the project was halted. The Arduino code and circuit were built, and the actuator was able to be controlled with the use of a push button (**See Figure 19**). The plan was to analyze the braking sub-system through physical testing, using an apparatus made to simulate the loads produced by the blades of the turbine. Through this testing, the material of the brake pads and the proper stroke and speed of the linear actuator would have been chosen. Since the factor of safety for the braking system is below the industry standard of 2 at max runaway speed of 25m/s, the braking system would need to be actuated during the ramp up phase at 18 m/s. This would require further testing to ensure that the sensing system used in the design could detect wind speeds of 18 m/s and actuate the actuator promptly.

7.2.4. Yaw (Lucas, Marina & Matt)

The yaw system was another subsystem that was put on the back burner while other subsystem was being completed. The plan was to 3D print the Yaw for the final assembly after spring break. Yaw would be tested via car testing with the final assembly. The team made a mount to attach to roof rack that would secure the turbine to car. The team would force the turbine to rotate through turns and high wind speeds. The teams most concern was making sure yaw's rail system did not shear. The team would experiment with different 3D print fills and try to test for shear points and fatigue life.

7.2.5. Shaft (Lucas, Marina & Matt)

The shaft subsystem testing was on hold until the brake system was completed. The teams main concerned was shearing while braking the turbine. The shaft would be tested via caring testing. The team would stop the turbine at various wind speeds and applied brake forces. It was determined through blade tests our shaft and the startup torque of the motor in use.

References

[1] National Renewable Energy Laboratory, "US Department of Energy Collegiate Wind Competition 2020," 2019.

2021 Collegiate Wind Competition Technical Report

NORTHERN ARIZONA UNIVERSITY

May 23, 2021



Team Member	Team and Title	Contact Information
	MECHANICAL TEAM	
Barry Benson	Machinist	bjb448@nau.edu
Tore Cadman	CAD Consultant	tsc97@nau.edu
Bryce Conner	Project Lead (Primary Author)	bsc225@nau.edu
Joseph Conroy	DAQ Developer	jc3552@nau.edu
Stanley Kennedy	Capstone Liaison	ask98@nau.edu
Aaron Zeek	Aerodynamicist	acz34@nau.edu
	ELECTRICAL TEAM	
Benjamin Allen	Software Developer	bra92@nau.edu
Noah Bell	Electrical Lead	nsb85@nau.edu
Evan Kramer	Budget Liaison	edk37@nau.edu
Nolan McNeil	Hardware Developer	npm53@nau.edu
Aidan Nash	Technical Lead	aen73@nau.edu
	ADVISORS	
David Willy	Principal Investigator	David.Willy@nau.edu
Venkata Yaramasu	Electrical Consultant	Venkata.Yaramasu@nau.edu
Sarah Oman	Senior Design Coordinator	Sarah.Oman@nau.edu
David Trevas	Senior Design Instructor	David.Trevas@nau.edu



CONTENTS

I Executive Summary 2

II Design Objective 3
II-A Summary of Regulations . . . 3

III Aerodynamics and Blade Design 3
III-A MATLAB BEM Algorithm . . . 3
III-B Q-Blade Analysis . . . 4
III-C Structural Analysis . . . 6
III-D Finalized Blade Shape . . . 7

IV Pitching 7
IV-A Driven Pitch System . . . 7
IV-B Driving Pitch System . . . 8
IV-C Pitch Sub-System Testing . . . 8

V Braking 9
V-A Floating Disk Brake . . . 9
V-B Pitching to Stall . . . 9
V-C Brake Static Performance . . . 9

VI Yawing 10
VI-A Passive Yaw Fin . . . 10
VI-B Nacelle-Tower Connection . . . 11
VI-C Stress Investigations . . . 11

VII Other Mechanical Components 12
VII-A Nacelle . . . 12
VII-B Hub . . . 12
VII-C Shaft . . . 12
VII-D Base-plate . . . 13

VIII Electrical Interface 13
VIII-A Component Analysis . . . 13
VIII-B Control Logic . . . 14

IX Design Overview 15
IX-A Existing Prototype and Testing Apparatus . . . 16
IX-B Design Inspection . . . 16
IX-C Commissioning . . . 17

X Dynamic Testing 18
X-A Vehicle Testing . . . 19
X-B Electrical Investigations . . . 19

XI Conclusions 19

References 20

I. Executive Summary

The following report is the summation of Northern Arizona University's efforts in the 2021 Collegiate Wind Competition (CWC) held by the United States Department of Energy (DOE). The CWC encourages students at a variety of wind energy institutions to design, fabricate, and test a micro-scale wind turbine within the boundaries prescribed by the DOE in the 2021 CWC rules and regulations (RR) [1]. Upon completion of the project, students were to attend the competition to test the developed turbines in a public and competitive environment. However, due to the unpredictable circumstances brought on by the global pandemic, this stage of the competition has been forgone. The DOE as well as advisers at the National Renewable Energy Laboratory (NREL) have encouraged independent testing of the turbines appropriate to each university's capacity. NAU has made efforts to develop a data acquisition (DAQ) system that has been utilized to provide informative data to the state and efficiency of the manufactured turbine.

The group's design goal is to produce a safe and efficient turbine. This is done through the optimization of all components relevant for testing, as discussed in Section II. After the identification of the team's objective, following sections are assigned to each critical sub-system. Within these individual sections the team's design, analysis, and static experimentation of said sub-systems are discussed. This begins with the blade design, where the team constructed and employed a MATLAB algorithm along with the open-source program Q-Blade to converge on an aerodynamically and structurally appropriate design. Next the pitch system is introduced. The driven pitch system was chosen to be a hybrid linear bearing connected to mounted bearings through Heim joints. The driving system of the pitch was selected as a stepper motor pushing a gear train of miter, spur, and rack gears. This design is complimented by static experimentation that lead the team to utilize a specific pitch orientation. The braking and yawing systems are then discussed. The brake uses a linear actuator to clamp a steel disk onto a rubber backing in the nacelle in tandem with the stalling of the blades to reduce torque production, resulting in high factors of safety (FOS) without the concern of sheering the blades. The yawing is enacted by a passive yawing fin and complimented by a nacelle-tower connection methodology that utilizes two steel bearings to pinch the nacelle into place once the designed retainer locks the mechanism. The remaining components of the turbine (nacelle, hub, shaft, and base-plate) follow these trends in a more condensed fashion, discussing the key engineering requirements of each part and how said requirements were met.

In the final sections of the report, the electrical subsystem, design overview, and dynamic testing results are explored. The electrical analysis does not only depict the layout chosen to transmit mechanical power to electric power, but also the considerations that were made to aid in the turbine's optimum performance through an extensive control algorithm in charge of monitoring and/or adjusting the status of the pitch, brake, load connection, and emergency push button. The mechanical and electrical components are then combined and visualized. The remainder of the overview section will then discuss the turbine's conformity to constraints established in the RR in terms of safety and installation. Lastly, the efforts depicted in these section are dynamically tested in the prescribed environments to confirm the validity of each sub-system on an assembly level.

II. Design Objective

The NAU 2021 CWC team's (AeroAXE) objective is to design, fabricate, and test a micro-scale wind turbine as per the specifications of the 2021 RR that will operate efficiency and safely among the other submissions from the prestigious wind energy institutions throughout the nation competing in this year's CWC. This will be achieved by addressing all categories listed in Table A-2 of the RR [1]. Although the global pandemic has rendered the rubric listed for the testing of the turbine in Table A-3 of the RR no longer applicable, the group will remain resilient and persist in this individualistic environment and design with these rigorous tests acting as the driving factors. The team will emphasize the brake safety and the development of an appropriate power curve, but all other sections including start-up, rated control, and overall durability will be addressed with the full intent of obtaining as many (theoretical) points as possible.

A. Summary of Regulations

The DOE puts forth many regulations in regard to the fabrication of the micro-scale wind turbine. These regulations are not only present for accurate comparisons of the different university's turbines, but to also ensure the safety of the students and faculty involved in the testing of said turbines. Table I summarizes these regulations.

TABLE I
Turbine Design Constraints

Description	Target
Aerodynamic	
Cut-in wind speed	2.5 - 5 m/s
Operating wind speed	5 - 11 m/s
Rated wind speed	11 m/s
Testing wind speed	$\leq$13 m/s
Theoretical wind speed	$\leq$22 m/s
Dimensional	
Rotor volume	45x45x45 cm
Rotor centerline height from base	60 (±3 cm)
Base-plate diameter	$<$15 cm
Base-plate thickness	$<$16.1 mm
Reference diameter for fasteners	4.5 in
Mounting bolt diameter	10 mm
Electrical	
DC output voltage	$<$48 V
Tower resistance to ground	$<$100 kΩ
Turbine side capacitance	$<$10 J
Turbine side battery capacitance	0 J
Load side AC supply voltage	120 V

III. Aerodynamics and Blade Design

The aerodynamics of the turbine were the first considerations made in the early design stages of the project. Although vertical axis wind turbines (VAWTs) show promise in reduced wake production and flexibility in erratic flow fields, the group's design quickly converged to a horizontal axis wind turbine (HAWT) in consideration of the typical inefficiencies associated with VAWTs. Utilizing the mathematically intensive process that is described in *Wind Energy Explained* [2], the group compiled a MATLAB algorithm that produced an ideal blade shape with tip loss and wake considerations. Blades that showed promising C_p vs λ curves were then replicated in Q-Blade to produce more comprehensive analyses. It was determined that the inclusion of a pitching system would greatly enhance the group's design. For the trade-off of mechanical complexity the turbine would still remain competitively efficient in terms of both start-up and operating conditions. Finally, a sturdy connection methodology that is able to resist the maximum centrifugal forces of the micro-scale wind turbine was developed through finite element analyses (FEA).

A. MATLAB BEM Algorithm

The blade element momentum (BEM) theory suggests that by breaking a blade into segments and examining the aerodynamic phenomena on a differential level, an optimum blade shape and its respective efficiency can be calculated. The algorithm's required inputs are as follows: blade radius (R), design tip speed ratio (λ), airfoil specifications at each segment, rated wind speed (U), and number of blades (B).

$$C_p = f(R, \lambda, c, C_D, C_L, U, B) \tag{1}$$

Where c, C_D, and C_L are the airfoil chord length, drag coefficient, and lift coefficient, respectively. The computationally challenging aspect of the algorithm is the calculation of lift and drag forces.

These forces are functions of the angle of attack (α) and the Reynolds number (RE). By identifying the α at which the maximum lift to drag ratio (C_L/C_D) occurs for different values of RE, the optimum twist can be found for each blade segment when considering the rated values for U and λ.

Therefore, in order to properly operate the algorithm needed an array of airfoil data at varying RE values. XFOIL is an interactive program for analyzing airfoils embedded within Q-Blade which produces these data sets. Starting at a RE value of 3000, RE values up to 150,000 were simulated with increments of 1000. These values enveloped all possible conditions according to the group's early calculations. This in tandem with a small increment produced a comprehensive data base that allowed the group to catch any aerodynamic consequences due to subtle geometry changes. Figure 1 displays the data used to locate the optimum α, at which point separate data sets containing individual C_L and C_D values were retrieved from directories called upon by the program.

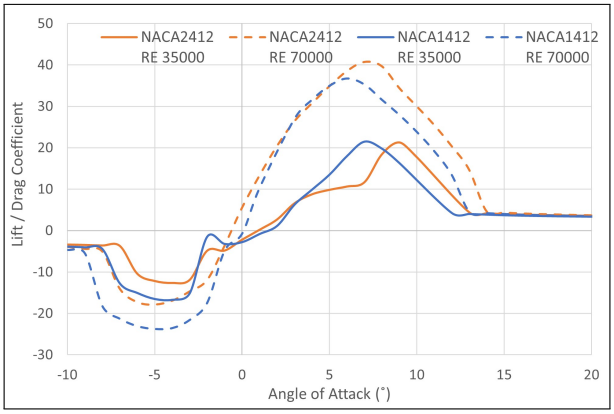


Fig. 1. C_L/C_D vs α

When considering the number of airfoils the group was interested in investigating along with the amount of data present in each file, the group stored over 80 data sets with each individual file consuming roughly 175 KB of storage. This resulted in extensive calculation times taking as long as two hours to converge. After adjustments to the algorithm's logic and convergence factor, run times as low as 30 minutes were experienced without any sacrifices in accuracy. After utilizing the algorithm many times, a three-bladed rotor with a design λ of 4 that incorporates the NACA2412 airfoil at its root and transitions to the NACA1412 for the mid-span and tip was selected. This combination resulted in a maximum aerodynamic efficiency of 43.1%, as supported by Figure 3 (seen in the following section comparing the algorithm results to a blade of the same shape using Q-Blade). This blade shape was selected not only for the high efficiency displayed, but also for the tendencies it exhibited prior to the operating λ, which indicated strong performance (C_p=25%) as early as $\lambda = 3$.

B. Q-Blade Analysis

Although the information produced by the team's MATLAB algorithm is vital to the production of the blade, extensive analysis needs to be performed outside the confines of the algorithm to understand the comprehensive characteristics of the blade. Torque production at lower wind speeds, inefficiencies at non-operating conditions, the benefits of pitching, and evaluation of runaway scenarios are all considerations that will prove beneficial to the team's design.

The first consideration is torque production at low winds speeds. As per the RR, the group is interested in power production at wind speeds as low as 2.5 m/s. In reflection of this, the group investigated the blade's performance at 3 m/s. According to static experimentation performed on the rotary system of the turbine, torque values should reach up to 0.02 N·m to produce any rotational movement. This is above the threshold exhibited by the MATLAB blade (Iteration I). Even after exaggerating the chord length at the root of the blade to increase solidity, therefore torque production, the inflated torque values the group attained were negligible at lower λ values. That is until the inclusion of pitching, which raised the torque differential of each blade from 0.4 N·mm to 5 N·mm when pitched 40°, as seen in Figure 2. Utilizing a pitching system, the rotor would ideally produce 0.0198 N·m at 3 m/s. In light of the drastic torque increase displayed by the magnified solidity, the geometry changes to the blade were implemented (iteration II) into the team's final design and were utilized in tandem with a pitching system to approach optimal start-up aerodynamics.

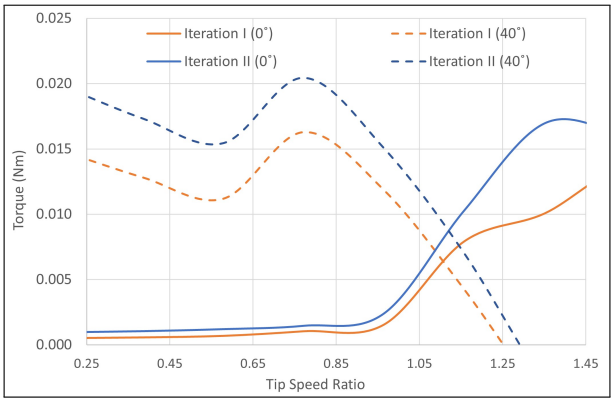


Fig. 2. Cut-in Torque Comparison at 3 m/s

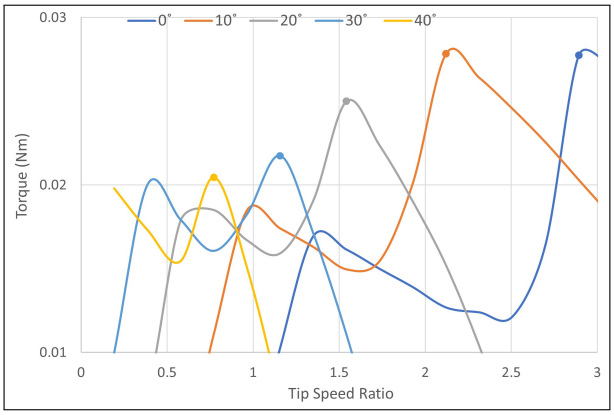


Fig. 4. Torque at 3 m/s with Varying Pitch (Iteration II)

Changes in geometry which aim to aid the conditions of certain operating scenarios often result in a decline in performance in other areas. However, blade iteration II displayed aerodynamic properties on par and even superior to iteration I (Figure 3). Apart from the design changes that will arise from a new ideal λ of 3.5 and the inefficiencies that appear after a λ of 4, the amended blade boasts a higher maximum efficiency of 45.1% along with more promising trends at lower rotational velocities.

The inclusion of an active pitching system solves one of the largest problems seen in lift machines by increasing torque production in low wind regimes, but introduces a considerable amount of complexity to the control algorithm. The complications arise from the relationship of torque with wind and rotational speed as exhibited in Figure 4. Until streamlines disconnect, increasing pitch will result in the maximum torque occurring at a lower λ at the cost of said torque's magnitude. The control algorithm would ideally start at a pitch of 40° and then adjust until operation conditions for that wind speed are achieved. However, the variables that are required to find optimum pitch vary frequently in flow fields of this size. This encouraged the group to make estimations of ideal conditions utilizing the turbine's power production, discussed further in Section VIII.

Before confirming the final design, it is pertinent to examine conditions in which the generator is disconnected from the load and is free to accelerate to the runaway λ value which will produce excessive centrifugal forces. The identification of this value relies on the convergence of the BEM iterator at rotational speeds that surpass rated λ. Since BEM iterators can have issues with stability

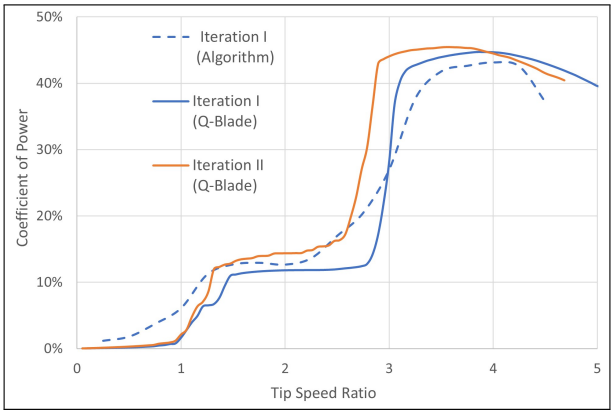


Fig. 3. C_p vs λ at 11 m/s

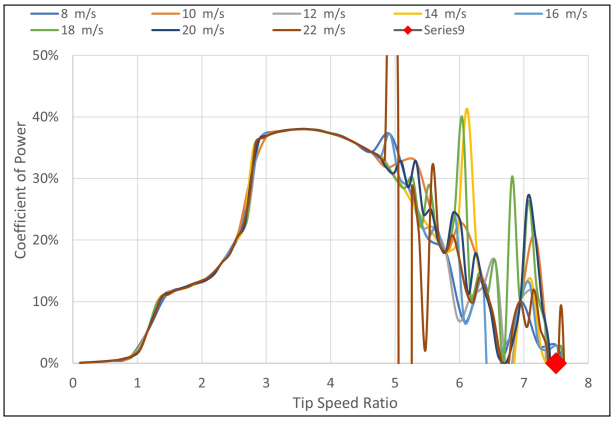


Fig. 5. Runaway λ Values for Different Wind Speeds

in this region, the group used several different C_p vs λ curves to approximate this value, as seen in Figure 5. It is apparent that most wind speeds have a runaway λ range that straddles 7.5. This results in rpm values up to 8100 when considering the existing geometry.

The final data that needed to be extracted from Q-Blade is the power curve and its respective annual energy production. Assuming operating conditions that would result in maximum power output for each wind speed, the turbine has a rated power output of 60 W. Using a variety of Rayleigh distributions, the annual energy production was derived assuming average wind speeds of the same range as seen in Figure 6.

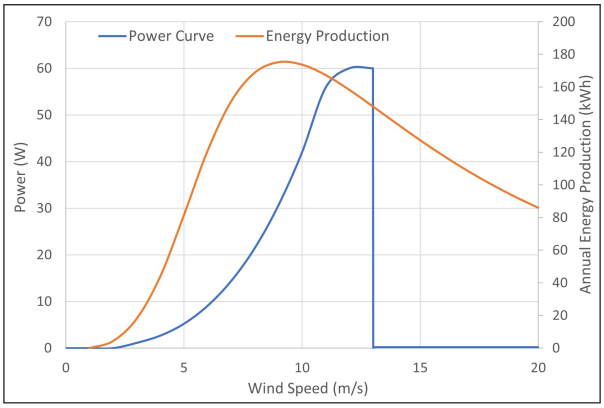


Fig. 6. Power and Energy Production vs Wind Speed

C. Structural Analysis

Any object placed within a flow field and expected to remain fastened to a single point will experience thrust forces. In regard to turbines, the calculation of this force is a function of the field's dynamic pressure and the axial induction factor (a).

$$T = \frac{1}{2}\rho A U^2 \left[4a\left(1-a\right)\right] \tag{2}$$

In parked conditions, the second half of the equation involving the axial induction factor becomes irrelevant and the maximum rotor thrust can be evaluated as 11.4 N. However, dynamic conditions will alter the inputs to this equation. Inclusion of an ideal axial induction factor (1/3) and the new swept area will result in forces on the order of 31.1 N.

The calculation of thrust production on the rotor is important for the safety of many sub-systems, but the largest stress sources stem from the centrifugal forces. This design will require stresses lower than the tensile strength of the final material to avoid catastrophic mechanical failure. The group predicts that with the existing blade geometry forces up to 6.2 kN could be experienced. This results in stresses up to 18.4 MPa. However, concentrations due to rapid changes in the blade's cross section still pose a threat beyond this. In order to confirm that the selected blade geometry can be supported by the available materials, an FEA analysis was performed implementing the maximum values of thrust and rotational velocity. Figure 7 shows that a majority of the mid-span experiences stresses on the order of what was predicted.

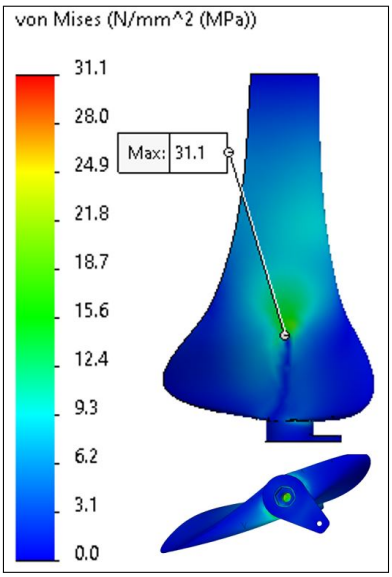


Fig. 7. Blade FEA Analysis

However, stress concentrations with magnitudes up to 31.1 MPa are found at the bolt connection. Referencing experimental data, the tensile strength of PLA is on the order of 36.5 MPa [3]. Therefore, the FOS is 1.17. As this phenomenon only occurs when the load disconnects, which will trigger the control systems to park the turbine, the FOS should prove sufficient considering the minimal exposure the turbine will have to these forces.

The group performed a strength test to confirm the above FOS. Seen in Figure 8, the blade was fastened upside down from a ladder suspended

wooden 2”x4”. Weights in the form of 80 lbs concrete bags were added to loading apparatus. For the safety of the on-site personnel, after every 80 lb bag was added, 80 lbs of lifting weights were added and removed in increments to confirm the blade was capable of suspending another bag. Due to spacial restrictions and the lack of proper facilities, only 480 lb (2.13 kN) was added before safety concerns arose. Although this did not reach the maximum forces predicted at 22 m/s for runaway, the achieved loading is 6.3 times the magnitude predicted in optimum operation and 0.98 times the maximum test runaway (13 m/s).

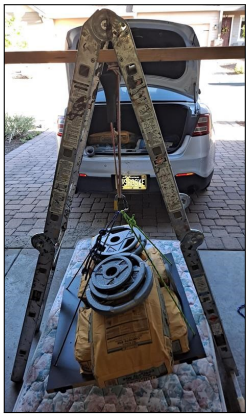


Fig. 8. Blade Loading

D. Finalized Blade Shape

The final design employs the shape that was developed through MATLAB and improved by Q-Blade iterations. The design also needed a connection methodology to the mounted bearings and Heim joints utilized in the driven pitching system, further discussed in Section IV. For the bearing connection, a 60 mm M6 bolt threads into carefully dimensioned plastic using a high torque drill in tandem with the presence of a hex bolt coupler secured with epoxy. The Heim joint connection is on a flange that extends from the base of the blade with a 30° offset from operating for optimum pitch range. In consideration of this offset, the group included a cut on the flange to signal the pitch position. All of these features are present in Figure 9. Table II also lists information regarding the chord length and twist at each segment along the blade. The fabricated blade is also shown in further detail within Section IX.

IV. Pitching

As derived in the previous section, the aerodynamic freedom that is introduced by the implementation of a pitching system encouraged the team to follow this design path. The system has the driven and

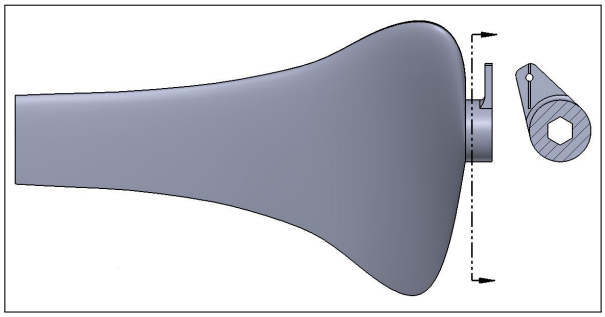


Fig. 9. Final Blade with Connections

TABLE II
Blade Dimensions

Radius mm	Airfoil	Chord mm	Twist °
0	Circular	25	N/A
11	Circular	25	N/A
30	NACA 2412	130	31.6
50	NACA 2412	105	22.5
70	NACA 2412	70	16.2
90	NACA 1412	60	13.4
110	NACA 1412	50	10.3
130	NACA 1412	44	8.0
150	NACA 1412	40	6.3
170	NACA 1412	38	4.9
190	NACA 1412	36	3.8

driving components. A modified swash-plate is used to connect these two systems. Heim joints and mounted bearings were then used to fasten the blades to the pitching system and hub. The inclusion of these kinematic devices allowed for multiple degrees of freedom to prevent binding of the driven system and reduced friction faced by the driving system, which consists of a stepper motor and gear train that allows for the linear movement along the shaft.

A. Driven Pitch System

The system was inspired by the previous 2020 NAU CWC team who attempted to utilize two linear actuators symmetric about the shaft to push a swash plate and alter the pitch by turning physical adapters between the hub and blades [4]. Upon reverse engineering, the group found several areas to improve upon.

Firstly, the previous team’s shaft was a thin steel shaft, in contrast to the thick aluminum shaft fabricated for this year’s competition. The clearance diameter of the previous swash plate

was too small for the newer shaft. However, swash plates of larger diameter showed a drastic increase in price. This reality, coupled with the fact that swash plates feature a 2nd degree of freedom required for cyclic pitching that is essential when operating helicopters but useless in micro-scale turbine application, the group decided to forgo an outsourced part and design a linear hybrid bearing that would grip the shaft allowing for extra support of the rotating axis, minimal resistive torque, and a more cost effective product. The final iteration of this part can be seen in Figure 10. The hybrid linear bearing was 3D-printed in four segments prior to the insertion of individual ball bearings and then sealed with epoxy in post processing.

The group also sought to include mechanisms to reduce the innate friction of the system. Rather than mounting the rotating component of the blade directly to the hub and relying on the power of the driving system to force rotation, the group used mounted bearings to connect the hub and blades. The use of Heim joints was then imitated and connected via 3D-printed couplers, as they proved efficient in the prevention of binding between the fastened parts.

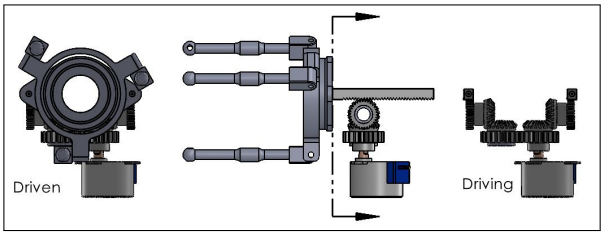


Fig. 10. Pitching System

B. Driving Pitch System

In regard to the driving pitching system, the group considered the use of linear actuators, but the lack of precise control available for actuators led the group to utilize a stepper motor to give the system more agency over pitch and therefore experienced aerodynamics. After some debate on the most spatially efficient way to translate the rotational movement to the desired linear movement, a gearing system that utilizes miter, spur, and rack gears was implemented. This methodology allowed for a compact design and served as the foundation of the upper nacelle blueprints. The fabricated system is also displayed in Section IX.

C. Pitch Sub-System Testing

A majority of the thrust force derived in Section III will be supported by the shaft or translated into the displacement of the blades. This displacement will be a phenomenon that the driving servo of the pitching mechanism will need to either support or counteract. Figure 11 shows the testing apparatus that was used to find the point at which the stepper motor failed to pitch forward. Varying sizes of Jenga blocks (12g-170g) were added to a 3D-printed platform that was inserted within the vertically oriented upper nacelle. The apparatus was powered by a 6V input and controlled by two push buttons to pitch forward and backward. In the process, the group found the implemented stepper motor failed to push loads above 3.3 N (0.74 lb). To account for the minimal holding torque derived through this experiment, the team chose a particular pitching orientation to compliment this constraint. The pitching mechanism will push when seeking to increase torque and pull when seeking to lower torque at low and high wind regimes, respectively. The idea of over pitching the blades to decrease torque production in strenuous flow conditions is discussed further in Section V. This methodology creates an environment where the driving system will not face extensive thrust forces when seeking

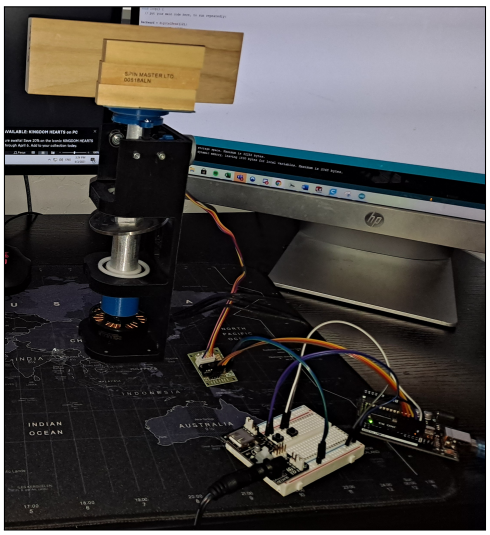


Fig. 11. Pitching Test Apparatus

to move forward and will only need to overcome the innate friction of the system while also utilizing said thrust forces when attempting to stall.

V. Braking

The braking system is a floating disk which uses a linear actuator to apply a clamping force to pinch a steel disk against a rubber brake pad and backing. In tandem with this stopping force, the inclusion of the pitching system allows for the natural decline of the aerodynamic forces acting upon the blades, greatly reducing the potential of shearing off the rotor due to the rapid change in rotational kinematics. The capabilities of these mechanisms are mathematically analyzed and statically exposed to the relevant forces. Due to the simplicity of the sub system, in place of a CAD drawing, the fabrication is seen in Section IX.

A. Floating Disk Brake

A standard floating disk brake system that applies a clamping force with an actuator is the primary means of parking the turbine. The group originally planned to use two actuators symmetric about the shaft. However, further investigation proved this method to be excessive. The finalized design features a rubber brake pad which pushes the disk against a rubber nacelle backing in place to prevent the excessive heating of the 3D-printed plastic used in the nacelle. The inclusion of this backing was inspired by test results of previous NAU CWC teams where parts were warped due to excess friction. With the 50 N axial force produced by a single PQ12-P Actuonix actuator, the minimum estimated friction factor between dry rubber and steel at 0.6 [5], and the acting distance of the actuator, the braking torque available to the system is on the order of 3.45 N·m. When comparing this to the expected maximum torque values at 22 m/s shown in Figure 12, the brake disk has a FOS of 2.3. The magnitude is increased further by the inclusion of the turbine's pitching capabilities.

B. Pitching to Stall

Another aspect of pitching was briefly discussed in Section IV, which is the ability to pitch the blades to stall. This gradually decreases torque production. If the blades are in operating conditions at 22 m/s, the turbine has the potential of producing up to 1.49 N·m of torque. After pitching forward 15°, this value occurs at a much lower λ with a magnitude of 0.44 N·m. Although continuing to increase pitch will result in a lowered maximum torque and ease of braking, the group has only allotted for 10° of control. This design was encouraged by the limited pitch range derived from the confined linear space available while taking into account the larger range required for desirable start-up characteristics as depicted previously in Figure 4. This lowers the maximum required torque production of the brake disk to 0.65 N·m, raising the FOS to 5.3. In addition to the lowered torque, the induced reduction in rotational velocity will lower the chances of a blade shearing off due to the sudden rotational deceleration.

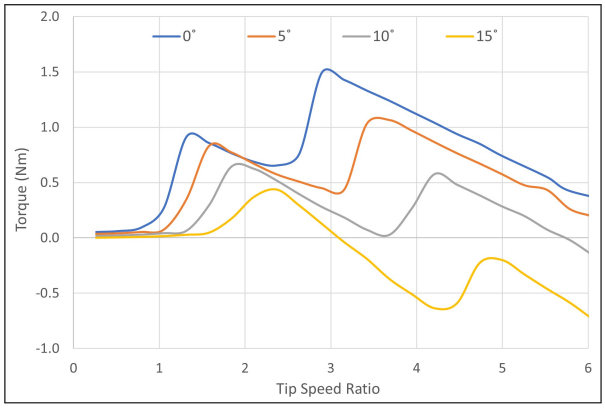


Fig. 12. Torques Reduced by Stall at 22 m/s

C. Brake Static Performance

The testing of these sub-systems prior to assembly will help ensure the validity of the braking process. Figure 13 is representative of the apparatus fabricated for testing the holding torque of the brake disk when clamped by the fully extended linear actuator powered by 6 V. The actuator is controlled by two push buttons that extend and retract the shaft. The weights are the same Jenga blocks implemented in the pitching tests. The upper nacelle is locked in place using duct tape. The lever arm designed for this experiment in tandem with the cardboard volume serving as a load capacity exert a natural torque of 0.21 N·m. After adding 26.9 N, the disk began to slip. The holding torque achieved was 2.64 N·m. This value is slightly lower

than the predicted values based on the spec sheets of the equipment, but still provides FOS of 1.8 and 4.1 when considering braking from operating and stalled conditions.

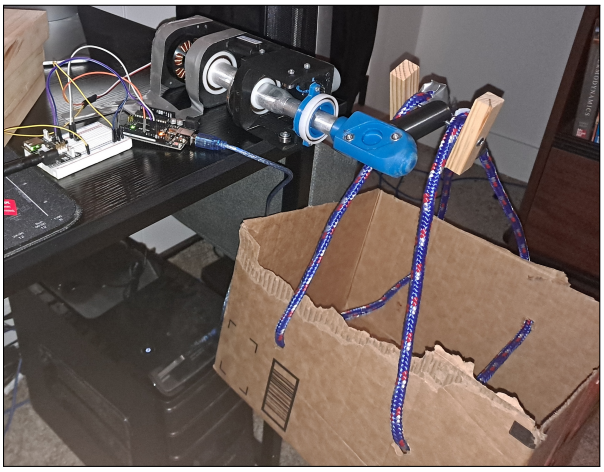


Fig. 13. Braking Test Apparatus

In regard to pitching, the group has seen superb results in static experimentation. The group confirmed that the stall was enough to prevent rotation up to 40 mph (17.9 m/s). Despite the strong performance, Figure 12 would predict similar results even at operating pitch conditions. Further confirmation of the aerodynamic response when stalling from high rotational velocity is required to confirm the mechanism's true effectiveness.

VI. Yawing

Yawing refers to the active or passive system utilized to ensure the orthogonal relationship between the rotor plane of the HAWT and the fluid direction. In micro-scale turbines, active yaw systems are cost inappropriate as well as unnecessary. Due to the loss of efficiency associated with down-wind rotors (one strategy for passive yawing) and the 45 cm range permitted to the team, the yawing fin design route was followed. Through trial and error, different iterations of the group's fin geometry was analyzed at different offsets from alignment and wind speeds until appropriate forces were achieved. To induce the rotation of the turbine, the nacelle's connection to the tower needed to employ mechanisms that permit said rotation. The structural integrity of said connection was then tested.

A. Passive Yaw Fin

The use of a passive yawing fin is common practice in small scale wind turbines. A surface area parallel to the flow field and extended from the axis of rotation (the tower) will result in a yawing system that employs the dynamic pressure innately available in the fluid. Mathematical modeling of this phenomenon requires considerations of the fin's geometry and position. Through augmentation of the equation for dynamic pressure, the team performed further analysis by means of Equation 3.

$$T_{yaw} = \frac{1}{2}\rho U^2 x_c(\theta) \int_0^{L(\theta)} z(x)\, dx \qquad (3)$$

Where the torque production of the yaw is a function of the fluid conditions and exposed area of the fin set by the angle at which the rotor and flow are offset from alignment (θ). In the case that the fin is not a uniform plate, the distance from the axis of rotation (x) will alter the height (z), which when integrated along the length of the exposed fin (L) will return the area. Finally, the force's magnitude is then scaled by the acting distance, identified by the exposed area's center of mass (x_c). In order to apply Equation 3, a preexisting geometry is required. Upon the third iteration of the fin, seen in Figure 14, sufficient torque production was seen to counteract the resistivity of the nacelle-tower connection along with the torque on the rotor due to induced thrust forces previously derived. The fin is split into two segments along the mid-span to allow for 3D-printing despite the size of the part. The wings are placed at an 8° offset to improve the performance of the fin at lower values of θ. The fin's wings also take the profile of the NACA0009 airfoil, as inspired by Pennsylvania State University's 2019 CWC design [6]. Drafts extend from the nacelle-fin connection point. These two aspects were included

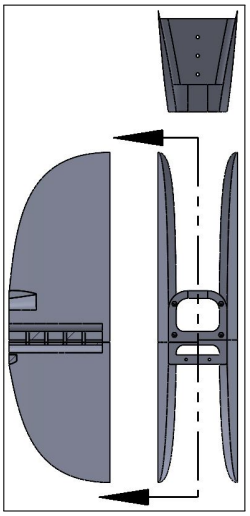


Fig. 14. Yawing Fin

in an attempt to reduce the formation of eddies behind the turbine. The fabricated yaw is depicted in Section IX.

B. Nacelle-Tower Connection

The inclusion of a yawing fin creates the need for a nacelle connection to the tower that permits rotation. A standard two-stage bearing train was implemented that feeds through an opening in the bottom of the lower nacelle. The tower diameter has a slight step down to secure the inner lip of the bottom bearing. The nacelle (not shown in Figure 15) is then inserted, followed by another bearing which clamps the nacelle using the outer lips of both bearings. In initial blueprints, the final steps were the inclusion of a retaining ring to secure the assembly and a slip ring placed atop the tower to allow for the rotation of the nacelle without the entanglement of wiring.

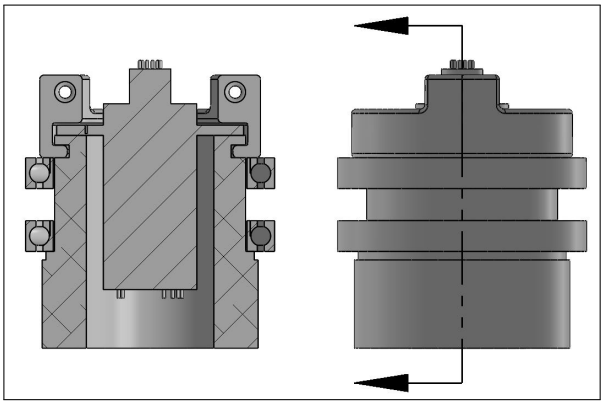


Fig. 15. Nacelle-Tower Connection

Through fabrication, the group found two issues with this methodology. The first is a tolerance issue that arose between the outsourced bearings, retaining ring, and machined tower. The available space resulted in excess tilt that reduced the efficiency of the turbine. The second issue was the minimal fastening methodologies available to the slip ring. The team addressed these aforementioned problems by developing a two-part retainer that would fill the entirety of the tower's indent, clamp down the slip ring, and align the top support bearing with the tower. By introducing a 3D-printed part to the sub-assembly, the team was capable of iterating on dimensions until an optimized system was fabricated without the consequences of purchasing inappropriate components or redoing cost intensive machining.

C. Stress Investigations

The component likely to fail under excessive shear stress within the sub-system is the *straddle* of the lower nacelle that is clamped by the bearings. An FEA was performed based on the induced torque from the thrust on the rotor. Figure 16 displays the results and indicate a FOS of 11.4.

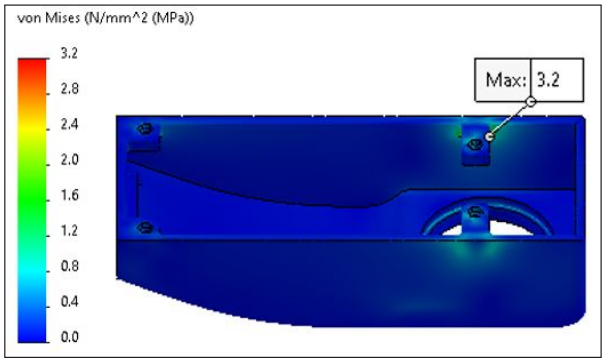


Fig. 16. Nacelle-Tower Connection FEA

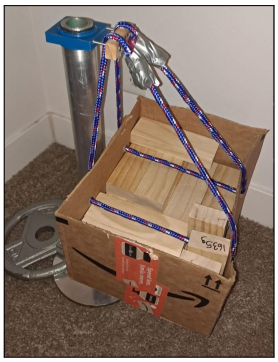


Fig. 17. Connection Testing

From there, static testing of the part exhibited the capability of the turbine to not only withstand the expected forces during operation but also confirmed the absence of any binding within the mechanism. Jenga blocks were added to a loading apparatus as seen in Figure 17. After each addition, the apparatus was rotated 360° four times to confirm that movement would not induce mechanical failure or binding. The group added 69.4 N before experiencing issues with the spatial loading capacity. This weight resulted in a torque value of 4.51 N·m. Although the group was unable to test until failure, the value reached is above that of the expected maximum 3.81 N·m calculated through thrust and geometric considerations.

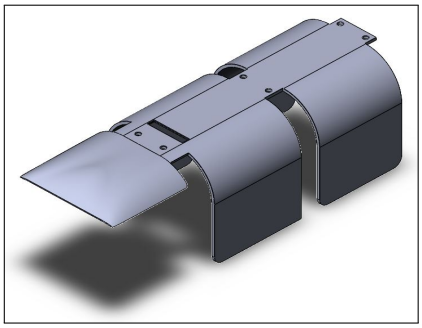


Fig. 18. Cover

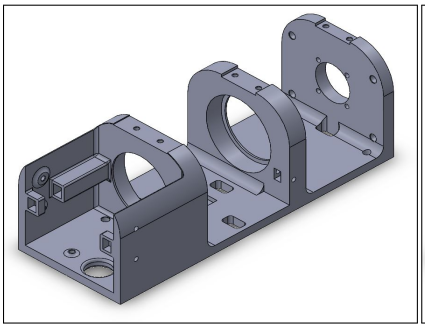


Fig. 19. Upper Nacelle

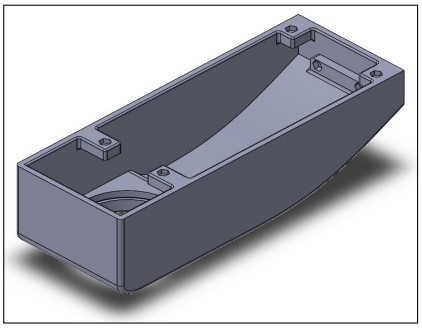


Fig. 20. Lower Nacelle

VII. Other Mechanical Components

Within the past year, the team has spent nearly 2600 hours researching, designing, and reporting on the contents of the turbine. The entirety of the story cannot be comprehensively expressed within twenty pages. The following section will report on components that received no less mathematical or engineering analysis than other sub-systems but do not highlight the more distinctive aspects of the team's design. All of these parts' printed/machined models can be seen in Section IX.

A. Nacelle

The nacelle can be dissected into three sections, the upper and lower nacelles along with the cover. The upper nacelle houses the brake disk, linear actuator, driving pitch system, generator, and support bearing. It also must connect to the lower nacelle, cover, and fin. The part needed to be carefully toleranced considering the amount of sub-systems that rely on the dimensions of the component. The part was 3D-printed four times before all aspects were appropriately sized with changes to the last iteration on the order of 0.15 mm.

The lower nacelle was previously shown in an FEA (Section VI). Apart from withstanding sheer stress, the lower nacelle needs to provide space for the slip ring, wiring, retainer, electrical headers, driver board, and stepper motor. Four connection points for the upper nacelle and two for the fin are also present. These connections utilize an epoxy secured hex nut but also thread into a portion of the plastic itself.

The cover is derived from the shape of the upper nacelle. The cover should not interfere with any of the components while making a semi-flush surface to prevent the formation of eddies within the sections of the nacelle.

B. Hub

Since the hub consumes space that is valuable to the translation of wind energy to mechanical power, it should be as minimal as possible without sacrificing structural stability. The hub provides a center clearance for the bolt head protruding from the mounted bearing and adjacent clearances for the hex couplers that secure said bearing to the hub. An adhesive FOS of 2.4 is obtained by maximizing the surface area of the epoxy secured coupler at the cost of no plastic threading. However, when considering runaway at the maximum theoretical wind speed, the hub has an insufficient FOS (0.54). Since RPM and voltage are directly related, this issue can be solved by the inclusion of an over voltage protection event that is discussed further in Section VIII. This raises the hub's FOS to 3.11.

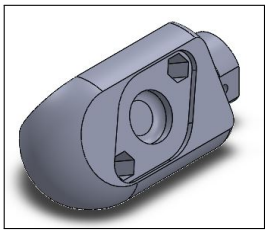


Fig. 21. Hub

C. Shaft

A plastic shaft was considered in the early stages of the project, but the weight of the rotor acting on the shaft caused bending, leading to an array of inefficiencies. The shaft includes several step downs to allow for insertion into the hub, brake disk, and generator coupler. A maximum stress of 1.4 MPa was identified through the use of previously derived

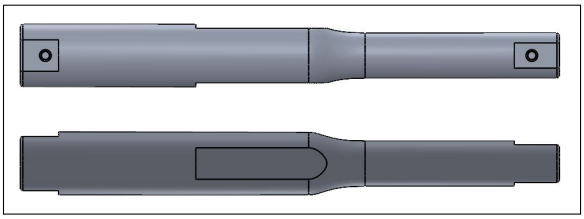


Fig. 22. Aluminum Shaft

values (Section III) in an FEA. When considering the tensile strength of aluminum, the FOS is 183.6 [7]. This exaggerated value is a result of initial dimensions assuming a plastic shaft. This drove the sizing of other components in the initial design phases, resulting in shaft geometry that had to be retained even after switching materials.

D. Base-plate

The aluminum tower was welded to an aluminum base-plate. Although this methodology results in an excessively large FOS of 24.5. The utilized manufacturing process was cost appropriate and simple for experienced welders. This part is seen manufactured in Section IX.

VIII. Electrical Interface

The fabrication of the electrical systems to transfer the mechanical energy produced by the turbine into usable electrical power is the final sub-system. This topology is depicted in Figure 23. This begins with the use of a 110 kV MAD generator selected for its strong performance at low rotational velocities. The FUS 45-0045B six diode rectifier was then utilized to convert the turbine's output from an AC to DC voltage. A DROK LTC1781 DC/DC step up converter is employed to reach a rated 30 V. Prior to this step up, voltage readings are sent to the Arduino Mega micro-controller (MCU) through an

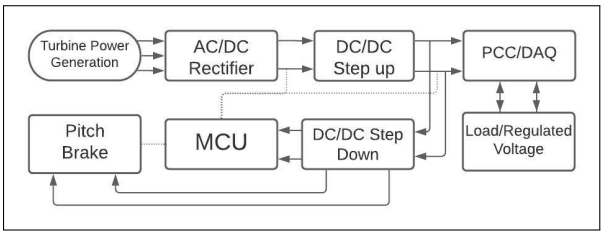


Fig. 23. Electric Topology

INA260 voltage sensor to be used in the control algorithm. This regulated voltage is then split into two separate circuits. The first is to the XL4015 DC/DC step down converter to power the MCU, the 28BYJ-48 stepper motor (pitching), and the PQ12-P linear actuator (braking). The second circuit leads to the point of common coupling (PCC) and load system developed by the group. Another INA260 power sensor is implemented prior to exiting the electrical housing to detect continuity between the turbine and PCC.

A. Component Analysis

The first step to the integration of the electrical and mechanical systems is the 3-phase generator. To perform efficiently at lower wind speeds, the group moved forward with an 110 kV generator. However, the lower kV rating resulted in lower FOS at higher rpm values. A runaway event at a wind speed of 22 m/s would result in a 72.7 V output from the turbine. This is not viable for any of the components implemented into the system, as seen in Table III. This table suggests a maximum value of 35 V.

TABLE III
Electrical Component Specifications

Component	Input	Output	Maximum
12 Ch. Slip Ring	-	-	10 A
18-Gauge Wiring	-	-	15 A
Rectifier	0-45 VAC	0-45 VDC	45 A
DC/DC Step Up	3-35 V	3-35 V	15 A
DC/DC Step Down	8-36 V	1.25-32 V	5 A
Voltage Sensor	0-36V	0-36V	15A
Load (0-4.75) Ω	-		100 W

This voltage production would be seen at a runaway event as early as 10.4 m/s, but would never occur within normal operating conditions. Therefore, in order to assure the safety of the electrical components within the circuit, an over-voltage protection event that will trigger the braking system at any voltage read out above 30 V prior to the DC/DC step up converter will be employed. In theory, the disconnection of the load would park the turbine before this command. The 5 V clearance has been implemented to raise the FOS (1.17) as well as account for any inaccuracy or delay added by the voltage sensor/MCU. An

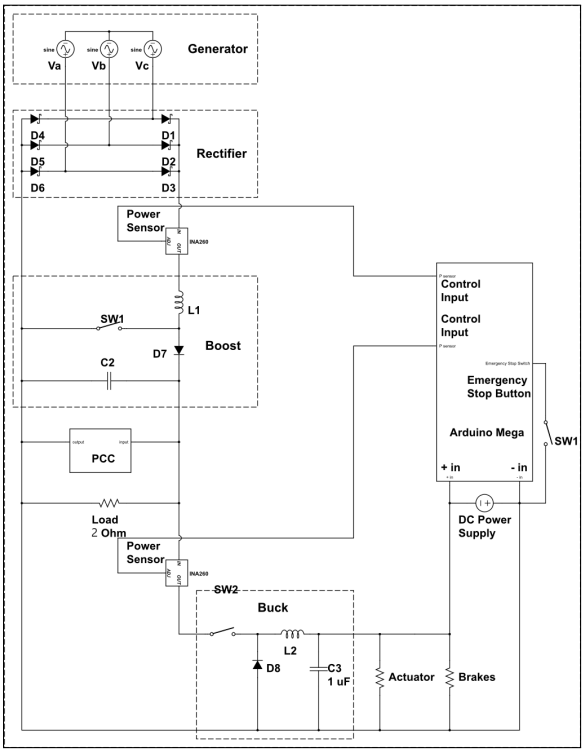


Fig. 24. Electric Diagram

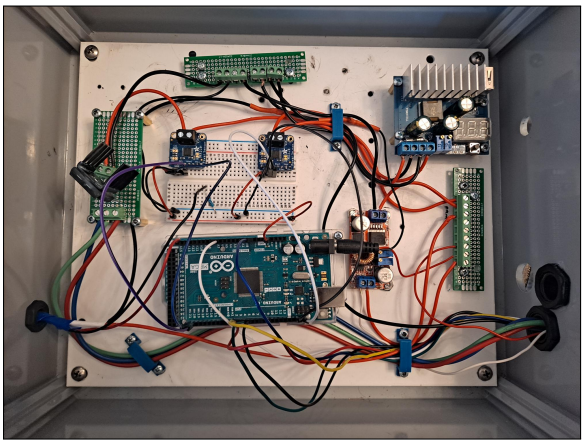


Fig. 25. Electrical Housing (Inner View)

electrical diagram of the components can be seen in Figure 24 along with the physical layout of the components seen in Figure 25.

Apart from the electrical housing, the NAU 2020 Energy Club fabricated a PCC for future CWC teams to use in testing. The team's PCC utilizes a LabVIEW UI and includes physical voltmeter and ammeters displays atop the housing to aid in troubleshooting. The PCC follows the connection methodology as described by the 2021 RR and has several extra ports for future teams to improve upon. One of the add-ons incorporated during the 2021 spring semester was a cup anemometer for wind speed readouts. Also included within the PCC black box is the emergency push button, which is another component that was handed down by previous NAU CWC teams.

The remaining electrical components of the system are the electrical loading and DC feedback. The loading should allow for optimum power output while ensuring current values below the maximums seen in Table III. With these considerations, a resistance of 2 Ω was selected. However, this is not the only safety concern associated with the loading. As testing is to occur within a vehicle, the group must safely secure the load within an enclosure so that no members or equipment are in danger when the turbine is in operation. The team utilized a metal enclosure handed down by previous NAU teams to ensure the safety of the involved individuals.

B. Control Logic

The turbine utilizes an Arduino Mega to control the turbine in operation. The algorithm will begin by checking the three shut down scenarios. The first is the over voltage protection event. If the voltage prior to the DC/DC step up is larger than 30 V, the turbine will pitch the blades to stall and then extend the actuator. However, because parking the turbine will reduce the voltage, the turbine would then inappropriately release the braking system in an over-speed event if the above condition was the only parameter for over-voltage protection. Therefore a manual aspect is introduced, where the emergency push button circuit must be opened and closed before operation is to resume. The same events will occur if the emergency button circuit has been opened (as per the RR) or the post DC/DC step up continuity returns an open circuit through the detection of voltage with no current. The algorithm will then loop itself until the emergency button is released and the load connection proves continuous, at which point the pitching loop will begin after releasing the braking system.

As mentioned in Section III, the variables that

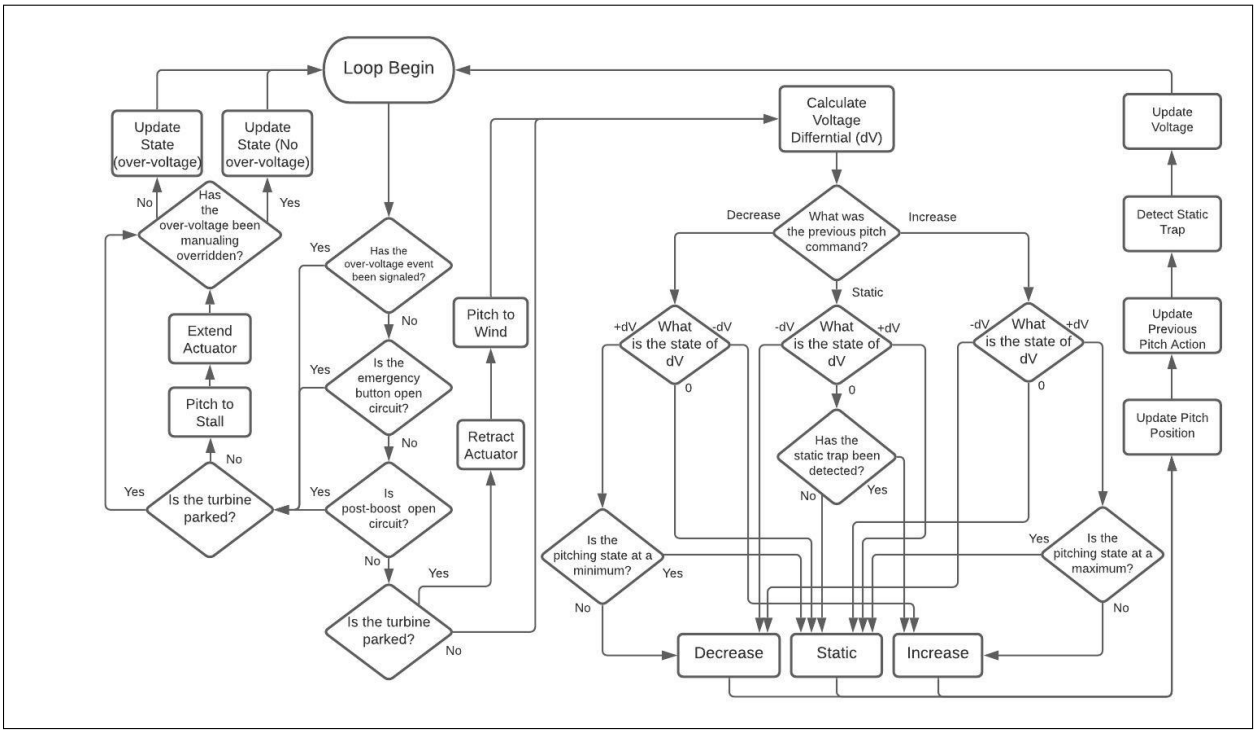


Fig. 26. Control Algorithm

determine the optimum pitch angle vary frequency and are challenging to accurately obtain in real time. In response to this, the group utilized a system that tracks the voltage differentials (dV) and compares them to the previous pitching action to determine the next appropriate command. For example, if the previous action pitched the blades closer to operating from a start up position (increase) and the voltage mirrored this magnification, it will once again *increase* the pitch. In contrast, if that increase produced a negative dV, the controls would then pitch from operating back to start up (decrease). If the magnitude of dV is below the designated threshold, the turbine will remain static. This logic is visualized in Figure 26.

There are several considerations that go into this logic that will optimize its performance and prevent it from malfunctioning. One of these considerations is the magnitude at which dV is considered non-zero. This value must be complimented by the incorporated delay as well as the increments at which the pitch is changed. Misalignment of these values can either result in a turbine that does not pitch and sits idol or one that is constantly pitching and drawing a needless amount of current. The team sets these values as 0.2 V with a 0.5 second delay in which the motor will pitch 1° ($\approx$ 6 steps). However, if the above logic was the extent of the algorithm, the unpredictable conditions of the wind could trap the turbine in a futile loop.

Assuming start-up position at the time of commissioning, the pitch position is tracked to avoid this. This allows the algorithm to prevent movement beyond the physically available pitching range. The final consideration is the static loop, where steady flow could result in the turbine remaining at sub-optimum pitch conditions. A tracking variable that persists for a number of loops will break this cycle if it is detected that the turbine has remained static with no voltage differential for too long. Although this has the potential to disrupt operating conditions, the algorithm will quickly return the turbine to ideal pitch positioning in that scenario.

IX. Design Overview

In the preceding sections, sub-systems have been individualistically discussed to justify the utilized

designs. This section will present the turbine in a comprehensive manner. This will be done through the visualization of the fabricated product as well as its accompanying testing apparatus. This is followed by an assessment of the turbine's conformity to the constraints established in Section II through the technical inspection checklist presented in Appendix B of the 2021 RR. This checklist will be shown in tandem with a summation of other safety measures mentioned throughout the document. The section will be concluded with the instructions for the turbine's commissioning.

A. Existing Prototype and Testing Apparatus

The blades, as well as their connection to the hub, are displayed in Figure 27. Following this, the pitching system is shown in Figure 28. The brake and generator mounting system (a sub-function of the upper nacelle) are highlighted in Figure 29. The yawing fin is displayed by a side view of the upper portion of the assembly in Figure 30. This figure also features the cover, which has been left out of other images for clear visibility. Figure 31 shows the management of wiring within the nacelle, as well as a portion of the nacelle-tower connection. Figure 32 displays not only the weldment and M10 clearence holes of the baseplate, but also depicts the apparatus used to prevent the crushing of wires when not in commission.

Accompanying the physical turbine are the electrical systems. The team's electrical housing, which contains all components listed in Table III other than the slip ring and variable load, is seen in Figure 33. Next is the Energy Club's PCC and resistive load, present in Figures 34 and 35. Note that the enclosure shown would have the lid bolted over the load when in commission. Finally, the group utilizes a Jeep Wrangler (Figure 36) with a detachable roof to attach a plywood apparatus atop the vehicle to test the turbine, the installation of which is precisely documented in the commissioning subsection to follow.

B. Design Inspection

The team's principal investigator acted as the judge for the unofficial technical inspection. All safety requirements have been met and most non-safety requirements have been either met or addressed.



Fig. 27. Rotor

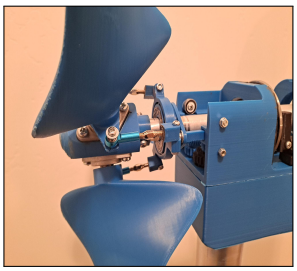


Fig. 28. Pitching System

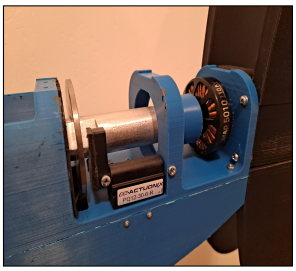


Fig. 29. Brake System

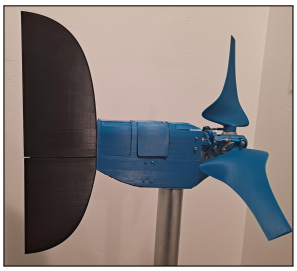


Fig. 30. Yaw Fin

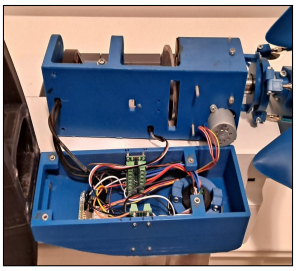


Fig. 31. Lower Nacelle

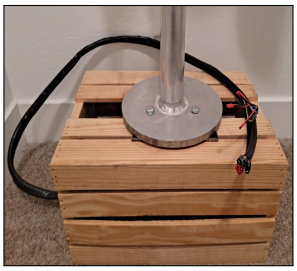


Fig. 32. Base Plate

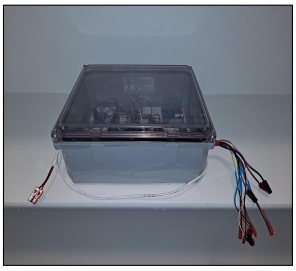


Fig. 33. Electrical Housing

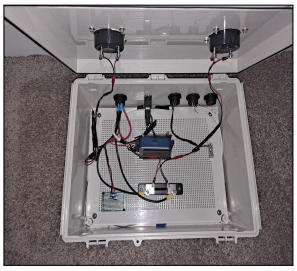


Fig. 34. In-House PCC

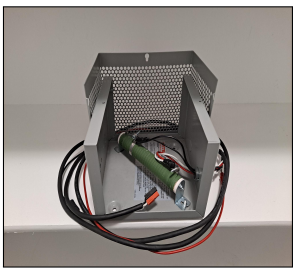


Fig. 35. Resistive Load

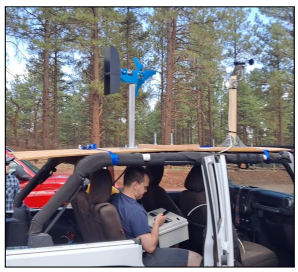


Fig. 36. Testing Apparatus

The following enumeration represents the only categories where the team's design strayed from regulation.

- The turbine mid-plane sits at 710 mm.
- The base plate diameter at 228 mm (9").

These anomalies are the result of prioritizing interfacing with the in-house apparatus. The rotor mid-plane sits at 710 mm from the base plate's bottom. This was done to retain the same height as the preexisting NAU Energy Club's anemometer equipment. Furthermore, the base plate's diameter was left at a larger diameter of 22.8 cm (9") to ensure a safer connection to the plywood apparatus.

Even beyond the official measures, the design of machines rotating at thousands of rpm need a considerable number of safety precautions. Parts discussed throughout the document have received both analytical and experimental verification of their performance under their most strenuous operating conditions. Those efforts are summarized in Table IV. Up until this point, presented FOS have only considered worst-case scenarios. For comprehensive documentation of the turbine, Table IV includes values for other relevant states of the turbine using the same analyses previously implemented. This includes situations that would theoretically not occur under the management of the control system. The team thought it valuable to understand where the turbine would fail even outside of designed operation. The only scenarios that are forgone are those where runaway conditions at 22 m/s still result in FOS above 10 (i.e. the shaft).

The final topics to address in this inspection are the designs inspired by previous CWC participants, both within and outside the confines of NAU. All inspired designs have been addressed in their respective sections, but the summation of these inspirations can be seen in Table V.

TABLE IV
MINIMUM FACTORS OF SAFETY

Part	Conditions	FOS
Blade	Runaway (22 m/s)	1.17
	Runaway (13 m/s)	3.67
	Operating (13 m/s)	15.87
	Operating (11 m/s)	21.47
	Voltage Protection	7.77
Hub	Runaway (22 m/s)	0.54
	Runaway (13 m/s)	1.63
	Operating (13 m/s)	6.58
	Operating (11 m/s)	9.16
	Voltage Protection	3.11
Brake	Operating (22 m/s)	5.31
	No stall (22 m/s)	2.32
	Operating (13 m/s)	14.38
	No stall (13 m/s)	6.60
Shaft	Runaway (22 m/s)	183.6
Base-plate	Operating (22 m/s)	24.5
Tower-Nacelle Connection	Operating (22 m/s)	11.4
Electronics	Runaway (22 m/s)	0.47
	Runaway (13 m/s)	0.80
	Operating (13 m/s)	1.72
	Operating (11 m/s)	2.03
	Voltage Protection	1.17

TABLE V
INSPIRED DESIGNS

Inspiration	Design Description
2020 NAU	Pitching that utilizes a swash plate
2020 NAU	Load safety enclosure
2020 NAU	Emergency stop button
2019 PSU	NACA0009 profile for fin wings
2018 NAU	Rubber backing for brake disk

C. Commissioning

When installing the turbine in the field, there are several considerations that need to be made. These considerations are not only for the safety of the students operating the machinery, but also for the ideal operation of the turbine.

Prior to moving the turbine, confirm that...

- the base-plate is mounted to the wooden support and all wiring is fed through the clearance hole so that no wires are crushed under the weight of the apparatus.
- the blades are pitched to stall so that any ambient wind will not cause rotation that could injure on-site technicians.
- all Anderson and/or JST interconnections between the turbine, electrical box, PCC, load, and power supply are disconnected.

While moving the turbine, be sure that...

- two people accompany the turbine at all times. One to support the weight of the turbine and maneuver through enclosures, another to open doors, keep the wiring from touching the ground, and aid the individual carrying the turbine in any manner required.
- other components can be moved by a single individual, but efforts should be made that no wiring is dragging behind the individual that could get caught on doors, furniture, etc.

The following instructions are specific to the team's testing apparatus that was previously displayed in Figure 36, but similar guidelines should be followed in any testing or operating environment. When installing the turbine...

- remove the roof of the testing vehicle. This should be done without any turbine components in the nearby vicinity.
- place the plywood frame atop the roofless vehicle and insert the 2"x4" anchor along the plywood over the center bolt holes.
- with one member within the vehicle and another accessing the top, feed the two M12 bolts through the clearance in the car's overhead frame, at which point the locking nuts can be wrenched down to the 2"x4" anchor.
- using ratchet straps, secure the plywood to the front and back of the vehicle. This should involve an extra wrap around any available sections of the vehicle frame.
- the anemometer can now be installed at any of the plywood corners. From within the vehicle, feed four M10 bolts through the plywood so an individual above the vehicle can secure them with locking nuts.
- the installation of the turbine should involve three individuals, one within the vehicle and two others outside supporting the weight of the turbine. Feed the cabling through the center clearance and align the 3 M10 bolt holes. Using M10 bolts, torque down the turbine with wing nuts to 50 N·m (If tooling is available).
- Prior to securing the final wing nut, insert the 12 mm ring terminal around the bolt. This is attached to an 18-gauge wire that acts as a tower ground and is fed directly into a JST outside the electrical box. There is a separate clearance for this wire in the plywood 5 cm outside the perimeter of the base-plate.
- Place all other components (electrical box, PCC, load, and power supply) within the vehicle and make all necessary connections. The turbine to electrical interface has 5 Anderson connections (3-Phase and 6V feedback) along with 6 JST connections (stepper control, actuator control, and tower ground). All are clearly labeled at each side of the connection.
- the electrical box to PCC to load connections all feature clearly labeled Anderson connections. The only remaining wiring is the parallel connection of the power supply to the load, which is done through typical color coded DC power supply headers. To power the supply within the vehicle, a 12 VDC to 120VAC inverter is required.
- once all components are secure within the vehicle and the blades have been repositioned to start up, the turbine is ready for operation. Be sure that the PCC is easily accessible so power production can be monitored and the emergency stop button is readily available.

X. Dynamic Testing

In midst of the global pandemic where access to wind tunnels is scarce, the team utilized a group member's personal vehicle to simulate a flow field as previously shown in Section IX. Figure 37 shows this vehicle on a secluded forest service road with the turbine in operation.



Fig. 37. Dynamic Vehicle Testing

A. *Vehicle Testing*

The group was capable of testing start up, operating, and parked conditions. The results of these tests are shown in Figure 38. Examining the raw data, parked conditions displayed promising results, keeping the turbine static at wind speeds up to 13 m/s with no significant power production. The trends in the other testing scenarios indicate issues with start up and power output at winds speeds at and above the rated regime despite the visually apparent rotational velocity obtained. The maximum power achieved was 11.14 W at a wind speed of 21.5 m/s. At this particular instance, the achieved voltage was 5.84 V. This explains why the control algorithm did not shut down the turbine, as substantial voltage losses were experienced and the system did not approach the over-voltage protection event despite the higher wind speeds.

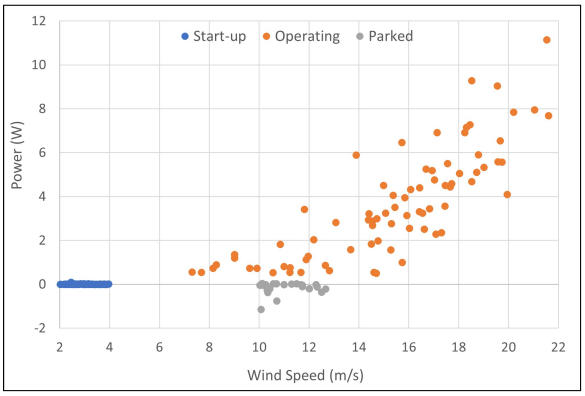


Fig. 38. Dynamic Testing Results

B. *Electrical Investigations*

This level of power production is an order of magnitude lower than Q-Blade estimations (425 W at 21.5 m/s). This drastic difference was a strong indication of a malfunctioning electrical component. In order to address some of the problems seen, the group re-examined the electronics in a comprehensive manner. The testing apparatus is seen in Figure 39. Once a steady rotational velocity was obtained by the dynamo-meter, the line to line 3-phase, pre-step up, and post-step up voltages were all read in tandem with the output of the PCC. Although the dynamo-meter was in use, the generator supplied power through the same configuration shown in Figure 31 with one extra terminal prior to the headers located in the lower nacelle.



Fig. 39. Electrical Testing Apparatus

It was discovered that the generator was out of phase and the line to line voltages were varying up to 1.5 V. After several tests were run consisting of three different generators of different kV rating and multiple electrical configurations to troubleshoot the experienced issues, the group theorized the problem was a faulty rectifier. After replacing the component, the group ran a full electrical system test that resulted the values present in Figure 40. The values obtained through testing are compared to the maximum power output that could be seen at that rotational velocity as derived by Q-Blade. This data shows a more appropriate capacity that will result in more appropriate power production in future vehicle tests.

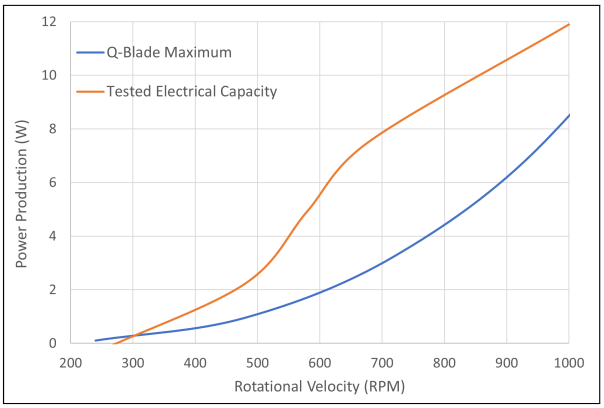


Fig. 40. Tested Electrical Capacity

XI. Conclusions

NAU's 2021 CWC turbine team has produced a mechanically and electrically functioning turbine

as per the regulations set forth by the DOE in the RR. The blades produced have a theoretical efficiency over 45% and have been tested and simulated to confirm the structural capability of the blade to withstand a variety of scenarios including rotational velocities up to 8000 rpm. A unique pitching system was then developed to increase the performance of the blades in a variety of scenarios, producing nearly 0.02 N·m of torque at wind speeds as low as 3 m/s and reducing torque down to 0.65 N·m in strenuous flow regimes (22 m/s). Other critical subsystems include the brake and yaw. The braking mechanism boasts a FOS of 5.31 after many safety precautions employed in the initial designs. The yaw system proved efficient in live testing in a variety of wind speeds with no signs of structural damage. These physical designs were then complimented by electrical systems and control algorithms that were carefully adjusted to withstand the expected scenarios and optimize the operation of the turbine. Live vehicle testing then highlighted ways to prevent power loss, which was then confirmed through the comprehensive testing of the electrical system in a controlled environment. The product seen documented throughout the report is not only a result of the efforts put forward by the group members, but also of the support the group received financially, academically, and emotionally from NAU faculty, DOE representatives, and the community developed by the CWC and the wind industry in Flagstaff and throughout the United States. The group looks forward to involving themselves with NAU's 2022 CWC team and act as that support as more young engineers explore the physics and design considerations that are embedded within the study and research of wind turbines.

REFERENCES

[1] U. D. of Energy, "Cwc2021 rules and requirements," 2021.

[2] J. F. Manwell, J. G. McGowan, and A. L. Rogers, *Wind energy explained: theory, design and application*. John Wiley & Sons, 2010.

[3] W. Shuhua, X. Qiaoli, L. Fen, D. Jinming, H. Jia, and X. Bingshe, "Preparation and properties of cellulose-based carbon microsphere/poly(lactic acid) composites," *Journal of Composite Materials*, vol. 48, 04 2014.

[4] L. Duncan *et al.*, "CWC20 NAU Technical Design Report," *United States Department of Energy*, 2020.

[5] M. Cruz Gómez, E. Gallardo-Hernández, M. Vite Torres, and A. Peña Bautista, "Rubber steel friction in contaminated contacts," *Wear*, vol. 302, no. 1, pp. 1421–1425, 2013, wear of Materials 2013. [Online]. Available: https://www.sciencedirect.com/science/article/pii/S0043164813001099

[6] A. Proulx, S. Rich, J. Kaewvichien *et al.*, "The Pennsylvania State University Wind Energy Club Technical Design Report," *United States Department of Energy*, 2019.

[7] B. Liu, R. Villavicencio, and C. Guedes Soares, "Failure characteristics of strength-equivalent aluminium and steel plates in impact conditions," 03 2013.

Northern Arizona University

2022 Collegiate Wind Competition

Turbine Team

Technical Design Report

For the United States Department of Energy

4/24/2022

Prepared by,

Owen Murphy	Mikela Petersen	Lucas Johnson	Graham Burnside	Dario DeDonato	Ben Coulter
ME Team Lead	Blades	Pitching	Foundation	Tower & Yaw	Brakes
jom28@nau.edu	mmp378@nau.edu	lbj38@nau.edu	gfb32@nau.edu	dgd53@nau.edu	bsc226@nau.edu

Samantha Nearing	Chase Hughes	Andrew Harper	Tyler Schwartz	Maxwell Fawcett
EE Team Lead	Diversion Load	DC/DC Converter	PCB Design	Arduino Control
sdn63@iris.nau.edu	cmh789@nau.edu	andrew.harper@nau.edu	tms579@nau.edu	mbf95@nau.edu

WindJa Energy Club at NAU

1 Contents

2 Executive Summary 3
3 Design Objectives 3
3.1 Turbine Objectives 3
3.2 Foundation Objectives 4
4 Blade Design 4
4.1 Geometry & Airfoil Selection 4
4.2 Aerodynamic Analysis 5
4.3 Composite Manufacturing 5
4.4 Blade and Hub Stress Analysis 6
5 Foundation Design 7
5.1 Initial Axial Thrust and Tower Drag Calculations 7
5.2 Axial Drag Reductions 8
5.3 Load Cell Testing 9
5.4 Design Iterations 9
5.5 Installation Procedure 10
5.6 Foundation Testing 11
6 Mechanical Design 12
6.1 Nacelle 12
6.2 Pitching 12
6.3 Brakes 14
6.4 Tower and Yaw 15
7 Electrical System Design & Analysis 16
7.1 Generator 16
7.2 AC/DC 16
7.3 DC/DC Boost Converter 16
7.4 Diverter Load 17
7.5 Printed Circuit Board 18
7.6 Load 18
8 Software Implementation and Testing 18
9 Field Testing 19
9.1 Procedure 19
9.2 Results 19
10 Changes from Last Year 20
11 References 21
12 Appendix/Photo Collection 22

2 Executive Summary

Northern Arizona University's WindJax team designed, analyzed, and tested a micro-wind turbine and foundation system for the 2022 Collegiate Wind Competition. This report discusses the design choices that the team made, what analysis methods were used to estimate turbine performance, and the testing procedures used to validate the design.

The turbine design consists of a three bladed horizontal axis wind turbine with composite blades, an active pitching system, and a disk brake. The airfoil selected was the GOE79, and the blades were manufactured by vacuum bagging a flax seed based composite structure called BComp around 3D printed cores.



Figure 1: Wind Turbine Full CAD Model Isometric

The variable pitch design was initially based on last year's swash plate system. However, the team made multiple design changes in order to improve performance and reliability. These changes included a hub diameter reduction, swash plate size reduction, switching from a PLA bearing to stainless steel, and directly mounting a linear actuator in place of last year's rack and pinion system.

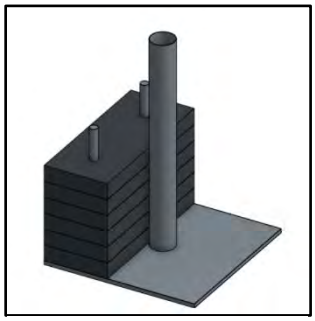


Figure 2: Foundation CAD Model

Due to the introduction of the foundation design requirements for this year's competition, the team prioritized early design prototypes and testing for this system. Additionally, significant efforts were put towards streamlining the turbine and tower to reduce drag forces. After thorough testing, the team settled on a gravity based, directional foundation design. This decision was made as none of the earlier designs tested met the expected moment produced in competition, and the team found that having a heavier foundation that is stable would provide more points than otherwise.

3 Design Objectives

3.1 Turbine Objectives

Looking at the three tasks that will be completed at competition that are specifically focused on the turbine, the team developed design specific objectives to optimize performance in each task. For the power curve performance task our turbine must produce maximum power between wind speeds of 5 m/s to 11 m/s. To accomplish this task, the team's main design objective is to maximize the turbine's coefficient of power. In order to meet this design objective, the team designed blades that maximize the lift coefficient to drag coefficient ratio at the expected Reynolds numbers based on the known wind speeds. The blade shape also maximizes the swept area, optimizing the energy captured from the wind. While the cut-in wind speed is not a measured task in the competition, the team is cognizant of our turbines cut-in wind speed and is aiming to have turbine startup in wind speeds less than 5 m/s. The turbines pitching system will reduce the cut-in wind speed, as well as improve the power output between 5 m/s to 11 m/s.

For the safety task, the wind turbine must be able to reach "shutdown" at wind speeds up to 22 m/s [1]. The design objective for the safety task is to have a braking system that can overcome the moment

created by the shaft at 22 m/s. The team accomplished this design objective by designing a disk brake system that works in conjunction with the pitching system. The pitching system in the stall position slows the rotation of the blades while the disk brake can further decelerate the turbine as necessary.

The durability task of the competition measures the change in foundation position after the completion of the previously mentioned tasks. The main design objective for this task is to minimize the drag on the nacelle and the tower. The design objective was accomplished by creating the most compact nacelle assembly possible. The team further reduced drag by creating a streamline attachment for the tower and the nacelle, thus minimizing the pressure drag.

3.2 Foundation Objectives

There are two tasks targeted towards the foundation, these being the durability task and the structure weight task. The first objective is to create a foundation that would move no more than 6mm during wind tunnel testing. The second objective was to make the foundation as light as possible while still fulfilling the durability objective. Lastly, the foundation must be fully installed within the 15 minutes of allotted time.

Ultimately, the team prioritized durability as this was more crucial to the safe operation of the turbine. Multiple lightweight foundation designs were tested, but the team determined that these lightweight designs did not fulfill the durability objective.

4 Blade Design

4.1 Geometry & Airfoil Selection

In order to design and analyze blades, the team used a Matlab code based on Blade Element Momentum theory (BEM). This code was created by the team and output initial chord lengths and angles of twist at each blade section. The twist angles and chord lengths as a function of radial position can be seen in Figure 3:

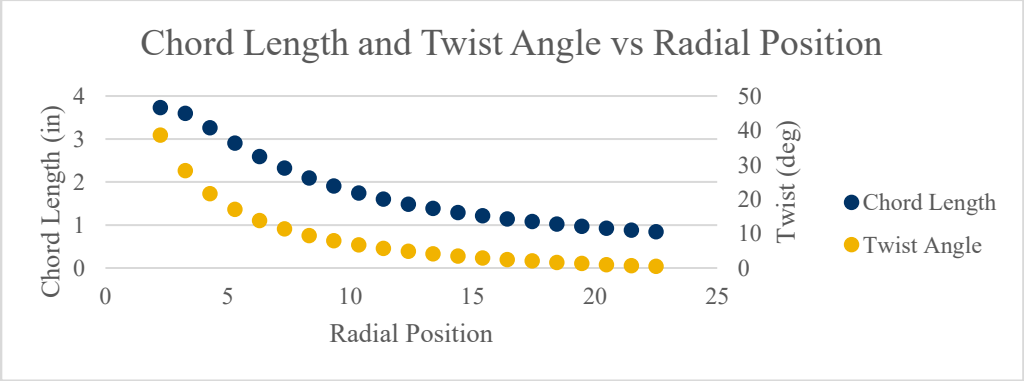


Figure 3: Chord Length & Twist vs Radial Position on the Blade

With these values, the Reynold's number range was calculated for the expected conditions at competition. The Reynold's number was used to evaluate various airfoils that were subsequently simulated using Q-Blade. This simulation data was used to estimate the Power Curve Performance Task score at competition. As a result of this process, the team settled on the GOE79 airfoil as it provided the best balance of manufacturability and performance [2].

4.2 Aerodynamic Analysis

Q-Blade simulations were used to estimate the Coefficient of Power, or Cp, of the blades at various tip speed ratios, or TSR's. As a result of these simulations, the team found a maximum Cp of approximately 0.44 at a TSR of 4.5. Additionally, due to the inclusion of an active pitching system in this year's turbine, Cp vs TSR curves were simulated for a variety of pitch angles relative to this maximum. These curves are overlayed in Figure 4 to visualize the change in performance for varying pitch angles and the ability to feather to turbine blades out of the wind. Similarly, the power curve from 5m/s to 22m/s was generated using simulations from Q-Blade. The rated power for the turbine is 54.3W as seen in Figure 5.

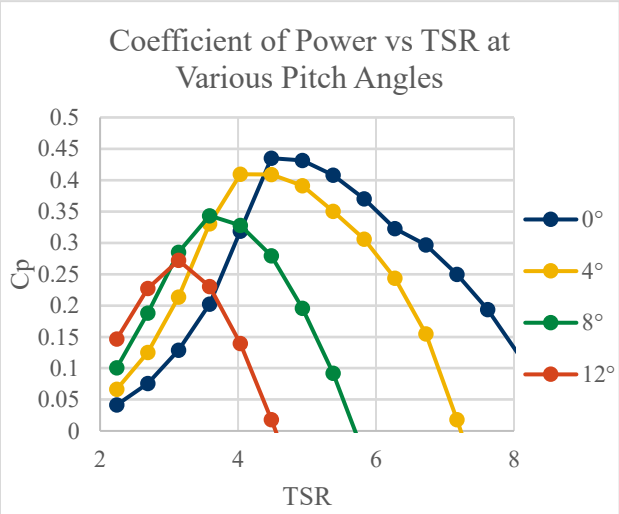


Figure 4: Power Coefficient vs Tip Speed Ratio at Various Pitch Angles

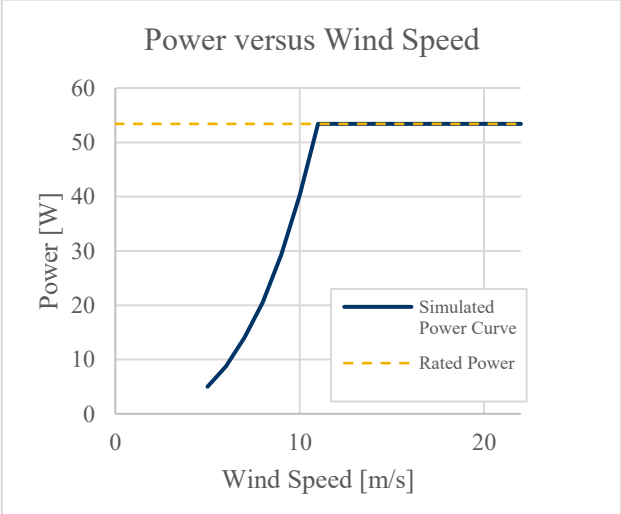


Figure 5: Power [W] vs Wind Speed [m/s]

4.3 Composite Manufacturing

After printing prototype blades, it was determined that fully 3D printed blades would not be suitable for the expected loads given the low percent thickness of the airfoil. After discussions with the composites sponsor, Gurit, the team decided to use BComp, a material similar to carbon fiber but sustainably made from flax seed. Without composite manufacturing experience, the team initially experimented with 3D printing split molds. However, due to the time commitment of designing and manufacturing new molds for every iteration of the blade design, the team decided to switch to vacuum bagging BComp around 3D printed cores. After countless attempts, the desired blade quality was eventually achieved through this method. The manufacturing process first involves hand laying-up the BComp around the cores, placing the blades in a sandwich of peel ply and breather fabric, and sealing the blades in a vacuum bag. Once the blades are removed, they are trimmed and additional coats of epoxy are applied to reach the desired surface finish.

The final blades have both a layer of unidirectional fabric and twill wrapped around a PLA core with a steel grommet inserted into the hub mounting point. The manufacturing process can be seen in Figure 6 with a final blade in Figure 7:



Figure 6: Blade Manufacturing Process



Figure 7: Final Blade

4.4 Blade and Hub Stress Analysis

Due to the complex nature of the composite blades, the team decided to do load calculations only on the mounting point and perform a series of tests on the rest of the blade structure. The load calculations were performed using the mass of the blade, location of the center of mass, and maximum angular velocity in order to find the maximum centripetal force. Using these calculations and the material properties provided by Gurit for the BComp fabric, the team estimated a factor of safety of 1.61.

In order to verify this factor of safety, the team mounted the entire shaft, hubs, and initial blades into a dynamometer and spun the blades until failure. The blades failed at 5306.1 rpm in the location expected, giving the blades a factor of safety of 1.3. As a result of this test, the team decided to alter the geometry of the blade by increasing the distance between the bottom of the blade and the mounting hole as well as imbedding a steel grommet to dissipate the centripetal load.



Figure 8: Blade Centripetal Force Testing Apparatus



Figure 9: Blade Centripetal Force Test Results

In addition to the centripetal test in the dynamometer, the team conducted a bending test. The blade bending test was completed by attaching a weight to the blade tip as seen in Figure 10. The calculated maximum bending stress was 255.02 kPa at 22 m/s, and the testing resulted in a bending stress of 1116.8 kPa before ending the test. This results in a factor of safety of at least 4.38 since blade failure was not reached.



Figure 10: Blade Bending Stress Testing Apparatus

The team also conducted separate hub tests in order to find a factor of safety for the hubs themselves. This was done by mounting weights at a known radius from the attachment point of the hubs and spinning them to a known angular velocity. Similar to the axial blade test, failure was not able to be reached. Due to limitations in the maximum dynamometer angular velocity, the hubs experienced a maximum of 721.2N of centripetal force, yielding a factor of safety of 12.1.

5 Foundation Design

5.1 Initial Axial Thrust and Tower Drag Calculations

When first prototyping foundation designs, the team needed an estimated of the loads the foundation must withstand in the conditions of a runaway event up to 22 m/s. The main sources of these forces were assumed to be the axial thrust of the turbine, the nacelle drag, and the drag on the tower as seen in Figure 11. These forces were estimated with the following equations:

$$T = \frac{1}{2}\rho A U^2[4a(1-a)] \quad \text{Eqn 1}$$

$$F_D = \frac{1}{2}\rho A U^2 C_D \quad \text{Eqn 2}$$

The axial force was estimated with equation 1, where T is the thrust force, ρ is the density of the air, A is the rotor area, U is the free stream velocity, and 'a' is the axial induction factor [2].

Operating at the Betz limit with 'a' = 1/3, sea level density $\rho = 1.23\frac{kg}{m^3}$, rotor area $A = \frac{\pi}{4}D^2$, and free stream velocity $U = 22$ m/s the maximum axial thrust force was calculated to be 42 N or 9.45 lbf. This procedure was done again using the power coefficient of the blades calculated through QBlade. The axial induction factor 'a' was then calculated to be 0.151, and thrust was solved for. MATLAB was used to create a plot of the estimated thrust forces from 0-22 m/s, shown in Figure 12. According to the QBlade limit, the maximum thrust force is 24 N, or 5.4 lbf.

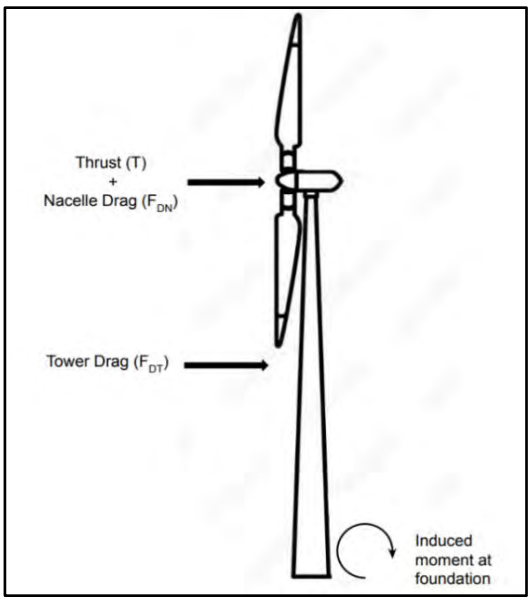


Figure 11: Nacelle and Tower Forces Diagram

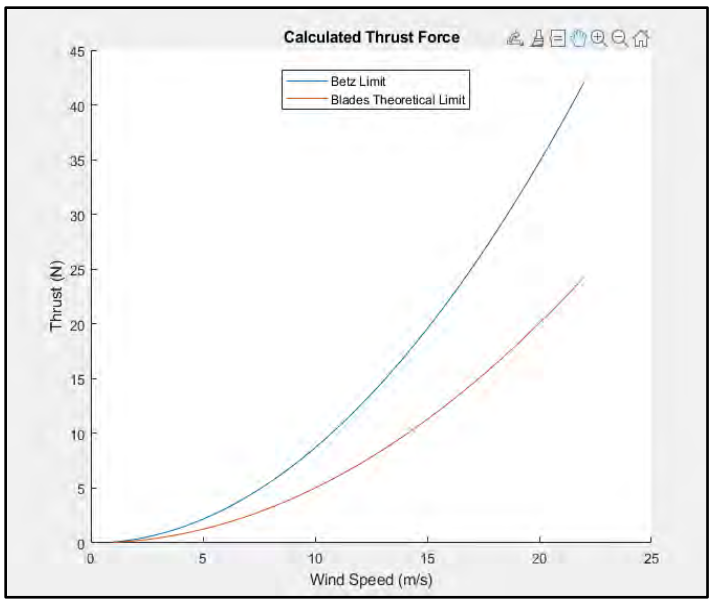


Figure 12: Thrust Force Testing Results

For the initial tower drag estimate, the team used equation 2, where C_D is the coefficient of drag, and A is the planform area of the cylinder. Initially, the tower was assumed to be a cylinder of 3.81 cm diameter with a height of 60 cm. At 22 m/s, the Reynolds number was calculated to be $5 * 10^4$, giving an estimated C_D of 1.1 [3]. Under these conditions, F_{DT} was estimated to be 7.5 N, or 1.7 lbf.

Lastly, the nacelle drag, or F_{DN}, was estimated. This was determined by modeling the nacelle as a simple cylinder of 10 cm diameter perpendicular to the wind, with a C_D of 1.2. Following equation 2 again, this gives a drag force of 2.8 N, or .63 lbf.

With these forces, the tipping moment at the foundation was calculated to determine the restoring moment needed to prevent the tipping of the foundation and turbine. Based on the estimated distance from the rotor center to the top of the sand as 1 m in the competition rules, the distance from the center of the tower would be approximately 0.7 m. By multiplying the forces with their respective lengths, the calculated maximum theoretical moment is 50 N*m, or 37 lbf*ft. Using the maximum Cp from Q-Blade, the maximum theoretical moment is 32 N*m, or 23.6 lbf*ft.

5.2 Axial Drag Reductions

After the initial forces were estimated, the team investigated ways to reduce these forces. Since the majority of the torque produced is from the thrust force of the rotor, the team looked at ways to reduce this thrust force. However, it was found that this would result in decreased performance in the power curve performance task. The team decided to prioritize decrease the drag on the nacelle and tower in order to improve the foundation durability without sacrificing power output.

To accomplish a reduction in drag on the tower, the team decided to create a streamline attachment to slide over the tower to reduce the pressure drag. The streamline chosen was an EPPLER 863 strut airfoil. This was chosen for two reasons. The first was due to the high percent thickness, allowing the full length of the airfoil to fit within the 15cm tower diameter requirement. A top view of this attachment can be seen in Figure 13. The second reason was the relatively low drag coefficient, minimizing the load on the foundation.

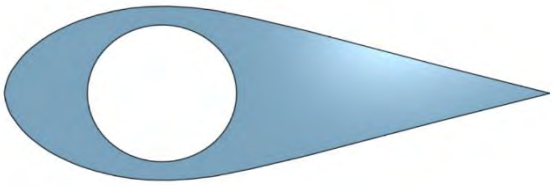


Figure 13: EPPLER 963 Airfoil Tower Attachment

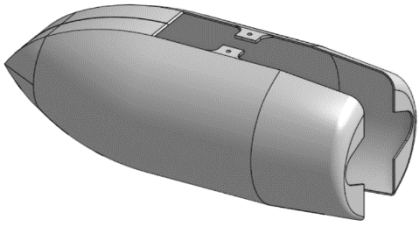


Figure 14: Streamlined Nacelle Covers

Similarly, the nacelle was also streamlined to reduce pressure drag. This was done through creating covers that tapered down to a point, mimicking the design of an airfoil, seen in Figure 14.

5.3 Load Cell Testing

To better determine the forces the foundation will be subject to, the team decided to devise a test to measure the horizontal drag forces. This was done through using a 10 kg load cell attached to the bottom of an extended tower that was designed to pivot about an axle. The turbine would then push against the load cell in the opposite direction of the incoming wind as seen in Figure 15. To calibrate the load cell, the team used a scale to pull at a known weight and inputted the value into the Arduino calibration code.

With this testing set up in combination with a cup anemometer, the team is able to estimate the drag forces on the turbine. After having done initial tests, the team noted that the maximum thrust output at approximately 15 m/s was on the order of 2 lbf, or 9 N. Referring to Figure 12 in section 5.1, this is slightly lower than the blades theoretical limit.

It should be noted that there are a few limitations with the current testing setup, mainly that the tower length above the pivot point is not identical to the competition tower length, and the drag on the tower below the pivot point will counteract the thrust force. Additionally, it was noted that the turbine created vibrations that are not easily replicable when testing the foundation.



Figure 15: Axial Thrust Force Testing Apparatus

5.4 Design Iterations

At the beginning of foundation testing, the team focused on the structure weight portion of testing. The first foundation prototype was a mesh box design intended to resist the predicted thrust force of 42 N. Due to the uncertainty of the sand properties, the team determined that it was essential to immediately begin testing procedures. After building the mesh prototype and testing apparatus similar to the one that will be present at the competition, foundation testing data could be collected. The mesh design resisted less than 4 N of force acting at the location of the hub and was therefore redesigned for a better performance.

The next design iteration made use of multiple “sand screws” that would be inserted into the ground and intended to maintain the stability of the foundation. 3D printed sand screws of various geometries were

created for testing purposes. After conducting similar testing to the mesh box, the team found that none of the sand screws designed were able to resist the estimated thrust loading.

The third design iteration was a steel box that would be inserted into the sand depth and then filled with sand to act as a weighted foundation. Multiple box geometries were created and tested including a box design with an angled backplate that was intended to make use of compressive forces in the sand. The highest amount of blade thrust force the box designs could resist was 11 N. The team tested the same steel box design and added 37.5 lbs of weights to the box. The weighted box resisted 42 Nm which had the best performance.

The design iteration process began with several lightweight structures that did not perform as well as anticipated. Due to potential improvements in the overall points scored at competition as well as preventing possible damage to the turbine, the priority shifted from weight reduction to durability.

The final design consists of a 25 x 25 cm 3/16 in thick steel plate with a 1.5 in steel tube welded to the center. Two threaded rods were then welded to the front half of the steel plate. Multiple 25 x 10 x 2.5cm steel blocks had holes drilled through them to allow them to fit over the threaded rods. A total of six blocks can be added, giving a final weight of 70 lbs, or 31.7 kg. Based on the maximum moment of 32 N*m calculated in Section 5.1, the factor of safety against tipping for this design is 1.84.

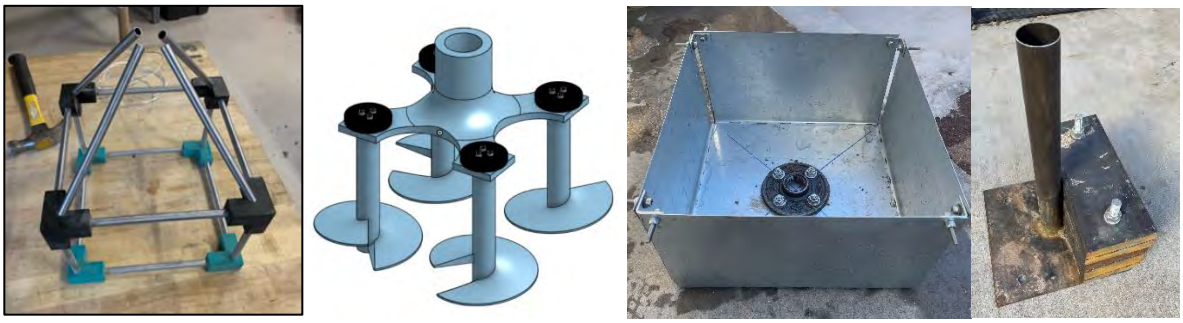


Figure 16: Foundation Design Iteration Method from Oldest (Left) to Most Current (Right)

5.5 Installation Procedure

The competition requires that the foundation design be installed into the testing facility without any of the team members' hands touching the water. For the installation process, the team has designed a square steel perimeter box (Figure 17) that slides into the sand. The steel perimeter box is dimensioned with an opening of 25 x 25cm that fits around the foundation and extrudes out of the water, allowing the team to hold onto it without touching the water. This installation tool also contains markings near the top of the waterline that depict how far into the sand the box should be installed.

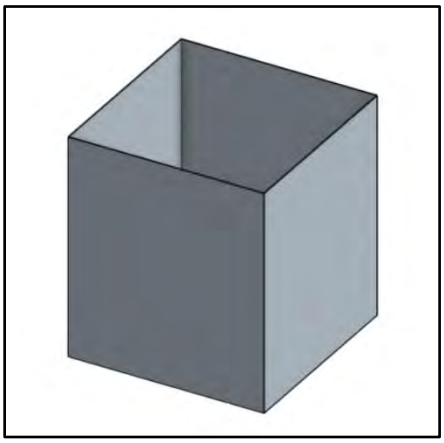


Figure 17: Installation Perimeter Box

The first step of installation is sliding the installation perimeter box into the sand until the waterline reaches the indicated marking. A long shovel is then used to dig out the sand within the box without touching the water. The sand removed from inside the box is simply dumped outside of the box. Once the team has dug out all the sand to the bottom of the perimeter box, a garden hoe is then used to remove any sand in the corners of the box. The garden hoe is

also used to pack down the sand at the bottom of the box and creates a flat surface for the foundation to rest. The foundation is then lifted by a team member and carefully dropped into the perimeter box until it is fully resting on the sand at the bottom. The perimeter box is then slid out of the sand and the excess sand surrounding the foundation is compacted. This completes the installation process.

5.6 Foundation Testing

The foundation was subjected to one test, a moment arm test. The foundation was installed as the team plans to do in competition. Then a fish scale was attached to the top of the tower, where the thrust force from the nacelle will act on the tower. The scale was then pulled until the tower moved more than 6 mm; the force needed to move the tower was recorded. The moment arm test was completed for every foundation design concept our team built.



Figure 18: Foundation Testing Setup

6 Mechanical Design

6.1 Nacelle

The nacelle is designed to provide mounting locations for both linear actuators, the generator, the shaft bearing, the linear bearings, the covers, and tower connection. The design went through two main iterations from the first to the second semester. The initial design consisted of a flat plate with slots to provide easy modification and design flexibility when designing the mounts for all subsystems. Once the team had decided on the overall nature of each subsystem, the nacelle went through a complete redesign.

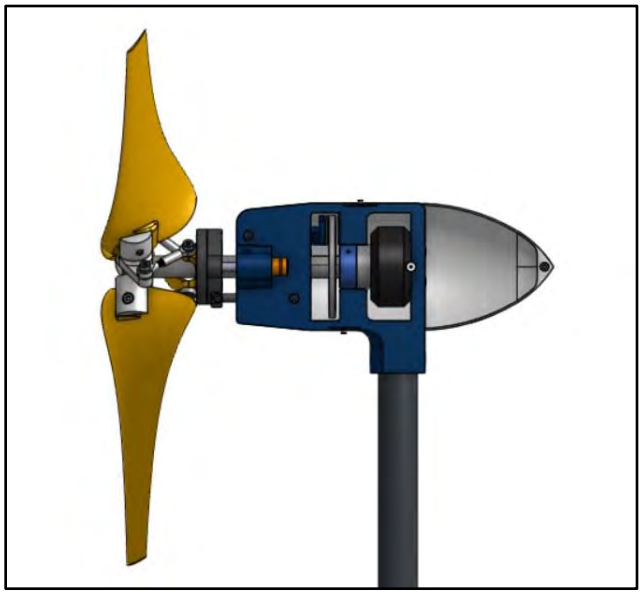


Figure 19: Wind Turbine Full CAD Model Internal View

This redesign was focused on reducing the size and part count of the turbine. Size reduction was prioritized in order to reduce the axial drag on the nacelle, and thus reduce the load on the foundation. The tower mount was also shifted towards the back of the nacelle in order to keep the mass of the turbine in front of the foundation's point of rotation. The current nacelle consists of only two 3D printed parts with various heat-set inserts used in order to provide reliable threads for subsystem attachment. The rear of the nacelle provides the mounting locations for the tower, generator, and stationary brake pad while the front holds the shaft bearing and linear bearings for the pitch system. Both actuators are imbedded within the front of the nacelle and various channels were designed to provide adequate cable management.

6.2 Pitching

The pitching system is designed to change the angle of all three blade simultaneously. The system will be used to prevent aerodynamic hysteresis and add redundancy to the braking system. The system is comprised of a linear actuator, a linear swash plate, three push rods, and three blade hubs. The blades are connected to the shaft via the hub pieces as seen in Figure 20, and these parts allow the blades to rotate around the bolt attaching the hub to the shaft. The push rods attach the hubs to the linear swash plate. The push rods are made up of two ball joints at each end of the rod, the ball joints allow the geometry of the system to change when pitching. The linear swash plate allows the inner disk to rotate with the rotation of shaft while holding the outside side steady in order to attach it to the linear actuator. The linear actuator is mounted to the nacelle and the piston rod is mounted to the linear swash plate. As the piston rod extends and retracts the blades all change angle in unison.

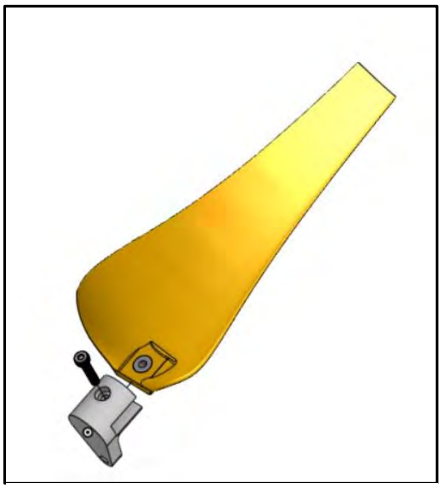


Figure 20: Blade and Hub Assembly

The entire system is controlled with a single linear actuator which means that the linear actuator chosen for the system must be able to withstand the force acting on it from the pitching moment. In order

to calculate the pitching moment created by the blades, the team had to first complete an analysis of the pitch mechanism geometry.

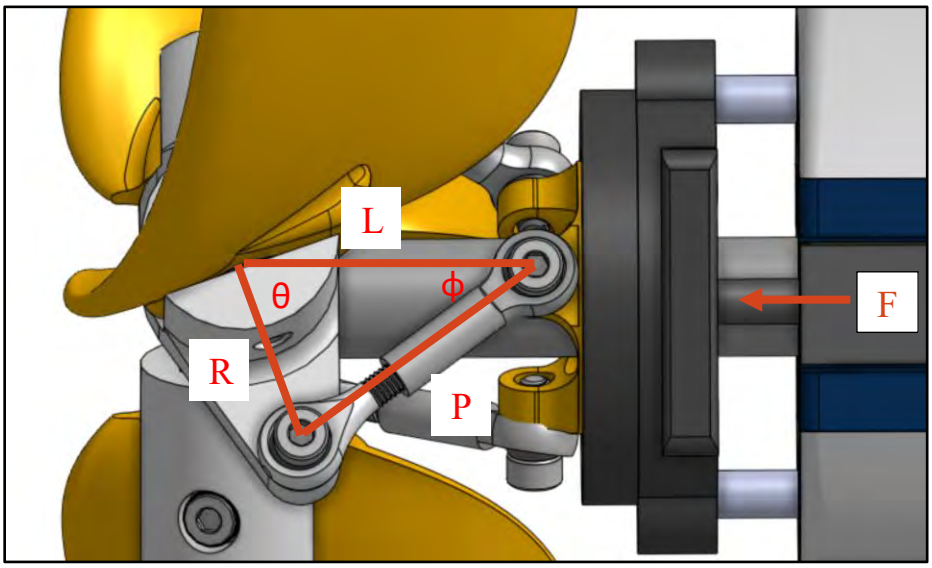


Figure 21: Pitching System Geometry

As seen in Figure 21, the pitch system has a constant hub length, R, and push rod length, P, but changes in length on the shaft, L, due to the change in the linear actuator piston rod length. The change in length causes the angles θ and φ to also change. The change in φ can be described using Equation 3. The total force can then be described using Equation 4, where M is the pitching moment for one blade. The force equation is specific to the geometry of the system. Once the previous two equations were developed, the total pitching moment for one blade was calculated elementwise using Equation 5.

$$\varphi = cos^{-1}\sqrt{1-(R/L)^2 \sin(\theta)^2} \qquad \text{Eqn 3}$$

$$F = \frac{3Mcos(\varphi)}{Rcos(90-\theta-\varphi)} \qquad \text{Eqn 4}$$

$$M = C_M(1/2)q_\infty {U_{rel}}^2 Ac \qquad \text{Eqn 5}$$

The variables in the Equation 5 are defined as follows: C_M is the moment coefficient of an airfoil at a specific Reynolds number, q_∞ is the dynamic pressure, U_{rel} is the wind speed relative to the blade, and A is the chord length, c, times the span, S. The geometry of the blade was gathered from the program QBlade, and the moment coefficient was gathered from Airfoil Toolbox [4] for a GOE79 airfoil. The team then calculated the relative velocity of the wind at each section of the blade, followed by calculating the pitching moment at each section of the blade. The air density was assumed to be standard air density at sea level. The following table shows the elementwise calculations for one blade:

Table 1: Blade Pitching Moment Analysis

	Blade Section	Chord Length (m)	Section Arean (m^2)	Local TSR	U relative (m/s)	Section Pitching Moment (Nm)
1	1	0.0491	4.9056e-04	0.5998	25.6540	0.0010
2	2	0.0523	5.2307e-04	0.8314	28.6103	0.0014
3	3	0.0511	5.1087e-04	1.0630	32.1073	0.0016
4	4	0.0480	4.8046e-04	1.2946	35.9879	0.0018
5	5	0.0445	4.4482e-04	1.5261	40.1410	0.0020
6	6	0.0410	4.0964e-04	1.7577	44.4902	0.0020
7	7	0.0377	3.7715e-04	1.9893	48.9834	0.0021
8	8	0.0348	3.4798e-04	2.2209	53.5844	0.0021
9	9	0.0322	3.2209e-04	2.4525	58.2676	0.0022
10	10	0.0299	2.9921e-04	2.6841	63.0148	0.0022
11	11	0.0279	2.7898e-04	2.9157	67.8124	0.0022
12	12	0.0261	2.6105e-04	3.1472	72.6505	0.0022
13	13	0.0245	2.4510e-04	3.3788	77.5215	0.0022
14	14	0.0231	2.3086e-04	3.6104	82.4196	0.0022
15	15	0.0218	2.1808e-04	3.8420	87.3402	0.0022
16	16	0.0207	2.0657e-04	4.0736	92.2798	0.0022
17	17	0.0196	1.9616e-04	4.3052	97.2353	0.0022
18	18	0.0187	1.8671e-04	4.5368	102.2046	0.0022
19	19	0.0178	1.7810e-04	4.7683	107.1856	0.0022
20	20	0.0170	1.7021e-04	4.9999	112.1769	0.0022
21	21	0.0163	1.6298e-04	5.2315	117.1771	0.0022

The summation of the pitching moment on each section of the blade was then used in the previous force equation with the system geometry to find the total force required for our linear actuator. Figure 22 describes the force required for the range of angles in our system.

The greatest force the linear actuator is required to hold is 11.17 N. The linear actuator being used is the PQ12-100-6-R Micro-Actuator. This linear actuator has a hold force of 50 N, giving the system a factor of safety of 4.48.

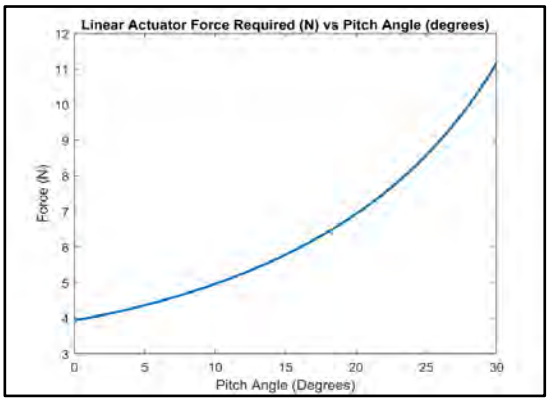


Figure 22: Linear Actuator Force Required vs Pitch

6.3 Brakes

The brakes use a linear actuator with a mounted brake pad to press against a sliding brake disc, compressing the disc with a secondary brake pad fixed to the nacelle. The actuator pad uses a 3D printed mount and both brake pads are made of neoprene rubber. The aluminum disc was manufactured using a CNC router. The chosen actuator is a micro linear servo capable of producing 50 N of force. The brake disc has a diameter of 7.2 cm giving the turbine a theoretical braking force of 3.6 N-m. The design was chosen by the equations for angular momentum and impulse.

The brake system also underwent two different tests: a static test and a dynamic test. The static test had the brake engaged and weight added to the radius of the disk brake. The weight on the radius of the disk brake created a moment on the system. Weight was added until the brake failed, in turn allowing the shaft to spin. While the static test did not show that the brake provided adequate force for the system, the dynamic car testing showed that the system sufficiently decelerated and could

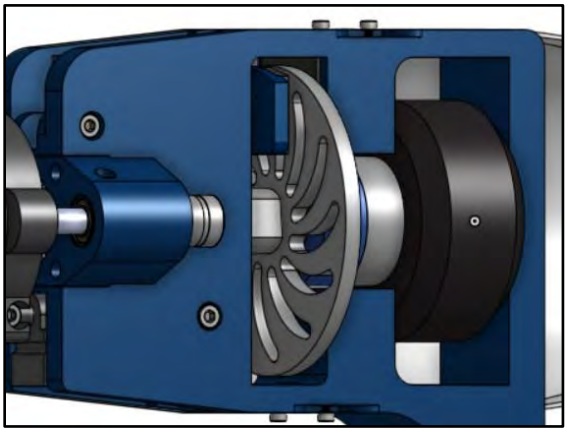


Figure 23: CAD Disc Brake Mechanism

withstand 22 m/s winds without brake failure. The team theorizes that this is due to rapidly decreasing the TSR of the blades and thus reducing the torque generated by the blades.



Figure 24: Static Brake Testing Apparatus

6.4 Tower and Yaw

The tower has been welded to a 0.5-inch-thick steel baseplate. In order to ensure that the weld can resist the forces acting on the tower, a load analysis was conducted to determine the minimum throat length of the weld necessary to maintain structural integrity. The forces acting on the tower were assumed to be equivalent to the axial thrust forces at the location of the nacelle (calculated previously as 42N). The force acting at the top of the tower, the diameter of the tower and the ultimate tensile strength of the welded material were used to estimate the specific weld size. The direct shear stress and bending tensile stress were calculated from Equations 6 and 7 and then combined in Equation 8 for a resultant stress at the weld location [5]. Eq. 9 was then used to find the minimum throat length to resist the estimated force.

$$\tau_s = \frac{Force}{Unit\ Throat\ Length} \quad \text{Eqn 6}$$

$$\tau_b = \frac{Moment * Y}{Unit\ Moment\ of\ Inertia} \quad \text{Eqn 7}$$

$$\tau_r = \sqrt{{\tau_s}^2 + {\tau_b}^2} \quad \text{Eqn 8}$$

$$throat = \frac{\tau_r}{Design\ Strength} \quad \text{Eqn 9}$$

From the above calculations it was determined that having a throat length of 3mm on for the weld will result in a factor of safety above 15. The team assessed this as adequate for maintaining the structural integrity of the tower and baseplate and moved forward with the weld design.

The yaw system is a simple bearing surface with a pin to prevent rotation after foundation installation. A loading force acting on the nacelle is expected to occur and cause stress at the location of the yaw. The team needed to assess the amount of force that could be placed on the yaw without causing the nacelle to fail. Through testing (Figure 25), the nacelle yaw was able to resist approximately 222 N of force. Compared to the expected thrust force acting on the nacelle of 42N, this is a minimum factor of safety of 5.



Figure 25: Nacelle Yaw Loading

7 Electrical System Design & Analysis

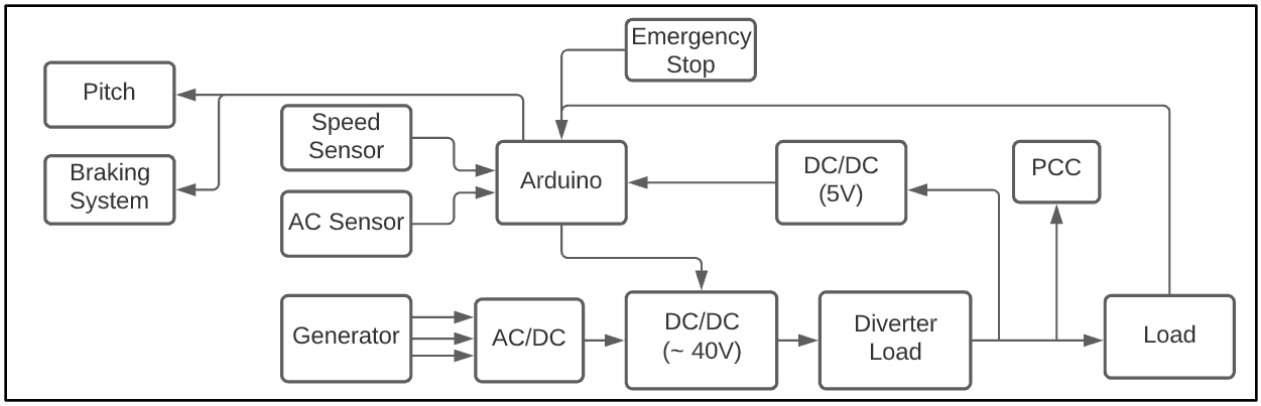


Figure 26: Electrical System Architecture

7.1 Generator

The selected generator for the electrical system was the MAD IPE 5012 160kV motor. The relatively low kv rating of the motor allows for the team to utilize a boost converter for all windspeeds expected at competition. The motor's higher efficiency than competitors at low RPMs made it an ideal candidate for selection in our design for the competition. Additionally, it only reaches about 54 °C after 5 minutes at maximum power output, which was significantly lower than that of its competitors [6].

7.2 AC/DC

A three-phase full wave bridge rectifier, Figure 27, is used to convert the three-phase output of the generator into a DC voltage. The DC voltage then goes through a capacitor of 10µF to help reduce the ripple created by the rectifier. This unit was purchased to help reduce the power losses compared to building one with 6 individual diodes.

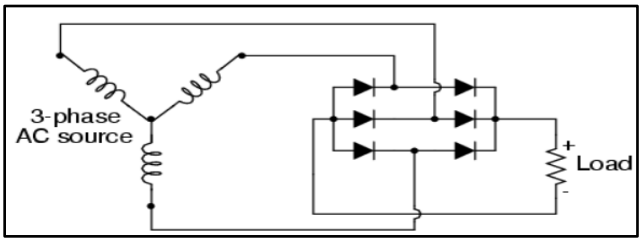


Figure 27: Three-Phase Full-Wave Bridge Rectifier

7.3 DC/DC Boost Converter

The main system is the DC/DC boost converter, Figure 26, this system consists of: 98.5µH inductor, N-channel power MOSFET, diode, and 100µF capacitor. The microcontroller in our system is the Arduino MEGA 2560 coded with MATLAB Simulink. The Arduino will take the output voltage from a voltage divider connected to the output of our system. Depending on the output voltage the duty cycle of the square wave going into the MOSFET will change from 20% to 60% as shown in Figure 28. This control in the duty cycle allows the voltage at the output to be controlled and limited to a maximum of 40 V.

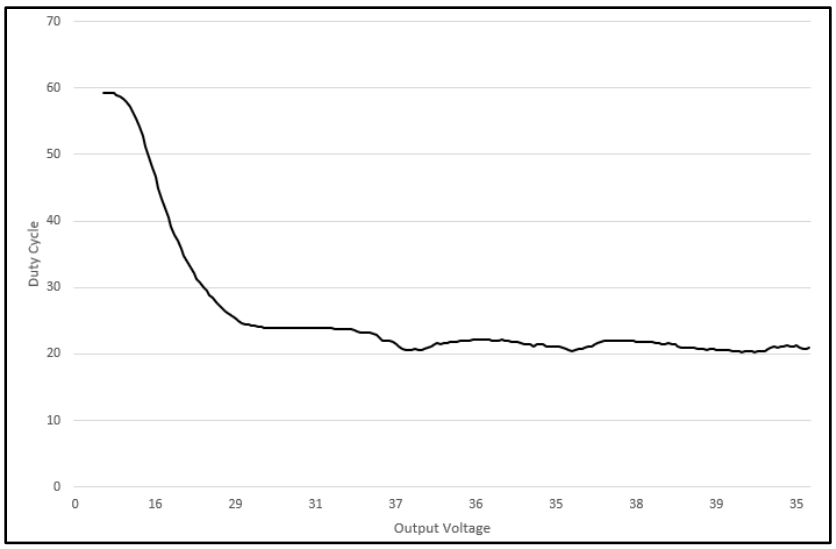


Figure 28: Duty cycle compared to Output Voltage

7.4 Diverter Load

Another important electrical system is the diverter load, Figure 26. The diverter load consists of twelve 10 Ω 100W rated resistors to make an equivalent resistance of 4Ω at 1200 W. This system is controlled by an N-channel power MOSFET used as a switch. The Arduino takes the output voltage and current sensor data to determine if a signal needs to be sent to the gate. If the current is zero, that indicates that the load is disconnected and the MOSFET will turn on, giving power to the diverter load. Within the Simulink code, power is also calculated. If output power reaches a certain value, in our case 40V to give the system some error before reaching the competition maximum of 48V in the case of a runaway or quick RPM boost, the MOSFET will turn on to not exceed that power output. Along with the DC/DC boost converter, this system will also regulate the system voltage when needed. It regulates the power of the system through the dissipation of heat into the large heat sink as seen in Figure 29.



Figure 29: Diversion Load

7.5 Printed Circuit Board

The system in Figure 26: Electrical System Architecture, is implemented onto a PCB. Wire connections are used for the generator, Arduino, diverter load, DC/DC buck converter, and load. The AC/DC Converter, DC/DC boost converter, and sensors are built onto the PCB. All the components on the PCB are through-hole compatible since through-hole components are easier to find higher rated devices for. The PCB is a 2-layer design with top traces shown in red and bottom traces shown in blue as seen in Figure 30. The traces are 1.02 mm equivalent to 18 AWG allowing the board to be rated for 10 Amperes. The board was purchased through JLC PCB.

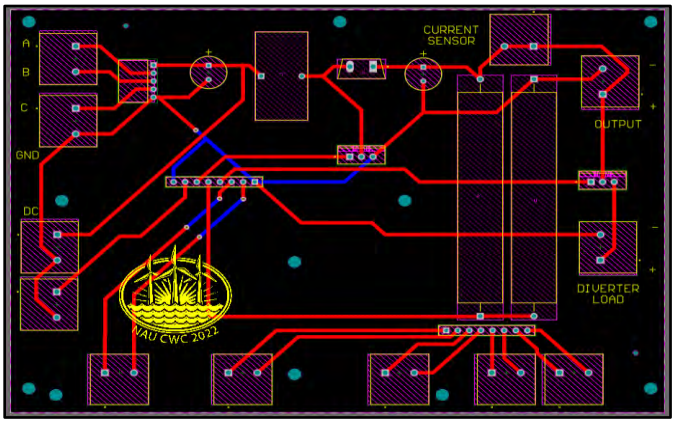


Figure 30: Electrical System Architecture

7.6 Load

The load for the system will be a power resistor capable of 200 W and around 2 Ω. When testing the system at different resistances such as: 15 Ω, 10 Ω, 4 Ω, and 2 Ω. It was found that at lower resistances the current drawn from the source and output current was much larger than when testing at higher resistances. Since the output current for our system can be a maximum of 10 A, the resistance of 2 Ω allows the most current: increasing our power output and efficiency.

8 Software Implementation and Testing

8.1 Software

The program that was used to control all electrical systems and the boosting of the boost converter was all done through MATLAB Simulink. Simulink allowed us to use block style programming and Arduino addon which helped make hardware uploading to the Arduino quite easy, this also helped make it easy to write the algorithms and was able keep everything clearly organized using subsystems for the various parts of the control system for the turbine shown in Figure 31. For testing, we

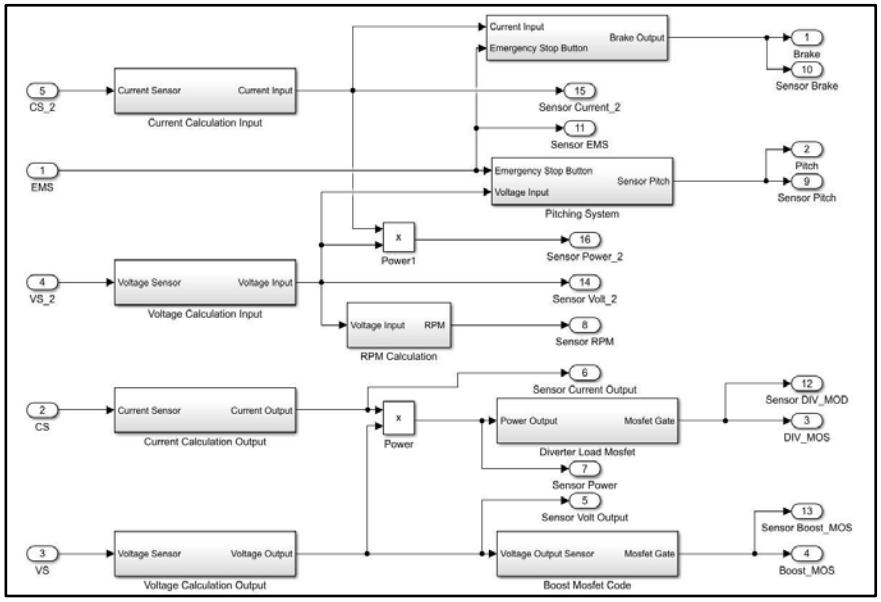


Figure 31: Main Control System Design

used sensor outputs that went to scopes in Simulink to help monitor the input and output data going to the Arduino. And we used another Arduino that read the actual pins going in and out of the main control Arduino and logged the data on an Excel spreadsheet.

9 Field Testing

9.1 Procedure

Before the completion of the full turbine testing, our team tested each subsystem individually. Each individual test allowed our team to gain a better understanding of what is to be expected in the full turbine test. The individual tests also provided our team with a factor of safety for each system, ensuring that each system will be strong enough before assembly. Each of the subsystem tests were completed multiple times to reduce random error with the exception of the tests that resulted in broken parts.



Figure 32: Car Testing Apparatus

Once the team completed individual tests for each subsystem and felt confident in the results gathered the team moved to full turbine testing. The full turbine test proved to be a challenge due to the wind tunnel at NAU not having a large enough test section for our turbine. As mentioned previously, our team designed and built an apparatus to mount our wind turbine on top of a car for testing as seen in Figure 32.

In preparation for car testing, our team assembled the entire turbine and mounted it to the testing apparatus, which was then mounted to the roof of a car. The wires for the motor and the two linear actuators were fed down the tower and into a window of the car. In the car, our team had all the electrical components, including our boost system, control system, and a PCC. A cup anemometer was also mounted in order to collect wind speed data. The PCC recorded the wind speed, voltage, and current of the turbine during each test. The pitch angle and the electrical resistance were changed independently, and values were recorded to compare the power output at various pitch angles and resistances. The axial drag induced on the foundation by the turbine was also tested in this system using the load cell discussed in section 5.3. The team then recorded the thrust force on the nacelle at wind speeds up to 22 m/s. The data provides an estimate for the moment that the turbine will experience at competition.

9.2 Results

During the car testing performed on the entire turbine system, the blades, pitch, brakes, and force acting on the foundation were assessed. Before car testing began, individual tests were conducted on the turbine subsystems to prove the durability and safety of each system. The following discussion determines the reliability and functionality of the designed wind turbine.

The primary form of testing conducted by the team was through car testing. The blade performance, pitch degree performance, and braking performance were all analyzed by this test. In addition to testing the individual subsystems, the overall functionality of the turbine was evaluated. All the subsystems were able to work in unison during car testing to generate power, resulting in a functional turbine. The pitch angle of the blades was changed to find the angle that would generate the greatest amount of power. The pitch angle for startup speeds and slow down speeds were also determined through car testing. It was determined that

the turbine could be completely stopped through the pitching mechanism. This reduces the rotation of the blades and allows for the disc brake system to act as an additional brake for safety purposes.

10 Changes from Last Year

This year's team was not involved with the design and construction of last year's turbine, so much of the current design is new. The four main subsystems that were inspired by previous years were the pitching, braking systems, and electrical system of last year and the composite blades from the 2014 team.

The pitching system from 2021 was designed around the traditional swash plate mechanism but was driven by a motor geared to a rack and pinion system. After discussions with the graduates of that team, it was found that they encountered difficulties in supplying enough force to counter the pitching moment of the blades with this design. Additionally, the design took up significant space inside the nacelle body. As a result, the team used the initial swash plate concept but redesigned with nacelle to accommodate a lead screw design initially, and eventually a linear actuator. The sliding disk brake was also inspired by last year, as well as the many other past teams from both NAU and other universities that utilized a similar system.

The electrical system took inspiration from the previous year's team with: the three-phase full wave bridge rectifier, DC/DC boost converter, and resistive load. The main changes for this year were: using MATLAB Simulink to code the Arduino MEGA 2560, designing the diverter load, designing the DC/DC boost converter, and designing a PCB for the system.

The manufacturing process of the blades was initially inspired by the 2014 team's split mold method. However, after initial prototype blades were made using this method, it was found that the process to re-manufacture the molds for new iterations of the blades was extremely time consuming. As a result, the team branched off into vacuum bagging composite material around a 3D printed core as this allowed for both rapid design iteration but also strong and rigid blades. This was an entirely new process for everyone on the team and took a significant amount of trial runs to reach the current state of the blades.

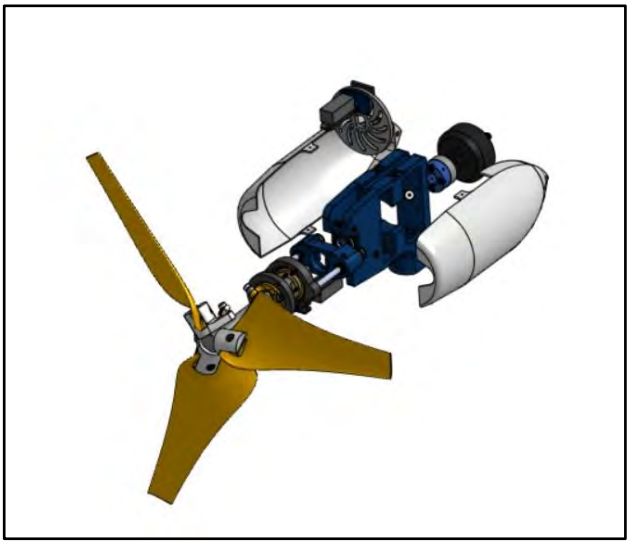


Figure 33: Turbine Exploded View



Figure 34: Assembled Turbine

11 References

[1] "U.S. Department of Energy Collegiate Wind Competition 2022," 14-Oct-2022. [Online]. Available: https://www.energy.gov/sites/prod/files/2020/10/f79/cwc-2021-rules-requirements.pdf. [Accessed: 29-Nov-2021].

[2] J. F. Manwell, J. G. McGowan, and A. L. Rogers, *Wind Energy explained*. Chichester: John Wiley, 2002.

[3] P. J. Pritchard, J. C. Leylegian, R. Bhaskaran, J. W. Mitchell, and R. W. Fox, *Fox and McDonald's introduction to Fluid Mechanics, 9th edition*. Wiley, 2015.

[4] "GOE79 (PFALZ 11) AIRFOIL," [Online]. Available: http://airfoiltools.com/airfoil/details?airfoil=goe79-il

[5] S. Ghosh, "Fillet weld strength calculation example for welded connection subjected to bending," *mechGuru*, 19-Oct-2019. [Online]. Available: https://mechguru.com/free-caculator/weld-strength-calculation-example-for-bending-moment-application/. [Accessed: 24-Apr-2022].

[6] "Amazon.com: Mad components 5012 IPE v3.0 160KV brushless ..." [Online]. Available: https://www.amazon.com/MAD-COMPONENTS-Multirotor-Quadcopter-Hexrcopter/dp/B08K482875. [Accessed: 25-Apr-2022].

12 Appendix/Photo Collection

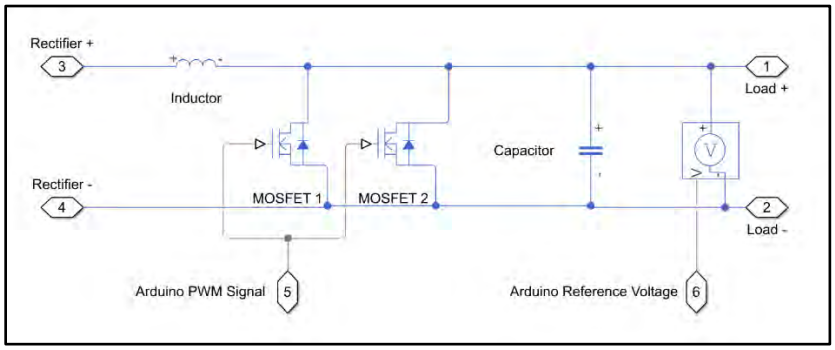


Figure A1: DC/DC Boost Converter

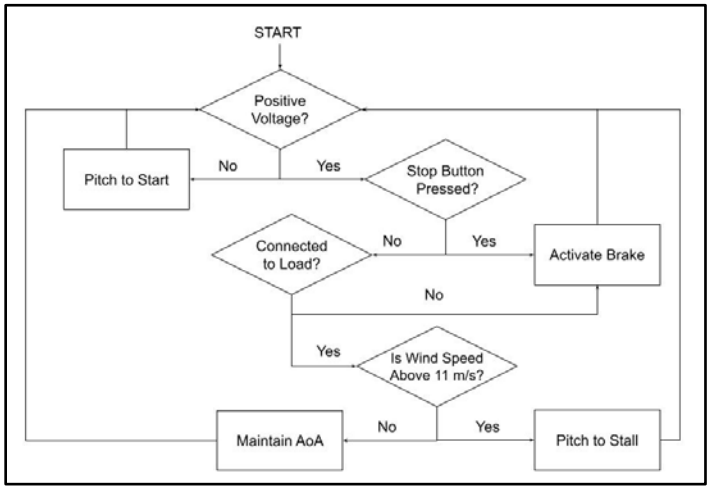


Figure A2: Control Flow Diagram